



HAL
open science

Role of SWI/SNF chromatin-remodeling complexes in tumorigenesis: insights in dedifferentiated melanoma and renal medullary carcinoma

Bujamin Vokshi

► **To cite this version:**

Bujamin Vokshi. Role of SWI/SNF chromatin-remodeling complexes in tumorigenesis: insights in dedifferentiated melanoma and renal medullary carcinoma. Agricultural sciences. Université de Strasbourg, 2020. English. NNT : 2020STRAJ116 . tel-03689309

HAL Id: tel-03689309

<https://theses.hal.science/tel-03689309>

Submitted on 7 Jun 2022

HAL is a multi-disciplinary open access archive for the deposit and dissemination of scientific research documents, whether they are published or not. The documents may come from teaching and research institutions in France or abroad, or from public or private research centers.

L'archive ouverte pluridisciplinaire **HAL**, est destinée au dépôt et à la diffusion de documents scientifiques de niveau recherche, publiés ou non, émanant des établissements d'enseignement et de recherche français ou étrangers, des laboratoires publics ou privés.

ÉCOLE DOCTORALE DES SCIENCES DE LA VIE ET DE LA SANTÉ

Institut de Génétique et de Biologie Moléculaire et Cellulaire

THÈSE présentée par :

Bujamin VOKSHI

soutenue le : **09 décembre 2020**

pour obtenir le grade de : **Docteur de l'université de Strasbourg**

Discipline : Sciences de la Vie et de la Santé

**Role of SWI/SNF chromatin-remodeling complexes
in tumorigenesis :
Insights in dedifferentiated melanoma cells and renal
medullary carcinoma**

THÈSE dirigée par :

M. DAVIDSON Irwin

Directeur de recherche CNRS, IGBMC, Illkirch

RAPPORTEURS :

Mme. CAMEL Julie

Chargée de recherche INSERM, CRCL, Lyon

M. BALLOTTI Robert

Directeur de recherche INSERM, C3M, Nice

AUTRES MEMBRES DU JURY :

M. COIN Frédéric

Directeur CNRS, IGBMC, Illkirch

INVITÉS :

Mme. BERGAMIN Elisa

Directrice de recherche CNRS, IGBMC, Illkirch

M. MALOUF Gabriel

Chargé de recherche INSERM, IGBMC, Illkirch

'Science is made up of so many things that appear obvious after they are explained.'

Frank Herbert

This manuscript is dedicated to all the people whose self-abnegation have allowed me to afford the luxury of sitting, thinking, writing and most of all learning.

Thank you.

ACKNOWLEDGEMENTS

As I write the last few lines of this manuscript and take a review of these intense years I would like to thank many different people without the support of which I would not have made it so far.

First, I would like to thank Dr. **Julie Caramel**, Dr. **Robert Ballotti**, Dr. **Elisa Bergamin** and Dr. **Frédéric Coin** for their critical evaluation of this manuscript. I feel deeply honored that such high-level experts have accepted to be members of my PhD committee and dedicate some of their time to my projects. When we first discussed who should be in my jury with my supervisor, their names came up very easily and it felt like an evidence that they were the best fit.

Talking about supervision, I've had the great luck to meet one of the best mentors in my PhD supervisor Dr. **Irwin Davidson**. Irwin, you represent for me the pinnacle of what a solid supervisor should be with the general sincerity, kindness and patience that characterize you. I am very grateful that you gave me a chance to stay in your team these past five years and work alongside you on those numerous interesting projects. Your trust and guidance have turned me into a confident young researcher and for that I will always be indebted to you. *Sapienter si sincere!*

Another person that gave robust guidance during the second half of my PhD was Dr. **Gabriel Malouf**, which I would like to warmly thank. Gabriel, you can be terrible at times with your ideas and you have pushed me at times; however I can say that I have never regretted discussing my projects with you as good always came out of it. Thank you for giving me the opportunity to work on some really interesting projects, which taught me a lot!

Next, I would like to thank all past and present members of the Davidson/Malouf team.

Gabrielle Mengus – Merci de m'avoir montré la manipulation des souris, c'était très enrichissant. Désolé pour toutes les fois où tu m'as vu mangé dans le laboratoire !

Isabelle Michel – Ah ma chère Isa, que ferions-nous sans toi dans le labo, tu étais là à mon arrivée et tu seras sûrement là longtemps après mon départ. Tu portes l'héritage des gens qui ont traversé ces palliasses, j'espère que je ne te laisserai pas un trop mauvais souvenir de mon passage. Merci pour tout !

Sébastien Coassolo & Thomas Kleiber – Merci aux anciens qui m'ont soutenu lorsque je n'étais qu'un débutant, votre bonne humeur et votre aide m'ont aidé à tenir quand c'était difficile !

Guillaume/Youenn Davidson – Avec moi, tu es la seule personne qu'on peut appeler par 2 prénoms différents !! Je ne regrette pas d'avoir voulu mieux te connaître, car sous tes airs timides se cache une personne bourrée de gentillesse et avec laquelle j'ai beaucoup de points communs. Merci beaucoup pour ton assistance sur tous mes projets, même quand je te demande des analyses pénibles à faire (avec un ton autoritaire !). Au fil des années, je peux dire que tu es devenu bien plus que le 'bioinformaticien du labo' pour moi, mais un véritable ami.

Justine Gantzer & Alexandre Haller – Un petit mot pour mes 'étudiants'. Mon aventure se finit bientôt, la vôtre ne fait que commencer, ainsi va la vie. Je vous souhaite d'y prendre autant de plaisir que moi !

Jonathan Thouvenin – On a commencé comme encadrant/apprenti, on a fini amis. Il y a des personnes avec lesquelles le feeling passe naturelle, tu en fais partie ! Je suis fier du travail que tu as accompli au labo, bon courage en Belgique !

Philippe Baltzinger – Phil, j’admire la sincérité et la bienveillance avec laquelle tu approches toute chose. Je te souhaite vraiment d’exceller durant ta thèse et d’avoir une belle carrière après, c’est tout le mal que tu mérites !

Alexandra Helleux – Sous tes airs de bretonne farouche, tu as un grand cœur! Merci pour ta collaboration sur mes projets. J’espère qu’un jour, je réussirai à te convaincre que je ne suis pas arrogant !

Dana Diaz – Danush, we became friends almost since we first met, and you have remained a faithful and reliable friend! I really appreciate our numerous discussions in your module!

Igor Martianov & Sehrish Bazai – Thank you for your help and your kindness, it was really appreciated!

I also would like to thank the members of the **Get Together crew** : Véronique Fischer, Duygu Yilmaz, Kenny Schumacher and Vincent Hisler. Preparing our monthly reunion was not always easy but I always enjoyed sharing a beer in your company. Thank you! Talking of Berico and Gambi, of course this PhD thesis cannot begin without a few words on my most loyal friends and labmates!

Giovanni Gambi & Pietro Berico – Guys, when I first met you both I sensed you might be bright students (despite your Italian accent!), let me say that I am still surprised every single day by the amount of work and intelligent ideas you guys are able to generate. I am convinced you will be absolutely brilliant scientists! You both are truly an inspiration for me at the lab but also personally. You were there on all the difficult moments during these last 4 years and helped me to restart every time, I am forever indebted to you guys and I am grateful to count you among my best friends! Also for the delicious pizzas, the pasta, the Cantillon and the numerous Prosecco! Grazie!

I would also like to acknowledge another person that I met in the lab and has ever since never left my side, Dr **Gizem Caliskan**. My love, words are lacking to express my gratitude for the relentless help, the support and the love you provided me with all along these past months, and especially during the writing of this manuscript. Your never-fading beautiful smile and your positivity always bring out the best in me. I look forward to sail for new adventures along you and share our passion for science!

Lastly, I would like to thank my family and close relatives.

Miriam & Ronan – Je n’ai pas toujours été très présent et je le regrette, mais je suis heureux et fier de vous compter parmi mes meilleurs amis depuis plus de 10 ans. Et j’ai hâte de passer des moments avec ma sublime nièce Esmé !

Leondrit – Je n’ai pas toujours été tendre avec toi, mais je peux dire aujourd’hui que je suis fier de ce que tu es devenu. J’espère qu’en lisant ce manuscrit, tu seras fier de moi aussi. Je t’aime frerot.

Sabahat & Ferid – Maman, papa, votre amour inconditionnel et votre soutien ont fait de moi la personne que je suis aujourd’hui. Si j’ai suivi ma passion, c’est grâce à votre soutien sans failles. Vous rendre fiers est la plus grande des récompenses de mon travail. Falemnderit, ju dua shumë !



Ce travail a été rendu possible grâce aux financements par la Ligue contre le Cancer et l'Agence Nationale de la Recherche qui m'ont permis d'effectuer ces 4 années de thèse dans les meilleures conditions possibles. Je leur suis extrêmement reconnaissant de m'avoir accordé leur confiance et pour l'intérêt porté à mon projet.

La qualité de mon travail résulte en partie de l'accueil de l'Institut de Génétique et de Biologie Moléculaire et Cellulaire (IGBMC) ainsi que l'ensemble de ses plateformes et de leurs membres qui par l'excellence de leur travail m'ont permis de faire ma thèse dans les meilleures conditions. De ce fait, je remercie de tout cœur toutes ces personnes qui ont contribué de près ou de loin à mon projet.

Je souhaiterais également remercier les membres de la section hygiène et sécurité de l'IGBMC ainsi que la cellule de crise qui font un travail formidable et dont l'existence s'est montrée essentielle durant ces temps difficiles de pandémie.

RÉSUMÉ EN FRANÇAIS

Rationale

Les complexes de remodelage de la chromatine sont d'importantes machineries moléculaires impliquées dans la régulation de l'expression génique. Chez l'Homme, la famille SWI/SNF (SWItch/Sucrose Non-fermentable) comprends au moins 3 sous-complexes (nommés cBAF, pBAF et ncBAF) de compositions différentes mais comprenant au moins une sous-unité catalytique SMARCA2 (BRM) ou SMARCA4 (BRG1) avec un domaine ATPase nécessaire à l'hydrolyse de l'ATP fournissant ainsi de l'énergie nécessaire au remodelage la structure de la chromatine.

Le séquençage des tumeurs humaines a mis en évidence une fréquence élevée de mutations sur un ou plusieurs sous-unités SWI/SNF. L'inactivation dans les modèles murins a validé les rôles majeurs de SMARCA4 et SMARCB1 (BAF47) respectivement dans le développement et l'oncogenèse. De nombreuses publications ont utilisé des approches biochimiques et génomiques pour associer la mutation d'une sous-unité à la déstabilisation de SWI/SNF et son ciblage différentiel sur la chromatine vers des régions associées à des oncogènes. Ma thèse se porte sur le rôle des complexes SWI/SNF dans 2 types de cancers différents : le mélanome de type dédifférencié et le carcinome médullaire du rein.

Partie I – Le mélanome dédifférencié

1.1. Contexte

Les mélanomes cutanés, issus de la transformation maligne des mélanocytes, sont parmi les cancers humains les plus agressifs et résistants aux traitements. Il est maintenant bien établi que les tumeurs de mélanomes sont très hétérogènes, et comprennent des cellules avec des propriétés invasives, prolifératives et tumorigènes différentes. Des analyses transcriptomiques ont permis plusieurs types cellulaires avec une expression différentielle des facteurs de transcription maîtres comme MITF et SOX10. Les cellules mélanocytiques expriment des niveaux élevés de ces facteurs avec un ensemble de marqueurs du lignage des mélanocytes. Les cellules de type crête neurale sont caractérisées par l'absence de MITF mais l'expression de SOX10. En revanche, les cellules

mésenchymateuses/dédifférenciées n'expriment ni MITF ni SOX10, mais SOX9. Chacun de ces phénotypes est caractérisé par une signature transcriptomique distincte en grande partie régulée par MITF et SOX10 quand ils sont exprimés, ou AP-1/TEAD dans les cellules dédifférenciées. Cette hétérogénéité moléculaire intra-tumorale est le résultat d'une plasticité cellulaire et une interaction entre les cellules tumorales et le stroma et/ou l'infiltrat immun.

De précédents travaux de notre laboratoire ont montré l'importance de SMARCA4 dans la survie et la prolifération des cellules de type différencié due à une interaction physique et fonctionnelle entre MITF et SOX10 et le complexe PBAF. Je me suis intéressé au rôle de SMARCA4 dans les cellules de mélanome de type dédifférencié. La présence de ces cellules est augmentée par différents traitements thérapeutiques et elles jouent un rôle clé dans la résistance aux thérapies.

1.2. Résultats

A – Rôle mineur de SMARCA4 dans la prolifération et la survie des cellules de mélanomes dédifférenciés dans des conditions de culture en 2D.

J'ai d'abord commencé par étudier l'expression des sous-unités SWI/SNF dans les 3 lignées dédifférenciées modèles : MM099, MM047 et MM029. Par RT-qPCR et immunoblot, j'ai pu montrer que toutes les lignées expriment SMARCA4, SMARCA2 et la majorité des autres sous-unités. J'ai par ailleurs montré que leur niveau d'expression est comparable aux cellules de mélanome différenciées. Par immunoprécipitation de SMARCA4, j'ai pu montrer que les complexes SWI/SNF sont structurellement intacts et ont une composition similaire dans toutes ces lignées.

Afin d'étudier le rôle des complexes SWI/SNF, j'ai réalisé une inhibition d'expression par siRNA des sous-unités catalytiques SMARCA2 et SMARCA4 dans 3 lignées dédifférenciées. Après avoir validé l'inhibition par RT-qPCR et immunoblot, j'ai mesuré l'effet sur la prolifération cellulaire par comptage et CellTrace. L'inhibition de SMARCA4, et non SMARCA2, réduit de façon mineure la prolifération des 3 lignées, expliquée en partie par une induction de la sénescence cellulaire.

L'analyse transcriptomique par séquençage d'ARN (RNA-seq) a montré que l'inhibition de SMARCA4 dans les cellules MM099 et MM047 entraînait la dérégulation significative d'une centaine de gènes, ce qui apparaît comme peu comparé au plus de 9000 gènes régulés par SMARCA4 dans les

cellules mélanocytiques. Parmi les gènes dérégulés, on trouve une surexpression des cytokines impliquées dans la sénescence (SASP) et une inhibition de régulateurs de la matrice extracellulaire (ECM) et de la motilité cellulaire.

B – SMARCA4 régule un programme essentiel à la migration, l'invasion et la formation des sphéroïdes tumoraux en 3D des cellules de mélanomes dédifférenciés

Afin de tester si SMARCA4 a un potentiel rôle dans la motilité de ces cellules, j'ai réalisé des tests scratch en culture 2D ainsi que des essais sur chambre Boyden avec ou sans utilisation de Matrigel. Ces analyses ont montré que la perte de SMARCA4 entraîne une forte augmentation des capacités migratoires et invasives des cellules dédifférenciées. Par immunoblot, j'ai pu démontrer que cela s'expliquait en termes moléculaires par des changements d'expression de régulateurs importants tels que la vimentine, la E-cadhérine, la claudine 1.

Poussés par ces observations et malgré son rôle mineur dans la prolifération 2D, nous avons voulu tester si SMARCA4 joue un rôle plus important en conditions 3D plus similaires aux conditions de formation tumorale in vivo. Les 3 lignées dédifférenciées forment facilement des sphéroïdes tumoraux. L'inhibition de SMARCA4, et non SMARCA2, dans ces mélanosphères diminue considérablement leur formation. Ces observations ont été validées indépendamment par l'utilisation des shRNA ciblant SMARCA4 permettant l'inhibition durable de son expression.

L'analyse transcriptomique des mélanosphères par RNA-seq et la comparaison avec les conditions 2D a permis de mettre en évidence les changements d'expression de nombreux gènes lors de la croissance en 3D. De plus, l'analyse des cellules en 3D par RNA-seq suite au siSMARCA4 a révélé que son inhibition entraîne la dérégulation de plus de 750 gènes essentiels à la formation et la croissance en 3D. Ces gènes sont impliqués majoritairement dans l'organisation de l'ECM, l'angiogenèse et la réponse immunitaire. Bien qu'il ne soit pas essentiel pour la prolifération des cellules de mélanome dédifférenciées en conditions de culture standard en 2D, SMARCA4 est donc un facteur clé pour l'expression de gènes nécessaire à la formation de sphéroïdes tumoraux.

C – Localisation génomique différentielle de SMARCA4 dans les cellules mélanocytiques et dédifférenciées.

Dans les cellules mélanocytiques, MITF et SOX10 dirigent la fixation génomique au niveau des éléments cis-régulateurs d'un ensemble de gènes formant la signature transcriptomique de ces cellules. Afin d'identifier les cibles directes et les voies moléculaires régulés par SWI/SNF dans les cellules dédifférenciées, j'ai cartographié les sites de fixation de SMARCA4 par immunoprécipitation de chromatine, suivi de séquençage (ChIP-seq). J'ai pu mettre en évidence un grand nombre de sites de fixation de SMARCA4 dont un sous-ensemble sont également fixés dans les cellules mélanocytiques. En revanche, on constate une perte des sites de fixation dépendants de MITF/SOX10 au niveau de gènes impliqués dans la prolifération cellulaire, la différenciation et la pigmentation et une occupation sélective au niveau des gènes impliqués dans la migration, l'invasion, la croissance tumorale, l'organisation de l'ECM ainsi que la réponse immunitaire. L'analyse bioinformatique des motifs retrouvés au niveau des sites de fixation a permis d'identifier les facteurs de transcription responsable du recrutement de SMARCA4 que sont AP-1, AP-2, TEAD, RUNX, PRRX1, ZEB1, SOX9, STAT et IRF. Bien que les rôles de AP1, TEAD et ZEB1 ont déjà été caractérisés, nous avons mis en évidence le rôle important de PRRX1. L'expression de ce facteur est augmentée lors de la croissance en 3D et j'ai montré que l'inhibition de son expression diminue fortement la croissance des mélanosphères. Ces résultats montrent que SMARCA4 est recruté aux éléments cis-régulateurs par un ensemble de facteurs de transcription essentiels à l'identité des cellules dédifférenciées. L'occupation génomique différentielle dans les cellules mélanocytiques et dédifférenciées est en forte corrélation avec les signatures caractéristiques de ces lignées.

Partie II – Le carcinome médullaire du rein

2.1. Contexte

Les carcinomes médullaires du rein (RMC) sont des tumeurs malignes très rares et agressives, décrite récemment en clinique et survenant généralement chez de jeunes adultes porteurs du trait drépanocytaire. La caractéristique principale des RMC est l'inactivation biallélique de SMARCB1 (BAF47) donnant aux cellules leur aspect rhabdoïde typique. Cette perte de la sous-unité SWI/SNF

intervient par chromothripsie à un jeune âge et constitue l'évènement-clé de la transformation des cellules. L'origine cellulaire du RMC n'est actuellement pas défini, ces tumeurs se localisent toujours dans la partie médullaire du néphron, connu pour être moins bien vascularisée et donc plus hypoxique et sensible à une ischémie chronique liée au trait drépanocytaire, bien qu'aucun lien direct n'ait encore pu être établi. Le RMC offre un système modèle idéal pour comprendre le rôle des complexes SWI/SNF dans l'oncogenèse avec l'évènement clé et unique de la perte de l'expression de la sous-unité SMARCB1.

L'objectif de mon second projet a été d'identifier les caractéristiques et l'origine cellulaire du RMC grâce à une approche translationnelle impliquant à la fois des données provenant de patients et de modèles cellulaires disponibles. Ces travaux permettront de mieux comprendre d'un point de vue biologique les mécanismes de l'oncogenèse et le lien causal entre SMARCB1 et RMC ainsi que les voies impliquées.

2.2. Résultats

A – Le carcinome médullaire du rein est caractérisée in vivo par une signature anti-ferroptotique et une identité mésenchymateuse.

Dans cette étude, j'ai intégré des données de patients avec des expériences sur des lignées cellulaires afin de comprendre les mécanismes impliqués dans la transformation. Afin d'identifier les caractéristiques de la RMC ainsi que son éventuelle hétérogénéité, nous avons réalisé un séquençage à cellule unique (scRNA-seq) sur une biopsie de RMC et du tissu normal adjacent (NAT). Nous avons pu identifier et répertorier les signatures moléculaires de 19 populations cellulaires correspondant aux types cellulaires qui composent les différentes structures du rein dont 3 dans l'échantillon tumoral qui correspondent aux cellules RMC, aux fibroblastes associés au cancer (CAF) et aux macrophages.

Les cellules RMC présentent une signature mésenchymateuse (expression de vimentine, fibronectine, N-cadherine) et anti-ferroptotique (expression de GPX4, FTH1). Ces résultats inédits furent confirmés par analyse SCENIC qui a révélé HIF1A (hypoxie), JUND (réponse au stress), IRF1 (interférons), MYC (prolifération), NFE2L2 (anti-ferroptose) comme des régulateurs clés dans ces cellules. En revanche, nous constatons une perte des régulateurs SMARCA4 (SWI/SNF) consistant avec

la perte de SMARCB1, ainsi que PAX2/8 (identité rénale) et TFCP2L1 (oncosuppresseur connu). Toutefois, peu d'hétérogénéité intra-tumorale a été détecté.

Afin de valider ces résultats, nous avons intégré ces données de scRNA-seq avec des données transcriptomiques issues de 2 cohortes indépendantes de patients RMC en France et aux USA. L'analyse de ces données a confirmé la spécificité des signatures issues de la scRNA-seq. Nous avons donc pour la première fois identifiée la cellule d'origine putative du RMC (cellules de la partie épaisse ascendante de l'anse de Henle ou mTAL) ainsi qu'une signature spécifique des RMC avec le gain ou la perte d'activité d'un ensemble de facteurs de transcription et l'association avec un programme anti-ferroptotique.

B – La perte de SMARCB1 induit une réorganisation des complexes SWI/SNF et du paysage épigénétique dans des cellules issues de carcinome médullaire du rein.

Afin d'identifier les mécanismes responsables des changements d'expression impliqués dans l'oncogénèse, nous avons étudié 2 modèles cellulaires dérivées de patients RMC. J'ai pu confirmer la perte de SMARCB1 dans ces lignés et mettre en évidence une perte concomitante de plusieurs autres sous-unités SWI/SNF, notamment SMARCA2, ARID1A, PBRM1 et DPF3, indiquant une réorganisation des complexes de remodelage SWI/SNF.

J'ai établi des lignées où la réexpression de SMARCB1 est inductible par doxycycline. J'ai montré que la réexpression de SMARCB1 permet la formation de complexes SWI/SNF fonctionnels soit en régulant l'expression des sous-unités, soit en régulant leur dégradation par le protéasome ou enfin par stabilisation structurale des complexes SWI/SNF en formation. Différentes approches fonctionnelles m'ont permis de montrer que l'induction de SMARCB1 induisait une forte mortalité cellulaire, en ligne avec un rôle oncosuppresseur. Notamment, j'ai pu mettre en évidence que SMARCB1 antagonise la fixation génomique et la fonction du complexe MYC/MAX dont l'importance a été mise en évidence par les données de scRNA-seq.

Afin d'identifier les conséquences de la réexpression de SMARCB1 sur le paysage épigénétique, j'ai intégré des données ChIP-seq de SMARCA4 avec ou sans expression de SMARCB1 avec celles de H3K27ac. Les analyses suggèrent que l'absence de SMARCB1 provoque une perte

importante de sites de fixation correspondant à des enhanceurs de gènes impliqués dans l'identité et la mort cellulaire.

C – SMARCB1 contrôle un programme oncosuppresseur via la régulation de l'identité épithéliale et de la ferroptose.

J'ai réalisé des RNA-seq à 12 et 48 heures après la réexpression de SMARCB1 mettant en évidence plus de 2000 gènes dont l'expression est dérégulée suite à la perte de SMARCB1. J'ai montré que SMARCB1 active l'expression de gènes impliqués dans l'adhésion et l'identité épithéliale, la sensibilité à la ferroptose et la réponse immunitaire, tandis qu'il réprime des gènes liés à la prolifération, le cycle cellulaire et la réparation de l'ADN.

Afin de confirmer ces résultats, j'ai réalisé des immunoblots qui ont montré que la réexpression de SMARCB1 induisait bien une élévation protéique de marqueurs épithéliaux et une baisse de marqueurs mésenchymateux. Par ailleurs, SMARCB1 semble réprimer directement MYC et NFE2L2. Enfin, j'ai montré grâce à l'utilisation de l'inhibiteur ferrostatin-1 que les cellules exprimant SMARCB1 deviennent sensibles à la mort cellulaire par ferroptose induite par une augmentation de ACSL4, un régulateur de la peroxydation membranaire. Ainsi, l'intégration des données transcriptomiques de patients et de scRNA-seq avec celles issues des lignées cellulaires expérimentales a donc permis de mieux comprendre comment SMARCB1 régule un programme oncosuppresseur et de sensibilité à la ferroptose.

Conclusion générale

L'ensemble des travaux menés durant ma thèse ont permis de mieux comprendre le rôle des complexes SWI/SNF dans l'oncogenèse et d'identifier les mécanismes moléculaires associées.

Les études menées dans le mélanome de type dédifférencié ont mis en évidence son rôle clé dans la régulation de l'expression des gènes nécessaires à la croissance en 3D. La transition phénotypique d'un mélanome différencié vers un mélanome dédifférencié s'explique par une extinction des programmes de MITF et SOX10 avec une perte des sites de fixation de SWI/SNF associées. Simultanément, la fixation génomique de SMARCA4 est dirigée par l'activation des programmes de

SOX9, PRRX1, ZEB1 afin de permettre le remodelage de la chromatine et l'expression de gènes nécessaires au maintien de l'identité mésenchymateuse/cellule souche et des capacités métastatiques. Ces résultats confirment le rôle pivot des complexes SWI/SNF dans la régulation du paysage épigénétique des mélanomes.

D'autre part, les travaux menés sur le RMC ont permis de mieux caractériser les mécanismes impliqués sous le contrôle de SMARCB1 et des complexes SWI/SNF. En effet, la perte des programmes TFCEP2L1, MITF, PAX2/8 entraîne une dédifférenciation des cellules médullaires de l'anse de Henle accompagnée en outre d'une résistance à la mort par ferroptose dont ces cellules semblent être sensibles de nature. Ces résultats pourraient si validés en clinique donner lieu à de nouveaux développements thérapeutiques pour le traitement de ce type de carcinome.

Table des matières

GENERAL INTRODUCTION

CHAPTER I. CHROMATIN STRUCTURE AND TRANSCRIPTION REGULATION

1.1. CHROMATIN IS A CENTRAL REGULATOR OF GENE EXPRESSION	27
<i>1.1.1. Compaction of the genetic information into chromatin</i>	<i>27</i>
1.1.1.1. Structure of chromatin	27
1.1.1.2. Function of chromatin	31
<i>1.1.2. The epigenetic code</i>	<i>33</i>
1.1.2.1. DNA methylation	33
1.1.2.2. The histone code	35
<i>1.1.3. Fundamental cellular processes associated with chromatin</i>	<i>37</i>
1.1.3.1. DNA replication	37
1.1.3.2. DNA repair	39
1.2. MECHANISMS OF RNA POLYMERASE II TRANSCRIPTION.....	41
<i>1.2.1. The Transcription machinery.....</i>	<i>43</i>
1.2.1.1. RNA polymerase II.....	43
1.2.1.2. Core promoters	45
<i>1.2.2. Mechanism of transcription</i>	<i>47</i>
1.2.2.1. Pre-initiation complex formation and transcription initiation	47
1.2.2.2. Elongation and termination	49
<i>1.2.3. Post-transcriptional regulation of gene regulation</i>	<i>53</i>
1.2.3.1. RNA splicing and spliceosome.....	53
1.2.3.2. RNA degradation pathways.....	57
1.3. CONTROL OF RNA POLYMERASE II TRANSCRIPTION ACTIVATION	59
<i>1.3.1. The enhancer code</i>	<i>59</i>
1.3.1.1. Cis-regulatory elements	61
1.3.1.2. Trans-regulatory elements	63
<i>1.3.2. Co-activators.....</i>	<i>67</i>
1.3.2.1. The Mediator complex.....	67
1.3.2.2. The SAGA and ATAC complexes	69
<i>1.3.3. Tridimensional genome architecture</i>	<i>71</i>
1.3.1.1. Phase separation: A new phase in cell biology.....	73
1.3.1.2. Topology-associated domains (TADs).....	75

CHAPTER II. CHROMATIN MODIFIERS AND REMODELERS

2.1. COVALENT HISTONE-MODIFYING COMPLEXES.....	81
---	-----------

2.1.1. <i>Histone acetylation</i>	81
2.1.1.1. Mechanism of acetylation	81
2.1.1.2. Acetyltransferases	83
2.1.1.3. Deacetylases	87
2.1.2. <i>Histone methylation</i>	91
2.1.2.1. Mechanism of methylation	91
2.1.2.2. Methyltransferases (MLL/COMPASS, Polycomb)	93
2.1.2.3. Demethylases	97
2.2. ATP-DEPENDENT CHROMATIN REMODELING ENZYMES	99
2.2.1. <i>The nucleosome positioning code</i>	101
2.2.1.1. Similarities and differences between remodelers	101
2.2.1.2. Mechanism of remodeling	101
2.2.2. <i>The INO80 family</i>	105
2.2.3. <i>The CHD family</i>	107
2.2.4. <i>The ISWI family</i>	109
2.3. FOCUS ON THE SWI/SNF CHROMATIN-REMODELING FAMILY	111
2.3.1. <i>Evolution from yeast to mammals</i>	111
2.3.1.1. Discovery	111
2.3.1.2. Evolution and conservation	113
2.3.2. <i>Human ubiquitous SWI/SNF complexes</i>	115
2.3.2.1. Human SWI/SNF sub-complexes: BAF and pBAF	115
2.3.2.2. The novel non-canonical BAF (ncBAF)	117
2.3.3. <i>Other SWI/SNF-related complexes</i>	119
2.3.3.1. Cell-type-specific SWI/SNF complexes	119
2.3.3.2. Interplay with other chromatin remodelers	121
2.4. STRUCTURE OF THE SWI/SNF FAMILY	123
2.4.1. <i>Domain organization</i>	123
2.4.1.1. Interactome-related domains	123
2.4.1.2. Genome targeting-related domains	125
2.4.2. <i>Combinatorial and modular assembly</i>	127
2.4.2.1. SWI/SNF modular organization	127
2.4.2.2. SWI/SNF assembly pathways	129
2.4.3. <i>Towards resolving SWI/SNF structure</i>	131
2.5. KNOWN BIOLOGICAL FUNCTIONS OF SWI/SNF REMODELERS	135
2.5.1. <i>Functional dynamics of SWI/SNF complexes</i>	135
2.5.1.1. Global and tissue-specific functions	135
2.5.1.2. Cooperative or antagonizing compensation?	137

2.5.2. Role in development and differentiation	141
2.5.3. Role in cancer	145

CHAPTER III. MECHANISMS OF CANCER : INSIGHTS INTO RENAL MEDULLARY CARCINOMA AND MELANOMA

3.1. RENAL MEDULLARY CARCINOMA	151
3.1.1. Tissue-of-origin	151
3.1.1.1. Anatomy of the kidney	151
3.1.1.2. Biology of inner medulla cells.....	155
3.1.2. Renal medullary carcinoma	161
3.1.2.1. Classification of kidney cancers	161
3.1.2.2. The genesis of renal medullary carcinoma	167
3.1.2.3. RMC treatments.....	173
3.2. MELANOMA	177
3.2.1. Cell-of-origin	177
3.2.1.1. Anatomy of the skin	177
3.2.1.2. Ontogeny of melanocytes	181
3.2.1.3. Melanocyte-Inducing Transcription Factor	185
3.2.2. The genesis of melanoma	189
3.2.2.1. Melanoma classification	189
3.2.2.2. Biology of melanoma development.....	195
3.2.2.3. Melanoma heterogeneity	199
3.2.3. Treatments and resistance	203
3.2.3.1. Immune checkpoint blockade	205
3.2.3.2. Targeted therapies.....	207

RESULTS

ESSENTIAL ROLE OF THE CHROMATIN REMODELER BRG1 FOR FORMATION OF TUMOR SPHEROIDS BY DEDIFFERENTIATED MELANOMA CELLS.	214
CHROMATIN REMODELING SUBUNIT SMARCB1 REGULATES CELL IDENTITY AND SENSITIVITY TO FERROPTOSIS IN RENAL MEDULLARY CARCINOMA	278

GENERAL CONCLUSIONS AND PERSPECTIVES

1 – SWI/SNF: IMPORTANT BUT DISTINCT ROLES IN ONCOGENESIS.	344
2 – MELANOMA ADDICTION TO CHROMATIN-REMODELING BY SWI/SNF	344
3 – EMT AND FERROPTOSIS : A NEW PARADIGM ?	345
4 – ROLE OF SWI/SNF : THE GLOBAL AND THE TISSUE-SPECIFIC	345
5 – SWI/SNF AS A TOOL TO IDENTIFY TUMOR VULNERABILITIES	346
6 – ON THE IMPORTANCE OF 3D SPHERE EXPERIMENTS.....	347

Liste des figures

Figure 1. Nucleosome and chromatin organization.....	28
Figure 2. Euchromatin and Heterochromatin.....	30
Figure 3. DNA methylation in normal cells versus cancer cells.....	32
Figure 4. Histone modifications.....	34
Figure 5. DNA replication through chromatin.....	36
Figure 6. DNA repair mechanisms.....	38
Figure 7. DNA double strand break repair; Non-homologous end joining process.....	40
Figure 8. Crystal structure of the 12-subunit yeast Pol II, coupling of Rpb4/7 binding and clamp closure, and upstream interaction face.....	42
Figure 9. Sequence motifs and localization of core promoters.....	44
Figure 10. Illustration of Pol II transcription cycle.....	46
Figure 11. Structure of eukaryotic Pre-Initiation Complex.....	46
Figure 12. Assembly of general transcription factors for RNA pol II transcription.....	48
Figure 13. Transition from Pol II pausing state to active elongation state.....	50
Figure 14. Assembly and catalytic cycle of spliceosome.....	52
Figure 15. Signals and mechanism of RNA splicing.....	54
Figure 16. Illustration of mRNA decay pathway.....	56
Figure 17. miRNA biogenesis pathway.....	58
Figure 18. Chromatin dynamics at tissue-specific enhancers during cell differentiation.....	60
Figure 19. Readout mechanisms.....	62
Figure 20. X-ray structures of the basic/helix-loop-helix/leucine zipper (bHLHZ) domains of Myc-Max and Mad-Max.....	64
Figure 21. DNA loop formation.....	66
Figure 22. Enhancers.....	66
Figure 23. Shared subunits of SAGA.....	68
Figure 24. Chromatin feature.....	70
Figure 25. Genome organization.....	72
Figure 26. Major subnuclear structures.....	74
Figure 27. Self-organization of chromatin.....	76
Figure 28. Histone modifications.....	80
Figure 29. Chromatid cohesion is promoted by acetylation of SMC3.....	82
Figure 30. Reactions of reversible lysine acetylation by HAT and HDAC enzymes.....	84
Figure 31. Domains of human HDACs.....	86
Figure 32. Illustration of HDACs and HDACi regulating different stages of cancer.....	88

Figure 33. Mono-, di-, trimethylation of lysine residues on core promoters and their functions.....	90
Figure 34. Functional PTM crosstalk between methylation and phosphorylation on non-histones substrates. ‘methylation-phosphorylation switch’.....	92
Figure 35. COMPASS complexes in mammals and their subunits composition.....	94
Figure 36. Methylation of arginine residues by PRMTs and addition of a citrullinyl group on arginine residues by PADs.....	96
Figure 37. ATP-dependent chromatin remodeling enzymes.....	98
Figure 38. ATPase subunits of remodelers with DExx and HELICc domains.....	100
Figure 39. Functional classification of remodelers.....	102
Figure 40. Functions of INO80 complex.....	104
Figure 41. CHD family.....	106
Figure 42. ISWI family chromatin remodeling complexes.....	108
Figure 43. SWI/SNF complexes in yeast.....	110
Figure 44. Evolution of SWI/SNF complex from yeast to mammals.....	112
Figure 45. Genes encoding SWI/SNF subunits, their aliases and presence of each subunits in specific complexes and modules.....	114
Figure 46. GBAF, BAF and PBAF complexes.....	116
Figure 47. Changing of BAF complex subunit composition during development.....	118
Figure 48. WSTF-containing chromatin remodeling complexes.....	120
Figure 49. Crosstalk between NuRD and SWI/SNF complexes.....	122
Figure 50. Protein domains in each subunits of mammalian SWI/SNF complex.....	124
Figure 51. Domain organization of DPF3 proteins.....	126
Figure 52. Modular organization of mammalian SWI/SNF complex.....	128
Figure 53. Mammalian SWI/SNF assembly pathways.....	130
Figure 54. Yeast SWI/SNF and human BAF complex.....	132
Figure 55. Model of the interaction of BAF complex with nucleosome core particle (NCP).....	132
Figure 56. Cryo-EM maps of BAF-NCP.....	134
Figure 57. Vulnerability of mutant SWI/SNF complexes in cancer.....	136
Figure 58. Hypothetical models of BRM-SWI/SNF function in BRG1-mutant cancers.....	138
Figure 59. SWI/SNF in early embryogenesis.....	140
Figure 60. SWI/SNF in neural development.....	140
Figure 61. Function antagonism between SWI/SNF and PRC2 Polycomb complexes.....	142
Figure 62. Mutation rate of mammalian SWI/SNF subunits.....	144
Figure 63. Competition of SS18-SSX fusion protein with the normal SS18 subunit for incorporation into the SWI/SNF complex.....	146
Figure 64. Anatomy of the kidney.....	150
Figure 65. Structure of the kidney nephron.....	152

Figure 66. Metanephric development in humans.....	154
Figure 67. Renal tubule cell nomenclature.....	156
Figure 68. Countercurrent multiplication.....	158
Figure 69. Major subtypes of renal cell carcinoma.....	160
Figure 70. The mutational landscape of clear cell RCC.....	162
Figure 71. Five-year survival rates of main RCC subtypes.....	164
Figure 72. Hematoxylin-eosin staining showing esmoplastic reaction to renal medullary carcinoma.	166
Figure 73. Model representing the role of SMARCB1 in enhancer regulation, which deregulation drives oncogenesis in MRT.....	168
Figure 74. Principle of Sickle cell anemia.....	170
Figure 75. Current model of RMC pathogenesis.....	172
Figure 76. Current diagnosis and management recommendations for RMC.....	174
Figure 77. Schematic cross section of the human skin.....	176
Figure 78. Stratified structure of the skin.....	178
Figure 79. Production pathways of pheomelanin and eumelanin.....	180
Figure 80. TGFb/BMP-SMAD pathways.....	182
Figure 81. Canonical WNT signaling pathway.....	182
Figure 82. Neural crest formation stages and gene regulatory networks.....	184
Figure 83. Structural characterization of the MITF DNA-binding and assembly region.....	186
Figure 84. Subtypes of cutaneous melanoma.....	188
Figure 85. MAPK/ERK and PIK3/AKT pathways.....	190
Figure 86. Driver mutations in melanoma.....	192
Figure 87. The Clark Model of melanoma progression.....	194
Figure 88. Linear development from melanocyte to metastatic melanoma.....	196
Figure 89. MITF rheostat model.....	198
Figure 90. Expression of MITF/SOX10 and melanoma heterogeneity.....	200
Figure 91. Melanoma cell dedifferentiation increases sensitivity to ferroptosis through upregulation of GPX4.....	202
Figure 92. Immunotherapies approved by FDA (in white) or in trials (in gray) for cutaneous melanoma treatment.....	204
Figure 93. Targeted therapies approved by FDA (in white) or in trials (in gray) for cutaneous melanoma treatment.....	206
Figure 94. BRAFi and MEKi induce melanoma cell death.....	206
Figure 95. Potential therapeutic vulnerabilities for cells resistant to MAPKi.....	208

INTRODUCTION

Chapter I. Chromatin structure and transcription regulation

Chapter I. Chromatin structure and transcription regulation

In 1665, scientist Robert Hooke observed under a microscope what he would call a “cell” and define as the universal indivisible unit of life. Cells are indeed the fundamental building blocks of living organisms. All cells have a membrane that delimitates the cytoplasm which contains and is itself structured by the cytoskeleton. All cells possess nucleus which stores nucleic acid molecules (e.g. DNA, deoxyribonucleic acid) that bear the hereditary information in the form of genes (genome) that are necessary to encode proteins that have various biochemical properties and all the regulatory factors that process the genome effectively. The genome is encapsulated by a dense, filamentous meshwork called nucleoskeleton, which located the inner nuclear membrane. And finally, they all are programmed by their genotype, carried in the DNA and present a phenotype which is the expression of their genotype in interaction with the environment. In eukaryotes, in order to fine-tune the gene expression of the cells, DNA structure is tightly controlled by a plethora of proteins and complexes.

1.1. Chromatin is a central regulator of gene expression

1.1.1. Compaction of the genetic information into chromatin

1.1.1.1. Structure of chromatin

Watson, Crick, Wilkins and Franklin discovered the double helix structure of DNA in which two antiparallel hydrogen-bonded polynucleotide chains are wound into a right-handed turn of 1.9 nm in diameter with 10.5 base pairs (bp) per turn (Crick and Watson, 1953). In average, each human cells contain 2m of DNA which has to be packaged into a nucleus only 5 to 20 μm in diameter. Thus, cells have found ingenious ways to fit the genetic material into the nucleus. Chromatin was first termed by the founder of cytogenetics Walther Flemming who described it as a macromolecular complex of DNA and proteins found in eukaryotic cells.

In 1884 the chemically acidic DNA was indeed found to be associated with small nuclear proteins of basic pH named histones (Olins and Olins, 2003) thus forming together the basic and repeating unit of chromatin; the nucleosome (Kornberg, 1974; Oudet, 1975). Over the past decades, it has become clear that these units are dynamically regulated and play a key role in the nuclear

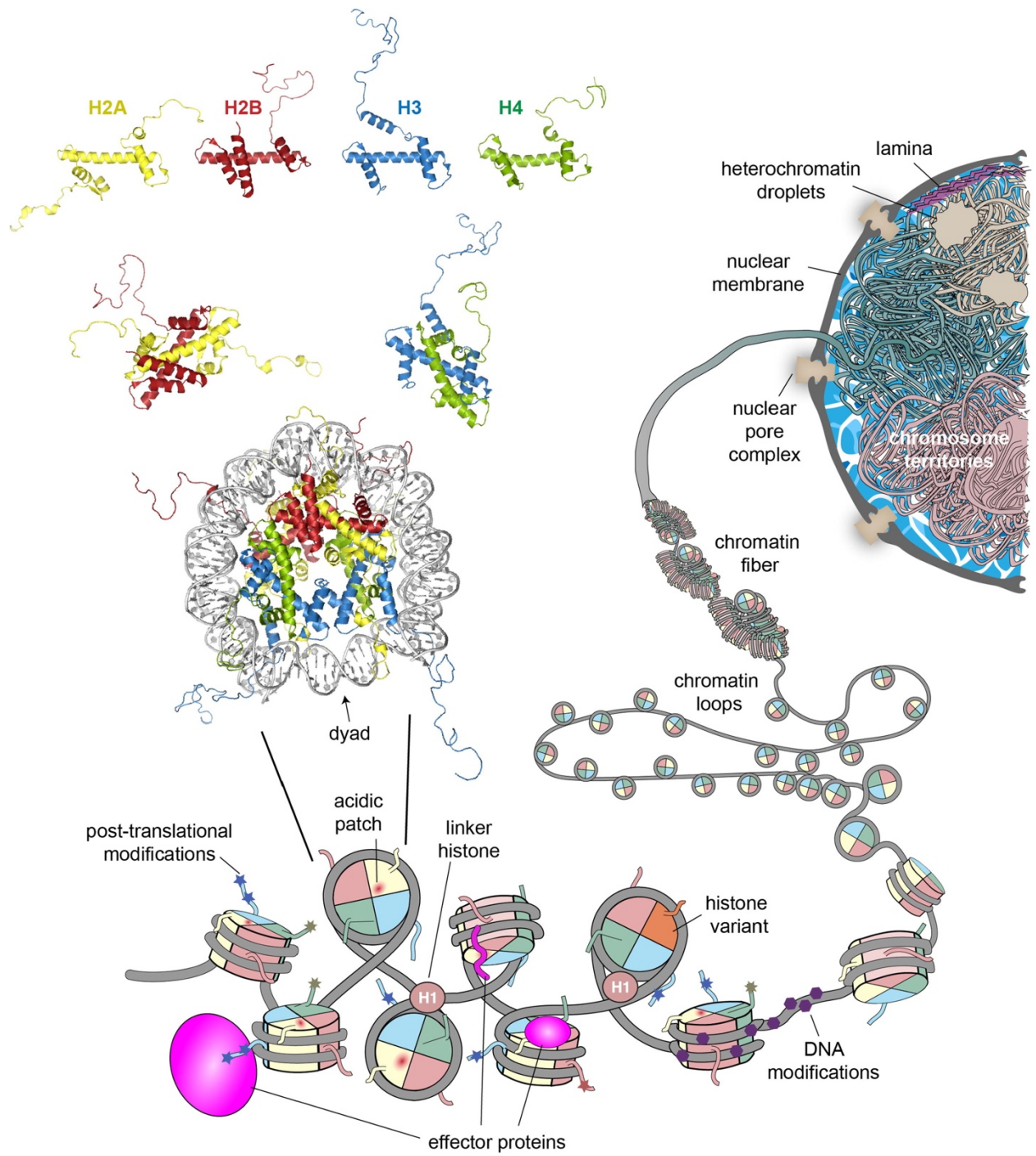


Figure 1. Nucleosome and chromatin organization.

From Emmerik and van Ingen, 2029.

organization and function.

The nucleosome core particle (NCP) consists of 147 base pairs of DNA wrapped in a 1,7 left-handed super-helical turn around an octamer of four core histones: H2A, H2B, H3 and H4 (McGinty and Tan, 2015). This octamer organizes symmetrically around two central H3 histones that each heterodimerize with two H4 forming a tetramer which in turn interacts with two H2A/H2B heterodimers. Interactions between dimerization partners is rendered possible by the so-called histone fold domains (HFD) which are extremely well conserved through evolution and were also found to be present in non-histone proteins. Structurally, each HFDs consists of three α -helices, two short and one central long helix connected by loops (Figure 1).

Small sections of nucleosome-free DNA serve to join the nucleosomes together taking a 'beads-on-a-string' structure and an additional linker histone H1 seals and stabilizes the wrapped DNA at the nucleosome entry and exit sites. The central DNA base pair at which the nucleosome can be separated in two symmetrical halves is defined as the nucleosome dyad and constitute the anchor point for linker histone H1. Overall the histone octamer interacts in 14 discrete places with the nucleosomal DNA at regular intervals mostly through arginine residues reaching out of the DNA phosphodiester backbone, resulting into one of the most stable DNA-protein associations. The human genome contains 10-20 copies per histone and their expression is regulated by the cell cycle as exponential production of histones are required to restore duplicated chromatin during S phase when DNA replication occurs. Along these canonical histones, a set of histone variants have evolved for histone H1, H2A and H3 (Yuan and Zhu, 2012; Weber and Henikoff, 2014). For instance, approximately 75% of histone H3 are deposited during DNA replication by histone chaperones, while the remaining 25% are histone variant H3.3 which is not coordinated with DNA synthesis (Talbert and Henikoff, 2017). Centromeres, which are specialized chromatin regions essential for mitosis, are characterized by nucleosomes in which CENP-A replaces H3 (Foltz *et al.*, 2006). Another well-characterized histone variant is H2A.Z which arises early during development and contains an extended acidic patch stimulating gene expression by recruitment factors responsible for the decompaction of chromatin (Guillemette *et al.*, 2005; Goldman, Garlick and Kingston, 2010; Marques *et al.*, 2010; Talbert and Henikoff, 2010).

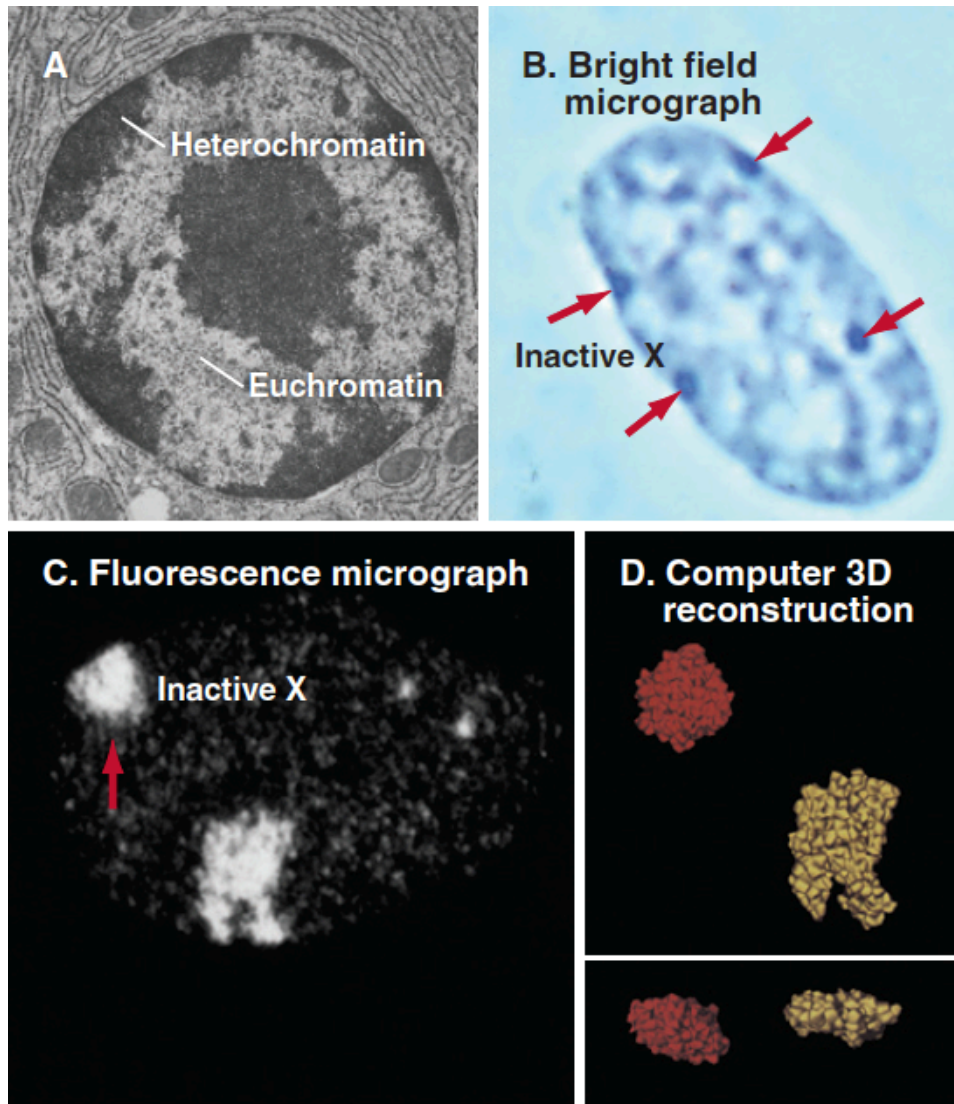


Figure 2. Euchromatin and Heterochromatin.

From Pollard, Thomas D., *et al. Cell Biology*, 2016.

A. Electron micrograph of a thin section of a plasma cell nucleus. **B.** Light micrograph of a female nucleus. **C.** Fluorescence micrograph of inactive X chromosome. **D.** Two different views of the X chromosomes.

1.1.1.2. Function of chromatin

Packaging DNA, aside from fitting the DNA inside the cell nucleus, allows for regulation of gene expression. Indeed, the level of chromatin compaction directly affects DNA accessibility and thus determines the functional output of the related biological processes.

Luckily nucleosomes can be dynamically evicted or shifted in position by different mechanisms such as chromatin remodeling and histone modifications. One of the key features of histone proteins, beside their HFDs, are their flexible extensions protruding out from the globular core nucleosome consisted of highly modifiable N-terminal and/or C-terminal histone tails which account for 20% of the entire histone octamer mass (McGinty and Tan, 2015; van Emmerik and van Ingen, 2019). These tails are known to be involved in the positioning of nucleosomes along the genome to allow further compaction in two main chromatin states.

The first state is the so-called heterochromatin which is a closed state and can be subdivided into facultative heterochromatin and constitutive heterochromatin. The latter is characterized a strong condensation of chromatin and is regarded as a mechanism to permanently silence genes such as centromere and telomere regions or repetitive DNA elements in all post-mitotic cells (Janssen, Colmenares and Karpen, 2018). Several isoforms of heterochromatin protein 1 (HP-1) are globally responsible for the formation and maintenance of heterochromatin in the nucleus (Lomberk, Wallrath and Urrutia, 2006). Facultative heterochromatin, the second type of heterochromatin, is composed of regions of genes that are differentially expressed in distinct cell-type or tissues. Thus, these regions are associated with repression of gene expression in some cells only. The Re1-silencing transcription factor (REST) and the related CoREST complex are involved in silencing the neuronal differentiation genes in non-neuronal cells (Ballas *et al.*, 2005).

The second state of chromatin is a more relaxed and open state called euchromatin (Figure 2). It is associated with all the regions that are actively expressed in a given cell. However, except for the housekeeping genes, not all genes are always expressed in the euchromatin as proper opening of the chromatin is essential. Many histone tails modifications are found in the gene bodies and regulatory elements within the euchromatin and are known to epigenetically regulate the structure of chromatin

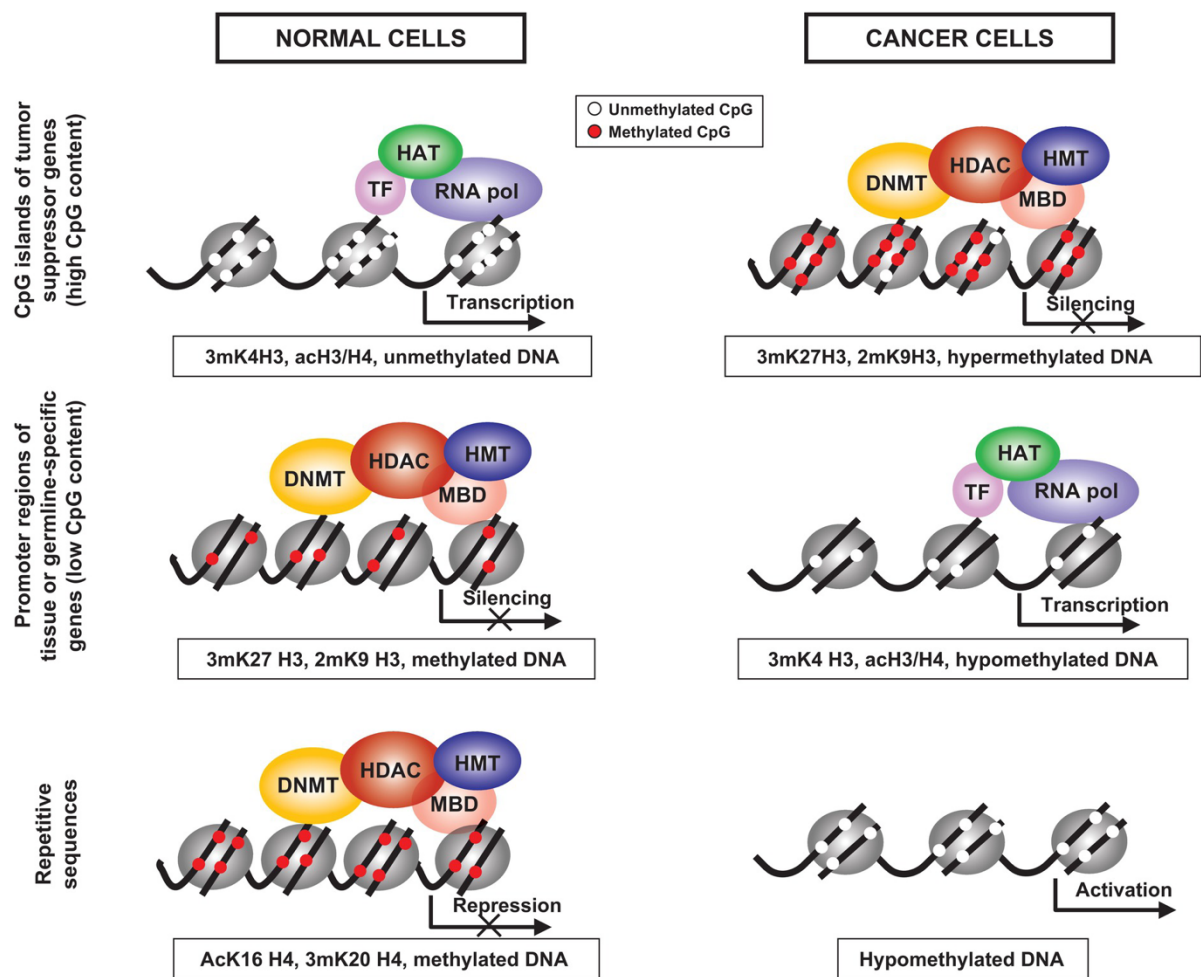


Figure 3. DNA methylation in normal cells versus cancer cells.

From Thiagalingam, *System Biology of Cancer*, 2015.

and the accessibility and readability of DNA sequences (Li, Carey and Workman, 2007; Bannister and Kouzarides, 2011).

1.1.2. The epigenetic code

In addition to the unique genetic code found in every single cell, the epigenetic code (epigenome) adds another layer of regulation which involves DNA methylation and histone modifications. It enables cells to integrate environmental signals in order to provide the best response through transient or permanent regulation of gene expression without alterations of the DNA sequence itself. The term epigenetics was first used by Conrad Waddington in 1942.

1.1.2.1. DNA methylation

Methylation is the only known reversible modification found on DNA and has major implications in gene regulation. In eukaryotes, DNA methylation involves most often the addition of a methyl group to carbon 5 of cytosine (5-methylcytosine), causing the methyl group to protrude into the major groove of the DNA helix. This reaction is catalyzed by enzymes known as DNA methyltransferases (DNMT1, -3A and -3B; DNMT2 being involved in RNA methylation) (Klose and Bird, 2006). The distribution of DNA methylation in eukaryotic genomes is not uniform but rather concentrated on both strands in CG-rich regions, called CpG islands, located most often at the 5' ends of gene promoters (Figure 3). 5% of cytosine residues are found methylated in the human genome. Evidence of a role for DNA methylation is based on a number of observations. First, the inactivated X chromosome in mammalian female cells are transcriptionally inactive and often heavily methylated. Second, DNA methylation patterns are tissue specific and once established are heritable to all cells of that tissue. During embryonic development, the early silencing of essential genes such as OCT4 and NANOG is associated with increased levels of DNA methylation at their promoter regions (Fouse *et al.*, 2008; Tsai *et al.*, 2012).

The removal of DNA methylation is rendered possible by the hydroxylation of 5' methylcytosine (5mC) by the ten-eleven translocation dioxygenases (TET1, -2 and -3) which is a key intermediate in demethylation pathways. The methylated cytosine can then either be passively depleted through DNA

A. Histone modifications create chromatin states

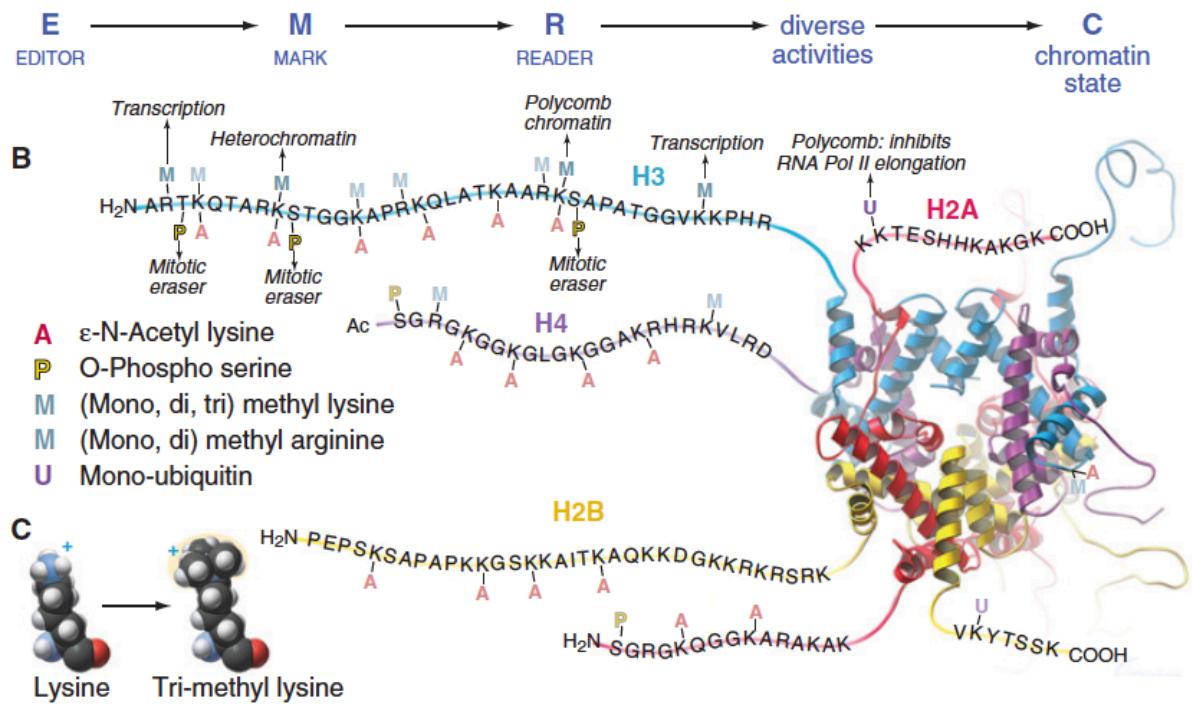


Figure 4. Histone modifications.

From Pollard, Thomas D., et al. *Cell Biology*, 2016.

A. Pathways of PTMs. **B.** Modifications of the amino and carboxyterminal domains of histones **C.** Structure of tri-methyl lysine.

replication or actively reverted to cytosine through oxidation and base excision repair (Kohli and Zhang, 2013). DNA methylation has been shown *in vitro* to inhibit the binding of transcription factors to DNA, however it may also recruit histone modifiers involved in gene repression (Klug *et al.*, 2016).

1.1.2.2. The histone code

In addition to DNA methylation, histone modification is an important epigenetic mechanism of gene regulation. The N-terminal histone tails consist of a disordered chain of aminoacids, rich in arginines and lysines, that protrude from the core nucleosome and can be subjected to various covalent post-translational modifications (PTMs). These PTMs are reversible and compose the so-called histone code which influence gene expression through two main mechanisms. First, histone PTMs directly modify the chemical charge of nucleosomes which alters the chromatin conformation by loosening the DNA-histone and histone-histone interactions (Li, Carey and Workman, 2007; Bannister and Kouzarides, 2011). Second, they can positively or negatively regulate the recruitment of downstream effector proteins which are able to read specific PTMs or complex combinations of histones, hence these proteins are termed 'readers'. More than 150 distinct readers have characterized with specific domains such as the Tudor domain, the MBT domain or the chromodomains (Klug *et al.*, 2016). *Per se*, histones are modified by editors which include 80 writers able to add a mark and 40 erasers responsible for controlled removal of histone PTMs (Figure 4). Of course, readers can also have writer or eraser activities, this can often be seen in multiprotein complexes such as NuRD or TIP60 complexes. Thus, it is possible that some histone marks influence the rate or efficiency with which later modifications are added in the vicinity.

To this day, the best characterized PTMs are the acetylation and methylation, but there also exists a plethora of others such phosphorylation, SUMOylation, ubiquitination, biotinylation, crotonylation, citrullination. Just as DNA methylation, these histone marks are not distributed randomly on the genome but rather associated with functional regions (McGinty and Tan, 2015; van Emmerik and van Ingen, 2019). For instance, the acetylation of lysine 27 of histone H3 (H3K27ac) is often associated with active gene expression, but the same lysine can be trimethylated (H3K27me3) which is then

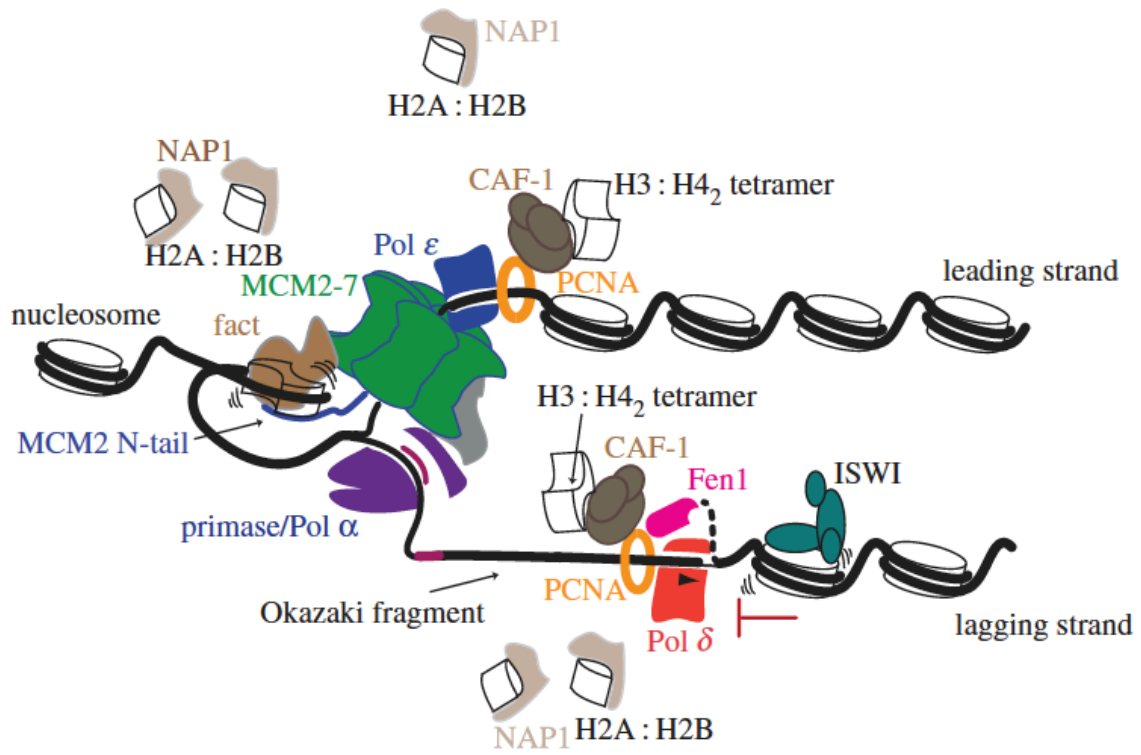


Figure 5. DNA replication through chromatin.

From Bellush and Whitehouse, 2017.

associated with silencing. This mutual exclusivity and antagonism regarding H3K27 marks is well-documented, however H3K27me3 can be found together with the activating mark H3K4me3 on so-called ‘bivalent promoters’, often in genes involved in pluripotency or gene imprinting. Importantly, three histone marks H3K36me3, H3K79me and H2Bub1 are found along bodies of active genes involved in various cellular processes (Li, Carey and Workman, 2007).

1.1.3. Fundamental cellular processes associated with chromatin

The ability to package DNA into chromatin has been selectively safeguarded through evolution with the increase of complexity in multicellular organisms. As mentioned before, the structure of chromatin tightly dictates the yields of fundamental DNA-based cellular processes which are replication, repair and transcription.

1.1.3.1. DNA replication

DNA replication is the process by which a cell duplicates its DNA prior to mitosis. Following the discovery of DNA structure, Watson and Crick had theorized that the specific base pairings within the double helix existed in order to ensure a controlled system of replication during cell division (Crick and Watson, 1953). However, definitive demonstration of such mechanism was made possible by Meselson and Stahl’s use of in vitro radioactive isotope labelling to show that DNA is indeed replicated in a semi-conservative manner (Meselson and Stahl, 1958). Years later Arthur Kornberg isolated DNA polymerase I, the enzyme that catalyzes the synthesis of DNA, for which he got the Nobel Prize in Physiology or Medicine in 1959.

In contrast to prokaryotes, eukaryotes use multiples origins of replication that all need to be fired together to efficiently duplicate larger chromosomes during S phase. Recently, it became apparent that the structure of chromatin profoundly influences the rate and timing of replication through control of replication origin binding by origin recognition complex (ORC) (MacAlpine and Almouzni, 2013) (Figure 5). Moreover, many replisome assembly units were found to display histone binding domains such as the CMG helicase subunit MCM2, but also the histone chaperone and chromatin-remodeling factor FACT (facilitates chromatin transcription) (Kurat *et al.*, 2017; Evrin *et al.*, 2018). The system is

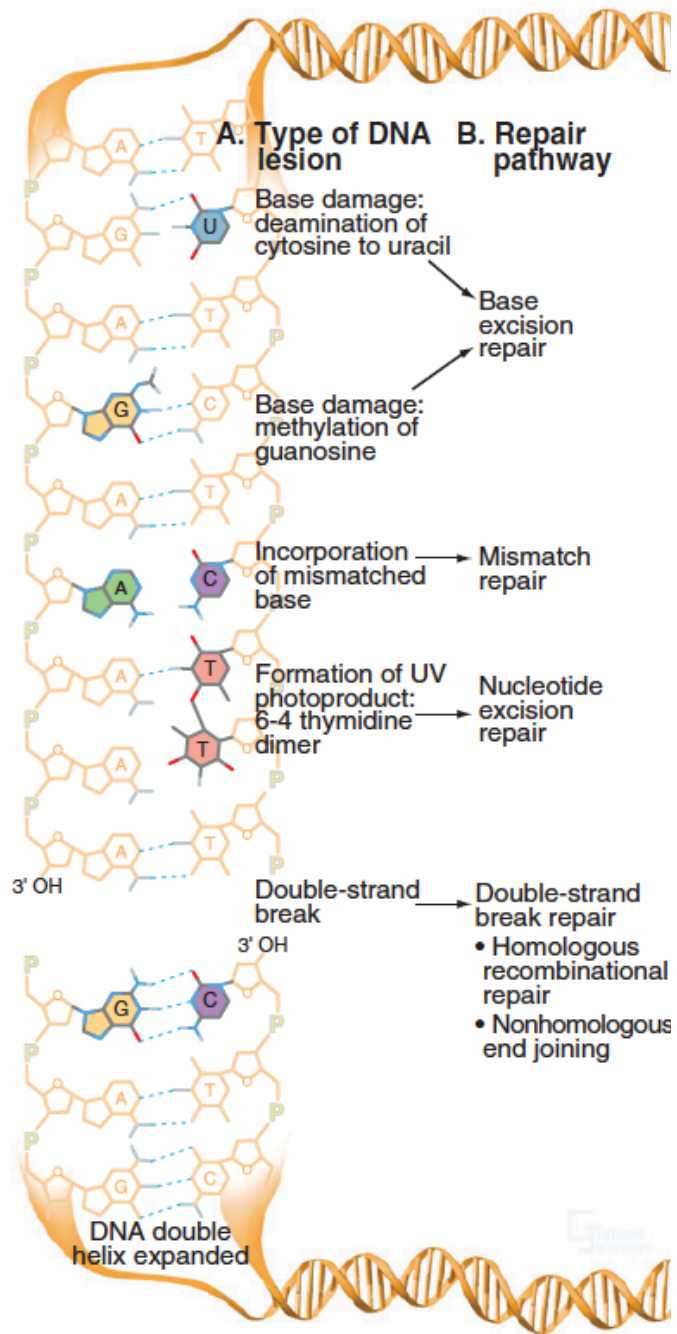


Figure 6. DNA repair mechanisms.

From Pollard, Thomas D., et al. *Cell Biology*, 2016.

tightly regulated to allow efficient nucleosome disassembly and re-assembly on the newly synthesized DNA, and failure to do so blocks the cell from dividing (Bellush and Whitehouse, 2017).

1.1.3.2. DNA repair

Another aspect of replicating DNA to allow inheritance of the genetic information in daughter cells is that first the replication machinery is not infallible and makes random errors here and there; and second that DNA itself is very sensitive to genotoxic-induced mutations.

From an evolutionary standpoint, this genetic instability is beneficial as it not only allows for more diversity and specification but also provides adaptive mutations. However, failure to repair DNA damages has been linked to many severe diseases such as Xeroderma pigmentosum or cancer (Jeggo, Downs and Gasser, 2017). Depending on the cause which can be endogenous or exogenous, the DNA damage response (DDR) differs and at least four main pathways have been documented from the simplest to more complex: direct reversal repair (DR), excision repair (ER), mismatch repair (MMR), DSB repair pathways (DSBR) (Chatterjee, N., Walker, 2017; Stadler and Richly, 2017) (Figure 6).

Direct reversal repair is the simplest form of repair which involves only a biochemical reaction of reversal to the original nucleotide by specialized enzymes such as the DNA alkyltransferases (MGMT) responsible for repair of alkylated guanines and indirectly the cause of resistance to alkylating mutagens used as anticancer treatments in patients (Hegi *et al.*, 2005).

Excision repair is subdivided into base excision and nucleotide excision repair pathways. The former, termed BER, relates to the detection of abnormal base and subsequent removal by AP-endonucleases and further repair by DNA polymerase. The latter is more complex and has been divided in two pathways: the global genomic NER (GG-NER) and the transcription-coupled NER (TC-NER). They differ in how DNA damage is recognized however they share the same downstream repair mechanisms which rely on the transcription factor complex TFIIH (Compe and Egly, 2012) coupling gene expression to repair.

MMR is activated in cases where DNA polymerases make errors while replicating, which results in mispairing of the double helix. This involves the MSH/MLH complexes and endonuclease-mediated removal of a large section around the mismatch and later complementary synthesis and ligation.

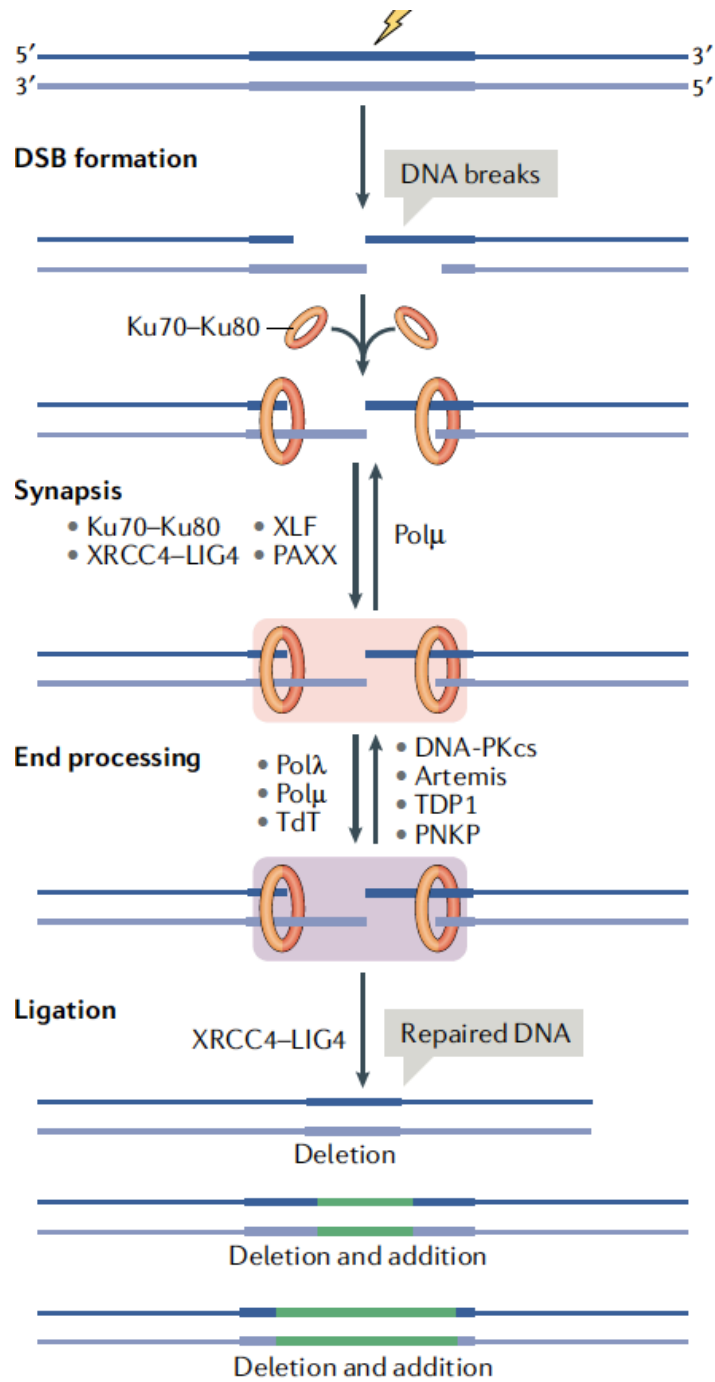


Figure 7. DNA double strand break repair; Non-homologous end joining process.

From Zhao *et al.*, 2020.

DSB repair. Mutations can also happen on both strands. Double strand breaks (DSB) are very hazardous X-rays induced mutations that can lead to genome rearrangements; thus 2 different pathways exist to repair them. Non-homologous end joining (NHEJ) is the major pathway which occurs at all cell cycle stages however it is referred to as ‘non-homologous’ because the break ends which are detected by KU70/KU80 proteins are directly ligated without the need for homologous template by DNA ligase IV and its cofactor XRCC4 (Zhao *et al.*, 2020). In contrast homologous recombination (HR) accounts for roughly 20% of DSB repairs as it can occur only at S/G2 phases when the chromatin is compacted into chromatid forms. DSBs are detected by ATM/ATR protein which phosphorylate S139 of histone variant H2AX which results in chromatin decondensation and recruitment of RAD50/BRCA1 complex that allow to repair DNA by using an intact chromatid as a template (Huang and Zhou, 2020). The fidelity of HR is thus higher than that of NHEJ (Figure 7).

Thereby, the dynamically changing structure of chromatin influences both DNA replication and repair throughout the cell cycle.

1.2. Mechanisms of RNA polymerase II transcription

Besides replication and repair, chromatin has also a fundamental and thoroughly studied role in a third nuclear DNA-mediated process which is transcription. RNA transcription is one of the pivotal steps in the transfer of sequence information as stated in 1958 in the central dogma of molecular biology by Francis Crick. Genes are detected by the transcription machinery and converted into RNAs which can be coding such as messenger RNA (mRNA) or non-coding such as transfer RNA (tRNA), ribosomal RNA (rRNA) and other less well-characterized non-coding RNAs by DNA dependent RNA polymerases. Thus far, three RNA polymerases (RNAP) have been described in eukaryotes (with 2 additional exclusive to plants). Transcription by RNAP I is exclusive to the synthesis of pre-rRNA 45S in the nucleoli, while RNAP III synthesizes tRNA and rRNA 5S in the nucleus and cytosol. Both are important for transcribing essential components of the cytosolic ribosomes, key enzymes for translating mRNAs to proteins. Since its purification by Robert Kornberg, by far the most studied RNA polymerases are class II RNAPs due to their high level of regulation required over transcription of all coding genes into mRNAs as well as some non-coding RNAs.

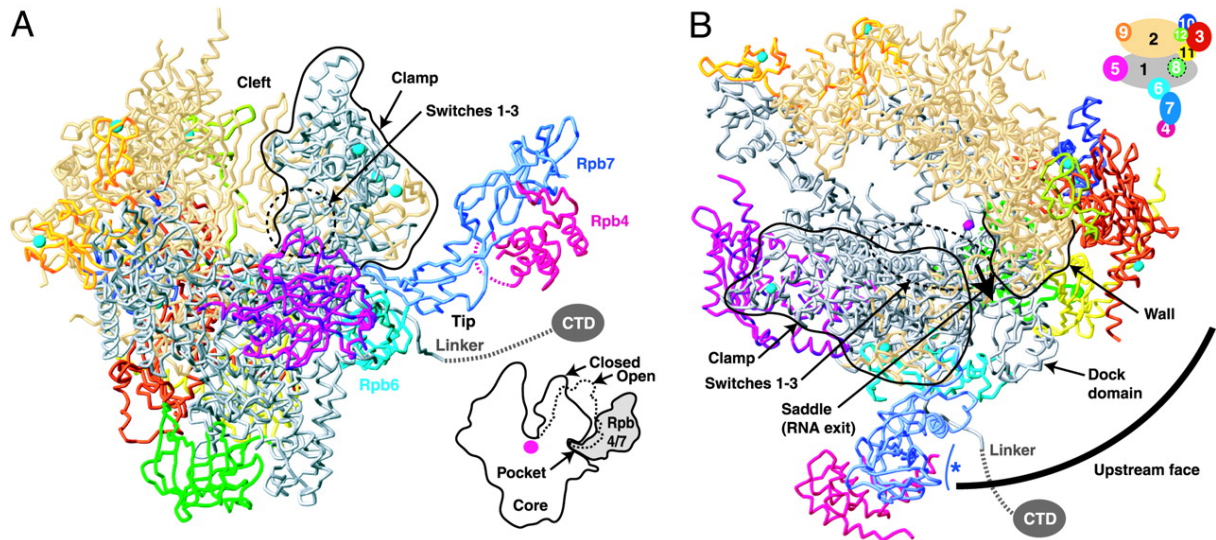


Figure 8. Crystal structure of the 12-subunit yeast Pol II, coupling of Rpb4/7 binding and clamp closure, and upstream interaction face.

A. Ribbon model of Pol II. **B.** Pol II upstream interaction face. Shown in a view of the model from the “top”. From Karim-Jean Armache *et al.*, 2003.

1.2.1. The Transcription machinery

1.2.1.1. RNA polymerase II

Isolated in 1969 by Roeder and colleagues, RNAPII is the enzyme responsible for synthesis of all mRNA as well as many non-coding RNAs. RNAPII is a 0,5MDa complex that is highly conserved from yeast to humans. It was found to be composed of 12 subunits termed RPB1 to RPB12, from high to low molecular weight (Roeder and Rutter, 1969; Kedinger *et al.*, 1970; Armache *et al.*, 2005; Werner and Grohmann, 2011). Only five subunits of RNAPII (RPB5, 6, 8, 10 and 12) are common to other RNAP such class I and III. It was also shown that a catalytic core consisting of 10 subunits without RBP4 and RPB7 is sufficient for in vitro transcription, however these subunits are required in vivo transcription (Armache *et al.*, 2005).

High-resolution structure of yeast RNAPII by Cramer *et al.* in 2000 revealed its distinct domain-like regions based on their functions (Cramer *et al.*, 2000) (Figure 8).

The first domain is the so-called ‘assembly platform’ composed by a dimer of RPB3-RPB11 on which the largest subunit RPB1 and RPB2 are anchoring to form a crab claw shaped clamp which harbors inside the catalytic center with two Mg^{2+} ions. The entry of DNA in this zone is controlled by the two jaws represented by RPB5 and RPB9. Together all these structures composed the RNAPII core which is headed by the stalk domain composed by RPB4 and RPB7. The stalk acts a recruitment and interacting platform for other factors such as transcription initiation factors and is also restricting the movement of the clamp during RNA synthesis. The nascent RNA transcript exits the RNAPII through a funnel close to the stalk domain. Also close to the stalk domain is the long C-terminal repeat domain (CTD) tail of RPB1 which is as the name indicated consists in a 52-fold repeat of a heptad sequence extremely rich in highly modifiable serine, threonine and tyrosine residues (i.e. Tyr-Ser-Pro-Thr-Ser-Pro-Ser) (Buratowski, 2009; Bartkowiak and Greenleaf, 2011). This tail is of great importance for transcription initiation (which I will be describing below).

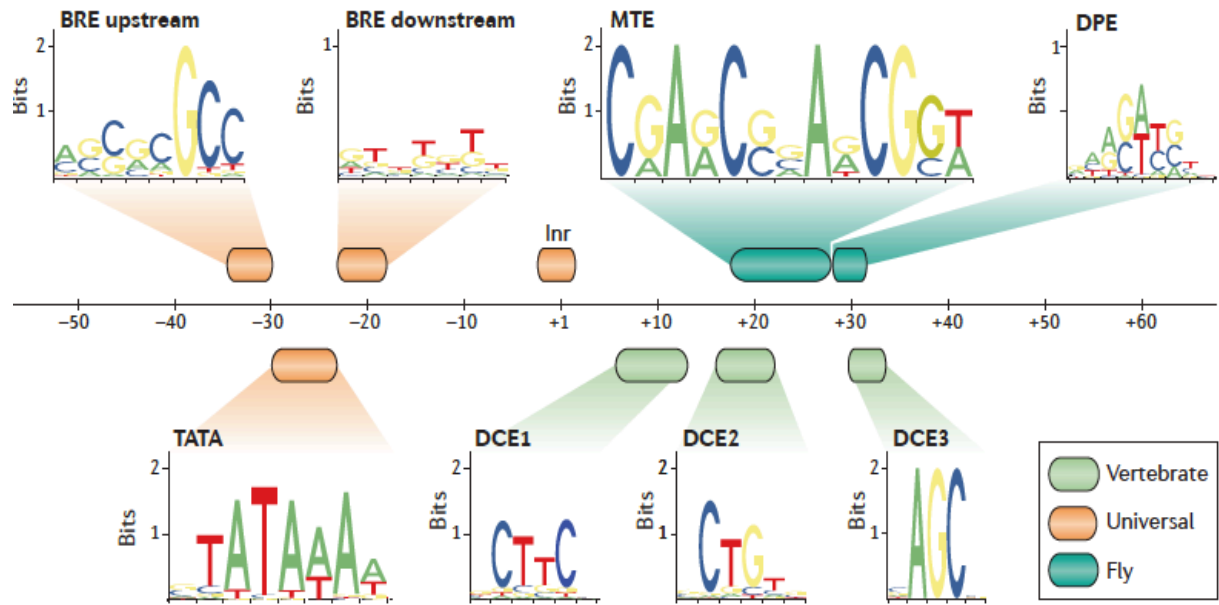


Figure 9. Sequence motifs and localization of core promoters.

From Lenhard *et al.*, 2012.

1.2.1.2. Core promoters

All eukaryotic genes have a promoter region depleted of nucleosomes, also called NDR, which defines where the transcription starts, defined as the transcription start site (TSS). At the end of a gene, there is a transcription termination site (TTS) and in between both site, there is an open reading frame (ORF). Promoters are crucial for gene regulation. They vary in terms of associated regulatory elements and sequence motifs. The consensus definition of a 'core promoter' is the minimal sequence that orchestrates transcription initiation and is located within 500 bp up and downstream of the TSS of a gene. Thus, core promoters are designed to recruit basal transcription machineries including RNAPII and their specificity is partly due to specific consensus elements. The TATA-box was the first core promoter element to be identified (Gannon *et al.*, 1979) which canonical sequence is TATAWAWR, where W stands for A/T and R for A/G. It is generally located 30bp before the TSS, however it is not present in all genes (Jin *et al.*, 2006; Kimura *et al.*, 2006; Yang *et al.*, 2007). Actually, the majority of genes harbors other elements, sometimes in combination, such as the Initiator (Inr), the BRE (TFIIB recognition element), the TCT (polypyrimidine initiator), the MTE (motif ten element), the DPE (downstream promoter element) and the DCE (downstream core element) motif (Basehoar, Zanton and Pugh, 2004; Kadonaga, 2012; Vo Ngoc *et al.*, 2017). Some genes do not have any detectable elements, suggesting these may not required for promoter function and transcription initiation (Hahn, 2004; Cramer, 2019). Other characteristics may also be in play such as AT-content and DNA bendability (Levens, Baranello and Kouzine, 2016; Haberle and Stark, 2018).

In addition, three core promoter architecture have been identified with distinct functions in eukaryotes. Sharp promoters with one or few strong TSSs within a narrow region which have been found in regulated tissue-specific genes harboring combination of TATA-box and other promoter elements (Ponjavic, Ponting and Lunter, 2007; Lenhard, Sandelin and Carninci, 2012). In contrast, broad promoters with several weak TSSs within a large locus associated with housekeeping or constitutive genes. Finally, mixture of both features can be found in so-called mixed promoters with broad pattern but one dominant TSS (Juven-Gershon and Kadonaga, 2010; Kadonaga, 2012; Lenhard, Sandelin and Carninci, 2012; Danino *et al.*, 2015) (Figure 9).

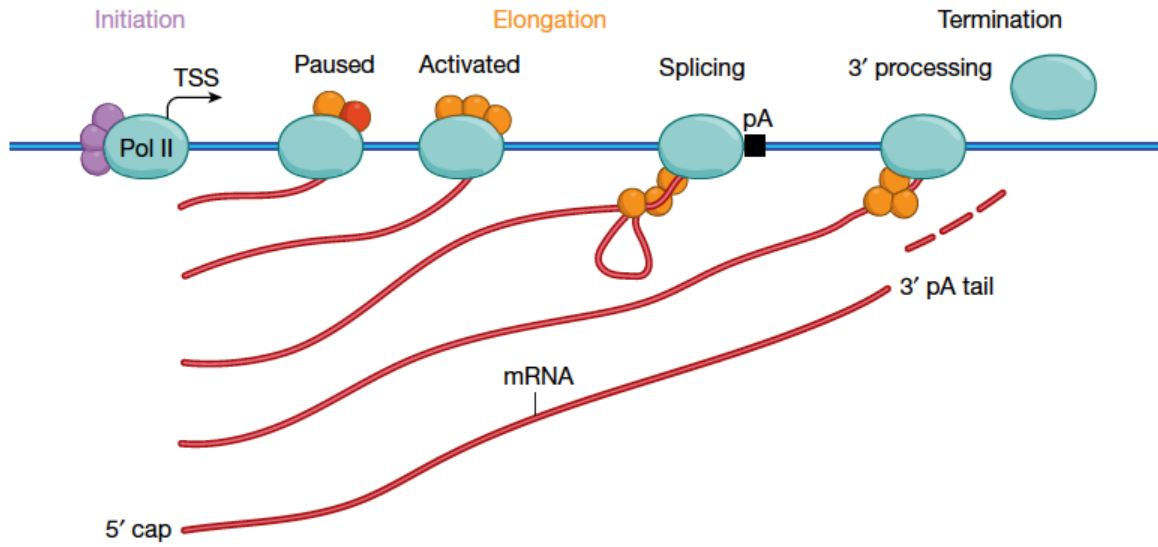


Figure 10. Illustration of Pol II transcription cycle.
From Cramer, 2019.

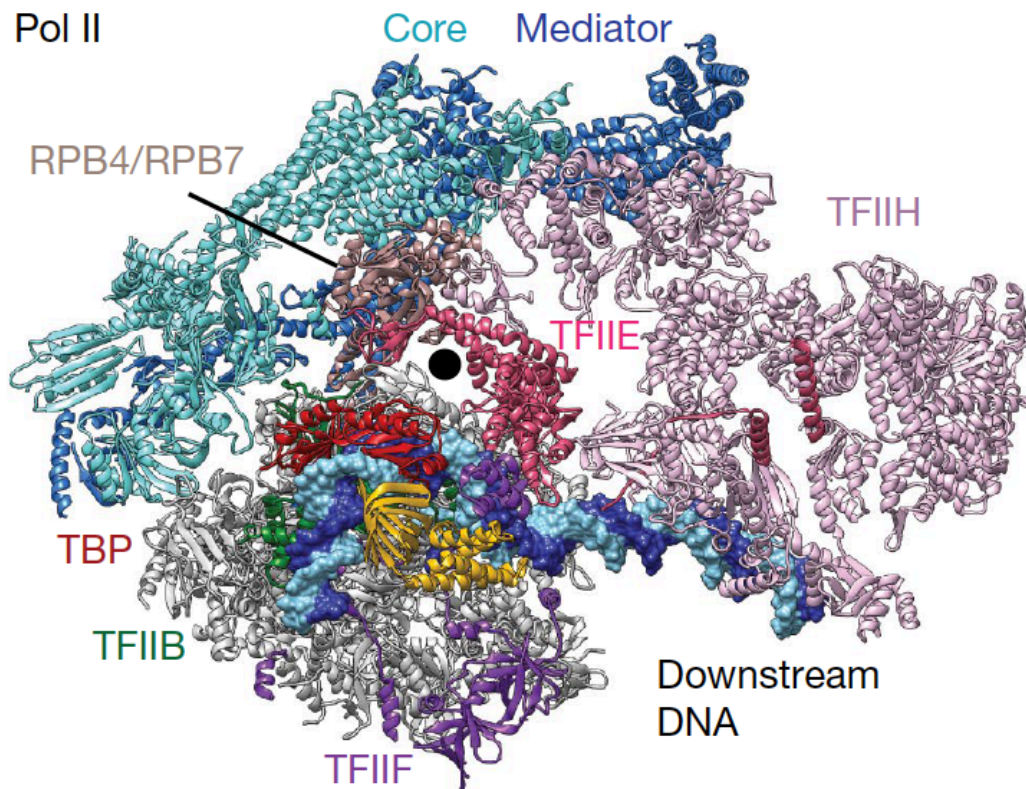


Figure 11. Structure of eukaryotic Pre-Initiation Complex.
From Cramer, 2019.

1.2.2. Mechanism of transcription

Transcription is mechanistically composed of three main steps: initiation, elongation and termination. Initiation is the most regulated step of transcription and requires factors commonly termed the pre-initiation complex and includes a pausing phase before elongating the RNA.

1.2.2.1. Pre-initiation complex formation and transcription initiation

Whilst RNAPII is necessary for synthesizing RNA, by itself it cannot bind to promoters, melt the DNA and find the TSS, which are required steps to initiate transcription. For that, it needs the assistance of several multiprotein complexes known as General Transcription Factors (GTFs) which are TFIIA, TFIIB, TFIID, TFIIE, TFIIF and TFIIH. Together these 6 GTFs with RNAPII formed what is called the Pre-Initiation Complex (PIC), representing a remarkable complex of more than 40 individual proteins (Figure 10 and 11).

TFIID loading on the promoter. The first step of PIC assembly is the binding of the GTF TFIID on the promoter through its TBP (TATA-box binding protein) subunit. TFIID is a highly conserved complex and the largest GTF composed of TBP and 13 TBP-associated factors (TAFs, named TAF1 to TAF13). Upon binding on the minor groove of DNA, TBP causes the promoter to tilt to a 90° angle with TFIID covering roughly 60bp around itself (Hahn, 2004).

TFIID acts a recruitment and interacting platform for many regulatory factors such as other GTFs but also coactivators and chromatin modifying complexes (which will be detailed in Chapter II of this manuscript).

TFIIA stabilizes TBP on DNA. TFIIA is a heterodimer of two subunits termed TFIIAab and TFIIAg. Upon recruitment, it binds to TBP and seals its interactions with DNA by changing the conformation of TBP-containing GTF TFIID. TFIIA is an auxiliary factor as it is not required for in vitro transcription.

TFIIB recruit TFIIF-RNAPII complex. Following TFIIA recruitment, TFIIB joins and interacts with TBP and the surrounding DNA further stabilizing the forming PIC (Werner and Grohmann, 2011). DNA bound by TFIIB can contain the aforementioned BRE (TFIIB recognition element) core promoter. The major role of TFIIB is to recruit the RNAPII-TFIIF complex. TFIIF is dimer of TFIIFa and TFIIFb which form a complex with free nucleoplasmic RNAPII via the aforementioned RBP4/7 stalk domain

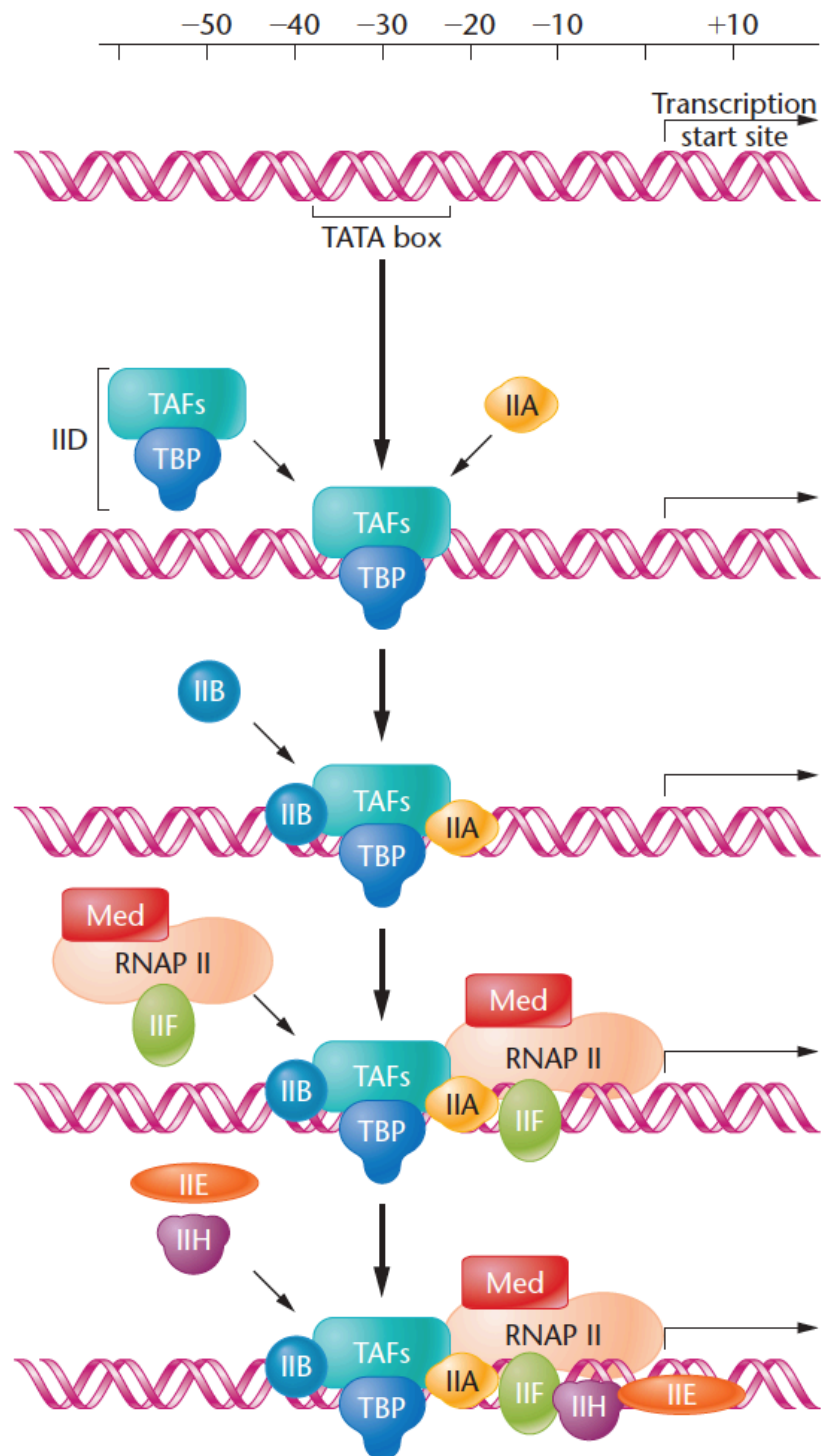


Figure 12. Assembly of general transcription factors for RNA pol II transcription.
From Pollard, Thomas D., et al. *Cell Biology*, 2016.

of RNAPII. Upon recruitment, TFIIF binds to TFIIB and DNA stabilizing the whole machinery.

TFIIE recruits TFIIF. The heterodimeric GTF TFIIE binds to gene promoters upstream of the TSS and makes contact with RNAPII on the opposing side of TFIIF (Sainsbury, Bernecky and Cramer, 2015; Hantsche and Cramer, 2017). TFIIE enables the recruitment of the last and second largest GTF, TFIIF, and forms interaction with it (Compe *et al.*, 2019).

Unwinding of DNA by TFIIF subunit XPB. TFIIF is composed of 10 subunits organized into two main domains: a trimeric kinase domain and a core domain. The latter is shaped as a ring and contains the two ATPase subunits XPB and XPD. XPB is a DNA helicase that uses ATP hydrolysis energy to unwind DNA thereby facilitating the formation of the ‘transcription bubble’, which is required for RNAPII to start transcribing one strand. Beside transcription initiation, TFIIF also has roles in transcription-coupled NER which requires its subunits XPB and XPD. The ATPase activity of XPB stabilizes TFIIF to the sites of DNA damage and the helicase activity of XPD is essential for efficient opening of the DNA at damage site (Coin, Oksenyich and Egly, 2007; Oksenyich *et al.*, 2009). Mutations in these key subunits of TFIIF are responsible for several DNA repair-related human diseases (Coin *et al.*, 1998; Oksenyich *et al.*, 2009; Egly and Coin, 2011).

CTD tail phosphorylation by TFIIF subunit CDK7. Another requirement for transcription initiation is fulfilled by the TFIIF kinase domain. This domain known as CDK-activating kinase (CAK) contains CDK7 which can phosphorylate Serine 5 residues of the CTD tail of RNAPII subunit RPB1. Following this sequential assembly and phosphorylation of CTD tail, RNAPII initiates RNA synthesis upon stimulation by TFIIB which is essential in stabilizing RNAPII into its elongating form. After the first 30 nucleotides (nt), RNAPII loses direct contacts with the PIC (Hahn, 2004) and the newly synthesized RNA is capped by addition of a methylated guanine in 7 (m⁷G) (Figure 12).

1.2.2.2. Elongation and termination

Around 60 nt downstream of the TSS, elongating RNAPII has been described to freeze known as promoter proximal pausing. This phenomenon has been described in *Drosophila* initially for heat shock genes (Spencer and Groudine, 1990) and is proposed as a mechanism to allow external stimuli integration and synchronicity in cells (Adelman and Lis, 2012; Mayer, Landry and Churchman, 2017).

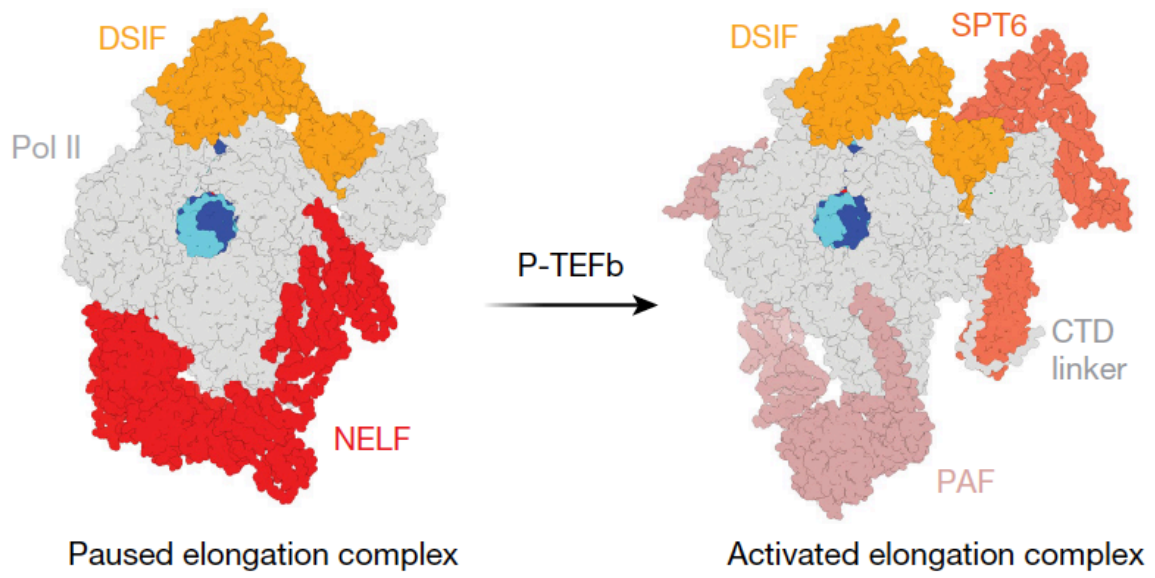


Figure 13. Transition from Pol II pausing state to active elongation state.

From Cramer, 2019.

The DRB-sensitivity inducing factor (DSIF) and the negative elongation factor (NELF) have been shown to pose RNAPII elongation (Aiyar *et al.*, 2004).

Release from this paused state is mediated through the action of CDK9 on the positive transcription elongation factor b (P-TEFb) (Luecke and Yamamoto, 2005). Thus, NELF dissociates with RNAPII and productive elongation proceeds (Levine, 2011; Nechaev and Adelman, 2011; Chen, Smith and Shilatifard, 2018). The rate of transcription elongation by RNAPII (also called 'processivity') has been estimated at a formidable average speed of 2 kb per minute (Singh and Padgett, 2009; Steurer *et al.*, 2018).

Elongation continues until RNAPII passes through a consensus sequence on the DNA AATAAA known as the polyadenylation signal (PAS). The PAS is then recognized on the transcript by cleavage and polyadenylation specificity factor (CPSF) which binds to AAUAAA and induces RNAPII pausing. Next, cleavage stimulatory factor (CSTF) binds to RNAPII through its CTD tail and interacts with CPSF which then dissociates from RNAPII leading to the cleavage of the pre-mRNA about 30bp downstream of the PAS (Richard and Manley, 2009; Porrua and Libri, 2015). Then, the 3'OH extremity of the pre-mRNA receives a poly(A) tail which consists of roughly 250 AMPs and is catalyzed by the poly(A) polymerase using ATP as source of energy. This poly(A) tail is essential as it allows the binding of the so-called poly(A) binding protein (PABP) which has 2 roles: 1) it stabilizes the RNA and avoids degradation from exonucleases; and 2) it is involved in the nuclear export and subsequent translation of the RNA molecule. However, some RNAs such as small nuclear RNAs or canonical histone mRNAs do not have this mechanism and termination happens in a poly(A)-independent manner. For instance, canonical histone mRNAs have other regulatory structures namely a 3' stem-loop and a downstream specific motif which are recognized by SLBP (stem-loop binding protein) and the spliceosome enabling to recruit the cleavage factors to release the RNA from the polymerase, thus histone mRNAs do not exhibit the classical poly(A) tail. Upon release of the transcript, RNAPII continues its elongation for a little while however the new RNA lacks the 5' cap and is rapidly degraded which causes the polymerase to detach from the DNA template (Figure 13).

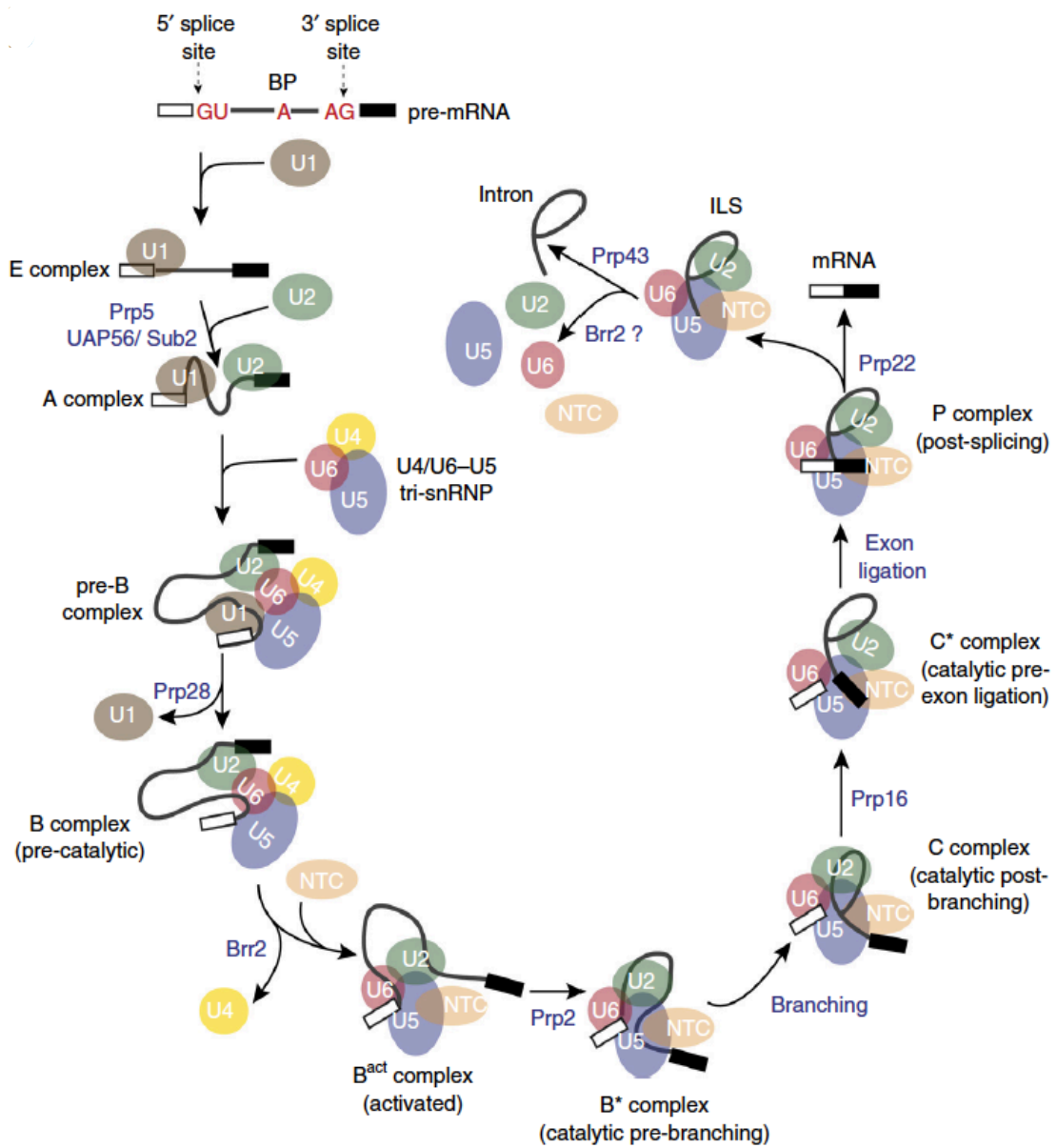


Figure 14. Assembly and catalytic cycle of spliceosome.
From Fica and Nagai, 2017.

Efficient termination is essential to avoid conflicts with neighboring transcription and to liberate RNAPII for subsequent rounds of transcription. 5'mG Capping and poly(A) tailing are two modifications that have often been called 'post-transcriptional', yet they are actually made co-transcriptionally: RNAs are capped just after transcription initiation while the latter is added after termination.

1.2.3. Post-transcriptional regulation of gene regulation

1.2.3.1. RNA splicing and spliceosome

Upon being transcribed, precursor messenger RNAs (pre-mRNAs) need to go through a step of processing called splicing in order to become mature mRNAs that can leave the nucleus to be translated in the cytoplasm by the ribosome machinery.

Pre-mRNAs are composed of distinct 2 parts: the intronic regions (introns) that are not found in the mature RNA and the exons which represent the coding part of the RNA. Whilst, pre-mRNAs are very heterogeneous in length, on average human exons tend to be only 150bp (Lander *et al.*, 2001). The variety of RNA sizes mostly stems from the introns which are very long and contain the necessary signals that allow the RNA to be processed.

Indeed, RNA splicing requires three consensus motifs found at or close to intron-exon junctions: the 5' splice site (5'SS, GU) on exon n, the 3' splice site (3'SS, YAG motif) on exon n+1 and the branch point (BP) 20 to 40bp before the 3'SS which always contains a A (Wahl, Will and Lührmann, 2009; Fica and Nagai, 2017). By base pairing, these three sites can be recognized by small nuclear RNAs (snRNAs) which are transcribed by RNAPIII and associate with proteins to form snRNP (small nuclear ribonucleoproteins). In mammals, there are five distinct snRNPs subcomplexes namely U1, U2, U4, U5 and U6 which together form *de novo* the spliceosome on every intron in a stepwise manner.

The formation of the spliceosome begins with the binding of snRNP U1 on the 5'SS end of the pre-mRNA which is immediately followed by U2 on the branch point. This sends a signal to recruit the preassembled U4/U6/U5 tricomplex of snRNPs which dislodges U1 from the 5'SS. Next, interactions between U6 and U2 lead to closing the gap and forces the spliceosome to undergo conformational changes and

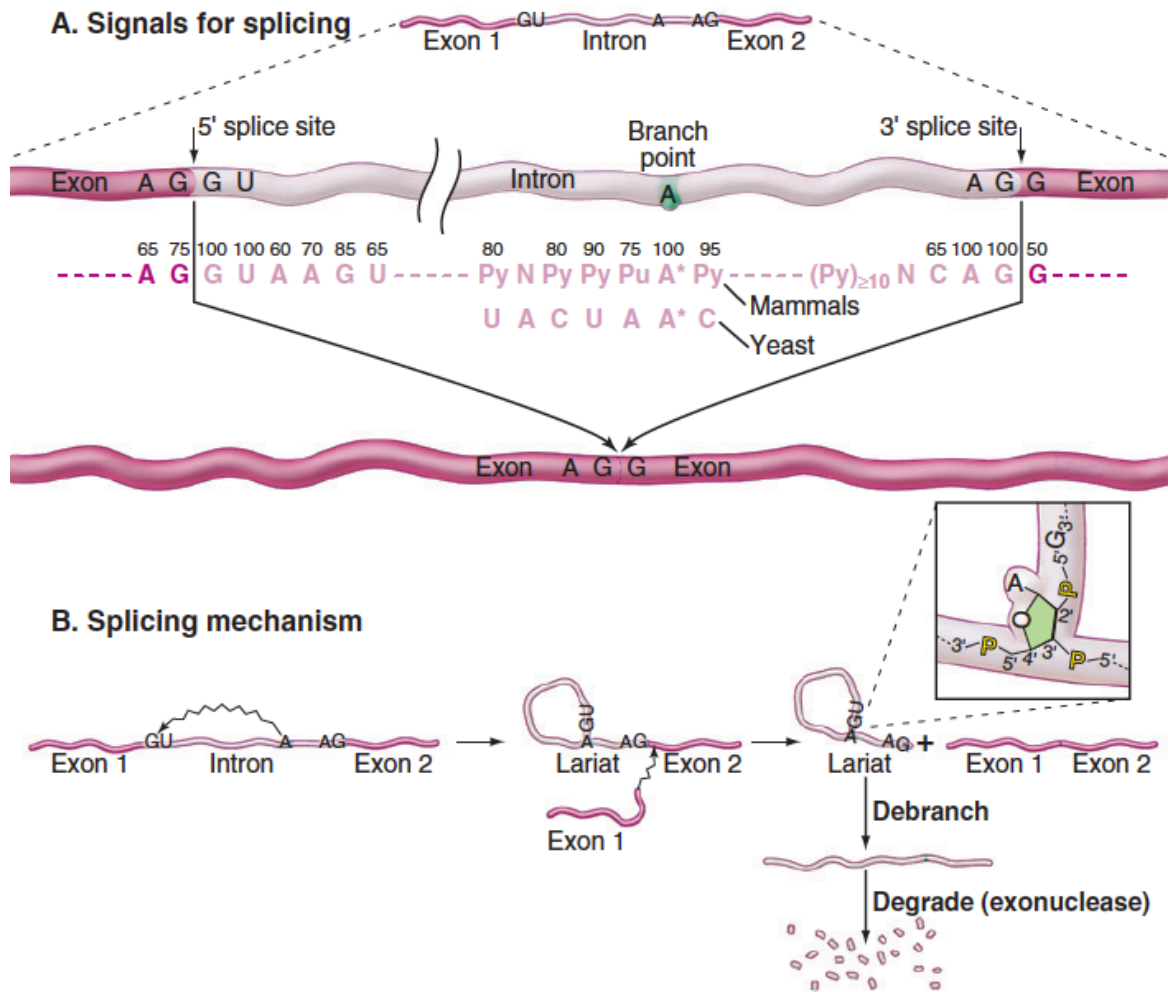


Figure 15. Signals and mechanism of RNA splicing.
 From Pollard, Thomas D., *et al.* *Cell Biology*, 2016.

U4 is released. Then, two esterification reactions are catalyzed by the now catalytically active spliceosome (which was repressed by U4).

The first reaction involves the phosphate group of the 5'SS G on exon n and the free hydroxyl group of A within the branch point which leads to the formation of the intron lariat formation. The second reaction sees the now free hydroxyl group of 5'SS on exon n chemically attack the 3'SS on exon n+1 which allows to splice both exons together while the intron lariat is evicted and degraded. When all exons of a gene are conserved in the mature mRNA, the splicing is qualified as constitutive.

However more than half of human genes use alternative splicing mechanisms where exons are omitted, or introns are kept in the final mRNA. This leads to a high degree of diversity in RNA sequences and gives rise to a considerable number of distinct isoforms for the same gene. Besides, alternative promoters can be found on a gene which increases the number of isoforms as alternative promoters and splicing can have additive effects which increases complexity. For instance, the Microphthalmia-inducing transcription factor (MITF, bHLHe32) is known to be driven by 9 alternative promoters which are activated in a tissue-specific manner however a total of 16 transcripts of this gene exist due to alternative splicing (Murakami, Iwata and Funaba, 2007).

Mutations in the spliceosome have been linked to disease and cancer as mis-spliced RNAs are usually detected and degraded via Non-sense Mediated Decay (detailed in 1.2.3.2.). An example of this has been described for SF3B1 which is a protein found in snRNP complex U2 and is the most highly mutated RNA splicing factor. Reports by Inoue et al. linked the most common SF3B1 mutation in uveal melanoma to mis-splicing and subsequent degradation of SWI/SNF subunit BRD9 which drives malignancy (Inoue *et al.*, 2019) (Figure 14).

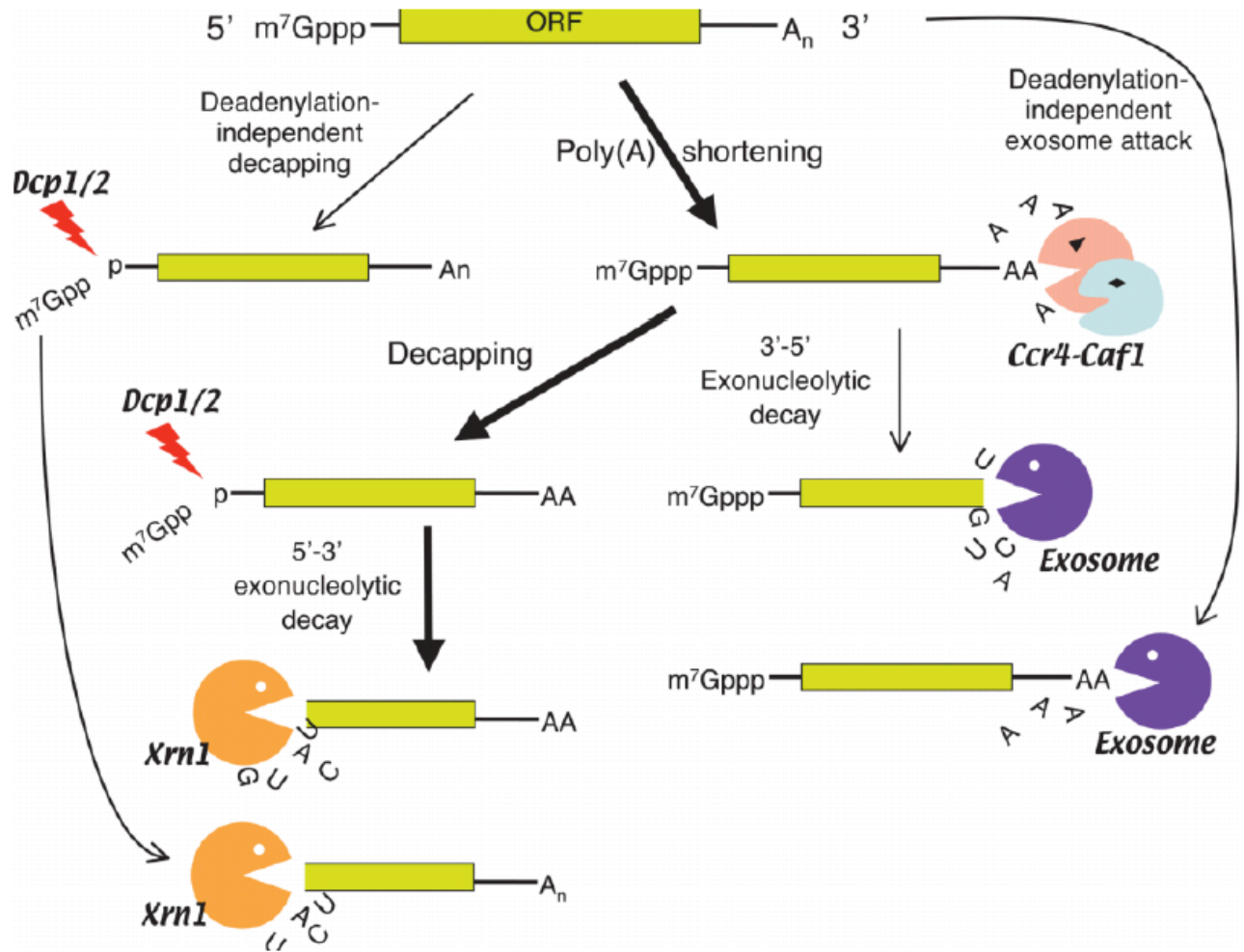


Figure 16. Illustration of mRNA decay pathway.
From Chen and Shyu, 2011.

1.2.3.2. RNA degradation pathways

Three distinct mechanisms of RNA degradation have been described: non-sense-mediated decay (NMD), deadenylation-dependent decay, ARE-mediated decay and miRNA-mediated decay.

Discovered in 1979, the aforementioned NMD pathway is one of the RNA surveillance mechanism which controls the quality of the new transcripts (Kuzmiak and Maquat, 2006). Newly spliced RNAs are widely bound by regulatory proteins on their exon junctions forming the Exon-Junction Complex (EJC) which in a normal context are displaced by the ribosome during translation of the mRNA. However, some mis-spliced RNA can include so-called poison introns bearing a premature stop codon (PTC) which blocks translation and leads to the recruitment of UPF factors (UPF1, 2 and 3) at the exon-junction complex (EJC). Subsequent phosphorylation of UPF1 will leads to the degradation of the mis-spliced RNA, this ensures high fidelity to the genetic material and proper function of the encoded protein (Wei-Lin Popp and Maquat, 2013).

Another mechanism of RNA degradation involves the poly(A) tail found on all mRNAs. The length of the poly(A) directly correlates to its half-life as it is gradually shortened in the cytoplasm by deadenylases such as the CCR4-NOT complex. When the tail becomes too short, the mRNA is either decapped by DCP1/2 factors and subsequently degradation by XRN1 exonucleases from 5' to 3' ; or the mRNA keeps its cap and is degraded by from 3' to 5' by the exosome and finally the cap is digested by DCPS factor (Chen and Shyu, 2011).

Additionally, some poly(A) tails harbors so-called ARE sequences (AU-rich element) which are recognized by ARE-binding proteins (AUBPs) such as ZFP36L1 and accelerate the shortening of the tail, thus destabilizing the RNA. These 3' ARE motifs can mostly found in short half-life RNAs which need a higher degree of regulation and recycling such as stress or environmental stimuli response (De Toeuf *et al.*, 2018).

A final level of regulation arises from the interfering RNAs. Indeed, along mRNAs and snRNA, RNAPII also transcribes some primary microRNA (pri-miRNA, 1000nt) which contain one or several hairpin structures.

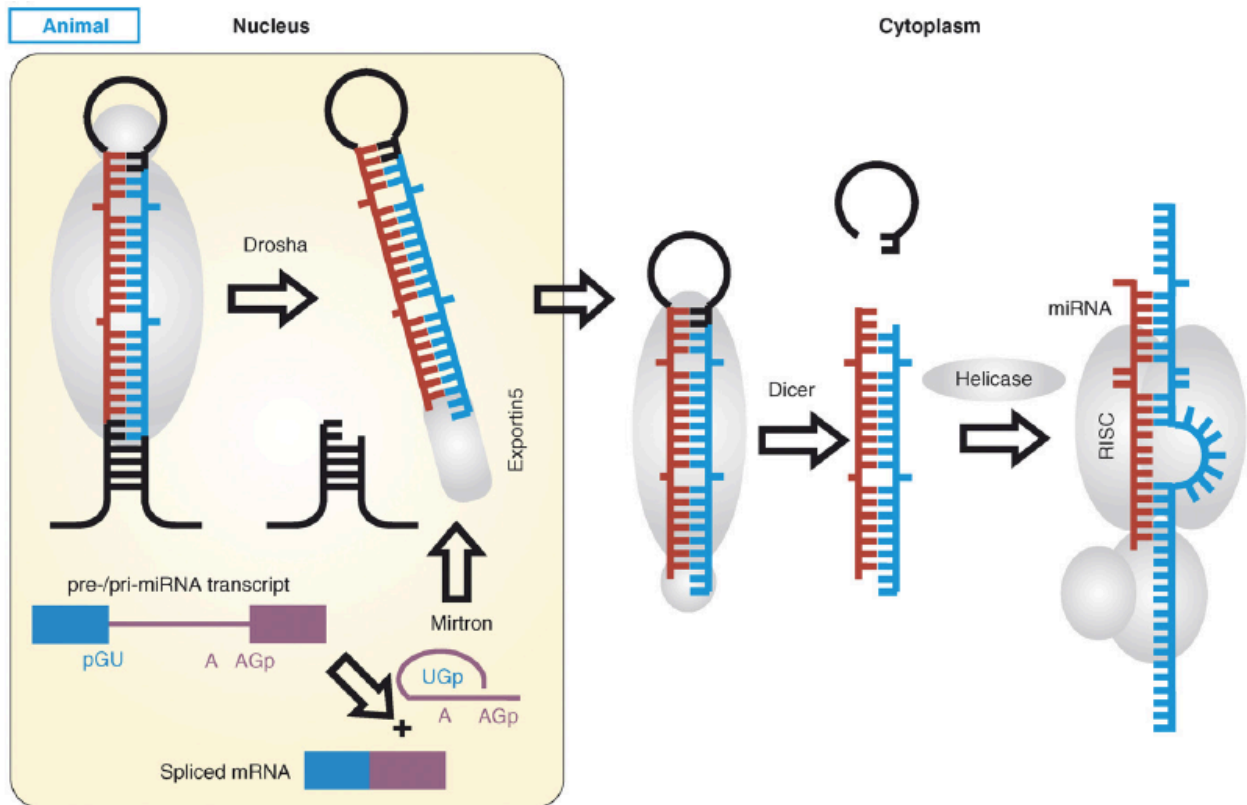


Figure 17. miRNA biogenesis pathway.

From Shabalina and Koonin, 2008.

These pri-miRNA are then cleaved by the RNase III (Drosha) into precursor miRNA of smaller size (100nt) which can be translocated to the cytoplasm where a second RNase III (Dicer) cuts the pre-miRNA into the mature miRNA) into a duplex of 20nt. Subsequently, the miRNA duplex is opened by a helicase and one of the single-stranded miRNA forms a complex with the RISC multiprotein complex (RISC micro-ribonucleoprotein).

Roughly 250 of these miRNA regulators are described in humans and they bind to their complementary messenger RNAs which then induces their degradation by the RISC subunit Argonaute. This mechanism known as RNA interference and is shared with the small interfering RNAs (siRNAs) which are mostly of viral origin and have been re-engineered for research purposes (Bentwich *et al.*, 2005; Shabalina and Koonin, 2008; Kleaveland *et al.*, 2018) (Figure 15).

These above mechanisms are essential post-transcriptional regulatory mechanisms of gene expression which contribute to the equilibrium between RNA synthesis and degradation and can lead to 'buffering' by lesser RNA degradation in abnormal cases where synthesis is defective (Timmers and Tora, 2018).

1.3. Control of RNA polymerase II transcription activation

Although post-transcriptional mechanisms have an important role, the highest conserved degree of regulation in transcription is concentrated in the control of the transcription initiation step. Thus, I will detail below the many layers of regulation of transcription initiation.

1.3.1. The enhancer code

The output of transcription is controlled via two well-characterized mechanisms: 1) DNA sequences found either in close proximity or further away from transcribed genes, which are termed cis-regulatory elements, 2) nuclear proteins that have chromatin binding abilities that act in 'trans' and are commonly called transcription factors.

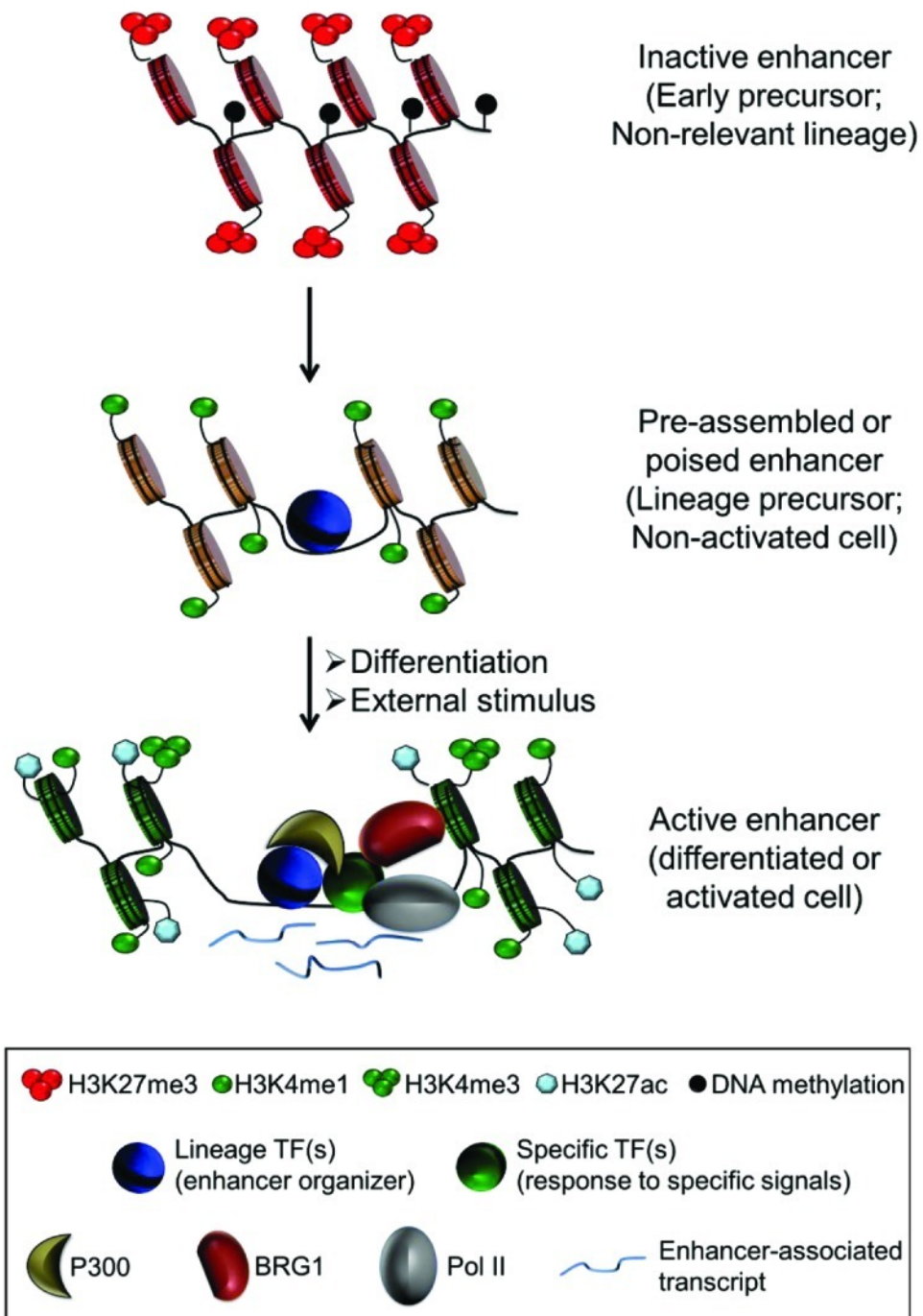


Figure 18. Chromatin dynamics at tissue-specific enhancers during cell differentiation.
From Spicuglia and Vanhille, 2012.

1.3.1.1. Cis-regulatory elements

Along with the aforementioned core promoters which are all proximal to the regulated gene, another type of cis-regulatory elements are enhancers. They are often referred to as distal regulatory elements; however, they can be localized either upstream or downstream of a gene, in intergenic regions, sometimes even in introns of unrelated genes or of the targeted gene itself.

By definition, they are short regions (50-1kb) of nucleosome-depleted DNA that can be bound by activators to increase the likelihood that a particular gene is transcribed and are found up to 1Mbp away from the TSS of the gene. The first discovery of enhancers within the SV40 genome which showed to have several enhancers increasing the expression of the beta-globin gene (Banerji, Rusconi and Schaffner, 1981; Benoist and Chambon, 1981). Typically, core promoters receive input from multiple enhancers which serve as amplifiers (Haberle and Stark, 2018).

In mammals, the total number of putative enhancers is estimated at roughly 1 million, by far outnumbering promoters of coding genes (Schoenfelder and Fraser, 2019). The activity of enhancers is partly dictated by the histone marks found around the nucleosome-depleted region (NDR) which contains the enhancer DNA sequence. Enhancers can exist in three states with distinct histone PTMs pattern (Spicuglia and Vanhille, 2012).

Active enhancers are typically rich in H3K27ac and H3K4me1, whereas inactive enhancers are repressed through methylation of H3K27 (Ernst *et al.*, 2011; Tee and Reinberg, 2014). A third state of enhancers are termed as 'poised' and harbor both active (H3K4me1) and repressive (H3K27me3) marks. These regions are associated with development and specification (Bernstein *et al.*, 2006; Barski *et al.*, 2007; Rada-Iglesias *et al.*, 2012).

However, recent studies revealed that this might be an oversimplification and described enhancers bearing no H3K27ac mark, but only H3K122ac (Pradeepa *et al.*, 2016). Moreover, selective reduction of H3K27ac in mouse embryonic stem cells by Zhang *et al.* showed that H3K27ac alone is not capable of functionally determining enhancer activity (Zhang *et al.*, 2020). Therefore, histone marks found on enhancers are likely read in combination with other PTMs (Figure 16).

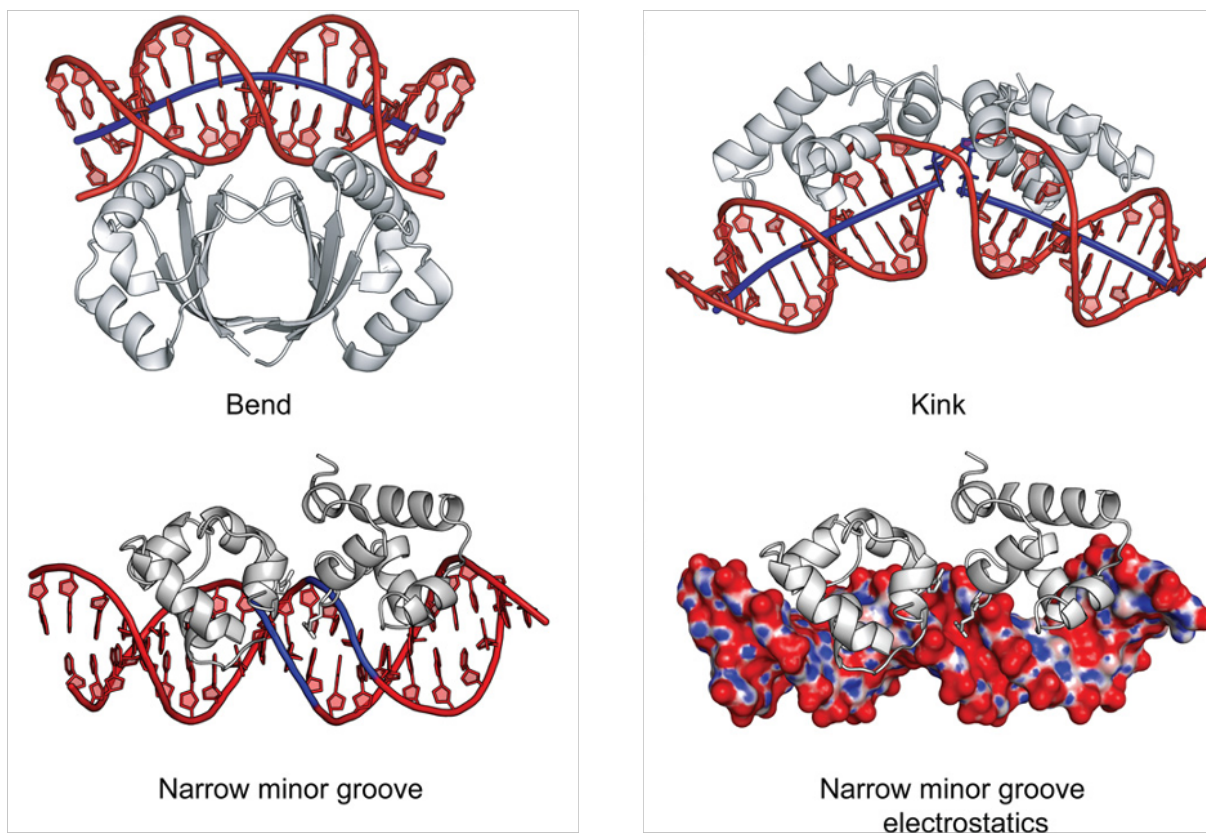


Figure 19. Readout mechanisms.

From Rohs *et al.*, 2020.

More recently, the term ‘super-enhancer’ (SE) has been introduced in 2004 by Chen and colleagues to describe large hyper-active regulatory domain consisting of a succession of enhancers, as defined by H3K27ac and/or Mediator complex occupancy (see 1.3.2.1.). Although their role is still debated, SEs have been implicated in regulating keys determinants of cell identity which are often deregulated during cancer development (Chen *et al.*, 2004; Lovén *et al.*, 2013; Whyte *et al.*, 2013; Wang, Cairns and Yan, 2019). Some known oncogenes such as c-MYC have been shown to be amplified in cancer cells through activation of a super-enhancer (Chen *et al.*, 2018; Jia *et al.*, 2020).

1.3.1.2. Trans-regulatory elements

Cis-regulatory elements are generally bound by specific trans-regulatory elements, or transcription factors, which in turn influence gene expression. TFs are nuclear multidomain protein containing three distinct parts: 1) a nuclear localization signal (NLS), 2) an effector domain which determines if the TF acts as an activation or repressor and 3) a DNA-binding domain (DBD) (Garvie and Wolberger, 2001) (Figure 17).

It is the DNA-binding capacity that makes TFs so special as they are able to detect specific loci by using two main mechanisms. Firstly, the DBD of a TF can recognize a specific nucleotide sequence found in its targeted genes; this is called “base readout” (Rohs *et al.*, 2010). Secondly, some DBDs can recognize specific structural features such as DNA-bending or unwinding which is known as “shape readout” (Stella, Cascio and Johnson, 2010). These two mechanisms can act in concert to regulate the expression of the TF target genes.

The most abundant class of DNA-binding proteins are zinc finger (ZF) family which are composed of several repeats of a short α -helix, two antiparallel beta-sheets and a central zinc ion. Such structures are found in GTF TFIIA giving its strong DNA-binding ability, but also the well-characterized nuclear receptors (Moras, 1998).

Another class of DNA-binding proteins are the basic helix-loop-helix (bHLH) family which is a large group of TFs found from yeast to humans and have critical roles in development. Members of this superfamily all share two highly conserved domains: 1) N-terminal ‘basic’ domain which allows DNA-binding to a specific sequence and 2) C-terminal ‘HLH’ domain which facilitates interactions with

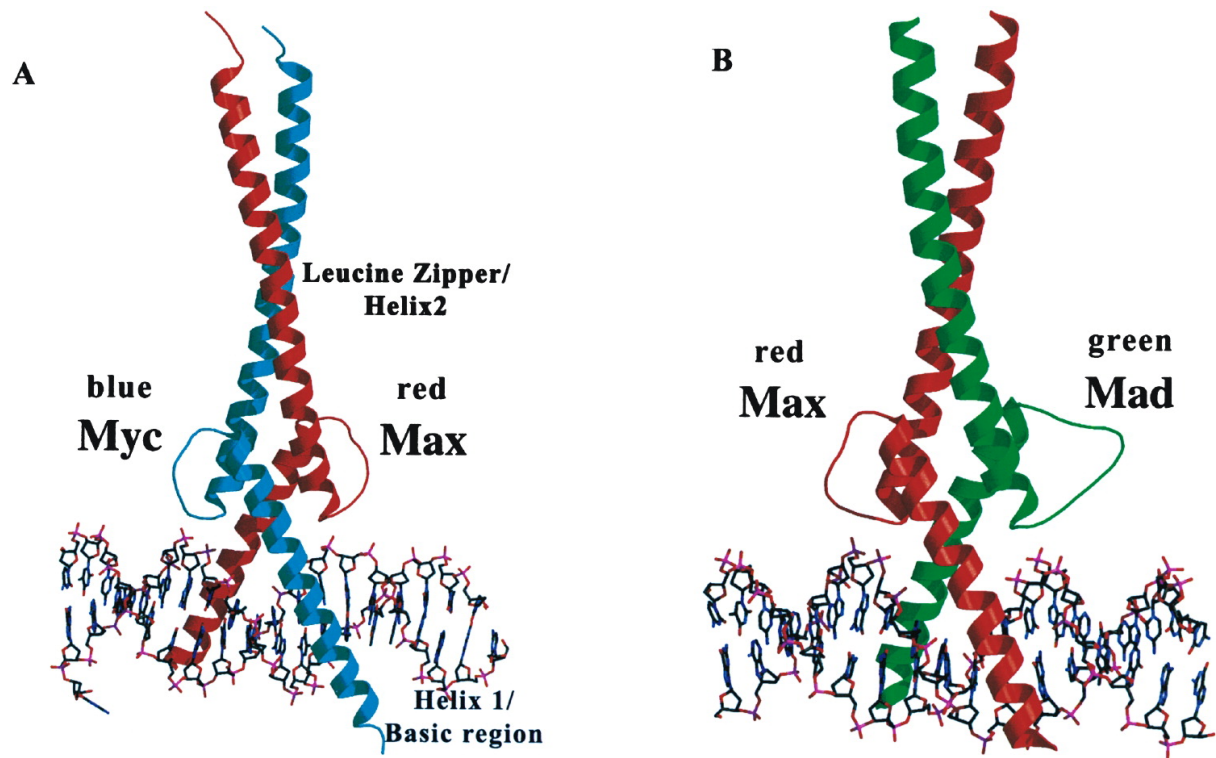


Figure 20. X-ray structures of the basic/helix-loop-helix/leucine zipper (bHLHZ) domains of Myc-Max and Mad-Max.

A. (bHLHZ) domain of Myc-Max and **B.** (bHLHZ) domain of Mad-Max heterodimers bound to their common DNA target (E-box). From Nair and Burley, 2003.

protein partners. The bHLH consensus motif is also known as the E-box ('Enhancer box', *CANNTG*) as first described by Murre and colleagues (Murre *et al.*, 1989). Well-characterized members of this family are MIST, TWIST, HIF, Hairy, MITF and MYC.

Transcription factor MYC was first discovered to be a proto-oncogene in Burkitt lymphoma patients where it regulates 15% of all coding genes (Ruf *et al.*, 2000). It has a slightly different structure compared to other bHLH members as it includes a leucine-zipper domain which mediates dimerization. Thus, MYC forms homo- or heterodimers with MAX and the dimerization is essential for proper function (Mathsyaraja *et al.*, 2019). Upon binding the MYC:MAX heterodimer recruits other proteins to E-boxes such as the NuA4 complex which contains the lysine acetyltransferase KAT5 (Tip60) in order to activate transcription of target genes. In a normal context, MYC is involved in angiogenesis through regulating the expression of vascular epidermal growth factor (VEGF) and is kept in check by tumor-suppressors ARF and p53. However, MYC is amplified in up to 40% of ovary and pancreatic adenocarcinomas and has been shown to drive oncogenesis via targeting cell cycle, DNA repair and metabolism (Stine and Dang, 2015; Kalkat *et al.*, 2018) (Figure 18).

MYC was also described as being part of the so-called Yamanaka factors, together with three other TFs which are OCT4, SOX2, KLF4. These factors were shown to be sufficient for transforming mouse embryonic but also human adult fibroblasts to pluripotent stem cells. Mechanistically, MYC interacts with many chromatin-modifying enzymes such as TRRAP-containing HAT complexes, CREB binding protein (CBP) and p300. Thus, the generation of induced pluripotent stem cells (iPS) is related to an induction of global acetylation by MYC, which allows the other Yamanaka factors to bind to their specific target loci (Takahashi and Yamanaka, 2006; Takahashi *et al.*, 2007).

The structure of chromatin plays an important role in TF binding to its cognate DNA sequence. Hence, TFs can be subdivided into three class: pioneers, settlers and migrants, depending on their binding capacities (Ernst and Kellis, 2013). So-called pioneer TFs have the ability to bind inaccessible DNA to promote remodeling of the regions and enhance accessibility for other TFs and co-factors. These factors are required for stem-cell pluripotency, cell differentiation and reprogramming (Magnani *et al.*, 2011; Zaret and Carroll, 2011). One good example is SOX2 which was shown to use binding energy to

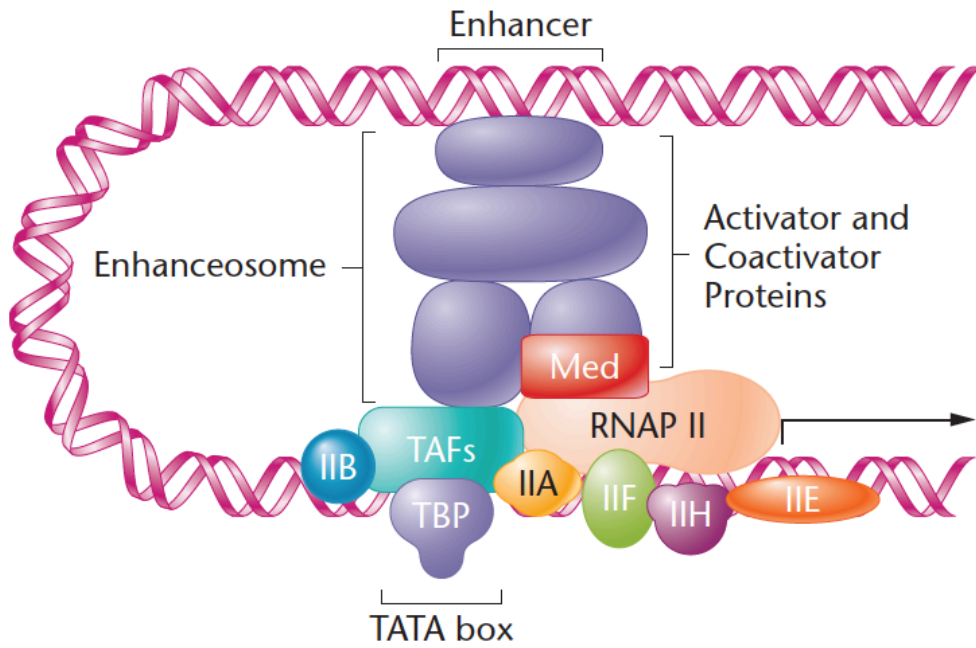


Figure 21. DNA loop formation.

From Pollard, Thomas D., et al. *Cell Biology*, 2016.

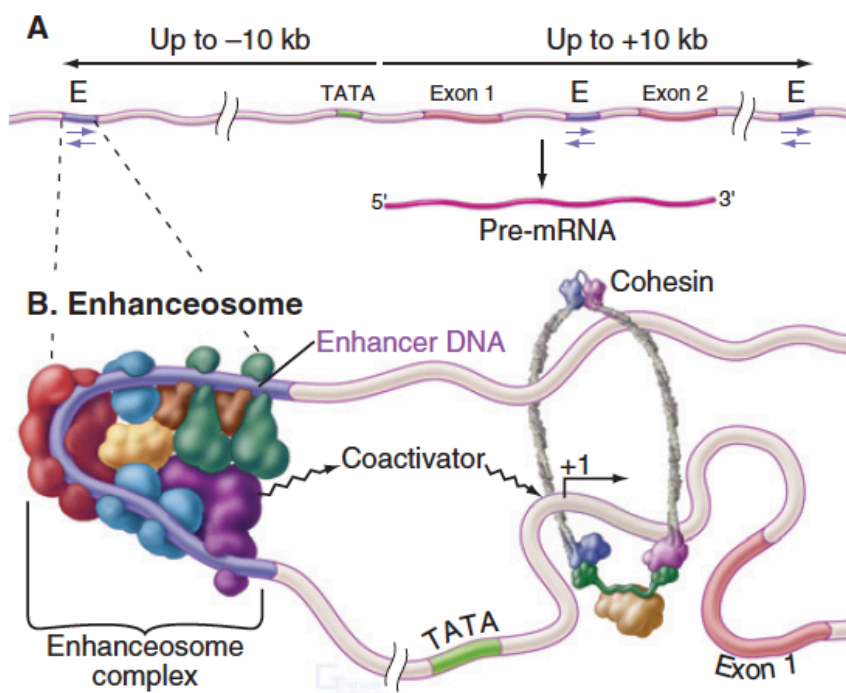


Figure 22. Enhancers.

A. Enhancers can be localized upstream or downstream of a gene. **B.** Forming enhanceosome. From Pollard, Thomas D., et al. *Cell Biology*, 2016.

locally distort and unwind DNA from nucleosomes in turn favoring DNA decompaction around its target genes (Dodonova *et al.*, 2020). In contrast, settler and migrant TFs only bind nucleosome-depleted regions but with a higher degree of selectivity for ‘migrant’ TFs depending on the cellular context and conditions, whereas settler rather bind all their accessible targets (Slattery *et al.*, 2014) (Figure 19).

Often, enhancer and promoter activities are dependent on the integration of multiple TFs input to precisely promote gene expression as shown by Minnoye and colleagues in the context of melanoma (Minnoye *et al.*, 2019). Currently two models were proposed to explain how this occurs: the ‘enhanceosome’ model and the billboard model. The enhanceosome model depends on the cooperative assembly of multiple TFs in a complex network of protein-DNA interactions.

However, this model requires highly organized TF binding sites at the enhancer region, which is quite rare, therefore these enhanceosome-like structures may only be found at developmental or differentiation genes where transcription is regulated in an ‘on/off’ binary manner (Thanos and Maniatis, 1995; Papatsenko and Levine, 2007; Chen *et al.*, 2014). In contrast, the billboard model allows for more flexibility in the combinatorial TF binding sites. In this model, TFs collaborate together to induce gene expression however cooperativity is not needed for function.

Thereby billboard-like structures are more common in genes which are regulated in a gradient manner, meaning that the expression levels of a gene increase with each activator TF that binds the enhancer (Kulkarni and Arnosti, 2003; Lorberbaum and Barolo, 2013) (Figure 20).

1.3.2. Co-activators

Transcription initiation involves co-activators which have important roles in accessibility of template DNA for the transcription machinery. They can act by remodeling or covalently modifying nucleosomes or by creating interactions between enhancers and promoters through chromatin loops (Näär, Lemon and Tjian, 2001).

1.3.2.1. The Mediator complex

First identified in yeast, Mediator is an evolutionary conserved, multiprotein complex consisting of 33 subunits (MED1 to -30) in mammals organized into four distinct modules : ‘head’, ‘middle’, ‘tail’ and ‘kinase’ containing CDK8

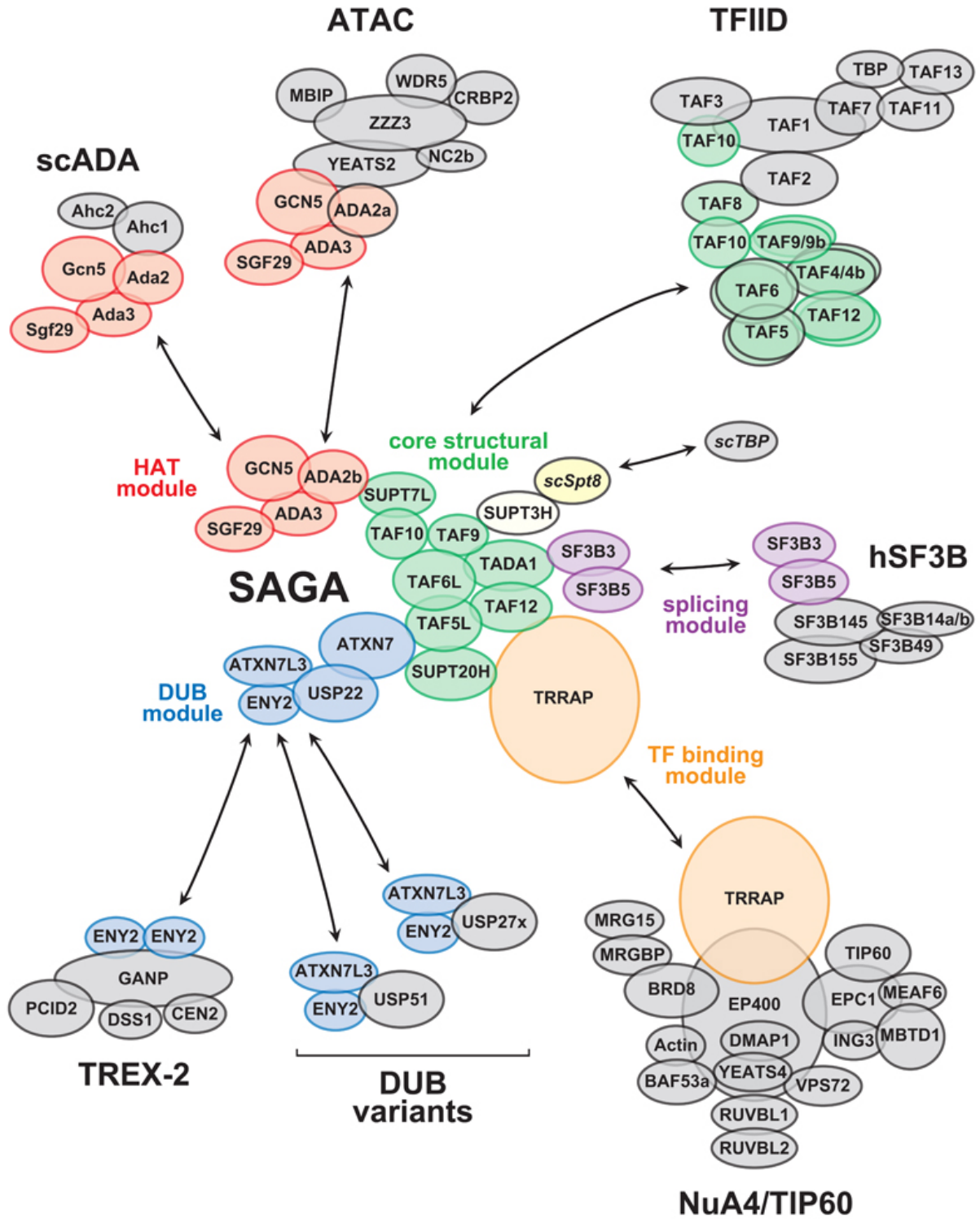


Figure 23. Shared subunits of SAGA.

(Kim *et al.*, 1994; Myers and Kornberg, 2000; El Khattabi *et al.*, 2019). This large complex acts as an adaptor protein between enhancer-bound TFs and GTFs at the promoter thus bridging enhancers to RNAPII and inducing transcription initiation (Hantsche and Cramer, 2017). In fact, Mediator complex also directly interacts with the RNAPII subunit RPB3 which has been shown to be required for RNAPII recruitment in vivo (Soutourina *et al.*, 2011). The CDK8 kinase module of Mediator is implicated in transcription repression, thus upon binding of Mediator on the pre-initiation complex, it loses its kinase module (Hsin and Manley, 2012). Consequently, the kinase module acts as a switch that controls Mediator-RNAPII interactions and perhaps explains why Mediator only dynamically interacts with the PIC during transcription initiation. However, it is now well established that Mediator is also important for transcription elongation by acting as a recruitment platform for elongation and RNA splicing factors as well as other chromatin- modifying and -remodeling complexes such as SAGA and SWI/SNF respectively (Lemieux and Gaudreau, 2004; Donner *et al.*, 2010; Plaschka *et al.*, 2015; Menezes *et al.*, 2017). Overall, this shows that Mediator is a co-activator complex required for RNAPII transcription.

1.3.2.2. The SAGA and ATAC complexes

The 1.8 MDa large Spt-Ada-GCN5 Acetyltransferase (SAGA) is an evolutionary conserved transcriptional co-activator complex composed of 18-20 subunits. Subunits are organized into distinct structural and functional modules : a structural core, a histone acetyltransferase (HAT), a histone deubiquitinase (DUB) and an activator binding module (Helmlinger and Tora, 2017).

Core module. Consist of 8 subunits which are TAF5L, TAF6L, TAF9, TAF10, TAF12, SUPT7L, TADA1 and SUPT20H. Histone fold domain (HFD)-containing subunits TAF9, TAF10 and TAF12 are shared with aforementioned the GTF TFIID complex, thus SAGA core module is often referred to as 'TFIID-like' (Figure 21).

Activator binding module. TRRAP is the biggest subunit of complex with 434 kDa molecular weight. It acts an adaptor by interacting with TFs such as MYC and E2F1 and recruits other SAGA modules and TIP60 to promoters (Lang *et al.*, 2001; Zhang *et al.*, 2014).

HAT module. It contains KAT2A/KAT2B, TADA2B, TADA3 and SGF29. KAT2A (GCN5 and its paralog KAT2B (PCAF) both exhibit histone acetyltransferase activities. They share 75% of sequence

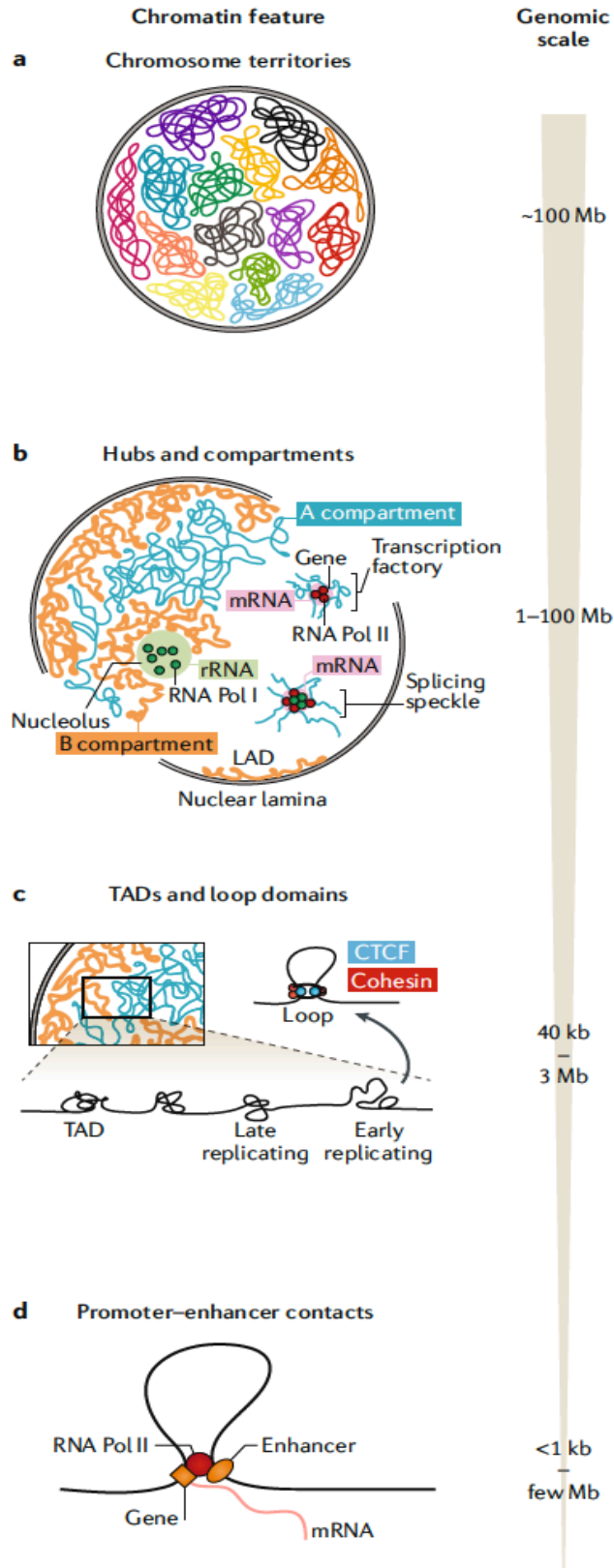


Figure 24. Chromatin feature.
From Kempfer and Pombo, 2020.

similarity and incorporated into SAGA HAT module in a mutually exclusive way. Adaptor subunits TADA2B and TADA3 facilitate the enzymatic activity of the HATs (Riss *et al.*, 2015). Finally, SGF29 interacts with chromatin through recognition of H3K4me3 and it is required for SAGA targeting (Bian *et al.*, 2011). HAT module of SAGA acetylate histone H3K9 and H3K19 lysine residues (Bonnet *et al.*, 2014; Feller *et al.*, 2015), which are marks recognized by the SWI/SNF chromatin-remodeling complex (Chandy *et al.*, 2006; Sanz *et al.*, 2016).

DUB module. USP22, ATXN7L1/2/3, ATXN7 and ENY2 form together the DUB module of SAGA which is responsible of histone H2B deubiquitination. USP22 is the catalytic subunit of the module however it was shown that deubiquitination requires module integrity.

Interestingly, ENY2 is a shared subunit with the nuclear pore-associated transcription export complex 2 (TREX-2) (Evangelista *et al.*, 2018), which is important for transcription-coupled mRNA export.

Recently, the co-activator Ada2a-containing (ATAC) complex has been found in mammals. Similarly to SAGA, ATAC HAT module displays acetyltransferase activity with a preferential acetylation of histone H4 (H4K5, H4k12, H4K16) (Suganuma *et al.*, 2008; Wang *et al.*, 2008). The unique feature of ATAC is that it harbors TADA2A, and not SAGA's TADA2B. Both ADA2 paralogs are responsible for anchoring HAT module to the corresponding specific complex. ATAC also contains six other subunits, YEATS2, ZZZ3, ATAC2, MBIP, DR1 and WDR5; the latter being shared subunits with COMPASS-like/MLL complexes. Recently, works have found ATAC complex to be involved in cancer. The YEATS2 subunit is an H3K27ac reader which was found to regulate an essential oncogenic program in non-small cell lung cancer (NSCLC) (Mi *et al.*, 2017).

1.3.3. Tridimensional genome architecture

The aforementioned factors and molecular machineries represent only a part of the bigger picture in transcription regulation (Figure 22). It is well established that the genome is organized by a non-random and high degree of order as : 1) the DNA itself which according to its compaction state (eu- or heterochromatin) has preferential location in the cell nucleus; 2) Chromatin-associated proteins are not randomly distributed but rather concentrated in subnuclear bodies such as the nucleolus, the Cajal

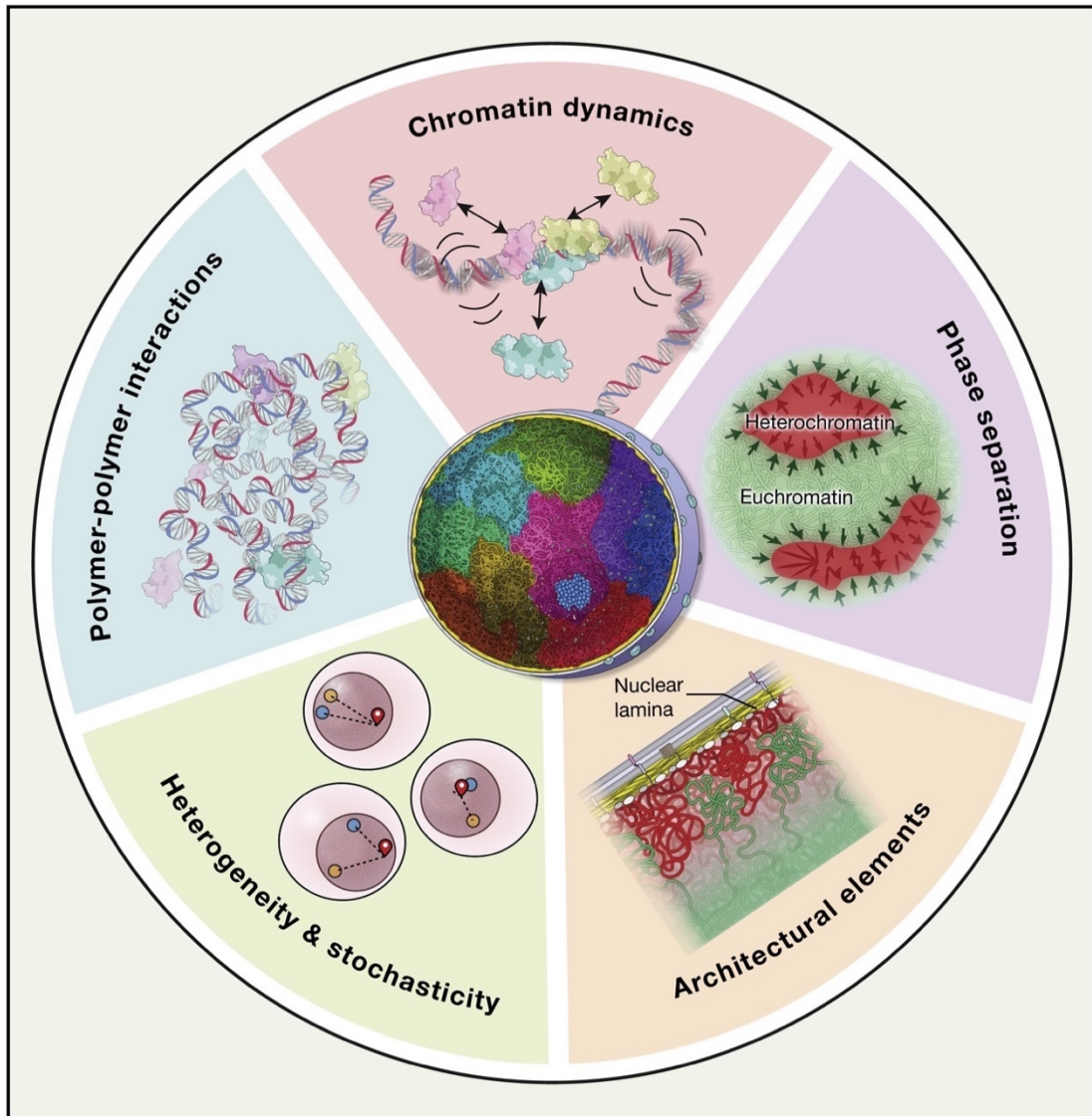


Figure 25. Genome organization.

From Mistelli, 2020.

body or speckles (Spector and Lamond, 2011; Staněk and Fox, 2017). In addition, the genome architecture is characterized by a high degree of variability and heterogeneity. For instance, two alleles of the same gene often differ in their 3D position in the same cell nucleus and the number of subnuclear bodies varies greatly among individual cells (Cattoni *et al.*, 2017; Finn and Misteli, 2019).

These observations led to the proposed hypothesis of ‘genome self-organization’ where chromatin is able to self-assemble into higher order of compaction under the sole influence of internal signals such as physical drivers (polymer interactions and phase separation) and constraints (nuclear lamina and subnuclear bodies). Thus, the chromatin architecture was subdivided into three layers from small to large scale: 1) chromatin loops which include promoter-enhancer interactions; 2) chromatin domains also known as topology-associated domains (TADs); and 3) chromatin compartments and chromosome territories.

1.3.1.1. Phase separation: A new phase in cell biology

Phase separation (PS) presents as an attractive model by which to explain nuclear compartmentalization (Gavrilov *et al.*, 2020). Recent developments in the field have proposed two distinct mechanisms of phase separation namely liquid-liquid PS (LLPS) and polymer-polymer PS (PPPS). PPPS is based on active bridging interactions relying on protein binders that tend to compact the chromatin fiber, whereas LLPS is driven by liquid-like multivalent interactions among soluble components that have distinct molecular composition and concentration. Both PPPS and LLPS can, in principle, promote the formation of nuclear compartments, however no definitive answer can be given currently and it might be that both mechanisms are unified into a single integrated system (Erdel and Rippe, 2018). Functional compartmentalization of the nucleus plays an important role in regulating transcription as it boosts its efficiency by accumulating enzymes and necessary factors in subnuclear bodies such as transcription factories. The basis of phase separation is the gradual demixing of distinct protein populations into two segregated, separated phases due their propensity to form homotypic rather than heterotypic interactions. Thus, PS promotes the formation of membraneless nuclear compartments by mediating the gradual aggregation of proteins (Banani *et al.*, 2017) (Figure 23).

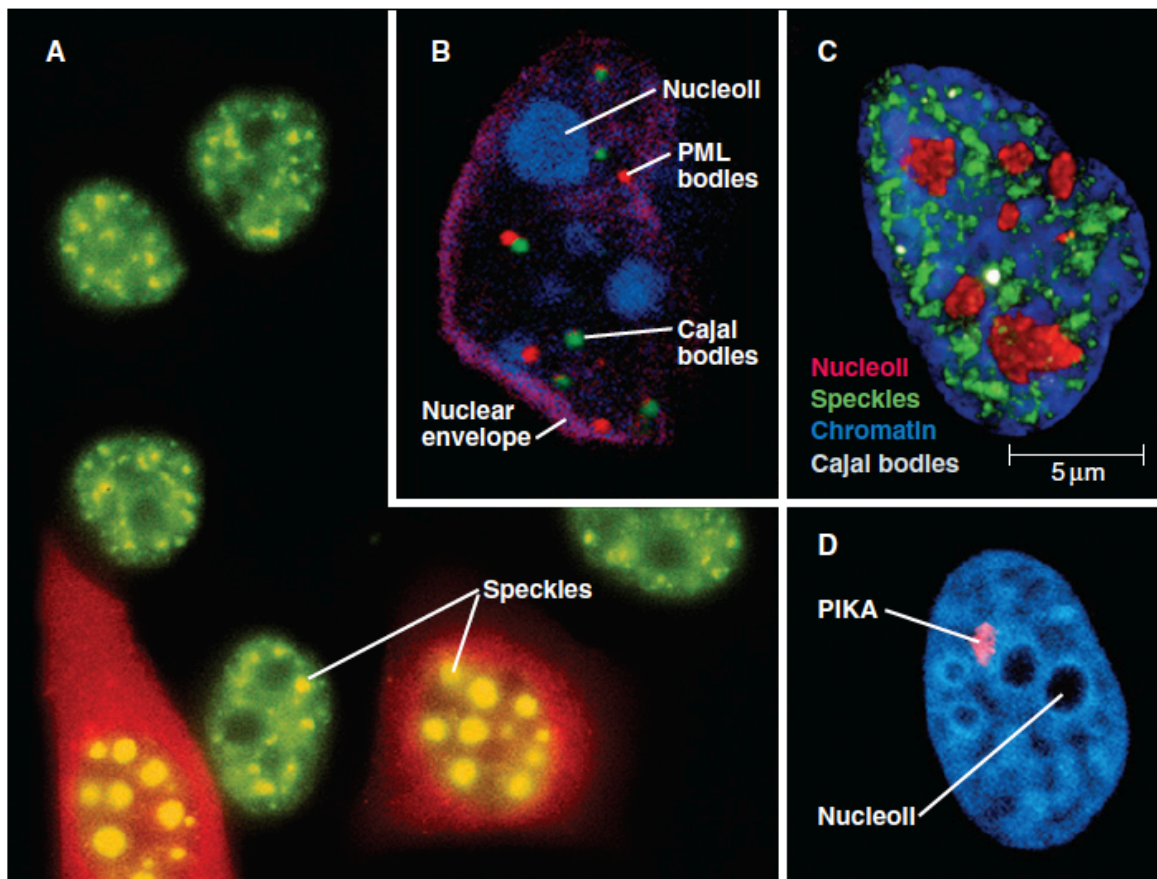


Figure 26. Major subnuclear structures.

From Pollard, Thomas D., *et al. Cell Biology*, 2016.

Nucleoli. Ribosomal DNA loci are the sites where RNAPI and ribosomal subunits are highly concentrated and tend to fuse (or ‘nucleate’) into a large rRNA transcription factory where ribosome subunits are efficiently synthesized and pre-assembled before export to the cytosol.

Speckles. At areas of low chromatin density, actively transcribed mRNA cluster together and bring in a plethora of RNA processing factors which form nuclear condensates called speckles. Therefore, RNA splicing is often coupled with transcription.

Heterochromatin. The aforementioned heterochromatin protein HP1a was shown to bind methylated chromatin and multimerizes, creating phase-separated droplets *in vitro* and *in vivo*. This tends to collect and all methylated loci such as repeated sequences together, further suggesting that the formation of heterochromatin is powered by phase separation (Larson *et al.*, 2017).

Transcription factories. Many other proteins and TFs that contain intrinsically disordered regions (IDRs) have the ability to phase separate. First discovered by Jackson *et al.* (1993), transcription factories are focal sites or ‘hubs’ of transcription within the nucleus which are believed to form via accumulation of RNAPII, Mediator and TFs such as BRD4 in protein-rich aggregated condensates. In fact, Mediator and RNAPII readily form small dynamic condensates which can be seen by light microscopy. This can also be seen for RNAPII and the Polycomb complex (Conte *et al.*, 2020). Strikingly, these transcription factories also involve the association of multiple super-enhancers, thereby explaining how several genes can be activated in a synchronized manner.

In a similar way, polymer physics and phase separation can explain the basis of how chromatin fluctuations can lead to intra-molecular interactions which give birth to loops and more sophisticated domains (Figure 24).

1.3.1.2. Topology-associated domains (TADs)

TADs constitute ‘self-interacting genomic regions’, meaning DNA regions within a TAD physically interact with each other more frequently than with regions outside the TAD. Evidence from microscopy and HI-C experiments allowed to visualize and better understand these sub-megabase structures. These domains present boundaries at both side which are conserved across species and are

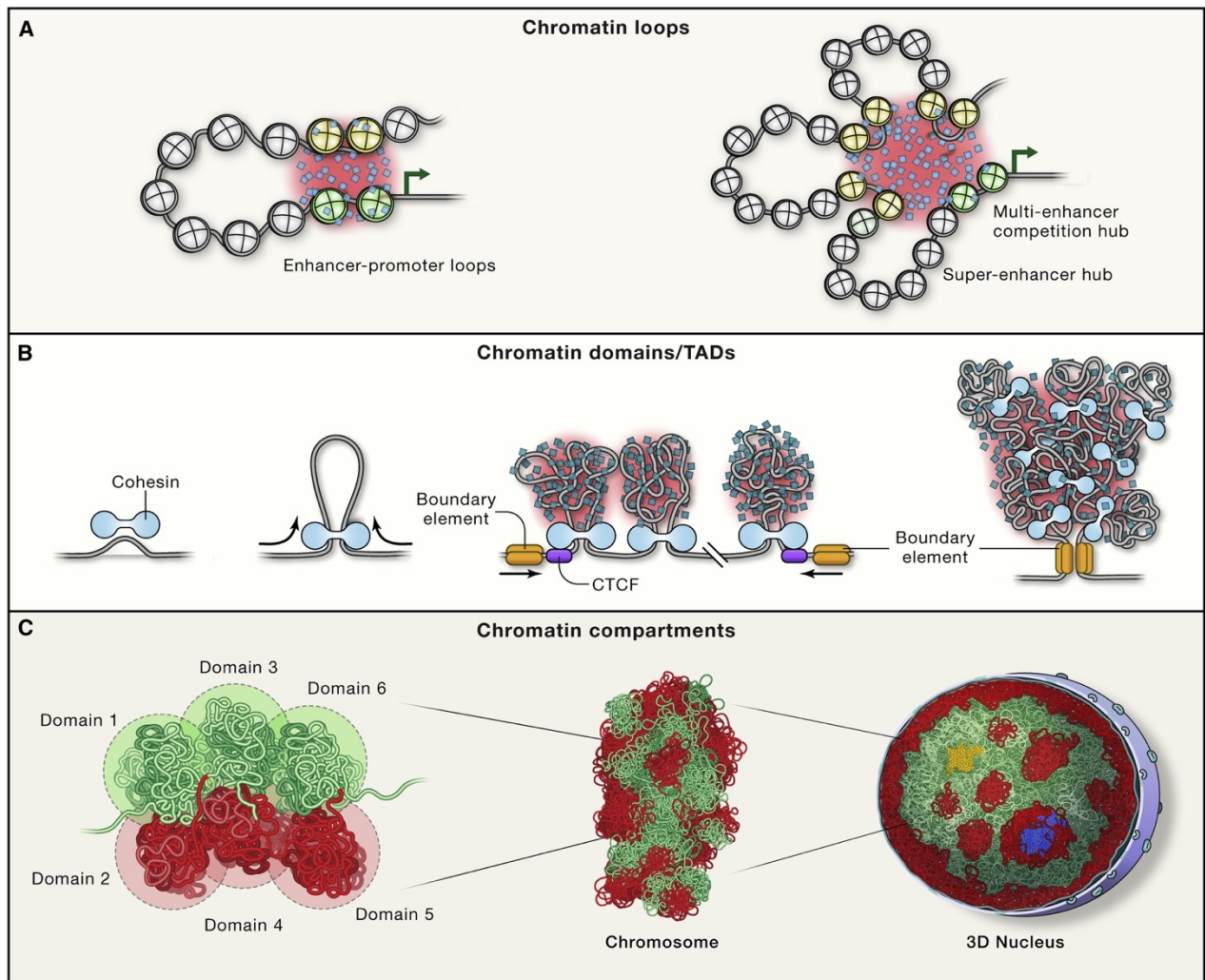


Figure 27. Self-organization of chromatin.
From Mistelli, 2020.

extremely enriched in CCCTC-binding factor (CTCF) and cohesion motifs (Dekker and Mirny, 2016; Rowley and Corces, 2018). A recent paper by Cavalli team provided insights on how CTCF and the cohesion complex play their role in TAD formation and integrity maintenance (Sati *et al.*, 2020). By combining super-resolution microscopy with selective depletion of CTCF or the cohesin complex subunit RAD21, they were able to show that cohesin generates chromatin contacts and allow intermingling within TADs; whereas CTCF prevents inter-TADs contacts by setting strict boundaries (also known ‘TAD insulation’).

The formation of TADs begins with extruding chromatin loops which are induced by polymer interactions and maintained via cohesin. Next, CTCF closes the gap between two boundaries allowing intermingling within a TAD neighboring. They also revealed that TADs are themselves organized into so-called chromatin nanodomains (CNDs), which as their name implies are smaller structures of 100kb (versus 900kb average for TADs). They showed that neither depletion of CTCF nor cohesin affected CNDs, which adds to complexity to the relationship between TADs and gene expression. Furthermore, treatment with an inhibitor of histone deacetylases (trichostatin A) lead to chromatin hyperacetylation which resulted in disruption of CNDs. This established that small 3D structures depend on chromatin interactions which are dictated by the epigenetic landscape and stabilized by phase separation.

In contrast, larger scale TADs are actively maintained via chromatin binders such as CTCF, cohesin and Mediator complex. However, despite CTCF and cohesin being major players in mediating chromatin interactions, it was suggested that additional yet undiscovered chromatin binders as well as non-coding RNAs might also contribute to the genome organization (Quinodoz *et al.*, 2018). Although the functions of TADs are not yet fully understood, it has been established that disruption of TAD boundaries via deletion of CTCF sites affects gene expression due to aberrant interactions between enhancers and promoters (Lupiáñez, Spielmann and Mundlos, 2016). The consequences of TAD boundaries perturbation have been linked to human limb malformations and even several types of cancers (Lupiáñez *et al.*, 2015; Flavahan *et al.*, 2016; Lupiáñez, Spielmann and Mundlos, 2016) (Figure 25).

Chapter II. Chromatin modifiers and remodelers

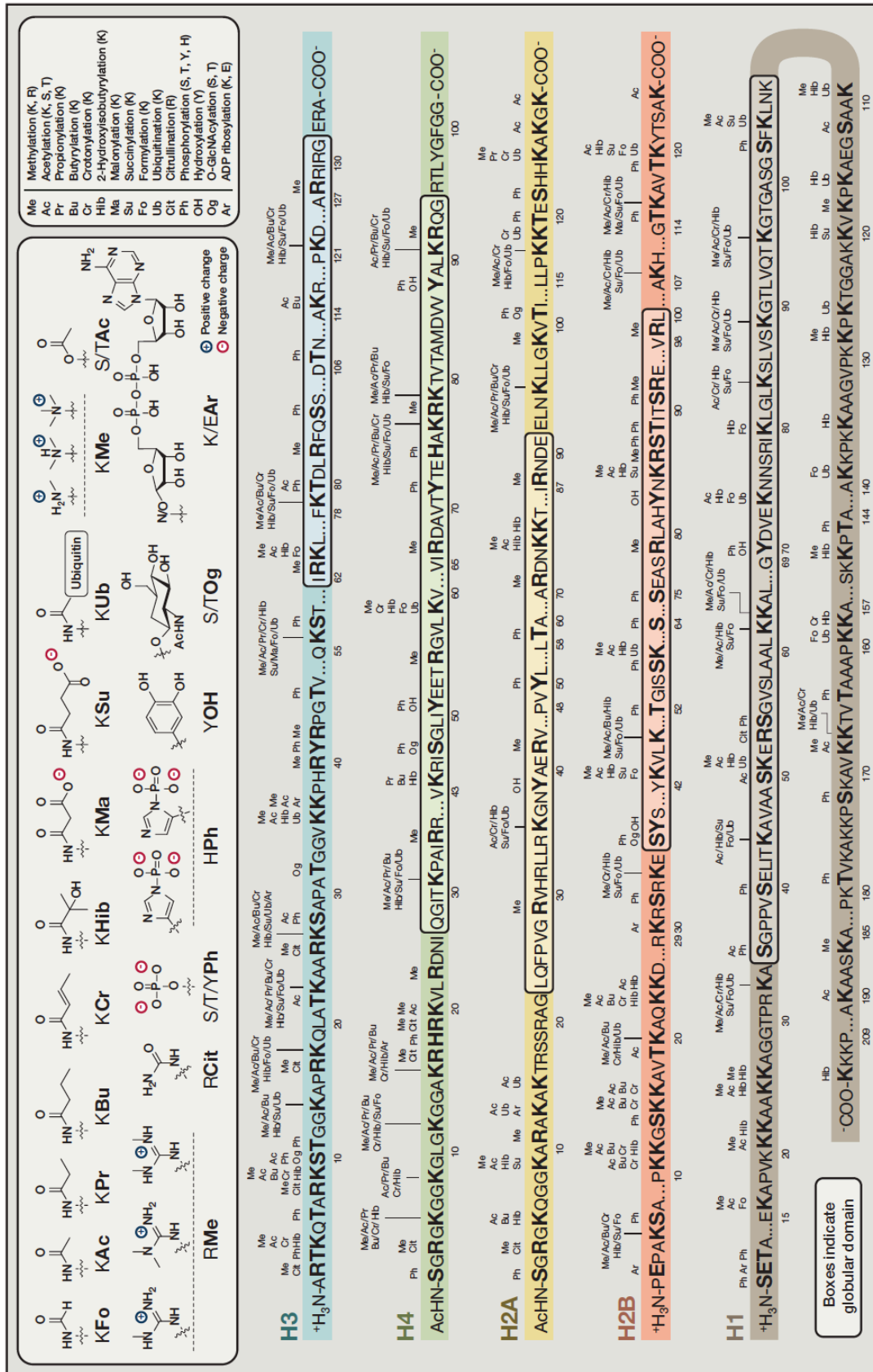


Figure 28. Histone modifications.

From Pollard, Thomas D., *et al. Cell Biology*, 2016.

Chapter II. Chromatin modifiers and remodelers

As mentioned in chapter I, the chromatin landscape plays an important role in the accessibility of DNA which in turn regulates transcription. One of the mechanisms of regulating chromatin accessibility is by covalent post-translational histone modifications (PTMs). Many different PTMs like acetylation (Allfrey, Faulkner and Mirsky, 1964), methylation (Murray, 1964), phosphorylation (Kleinsmith, Allfrey and Mirsky, 1966), ubiquitination (Goldknopf and Busch, 1977), sumoylation (Nathan *et al.*, 2006), ADP-ribosylation (Hassa *et al.*, 2006), and deamination (Cuthbert *et al.*, 2004) have been characterized with their diverse effects on transcriptional activity (Figure 28). One of the best characterized modifications is histone acetylation which is generally associated with active transcription.

2.1. Covalent histone-modifying complexes

2.1.1. Histone acetylation

2.1.1.1. Mechanism of acetylation

Acetylation consists in the addition of a functional acetyl group (COCH₃) on the ε-amino group of lysine residues. It is catalyzed by histone acetyltransferases (HATs) using acetyl-coenzyme A as a co-factor, which is a metabolite derived from energy generation. The addition of the acetyl group has for consequence to neutralize the positive charge of lysines, which are very abundant in proteins. It has been established that acetylation of histones is linked to gene activation as it remodels the chromatin fiber. A well-studied example is the X chromosome inactivation that occurs in mammals, where the formation of the so-called Barr body is known to be controlled by histone acetylation dynamics. X chromosome inactivation depends on the expression of a non-coding RNA called XIST (X inactivation specific transcript) which loci are localized in the so-called X inactivation center (XIC) of Xq. This region is about 1Mb and contains several regulatory elements. One of such elements is the promoter of XIST which has been shown to be hyperacetylated on histones H4 resulting in a strong expression of the ncRNA (O'Neill *et al.*, 1999). Once expressed, XIST plays a key role in promoting the formation of X chromosome constitutive heterochromatin, paradoxically by inducing deacetylation of histones.

Acetylation can also occur on non-histone proteins, consequently the nomenclature of HATs has been modified to KATs or lysine acetyltransferases ('K' is the symbol for lysine aminoacids). Many

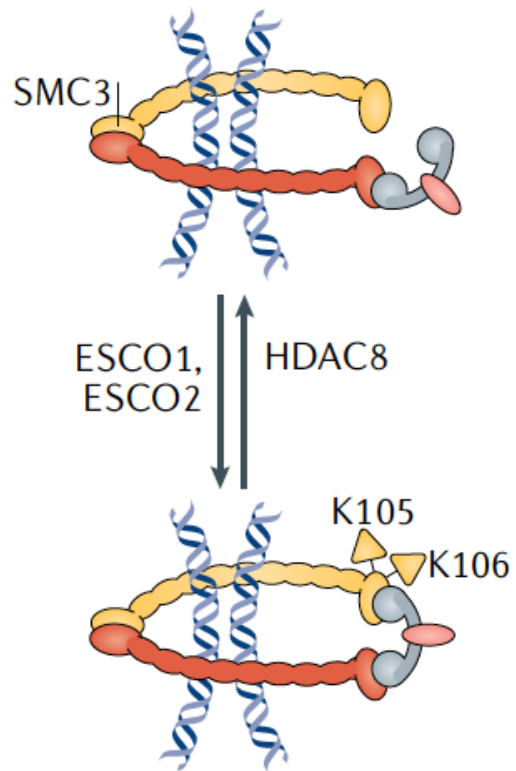


Figure 29. Chromatid cohesion is promoted by acetylation of SMC3.
From Narita *et al.*, 2019.

non-histone proteins are known to be acetylated (Downey, 2020). One example of this is component of the cohesin complex, structural maintenance of chromosomes protein 3 (SMC3) which acetylated on two conserved DNA-sensing residues K105 and K106. During DNA replication, sister chromatids have to be paired together by the cohesin complex in order to allow separation during mitosis. After being acetylated, SMC3 stably binds sister chromatids together by locking the cohesin ring. Additionally, other major cell cycle regulators including Aurora kinases (A and B) and CDK1/2 are subject to acetylation which highlights the important role of non-histone protein acetylation in cell cycle and mitosis (Narita, Weinert and Choudhary, 2019) (Figure 29).

Acetylation is also known to crosstalk with other PTMs such as methylation and phosphorylation. Regulation of p53 protein is an archetype of such crosstalk. In normal condition, p53 is bound by MDM2 which catalyzed ubiquitylation thereby promoting proteasome-dependent degradation. In stress condition, p53 is acetylated which impedes with MDM2-mediated degradation and allows p53 to bind and activate its targets. Acetylation of p53 on K382 has been shown to be stimulated via phosphorylation of S46 which brings in p300 acetyltransferase. As a result of this important crosstalk, acetylated and phosphorylated p53 is a key regulator of the induction of cell death by apoptosis (Habibian and Ferguson, 2019).

2.1.1.2. Acetyltransferases

Although their exact number is currently unknown, more than 20 canonical KATs have been reported to this day and are classified into four main families: GNAT (GCN5-related acetyltransferases), p300/CBP, p160/SRC and MYST. Other distinct KATs exist but are less well studied, namely TAT1, ESCO1/2 and KAT1. All KATs are primarily localized in the nucleus, except for TAT1 who is cytoplasmic, and they catalyze the acetylation of a plethora of histones and non-histone proteins. Distinct KATs have non-overlapping substrates, however some KAT paralogs exist and can show functional redundancy. For instance, aforementioned SAGA and ATAC complex subunits KAT2A and KAT2B are both capable of acetylating H3K9, a mark associated with euchromatin (Lu *et al.*, 2011; Sandoz *et al.*, 2019). In addition, both ESCO1 and ESCO2 acetyltransferases are responsible for SMC3 K105 and K106 acetylation (Alomer *et al.*, 2017; Kawasumi *et al.*, 2017) . Another example is the MYST family

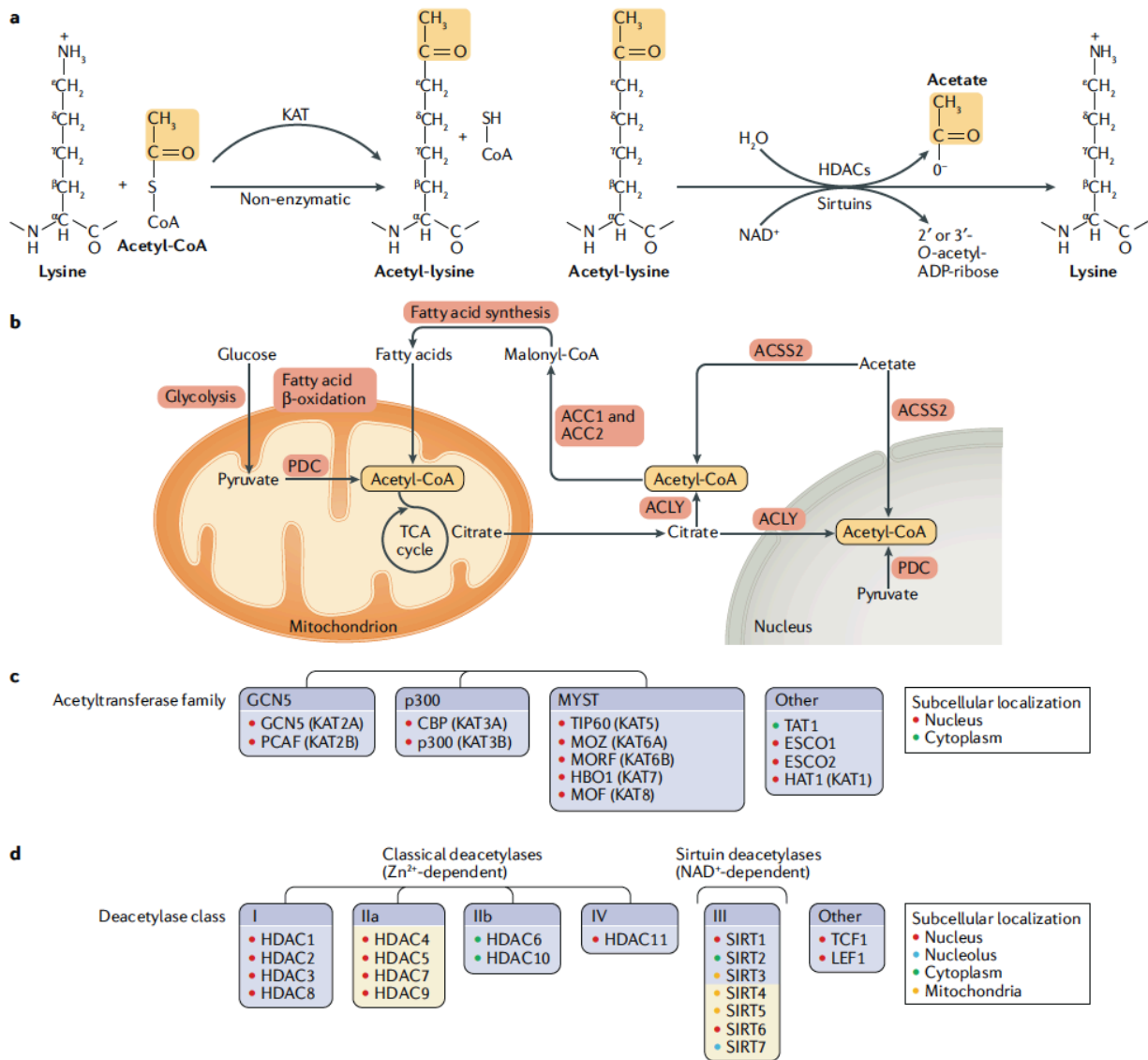


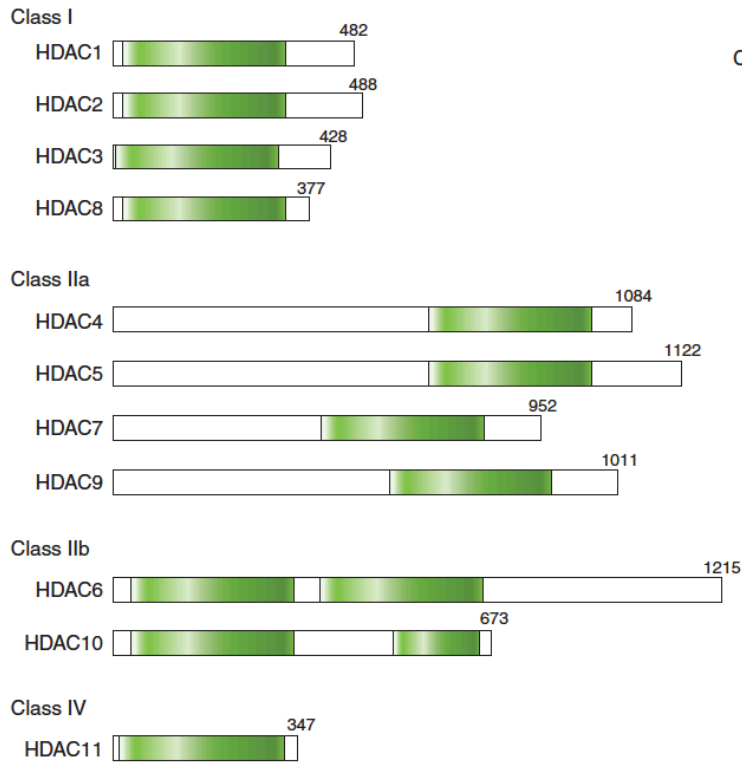
Figure 30. Reactions of reversible lysine acetylation by HAT and HDAC enzymes.

From Narita, Weinert and Choudhary, 2019.

KAT6A and KAT6B which are component of the MOZ and MORF complex, respectively and are both able to acetylate H3K23 (Huang *et al.*, 2016; Narita, Weinert and Choudhary, 2019). Finally, the CREB-binding protein (CBP, also known as KAT3A) and p300 (KAT3B) are known for H3K18 and H3K27 acetylation (Figure 30).

Roughly 90% of all acetylations are catalyzed by just five KAT (CBP, p300, KAT2A, KAT2B and KAT5). Amongst these, perhaps the best characterized KATs are the ubiquitously expressed p300 and CBP proteins, due to their key function in transcription regulation. Importantly, the inactivation of both genes leads to embryonic lethality in mouse models (Al, 1998; Tanaka *et al.*, 2000) and heterozygous mutations in CBP, and to a lesser extent p300, cause the Rubinstein-Taybi syndrome which is characterized by severe mental retardation and an elevated risk for several cancers such as acute myeloid leukemia (AML) and lymphoma (Petrif *et al.*, 1995). CBP and p300 share highly conserved domains critical for acetyltransferase activity and for transactivation activity via interactions with a plethora of transcription factors, therefore they are often considered as co-activators. Thus, p300/CBP has been described to serve as a bridging factor between promoter-specific TFs and the PIC by directly interacting with TBP, TFIIB and subunits of RNA polymerase II (RNAPII) and by acetylating TFIIE and TFIIIF (Goodman and Smolik, 2000; Janknecht, 2002). However, it is also possible that P300/CBP acts as scaffold to nucleate the assembly of diverse co-factors into a single co-activator complex to enhance transcription. For instance, p300/CBP has a role in antiviral response by acting as a recruitment platform for stress-response TFs such as AP-1, NFkB and IRF1 which all assemble in an enhanceosome-like structure to activate the *IFN-β* gene (Munshi *et al.*, 1998). Yet another important mechanism of transcription regulation by the p300/CBP family is the acetylation of H3K27 which has been shown to directly recruit the SWI/SNF histone reader and chromatin remodeling complexes through their bromodomain subunits (Kwon and Jewett, 2015). That being said, p300/CBP are also responsible for acetylating many non-histone proteins such as the aforementioned p53 protein (Soutoglou, Ktrakili and Talianidis, 2000), highlighting the highly versatile roles of these KAT families in transcription regulation (Chan and La Thangue, 2001).

Classical HDACs (histone deacetylase family)



Sirtuins (Sir2 regulator family)

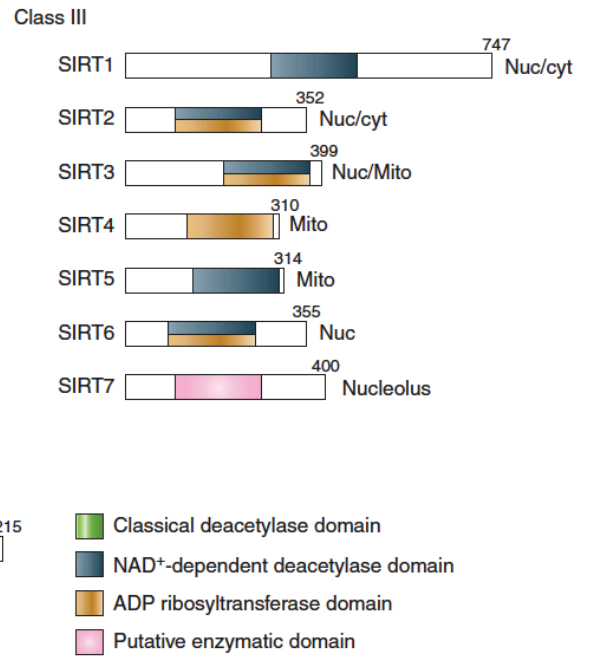


Figure 31. Domains of human HDACs.

From Seto and Yoshida, 2014.

2.1.1.3. Deacetylases

Acetylation is a highly dynamic and reversible process. Acetyl group removals are catalyzed by deacetylases (HDACs, or KDACs according to the recent nomenclature). In humans 18 enzymes have been reported thus far and are subdivided into four classes by phylogenetic analyses : class I to IV (Gregoretta, Lee and Goodson, 2004). However class I, II and IV HDACs share high sequence homology and are often termed the classical HDACs (1 to 11); in contrast with class III Sirtuins which have unrelated structural domains (SIRT1 to 7).

HDACs. The class I, II and IV HDACs belong to the arginase/deacetylase superfamily of proteins which unique feature is their requirement for a Zn^{2+} in order to mediate the removal of the acetyl group from lysine-containing substrates. The classical HDAC are often subdivided according to their structural homology with yeast proteins. Class I HDACs comprise HDAC1, -2, -3, -8 and share high sequence homology with yeast Rpd3. HDAC1 was the first to be identified and characterized for its histone deacetylase activity (Taunton, Hassig and Schreiber, 1996). Class I HDACs are ubiquitously expressed and located in the nucleus where they generally exert a co-repressor activity on transcription by deacetylating H3K27 and thereby promoting chromatin compaction. Class II HDACs comprise HDAC4, -5, -7, -9 and are homologous to yeast Hda1 (Yang and Seto, 2008). Just like class I, they are ubiquitously expressed and acts as co-repressor, however they have been uniquely shown to shuttle between the nucleus and the cytoplasm in response to signals, suggesting they might have extranuclear protein targets (Seto and Yoshida, 2014). Class IV HDACs is a poorly characterized family as only HDAC11 has been described for this class. They share homology with both class I and II and are homologous to yeast Hos3. Just as class I and II HDACs, this group is only nuclear (Gao *et al.*, 2002; Narita, Weinert and Choudhary, 2019) (Figure 31).

SIRTs. The class III sirtuins share homology with yeast Sir2 (silent information regulator 2). They belong to the deoxyhypusine synthase-like NAD/FAD-binding domain superfamily (Brachmann *et al.*, 1995; Frye, 1999). The catalytic activity of this family of HDACs depends on the presence of the oxidized form of nicotinamide adenine dinucleotide (NAD⁺) as a receiving co-factor for the acetyl group. To this day, 7 sirtuins have been reported in mammals with SIRT1 being the most similar to yeast Sir2 and the best characterized to this day. They are localized in different cellular compartments

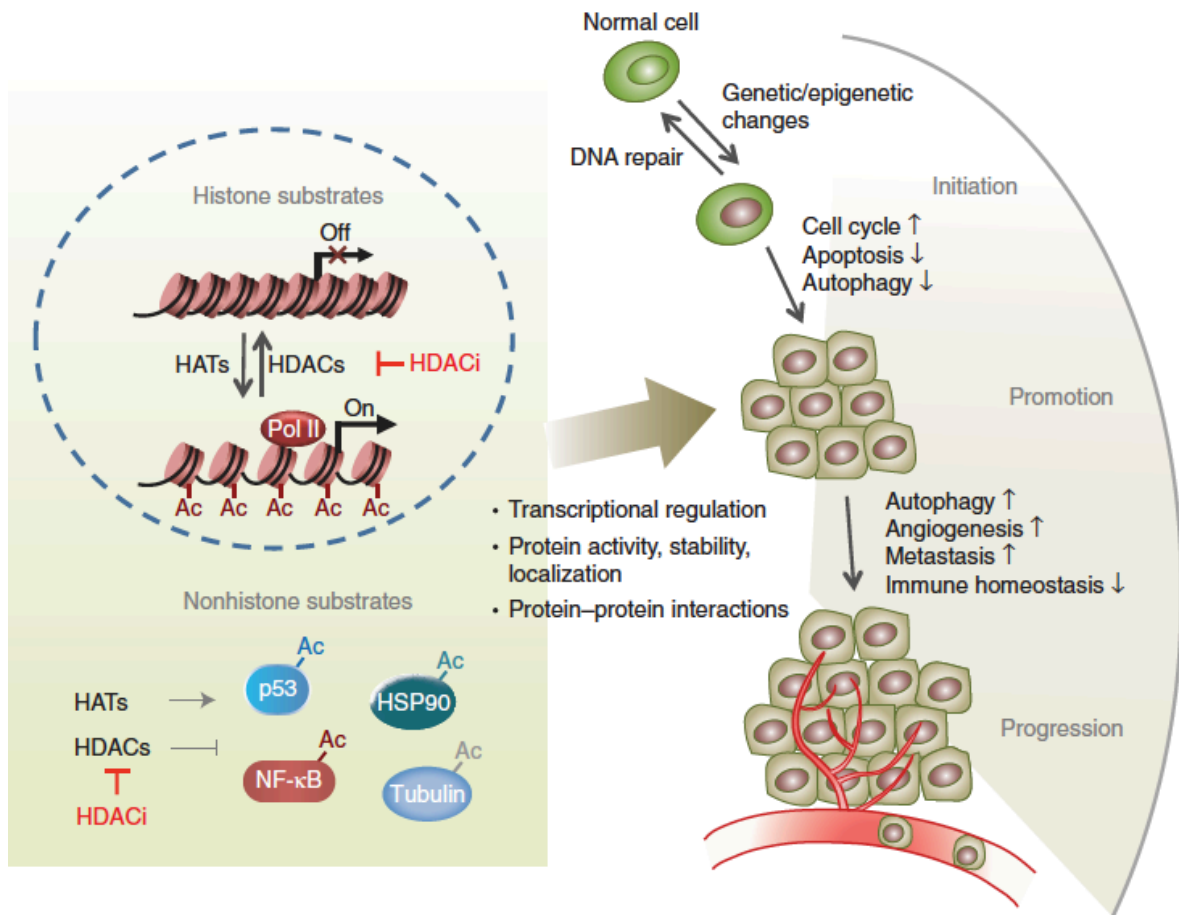


Figure 32. Illustration of HDACs and HDACi regulating different stages of cancer.

From Li and Seto, 2016.

including nucleus (SIRT1 and -6), nucleolus (-7), cytoplasm (-2) and mitochondria (-3, -4, and -5) (Houtkooper, Pirinen and Auwerx, 2012). Most SIRT histone targets have been well characterized, with H3K9ac, H3K16ac and H3K18ac being most represented. However SIRT4 and SIRT5 have only weak deacetylase activity and target other types of acylation, for instance SIRT5 functions as a desuccinylase, demalonylase and deglutarylase (Du *et al.*, 2011; Narita, Weinert and Choudhary, 2019).

Regulations of HDAC activity. Deacetylases are regulated through two mechanisms. Firstly, they are targeted by PTMs such as phosphorylations; for instance SIRT1 contains 13 residues that can be phosphorylated according to mass spectrometry data (Sasaki, Yamagata and Mitani, 2008). Casein kinase 2 (CK2)-mediated phosphorylation of SIRT1 increases its deacetylase activity and mediates the deacetylation of p53 which protects cell from apoptosis after DNA damage (Kang *et al.*, 2009). Secondly, some deacetylases have been reported as components of large multiprotein complexes. For example, HDAC1 and -2 are associated with at least three complexes called SIN3, NuRD and CoREST complexes. These complexes comprise regulatory subunits such as the MBD3 subunit in NuRD that targets methylated CpG DNA sequences, thus allow the specific targeting of HDACs on the genome.

HDAC inhibitors. Inhibitors of HDAC (HDACi) activity were indirectly discovered when it was found that n-butyrate induced accumulation of acetylated histones (Riggs *et al.*, 1977). However the first potent HDAC inhibitor was trichostatin A (TSA) isolated from *Streptomyces* strain and was originally used as an antifungal. HDAC inhibitors have been proposed as putative treatment in numerous tumor types with high acetylation dependency which have been shown to be sensitive (Strub, Ballotti and Bertolotto, 2020). One well-characterized example is the SWI/SNF subunit SMARCA2 which expression and activity are regulated both at the transcriptional and post-translational level especially by HDAC2, HDAC3 and HDAC9 (Gramling *et al.*, 2011; Kahali *et al.*, 2012). Using targeted inhibitors, researchers were able to pharmacologically reverse the epigenetic silencing of SMARCA2 which had tumor-suppressor effects in SMARCA2-deficient clear cell renal cell carcinoma (Fang *et al.*, 2020) (Figure 32).

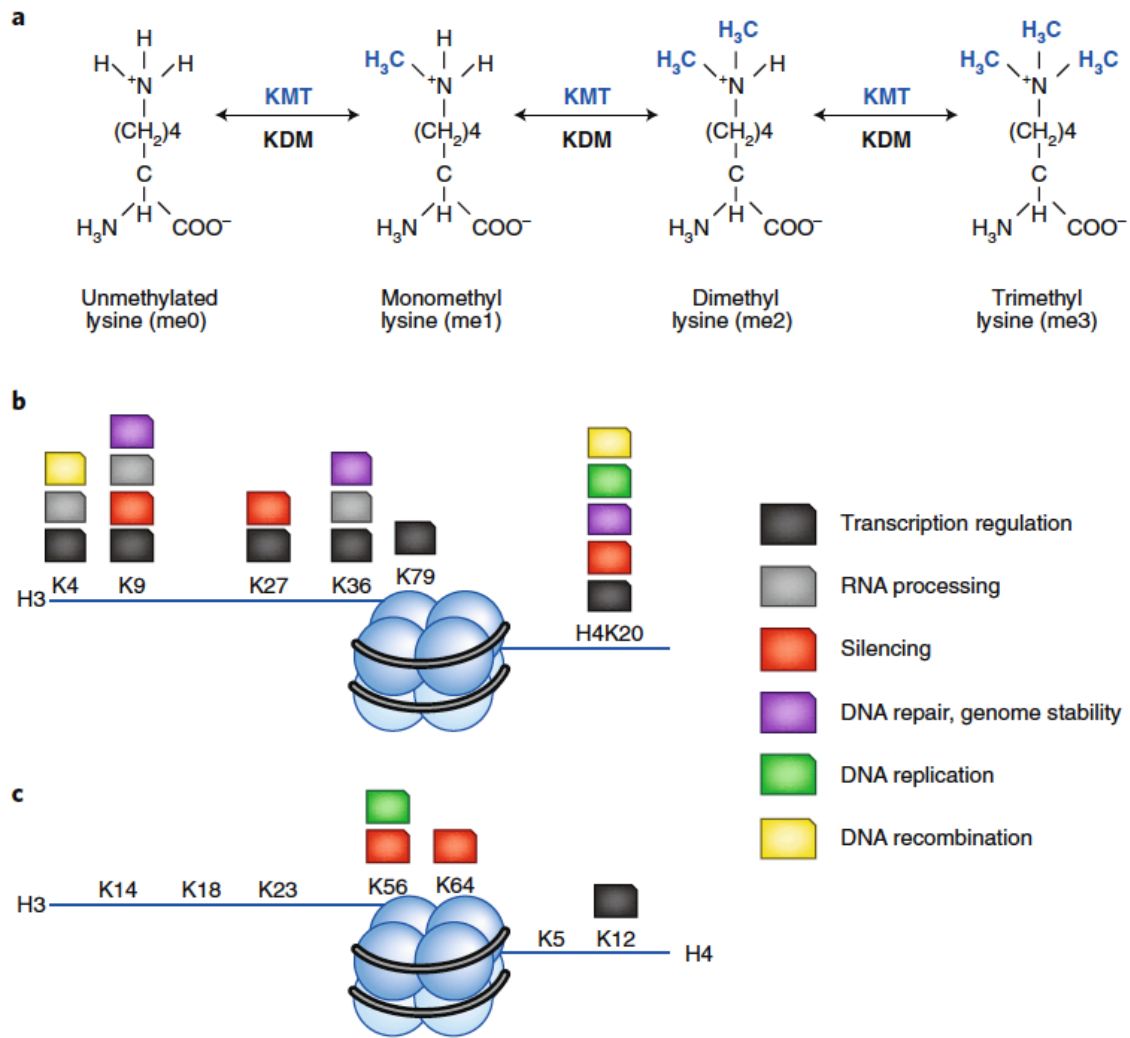


Figure 33. Mono-, di-, trimethylation of lysine residues on core promoters and their functions. From Husmann and Gozani, 2019.

2.1.2. Histone methylation

2.1.2.1. Mechanism of methylation

Histone methylation consists in the addition of a methyl group (-CH₃) on the ε-amino group of lysine residues (Allfrey, Faulkner And Mirsky, 1964; Murray, 1964). In contrast to acetylation, histone lysines can be methylated three times in total, going from an unmethylated state to mono-, di- and trimethylated forms. In addition, histone methylation can also take place on arginine residues which can be mono- or dimethylated in a symmetric or asymmetric way (Figure 33). Thus, methylation adds several important layers of complexity to the histone code (Bannister and Kouzarides, 2011). Again in contrast to acetylation, methylation is found in transcriptionally active as well as inactive regions. For instance H3K4me₁ and H3K20me are widely considered hallmarks of active chromatin (Ruthenburg *et al.*, 2007); whereas H3K9me₃ and H3K27me₃ are major marks of transcription repression (Schotta *et al.*, 2004; Kim and Kim, 2012). Histone methylation on lysine and arginine residues is carried out by lysine methyltransferases (KMTs) and PRMTs (protein arginine methyltransferases), respectively. Just as acetylation, methylation is a reversible process and specialised enzymes called LSD1-type KDMs (lysine demethylases) remove only lysine methyl groups. For arginine residues, the methyl group can be removed either by jumonji domain-containing (JmJC)-type arginine demethylases (RDMs) or by citrullination by protein arginine deiminase type 4 (PADI4).

Perhaps due to its major role in heterochromatin maintenance, histone methylation has been long considered as relatively stable. Yet, recent studies have revealed that cycles of methylation-demethylation can be highly dynamic. One example is the circadian clock-controlled histone modifying complex mixed lineage leukemia 3 (MLL3) which regulates the rhythmic oscillation of over a hundred circadian genes via methylation-demethylation of H3K4 in particular (Valekunja *et al.*, 2013).

Just like acetylation, methylation can also occur on non-histone proteins. It is revealed that regulators of DNA repair were methylated during DNA damage response (Liu, Kim and Oberdoerffer, 2013). Another example is the link between methylation and regulation of apoptosis through Numb, a protein partner of p53, as the methylated form of Numb loses its ability to bind p53 thus exposing the latter to ubiquitination and proteasomal degradation (Dhami *et al.*, 2013; Weirich *et al.*, 2015).

Methylation–phosphorylation crosstalk

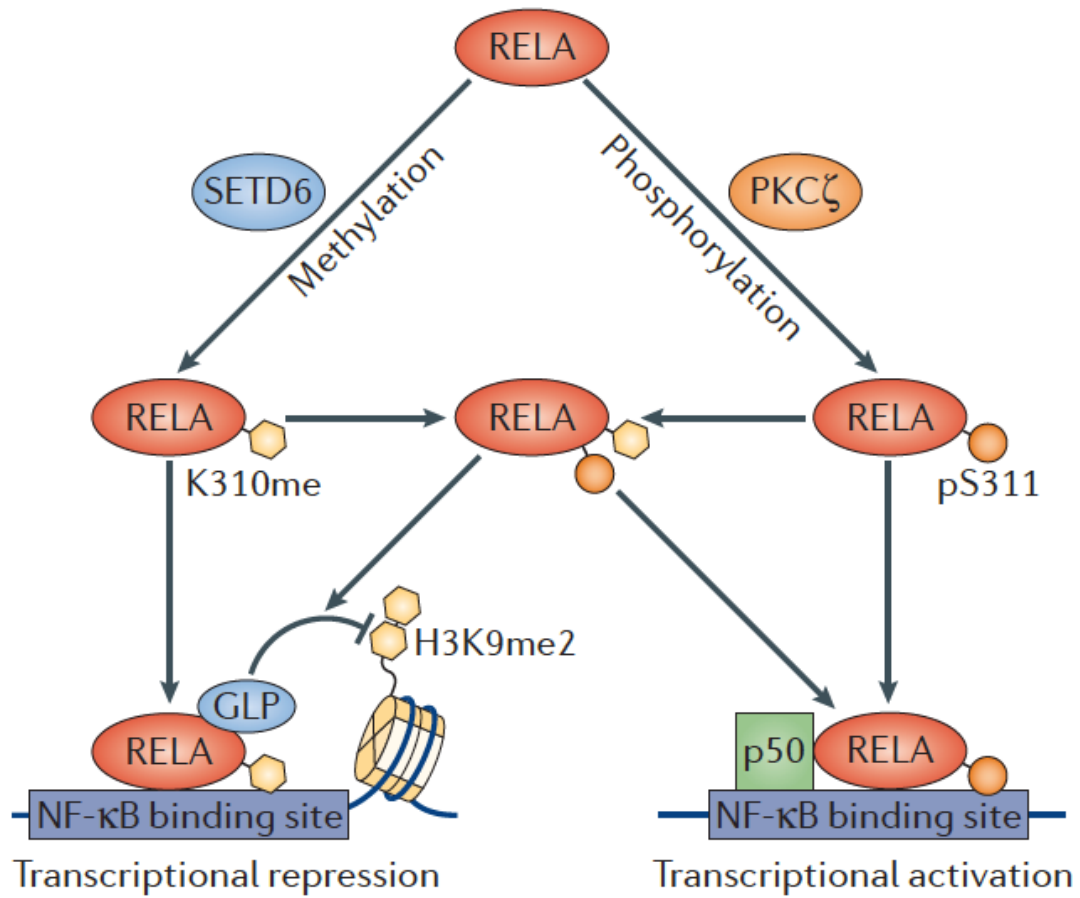


Figure 34. Functional PTM crosstalk between methylation and phosphorylation on non-histones substrates. ‘methylation-phosphorylation switch’.

From Biggar and Li, 2015.

Despite being far outnumbered by tyrosine phosphorylation sites, there are currently more than 1000 lysine and 2000 arginine methylation sites in about a thousand human proteins, with most being non-histones substrates (Moore and Gozani, 2014). Mapping of methyltransferase-substrates indicated that a large array of cellular functions is regulated through protein methylation ranging from chromatin remodelling to transcription, cell cycle, apoptosis, translation and signal transduction (Biggar and Li, 2015). Extensive crosstalk has been found between methylation and other PTMs such as phosphorylation, ubiquitylation and acetylation. One reported example concerns the ATXR5 methyltransferase whose activity was shown to be inhibited by the presence of neighbouring H3K27 acetylation (Bergamin *et al.*, 2017). Direct interactions between neighbouring methylation and phosphorylation sites represent a distinct class of PTM crosstalk referred to as the ‘(Sabbattini *et al.*, 2014). Such a switch exists in the NFκB p65 subunit (also known as RELA) which K310 monomethylation results in recruitment of its partner protein, the H3K9-methyltransferase GLP, leading to chromatin condensation and repression of NFκB genes. However, when neighbouring S311 is phosphorylated, GLP is unable to bind RELA which relieves repression and allows RELA to activate NFκB target (Duran, Diaz-Meco and Moscat, 2003; Biggar and Li, 2015) (Figure 34).

2.1.2.2. Methyltransferases (MLL/COMPASS, Polycomb)

Although we knew since the 1960s that transcription was modulated by histone methylation, the first histone KMT (KMT1A, also known as SUV39H1) was identified fairly recently by Jenuwein and colleagues (Rea *et al.*, 2000; Jenuwein, 2006). After the discovery of KMT1A, several other KMTs were identified through homology screens with the enzymatic SET (Su (var)3-9, Enhancer of Zeste and Trithorax) domain. All KMTs, with the exception of DOT1L, possess a SET domain subunit and use S-adenosylmethionine (AdoMet) as the methyl donor (Nguyen and Zhang, 2011). The role of SET domain is to transfer a methyl group from AdoMet to the protein lysine residue, leaving a methylated lysine and the co-factor byproduct S-adenosyl-L-homocystein (AdoHcy). Most SET-domain proteins cluster in seven main families : the SUV39, SET1, SET2, EZ, RIZ, SMYD and SUV4-20 families as well as the few orphan members such as SET7/9 or SET8 (Dillon *et al.*, 2005; Husmann and Gozani, 2019).

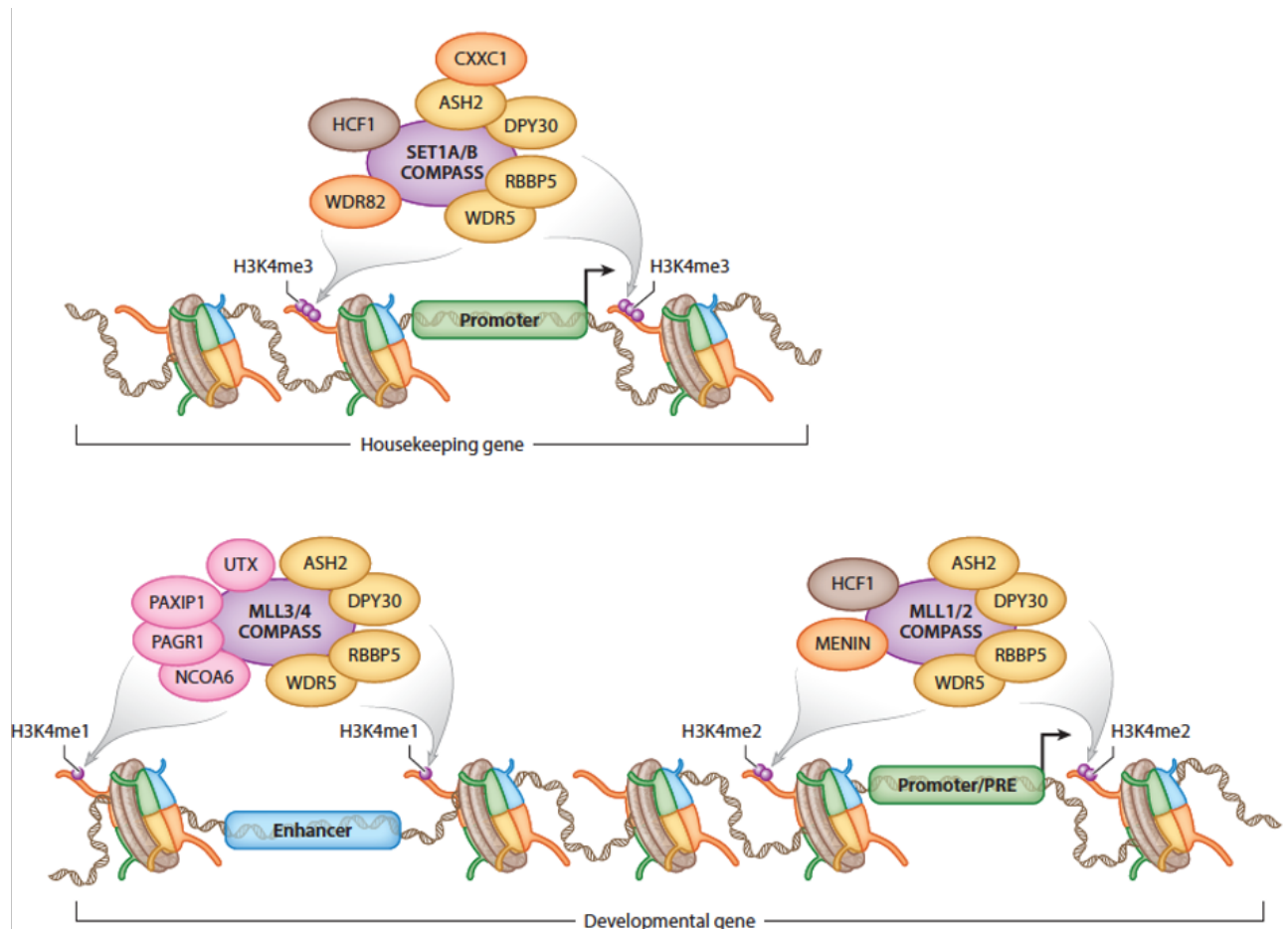


Figure 35. COMPASS complexes in mammals and their subunits composition.
From Meeks and Shilatifard, 2017.

SUV39 family. As mentioned before, SUV39H1 was the first KMT to be identified. Other members of this family include SUV39H2, G9A, GLP, SETDB1/2 which are all capable of H3K9 methylation.

SET1 family. In humans, there are six SET1-related methyltransferases: SETD1A (KMT2F), SETD1B (KMT2G), MLL1 (KMT2A), MLL2 (KMT2B), MLL3 (KMT2C) and MLL4 (KMT2D). These proteins are part of the well characterized SETD1-containing COMPASS complexes and the MLL-containing COMPASS-like complexes (Meeks and Shilatifard, 2017). Interactions among several subunits of this family, of methyltransferases were shown to be mediated by β -propeller domains which are repeated units consisting of four anti-parallel β -strands (Bergamin, Blais and Couture, 2014). These chromatin-modifying complexes were found to be essential for development as inactivation of core components such as MLL1 or SETD1A leads to embryonic lethality (Lee *et al.*, 2013; Bledau *et al.*, 2014). While COMPASS complexes mediates H3K4me₃ at gene promoters of especially housekeeping genes, COMPASS-like complexes were described to specifically mediate H3K4me at promoter and enhancer elements of developmental genes, such as Hox genes (Figure 35).

EZ family. Just like the SET1 family, methyltransferases EZH1 and EZH2 are both components of the evolutionary-conserved Polycomb Repressive Complex 2. PRC2 further contains core members SUZ12, EED as well as other accessory subunits such as JARID2 and AEBP2. First discovered in *Drosophila*, the role of Polycomb complexes has been thoroughly studied in development as it is critical for establishing the trimethylation of H3K27 (Margueron and Reinberg, 2011). Interestingly, JARID2 is a founding member of the Jumonji family which catalyzes protein demethylation, however it lacks a key residue for co-factor binding and is thus completely devoid of demethylase activity. Yet JARID2 contains a AT-rich interaction domain (ARID) which was shown to be essential for DNA binding of the PRC2 complex.

Cells also comprise non SET domain-containing methyltransferases such as the DOT1L enzyme and the PRMT families.

DOT1L. This enzyme is an evolutionarily conserved KMT that was identified in yeast as a disruptor of telomeric silencing. It was shown to be critical for methylating H3K79. DOT1L does not include a SET-

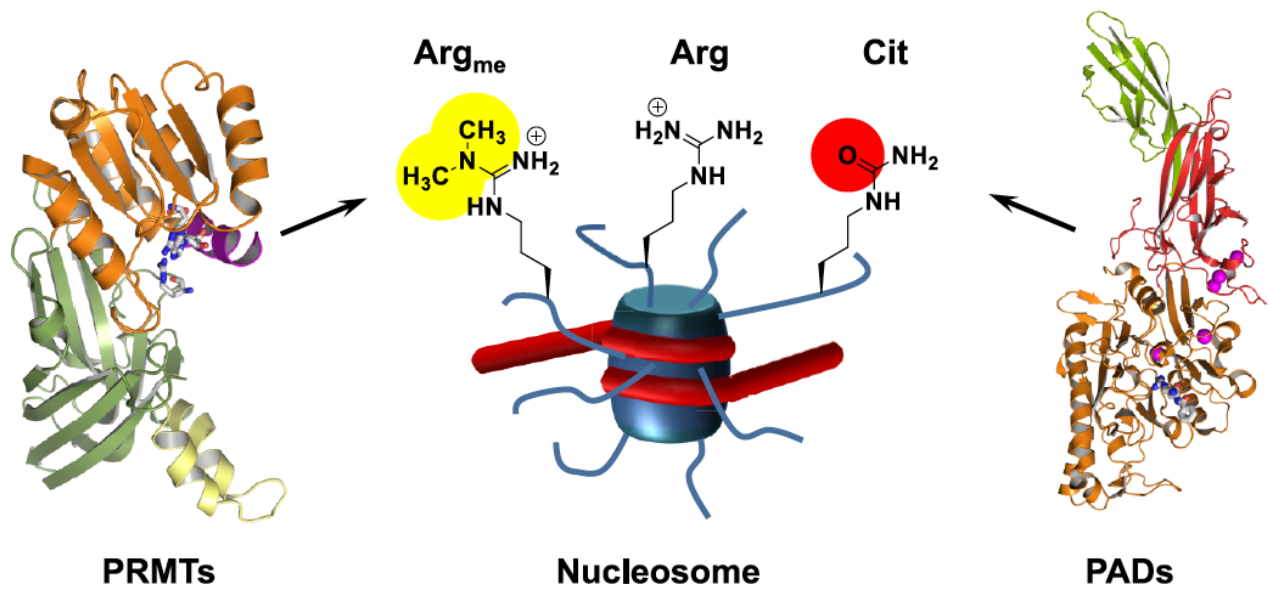


Figure 36. Methylation of arginine residues by PRMTs and addition of a citrullinyl group on arginine residues by PADs.

From Fuhrmann and Thompson, 2016.

domain, but a seven-stranded β -sheet that is also a characteristic of PRMTs (Cheng, Collins and Zhang, 2005).

PRMTs. Protein arginine methyltransferases are essential to catalyze mono- and dimethylation of arginine residues. Currently, seven mammalian PRMT genes have been described and are classified in four classes (I to IV). Amongst these, PRMT1 is the predominant arginine methyltransferase in humans as it is responsible for roughly 85% of all arginine methylation (Tang *et al.*, 2000). PRMT1 is essential during development and has been implicated in neuronal differentiation. It also has known non-histone substrates such as FGF2, STAT1 and SPT5 (Cheng, Collins and Zhang, 2005) (Figure 36).

2.1.2.3. Demethylases

After three decades of debates regarding the existence of lysine demethylases, Yang Shi and colleagues identified the first histone KDM which was termed KDM1A (or LSD1) as part of the C-terminal binding protein 1 (CtBP1) corepressor complex (Shi *et al.*, 2004). Eight KDMs has thus far been reported to be responsible for the removal of methyl groups and they are classified in two major families: the LSD1/KDM1 demethylases and the JmJC domain-containing demethylases.

LSD1 family. These enzymes belong to the amine oxidase superfamily as they oxidatively demethylate H3K4me_{1/2} and H3K9me_{1/2} by a mechanism that depends on the presence of flavin adenine dinucleotide (FAD) co-factor. Demethylation by LSD1 results usually in transcription activation. This family only contains two members: KDM1A and KDM1B, with the latter still being only poorly characterized.

JMJC family. This is the largest group of demethylases as it comprises 20 enzymes which are usually subdivided into JMJD demethylases (e.g. KDM3, KDM4A/B/C/D) and JARID1 demethylases (e.g. KDM5A/B/C/D). These enzymes belong to the 2-oxoglutarate-dependent dioxygenases and required Fe²⁺ and oxygen to remove the methyl groups.

Besides these classical demethylases, there are also the peptidyl arginine deiminases (PADIs) which are enzymes catalyzing the addition of a citrullinyl group on arginine residues of histones and non-histone proteins. To this day, five PADIs (1 to 4 and 6) have been identified and constitute yet another mechanism of arginine demethylation. Consistent with this hypothesis is the observation that

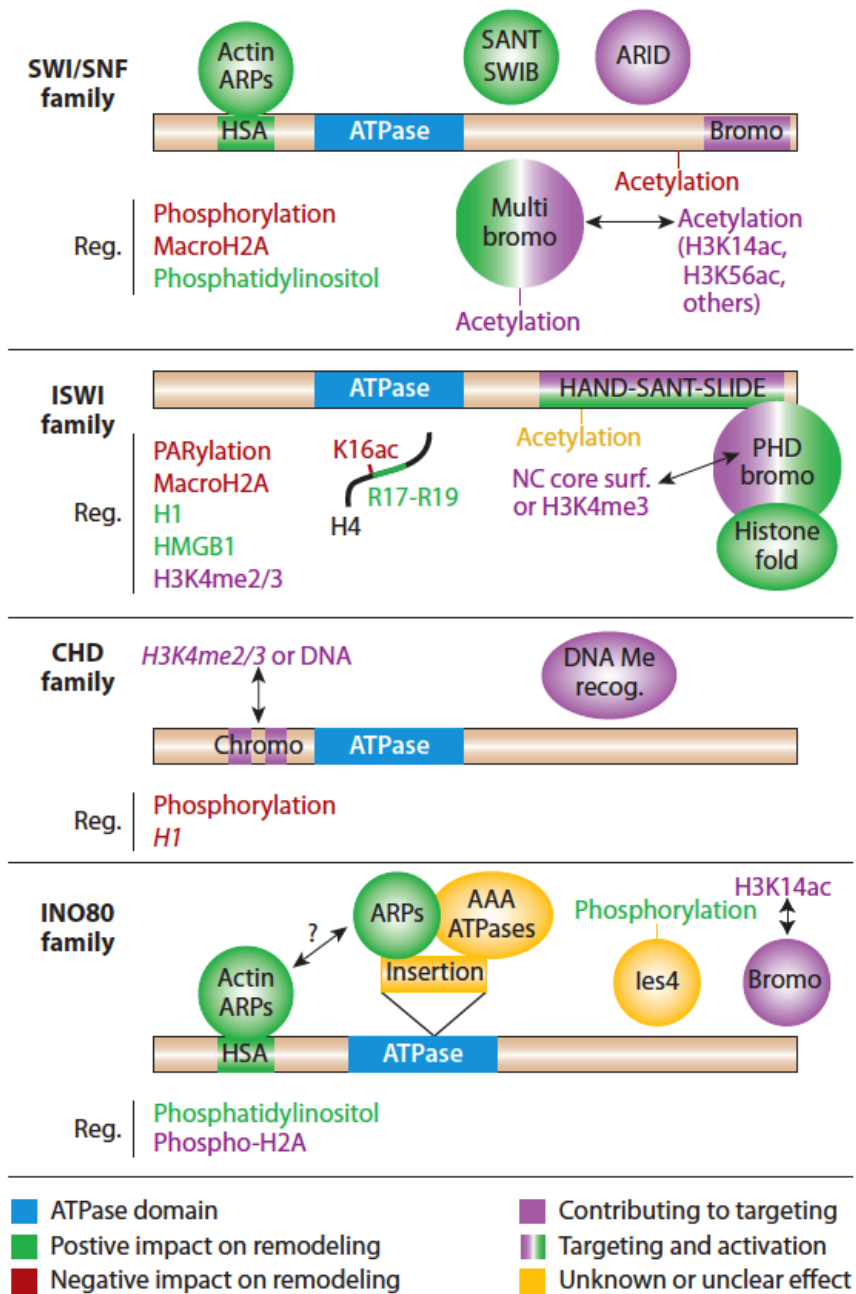


Figure 37. ATP-dependent chromatin remodeling enzymes.

From Clapier and Cairns, 2019.

induction of PADI4 results in a global increase of citrullinated histones and a decrease of arginine methylation, suggest PADI4 might also use methylated arginines as substrates for deimination. Yet, it is still debated how these citrullinated histones are to be replaced by unmethylated arginines to restore the normal epigenetic landscape and thus it is not considered as a canonical demethylation system (Fuhrmann and Thompson, 2016).

Aside from controlling the structure of chromatin, the equilibrium between KMTs and KDMs is crucial in regulating cell cycle. In humans, KMT6 is a key regulator of cell cycle genes such as CCNA2, CCND1 and CCNE1 (Bracken *et al.*, 2003). The demethylase KDM7B (PHF8) also contributes by regulating the well-known cycle regulator E2F1 during G1/S transition.

Demethylases are regulated by a plethora of mechanisms ranging from ubiquitination to metabolites as it is dependent on a set of metabolic byproduct co-factors such as AdoMet or FAD (Shi and Whetstone, 2007).

2.2. ATP-dependent chromatin remodeling enzymes

So far, we have described the multiple chromatin-modifying enzymes and complexes that covalently alter the composition of chromatin by regulating the dynamic and controlled flux of addition and removal of epigenetic marks on histone tails which globally constitute the histone code. Yet, there exist another mechanism by which the chromatin structure can be reversibly modified by actively remodeling the nucleosomes by using ATP as the energy source. This task is the responsibility of ATP-dependent chromatin-remodeling complexes that fine-tune the composition and the positioning of nucleosomes, which in itself constitutes yet another layer of transcription regulation often referred to as the ‘nucleosome spacing (or positioning) code’ (Segal *et al.*, 2006). However, this type of chromatin remodeling is not to be confused with ATP-independent remodeling which can occur from pioneer TFs (such as the aforementioned SOX2) shifting the position of nucleosome as a consequence of DNA binding (Workman and Kingston, 1992; Dodonova *et al.*, 2020) (Figure 37).

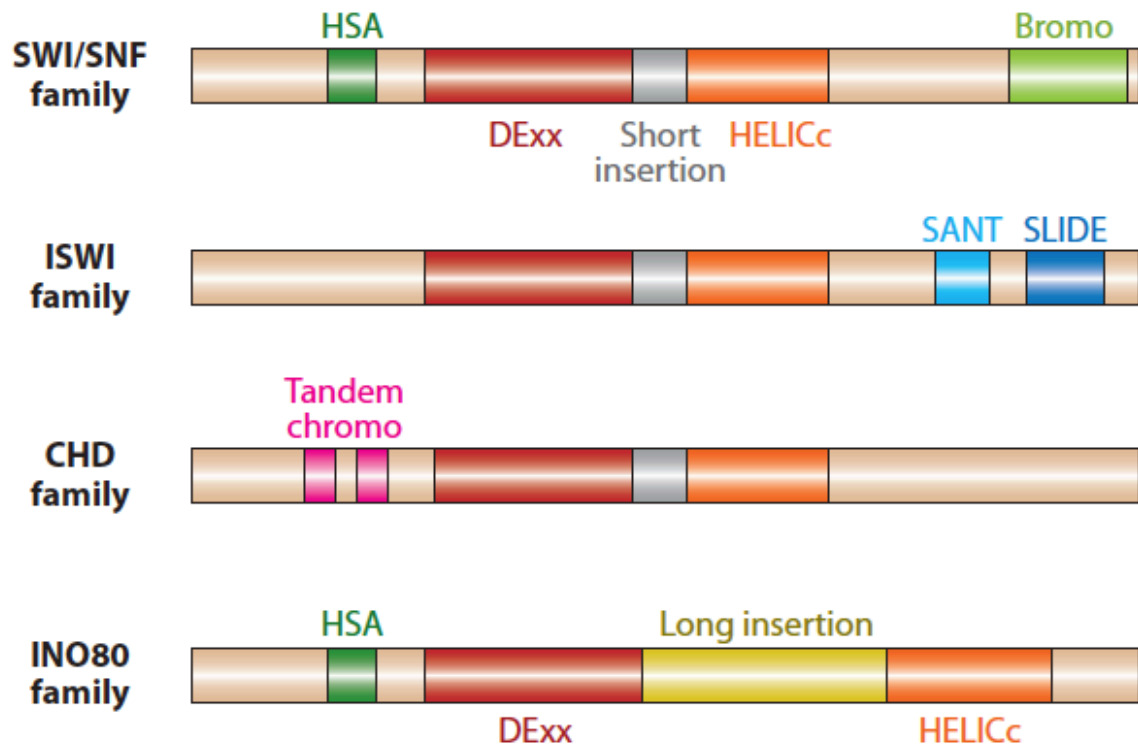


Figure 38. ATPase subunits of remodelers with DExx and HELICc domains.
 From Clapier, 2017.

2.2.1. The nucleosome positioning code

2.2.1.1. Similarities and differences between remodelers

ATP-dependent chromatin remodelers share some common features. They all function by utilizing energy from ATP hydrolysis and disrupt contacts between histone proteins and DNA resulting in an altered nucleosome structure (Kingston and Narlikar, 1999; Wang, 2003). They all possess an ATPase subunit with DExx and HELICc domains which are involved in DNA binding, DNA unwinding and ATP hydrolysis. Due to their similarities, chromatin remodelers may often compensate for each other and display a certain level of functional redundancy. However, based on the nature of additional function domains in the catalytic ATPase subunit, four families of such remodelers were identified and classified: ISWI, CHD, SWI/SNF and INO80. In metazoans, cell-type and development-specific subfamilies were described as well as orphan remodelers which cannot be classified into any of the main families (Clapier *et al.*, 2017). Although all chromatin remodelers independently of the family contain an ATPase-translocase motor, only members of the INO80 subfamily were reported to have the capacities of editing canonical nucleosomes with histone variant-containing dimers. Members of the ISWI and CHD subfamilies are mainly involved in nucleosome assembly and spacing, in contrast to SWI/SNF complexes which typically promote chromatin accessibility and maintain NDRs at regulatory elements (Clapier *et al.*, 2017) (Figure 38).

2.2.1.2. Mechanism of remodeling

Until now, three alternative mechanisms of action of remodeling have been described by the remarkable work of Clapier and colleagues: nucleosome assembly, nucleosome accessibility and nucleosome editing (Clapier and Cairns, 2009; Clapier *et al.*, 2017).

Nucleosome assembly. Following DNA replication, histone partner proteins called ‘histone chaperones’ - such as the FACT complex (Winkler and Luger, 2011) – have for task to bring histone complexes (H3-H4 tetramers and H2A-H2B dimers) to nascent DNA in order to recompact it (Gurard-Levin, Quivy and Almouzni, 2014). Chromatin remodelers have a major role to play in this essential process. In particular ISWI and CHD families of complexes have been shown to be required for at least two functions: 1) the formation of the canonical octameric nucleosomes; 2) the correct spacing of nucleosomes at relatively

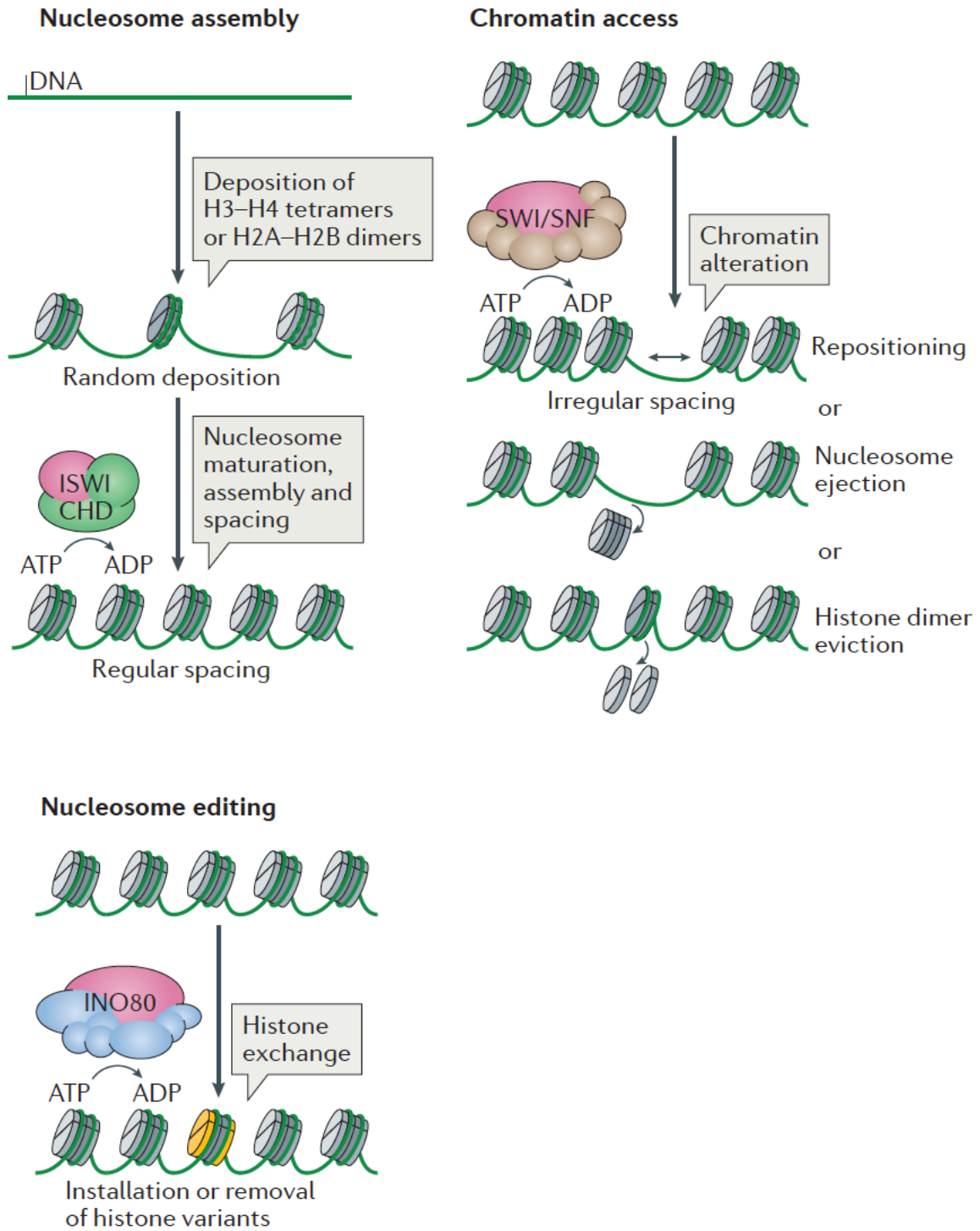


Figure 39. Functional classification of remodelers.

From Clapier, 2017.

fixed distances (Corona *et al.*, 1999; Clapier *et al.*, 2017). More recently, the SWI/SNF family has also been shown to be able of generating stable nucleosome-like particles, referred to as ‘remosomes’ (Shukla *et al.*, 2019). Nucleosome assembly is thought to primarily promote gene silencing through the creation of tightly packed nucleosome array impeding with the accessibility of TFs and RNAPII.

Nucleosome accessibility. As discussed previously, transcription is very dependent on the accessibility of naked DNA for regulatory proteins and RNAs to bind it. Making the chromatin more accessible can be achieved through three distinct ways: 1) simply sliding a nucleosome along the DNA up- or downstream of the targeted sequences; 2) evicting nucleosome components (most often H2A-H2B dimers) in order to destabilize DNA-nucleosome interactions; or 3) fully ejecting the entire histone octamer leaving a nucleosome-depleted region (NDR). Virtually all chromatin remodelers participate in this process, however SWI/SNF is responsible for most of it (Boeger *et al.*, 2004). One debated idea in the field is the correlation between nucleosome accessibility and activation of transcription. Although the opening of chromatin is indeed a requirement for transcribing genes, NDRs are accessible for both activator and repressor TFs which can lead to different gene expression outcomes.

Nucleosome editing. The last described mechanism of remodeling consists in altering the composition of nucleosomes by replacing a particular histone with either another canonical or a variant histone such as H2A.Z or H3.3. Currently, this type of activity has been reported only for members of the INO80 remodeler family (Obri *et al.*, 2014; Latrick *et al.*, 2016). The inclusion of histone variants at single nucleosomes or at an array of nucleosomes can effect TF recruitment and binding to chromatin. One good example is the role of H2A.Z in recruiting cell cycle effectors E2F proteins and bromodomain-containing BRD2 which has crucial role in melanoma metastasis and resistance to drugs (Vardabasso *et al.*, 2015) (Figure 39).

In spite of their similarities, chromatin remodelers use different modes of action. Further works will perhaps allow to uncover even more mechanisms. Due to their distinctive features, three of remodeler families will be detailed below: ISWI, INO80, CHD and SWI/SNF.

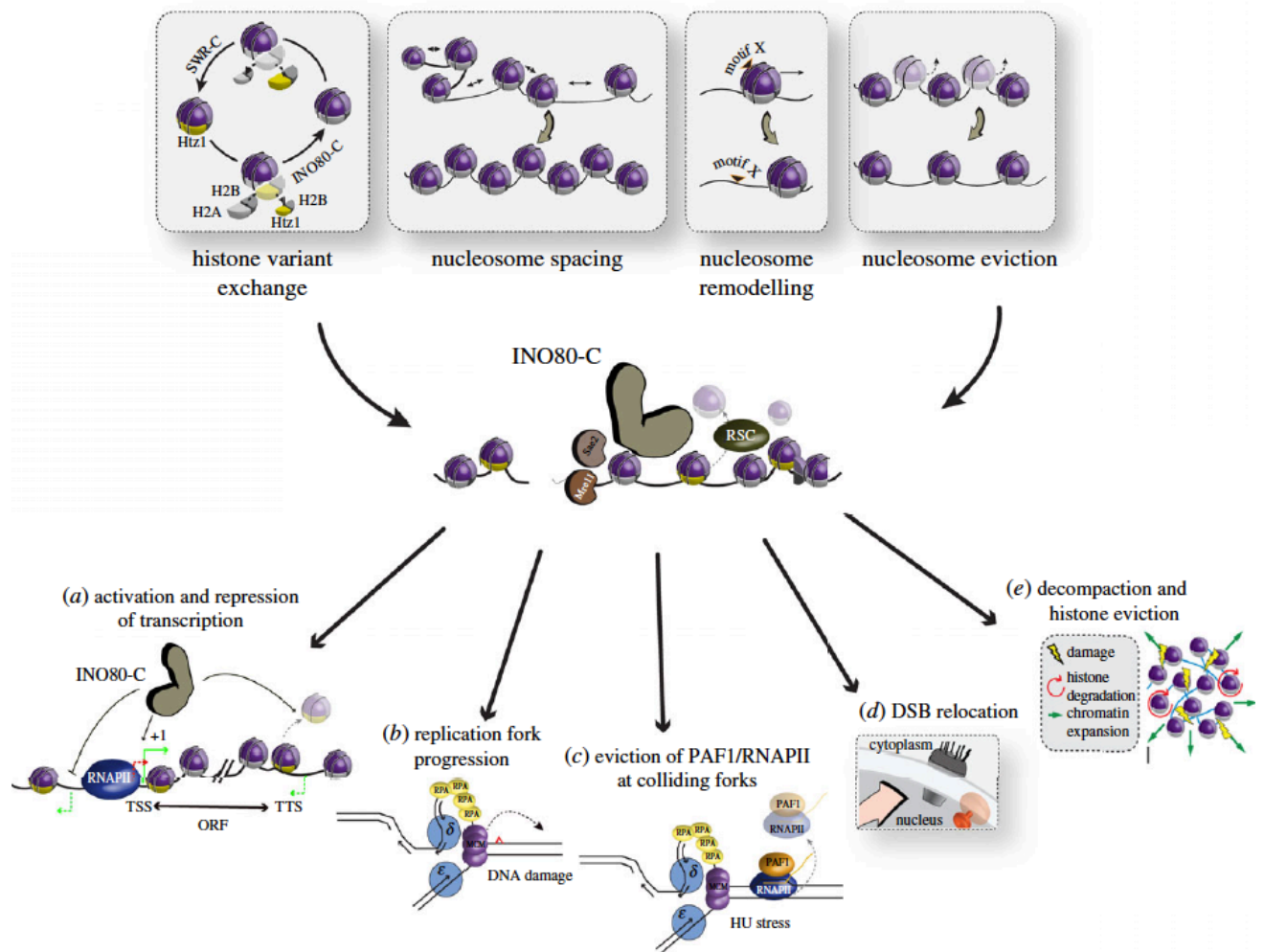


Figure 40. Functions of INO80 complex.

From Poli *et al.*, 2017.

2.2.2. The INO80 family

The mammalian INO80 (Inositol required 80) remodeler family comprises more than 10 subunits which assemble into three distinct subcomplexes : INO80, SRCAP and TIP60 (Clapier and Cairns, 2009). They all possess a shared core composed of a dimer of RUVBL1/RUVBL2 and an ARP module with ACTB and ACTL6A (similar to SWI/SNF). However, each subcomplex differ by their ATPase subunit namely hINO80 in INO80 complex, SRCAP in SRCAP complex and p400/DOMINO in TIP60 complex. Importantly the specific composition of the three subcomplexes was shown to influence their differential role in H2A.Z variant homeostasis. As the H2A.Z writer YL1 is in SRCAP and TIP60 complex (but not INO80 complex), while only TIP60 complex contains the H2A.Z eraser subunit ANP32E (Obri *et al.*, 2014; Latrick *et al.*, 2016) (Figure 40).

A unique feature of INO80 family members is the presence of an extended insertion within the ATPase domain, referred to as the ‘split ATPase domain’, which allows the ATPase domain to retain its catalytic activity while also enables the RUVBL dimer and ARP module to anchor on it, an important step for complex formation (Ikura *et al.*, 2000; Bao and Shen, 2007; Clapier and Cairns, 2009). Another key feature of the INO80 ATPase subunits is its DNA helicase activity which preferentially binds to four-way junction DNA structures *in vitro*, consistent with its function in DNA replication (Watanabe *et al.*, 2010; Papamichos-Chronakis *et al.*, 2011). It also has a greater affinity for H2A variants such as the aforementioned H2A.Z but also H2A.X, thus INO80 has been described to play an important role in mediating nucleosome eviction during DNA repair, especially in GG-NER and DSB repair (Wang *et al.*, 2014; Poli, Gasser and Papamichos-Chronakis, 2017). Perhaps the best characterized INO80 subcomplex is the TIP60 complex.

The mammalian TIP60 coactivator complex is composed of at least 18 subunits centered around the ATPase p400. This subcomplex is homologous to the 13-subunit yeast NuA4 complex (Doyon *et al.*, 2004; Sapountzi and Côté, 2011). Importantly, this complex also possess an chromatin-modifying activity which is allowed by the name-giving subunit TIP60 (KAT5) which belongs to the MYST family of HAT and mainly modifies lysine residues of histone H2A and H4 (Sapountzi and Côté, 2011). Intriguingly, TIP60 complex shares a subunit with the aforementioned coactivator complex SAGA

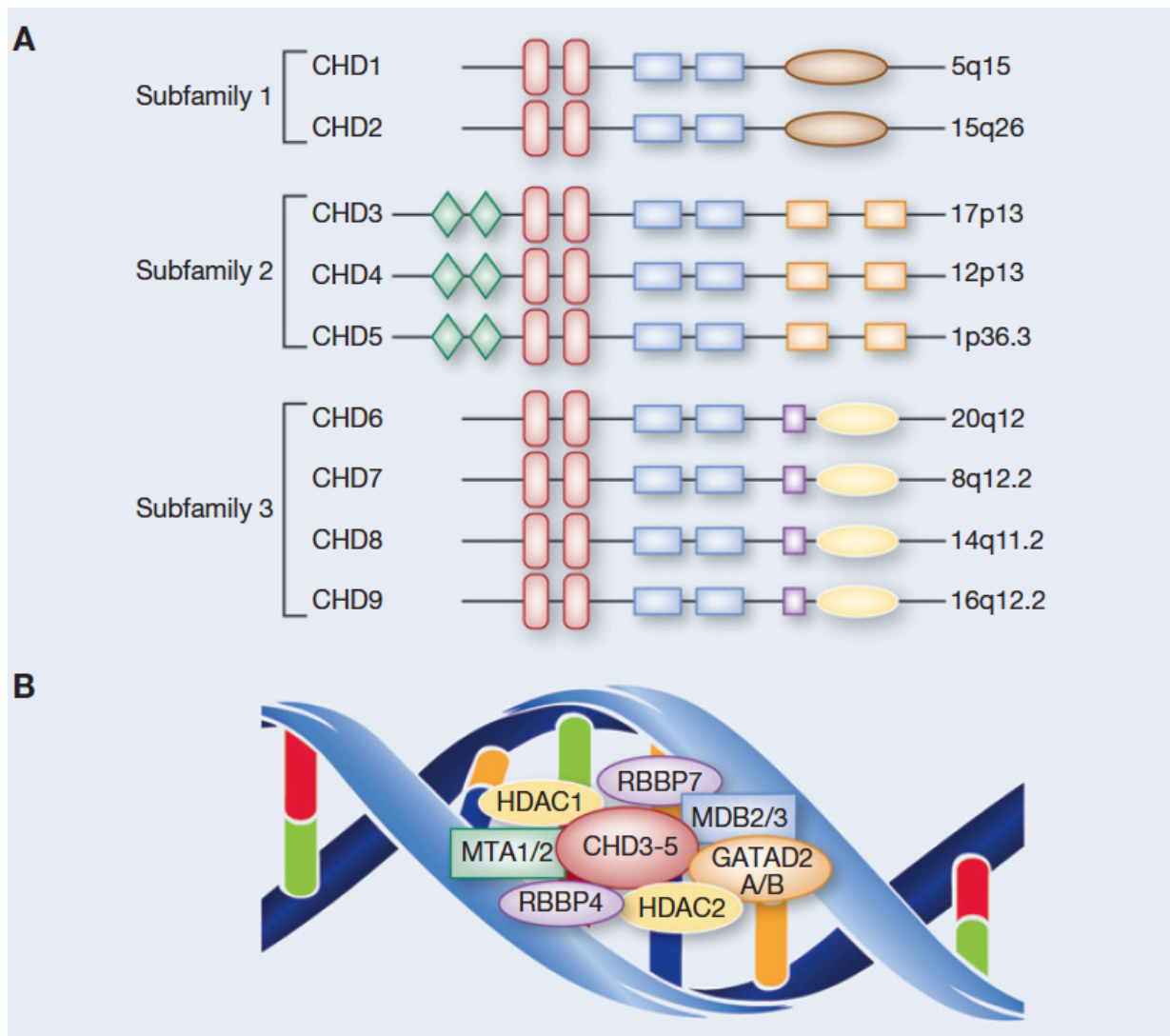


Figure 41. CHD family.

A. Three subfamilies and members of CHD family. **B.** CHD(3-5)-NuRD complex. From Kolla *et al.*, 2014.

which is TRRAP, a 0,5 kDa large protein that was shown recently to serve as a complex assembly platform together with the ATPase p400 (Helmlinger and Tora, 2017).

2.2.3. The CHD family

The chromodomain helicase DNA-binding (CHD) family comprises nine different ATPases (CHD1–9). All CHD proteins all share two features: 1) a CHROMatin Organizing (CHROMO)-domain that specifically recognizes methylated lysines (such as H3K4me_{2/3}); and 2) a SNF2-like ATPase domain that facilitates nucleosome mobilization (Marfella and Imbalzano, 2007). CHD family members are classified into 3 subfamilies based on structural features and sequence homology.

Subfamily I. This subfamily includes CHD1 and CHD2 which contain specific DNA-binding motif domain (Delmas, Stokes and Perry, 1993).

Subfamily II. It comprises CHD3 to -5 and contain notably Plant HomeoDomain (PHD).

Subfamily III. Composed by CHD6 to -9 with a specific Swi3, Ada2, N-CoR, TFIIB (SANT) and a BRK domain (Kolla *et al.*, 2014). The Nucleosome Remodeling and Deacetylase (NuRD) subcomplex is perhaps the best characterized chromatin-remodeling of the CHD family (Figure 41).

The NuRD complex is 1MDa multicomponent complex that highly conserved among higher eukaryotes and expressed in a large variety of tissue (Zhang *et al.*, 1999; Clapier and Cairns, 2009). The complex is composed of one copy of either CHD3, CHD4 or CHD5 ATPase subunit, one copy of HDAC1 or HDAC2, DOC1, GATAD2, several specific DNA-binding MTA1/2/3, several CpG-binding proteins MBD2/3 and several histone chaperones RbAp46/48 (Kloet *et al.*, 2015; Mohd-Sarip *et al.*, 2017). The incorporation of CHD3 is mutually exclusive with CHD4 thereby cells comprise a heterogeneous mix of both CHD3- and CHD4-containing complexes that may have redundant but also specific functions, yet to be discovered. Moreover, and similarly to the TIP60 complex, NuRD displays at least two enzymatic activities as the mutually exclusive ATPase subunits CHD3/4 enable the ATP-dependent chromatin remodeling activity and aforementioned HDAC1/2 catalyze protein deacetylation. (Bowen *et al.*, 2004; Torchy, Hamiche and Klaholz, 2015). A potential reason is that ATP-remodeling activity is necessary for the HDACs subunits to access their target (Pegoraro *et al.*, 2009).

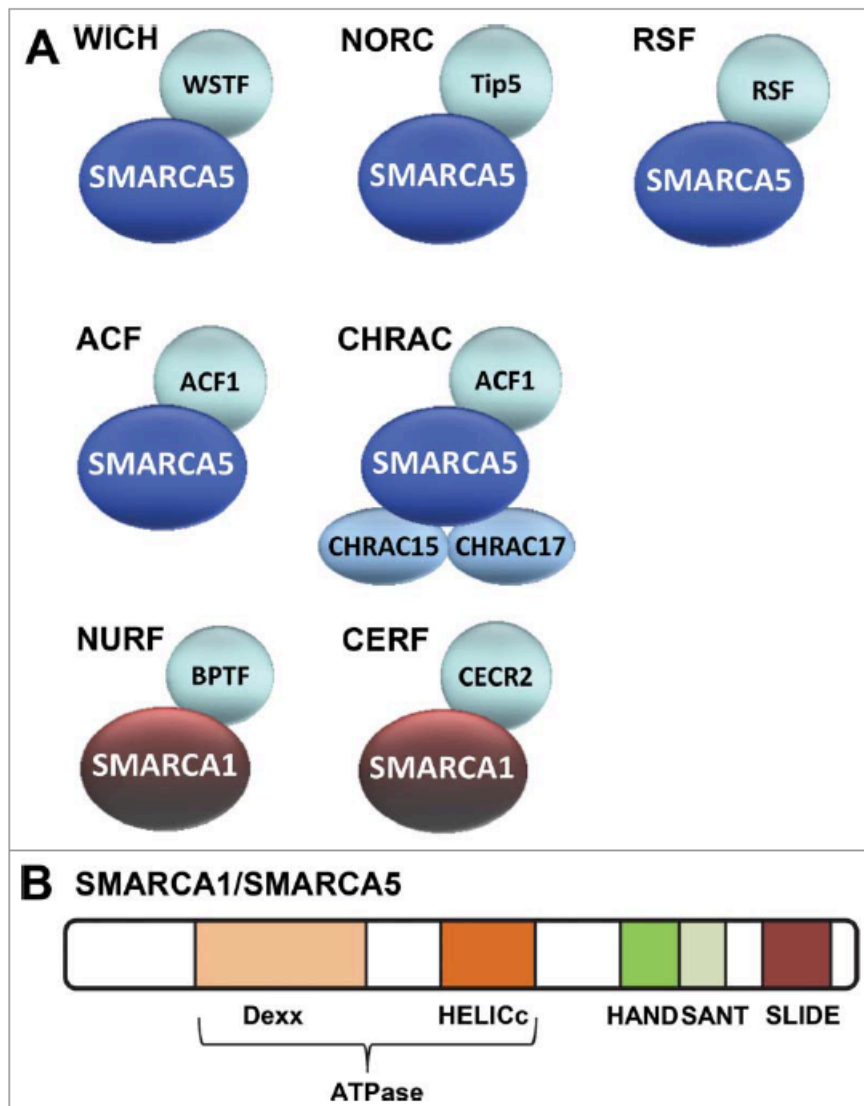


Figure 42. ISWI family chromatin remodeling complexes.

A. Seven mammalian ISWI family containing either SMARCA1 or SMARCA5. **B.** Domains of SMARCA1 and SMARCA5. From Aydın *et al.*, 2014.

2.2.4. The ISWI family

The mammalian ISWI (Imitation Switch) family of chromatin remodelers includes NURF, CHRAC and ACF complexes. They are characterized by the presence of the SANT and SLIDE domains which help in the preferential interaction with nucleosomes containing linker DNA over core nucleosomes (Corona *et al.*, 1999). Mammalian cells contain two isoforms of the ISWI ATPase encoded by two related genes Snf2L/SMARCA1 and Snf2H/SMARCA5. These ATPases show intrinsic chromatin remodeling activity. They were purified from cells as complexes that contain at least one additional accessory subunit (Clapier and Cairns, 2009). Those complexes are recruited to chromatin through a variety of mechanisms including modified histones, DNA binding proteins or specific DNA sequences. Once recruited they modulate accessibility to DNA by nucleosome assembly or sliding to ultimately regulate DNA-dependent processes (Becker and Workman, 2013). Additionally, the ISWI family has been described as one of the major ATP-dependent chromatin remodeling complex families that functions in the response to DNA damage as it is implicated in homologous recombination, non-homologous end-joining and nucleotide excision repair (Aydin *et al.*, 2014) (Figure 42).

In mammals, the Nucleosome Remodelling Factor (NURF) complex is the major ISWI chromatin remodeling complex involved in the regulation of gene expression. First identified in *Drosophila* (Tsukiyama and Wu, 1995; Tsukiyama *et al.*, 1995), NURF complexes comprise BPTF Bromodomain PHD-finger Transcription Factor (BPTF), RbAp46/48 along with the SMARCA1 ATPase subunit (Xiao *et al.*, 2001; Wysocka *et al.*, 2006; Alkhatib and Landry, 2011; Koludrovic *et al.*, 2015). BPTF contains multiple highly conserved domains essential for NURF interactions with a variety of transcription factors, thus promoting NURF recruitment to specific DNA sequences (Jones, Hamana and Shimane, 2000; Xiao *et al.*, 2001). BPTF can also interact with H3K4me3- and H4K16ac-modified histones through the C-terminal PHD finger and the bromodomain, respectively (Wysocka *et al.*, 2006; Ruthenburg *et al.*, 2011). It was recently shown that BPTF preferentially localizes to gene bodies but can also be found in promoters and enhancers. While its chromatin remodeling activity is constrained to the promoters, BPTF is required for exon splicing and intron removal within gene bodies during mRNA processing (Alhazmi *et al.*, 2018). In human melanoma, the gene encoding BPTF is amplified around 5–7% (Akbari *et al.*, 2015) and BPTF expression can be upregulated during tumor progression, an event

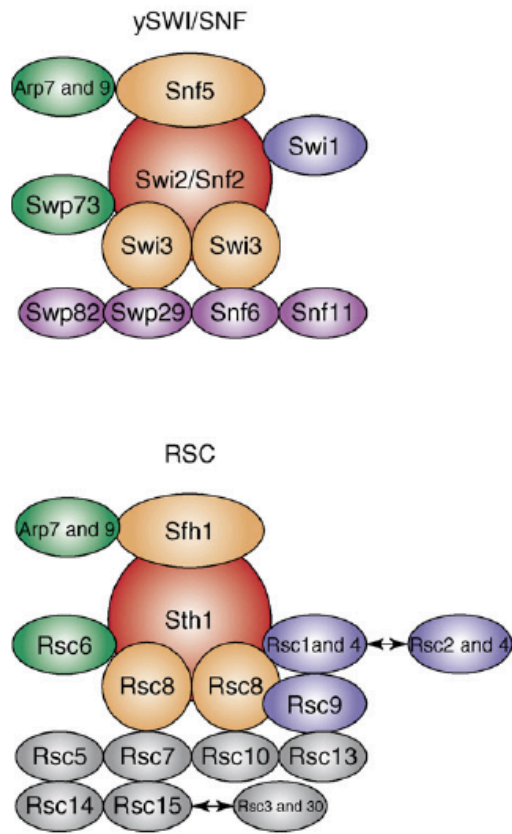


Figure 43. SWI/SNF complexes in yeast.

From Kwon and Wagner, 2007.

associated with poor prognosis and resistance to BRAF inhibitors (Dar *et al.*, 2015). Additionally, BPTF/NURF was shown to associate physically and functionally with the melanocyte regulator MITF to co-regulate genes involved in the proliferation of melanoma cells (Koludrovic *et al.*, 2015). In the same study, authors showed that BPTF is not required for melanoblast development in mice but for the generation of melanocytes from the adult melanocyte stem cell population.

While the key characteristic of NURF and ISWI family is their contribution to assemble nucleosomes, the last remodeler family SWI/SNF, which will be discussed below, has the opposite function which is to disassemble nucleosomes to permit accessibility.

2.3. Focus on the SWI/SNF chromatin-remodeling family

2.3.1. Evolution from yeast to mammals

2.3.1.1. Discovery

First characterized by Carlson and Botstein in 1983, *S. cerevisiae* invertase (coded by the SUC2 gene) is a key enzyme for glucose metabolism. Early screening for mutations causing defective sucrose fermentation by Neigeborn and Carlson identified 5 relevant genes designated Snf2-6 Sucrose Non-Fermenting 2-6 (Snf2-6) (Neigeborn and Carlson, 1984). In the same year, Stern and Herskowitz independently found that 3 of those genes (they named Swi1-3) were also important for yeast mating type switching. Almost a decade forward in 1992, Peterson and Herskowitz showed by second mutations in histone genes that Swi and Snf genes actually associate with one another to form a chromatin remodeling unit, leading to the term SWI/SNF (complex later isolated by (Cairns *et al.*, 1994)) (Peterson and Herskowitz, 1992) . A couple of years later, the Kornberg team isolated another SWI/SNF-like complex, based on homology with Snf2 ATPase protein, that they called Remodels Structure of the Chromatin (RSC). This novel complex shared some subunits with Swi2/Snf2 complex but was far more abundant in yeast and revealed to be required for cell viability (Cairns *et al.*, 1994) (Figure 43).

Within a few years, similar complexes were discovered in *Drosophila* in screens for genes opposing Polycomb-mediated repression of homeotic genes. Notably, Tamkun *et al.*, identified the gene Brahma (Brm) to be the orthologue of Swi2 (also called Snf2) (Tamkun *et al.*, 1992).

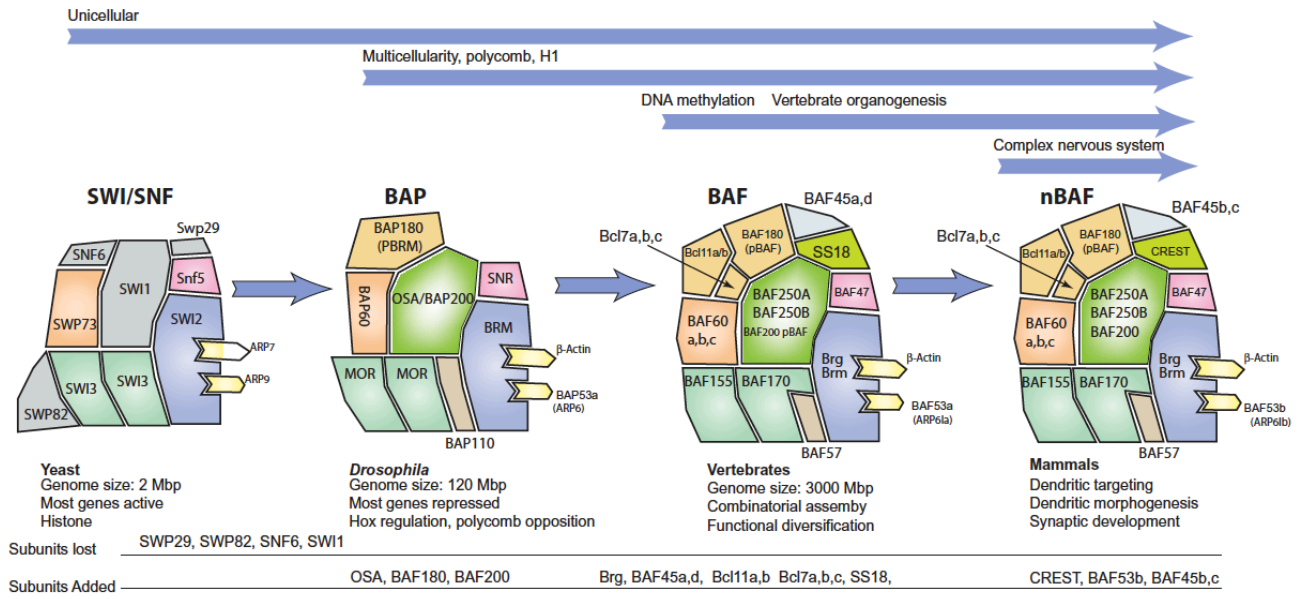


Figure 44. Evolution of SWI/SNF complex from yeast to mammals.

From Kadoch and Crabtree, 2015.

These Brm-containing complexes were Brm-associated protein (BAP) and polybromo-BAP (pBAP), homologs of SWI/SNF and RSC complex respectively. In mammals, early sequencing efforts identified 29 non-redundant genes encoding proteins similar to the yeast SWI2/SNF2. Over the years, biochemical studies of these genes led to the characterization of their associated chromatin-remodeling complexes.

2.3.1.2. Evolution and conservation

The mammalian SWI/SNF complex is the most well studied remodeler and has been evolving from unicellular organisms to metazoans and mammals (Figure 44).

During its 1,5 billion years of evolution, the SWI/SNF complex has been changing in composition and diversifying in function. As mentioned before, ySWI2/SNF2 contains the ATPase subunit SWI2 in complex with SWI1, two copies of SWI3, SNF5, SNF6, SWP29, SWP73, SWP82 and two actin-regulated genes ARP7 and ARP9. In *Drosophila*, BAP and pBAP complexes both contain BRM (SWI2), 2 copies of BAP155 (also called MOR, orthologue of SWI3), BAP47 (ARP7), BAP55 (ARP9), BAP60 (SWP73), BAP45 (SNF5) and newly gained subunits, BAP111 and ACTB. However, BAP and pBAP interestingly differ by their alternative incorporation of either OSA (orthologue to SWI1) alone or BAP180 (RSC1) together with BAP170 (RSC9) and SAYP (PHF10), respectively. The evolution from yeast to fruit fly rendered the SWI/SNF complexes more diverse by adding new subunits and by allowing alternative compositions to be determined by few unique subunits like AT-rich interaction domain (ARID)-containing proteins, OSA and BAP170. In turn, similar SWI/SNF sub-complexes were purified from human cells and revealed this chromatin-remodeler family to be highly conserved throughout evolution from yeast to fruit flies, *C. elegans*, vertebrates and mammals.

In mammalian complex nervous systems where SWI/SNF genes have the highest level of expression, the composition of the SWI/SNF complexes is the most diverse and has been shown to finely tune the differentiation of neurons, causing intellectual disability when defective. During neural development, the transition from neural progenitors to post-mitotic neurons requires a switch in subunit composition of the neural progenitor-BAF (ncBAF) towards neural-BAF (nBAF) complexes. Indeed, npBAF specifically ACTL6A, PHF10 and SS18 proteins which are exchanged when adult neurons exit cell cycle for alternative paralogs BAF53B, BAF45B/C and SS18L1 (also called CREST). This goes to

	Gene	Alias	mSWI/SNF complex	Module
Common subunits	ACTB		cBAF, PBAF, ncBAF	ATPase
	ACTL6A	BAF53A	cBAF, PBAF, ncBAF	ATPase
	ACTL6B	BAF53B		
	BCL7A		cBAF, PBAF, ncBAF	ATPase
	BCL7B			
	BCL7C			
	SMARCA2	BRM	cBAF, PBAF, ncBAF	ATPase
	SMARCA4	BRG1		
	SMARCC1	BAF155	cBAF, PBAF, ncBAF	BAF core
	SMARCC2	BAF170	cBAF, PBAF	
	SMARCD1	BAF60A	cBAF, PBAF, ncBAF	BAF core
	SMARCD2	BAF60B		
SMARCD3	BAF60C			
Complex-Specific subunits	ARID1A	BAF250A, OSA1	cBAF	cBAF-specific
	ARID1B	BAF250B, OSA2		
	ARID2	BAF200	PBAF	PBAF-specific
	BICRA	GLTSCR1	ncBAF	ncBAF-specific
	BICRAL	GLTSCRL1		
	BRD7		PBAF	PBAF-specific
	BRD9		ncBAF	ncBAF-specific
	DPF1	BAF45B, NEUD4	cBAF	cBAF-specific
	DPF2	BAF45D, REQ, UBID4		
	DPF3	BAF45C, CERD4		
	PHF10	BAF45A	PBAF	PBAF-specific
	PBRM1	BAF180	PBAF	PBAF-specific
	SMARCB1	BAF47, INI1	cBAF, PBAF	BAF core
	SMARCE1	BAF57	cBAF, PBAF	BAF core
	SS18	SSXT, SYT	cBAF, ncBAF	ATPase
	SS18L1	CREST		

Figure 45. Genes encoding SWI/SNF subunits, their aliases and presence of each subunits in specific complexes and modules.

From Centore *et al.*, 2020.

show that the incremental gains of SWI/SNF subunits throughout evolution led to a multiplication of alternative complex compositions which have biological relevance.

2.3.2. Human ubiquitous SWI/SNF complexes

2.3.2.1. Human SWI/SNF sub-complexes: BAF and pBAF

In humans, SWI/SNF genes are ubiquitously expressed in all cell types with highest levels in the brain. Since the Crabtree team first purified the human SWI/SNF, we know that there are also at least two sub-complexes that were tagged SWI/SNF-A and SWI/SNF-B corresponding to the BRG1-associated factor (BAF) complex (orthologue of yeast SWI/SNF and fly BAP) and the polybromo-BRG1-associated factor (pBAF) complex (orthologue of yeast RSC and fly pBAP) respectively. Both sub-complexes contain one of the two paralogue ATPase subunits, BRM (SMARCA2) or BRG1 (SMARCA4), which share over 70% sequence identity and display similar biochemical activities *in vitro* (Khavari *et al.*, 1993; Randazzo *et al.*, 1994; Phelan *et al.*, 1999). However, it quickly became clear that BRG1 and BRM are unable to functionally compensate for one another to various cellular processes including proliferation and differentiation (Reyes *et al.*, 1998; Bultman *et al.*, 2000; Kadam and Emerson, 2003) (Figure 45).

Similar to *Drosophila*, what makes BAF and pBAF different is their differential incorporation of the ARID-containing subunits: ARID1A or 1B in BAF (Nie *et al.*, 2000) and ARID2 in pBAF (Yan *et al.*, 2005) respectively. Inclusion of ARID2 in pBAF also brings 2 other pBAF-specific interactors polybromo-containing protein PBRM1 (BAF180) and BRD7 (Kaeser *et al.*, 2008). Early biochemical studies seem to also imply that pBAF complexes have an exclusive affinity for BRG1 as the ATPase, but it is yet unclear if this is always valid due to inconsistencies in more recent analyses. In 2009, the Crabtree team identified several novel subunits of SWI/SNF including SS18, SS18L1, BCL7A, GLTSCR1 and BRD9 (Ho *et al.*, 2009). A few years after, proteomic analysis of the synovial sarcoma protein SS18 showed that it only precipitates with ARID1-containing BAF complexes. Of note, they also showed that PHF10 (BAF45A) is specific to PBAF complex whereas, the other paralogs DPF1, 2 and 3 (BAF45B, C and D) are mutually exclusive subunits of BAF complex (Middeljans *et al.*, 2012).

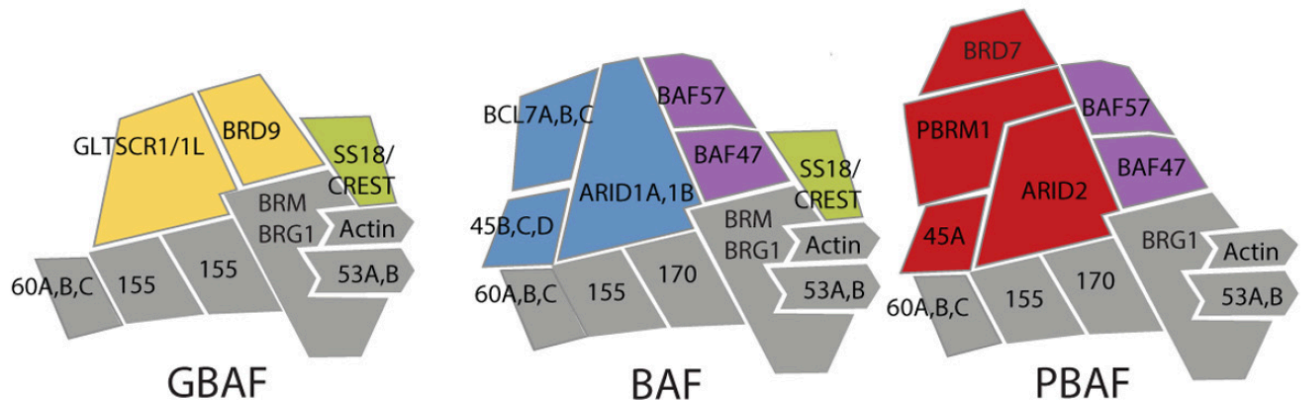


Figure 46. GBAF, BAF and PBAF complexes.

GBAF specific subunits are in yellow, BAF specific subunits are in blue, PBAF specific subunits in red, sharing subunits between GBAF and BAF are in green, sharing subunits between BAF and PBAF in purple. From Alpsy and Dykhuizen, 2018).

Taken together, biochemical and proteomic analyses have revealed the specific composition of the SWI/SNF sub-complexes, both containing a functional core composed of SMARCA4 or SMARCA2, BCL7A, B or C, ACTB, ACTL6A or B (BAF53A or B), SMARCC2 (BAF170), SMARCC1 (BAF155), SMARCD1, 2 or 3 (BAF60A, B or C), SMARCE1 (BAF57) and SMARCB1 (BAF47). Specific subunits of BAF complex are ARID1s, DPFs and SS18 whereas ARID2, PHF10, PBRM1 and BRD7 are found only in PBAF complexes.

2.3.2.2. The novel non-canonical BAF (ncBAF)

In 2013, Kadoch and Crabtree confirmed by proteomic analysis several mammalian-specific proteins to be part of the SWI/SNF complexes including GLTSCR1 and BRD9 (Kadoch *et al.*, 2013). However the exact composition of such BRD9-containing complex remained unclear until recently when the Dykhuizen team published their work on the glioma tumor suppressor candidate region gene 1 (GLTSCR1) and its mutually exclusive paralog GLTSCR1L (Alpsoy and Dykhuizen, 2018). By tandem purification analysis they identified a novel and smaller SWI/SNF sub-complex they termed GBAF as it specifically contained GLTSCR1 and BRD9 but not the core subunits BAF45, BAF47 and BAF57. Interestingly, GBAF complex were shown to display normal *in vitro* ATPase activity even without core subunits such as BAF47 and BAF57 which were thought to be required to enhance the remodeling activity of BRG1/BRM *in vitro* (Phelan *et al.*, 1999). Of note, they also showed that GLTSCR1 structurally replaces the ARID subunit in GBAF complex. Several publications confirmed these observations and revealed that BRD9 may be responsible for targeting this non-canonical BAF complex to specific genome localizations via interactions with BRD4 (Brien *et al.*, 2018; Gatchalian *et al.*, 2018). Later on, the Roberts team showed that loss of SMARCB1 in malignant rhabdoid tumors induces higher incorporation of BRD9 into SWI/SNF, indicating structural competitiveness between subunits (Michel *et al.*, 2018; Wang *et al.*, 2019) (Figure 46).

Altogether, several years of proteomic analysis have characterized the composition of 3 distinct SWI/SNF sub-complexes, all containing an ATPase core with BRG1/BRM, BCL7, ACTB and BAF53. The ubiquitous non-canonical BAF is closer to the canonical BAF than pBAF as it contains SS18 instead

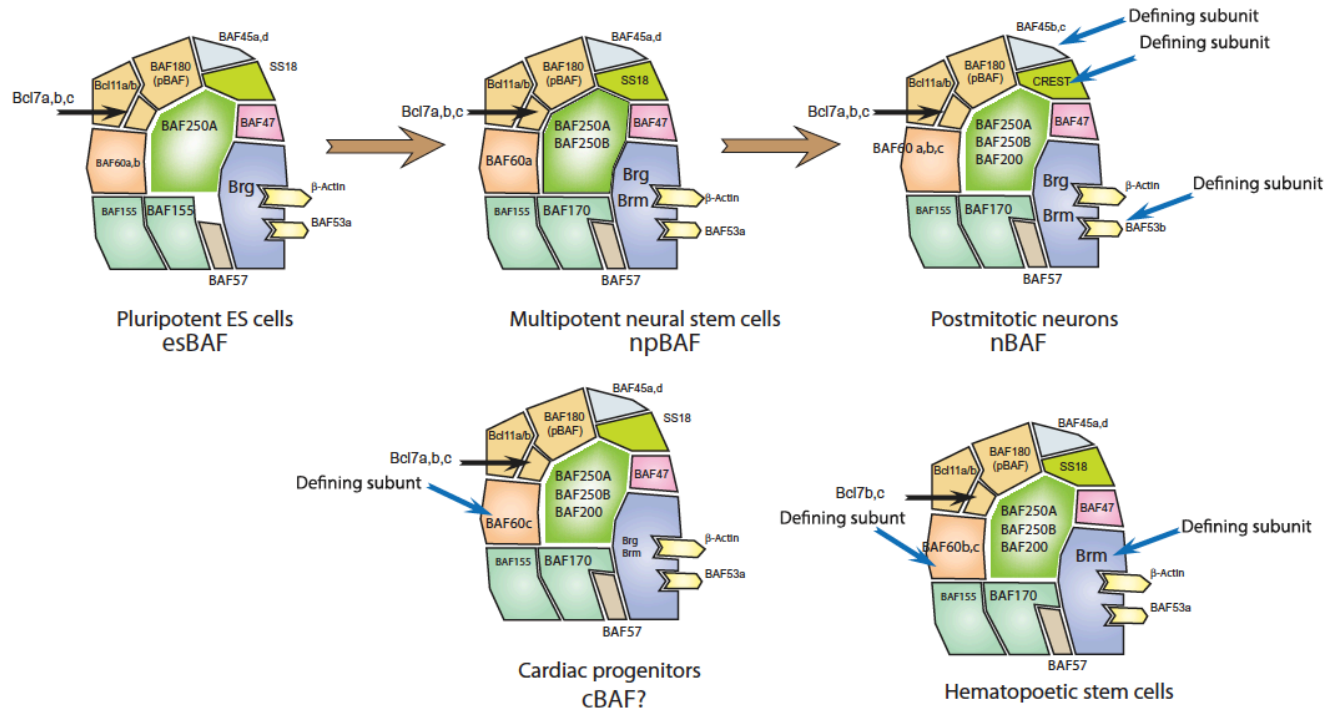


Figure 47. Changing of BAF complex subunit composition during development.

From Kadoch and Crabtree, 2015.

of PBRM1 and the core subunits BAF155 and BAF60. However GLTSCR1 and BRD9 are unique features of ncBAF, a new member in the ubiquitously expressed SWI/SNF complexes.

2.3.3. Other SWI/SNF-related complexes

2.3.3.1. Cell-type-specific SWI/SNF complexes

I previously described the 3 mammalian SWI/SNF sub-complexes that were identified and characterized in a plethora of human cell lines. These sub-complexes are ubiquitous and abundantly expressed in all cells, they are pan-cell-type SWI/SNF complexes which are required in fundamental cellular processes such as transcription regulation, growth and development. However, at least 6 sub-complexes with lineage-specific functions were previously described in cardiac cells (cardiac BAF, containing BAF45C and BAF60C), neural progenitors (npBAF, containing BAF45A and BAF53A), neural cells (nBAF, containing BAF45B and BAF53B), hematopoietic stem cells (hscBAF) and ES cells (esBAF, containing BAF155 but not BAF170) (Klein and Hainer, 2020) . Another one of those cell-type-specific SWI/SNF may be the BRG1-containing WINAC complex (Figure 47).

In 1994, a 1.5 Mb heterozygous deletion of roughly twenty genes on chromosome 7 were identified in 100% of genetic screens of patients with Williams syndrome, a genetic disorder associated with intellectual disability, facial and cardiac developmental problems (Ewart *et al.*, 1994). Years later, Lu *et al.* identified one of those deleted genes which was Williams syndrome transcription factor (WSTF), a ubiquitously expressed protein important during development (Lu *et al.*, 1998). In mice, WSTF homozygous knockouts leads to premature neonatal death associated with severe heart defects (Yoshimura *et al.*, 2009). The WSTF (also called BAZ1B) protein belongs to the BAZ family and was described to interact with SWI/SNF ATPase BRG1 and BRM to form the WSTF-including nucleosome assembly complex (WINAC). This complex is a canonical SWI/SNF-related complex that contains the core SWI/SNF subunits BRG1, BAF170, BAF155, BAF60A, BAF250A and BAF53 together with WSTF, TOP2B, the CAF1 complex p150 subunit and the FACT complex p140 subunit (Barnett and Krebs, 2011a). DNA topoisomerase 2B (TOP2B) is an important enzyme for its role in controlling DNA topology during transcription and replication (Salceda, Fernández and Roca, 2006). The Facilitates chromatin transcription complex (FACT) was identified by the Reinberg group and is known to be

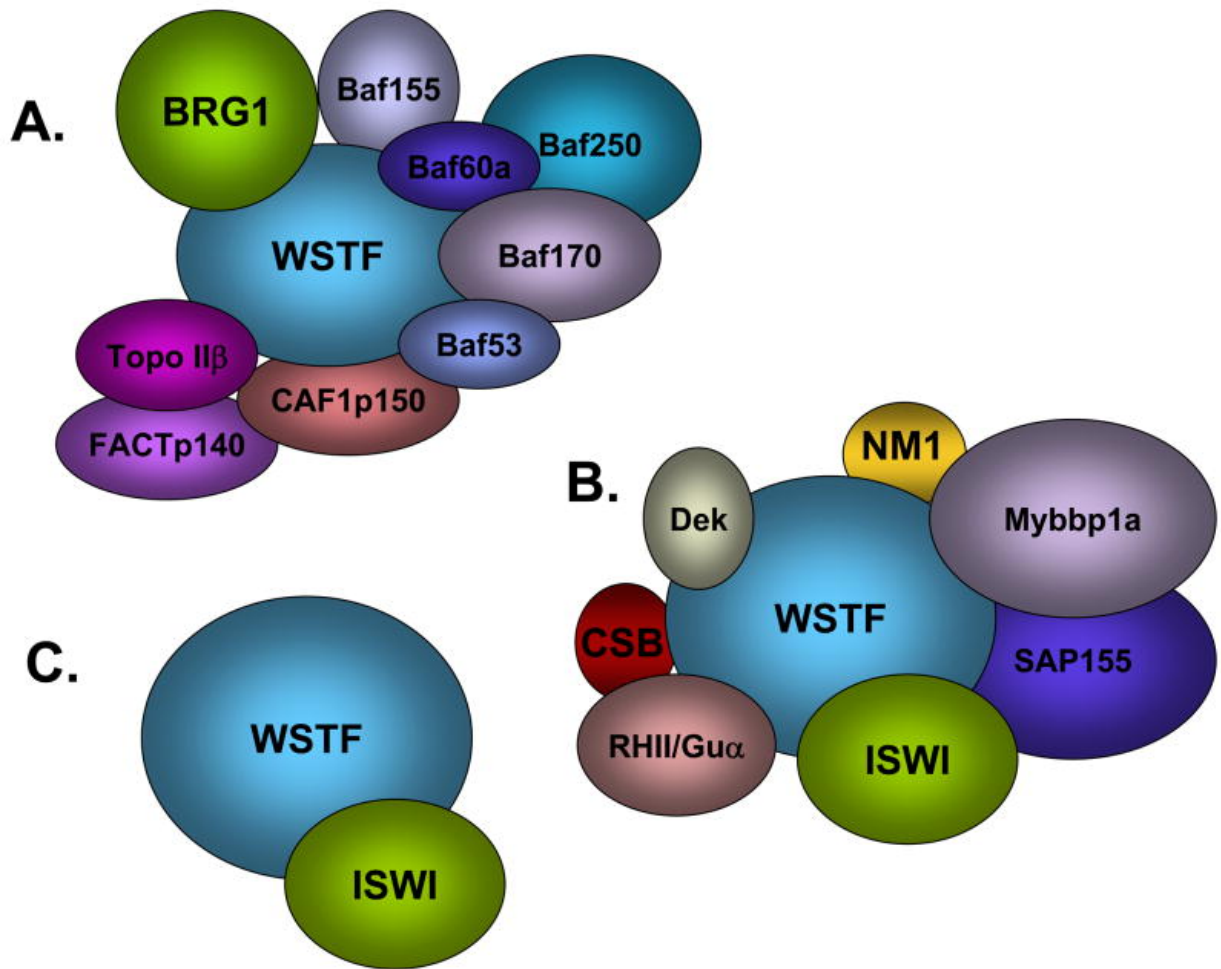


Figure 48. WSTF-containing chromatin remodeling complexes.

A. WINAC complex **B.** B-WICH complex **C.** WICH complex From Barnett and Krebs, 2011b.

essential for RNA polymerase II elongation (Belotserkovskaya *et al.*, 2003). The Chromatin assembly factor 1(CAF-1) was described for its involvement in chromatin assembly during DNA replication (Smith and Stillman, 1989). The chimeric WINAC complex has been shown in MCF7 cells to be involved in replication and transcription regulation through its chromatin assembly and remodeling activities. However, its role seems to be tightly related to the vitamin D receptor (VDR) targets, suggesting WINAC may only be a cell type-specific complex found in VDR-expressing lineages such as endocrine and gastrointestinal tissues (Figure 48).

2.3.3.2. Interplay with other chromatin remodelers

If the idea of a regulated interplay between different chromatin remodeling families seemed obvious in the tightly orchestrated cellular machinery, for a while evidence of such mechanism was lacking. In 2013, the Peterson group showed that DNA repair in yeast required the recruitment of both INO80 and SWI/SNF (Chambers *et al.*, 2012; Bennett, Papamichos-Chronakis and Peterson, 2013; Bennett and Peterson, 2015). A similar mechanism was found by (Ford, Odeyale and Shen, 2008) for the recruitment at the promoter of yeast INO1 gene, responsible for glucose metabolism, suggesting cooperativity between INO80 and SWI/SNF complexes. Another very recent study of the Clapier and Cairns group showed that the yeast RSC complex (homolog of human pBAF) preferentially binds to and ejects H2A.Z-marked nucleosomes (Cakiroglu *et al.*, 2019), which is a histone modification deposited by complexes of the INO80 family (Wang *et al.*, 2014; Latrick *et al.*, 2016; Brahma *et al.*, 2017; Shin *et al.*, 2018). This may represent a cooperative mechanism orchestrated by transcription factors responsible for sequential recruitment of these distinct chromatin remodelers in order to open the chromatin and allow transcription of stress-response genes (Sura *et al.*, 2017).

That being said, the interplay between remodelers is not always cooperative. As stated previously, the ISWI family is critical for nucleosome assembly and spacing, whereas SWI/SNF complexes are excellent nucleosome evictors and are known – at least in yeast – to be required in order to activate gene expression (Lorch and Kornberg, 2017). This functional antagonism was demonstrated by several independent studies conducted in yeast where genes such as RNR3 are repressed by ISWI

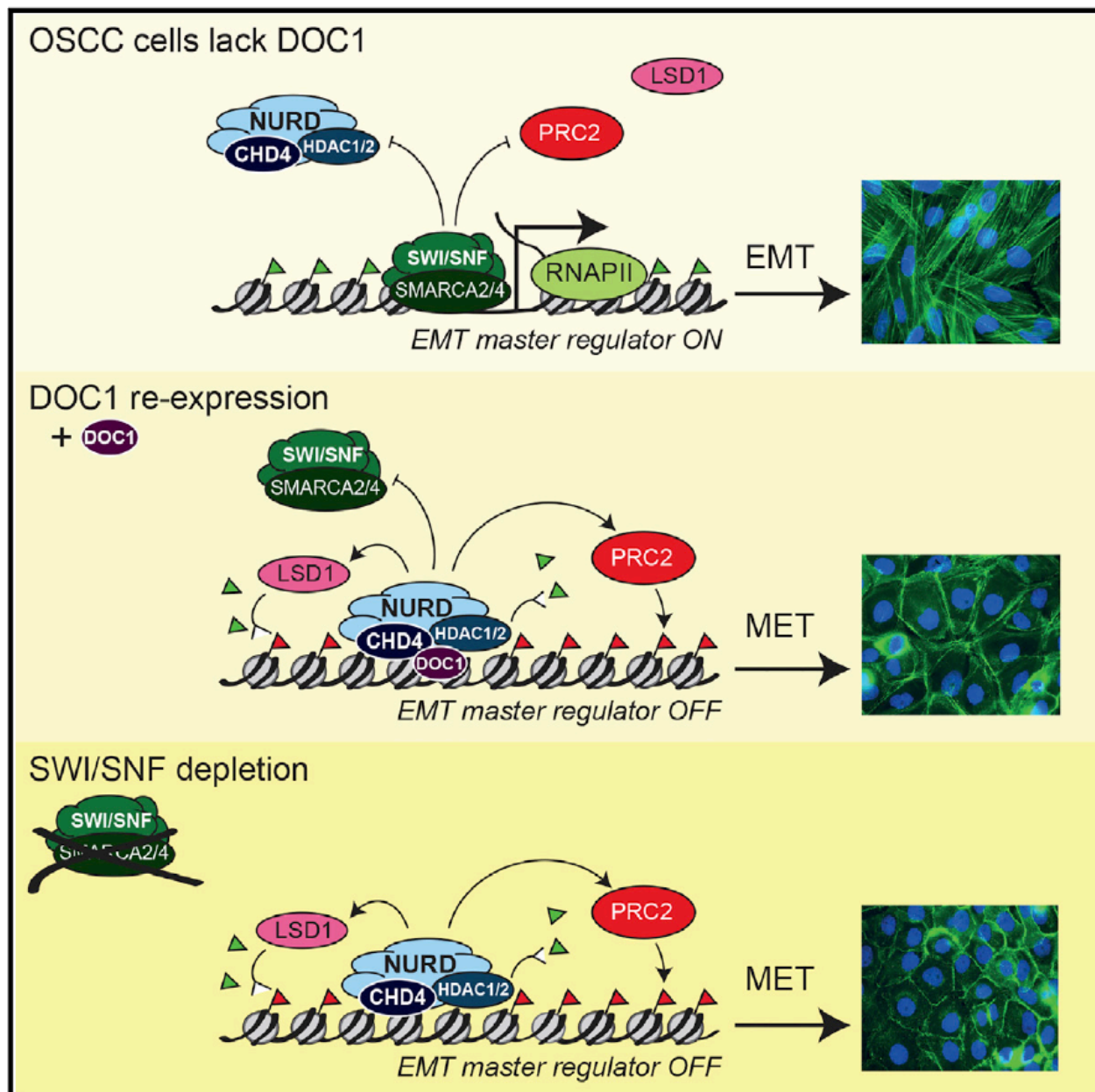


Figure 49. Crosstalk between NuRD and SWI/SNF complexes.

From Mohd-Sarip *et al.*, 2017.

complexes through nucleosome positioning at promoters which indirectly antagonizes SWI/SNF recruitment (Tomar *et al.*, 2009; Parnell *et al.*, 2015).

Similar antagonistic crosstalk has been discovered between NuRD complexes (CHD family) and SWI/SNF. As its name indicates, the NuRD subunit DOC1 was found to be lost in most human oral squamous cell carcinomas and correlated with tumor invasion and poor prognosis (Shintani *et al.*, 2001). Loss of DOC1 in oral cancers impacts NuRD recruitment to cell cycle and EMT genes. Work by Verrijzer group showed that at these specific loci, loss of NuRD recruitment results in SWI/SNF recruitment and formation of open chromatin which allows transcription. This indicates that NuRD mediates repression through both its histone deacetylation activity and by recruitment of the Polycomb complex and KDM1A (Mohd-Sarip *et al.*, 2017; Bracken, Brien and Verrijzer, 2019). This elegantly revealed the relevance of chromatin remodeling family crosstalk in cancer initiation and progression (Figure 49). Taken together, these works emphasize the emerging importance of chromatin balance in transcription control through cooperative and/or antagonistic interplay between different chromatin remodeling complexes.

2.4. Structure of the SWI/SNF family

2.4.1. Domain organization

SWI/SNF complexes are made up of a dozen subunits that harbor specific protein domains which all together influence the global activity of the complex. Given their high conservation between different species, this section will focus on analyzing the domain composition of the human SWI/SNF sub-complexes. Since the catalytic domains have already been extensively presented above, now other types contained in SWI/SNF responsible for complex assembly and targeting will be mentioned.

2.4.1.1. Interactome-related domains

Interactome-related domains are divided in two groups: domains that are critical for SWI/SNF complex formation; and domains responsible for interacting with signaling partner proteins. Structural subunits such as SMARCC paralogs or SMARCB1 contain coiled coil domain which allow oligomerization and protein-protein interaction, and were described to be important for SWI/SNF complex early assembly. Moreover, SMARCC subunits also have two domains: SWIRM, a small alpha-

SWI/SNF subunit	Domains
BRG1 or BRM	DNA-dependent ATPase, bromodomain, HSA, BRK, SnAC
BAF53 (A or B)	Actin fold
β -actin	Actin fold, ATPase
SNF5	SNF5 domain
BAF170	Chromo-related domain, SWIRM, SANT, Leucine zipper
BAF155	
BAF60 (A, B, or C)	SWIB/MDM2 domain
BAF57	HMG box
BAF45 (A, B, C, or D)	Tandem PHD domains, zinc finger
ARID (1A, 1B, or 2)	ARID/BRIGHT DNA binding domain
BCL7 (A, B, or C)	N-terminal conserved region
SS18 or CREST	N-terminal conserved region
BRD (7 or 9)	Bromodomain
PBRM1	Six bromodomains, BAH, HMG box
BCL11 (A or B)	Zinc fingers

Figure 50. Protein domains in each subunits of mammalian SWI/SNF complex.
From Hohmann and Vakoc, 2014.

helical domain of 85 amino acid residues and SANT which consist of 50 amino acids forming three alpha helix, both mediating protein-protein interaction, making them critical for complex formation. The former has been shown to be important for forming a complex between SMARCC subunits and the C-terminal SNF5 domain of SMARCB1, while the latter is involved in stabilizing the interactions between SMARCC subunits and the ATPase, BRM or BRG1. Another domain involved in interacting with the ATPase the SNH domain in SS18 which was shown to allow complexation with the ATPase.

Besides being important for complex assembly, several domains have been implicated in specific interactions with signaling partners and transcription factors. One example is the Requiem domain of DPF paralogs which was found to be a mediator between SWI/SNF and RELB involved in the NFkB pathway (Tando *et al.*, 2010; Huber *et al.*, 2017). The SAY domain, found exclusively in the pBAF-specific PHF10 subunit and not found in cBAF-specific DPFs, is responsible for interactions between the ARID2 subunit of pBAF and TAF5 subunit of the TFIID complex (Vorobyeva *et al.*, 2009). Another important domain is the LXXLL motif found in ARID subunits which have been shown allow interaction with nuclear receptors from the glucocorticoid family (Savkur and Burris, 2004; Sandhya *et al.*, 2018) (Figure 50).

2.4.1.2. Genome targeting-related domains

SWI/SNF complexes also contain a series of domains critical for its targeting, as their function is tightly related to the chromatin. These targeting domains can be subdivided according to their nature in two groups: nucleic acid binding and histone binding. The histone binding capacity of SWI/SNF was known since its discovery in yeast where mutations in histones disrupted its genome targeting (Cairns *et al.*, 1994; Peterson, Dingwall and Scott, 1994). For example bromodomains are 110-amino-acid protein domains able to recognize acetylated histone tails. These particular domains were first discovered in the *Drosophila* transcriptional activator gene *Brahma* which actually gave the name to the domain (Tamkun *et al.*, 1992; Shen *et al.*, 2007). Histone acetylation being mostly associated with active transcription, bromodomains of the ATPases may help target SWI/SNF to regions where nucleosomes need to be evicted to allow binding of the PIC complex. Other SWI/SNF subunits such as BRD7, BRD9

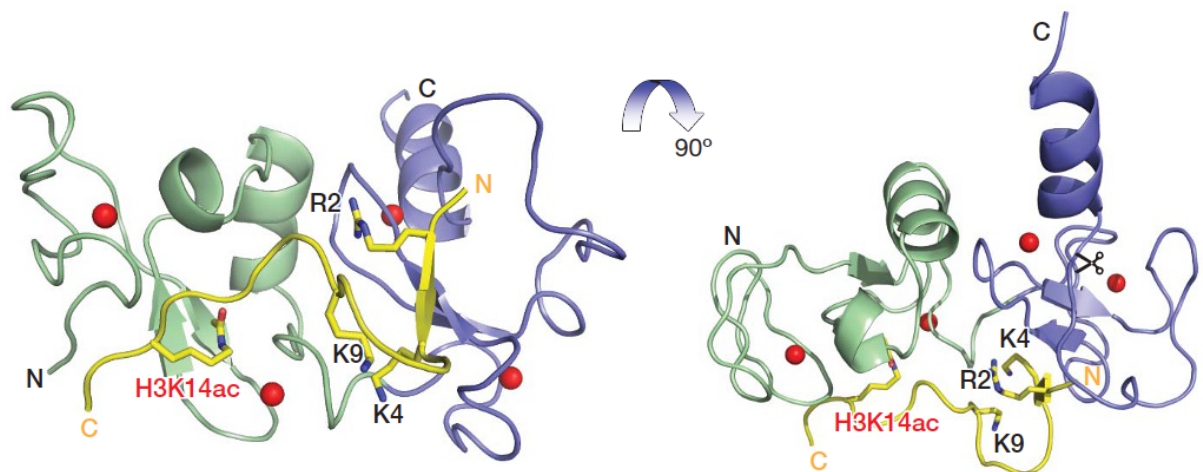
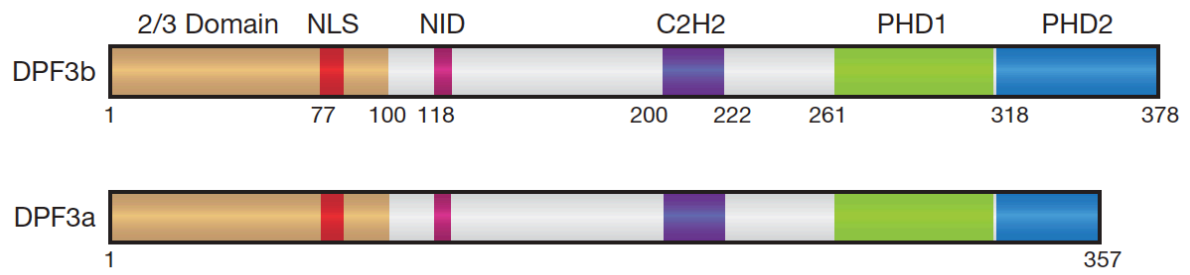


Figure 51. Domain organization of DPF3 proteins.

Domain organization of DPF3 proteins (upper) and NMR structure of the PHD12 bound to an H3K14ac peptide (lower). Red spheres are the zinc atoms. From Zeng *et al.*, 2010.

and PBRM1 also harbor one or several bromodomains, PBRM1 being the only known protein to contain six, although their precise role has not yet been elucidated (Filippakopoulos *et al.*, 2012).

Another important domain for histone binding is the C-terminal double PHD (plant homeodomain) found in PHF10 and DPF subunits. This specific domain was shown to recognize both acetylated and methylated histones such as H3K14ac and H3K3me3 (Zeng *et al.*, 2010; Palomera-Sanchez and Zurita, 2011) (Figure 51).

If for the sake of clarity, I clustered the SWI/SNF targeting domains as either histone binding or nucleic acid binding, this does not imply that these functions are always exclusive. Indeed, a recent paper from the Crabtree group revealed that the ATPase bromodomain binds to both histones and DNA simultaneously. They show that the histone-binding activity is not sufficient for nucleosome targeting *in vitro* and that the bromodomain also makes contact with DNA which stabilizes the interaction, together with the nearby AT-hook present in ATPases BRG1 and BRM (Morrison *et al.*, 2017). Other SWI/SNF subunits harbor DNA binding domains such as the AT-rich interaction domain of ARID1/2, the HMG boxes found in SMARCE1 and PBRM1, the SMARCB1 winged helix domain or the C2H2-type Krüppel zinc finger of DPF paralogs (Allen *et al.*, 2015; Sandhya *et al.*, 2018). Of note, these DNA-binding domains are generally capable of binding RNAs.

2.4.2. Combinatorial and modular assembly

2.4.2.1. SWI/SNF modular organization

Assembly of multiprotein complexes often occurs in a directed modular manner with defined and evolutionarily conserved subcomplexes (Marsh and Teichmann, 2015), however until recently this was unclear for SWI/SNF. In 2018, the Kadoch group published their BS3-crosslinked mass spectrometry results from human embryonic kidney cells (HEK293T) using DPF2 and SS18 as baits to identify the SWI/SNF intracomplex contacts. By Louvain two-nearest-neighbor analysis, they revealed that SWI/SNF complexes globally have a modular architecture. First, the ATPase module is composed of either SMARCA2 or SMARCA4 together with ACTB, one ACTL6 paralog (A or B) and one DPF paralog (1, 2 or 3). This module is responsible for the ATP-dependent chromatin remodeling activity and was shown to be sufficient *in vitro*. Second, the core module is critical for the assembly of holo-

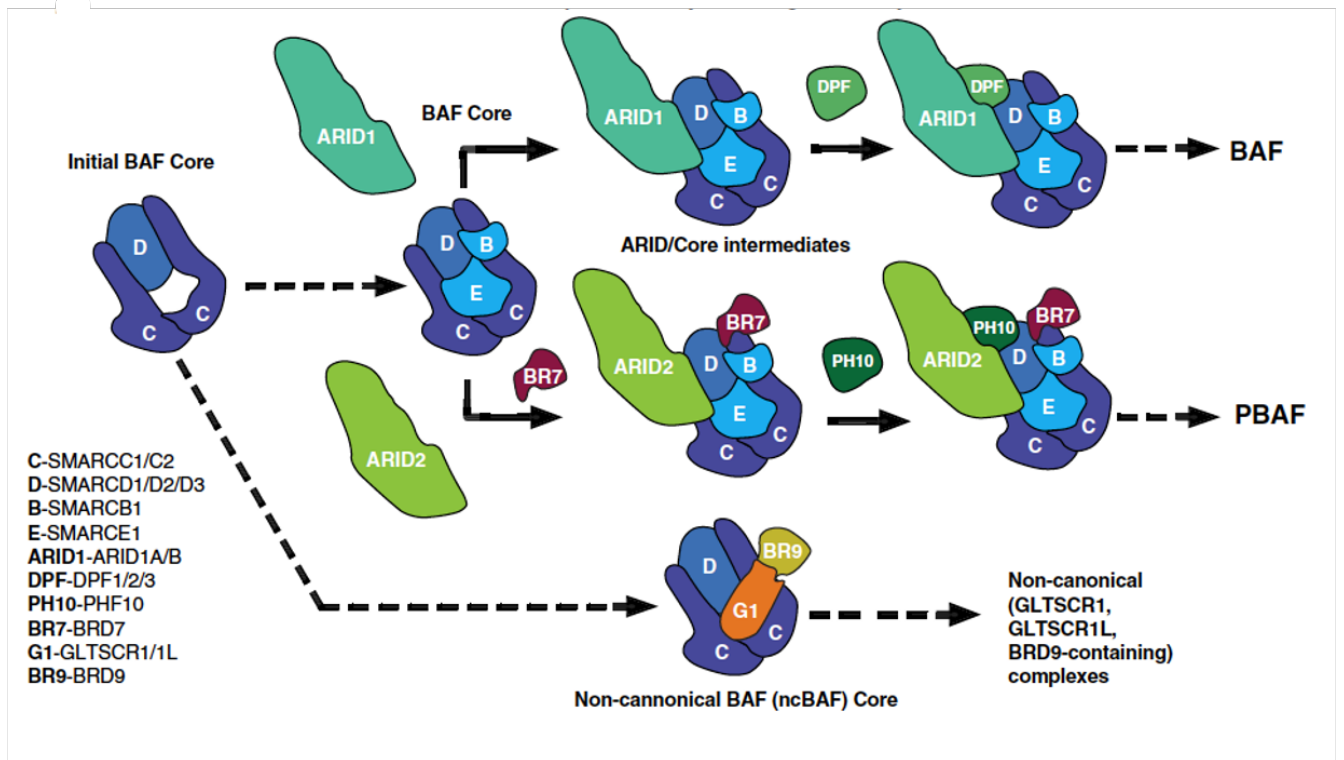
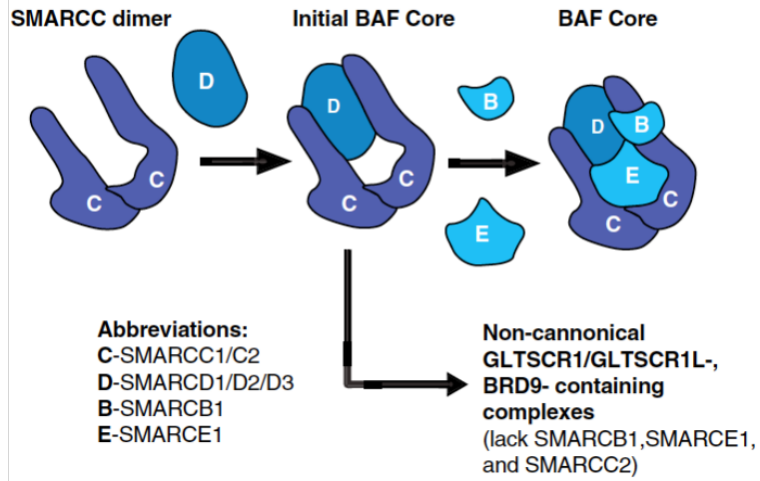


Figure 52. Modular organization of mammalian SWI/SNF complex.

Model for core formation (upper). Branching points of complex assembly (lower). From Mashtalir *et al.*, 2018.

SWI/SNF complexes and is defined by two copies of SMARCC paralogs (usually 1 and 2), one SMARCD1 paralog, SMARCE1 and one ARID paralog. The third and final module is SMARCB1 with one paralog of BCL7. They also conducted similar experiments in *Drosophila* and yeast, and showed highly conserved modularity for at least the ATPase module and the core module between all 3 species, underlying the functional relevance of such specific organization (Sen *et al.*, 2017). Consistent with these proteomic analysis, density sedimentation of SMARCD1-containing complexes spread across a gel gradient going from low-molecular weight free subunits to intermediate complexes and high-molecular weight fully-assembled SWI/SNF complexes. This highlights the existence of intermediate-molecular weight SWI/SNF modules in cells (Mashtalir *et al.*, 2018). A year later, another paper by the same group used the same proteomic approaches in small cell carcinoma of the ovary, hypercalcemic type (SCCOHT) cell lines, which are characterized by dual loss of both ATPase subunits, SMARCA2 and SMARCA4. Moreover, they revealed that in those cancer cells loss of ATPase subunits defined two groups of SWI/SNF subunits: those whose interactions were ATPase-dependent (ACTL6, BCL7, PBRM1 and SS18) and those whose interactions were ATPase-independent (SWI/SNF core module subunits). Thus they confirmed the existence of intermediate sub-complexes, consistent with the SWI/SNF modular organization. Functional characterization of these residual complexes revealed that these modules were not essential to SCCOHT cell proliferation (Pan *et al.*, 2019), in contradiction with previous hypothesis stating these aberrant SWI/SNF complexes may be directly driving oncogenesis (Hoffman *et al.*, 2014; Wilson *et al.*, 2014). However, it might be possible that these aspects may differ depending on the cell-type specific epigenetic landscape (Figure 52).

2.4.2.2. SWI/SNF assembly pathways

If the modular nature of SWI/SNF seemed conceivable early on in 1999 with the reconstitution by Phelan *et al.* 1999 of a minimal ‘core’ complex capable of chromatin-remodeling activity, the exact manner in which SWI/SNF complexes are formed was poorly understood. Besides revealing their modular architecture, the Kadoch group also characterized the assembly pathways of mammalian SWI/SNF sub-complexes cBAF, pBAF and ncBAF. To determine the order of assembly, they systematically deleted each SWI/SNF component using CRISPR-Cas9, removing all paralogs of a

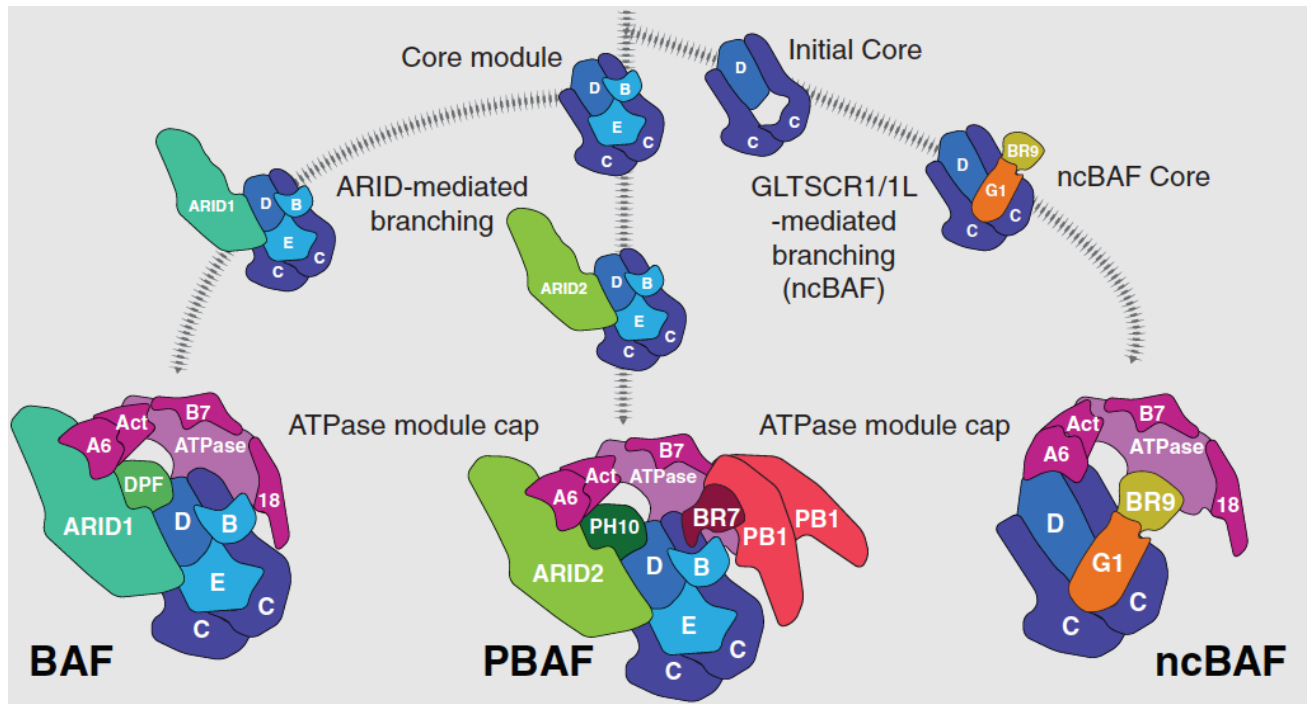


Figure 53. Mammalian SWI/SNF assembly pathways.

From Mashtalir *et al.*, 2018.

subunit whenever necessary as to avoid any structural redundancy. Serial immunoprecipitation and density sedimentation experiments followed with mass spectrometry revealed that deletion of SMARCC disrupts the formation of all SWI/SNF sub-complexes. Besides, by fluorometric analysis of purified complexes, they found that all components of SWI/SNF are present in a 1:1 stoichiometry, with the exception of SMARCC subunits (factor 1:1.6), indicating their dimerization.

These results revealed that the SWI/SNF complex initially starts forming around a dimer of two SMARCC paralogs (1 or 2 depending on the cell-type), after which one paralog of SMARCD will bind to that SMARCC dimer to form the 'initial SWI/SNF core' acting as a structural platform for the assembly of the complex. Then, a divergent point for the ncBAF sub-complex is the insertion of a GLTSCR1 paralog which primes the initial core towards adding more ncBAF-specific subunits. On the other hand, cBAF and pBAF continue their assembly with the addition of two core members: SMARCB1 and SMARCE1. At this point, the alternative incorporation of either one ARID1 paralog (A or B depending on the cell-type) or one copy of ARID2 will commit the core complex towards either forming cBAF or pBAF respectively. Canonical BAF final form (~1MDa) is achieved through addition of one DPF paralog (1, 2 or 3) and binding to this cBAF core platform of the ATPase module (containing BRG1 or BRM, ACTB, one SS18 paralog, one BCL7 paralog and one ACTL6 paralog). The formation of polybromo-BAF requires first the addition of BRD7 before PHF10 can bind and allow docking of the ATPase module. Final form of pBAF (~2MDa) is completed by the incorporation of 2 copies of PBRM1 subunits on the ATPase module. Formation of final ncBAF complex (~0,9MDa) follows an alternative routine, after addition of GLTSCR1 paralog, BRD9 binds to this ncBAF core before docking of the ATPase module. Therefore, the existence of multiple paralogs across these three complexes increases the diversity of SWI/SNF with an estimated total of 1452 possible combinations (cBAF: 1296, pBAF: 108, ncBAF: 48). Similar studies in yeast have shown this sequential and modular assembly to be conserved through evolution (Mashtalir *et al.*, 2018) (Figure 53).

2.4.3. Towards resolving SWI/SNF structure

To gain insights into the functions of SWI/SNF complexes, researchers have been studying the structure of all its components separately since the identification and the purification of yeast SWI/SNF

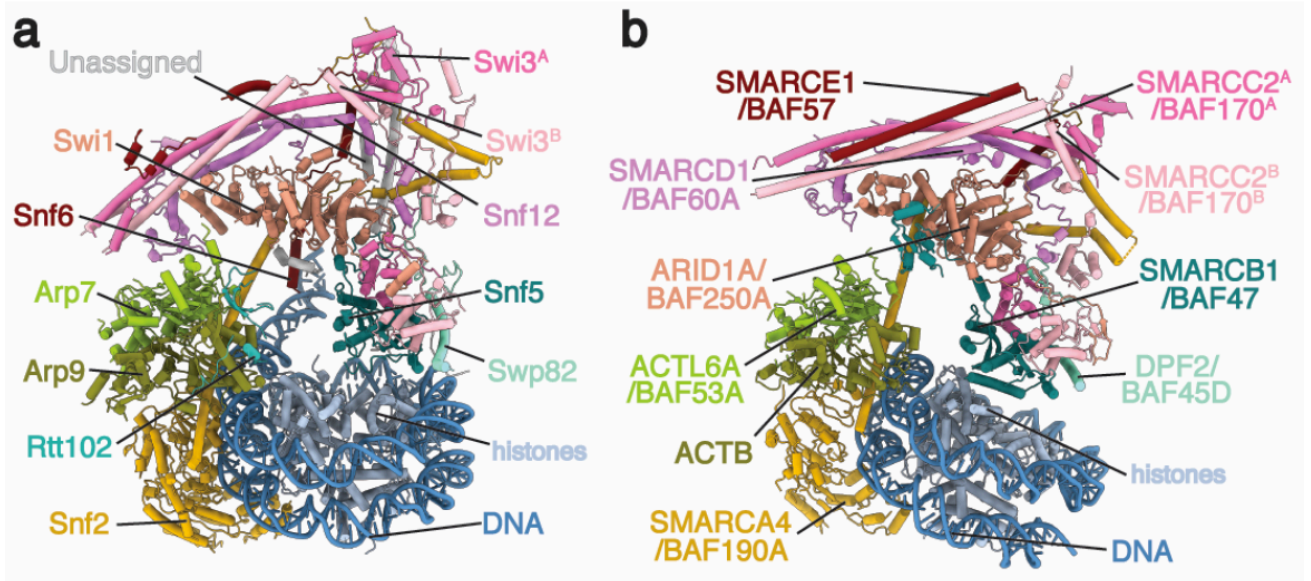


Figure 54. Yeast SWI/SNF and human BAF complex.

Comparison between **a.** yeast SWI/SNF and **b.** human BAF complex. From Marcum *et al.*, 2020.

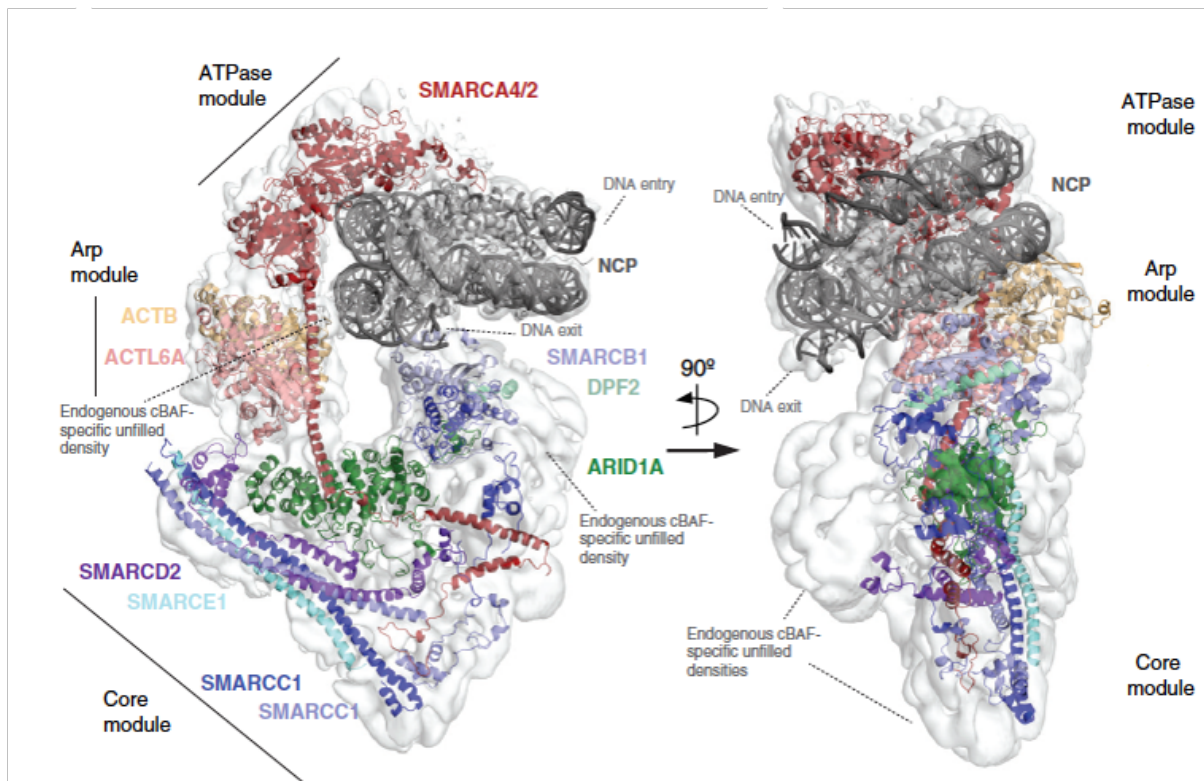


Figure 55. Model of the interaction of BAF complex with nucleosome core particle (NCP).

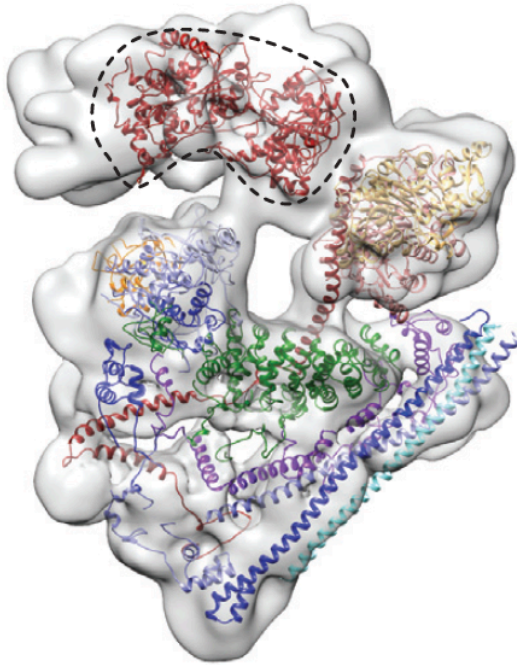
From Mashtalir *et al.*, 2020.

by Cairns *et al.* Several teams have attempted to look at the bigger picture and studied the structure of the whole complex (Asturias *et al.*, 2002; Chaban *et al.*, 2008; Dechassa *et al.*, 2008). However, only low resolution structures were available for almost a decade, researchers achieving higher resolution only for fragments such as the yeast ATPase module (Schubert *et al.*, 2013). Resolving the structure of SWI/SNF would have tremendous impact on many fields where its function is deregulated.

Recent cryo-EM studies allowed the visualization of yeast and human SWI/SNF complexes revealing the intriguing manner in which they engage with the core nucleosome (Patel *et al.*, 2019; Ye *et al.*, 2019; Han *et al.*, 2020; He *et al.*, 2020; Wagner *et al.*, 2020). Structural similarities between yeast and human SWI/SNF include; 1) the engagement of the ATPase with nucleosomal DNA on superhelical location 2 (SHL2) position (roughly 20 base pairs downstream of the nucleosome dyad); 2) contacts between the H2A/H2B acidic patch of the nucleosome and subunits of the core module containing positively charged residues; and 3) the ‘sandwiching’ of the nucleosome by two modules: one containing the ATPase and another composed of the core module, both being connected by the ARP module (Figure 54 and 55).

In humans, this tripartite engagement of the nucleosome, also known as ‘nucleosome C clamp’ was observed by high-resolution structural analyses of human recombinant SWI/SNF complex by (He *et al.*, 2020) and an endogenous model by (Mashtalir *et al.*, 2020). The nucleosome was shown to interact with both the C-terminal α -helix of SMARCB1 and the C-terminal SnAC ATPase domain of SMARCA2/4. These two modules are bridged by the ARP module comprising actin and ACTL6A via the HSA domain of SMARCA4, which is stabilized by interactions with the ARID subunit. The core module includes SMARCB1, SMARCE1, two SMARCC subunit, one DPF paralog, one SMARCD subunit and is stabilized by the Armadillo (ARM) domain of the large ARID subunit. While the core module forms the rigid scaffold unit within SWI/SNF, the ARP and ATPase modules seem to be more flexible and allowed remodeling activity by changing conformation. In fact, both structural and crosslinked mass spectrometry evidence seem to suggest that the ATPase module has to rotate as to create enough space for the nucleosome to dock on the core module. Next, SMARCA4 and SMARCB1 forms the clamp-like structure around the nucleosome, and further ATP hydrolysis results in another

BAF complex (unbound,
free state)



BAF complex (NCP-bound state)

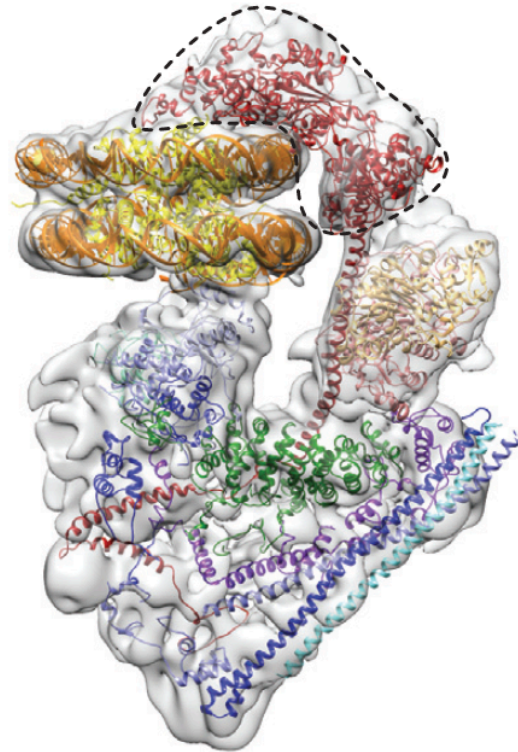


Figure 56. Cryo-EM maps of BAF-NCP.
From Mashtalir *et al.*, 2020.

change of conformation which pumps the DNA toward the nucleosome dyad and generates DNA translocation and then remodeling (Figure 56).

These insights into the ultrastructure of SWI/SNF allowed to enhance our understanding on the role of each subunit within the complex; which in part explain the higher frequency of mutations seen for some subunits such as ARID1A or BCL7A. The latter is recurrently mutated in lymphoma (Baliñas-Gavira *et al.*, 2020). The endogenous structure by (Mashtalir *et al.*, 2020) showed that BCL7A interacts with the ATPase module and the nucleosome and they suggested that it may act as a binding platform for specific TFs. Yet, to this day it remains unclear how BCL7 paralogs fit into the complex and how they contribute to oncogenesis.

2.5. Known biological functions of SWI/SNF remodelers

2.5.1. Functional dynamics of SWI/SNF complexes

2.5.1.1. Global and tissue-specific functions

Insights into the structure and modular assembly of SWI/SNF shed light on the potential difficulty to define a global role for the complex. With roughly 1500 different combinations, the SWI/SNF complex might be extremely heterogeneous *in vivo* and different compositions can result in distinct functional output. One good example is the current debate regarding the association between SWI/SNF mutations and the clinical response to immunotherapy. A landmark study published in Science showed that inactivation of PBAF-specific subunits PBRM1, ARID2 and BRD7 in murine melanomas lead to activation of the interferon γ -JAK-STAT pathway and overexpression of PDL1 on tumor cell surface (Pan *et al.*, 2018). In turn, the authors found that this was associated with enhanced secretion of chemokines that recruit cytotoxic T cells and thus better response anti-tumoral response. Several clinical studies confirmed this and found an association between PBRM1 loss and response to anti-PD1 immunotherapy in metastatic clear cell renal cell carcinoma, a type of kidney cancer with recurrent PBRM1 mutations (Miao *et al.*, 2018; Braun *et al.*, 2019). However, no positive association was found in a study on non-small cell lung cancer (NSCLC) (Zhou *et al.*, 2020), where the authors even concluded that PBRM1 mutations were predictive of resistance to anti-PD1 therapies.

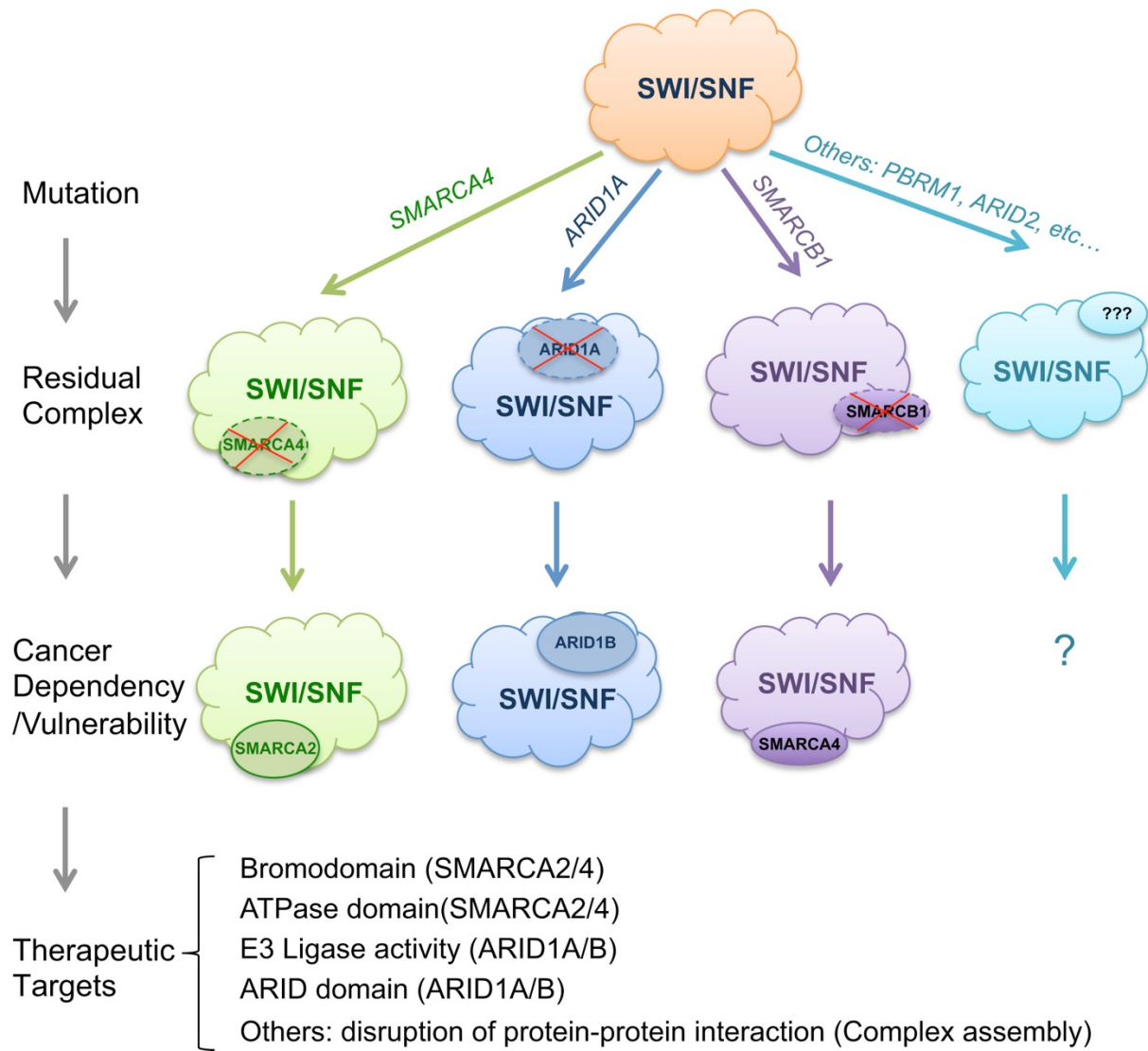


Figure 57. Vulnerability of mutant SWI/SNF complexes in cancer.

From Helming, Wang and Roberts, 2014.

A potential cause of these divergent observations may be related to differences in clinical study design. However, an important factor to take into account is tissue- or cell specificity. Tissue specificity may exert fundamental influence on gene expression through 1) expressing specific transcription factors, 2) establishing a unique epigenetic landscape (chromatin state); 3) expressing distinct SWI/SNF paralogs. It is well established that TFs and epigenetic marks are two important mechanisms for recruiting the SWI/SNF complex which may explain differences in function. However, another layer of complexity is added by the SWI/SNF genes expression patterns in different tissues but also at different stages of development. For instance, the expression of BCL11 paralogs is generally very low except in specific cells such as neurons and most hematopoietic cells (Yu *et al.*, 2012). It is often overexpressed in acute myeloid leukemia (AML) where it was found to inhibit p53 and lead to activation of cell cycle. Many SWI/SNF subunits have been described to mediate specific interactions with TFs or histone marks, thus tissue specificity may result in functional discrepancies.

2.5.1.2. Cooperative or antagonizing compensation?

While the SWI/SNF ATPases SMARCA2 and SMARCA4 share 75% sequence identity and have in common their mechanism of action for chromatin remodeling, they do not integrate the complex together. Virtually all SWI/SNF paralogs share this feature of being mutually exclusive within the complex. For instance, large-scale screens for cancer vulnerabilities (Project Achilles) found that tumor cell lines with ARID1A loss become dependent of its paralog ARID1B (Cheung *et al.*, 2011; Helming, Wang and Roberts, 2014) (Figure 57). Authors found that in tumors bearing ARID1A loss, targeting ARID1B might represent a potential therapeutic target. Furthermore, SMARCB1-deficient rhabdoid tumors were shown to be dependent on alternative BRD9-containing SWI/SNF complexes (ncBAF) and proliferation of these tumors was abrogated when treating a drug capable of specifically degrading BRD9 protein *in vivo* (dBRD9) (Michel *et al.*, 2018). Other synthetic lethalties such SMARCC1-SMARCC2, SMARCA4-ARID2 and SMARCA4-SMARCA2 were recently also described in a large-scale screen in cancer SWI/SNF knockout cell lines (Schick *et al.*, 2019). In the same study, the authors reported that loss of paralogous subunits such as SMARCA2/4 occupying the same key positions within

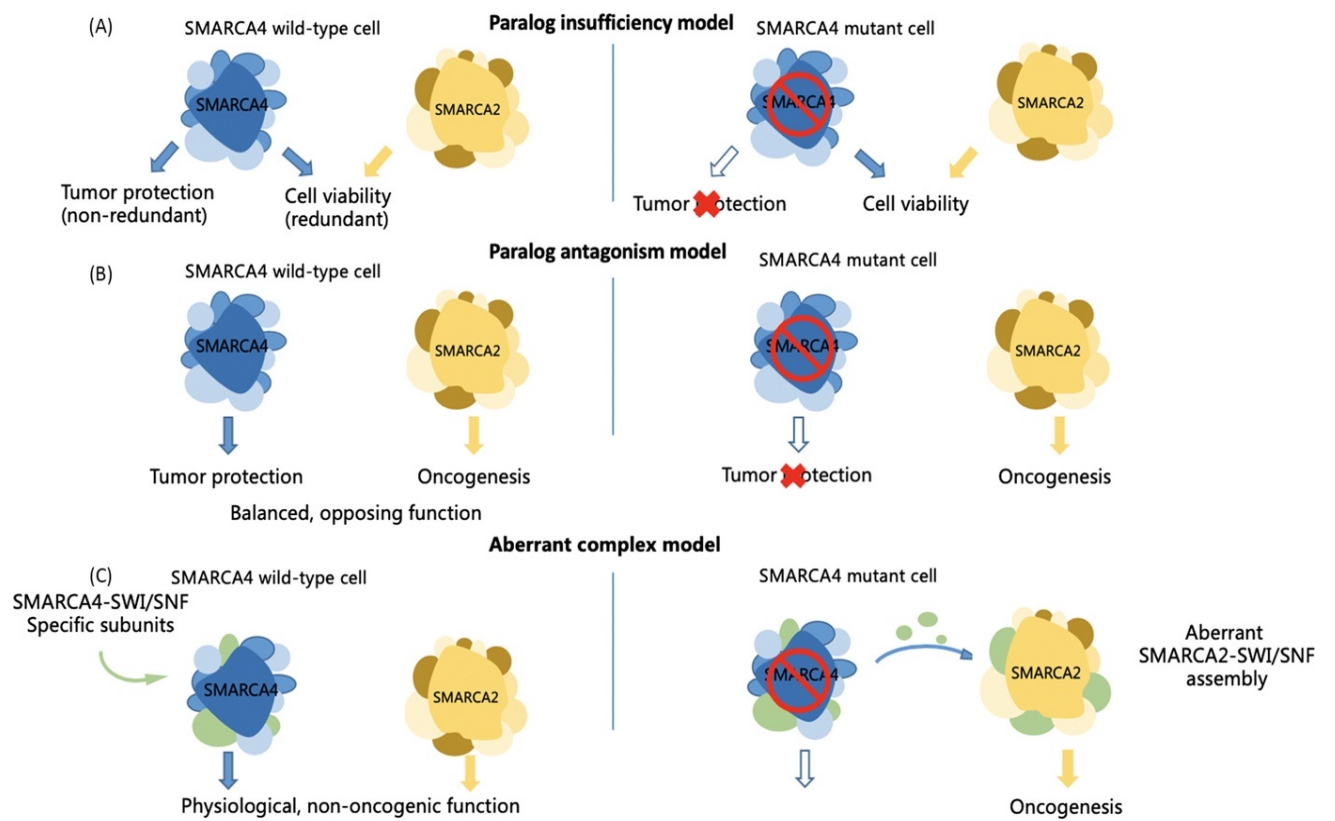


Figure 58. Hypothetical models of BRM-SWI/SNF function in BRG1-mutant cancers.

From Hu *et al.*, 2020.

the complex are compensated by increased expression and incorporation of the remaining paralogs. These findings are of importance as they show the dynamics of SWI/SNF compensation, which could drive tumorigenesis (Mittal and Roberts, 2020). Currently, three models were proposed to explain how the ATPase subunits may contribute to tumorigenesis (Hu *et al.*, 2020): the paralog insufficiency, the paralog antagonism and the aberrant complex model.

Paralog insufficiency. In the paralog insufficiency model, both ATPases have overlapping (cell cycle) but also distinct functions (tumor suppression). When the ATPase that has tumor-suppressor function is lost, the other ATPase incorporates within more SWI/SNF complexes and drives its targets (cell cycle) which leads to oncogenesis due to lacking tumor-suppressor program.

Paralog antagonism. In this model, both ATPases have antagonistic functions such as tumor-suppression and oncogenesis. In the normal context, both ATPases are expressed which maintains a balance of opposing programs within cells. However, if the ATPase that has tumor-suppressor activity is mutated and lost, cells have too much oncogenic signals which leads to cancer.

Aberrant complex. This model states that both ATPases have preferential interactions with specific SWI/SNF subunits which in the physiological context is necessary for maintaining a diverse transcriptional program. However, when one ATPase is lost, subunits of that subcomplex might try to incorporate and perhaps replace other mutually exclusive paralogs within the remaining ATPase subcomplexes and thus drive an aberrant oncogenic program. This model has been favored in several studies notably in pediatric rhabdoid tumors where SMARCB1 loss was shown to drive oncogenesis through a residual aberrant SWI/SNF complex (Sen *et al.*, 2017) (Figure 58).

However, while we know that SMARCA2/BRG1 and SMARCA4/BRM compensate for each other within SWI/SNF (Willis *et al.*, 2012), it is still largely unknown how much of their functions are redundant and if they may perhaps have antagonistic programs. One important paper by (Raab *et al.*, 2019) tried to tackle this question and they concluded that BRG1 and BRM genome binding sites largely overlap in HepG2 cells. Yet, although they bind to the same loci, they can have antagonistic effects on transcription. For instance, by integrating their ChIP-seq and RNA-seq data, they revealed that in loci where both ATPases colocalized distinct effects result from silencing BRG1 or BRM. For example, siRNA-mediated BRG1 silencing leads to activation of TNF α pathway by BRM, and *vice versa* when

BRM was silenced, BRG1 upregulates fatty acid metabolism which is normally repressed by BRM. They explain this by a model in which both ATPase have specific interactions between each other and with site-specific cofactors that mediate either activation or repression on a given gene loci (Wang *et al.*, 2018; Raab *et al.*, 2019). Yet, the fact that BRM could drive oncogenesis in tumors with BRG1 loss is still debated (Jancewicz *et al.*, 2019).

2.5.2. Role in development and differentiation

Historically, SWI/SNF complexes have also been involved in cell cycle due to the interaction with the Retinoblastoma protein (Rb) which is a major G1/S checkpoint regulator (Muchardt and Yaniv, 2001). Furthermore, SWI/SNF subunits have been shown to be essential for murine development as inactivation of BRG1, BAF47, BAF155, BAF60C, or BAF180 are embryonic lethal. Strikingly, BRM inactivation in mice produces only mild effects (Reyes *et al.*, 1998). Studies indicate that SWI/SNF enzymes are required for both embryonic stem cell pluripotency as well as cellular differentiation (De La Serna, Ohkawa and Imbalzano, 2006; Hota and Bruneau, 2016) (Figure 59).

Neural development. As mentioned above, SWI/SNF genes is involved in both neural and glial development where their expression is the highest in mammals (Matsumoto *et al.*, 2006; Marathe *et al.*, 2013). Besides the paralogous switch between npBAF (neural progenitor-BAF) towards nBAF (neural-BAF) complexes that I described previously, the role of SWI/SNF was also described to be mediated by specific TFs. For instance, BRG1 was shown to be interact with SOX10 via its BAF60A subunit which results in targeting to enhancers of genes encoding Schwann cell differentiation and maturation (Weider *et al.*, 2012; Bischof *et al.*, 2015). Consistently, many SWI/SNF mutations are associated with intellectual disabilities such as Coffin-Siris and Nicolaides-Baraitser syndromes (Mari *et al.*, 2015) (Figure 60).

Neural crest cells development. In the zebrafish model, Brg1-mutated embryos showed defects in the development of pigment cells and retina, the tissues expressing MITF. This work suggests that Brg1 is involved in neural crest induction, and consequently in the development of neurons, glia, and pigment cells (Eroglu *et al.*, 2006). In mammals, SWI/SNF chromatin remodeling enzymes play an important role in the promotion of activation of melanocyte specific genes by cooperating with MITF. MITF promotes

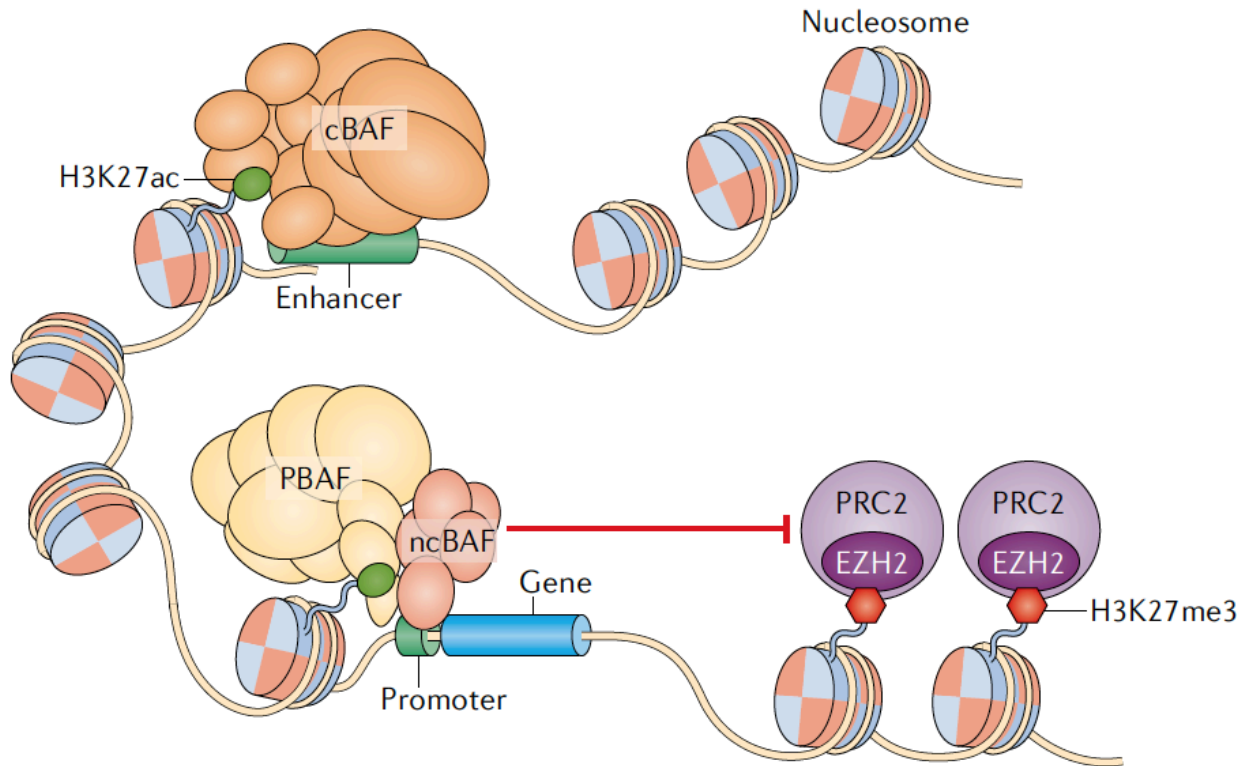


Figure 61. Function antagonism between SWI/SNF and PRC2 Polycomb complexes.

From Mittal and Roberts, 2020.

the recruitment of SWI/SNF to target genes involved in the synthesis of melanin pigment by remodeling the chromatin structure (De La Serna, Ohkawa and Imbalzano, 2006; Keenen *et al.*, 2010; Laurette *et al.*, 2015).

Muscle differentiation. The SWI/SNF complex has been described as a key regulator of skeletal muscle differentiation, especially BRM and BAF60C interact with myogenic factors such as MYOD1 to activate required gene expression programs at different stages of skeletal myogenesis (Cohet *et al.*, 2010; Albini *et al.*, 2015). Furthermore, BRG1 is a critical regulator of cardiomyocyte gene expression and differentiation as deletion of Brg1 in mice leads to abnormalities in cardiac morphogenesis (Takeuchi *et al.*, 2011). Other subunits are involved in the cardiomyocyte differentiation and cardiac morphogenesis such as ARID1A, ARID2, PBRM1 and BAF60C. Similarly to neural differentiation, SWI/SNF paralogs switches are used as pivotal developmental tools as ectopic expression of BAF60C in developing embryos, instead of BAF60A, leads to beating cardiomyocytes (Klein and Hainer, 2020).

Immune cell development. SWI/SNF influence the development of various immune cell types by controlling the differentiation of hematopoietic stem cells (HSCs) to different B- and T-cell lineages (Bultman *et al.*, 2006; Vradii *et al.*, 2006). BRG1 and the core subunit SMARCC1 have been implicated in regulating early stages of B-cell development as their inactivation leads to defective cell proliferation and differentiation (Choi *et al.*, 2012).

Since its discovery, the role of SWI/SNF has always been intertwined with that of the Polycomb repressive complexes (PRC) (Ingham, 1983; Jürgens, 1985). Accumulating evidence show that both complexes have antagonistic functions during development which are conserved in drosophila and mammals (Kadoch *et al.*, 2017; Stanton *et al.*, 2017). Furthermore, recent studies revealed that 1) a high concentration of SWI/SNF complexes is required to oppose PRC-mediated repression in vivo (Vaart *et al.*, 2020); and 2) mechanistically, the antagonism might be mediated through eviction of core PRC2 component EED by SWI/SNF subunit DPF2 (Zhang *et al.*, 2019). These studies were particularly informative about the role of SWI/SNF under physiological conditions and provided an explanation for SWI/SNF complex deficiency in some cancers, such as SMARCA-deficient sarcoma, rhabdoid tumors or synovial sarcoma (Alfert, Moreno and Kerl, 2019) (Figure 61).

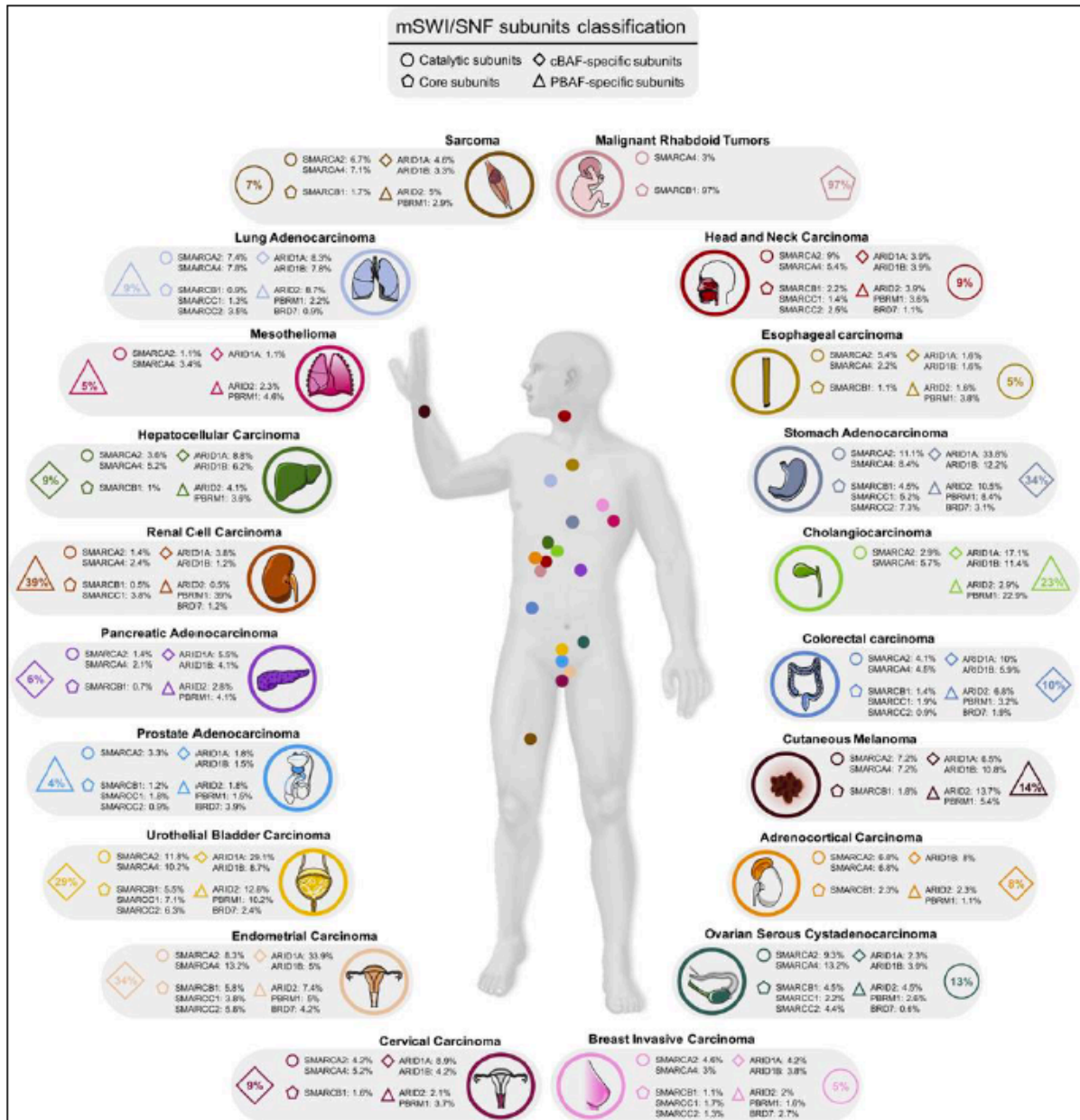


Figure 62. Mutation rate of mammalian SWI/SNF subunits.

From Chabanon, Morel and Postel-Vinay, 2020.

2.5.3. Role in cancer

As a regulator of differentiation and proliferation, SWI/SNF was found to be implicated in cancer. Mutations in at least nine SWI/SNF genes have been found in nearly 25% of human cancers (Kadoch *et al.*, 2013; Shain and Pollack, 2013; Vangamudi *et al.*, 2015) (Figure 62). This suggested that the complex might act as a tumor-suppressor, which is likely attributable to its role in facilitating the binding of specific TFs regulating differentiation, cell cycle and DNA repair (Mittal and Roberts, 2020). One of the most well-studied mechanisms of tumor-suppressor function comes from the biallelic inactivation of SMARCB1 in virtually 100% of malignant rhabdoid tumors (MRT) where SWI/SNF was shown to regulate the binding of Polycomb on differentiation and mitosis genes (Versteeg *et al.*, 1998; Roberts *et al.*, 2000; Wilson *et al.*, 2010).

SMARCB1, but also SMARCA4, are considered as ‘defining features’ for some types of cancers. SMARCB1 mutations are found in virtually all MRTs, atypical/rhabdoid tumors (ATRTs), epithelioid sarcomas and renal medullary carcinoma (RMC). SMARCA4 mutations are the hallmark of SMARCA4-deficient thoracic and uterine sarcomas, SMARCA4-deficient rhabdoid tumors and small cell carcinoma of the ovary, hypercalcemic type (SCOOHT). Germline mutations of SMARCA4 are also implicated in hereditary cancer syndrome (Connor *et al.*, 2020). Of note, SMARCA4-deficient tumors were reported to harbor concomitant loss of SMARCA2 (Jelinic *et al.*, 2016), however it is unknown if it is also the case of SMARCB1-deficient tumors. Importantly, both SMARCA4- and SMARCB1-deficient tumors have been described as bearing generally low mutation burden (Mittal and Roberts, 2020). However, the most commonly affected SWI/SNF subunits are ARID1A and ARID2. ARID1A mutations are frequent in ovarian cancers, whereas ARID2 are found mostly in melanomas (Pierre and Kadoch, 2017). Mutations of these subunits is mostly associated with loss-of-function which was proposed to lead to destabilization of the SWI/SNF core module (Mashtalir *et al.*, 2018). Yet, it is unclear to what extent these mutations are directly causing tumorigenesis as some cases present concomitant loss of the tumor-suppressor p53 (Shain and Pollack, 2013).

The role of SWI/SNF in cancer is not just limited to loss-of-function mutations. An excellent example of acquired oncogenic properties of the SWI/SNF complex was revealed by the discovery of

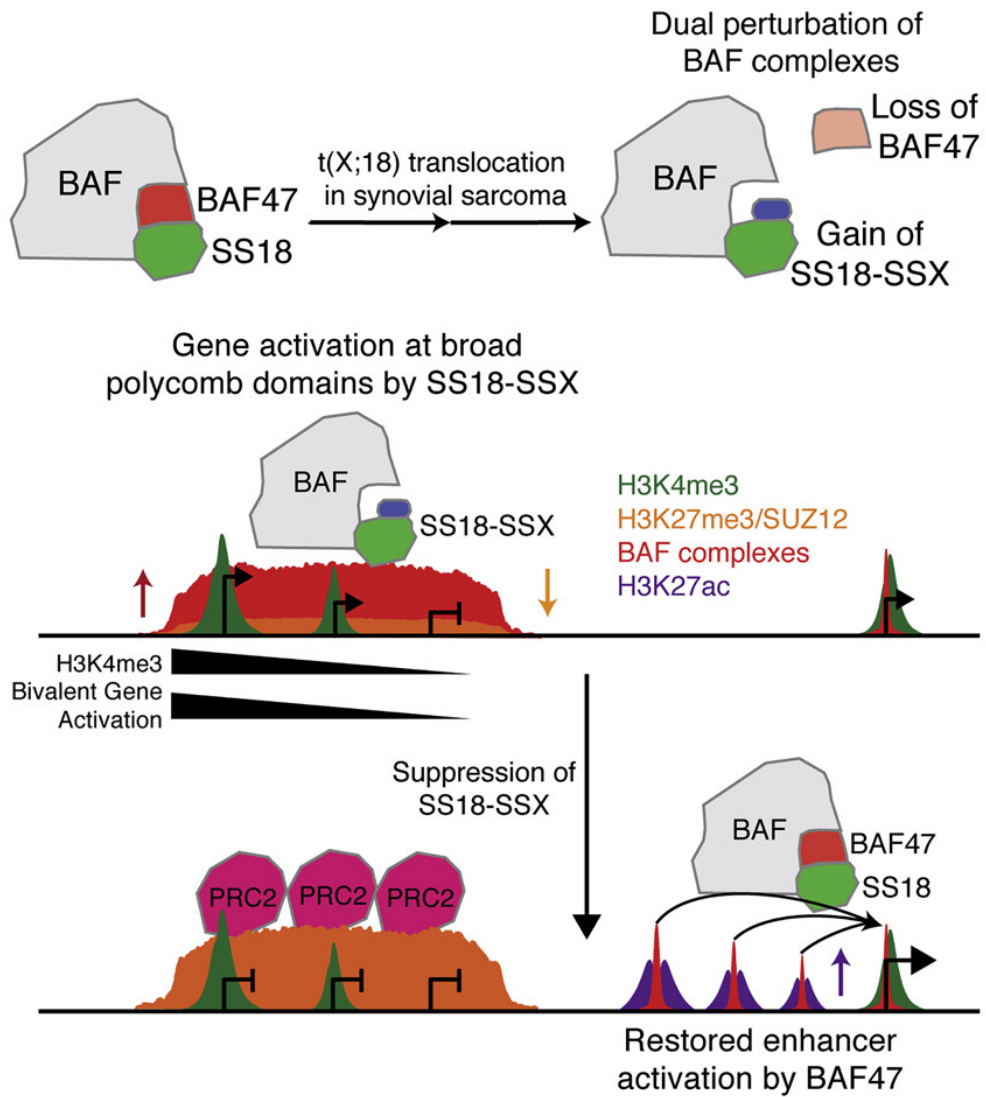


Figure 63. Competition of SS18-SSX fusion protein with the normal SS18 subunit for incorporation into the SWI/SNF complex.

From Kadoch and Crabtree, 2013.

SS18-SSX fusion protein. SS18 is the last characterized SWI/SNF subunit to date (Kadoch and Crabtree, 2013). The SS18 gene was first identified in synovial sarcoma in which a chromosomal translocation provoked the fusion of SS18 (chr8) to SSX (chrX) (Clark et al., 1994). In their landmark study, Kadoch and Crabtree demonstrated that the SS18-SSX fusion protein competes with the normal SS18 subunit for incorporation into the SWI/SNF complex. As a result, and likely owing to the large size of the fusion protein, the BAF47 subunit is evicted from the aberrant complex and subsequently degraded which was thought to give rise to oncogenesis in a loss-of-function manner similar to MRTs (Kadoch and Crabtree, 2013). However, a few years later, the Kadoch group demonstrated that SS18-SSX incorporation within the SWI/SNF complex leads to a gain-of-function of the complex with a global retargeting towards oncogenes that was driven by SSX DNA-binding domain (McBride *et al.*, 2018) (Figure 63).

**Chapter III. Mechanisms of cancer: insights
into renal medullary carcinoma and melanoma**

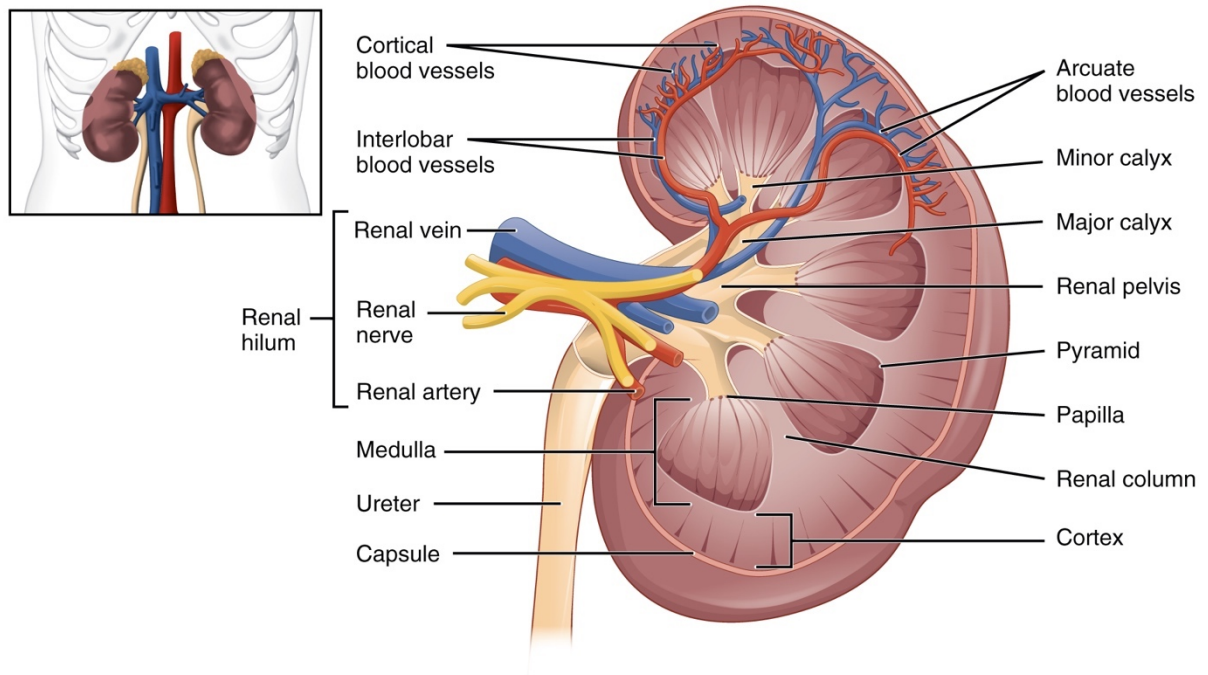


Figure 64. Anatomy of the kidney.

From <https://opentextbc.ca/anatomyandphysiology/chapter/25-3-gross-anatomy-of-the-kidney/>.

Chapter III. Mechanisms of cancer: insights into renal medullary carcinoma and melanoma

3.1. Renal Medullary Carcinoma

This chapter will focus on a rare type of kidney cancer called renal medullary carcinoma (RMC). Where does it come from and does it progress? To answer these questions, the anatomy of kidney and the putative cell-of-origin of RMC will first be discussed before diving deeper into the mechanisms of the genesis of the disease.

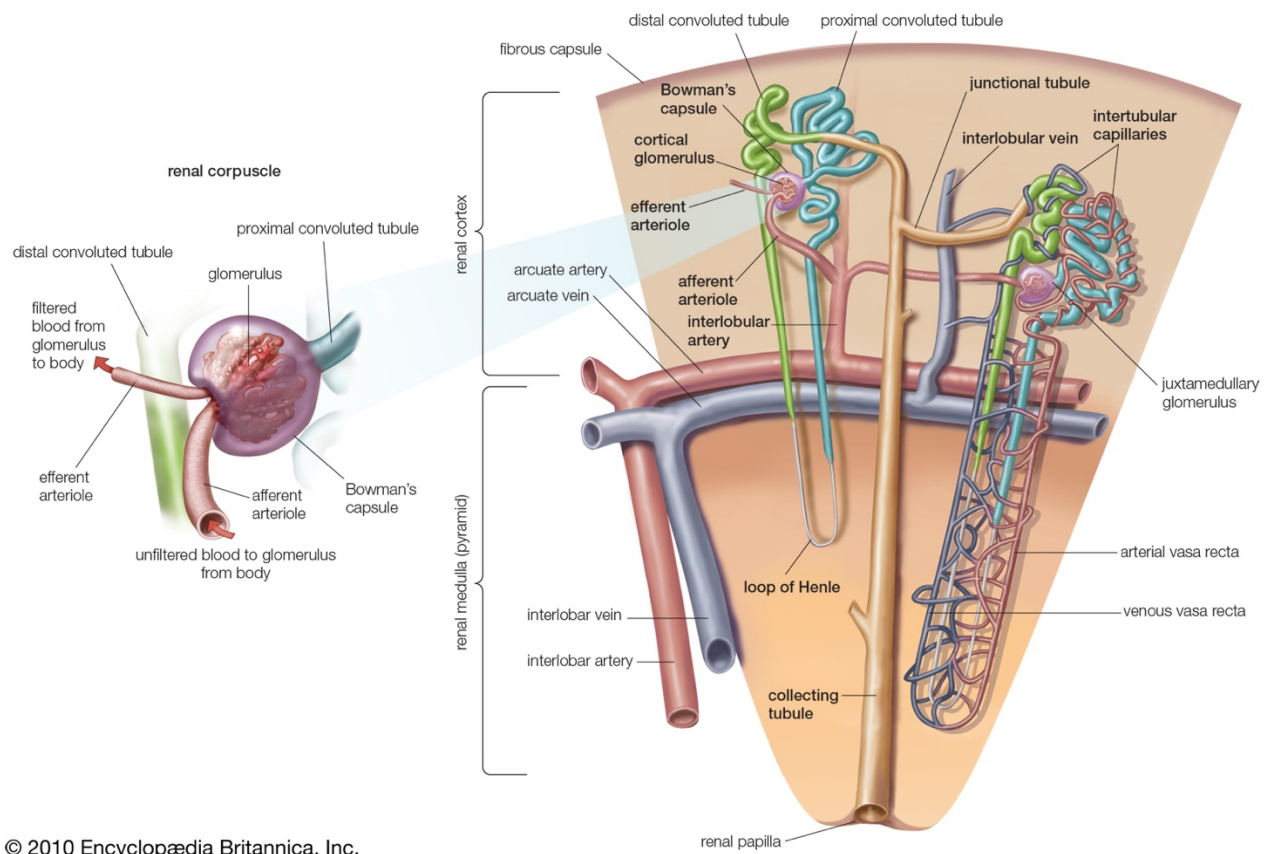
3.1.1. Tissue-of-origin

3.1.1.1. Anatomy of the kidney

A. Histological structure and cellular components

The kidney is a complex organ, located at the rear of the abdominal cavity in the retroperitoneum. Of note, normally-constituted humans possess two kidneys, the left being anatomically located higher than its right counterpart, which have redundant functions. The kidneys play crucial roles in the maintenance of the homeostasis including the regulation of blood pressure (salts and water balance), the modulation of acid-base balance and the elimination of wastes derived from the metabolism. The tightly controlled balance between glomerular filtration, tubular excretion and reabsorption constitutes the basis of kidney functions and importance. Around 40 highly specialized cell types are organized in peculiar compartments of the kidney to exert all these functions. The kidney has also endocrine functions: it produces erythropoietin which is responsible for inducing red blood cells maturation as well as active Vitamin D that participates to the homeostasis of calcium and phosphorus, and renin, an active actor in the blood pressure regulation (Wallace 1998).

Histologically, the functional substance of the kidney (or renal parenchyma), encapsulated in a fibrotic capsule, is divided into two major structures: the outer renal cortex and the inner renal medulla. Grossly, these take structures are organized in eight to twenty cone-shaped renal lobes each containing a portion of medulla called a renal pyramid which is surrounded by renal cortex. The tip of each pyramid, called renal papilla, empties urine into the renal pelvis that is connected to a ureter, the tube that carries excreted urine to the bladder. The kidney is vascularized through the hilum by the renal artery and vein that distribute especially well throughout the renal cortex (Figure 64).



© 2010 Encyclopædia Britannica, Inc.

Figure 65. Structure of the kidney nephron.

From <https://www.britannica.com/science/Bowmans-capsule>.

The functional unit of the kidney is the nephron, a structure that spans the cortex and medulla. Each human adult kidney contains around 1 million nephrons, which can be of short- or long-type depending on how far they reach into the medulla. All nephrons are divided into two parts: the blood-filtrating unit called the renal corpuscle located in the cortex, and a tubular part in charge of processing the primary urine filtered by the corpuscle. The renal corpuscle (or Malpighian corpuscle) consists of a glomerulus which is a tuft of capillaries composed of endothelial cells, and the glomerular capsule known as Bowman's capsule. The latter can be decomposed into three cell populations: i) the podocytes (also known as visceral epithelial cells) that form the epithelial lining of the capsule, ii) the podocyte progenitors called the parietal epithelial cells, and iii) the mesangial cells that are specialized contractile pericytes that together form a continuum with the smooth muscles (Liebich and Först 1990). The epithelial tubular portion of the nephron is divided into successive segments, composed of highly specialized tubule cells starting from the Bowman's capsule: the proximal tubule cells (convoluted and straight), the loop of Henle (descending and ascending limbs) and the distal convoluted tubule cells. The tubular part is connected to the renal papilla and the collecting duct system which consists of connecting tubule cells and the collecting ducts that come in two cell-types: principal and intercalated cells with distinct functions. The collecting ducts are subdivided into three segments: cortical, medullary and papillary (also called ducts of Bellini) that transition into the urothelium (Chen et al. 2019) (Figure 65).

B. Kidney development from embryo to adult

In humans and mammals alike, kidney development is a morphogenetic process that begins with the formation of three successive structures: the pro-, meso- and metanephros. They develop following a rostral-caudal pattern, the pronephros being the most rostral. During evolution, these embryonic renal structures have been adapted to play a functional role. For instance, the pronephros and mesonephros are the functional kidney in the fish larvae and adult fish respectively (Drummond and Davidson 2010). In mammals, while the pro- and mesonephros are only transient structures, the metanephros will give rise to the definitive kidney. The metanephros is formed of two compartments: the ureteric bud derived from the epithelial nephric duct and the metanephric mesenchyme, a structure arising from the intermediate mesoderm (Shah et al. 2009). The formation of the mature kidney starts with the

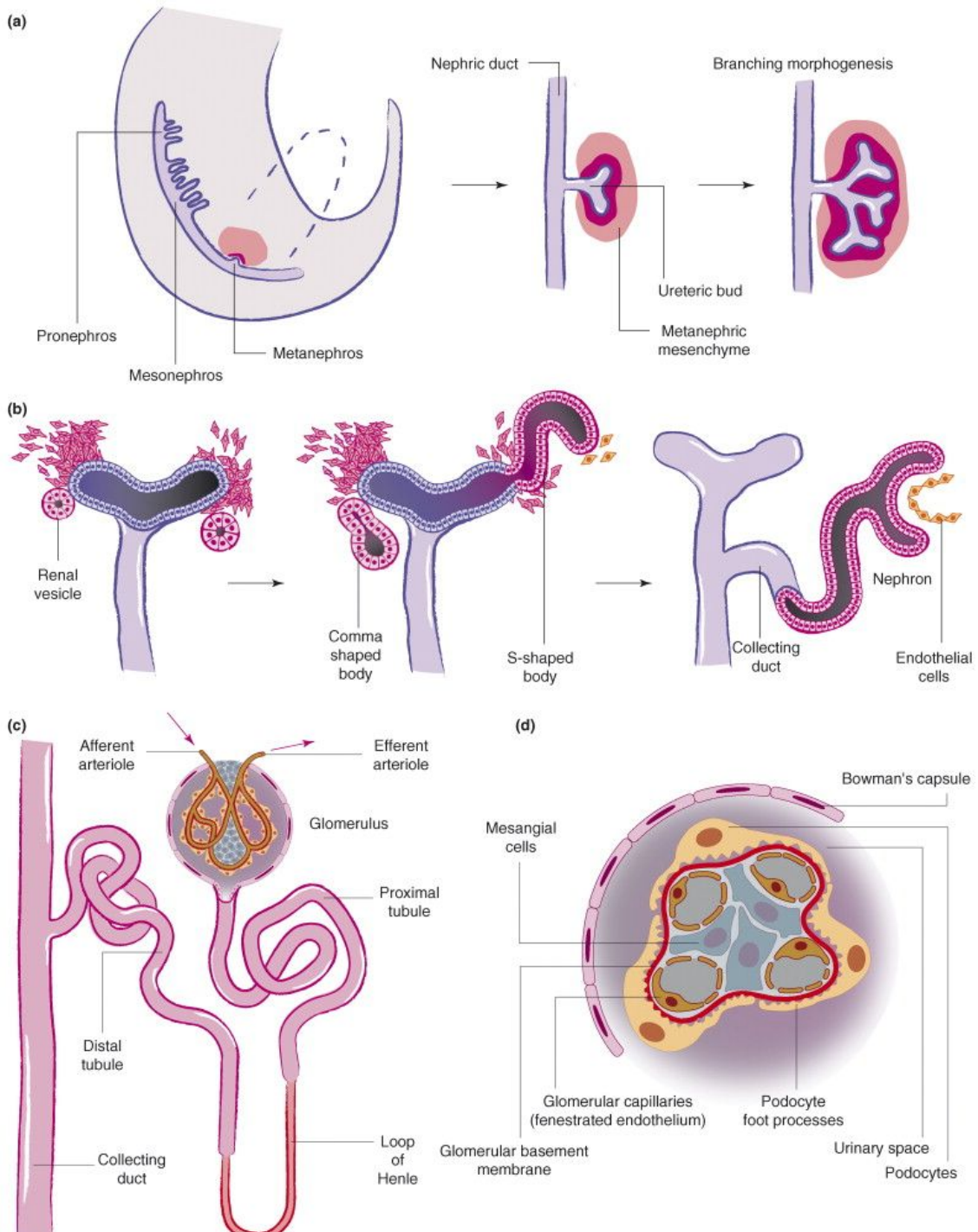


Figure 66. Metanephric development in humans.

specification of a condensed cluster of cells in the metanephric mesenchyme through a complex spatiotemporal organization largely dependent on key transcription factors (Joseph, Yao, and Hinton 2009). Key specifying factors such as PAX2, PAX8, HOX11, SOX9 and GATA3 allow the activation of the glial-cell-derived neurotrophic factor (GDNF) that is required for the subsequent emergence of the ureteric bud. Importantly, inactivation of GDNF leads to defective renal formation due to absence of ureteric bud emergence (Grote et al. 2008; Sanchez et al. 1996).

Immediately after the emergence of the ureteric bud, the metanephric mesenchyme begins to condensate around the tip to form the cap mesenchyme. These cells express high levels of SIX2/CITED1 which maintains their mesenchymal identity and stem-cell features (Kobayashi et al. 2008). In turn, interactions between the ureteric bud and cap mesenchyme induces the repression of SIX2/CITED1 through WNT signaling (Carroll and Das, 2011). The cap mesenchyme undergo mesenchymal-to-epithelial transition to generate the renal vesicle which continues its maturation into the so-called ‘comma-shaped’ and ‘S-shaped’ bodies. Close to the S-shaped body starts the development of the glomerulus due to major regulators notably WT1, PAX3 and VEGFA. Next, nephrogenesis involves the patterning of each cell-types depending on their relative location to the glomerulus. Cells proximal to the glomerulus will give rise to the Bowman’s capsule, while the proximal tubules and Henle’s loop derive from cells in the middle, and the remaining distal ends form the distal tubules. Lastly, the ureteric bud will further pattern to form the collecting ducts that fuse to the distal tubules, resulting in the mature nephron (Figure 66).

3.1.1.2. Biology of inner medulla cells

A. Role of inner medulla cells

Histologically, the kidney medulla is composed three layers: the inner medulla and the outer medulla which is itself subdivided into inner and outer stripe regions. These structures contains the straight segment of proximal tubule cells, the loop of Henle, the medullary collecting ducts and the medullary interstitium that acts as a connective tissue (Lamley and Kriz 1991). This stromal interstitium is composed specialized lipid droplet-containing interstitial cells (called ‘lipid-laden’ cells), endothelial cells of the vasa recta, macrophages, pericytes and some extracellular components (fibrillar reticulum

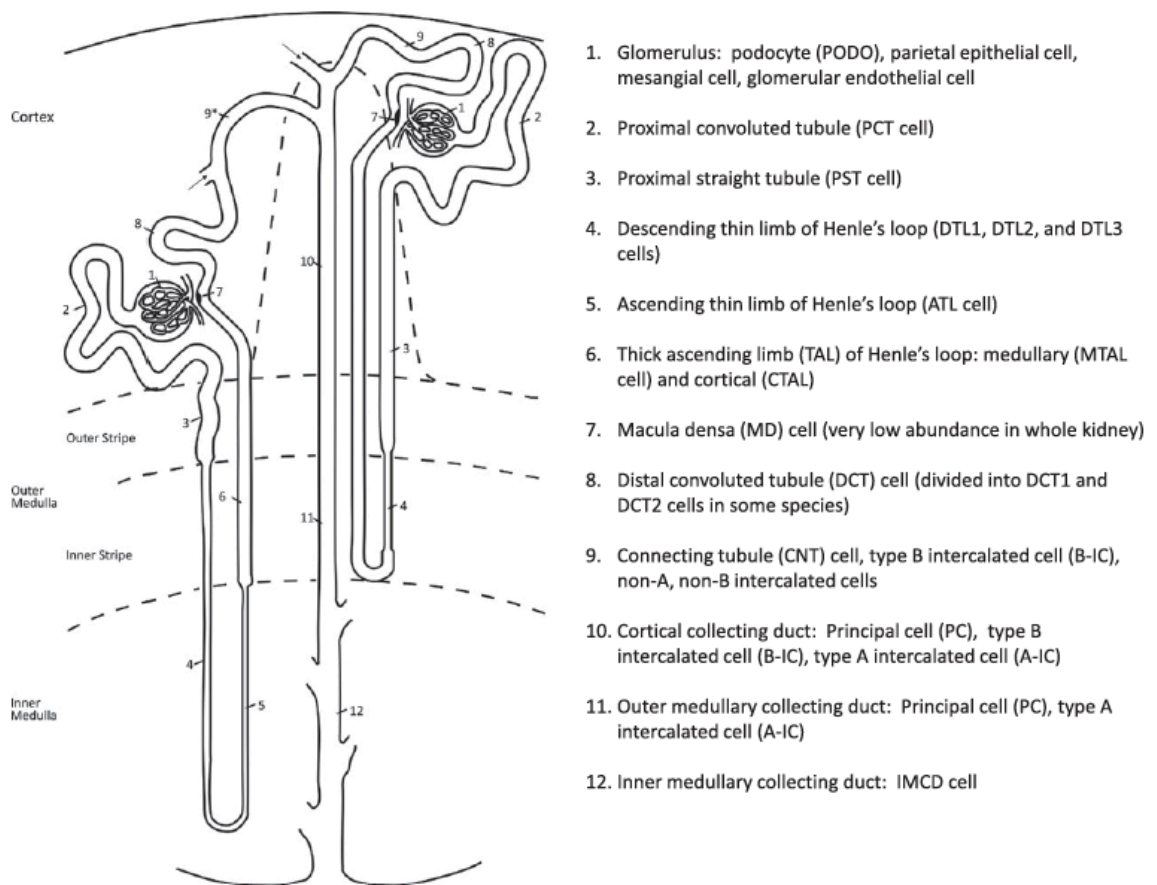


Figure 67. Renal tubule cell nomenclature.

From Chen *et al.*, 2019.

and interstitial fluid). Although proximal straight tubule (PST) cells are found in the outer stripe, only the loop of Henle and collecting duct system dives deeply into the inner medulla.

The loop of Henle segment is subdivided into three components from PST cells: the thin descending limb (DTL), the thin ascending limb (ATL) and the thick ascending limb (TAL). The TAL portion reaches out into the cortex to connect with the distal convoluted tubule (DCT) cells. Thus, TAL has been segmented into its medullary (mTAL) and cortical (cTAL) components. Of note, cTAL are often referred to as distal straight tubule (DST) cells. Also, short-type nephrons the ascending thin limb of Henle's loop (ATL) are not present, meaning DTL immediately transitions into TAL cells. The role of the loop is instrumental for kidney function as it regulates the concentration or dilution of urine through a mechanism known as the 'countercurrent multiplication' involving water and solute exchanges (Sands & Kokko, 1996). Functionally, the descending (DTL) and ascending (TAL) portion of Henle's loop have very distinct functions. DTL are very permeable to water but not to solutes which allows for progressive concentration of the urine reaching its maximum as the tip of the loop. In contrast, the situation is reversed in TAL: the tubules become impermeable to water and permeable to solutes principally via active transports. The urine solutes are reabsorbed mainly via the $\text{Na}^+/\text{K}^+/\text{2Cl}^-$ cotransporter (SLC12A1), localized at their apical pole. The intracellular ion gradient is maintained by a Na^+/K^+ ATPase found on their basolateral pole, that actively ejects Na^+ ions into the renal interstitium, that will ultimately be reabsorbed by the vasa recta (Sands and Layton 2009) (Figure 67).

The second epithelial population present in the inner medulla are the collecting ducts (CD). This set of tubules collects the urine produced by the nephrons and brings it via a series of structures (the pyramids, the calices, the pelvis and the ureter) into the bladder. The CD have a different embryonic origin than the other tubule cells as aforementioned. They can be divided into cortical and medullary collecting ducts, according to the kidney compartments it crosses. In terms of cell populations, CD are composed mainly of 'principal cells' (PC, roughly 60%), rich in Na^+/K^+ channels and water transporters known as aquaporins (AQP2 and -3). Hormones such as aldosterone and vasopressin are key regulators of collecting ducts which influence the final urine volume and concentration (Ranieri 2019). The remaining 20% of CD cells are the so-called 'intercalated cells' (IC) type α and β which intercalate in

between 'principal cells'. IC contribute to the acid-base homeostasis by regulating the secretion and reabsorption of acid and bicarbonates (Lee Hamm, Nakhoul, and Hering-Smith 2015).

B. Kidney medulla and hypoxia

The kidneys weigh less than 0,5% of an average human body weight, but receive about 25% of the cardiac output at rest. Thus, per gram of tissue, the kidney is among the most highly oxygenated organs in the body. However, the kidney, and particularly the medulla, are very susceptible to hypoxia which is the cause of both acute kidney injuries (AKI) and chronic kidney disease (CDK) (Kawasumi et al. 2017; Liu et al. 2017). Recently, the reasons underlying such vulnerability to hypoxia have been elucidated and they are numerous (Evans 2019).

First, the renal tubules are extremely demanding in oxygen due to their metabolic activity and some tubules are obligate aerobic metabolizers, just like the brain. Yet, Henle's loop TAL cells have the ability to generate ATP in absence of oxygen, however their transport activity can only be maintained through oxidative metabolism and they become damaged in hypoxic conditions (Epstein 1997). Second, oxygen delivery is limited by the density of peritubular capillaries which decreases due to a phenomenon called 'capillary rarefaction' that is thought to stem from interstitial inflammation and fibrosis (Prommer et al. 2018). The adult kidney has very poor capacity for angiogenesis as renal endothelial cells are relatively insensitive to proangiogenic factors such as VEGF. This specific feature of renal endothelial cells originates from the function of the kidney cells in the regulation of erythropoiesis through the secretion of the hypoxia-induced erythropoietin (Lee et al. 2019). Thus, the poor angiogenic ability of the kidney represents an evolutionary tradeoff for systemic control of erythrocyte production.

The third reason why the kidney medulla is so vulnerable to hypoxia stems from its intrinsic function in urine concentration via the countercurrent multiplication mechanism (Figure 68). This system is rendered possible by the countercurrent arrangement of arteries and veins of the medullary vasa recta. However, the consequence of such organization is arterial-to-venous oxygen shunting as some of the oxygen in renal arterial blood never reaches renal tissues and is instead 'stolen' by nearby veins (Pallone, Robertson, and Jamison 1990). Lastly, another reason underlying the hypoxia vulnerability of some medullary tubules is their spatial distance relative to capillaries.

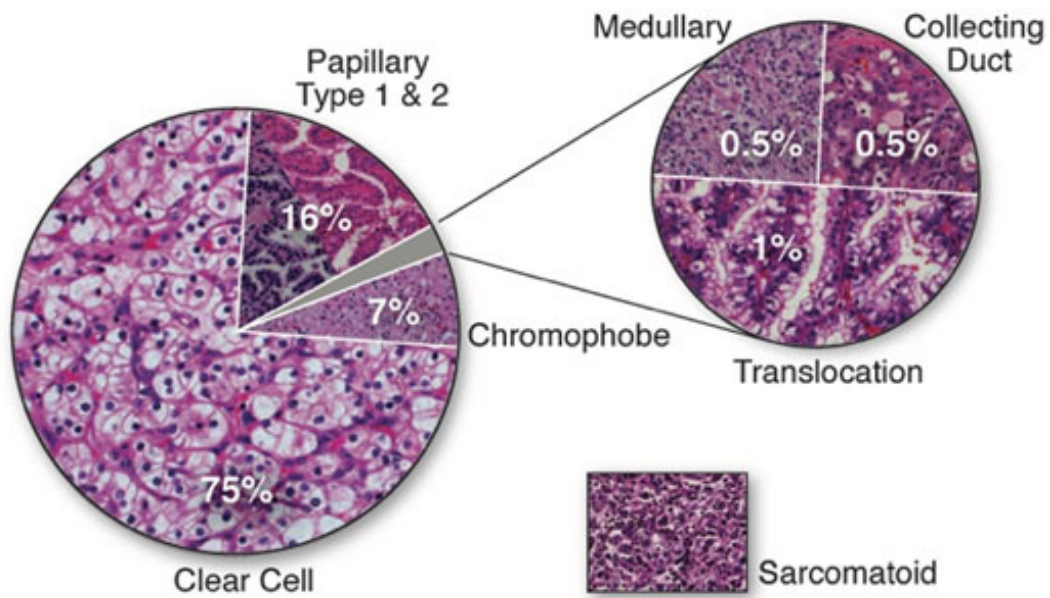


Figure 69. Major subtypes of renal cell carcinoma.

From Shuch *et al.*, 2014.

Therefore, due to their peripheral position in the inner stripe, the medullary TAL cells have the highest predisposition to the development of hypoxia (Fry et al. 2014). This is consistent with the common findings of damage to medullary TAL in human acute kidney injury (Heyman, Rosenberger, and Rosen 2010). One physiological benefit of being located far from capillaries is that it results in a lateral osmotic gradient that promotes sodium reabsorption in TAL cells (Pallone 2014).

3.1.2. Renal medullary carcinoma

3.1.2.1. Classification of kidney cancers

A. Clear-cell renal cell carcinoma

Renal cell carcinoma (RCC) is a diverse group of malignant tumors found in the kidney. The worldwide incidence of RCC is about 400,000 new cases annually for an estimated 150,000 annual deaths, making it the 9th most common cancer (Padala et al. 2020). Although RCC accounts for 2% of global cancer diagnoses and death, it has more than doubled in incidence in developed countries over the last two decades. Most cases of RCC are discovered incidentally on imaging, and survival is highly variable depending on the stage at diagnosis, with the metastatic disease having only a 12% five-year survival rate. The majority (65%) of RCCs are diagnosed in men, and the average age of diagnosis is 64. Known risk factors for RCC include smoking, obesity, hypertension, diet and alcohol consumption. Historically the first subtype of RCC was described in 1883 with a pathological description of a clear cell renal tumor (Grawitz, 1883). With the advent of more advanced molecular methods the genomic investigations of RCCs have clarified the molecular basis of several subtypes of RCC, mainly by the investigations into their hereditary forms (Linehan et al. 2004; Shuch et al. 2015). The 2016 World Health Organization (WHO) classification of kidney tumors currently recognizes no less than 55 different entities in adults and children of which 40 subtypes are malignant (Moch et al. 2016). Clear cell RCC represent about 75% of all RCC, while the remaining 25% are often grouped together and referred to as 'non-clear cell RCC' (Figure 69).

Clear cell RCC (ccRCC). They are associated with mutations in the Von Hippel-Lindau (VHL) gene in 91% of cases (Nickerson et al. 2008). The VHL gene, found on chromosome 3p25 is a tumor

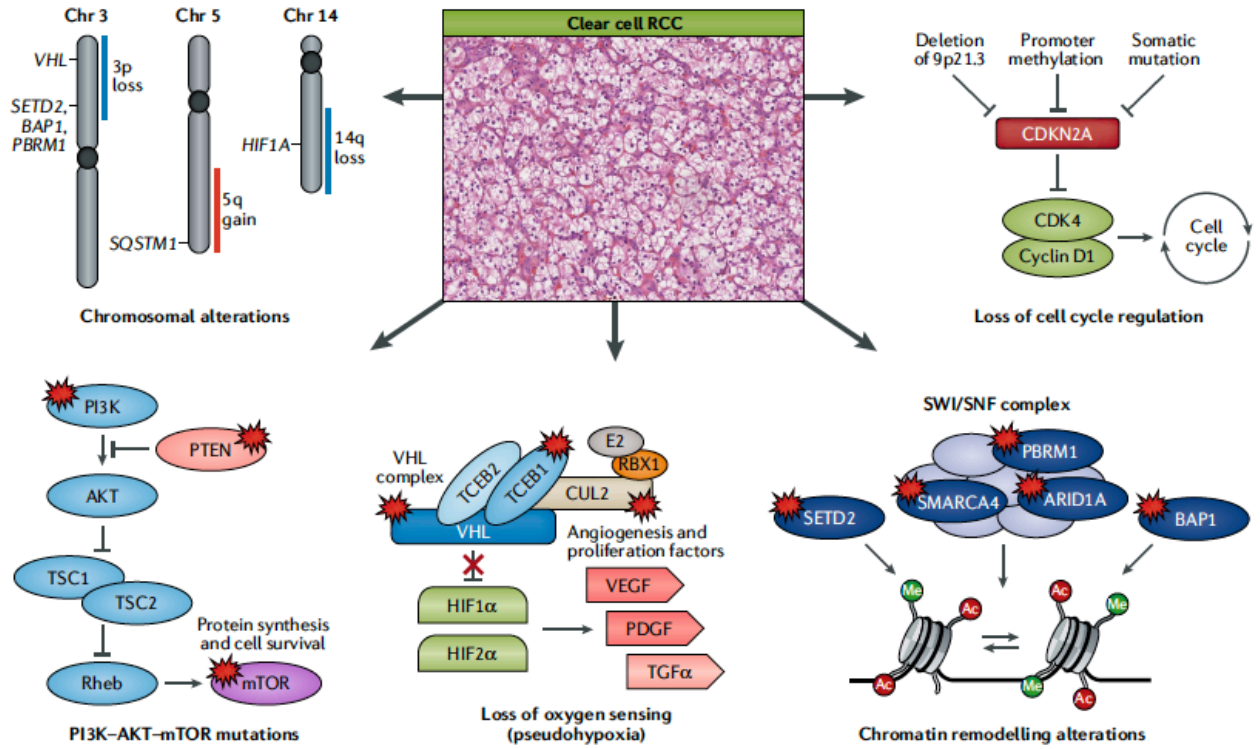


Figure 70. The mutational landscape of clear cell RCC.

From Linehan & Ricketts, 2019.

suppressor gene first described in 1993 by Linehan and colleagues who determined its association to the Von Hippel-Lindau syndrome (Grubb et al. 2005). The main pathway of ccRCC pathogenesis is through a biallelic inactivation of the VHL gene which in turn deregulates the hypoxia-inducible factor (HIF) protein, in particular HIF2 α , resulting in upregulation of downstream factors (Lara et al., 2015). Other frequently associated genes with sporadic ccRCC oncogenesis include chromatin-modifiers and -remodelers PBRM1, SETD2, JARID1C and BAP1 (Cancer Genome Atlas Research, 2013). Of note, ccRCC transform from proximal tubule cells. Gross features of ccRCC are globular growths from the renal cortex with tumor borders being sharp against the normal parenchyma. The tumor itself is yellow in color, often showing areas of hemorrhage and necrosis. Microscopically a typical clear cytoplasm ('clear cell') due to lipid and glycogen deposits. Importantly, ccRCC were shown to have higher metastatic rates as compared to both papillary and chromophobe RCCs, making them harder to treat (Leibovich et al. 2010).

B. Non-clear renal cell carcinomas

Non-clear RCC is represent up to 25% of all RCCs. Despite often being clustered as a single entity, nccRCC constitutes an heterogenous group of kidney cancers that encompasses multiple histologies with distinct molecular features. Their lower incidence and heterogeneity have resulted in a considerable gap of knowledge for each subtype. The main subtypes are papillary RCC (15%), chromophobe RCC (5%), collecting duct carcinomas (<1%), renal medullary carcinomas (<1%) and MiT/TFE translocation RCC.

Papillary RCC (pRCC). The second most common subtype is pRCC that is seen in 10-15% of cases (Patard et al. 2005; Steffens et al. 2012). These tumors can be subdivided into pRCC type-1 and type-2, both are thought to transform from proximal tubules. Gross features of both pRCC tumor types show a varying consistency with a brown color. Microscopically both tumor types display papillary architecture with occurrence of calcifications, necrosis, and macrophage infiltration. Distinct microscopic features of type-1 tumors are single-layered papillae with clear cytoplasm while type-2 tumors appear with thicker papillae and heterogenous cytoplasm. Recently Linehan and colleagues performed an extensive molecular characterization of pRCC concluding that 81% of type-1 pRCCs have

Histologic Cell Type	Survival	Frequency (%)	Syndrome	Gene	5 Years
Clear cell		60–75	VHL disease/HP FCRC	VHL/SDHB 3p del	~60%
Papillary		12	HPRC HLRCC	MET FH	~80%
Chromophobe		4	BHD syndrome	BHD	~90%
Oncocytoma		4	BHD syndrome	BHD	Benign
Collecting Duct		<1	–	–	<5%
Medullary		<1	–	Sickle trait	Rare

FCRC, familial clear cell renal cancer; FH, fumarate hydratase; HLRCC, hereditary leiomyomatosis and renal cell cancer; HP, hereditary paraganglioma; HPRC, hereditary papillary renal carcinoma; SDHB, succinate dehydrogenase B.

Figure 71. Five-year survival rates of main RCC subtypes.

From Qian *et al.*, 2020.

a gain in chromosome seven which includes the c-MET proto-oncogene. They further analyzed type-2 pRCC genomics finding their association with mutations found of the NRF2-ARE pathway genes. In their analysis type-1 pRCC was found to have a more favorable prognosis than type-2 (Linehan et al., 2016).

Chromophobe RCC (ChRCC). Being the third most common subtype, chRCC originates from the renal collecting ducts cells and accounts for approximately 5% of RCC cases (Amin et al. 2008; Capitanio and Montorsi 2016). Gross features of chRCC is large and well-circumscribed tumors with a brown color. The genomics of sporadic chRCC accredits alterations, deletions in chromosomes 1, 2, 6, 10, 13 and 17, to the oncogenesis of these tumors. A multi-omic analysis demonstrated that the majority of chRCC bear p53 and PTEN mutations (58% and 24%, respectively) (Casuscelli et al. 2017). A unique feature of these tumors is their indolent course, despite larger tumors compared to other RCCs.

The three subtypes mentioned above namely clear cell, papillary and chromophobe RCCs account for about 98% of cases, but other less frequent subtypes are noteworthy due to their aggressivity. For a long time these RCC remained unclassified, however with the advent of modern genomics, these rare subtypes are being investigated increasingly. They include collecting duct carcinomas, renal medullary carcinomas, MiT/TFE translocation carcinomas, sarcomatoid RCC (sRCC) as well as several hereditary RCC which bear specific germline mutations.

Collecting duct carcinomas (CDC). Just like chRCC and their name indicates, collecting duct carcinomas (or Bellini duct carcinomas) originates from the collecting ducts and are diagnosed in less than 1% of cases. However these tumors are characterized by their extremely aggressive nature. Most CDC are diagnosed in men (2.3:1) and have poor survival with a median of 44 weeks. Microscopically, CDC have a tubulopapillary structure with high desmoplasia and tumor cells present high-grade cytology (Malouf et al. 2016; Qian et al. 2020).

MiT-translocation RCC (tRCC). They represent a newly-recognized subtype of RCC bearing chromosomal translocations involving TFE3 (Xp.11). The TFE3 gene maps to the X chromosome (Xp.11) and is a member of the MiT family of transcription factors with MITF, TFEB and TFEC. Chromosomal rearrangements in tRCC results in the overexpression of several fusion proteins which

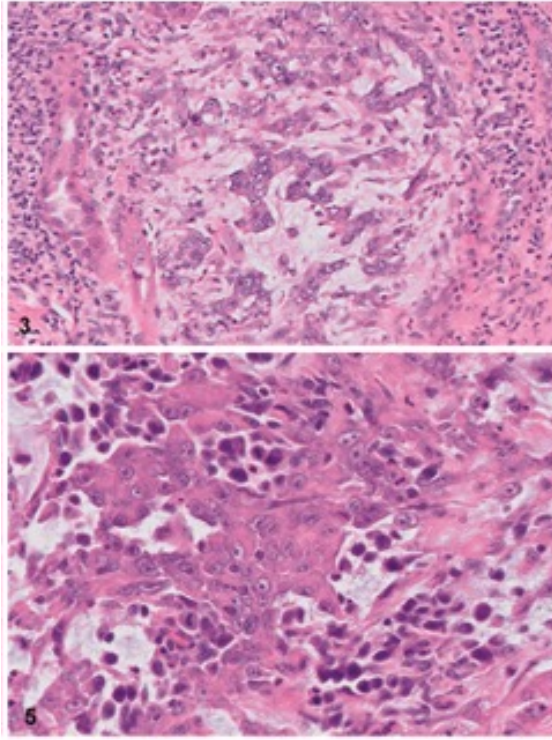


Figure 72. Hematoxylin-eosin staining showing esmoplastic reaction to renal medullary carcinoma.

From Elliott & Bruner, 2019.

retain the c-terminal domain of TFE3. Several fusion gene partners have been reported including LUC7L3, PRCC, ASPL, NONO and SFPQ (Caliò et al. 2019; Zhong et al. 2012). Microscopically, tRCC are characterized by an heterogeneous morphologies with larger epithelioid cells and smaller eosinophilic cells clustered into spheres. The mechanism of oncogenesis still remain poorly understood.

3.1.2.2. The genesis of renal medullary carcinoma

A. Clinical features of RMC

First described in 1995, renal medullary carcinoma (RMC) is a form of lethal malignant neoplasm arising from the kidney medulla region (Davis, Mostofi, and Sesterhenn 1995). Despite overall relatively rare (<0,5% of all RCCs), RMC is the third most common kidney malignancies in young adults. It typically afflicts young patients of African descent at median age of 28 years old. Virtually all patients have sickle cell traits, less often sickle cell disease. In fact, roughly 1 in 20,000 individuals with sickle cell trait develop RMC. The disease displays 10:1 male-to-female ratio and the majority (75%) of cases affect the right kidney. Initial clinical symptoms are various with flank pain and hematuria being the most common. RMC is one of the most aggressive disease among kidney cancers, with a median survival of 8 months (Alvarez et al. 2015; Beckerman et al. 2017). Most patients present metastatic disease at the time of diagnosis with most common sites being the liver, lungs, bones and adrenal glands (Elliott and Bruner 2019). At the histopathological level, tumors have been reported as an ill-defined and poorly circumscribed mass of 7 cm in average size that occupies most of the renal medulla (Schwartz et al. 2002). The tumor tissues resemble a high-grade carcinoma exhibiting reticular or cribriform patterns and were described as 'poorly differentiated' by Rao *et al.* due to expression of OCT3/4 as detected by immunohistochemistry (Rao et al. 2013). RMC usually also stain positive for VIM, MUC1, pankeratins, PAX8, HIF1 α and VEGF, markers that serve during the differential diagnosis (Gupta et al. 2012). Importantly, other distinctive histological features of RMC are a strong desmoplastic stromal response, a prominent inflammatory infiltrate as well as the frequent presence of sickled red blood cells (Dimashkieh, Choe, and Mutema 2003).

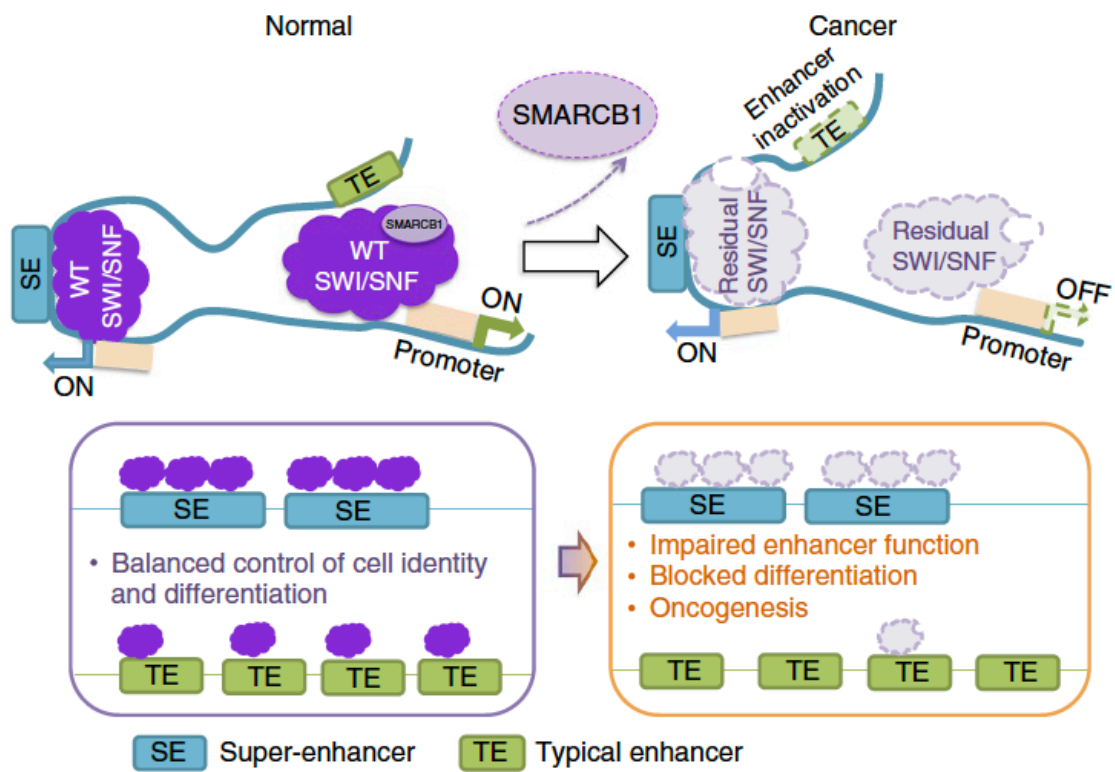


Figure 73. Model representing the role of SMARCB1 in enhancer regulation, which deregulation drives oncogenesis in MRT.

From Wang *et al.*, 2017.

B. Molecular hallmarks of RMC

The hallmark of RMC tumors is the loss of expression of SMARCB1, a potent tumor-suppressor, which is believed to be the oncogenic driver. SMARCB1 gene maps to the long arm of chromosome 22 (22q11.23) and several mechanisms have been associated with its loss in RMC including deletions, point mutations, inactivating translocations and loss-of-heterozygosity (Msaouel, Tannir, and Walker 2018). Besides RMC tumors, loss of SMARCB1 occurs in the majority of malignant rhabdoid tumors (MRTs), atypical teratoid/rhabdoid tumors (ATRTs) and epithelioid sarcomas (ESs). Historically, SMARCB1 has been first described in MRT which is an extremely aggressive malignancy affecting children. MRT and RMC share common features such as their renal origin and their particularly low mutation burden (Msaouel et al. 2020). Most of what is known about SMARCB1 comes from studies done with MRT tumors where it was shown to be a potent tumor-suppressor gene (Caramel et al. 2008; Nakayama et al. 2017; Versteeg et al. 1998). Mechanistically, the inactivation of SMARCB1 in MRT results in deregulated targeting of SWI/SNF complex leading to uncontrolled progression through the cell cycle. More recently, multi-omic analytic efforts by Msaouel *et al.* shed lights on several molecular characteristics of RMC with notably a chromosome 8q gain associated with an amplification of MYC (Msaouel et al. 2020). Another important discovery is that RMC tumors have a distinct immune profile with high inflammatory infiltrate associated with activation of the cGAS-STING pathway, although its exact role in pathogenesis is not yet elucidated.

cGAS-STING pathway. It has fundamental role in innate immune response that detects the presence of exogenous cytosolic DNA and, in response, triggers expression of type I interferon response that lead to senescence or activation of defense mechanisms. Upon binding of cytosolic DNA, the cGAS protein catalyzes the formation of cyclic GMP-AMP from GTP and ATP. cGAMP then binds to Stimulator of Interferon Genes (STING). Human TMEM173 gene encodes for STING, a protein consisting of 379 aminoacids which is characterized by three functional domains: a cytoplasmic c-terminal tail, a central globular domain, and four N-terminal transmembrane motifs that anchors STING into the endoplasmic reticulum. Upon binding of cGAMP, STING triggers the phosphorylation of IRF3 which translocates into the nucleus and activate the expression of inflammatory genes (Chen et al. 2016).

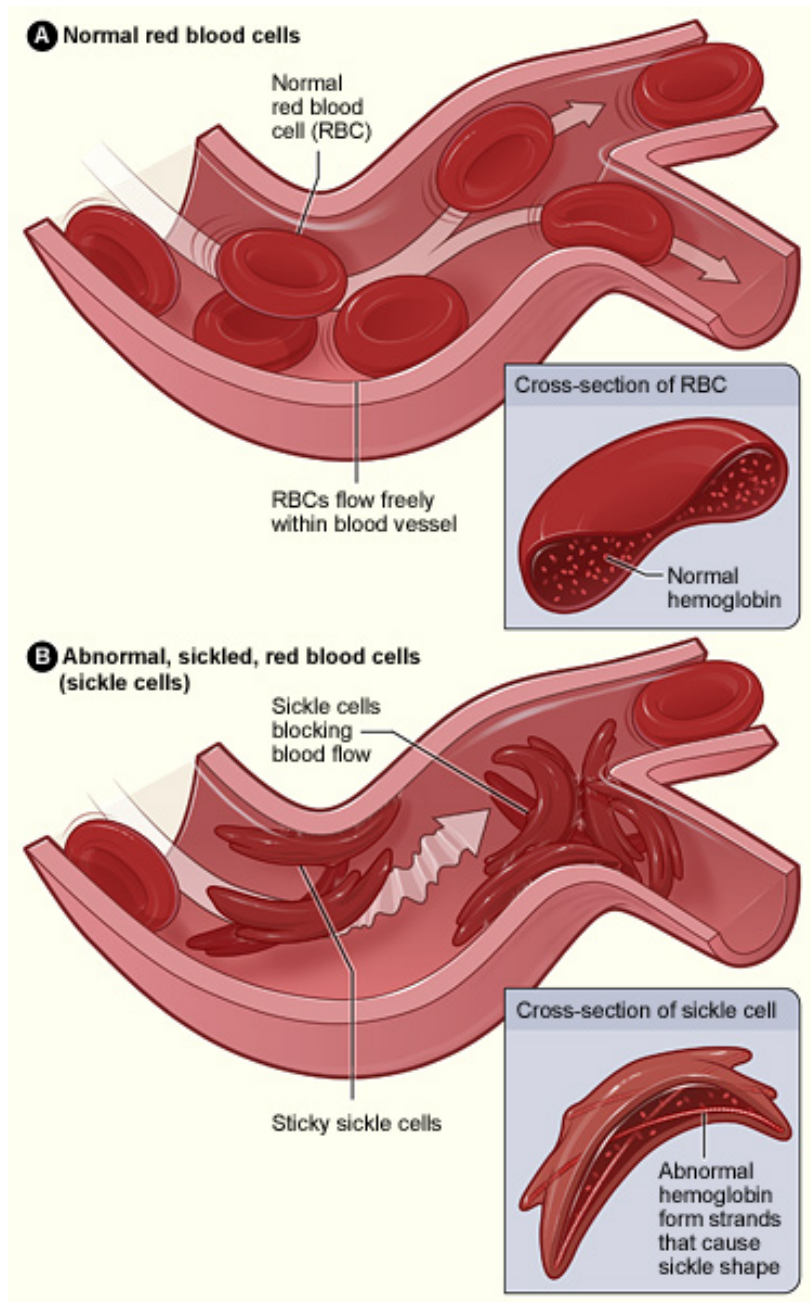


Figure 74. Principle of Sickle cell anemia.

From The National Heart, Lung and Blood Institute (NHLBI).

C. Mechanisms of pathogenesis

The question of the cell-of-origin is an important aspect when discussing the genesis of RMC. It was recently suggested that RMC may transform from collecting ducts, similarly to collecting duct carcinomas (Msaouel et al. 2020). Other have speculated that instead distal convoluted tubules might be the candidate cell-of-origin of RMC (Beckerman et al. 2017). Nevertheless, we can say with a relative degree of certainty that RMC derives from the kidney medulla due to the localization of the primary tumors. The kidney medulla is thought to be the most hypoxic microenvironment in the organism for many physiological reasons (Evans 2019). This is very important considering that virtually 100% of RMC patients present sickle hemoglobinopathies.

Sickle cell anemia. It is a genetic and hereditary disease affecting 50 million people around the world particularly in the African continent and ranked as the fourth priority by the WHO. It is produced by a single nucleotide mutation in the β -globin gene resulting in the substitution of glutamic acid by valine at the sixth position of this β chain. In this state, the hemoglobin is called hemoglobin S (HbS) (Murayama 1966). Sickle cells occur when a person inherits an abnormal copy of the hemoglobin gene from each parent (recessive disease). A person with a single abnormal copy (heterozygous for HbS) usually does not have symptoms and is said to have 'sickle-cell trait'. Instead, a person presenting homozygosity develops sickle cell disease. In the absence of oxygen, the hydrophobic valine causes HbS to agglomerate and form fibers that destructure erythrocytes (Ballas and Smith 1992). This phenomenon is reversible, because in the presence of oxygen, the fibers dissolve and sickle erythrocytes return to their original discoid shape. However, several cycles of oxygenation and deoxygenation causes the sickle erythrocytes to gradually become rigid. As a consequence, hemolysis of sickle cells frequently occurs resulting in a shorter erythrocyte lifespan of only 15 days compared to 120 days for a normal RBC (MacCallum et al. 1975). Thus the average hematocrit in people with SCA is ~25%. Of note, the blood hematocrit is sensed by the kidney medulla (Evans 2019).

Due to its central role in urine concentration, the kidney medulla is characterized by increasing interstitial sodium levels which results in DNA double strand breaks in renal medulla cells. In a person presenting no sickle cell trait, those DSBs are readily repaired by homologous recombination. However,

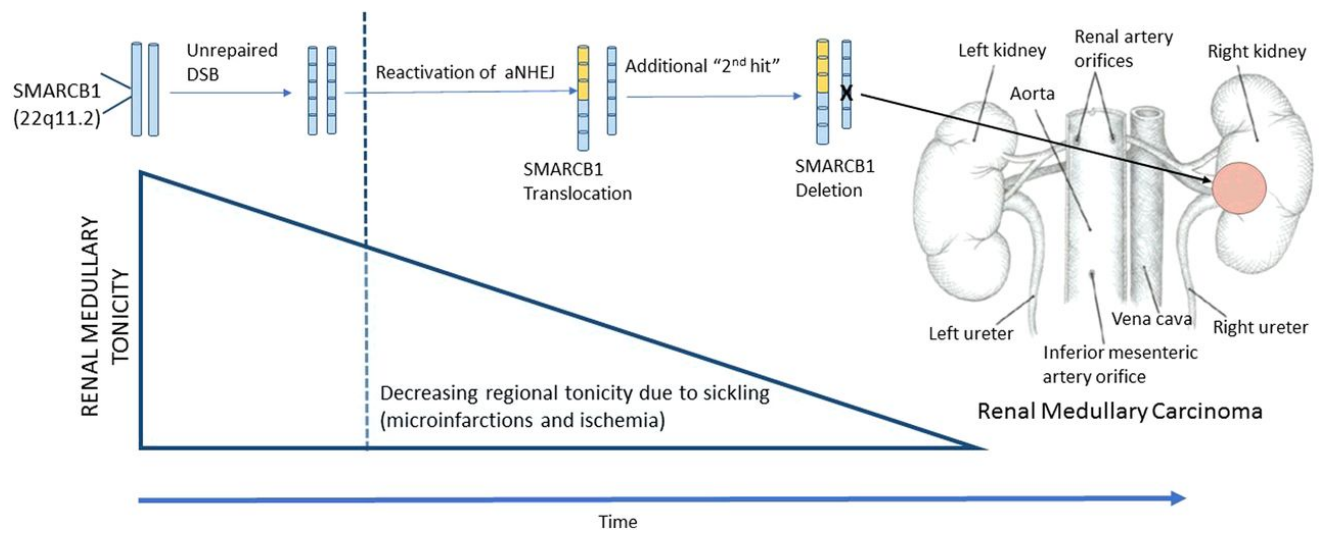


Figure 75. Current model of RMC pathogenesis.

From Msaouel *et al.*, 2018.

according to the current model of RMC pathogenesis, the extreme hypoxic conditions in the medulla induce sickling of erythrocytes in patients presenting sickle hemoglobinopathy which results in recurrent local ischemia and microinfarctions (Msaouel et al. 2018). In turn, ischemia-induced acute hypoxia favors the activation of the non-homologous end-joining (NHEJ) DNA repair pathway due to repression of BRCA1 and RAD51. This error-prone pathway likely produces translocations and deletions, particularly in fragile regions such as chromosome 22q where the SMARCB1 locus is located. The chromosome 22q is considered as fragile as it contains palindromic AT-rich repeats (PATRRs) and eight low copy repeat elements (LCRs) which predispose to random and recurrent translocations and deletions via the NHEJ repair pathway. Of note, deletion of 22q is part of the DiGeorge syndrome which constitutes the most common chromosomal microdeletion disorder occurring in 1 in 1000 fetuses. Thus, this model links sickle hemoglobinopathies to loss of SMARCB1 in renal medulla cells which triggers the oncogenic transformation resulting in RMC.

3.1.2.3. RMC treatments

Renal medullary carcinoma is a notoriously aggressive malignancy and has been found to be resistant to many conventional chemotherapeutic agents. The best available cytotoxic chemotherapy regimens produce a typically brief objective response in 30% of cases (Shah et al., 2018). The outcome at diagnosis remains extremely poor with a median of 17 months in metastatic-free patients and 4 months in patients with metastases (Iacovelli et al. 2015). Notably, patients receiving platinum-based chemotherapy benefitted of prolonged survival (12 months) compared with topoisomerase inhibitor therapy (7 months) or methotrexate-vinblastine-doxorubicin-cisplatin therapy (4 months). Currently the standard of care is an upfront systemic platinum-based chemotherapy followed by radical nephrectomy if the tumor response to chemotherapy was satisfactory (Msaouel et al. 2018).

There are currently several on-going clinical trials for RMC patients, including three trials using immune checkpoint inhibitors. This is largely based on reports of complete response of recurring metastatic RMC to PD-1 inhibitor, nivolumab, 9 months after initiation of therapy (Beckerman et al. 2017). Another promising trial currently in phase II relies on the use of second-generation proteasome

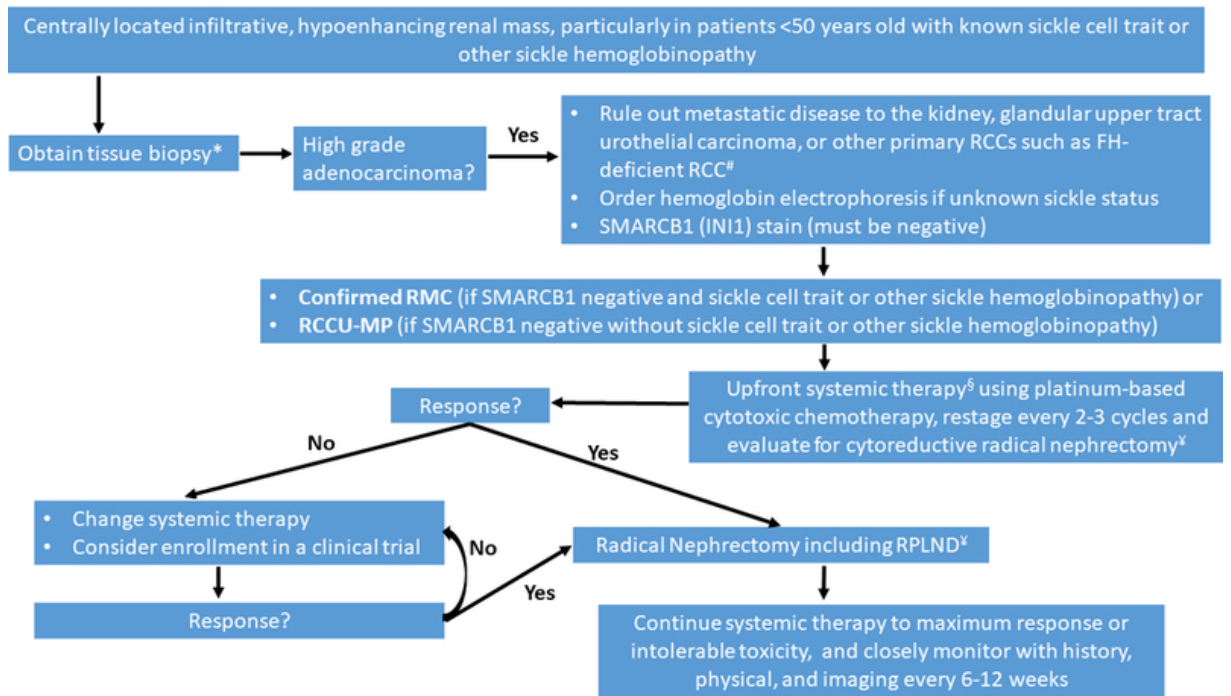


Figure 76. Current diagnosis and management recommendations for RMC.

From Msaouel *et al.*, 2019.

inhibitor, ixazomib, as it was shown that SMARCB1 loss leads to increased protein anabolism which renders tumor cells susceptible to proteostatic disruption (Hong et al. 2019).

A promising therapeutic target in RMC could be EZH2, the catalytic subunit of the PRC2, that is known to antagonize SWI/SNF complexes. Preclinical data show that EZH2 inhibition leads to apoptosis and differentiation in cell lines with SMARCB1 expression loss and may play a role in the treatment of RMC (Knutson et al. 2013). However, clinical trials using EZH2 inhibitors have been halted as studies in mice have suggested that it leads to hematologic malignancies (Simon et al. 2012). Similarly, anti-angiogenic therapy, a standard of care in ccRCC, has failed to prove its efficacy for RMC (Shah et al. 2017). Consequently, effective treatment strategies are urgently needed for RMC.

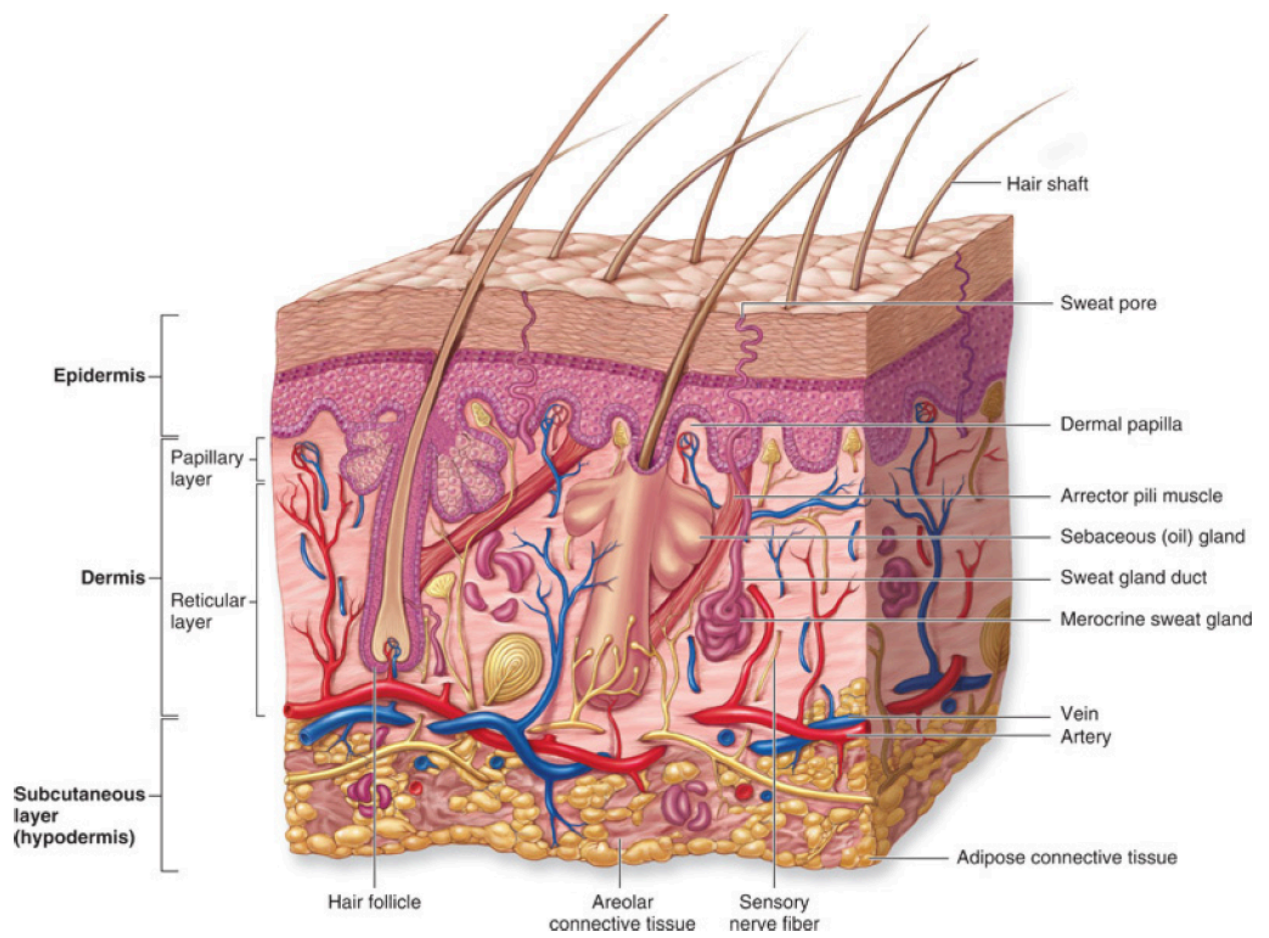


Figure 77. Schematic cross section of the human skin.

From ©The McGraw-Hill Companies, Inc.

3.2. Melanoma

This chapter will focus on melanoma which is the deadliest form of skin cancer. Where does it come from? How does it progress and what are the current treatments? To answer these questions, the anatomy of skin and the cell-of-origin of melanoma will first be discussed before diving deeper into the mechanisms of melanomagenesis.

3.2.1. Cell-of-origin

3.2.1.1. Anatomy of the skin

A. Histological structure and cellular components

The skin is the largest organ of the human body and as such the first line barrier protecting the organism from its environment. Known functions of the skin include protection from external physical and chemical assailants, sensation, hydro- and thermoregulation, important metabolic functions (such as vitamin D production) as well as interactions with the microbiota (Gallo 2017; Zimmerman, Bai, and Ginty 2014). This complex organ is constituted by cells of different embryonic origins and is structured into three primary layers (Figure 77).

Hypodermis. This is the innermost layer that anchors the skin to underlying tissues such as skeletal muscles, bones and organs. It is a highly vascularized connective tissue essentially composed of sweat glands and adipocytes specialized in fat storage and acting as energy reserve and heat insulators.

Dermis. The dermis is the layer of dense connective tissue that sits on top of the hypodermis and constitutes the thickest part of the skin. It is derived from the embryonic mesoderm and can be divided into two regions: the papillary dermis (superficial region) and the reticular dermis (deeper region) (Smith and Holbrook 1986). The main dermal components are skin fibroblasts that produce the extracellular matrix (ECM, such as collagen and elastin fibers), which provide both strength and elasticity. Other components are blood and lymphatic vessels, immune cells, sensory receptors and epidermal appendages such as nails, hair follicles, sebaceous glands and sweat glands.

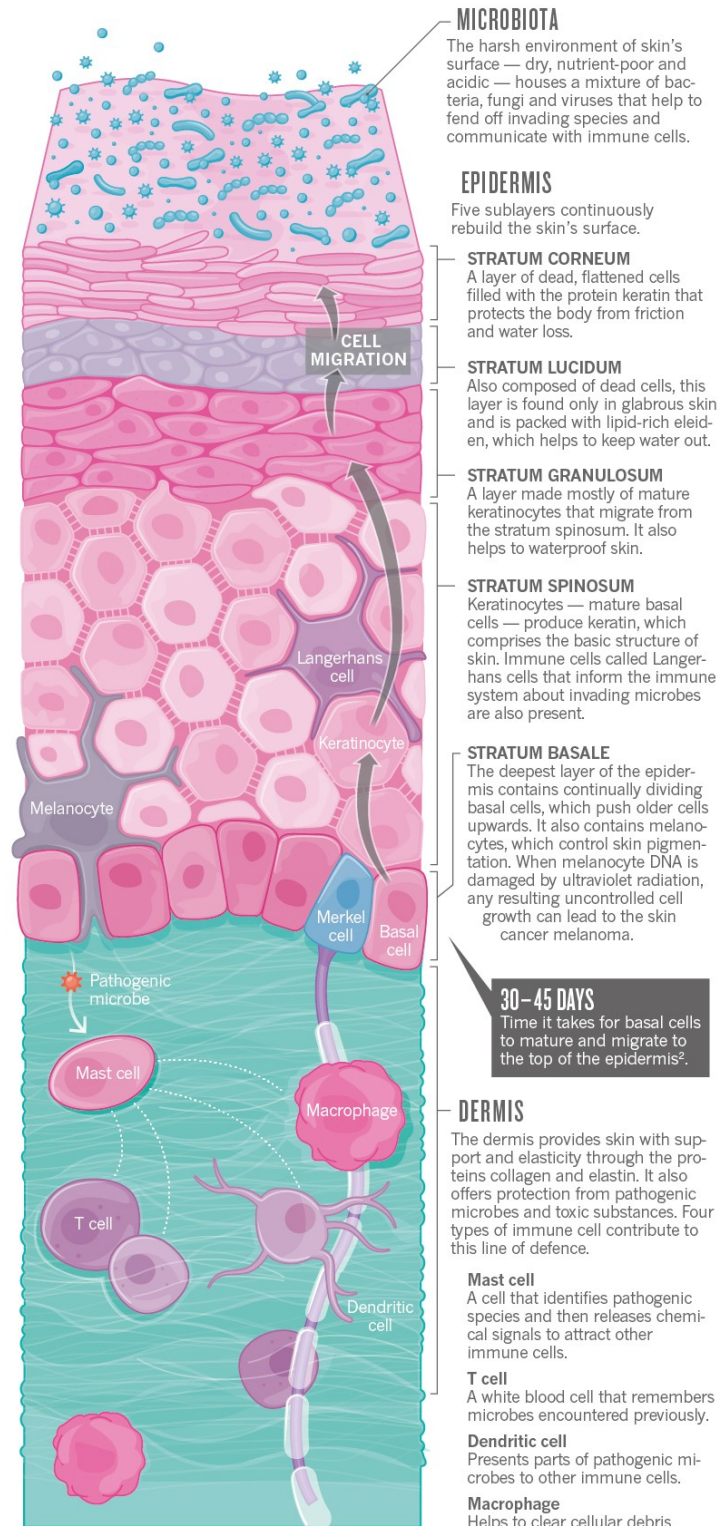


Figure 78. Stratified structure of the skin.

From Gould, 2018, Nature Outlook: Skin.

Epidermis. The epidermis is the outermost part of the skin which is separated from the underlying dermis via the dermo-epidermal junction. This junction is made of fibrillar ECM and has a fundamental role in the architecture of the epidermal components. The epidermis is a stratified squamous epithelium consisting of a constellation of keratinocytes which synthesize keratin, a filament-forming protein that ensures most protective functions of the skin. Due to poor vascularization, the epidermis relies solely on the blood supply from the dermis for nutrient and oxygen delivery (Baroni et al. 2012; Proksch et al. 2009).

Although keratinocytes represent about 90% of epidermal cells, the epidermis also contains other important populations such as the Langerhans cells (4%), the Merkel cells (3%) and melanocytes (3%) which have diverse embryonic origins (Madison 2003) (Figure 78).

Keratinocytes. They derived from the embryonic ectoderm. They proliferate upwards starting from the dermo-epidermal junction and undergo multiple stages of cell differentiation. Terminally differentiated keratinocytes, also called corneocytes, are dead cells filled with keratin that are continuously lost through desquamation, which are replaced by new layers in about 3 weeks.

Langerhans cells. They are dendritic cells derived from hematopoietic stem cells of the bone marrow. They reside in the epidermis as a dense network of mobile sentinels that sustain immune or allergic response.

Merkel cells. The origin of Merkel cells has been debated over the last 20 years, as they display both epidermal and neuroendocrine features. Current evidence suggests they may be derived from embryonic ectoderm or alternatively from the neural crest. These cells are present in the basal layer of the epidermis, concentrated in touch-sensitive areas close to sensory nerve endings (Polakovicova et al. 2011).

B. Role of melanocytes

Melanocytes are the fourth and last epidermal population. They are dendritic cells specialized in pigment production and can be found in the epidermis and hair follicles as well as in the inner ear, eyes, bones and the heart where their role is less understood (Goding 2007; Thomas and Erickson 2008). In human skin, melanocytes reside at the dermo-epidermal junction, regularly spaced by 10-15 keratinocytes and contacting up to 40. Once terminally differentiated, they synthesize the melanin

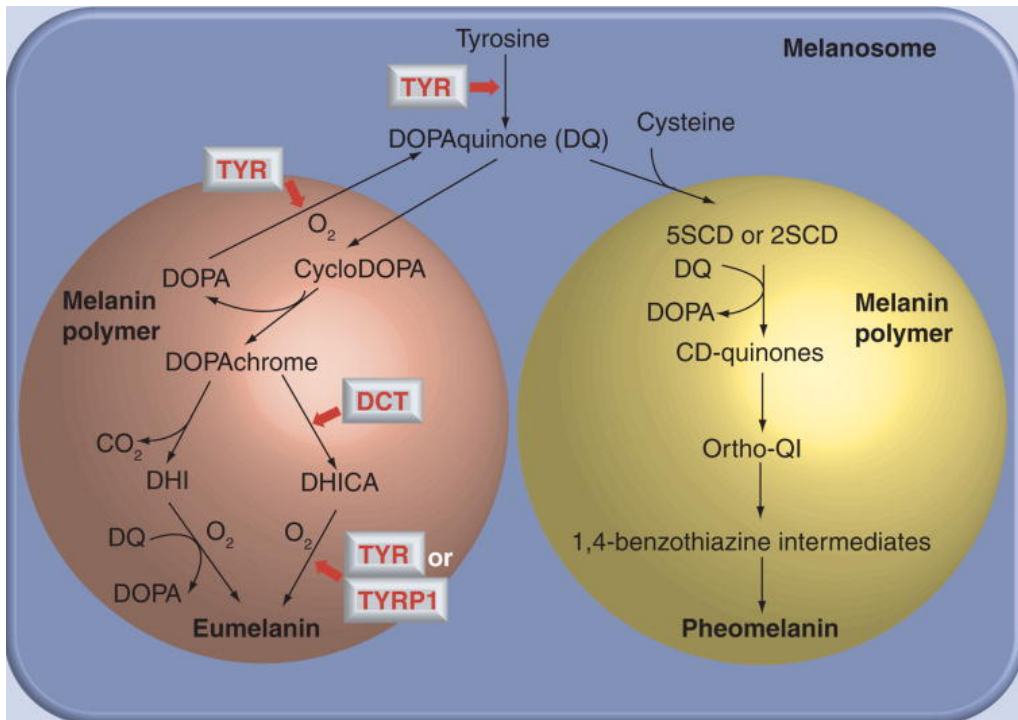


Figure 79. Production pathways of pheomelanin and eumelanin.

From Kondo and Hearing 2011.

pigment, in a process called 'melanogenesis', however they divide less than twice a year (Jimbow et al. 1976; Vandamme and Berx 2019). Melanin is the main contributor to pigmentation of skin and hair providing protection from ultraviolet radiation (UVR) damage due to its photoabsorbent and antioxidant properties (Brenner and Hearing 2008; Costin and Hearing 2007). Skin color and ease of tanning determine the skin 'phototype' which constitutes the most useful predictor of skin cancer risk within the population (Fitzpatrick 1988). Thus, populations can be classified in six phototypes (I to VI, pale white to black); the higher the type the lower the risk of sunburn and UVR damage (Bush and Simon 2007). Phototypes are the direct reflection of the distribution and melanin content of melanosomes, which is the result of the production ratio between pheomelanin (red to yellow shades) and eumelanin (brown to black shades), two types of melanin which can alternatively be synthesized (Kondo and Hearing 2011) (Figure 79).

Melanogenesis of both pheo- and eumelanin involve a tyrosine-dependent multistep reaction catalyzed by several key enzymes such as tyrosinase (TYR), tyrosinase-related protein 1 (TYRP1) and DCT (Land, Ramsden, and Riley 2003). Of note, melanogenesis is triggered several paracrine cytokines such as the melanocyte-stimulating hormone (α -MSH) which is secreted by keratinocytes that are exposed to UVB. After synthesis, melanin is packed into lysosome-like structures called 'melanosomes' and transported through the melanocytic dendrites to be delivered to adjacent keratinocytes (Dell'Angelica 2003; Schiaffino 2010). During their transport, melanosomes undergo a multistage maturation from immature endoplasmic vesicles to fully structured and pigmented organelles (Wasmeier et al. 2008). Upon being phagocytosed in keratinocytes, melanosomes are not distributed randomly and strategically concentrated over the UV-exposed side of nuclei in umbrella-like structures (Lin and Fisher 2007).

3.2.1.2. Ontogeny of melanocytes

During gastrulation, the embryo develops into three fundamental germ layers which are the endoderm, mesoderm and ectoderm. Endoderm forms the inner lining of the organism and gives rise to the digestive tube and the epithelial layer of respiratory, excretory and reproductive systems. As the name indicates, the mesoderm constitutes the middle tissues from which arise the muscles, connective

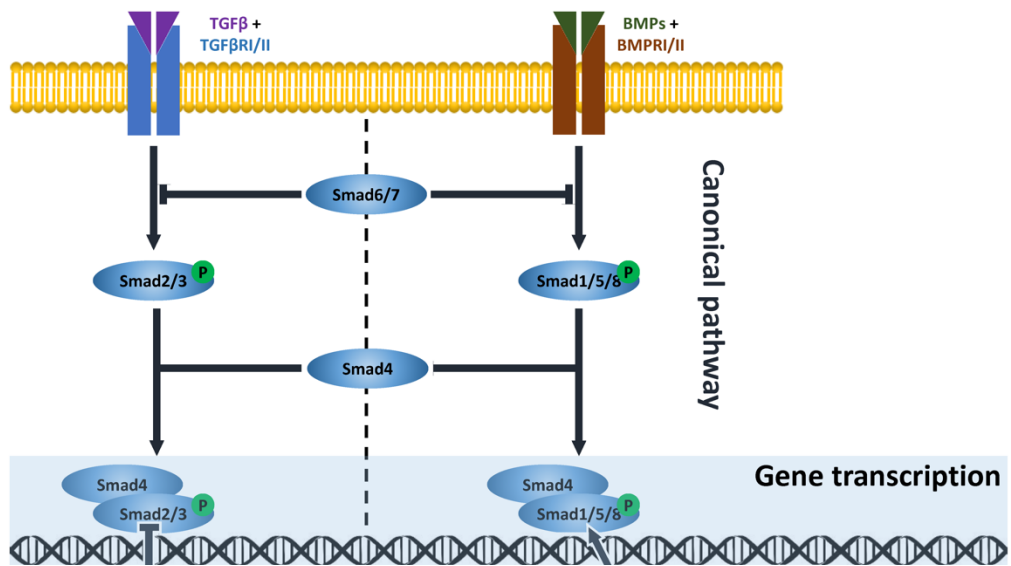


Figure 80. TGFβ/BMP-SMAD pathways.

From Dituri et al., 2019.

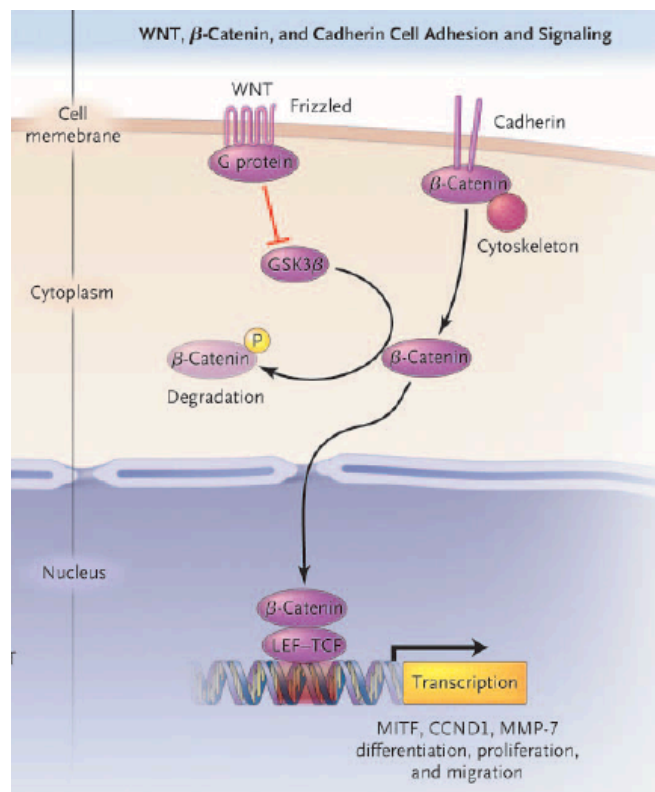


Figure 81. Canonical WNT signaling pathway.

From Miller and Martin, 2001.

tissues, bones and circulatory systems (lymph and blood). Lastly, the ectoderm is the outer body tissues which give rise to skin epidermis, nails, teeth as well as the nervous system. All melanocytes arise from neural crest cells (NCCs) which are induced during gastrulation and initially reside in the neural plate border territories within the ectoderm (Dupin, Creuzet, and Le Douarin 2006). Soon after gastrulation, the first step of organogenesis starts with primary neurulation, a process during which the ectoderm divides into three sets of tissues: the neural tube, the epidermis and the neural crest cells (Bronner and LeDouarin 2012). The formation of the neural tube was shown to be dependent on N-cadherin, a type of adhesion protein that holds the primary nerve cells together. Early induction of the neural crest relies particularly on crucial signals from the WNT and BMP pathways (Figure 80 and 81).

BMP pathway. The bone morphogenetic proteins are a group of growth factors first discovered for their ability to induce the formation of bone and cartilage, now considered to be pivotal in morphogenesis. Currently, thirteen have been described and all belong to the transforming growth factor beta (TGF β) superfamily. Upon interacting with their specific receptors, BMPs induce the phosphorylation of SMAD proteins and subsequent nuclear translocation. The SMAD signaling pathway consists in a complex network of nuclear TFs integrating inputs from both TGF β and BMPs. While the TGF β pathway relies on SMAD2/3:SMAD4 complexes, BMPs depend on SMAD1/5/8:SMAD4 complexes (Guo and Wang 2009). Of note, BMP4 was shown to be instrumental in inducing epidermis and neural crest cells as its inhibition by chordin, noggin and follistatin results in neural differentiation (Wilson et al. 1997).

WNT pathway. Several modes of WNT pathway activation have been described and the canonical WNT/ β -catenin pathway is the most well-understood. The WNT/ β -catenin pathway is essential for neural-crest induction and development of the melanocyte lineage. The human genome encodes 29 WNT cysteine-rich glycoproteins which are fundamental in activating the downstream pathway which depends on β -catenin, a member of the armadillo repeat motif (ARM) superfamily. In absence of triggering signal, β -catenin is associated with GSK-3 β , APC and axin in the cytoplasm. GSK-3 β phosphorylates β -catenin targeting it for ubiquitination and subsequent proteasomal degradation (Goding 2000; Saito-Diaz et al. 2013). Upon interaction of WNTs with their receptor Frizzled, the Dishevelled kinase is activated. This protein will phosphorylate and inhibit GSK-3 β resulting in accumulation and

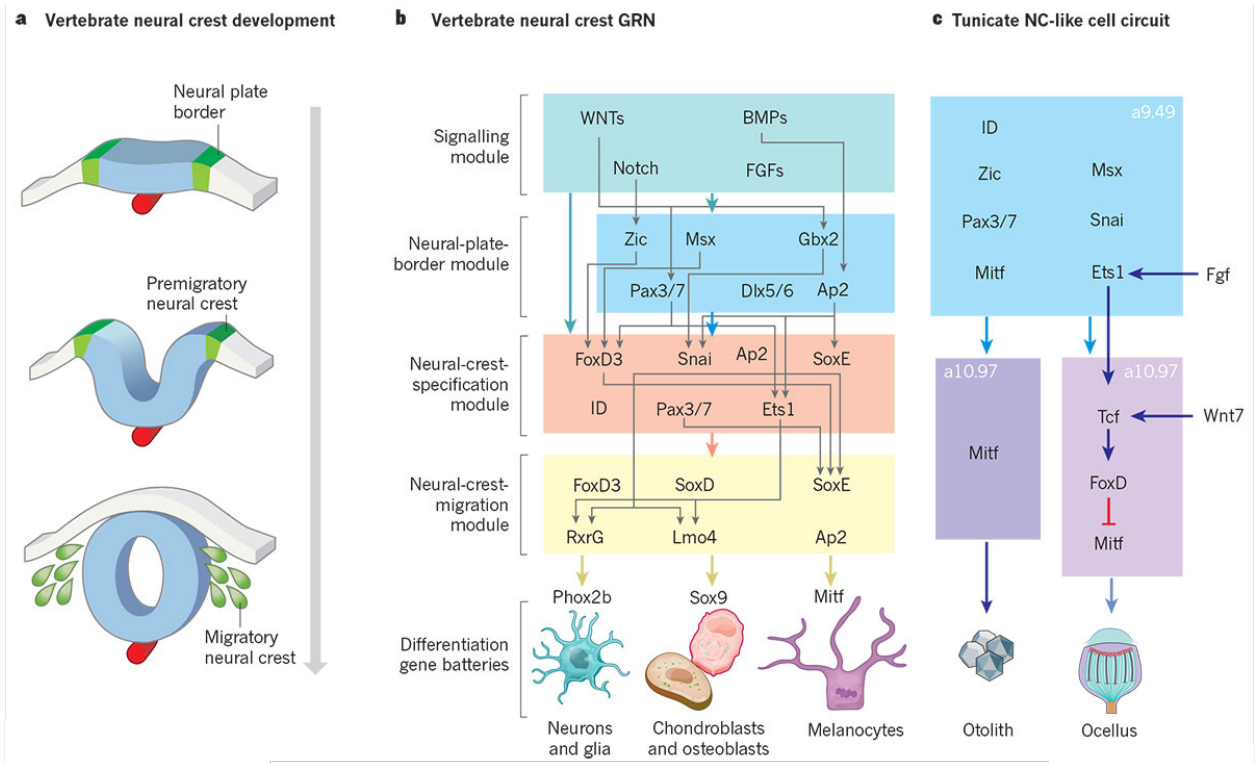


Figure 82. Neural crest formation stages and gene regulatory networks.

From Green, Simoes-Costa, and Bronner 2015.

nuclear translocation of β -catenin where it co-operates with LEF/TCF transcription factors and CBP/p300 co-activators to activate its target genes (Larue, Kumasaka, and Goding 2003). Of note, WNT1 or WNT3A and β -catenin have been shown to be essential for neural crest differentiation (Dorsky, Moon, and Raible 1998; Makoto et al. 1997).

After neural tube closure, specification of neural crest cells is allowed by induction of the expression of pre-migratory neural crest TFs such as FOXD3, TFAP2A, SOX10 and PAX3. However, NCCs are pluripotent progenitor cells that give rise to several lineages in distant sites of the organism (Mayor and Theveneau 2012). Thus, in order to acquire migratory properties required to colonize their target sites, NCCs undergo type I epithelial-to-mesenchymal transition (EMT) through induction of migratory neural crest TFs such as SNAIL, SLUG, RXRG and SOX9. Their migratory trajectory is critically connected to the face of the cells and takes place along two major paths either dorsoventrally between the neural tube and somites or dorsolaterally between somites and the ectoderm (Pla and Monsoro-Burq 2018; Vega-Lopez, Cerrizuela, and Aybar 2017). Most NCCs migrate dorsoventrally to give rise to multiple cell types like Schwann cells, smooth muscle cells, peripheral neurons or adipocytes; while cells taking the dorsolateral path give rise to skin melanocytes precursors referred to as melanoblasts (Ernfors 2010) (Figure 82).

In mammals, melanoblasts are specified from NCCs due to induction of the activity of the melanocyte master regulator MITF.

3.2.1.3. Melanocyte-Inducing Transcription Factor

First discovered in mice exhibiting loss of pigmentation and small ‘microphthalmic’ red eyes, the Melanocyte-inducing transcription factor (MITF) gene is located on chromosome 3q13. A peculiarity of the MITF locus is its organization in nine alternative promoters giving rise to nine splicing variants differing by their N-termini and expression patterns (Hershey and Fisher 2005; Steingrímsson 2008). MITF isoforms are expressed in a wide range of cells including melanocytes, osteoclasts, mast cells, retinal pigment epithelium and kidney cells, which explains how MITF mutations can lead to complex phenotypes with defective pigmentation, deafness and small eyes. Melanocytes almost exclusively express the M-isoform which is the most well-studied isoform to this day

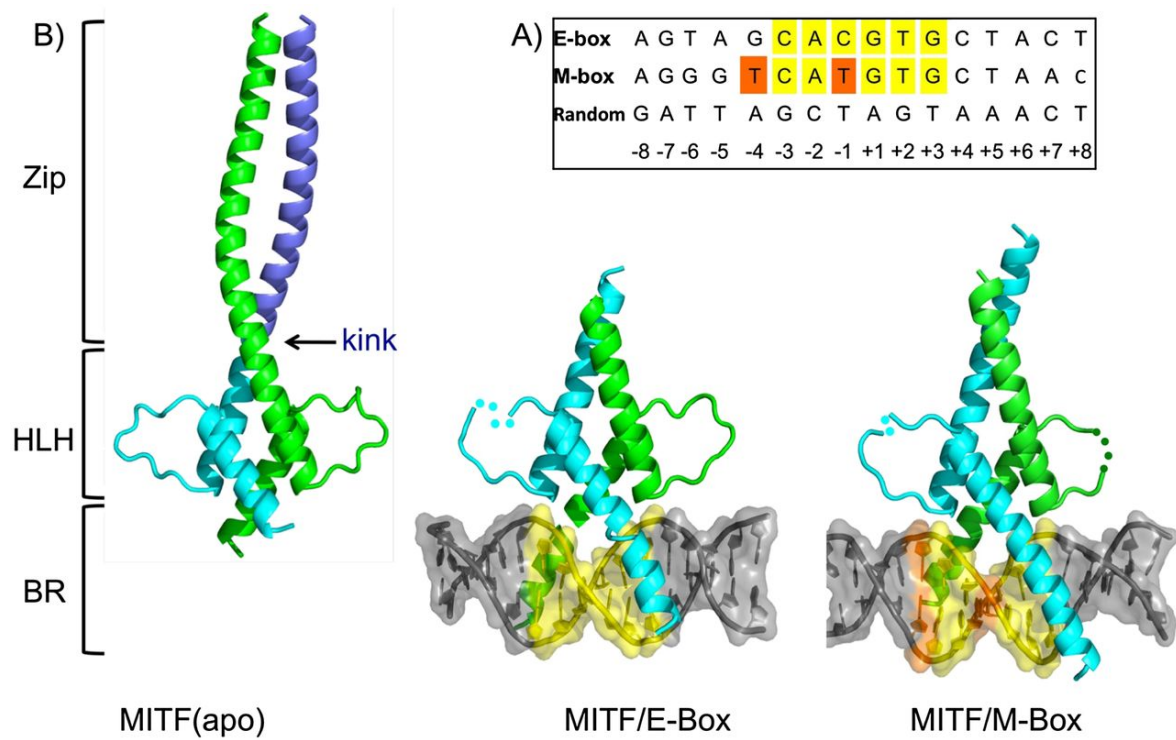


Figure 83. Structural characterization of the MITF DNA-binding and assembly region.

A. E-/M-box DNA sequences. **B.** Crystal structure of MITF in the absence and presence of DNA. From Pogenberg *et al.*, 2012.

(Hershey and Fisher 2005). MITF is a basic helix-loop-helix leucine zipper (bHLH-LZ) transcription factor that belongs to the MYC superfamily.

MITF can bind DNA as a homo- or a heterodimer with the highly related TFEB, TFE3 and TFEC transcription factors (Transcription factor B, 3 and C) which together form the MiT subfamily. In contrast, MITF does not form heterodimers with other bHLH-L2 TFs such as MYC, MAX, or USF as it harbors a three-residue insertion in its leucine zipper domain that creates a restrictive kink (Hemesath et al. 1994; Pogenberg et al. 2012). The MITF bHLH domain allows for recognition of E-box sequences (CACGTG) present in a set of its target genes. However, MITF displays higher affinity for the extend asymmetric E-box called 'M-box' (TCATGTG) as it is specifically present in promoters of genes associated with melanogenesis (Bentley, Eisen, and Goding 1994; Bertolotto et al. 1998). To regulate gene expression of its targets, MITF interacts with various co-factors. It is well established that MITF is largely dependent on chromatin-modifying and -remodeling complexes such as CBP/p300, NURF and BRG1-containing PBAF complexes (Koludrovic et al. 2015; Laurette et al. 2015). Of note, MITF finely regulates itself at a transcriptional level by a negative feedback loop (Louphrasitthiphol et al. 2019) or by various known activators and repressors such as SOX10, PAX3, CREB, β -catenin, STAT3, FOXD3, ZEB2, BRN2. In addition, several post-translational modifications notably by the c-KIT/MAP kinase pathway have been involved in regulating MITF activity (Goodall et al. 2008; Shibahara 2001; Thomas and Erickson 2009) (Figure 83).

MITF plays a pivotal role in melanocytes as it regulates several key gene networks (Goding 2000). Aforementioned pigmentation genes including TYR, TYRP1, DCT, PMEL, and MLANA are all under transcriptional control of MITF and they are crucial for melanocyte differentiation (Cheli et al. 2010). Moreover, MITF is also involved in the production and the trafficking of melanosomes to adjacent keratinocytes (Strub et al. 2011). Another key function of MITF is the regulation of cell cycle and mitosis genes in cooperation with SOX10 and chromatin remodelers. For instance, MITF activates the expression of cell cycle regulators such as CDK2, CCNB1 and CCND1 (Prince et al. 2004; Strub et al. 2011). Given that MITF is the master regulator of melanocyte proliferation and differentiation, it was

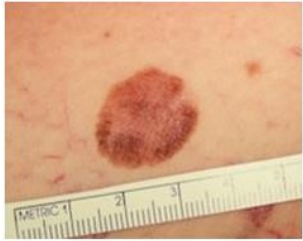



<p><i>Superficial spreading melanoma</i></p>  <ul style="list-style-type: none"> - Most Common - Flat and irregular in shape & color - Shades of black and brown 	<p><i>Nodular melanoma</i></p>  <ul style="list-style-type: none"> - Usually starts as a raised area - Dark black/blue or bluish/red - Some are not colored 	<p><i>Lentigo maligna melanoma</i></p>  <ul style="list-style-type: none"> - Usually occurs in older skin types - Commonly on face, neck, arms, etc - Abnormal skin areas usually large, flat, and tan with areas of brown 	<p><i>Acral lentiginous melanoma</i></p>  <ul style="list-style-type: none"> - Least common - Usually found on palms, soles, and even under fingernails
---	--	--	---

Figure 84. Subtypes of cutaneous melanoma.

From <https://www.oakwoodsolicitors.co.uk/service/melanoma-skin-cancer/>

without surprise that increasing evidence has reported its involvement in promoting melanoma (Hartman and Czyz 2015; Levy, Khaled, and Fisher 2006).

3.2.2. The genesis of melanoma

3.2.2.1. Melanoma classification

A. Main subtypes

Cutaneous melanoma is a malignant tumor that results from uncontrolled proliferation of skin melanocytes. It is the most lethal form of skin cancer responsible for nearly 75% of all skin cancer deaths. In the past 50 years its incidence rose faster than that of any other cancer (Jemal et al. 2011). If melanoma is diagnosed in its early stages, resection of the lesion usually results in relatively favorable prognosis. However, due to its ontogeny, melanoma have high EMT and migratory properties which are responsible for metastatic progression beyond its primary site. Once melanoma has metastasized, surgery is no longer an option and the disease becomes difficult to treat and is associated with poor prognosis (WH and JM 2017). It is important to be point out that the hyperproliferation of melanocytes can result in melanocytic neoplasms that range from benign lesions, termed melanocytic nevi, to malignant ones, termed melanoma. Although melanomas can arise from pre-existing nevi (about 30%), most primary melanomas arise de novo from skin not exhibiting any melanocytic neoplasm (Gandini et al. 2005; Weatherhead, Haniffa, and Lawrence 2007). Nevus-associated melanomas was found to commonly localize on the extremities and the trunk, whereas de novo melanomas are mostly found in the head and neck and the acral region. However, no differences in terms of prognosis and clinical features were found (Duman et al. 2015).

Four major subtypes of melanoma exist as proposed by the Clark & Reed classification based on their morphology and primary site : superficial spreading melanoma (SSM, 70%), nodular melanoma (NM, 20%), lentigo malignant melanoma (LMM, 10%) and acral lentiginous melanoma (ALM, 5%) (Clark et al. 1969) (Figure 84). These subtypes have well recognized clinical and histopathological characteristics. In addition, works by the Bastian group have highlighted the correlation between site of origin and somatic mutations. Melanoma arising from chronically sun damaged (CSD) sites bear a

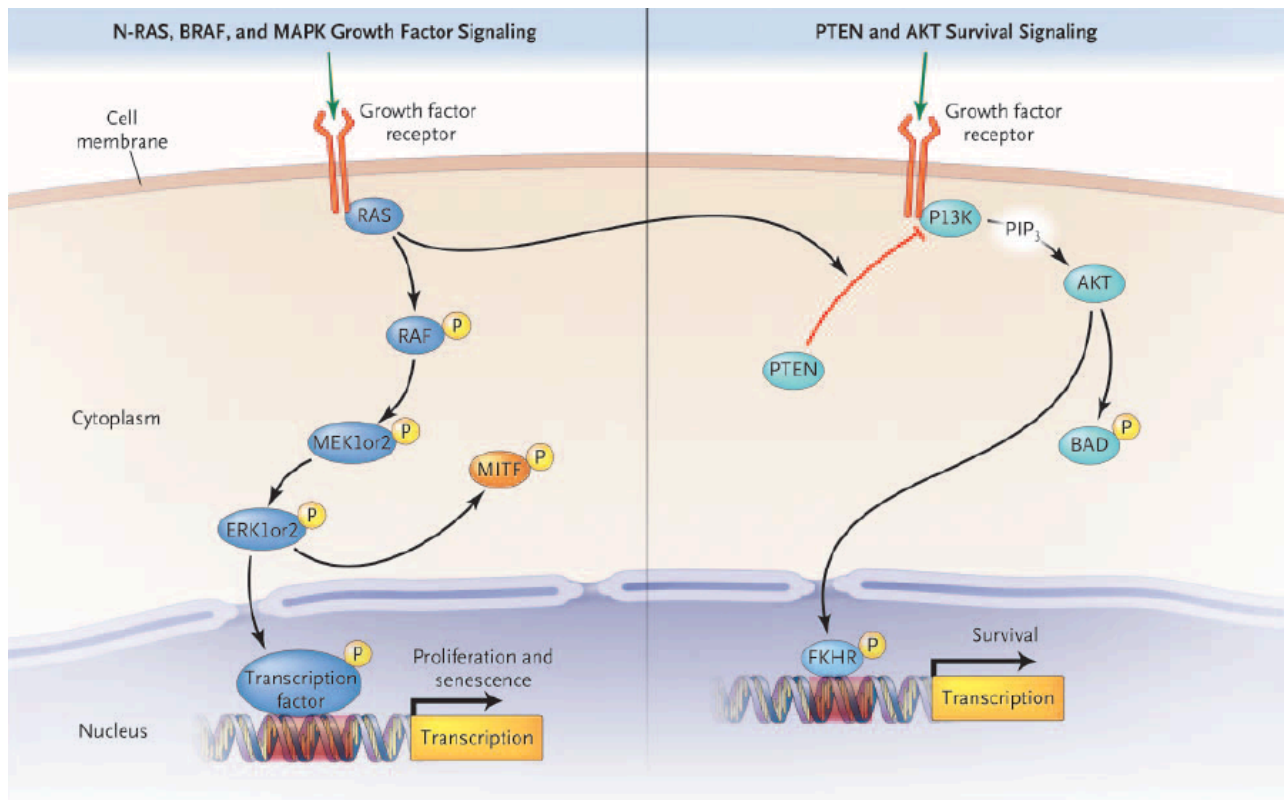


Figure 85. MAPK/ERK and PIK3/AKT pathways.

From Miller and Martin, 2001.

higher mutational burden than tumors arising from non-sun exposed sites. This can be explained by UV-induced C > T transitions at dipyrimidines which constitute the dominant mutational signature of CSD melanoma. CSD and non-CSD melanomas differ from their anatomical site of origin, degree of cumulative exposure to UV radiations, host age, mutation burden and type of oncogenic alterations (Curtin et al. 2005; Shain and Bastian 2016). Indeed, CSD melanomas typically originate from the head and neck region in older individuals (> 55 years old). In contrast, non-CSD melanomas often affect intermittently sun-exposed areas such as the trunk and legs in younger individuals (< 55 years old) that do not show marked actinic elastosis (skin photoaging).

B. Driver mutations

Melanomas are notorious for exhibiting one of the highest somatic mutation burden of all human tumors. The large majority (90%) of melanoma driver mutations typically lead to the aberrant activation of the MAPK and the PI3K/AKT pathways which are responsible for sustained activation of proliferation, cell growth and survival (Chappell et al. 2011; Wellbrock et al. 2004).

MAPK/ERK pathway. The MAP kinases pathway regulates cell fate decisions downstream of receptor tyrosine kinases, cytokines and heterotrimeric G-protein-coupled receptors (Wellbrock et al. 2004). In normal melanocytes, this pathway is activated by growth factors such as stem cell factor (SCF), fibroblast growth factor (FGF) and hepatocyte growth factor (HGF) (Bohm et al., 1995). A combination of these factors is required to stimulate strong ERK activity in melanocytes (Geissinger et al. 2002). Activated ERK translocates to the nucleus where it activates transcription factors important for cell proliferation (Figure 85).

PI3K/AKT pathway. The phosphoinositide-3-OH kinase (PI3K) pathway converts membrane phosphoinositides into secondary messengers through hyper-phosphorylation. These secondary messengers activate numerous downstream effector pathways such as AKT (protein kinase B) (Cully et al. 2006). Activated AKT regulates a network of factors that control cell proliferation and survival. Importantly, the activity of AKT is inhibited by the lipid phosphatase PTEN (phosphate and tensin homologue) which thus acts as a tumor-suppressor. Consistently, PTEN function was shown to be lost in late stage melanomas (Wu, Goel, and Haluska 2003).

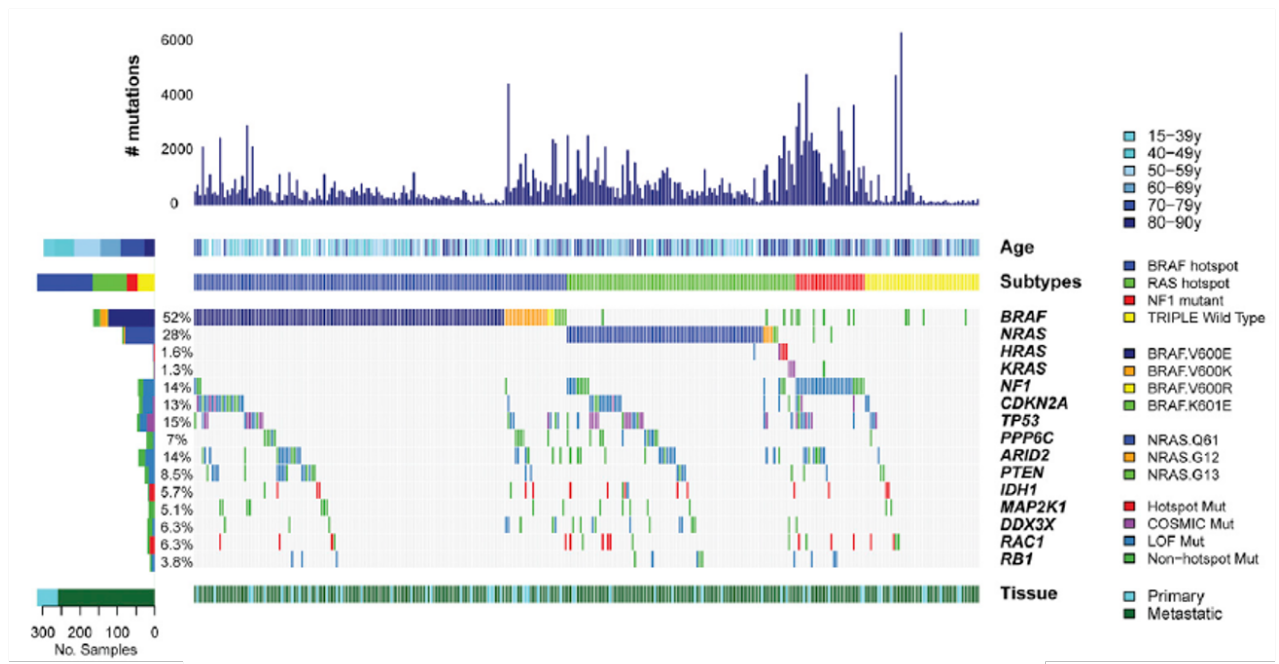


Figure 86. Driver mutations in melanoma.

From Akbani *et al.*, 2015.

Based solely on the occurrence of driver mutation, melanomas have been classified into four genomic subtypes : BRAF-mutant, NRAS-mutant, NF1-mutant and triple wildtype (Akbani et al. 2015). This classification is based on whole genome sequencing of 333 primary and metastatic cutaneous melanomas which revealed that the most frequent mutations affect BRAF (50%, predominantly V600E), NRAS (25%, predominantly G12 or Q61), NF1 (5-10%, loss of function) and KIT (2-8%, amplifications). Other mutations frequently encountered comprise ARID2, CDKN2A, PTEN, TP53 and RAC1. While NF1 and NRAS mutations are found predominantly in CSD-type melanomas, BRAF^{V600E} mutations constitute the hallmark of non-CSD melanomas afflicting young individuals (Birkeland et al. 2018; Curtin et al. 2005). Importantly, triple wildtype melanomas do not exhibit a UV-induced damage signature and are often more difficult to treat (Figure 86).

BRAF mutations. The RAF family comprises 3 members ARAF, BRAF and CRAF, however only BRAF is frequently mutated in melanomas. BRAF is a serine/threonine protein kinase organized in three domains: two domains with regulatory function and one catalytic domain responsible for MEK phosphorylation. The catalytic domain is also responsible for maintaining the protein in its inactive conformation through an hydrophobic interaction between the so-called glycine-rich loop and the activation segment, making it non accessible to ATP binding (Davies et al. 2002). In the mutated form BRAF^{V600E}, the hydrophobic valine is replaced by polar hydrophilic glutamic acid resulting in an abnormal flip of the catalytic domain that generates a constitutive active conformation with a kinase activity 500-fold higher than that of the wild-type BRAF kinase (Richtig et al. 2017; Wan et al. 2004).

NRAS mutations. The RAS subfamily contains 3 isoforms HRAS, KRAS and NRAS which are small GTPase proteins involved in signal transduction. In melanomas, the most frequently mutated RAS isoforms is NRAS. Mutations of codon Q61 in NRAS lead to the constitutive inhibition of GAP proteins which are responsible for GTP hydrolysis. This allows NRAS^{Q61*} to permanently remain in an active GTP-bound state, abnormally maintaining both the MAPK and the PI3K pathways activated. Importantly, NRAS and BRAF mutations are considered mutually exclusive (Fedorenko, Gibney, and Smalley 2013; Hodis et al. 2012).

NF1 mutations. The NF1 (Neurofibromin 1) is a GTPase-activating protein that inactivates the RAS family by facilitating hydrolysis of its bound GTP to GDP, thereby inhibiting downstream RAS

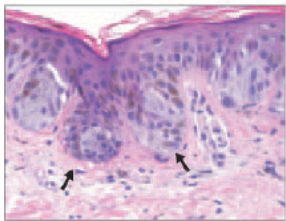
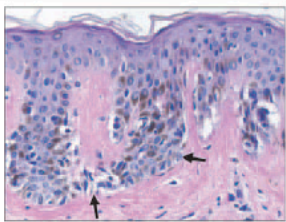
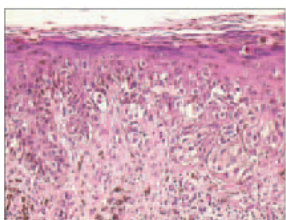
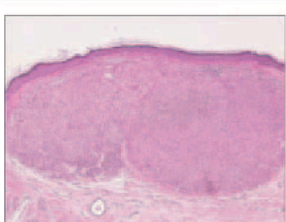
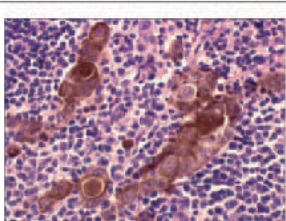
Histopathological Appearance	Description	Histologic Features
 <p data-bbox="309 483 432 506">Benign nevus</p>	<p data-bbox="576 255 635 277">Step 1</p> <p data-bbox="576 280 1070 450">The first event is a proliferation of structurally normal melanocytes leading to the benign nevus. Clinically, these nevi present as flat or slightly raised lesions with either uniform coloration or a regular pattern of dot-like pigment in a tan or dark brown background. Histologically, such lesions have an increased number of nested melanocytes along the basal layer (arrows).</p>	<p data-bbox="1129 255 1369 304">Proliferation of melanocytes Benign lesions</p>
 <p data-bbox="309 759 432 781">Dysplastic nevus</p>	<p data-bbox="576 530 635 553">Step 2</p> <p data-bbox="576 555 1070 703">The next step is the development of aberrant growth. This may occur within a preexisting benign nevus or in a new location. Clinically such lesions may be asymmetric, have irregular borders, contain multiple colors, or have increasing diameters. Histologically, such lesions have random and discontinuous cytomorphologic atypia (arrows).</p>	<p data-bbox="1129 530 1262 580">Dysplastic cells Random atypia</p>
 <p data-bbox="280 1034 464 1057">Radial-growth phase</p>	<p data-bbox="576 806 635 828">Step 3</p> <p data-bbox="576 831 1070 1001">During the radial-growth phase, cells acquire the ability to proliferate intraepidermally. Clinically, they sometimes present as raised lesions. These lesions no longer display random atypia and instead show cytomorphologic cancer throughout the lesion. In addition to the intraepidermal cancer, the cells can penetrate the papillary dermis singly or in small nests but fail to form colonies in soft agar.</p>	<p data-bbox="1129 806 1321 855">Intraepidermal growth Continuous atypia</p>
 <p data-bbox="280 1310 464 1332">Vertical-growth phase</p>	<p data-bbox="576 1081 635 1104">Step 4</p> <p data-bbox="576 1106 1070 1254">Lesions that progress to the vertical-growth phase acquire the ability to invade the dermis and form an expansile nodule, widening the papillary dermis. The cells can also extend into the reticular dermis and fat, are capable of growth in soft agar, and have the capacity to form tumor nodules when implanted in nude mice.</p>	<p data-bbox="1129 1081 1273 1104">Dermal invasion</p>
 <p data-bbox="280 1585 464 1608">Metastatic melanoma</p>	<p data-bbox="576 1357 635 1379">Step 5</p> <p data-bbox="576 1382 1070 1529">The final step in the model is the successful spread of cells to other areas of the skin and other organs, where they can successfully proliferate and establish a metastatic focus. These cells can grow in soft agar and can form tumor nodules that may metastasize when implanted in nude mice.</p>	<p data-bbox="1129 1357 1225 1379">Metastasis</p>

Figure 87. The Clark Model of melanoma progression.

From Miller and Martin, 2001.

signaling. NF1 mutations are found in 46% of melanomas expressing wildtype BRAF and NRAS. Most often, these alterations results in loss-of-function that drives the hyperactivation of NRAS protein and subsequently increases MAPK and PI3K pathways signaling (Krauthammer et al. 2015; Nissan et al. 2014). NF1 loss was shown to cooperate with BRAF to drive melanoma development and acquired BRAF inhibitor resistance (Maertens et al. 2013; Whittaker et al. 2013).

More recently, RNA and DNA sequencing of 133 single-cell melanocytes allowed the Shain group to propose a two-hit model of transformation highlighting once more the central role of the MAPK pathway. In this model, mutations affect either a single melanocyte or an array of neighboring melanocytes, thus constituting a 'field' for malignant transformation upon secondary mutations. It was notably found that mutations not targeting the MAPK pathway such as ARID2 or CDKN2A were enriched in those readily transformable melanocyte fields.

3.2.2.2. Biology of melanoma development

In 1984, Clark et al. proposed a multi-step progression model described the genetic basis of melanoma initiation and progression, which despite being relatively old, remains valid to this day and widely accepted in the field (Greene et al. 1984). According to the Clark model, melanogenesis follows a five-step development from melanocyte to metastatic melanoma (Figure 87).

MAPK mutation. The initial oncogenic event is associated with a strong MAPK mutations such as BRAF^{V600E} which leads to the development of a nevus (Pollock et al. 2003). However, the initial growth of the nevus is followed by stabilization of the size and loss of most proliferative activity due to oncogene-induced senescence (Michaloglou et al. 2008). Thus, the nevus is considered benign at this stage and may stay dormant for an extended amount of time before undergoing additional changes.

Senescence escape. The second event of melanoma development consist in senescence escape and growth of a dysplastic nevus that may arise from a preexisting melanocytic nevus or as a new lesion. Senescence escape is achieved through the disruption of the Retinoblastoma (Rb) pathway, mostly by the inactivation of CDKN2A (cyclin-dependent kinase Inhibitor 2A, p16), a gene encoding p16INK4a and p19ARF. Alternatively, PTEN is inactivated which leads to hyperactivation of PI3K/AKT as mentioned before.

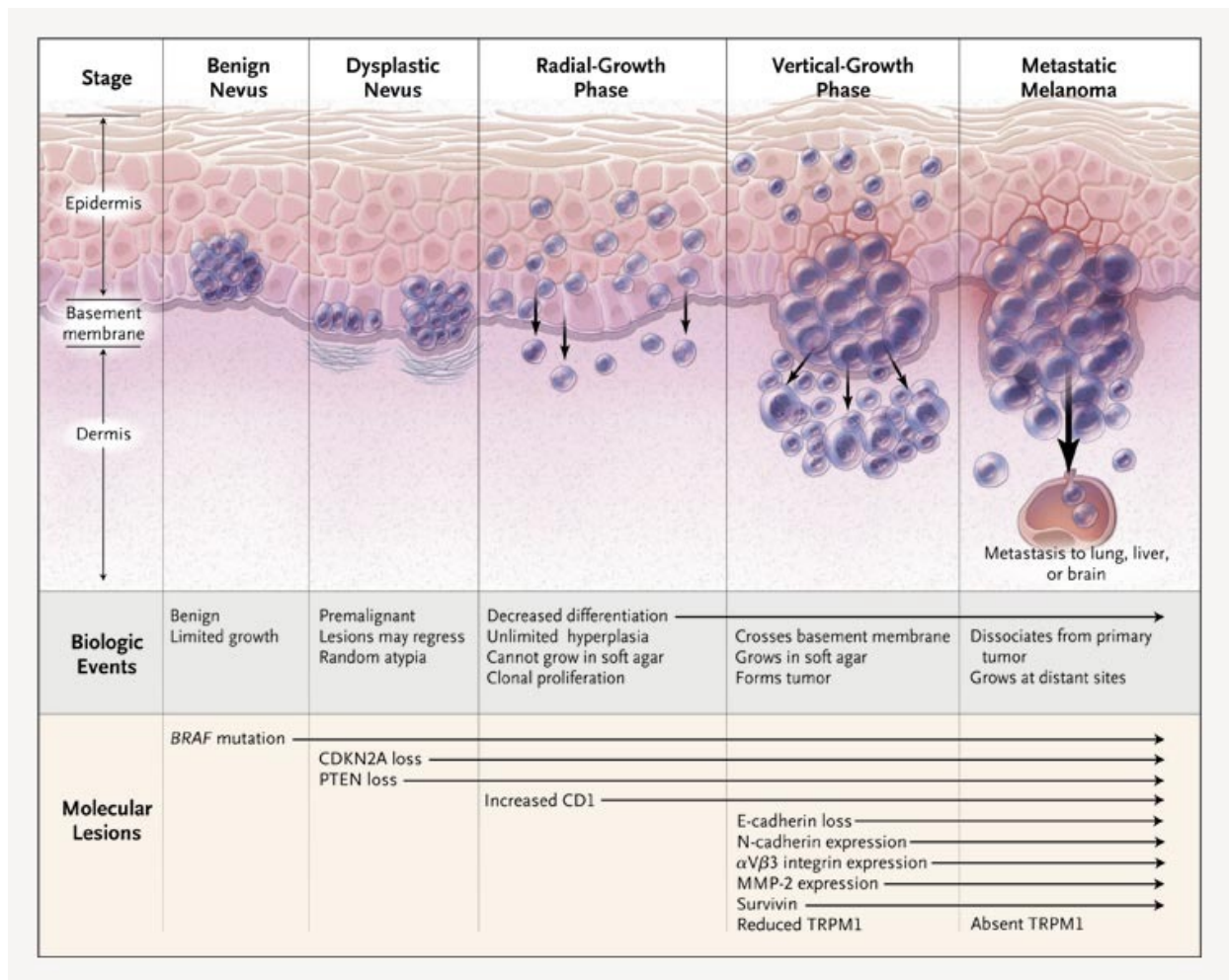


Figure 88. Linear development from melanocyte to metastatic melanoma.

From Miller and Martin, 2001.

Radial Growth Phase. Following the senescence escape, the third step in progression is the so-called radial growth phase (RGP) of melanoma as the disease spreads radially within the epidermis, as it cannot cross the dermo-epidermal junction. It was also found that at this stage, tumor cells are not able to grow in soft agar. In this phase of progression, the tumors are composed of a bulk of immortalized and highly proliferative cells. The clonal proliferation is fueled by the MAPK pathway as well as frequent amplifications of cell cycle regulators such as CCND1 or CDK4 (Sviderskaya et al. 2003).

Vertical Growth Phase. In the fourth stage, the rapidly-growing tumors irremediably enter the vertical growth phase (VGP) in which the tumors grow vertically and dive deep into the dermis. This step requires a drastic epigenetic reprogramming often referred to as ‘pseudo-EMT’ as melanocytes are not epithelial cells *per se*. During this process, the tumors are marked by the loss of differentiation markers and the expression of MMPs and integrins which contribute to the destruction of the dermo-epidermal junction. Consistently, tumor cells at this stage are capable of forming colonies in soft agar.

Metastatic progression. In the final stage of the Clark model, the tumor cells have acquired high invasive properties through pseudo-EMT and progressively spread in the surrounding region until they reach blood or lymphatic vessels. Additionally, pro-angiogenic signals such as VEGF were shown to be secreted by the tumors to induce formation of blood vessels (Murukesh, Dive, and Jayson 2010). Once their intravasation is completed, tumor cells circulate freely until they reach a favorable environment to form metastatic foci in other organs. The most common sites of melanoma metastases are distant cutaneous sites, the lung, the liver, the brain, bones, the gastrointestinal tract (Figure 88).

Thus, according to the Clark model, melanoma cells progress from a proliferative/weakly metastatic state to an invasive/strongly metastatic state through the accumulation of molecular changes (mutations and epigenetic changes). While it fits well with clinical observations, this linear evolution model was revamped over the years due to the advent of single-cell technologies. Some have proposed the existence of cancer stem cells that drive tumorigenicity, however such as model is still largely under debate and stem cells do not give satisfactory explanations for metastatic progression . Current models favor a branched clonal evolution of cancer cells where cells expand into multiple subtypes due to the integration of endogenous and exogenous signals, resulting in a co-existing ecosystem of tumor cells with distinct phenotypes.

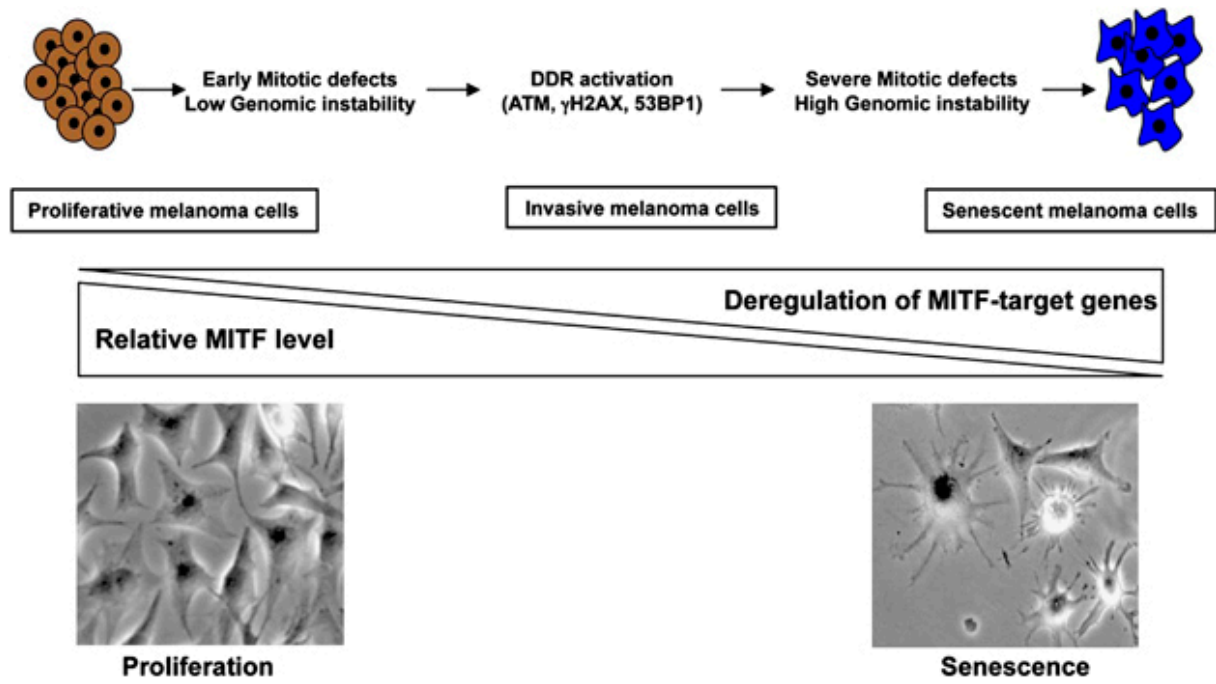


Figure 89. MITF rheostat model.

From Strub *et al.*, 2011.

3.2.2.3. Melanoma heterogeneity

Melanoma is among the most aggressive and therapy-resistant cancers. Thus, intratumoral heterogeneity is the most pressing issue for all types of therapy. Historically melanoma has been one of the fields that contributed the most to understand tumor heterogeneity, due in part to the relative ease of sample availability.

A. MITF rheostat

Phenotypic diversity in melanoma has been described decades ago (Barnes et al. 1981), but only the advent of high-throughput sequencing allowed the in-depth study and characterization of the different melanoma states. A first key study in 2006 by Hoek et al. identified three main cohorts (A, B and C) of 86 cultured melanoma cell lines based on their gene expression profiles (Hoek et al. 2006). This and subsequent transcriptomics studies have revealed that cells from lines in ‘cohort A’, express high levels of the melanocyte lineage-specific TF MITF and the neural crest-specific TF SOX10 (Hoek et al. 2008; Widmer et al. 2012). These cells are known to display high proliferation rates but poor migratory and invasive properties (Hoek et al. 2006; Verfaillie et al. 2015; Wouters et al. 2020). It was shown that the proliferative signature genes are targets of WNT signaling, MITF, SOX10 or PAX3 which are all highly active in these cells which is why they were termed proliferative or melanocytic (MEL) (Figure 89).

On the other hand, cells in ‘cohort C’ express low levels of MITF and SOX10, but high amounts of EMT-TFs ZEB1 and SOX9 as well as several TGF β target genes involved negative regulation of WNT signaling (WNT5a, DKK1, CTGF) and extracellular matrix remodeling (INHBA, COL5A1, and SERPINE1). Cohort C cell lines were also found to divide rather slowly displaying mesenchymal-like properties with higher migratory, invasive and therapy-resistance abilities (Konieczkowski et al. 2014). For these reasons, they are referred to as invasive or mesenchymal-like (MES) or dedifferentiated state. Importantly, melanoma cells with low MITF express higher levels of the receptor tyrosine kinase AXL, which has been linked to intrinsic resistance to MAPK inhibitors (Müller et al. 2014). Further epigenomic studies based on H3K27ac mapping and ATAC-seq data of the MEL and MES states revealed that they are regulated by SOX10, MITF, TFAP2A, and AP-1, TEAD4, RUNX2, respectively (Hoek et al. 2006; Verfaillie et al. 2015; Wouters et al. 2020). Moreover, it was found that tumor

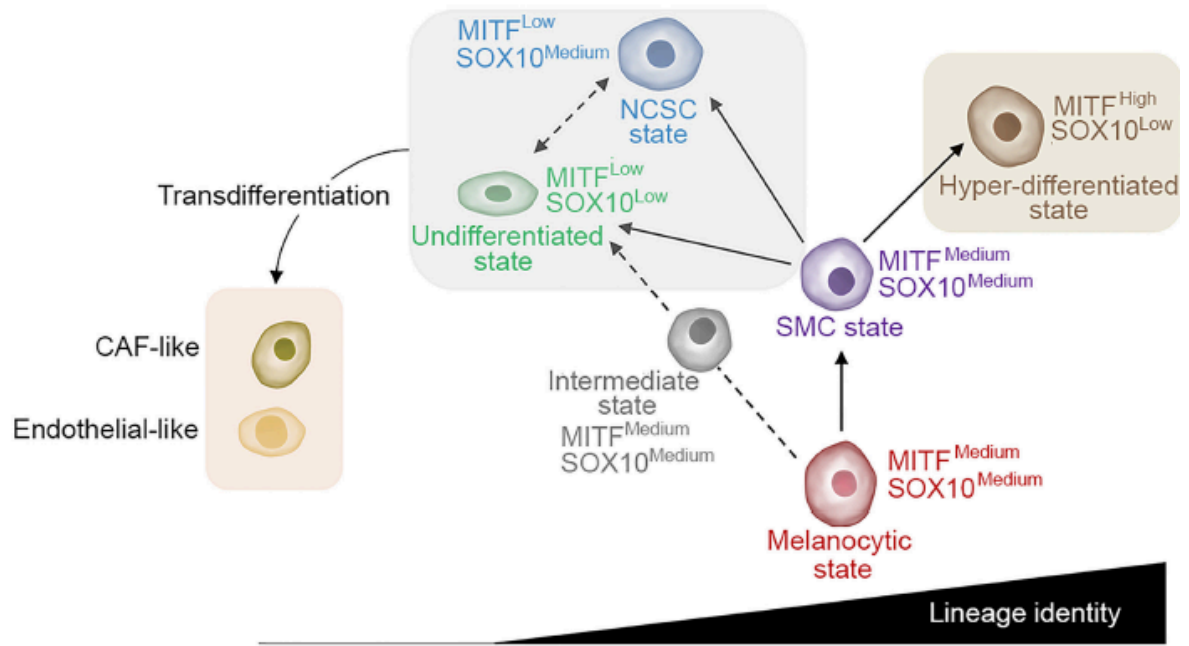


Figure 90. Expression of MITF/SOX10 and melanoma heterogeneity.

From Rambow *et al.* 2018.

inflammation promotes phenotypic plasticity as pro-inflammatory cytokine such as TNF- α instigate gradual suppression of MITF expression through JUN/AP-1, thereby making the connection between immune cell infiltration and melanoma heterogeneity (Riesenberg et al. 2015). These observations confirm that cells can dynamically switch their MITF expression which led to the proposed ‘rheostat model’ in which the activity of MITF determines many biological properties of melanoma cells (Carreira et al. 2006). High MITF activity promotes terminal differentiation and cell cycle exit, intermediate activities correlate with high proliferation, while lower MITF activity results in slow-cycling invasive cells. Early single-cell gene expression analysis demonstrated the heterogeneous expression of MITF *in vivo* (Davidson et al. 2019; Ullrich et al. 2015).

B. Phenotype switching

The increasing evidence demonstrating the MITF-dependent cell plasticity in melanoma were in support of a ‘phenotype switching’ model. It predicts that MITF-low and MITF-high subpopulations are only temporarily distinct and that these cells can reversibly and dynamically switch transcriptional programs between proliferative and invasive states in response to different cues (Hoek and Goding 2010; Quintana et al. 2010). *In vivo* analyses later on showed that melanoma tumors typically include cells of both phenotypes that can switch between the two phenotypes (Eichhoff et al. 2010; Hoek et al. 2008). In addition, Shaffer et al. showed that the switch to a resistant phenotype can be induced by drugs and they observed a rare transient subpopulation of cells that showed predisposition for switching (Shaffer et al. 2017) (Figure 90).

In their landmark study, Rambow *et al.* combined patient-derived xenografts models with single-cell RNA-seq to study the biology of melanoma minimal residual disease (MRD). MRD is a mechanism by which clinical relapses are driven in a mutation-independent way by a small subset of residual or ‘drug-tolerant cells’ (Luskin et al. 2018). By analyzing the gene expression kinetics after MAPK-targeted therapy, they highlighted the complex drug-induced heterogeneity *in vivo* with distinct subpopulations including MITF^{high}/SOX10^{low} terminally differentiated cells, SOX10^{high}/MITF^{low} neural crest cell-like cells and SOX10^{low}/MITF^{low}/AXL^{high} mesenchymal-like cells. Authors concluded that at least some of these drug-resistant states are due phenotypic reprogramming and subsequent ‘Lamarckian

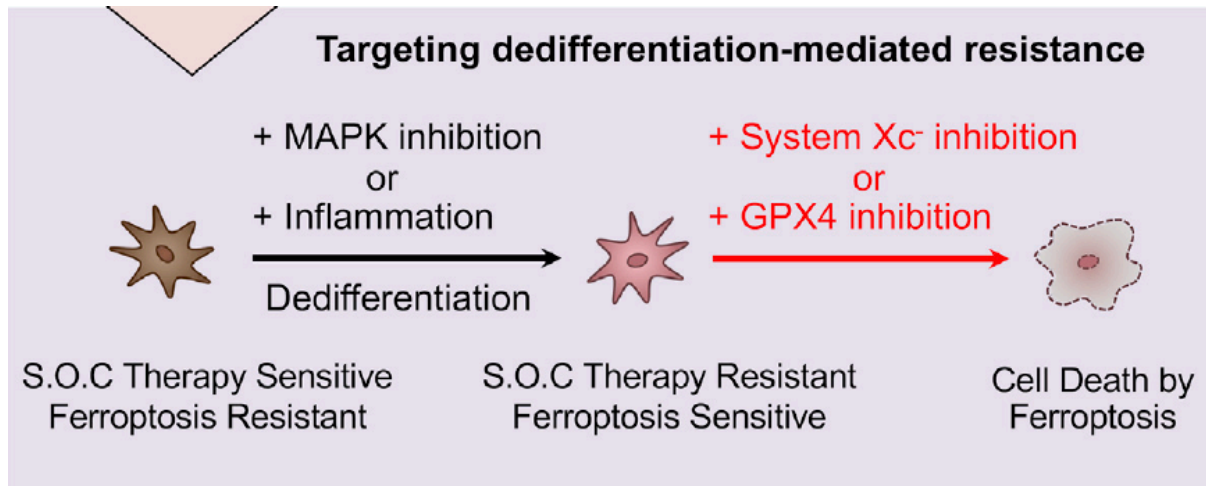


Figure 91. Melanoma cell dedifferentiation increases sensitivity to ferroptosis through upregulation of GPX4.

From Tsoi *et al.*, 2018.

selection' of specific cell states that are best adapted to survive in those conditions (Rambow et al. 2018). The novel neural crest cell-like phenotype is thought to represent one of the intermediates between melanocytic and dedifferentiated states which was observed *in vivo* in other single-cell datasets (Jerby-Arnon et al. 2018; Tirosh et al. 2016; Wouters et al. 2020). In their works, Tsoi *et al.* confirmed the existence of an intermediate neural crest signature and demonstrated that melanoma cell dedifferentiation increases sensitivity to ferroptosis through upregulation of GPX4 (Tsoi et al. 2018). Importantly, the phenotype switch from the melanocytic to mesenchymal state phenotypically and functionally resembles type III EMT often observed in cancer (Rambow, Marine, and Goding 2019) (Figure 91).

Altogether, phenotype switching in melanoma favors a model in which cell state transition is dependent on reprogramming of the transcriptome rather than being dictated by the acquisition of specific DNA mutations, although specific genetic lesions may actually render melanoma cells susceptible to such reprogramming as was shown for BRAF mutations (Caramel et al. 2013). Understanding of the molecular mechanisms underpinning phenotype-switching in melanoma is essential to developing novel therapeutic approaches aimed at eradicating therapeutically resistant cells with high metastatic potential.

3.2.3. Treatments and resistance

Local surgical excision represents the treatment of choice that is indeed curative for the majority of patients with newly-diagnosed melanomas at early stages (Gershenwald and Ross 2011). Furthermore, for patients with a solitary melanoma metastasis, metastasectomy is part of the standard of care, while in some metastatic cases chemotherapy may also be considered (Batus et al. 2013). Also, despite being rarely indicated for primary tumor treatment, radiotherapy has been considered for the treatment of skin, bone, and brain metastases (Garbe et al. 2016).

However, during the last decade, the development and approval of novel highly effective targeted therapies and immunotherapies has led to a clinical revolution for patients facing advanced-stage melanomas. Nowadays, immunotherapy and targeted therapies constitute the backbone of melanoma systemic therapy (Domingues et al. 2018).

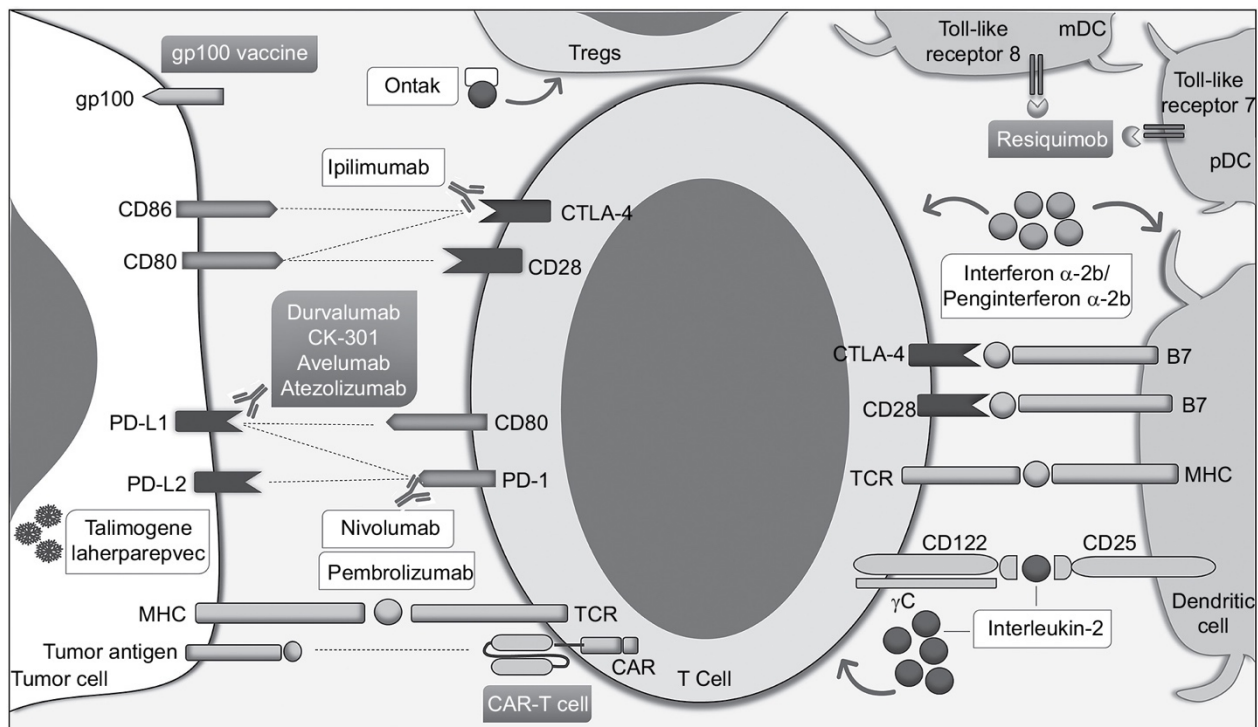


Figure 92. Immunotherapies approved by FDA (in white) or in trials (in gray) for cutaneous melanoma treatment.

From Domingues et al. 2018.

3.2.3.1. Immune checkpoint blockade

The concept that cancer and immune system are closely related is not new and was based on the frequent appearance of tumors at the sites of chronic inflammation and the presence of immune cells in tumor tissues (Balkwill and Mantovani 2001). In antitumoral responses, T lymphocyte cells recognize tumor-specific antigens which can activate them subsequently inducing their proliferation and differentiation in order to acquire the capacity to destroy targeted tumor cells. T-cell activation begins with the binding of a specific T-Cell Receptor (TCR) to its cognate peptide-major histocompatibility complex (MHC) presented on the surface of an antigen-presenting cell (APC). However, T-cell activation is regulated by a number of co-stimulatory and co-inhibitory signals. Some of the most studied immune checkpoint inhibitors are CTLA-4 and PD-L1 (Fife and Bluestone 2008).

Targeting CTLA-4. CTLA4 (cytotoxic T-lymphocyte-associated antigen-4) is an inhibitory molecule expressed on T cells that is involved in the early negative regulation of the T cell interaction with antigen presenting dendritic cells. Cancer cells express the B7 proteins (CTLA-4 ligands) to look like APCs and escape T-cell targeting. CTLA-4 inhibitors such as Ipilimumab, a monoclonal antibody, bind to CTLA-4 and thus enhance antitumoral T-cell response (Domingues et al. 2018).

Targeting PD-L1. PD-1 (programmed cell death protein-1), like CTLA-4, inhibits T-cell activity however, PD-1 negatively regulates TCR-signaling events at a later stage in peripheral tissues. Elevated PD-L1 expression was observed on both tumor cells and immune cell infiltrates in many different cancers including melanoma (Kaunitz et al. 2017). Anti-PD-1 monoclonal antibody such as nivolumab that blocks the interaction between PD-1 and PD-L1 result in higher antitumoral immune response that reduces tumor progression (Melero et al. 2013; Speckenier 2016) (Figure 92).

Importantly these two immune pathways can be targeted alternatively as pembrolizumab, an anti-PD-1 antibody, was approved for the treatment of advanced melanomas and may turn into a new standard for the treatment of melanomas resistant to CTLA-4 blockade (Ribas et al. 2015; Robert et al. 2015). Therefore, several clinical trials are ongoing assessing the clinical relevance of combination of anti-PD-1 antibodies with other immune checkpoint inhibitors or targeted therapies (Domingues et al. 2018). Unfortunately, only a subset of melanoma patients respond to immune checkpoint inhibitors for reasons yet to be elucidated. In addition, severe immune-related Adverse Events (irAEs) appear in some

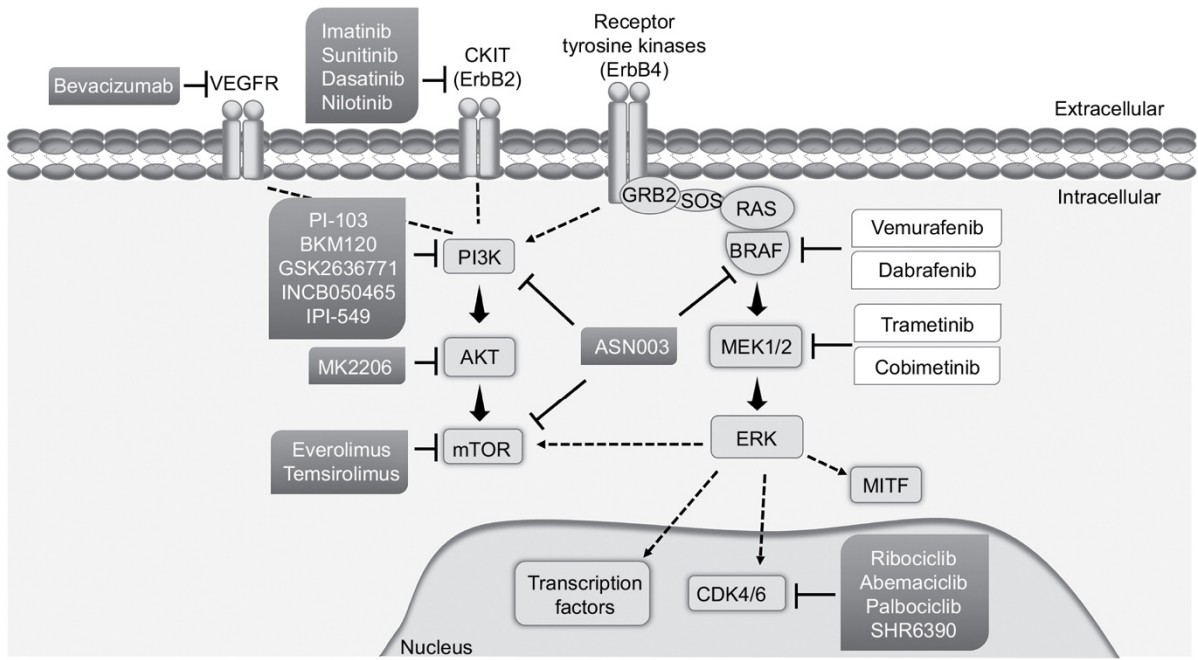


Figure 93. Targeted therapies approved by FDA (in white) or in trials (in gray) for cutaneous melanoma treatment.

From Domingues et al. 2018.

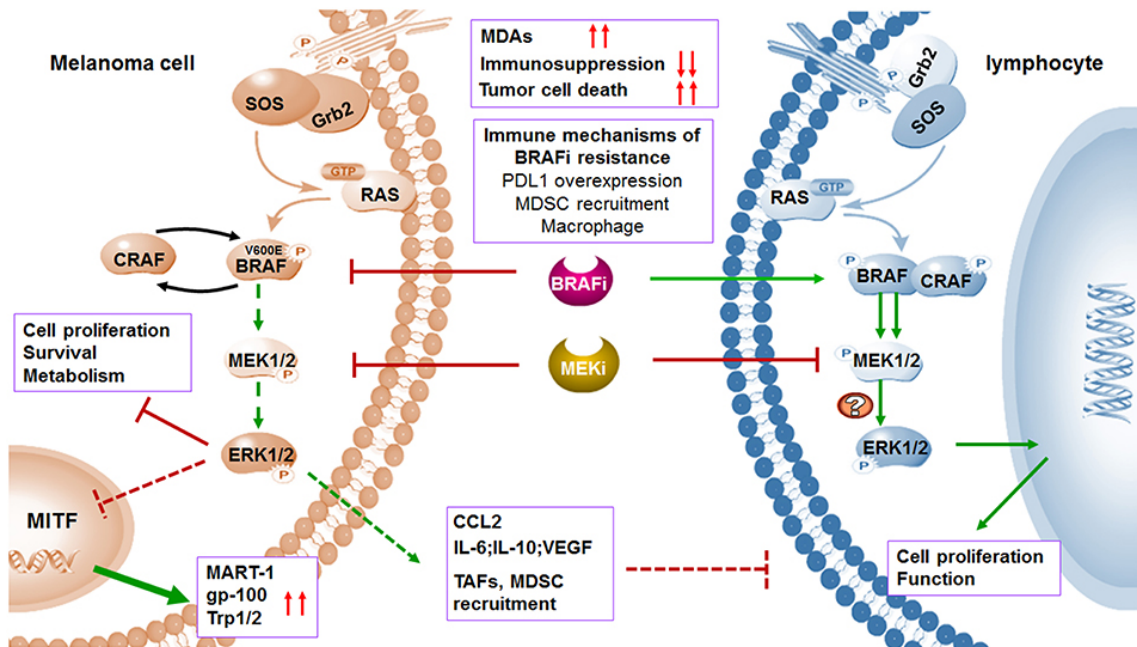


Figure 94. BRAFi and MEKi induce melanoma cell death.

From Yu et al., 2019.

patients, highlighting the necessity to identify predictive markers for treatment efficacy/safety and develop strategies to overcome such resistance.

3.2.3.2. Targeted therapies

As described before, about half of all melanoma driver mutations result in constitutive activation of BRAF and subsequently the MAPK pathway. This discovery led to the development of targeted inhibitors of the BRAF protein (BRAFi) namely vemurafenib and dabrafenib. As compared to chemotherapy, treatment with vemurafenib in monotherapy was shown to induce significant reduction of tumor size (roughly 50%). Dabrafenib had similar response rates to treatment as vemurafenib, but it showed less severe adverse effects and was shown to be effective in treatment of melanoma brain metastasis (Shah and Dronca 2014). However, in both cases, all patients, including the ones with strong/full response rates, eventually relapse after a median of 6 to 7 months (Chapman et al. 2011; Hauschild et al. 2012). The short-lived responses are in part due to alternative reactivation or bypassing of the MAPK pathway. Trametinib is a potent and highly sensitive MEK1/2 inhibitor (MEKi) and was shown to have better effect on the overall survival than chemotherapy (Flaherty et al. 2012). Importantly, combinations of BRAFi with MEKi have been shown to be more effective and no more toxic than either of the inhibitors alone (King et al. 2013; Wood and Luke 2017). Subsequently, several combination therapies with BRAF and MEK inhibitors became a worldwide standard of care for BRAF mutation-positive advanced or unresectable melanomas (Flaherty et al. 2012; Pavlick et al. 2015; Sullivan and Flaherty 2015) (Figure 93 and 94).

Additionally, since cKIT mutations or amplifications in melanoma led to the constitutive ligand-independent activation and upregulation of the MAPK and PI3K/AKT pathways, this receptor was also considered for targeted therapies. However, only Imatinib as cKIT inhibitor revealed significant activity in patients with metastatic melanoma harboring cKIT aberrations. Other multikinase inhibitors such as sunitinib, dasatinib and nilotinib, potentially efficient in patients with melanoma harboring cKIT mutations, are in clinical trials in combination with immunotherapies (Hsueh and Gorantla 2016).

With new insights brought by single-cell datasets, it became clear that targeting one subpopulation may not be sufficient and future strategies will aim at combining drugs targeting several

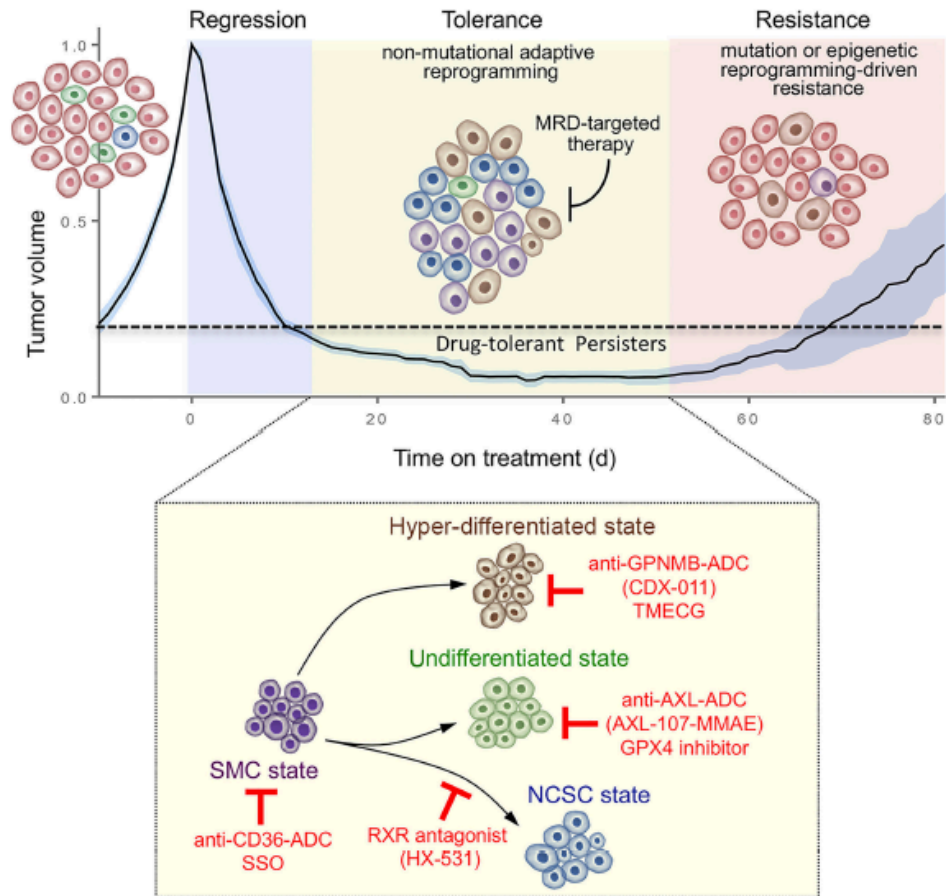


Figure 95. Potential therapeutic vulnerabilities for cells resistant to MAPKi.

From Rambow *et al.*, 2019.

or all of the characterized subpopulations co-existing in the tumors (Mukherjee et al. 2017; Rambow et al. 2018). Drugs targeting the vulnerabilities of dedifferentiated cells such as AXL (AXL-107-MMAE) or GPX4 (RSL3 or Erastin), or anti-RXR (HX-531) in the case of neural crest-like cells, will be tested in the future to assess whether they provide additional clinical benefit when combined to MAPK inhibitors to de-bulk the tumors (Boshuizen et al. 2018; Rambow et al. 2019; Tsoi et al. 2018) (Figure 95).

RESULTS

**PART I. Role of BRG1 in dedifferentiated
melanomas cells**

Essential role of the chromatin remodeler BRG1 for formation of tumor spheroids by dedifferentiated melanoma cells.

Bujamin Vokshi ¹, Guillaume Davidson ¹, Sébastien Coassolo ¹, Alexandre Haller ¹, Justine Gantzer ^{1,2}, Gabriel Malouf ^{1,2} and Irwin Davidson ^{1,3#}.

¹ Institut de Génétique et de Biologie Moléculaire et Cellulaire. 1 rue Laurent Fries, 67404 Illkirch Cedex, Strasbourg, France.

² Institut de Cancérologie Strasbourg Europe, 17 rue Albert Calmette, 67200 Strasbourg, France.

³ 'Equipe Labellisée' Ligue National contre le Cancer. Paris, France.

To whom correspondence should be addressed

E mail: irwin@igbmc.fr

Fax: +33 3 88 65 32 01. Tel: +33 3 88 65 34 45

Running Title: BRG1 in dedifferentiated melanoma cells

Key words: chromatin remodelling, SMARCA4, PRRX1, CLDN1, interferon response

The authors declare no potential conflicts of interest.

Abstract.

Introduction. Melanomas are highly heterogeneous and characterized by their cell plasticity partly dependent on MITF activity. Targeted therapy using BRAF/MEKi gives rise to resistant cells which lose their differentiation program and acquire a mesenchymal-like phenotype. The SWI/SNF chromatin-remodelling component BRG1/SMARCA4 is an essential cofactor of MITF for driving melanoma proliferation in differentiated/melanocytic melanoma cells. Herein we aimed at characterizing the role of BRG1 in dedifferentiated/mesenchymal melanoma cells.

Method. To address this question, we took advantage of several established patient-derived dedifferentiated melanoma cell lines which were used as a model of disease. We performed numerous functional assays on standard monolayer and in tri-dimensional cultures and characterized the effects of siRNA-mediated BRG1 silencing in both conditions by several approaches: i) transcriptome analysis; ii) profiling genomic localisations; iii) motif enrichment analysis.

Results. We show that while BRG1 plays only a minor role in regulating proliferation and gene expression in 2D conditions, it strongly regulates cell migration, invasion as well as 3D sphere formation. Comparative genome localisations of BRG1 in melanocytic/mesenchymal cells revealed the loss of BRG1 on MITF-dependent cell cycle and pigmentation genes with a relocation to genes associated with migration, angiogenesis and extracellular matrix organization. Integration of our data allowed the identification of a novel BRG1 target PRRX1 and we characterized its essential function for driving cell migration, invasion and 3D sphere formation. We further investigated the mechanism of action and highlighted the contribution of CLDN1 in the regulation of 3D sphere formation.

Conclusion. These data provide a better understanding on the interplay between BRG1, PRRX1 and CLDN1 in dedifferentiated cells which could be potentially exploited for the treatment of these hard-to-treat melanoma cell-types.

Introduction.

Melanoma is the most aggressive skin cancer arising from the oncogenic transformation of melanocytes by several recurrent somatic mutations, the most frequent of which are *BRAF*^{V600E} an activating mutation found in 50-60% of tumours, *NRAS* (\approx 20% of tumours) and loss of function mutations in *NFI* (\approx 10%)¹. Despite progress in patient outcome through the use of targeted kinase inhibitor and immune checkpoint therapies, a large number of patients acquire resistance or are considered as non-responders². One of the major factors leading to resistance is cellular plasticity and heterogeneity³. A large number of studies have now characterised in detail cellular heterogeneity and plasticity in melanoma defining cell populations with different epigenetic profiles and transcriptional signatures^{4,5}. RNA-seq and epigenetic profiling of cell lines and single cell profiling of tumours or patient derived xenografts (PDX) have identified multiple cell states the most studied of which are; melanocytic/proliferative, neural crest type, de-differentiated/mesenchymal and intermediate^{6,7}. The identities of each cell type are determined by the expression and activity of several key transcription factors^{9,10,11}.

We have characterized the action of MITF and SOX10 that drive the melanocytic/proliferative program, through ChIP-seq defining their genomic binding sites and RNA-seq after their siRNA mediated silencing to identify a large set of direct target genes both coding and non-coding that drive melanoma proliferation and survival^{12,13}. We also performed proteomics to identify the protein cofactors for MITF and SOX10 involved in their transcriptional activity. The PBAF chromatin remodelling complex, a member of the SWI/SNF family, interacts with both MITF and SOX10 in human melanoma cells¹⁴. Its catalytic subunit BRG1 is essential for proliferation of MITF-high cells and immortalised Hermes-3A melanocytes. Both MITF and SOX10 actively recruit BRG1 to chromatin to establish the epigenetic landscape of proliferative melanoma cells. In mouse, somatic Brg1 inactivation in the melanocyte lineage leads to loss of developing melanoblasts and the resulting animals lack pigmentation.

We also found that the NURF chromatin remodelling complex interacts with both MITF and SOX10. BPTF, the scaffolding subunit of the NURF complex co-regulates a subset of MITF target genes involved in proliferation of melanoma cells. However, in contrast to Brg1, Bptf is not required for mouse melanoblast development, but is required for generation of melanocytes from the adult melanocyte stem cell population¹⁵. These two chromatin-remodelling complexes therefore play distinct but complementary roles in the establishment and renewal of the melanocyte lineage and in human melanoma.

We also showed that Brg1 and Bptf are required for melanoma in the BRAF/PTEN mouse model. In these animals, melanoma is initiated by inducible somatic expression of oncogenic BRAF^{V600E} and deletion of Pten in adult melanocytes¹⁶. While the initial tumours are pigmented and show the characteristics of melanocytic/proliferative type cells, the invading cells undergo an epigenetic switch and rapidly lose pigmentation and expression of MITF and melanocyte markers, but retain SOX10 expression and thus adopt a neural crest-like identity. This switch can be reversed when tumour cells are grown in vitro with re-expression of MITF and melanocyte markers. Somatic inactivation of Brg1 or Bptf in these animals or in the cultured tumour cells blocks tumour formation. Thus, Brg1 and Bptf are required in human and mouse melanocytic type cells as well as in murine neural crest type melanoma cells.

Here we have addressed the role of BRG1 in de-differentiated/mesenchymal melanoma cells that express neither MITF nor SOX10. We show that BRG1 silencing in de-differentiated cells has only a moderate effect on cell proliferation and gene expression in contrast to the major role described in melanocytic type cells. Nevertheless, we demonstrate that BRG1 is required for formation of 3D melanospheres by de-differentiated cells. BRG1 ChIP-seq shows re-localization of BRG1 over the genome in de-differentiated cells and integration with RNA-seq following BRG1 silencing in 3D melanospheres identifies several gene expression programs regulated by BRG1 in collaboration with different transcription factors including PRRX1 that is essential for 3D spheroid growth.

Results.

BRG1 is required for optimal growth of de-differentiated melanoma cells.

To address the function of BRG1 in de-differentiated melanoma cells, we used 3 previously characterised primary cultures MM099, MM047 and MM029¹⁷. Each of these lines showed a gene expression signature and epigenetic profile characteristic of de-differentiated melanoma cells¹⁸. In contrast, they harboured different oncogenic mutations, BRAF^{V600*} in MM099 and MM029, and NRAS^{Q61*} in MM047¹⁹. Immunoblot experiments confirmed the lack of detectable MITF and SOX10 expression, that rather expressed SOX9, whereas the opposite was seen in melanocytic type 501Mel cells (Fig. 1A). In contrast, similar levels of expression of SWI/SNF subunits including BRG1, BRM, BAF170, BAF155 and BAF53 were seen in both cell types.

To address the role of BRG1, we performed siRNA-mediated silencing of BRG1, BRM or control siRNA (siC). Each siRNA selectively targeted either BRG1 or BRM with no change in the RNA level of BRM upon BRG1 silencing and *vice versa*. (Fig. 1B). BRG1 silencing did however lead to BRM protein accumulation without affecting mRNA level and *vice versa* suggesting a competition between the catalytic subunits for SWI/SNF complex formation (Fig. 1C). BRG1 silencing had only minor impact on proliferation of MM099 and MM029 cells with a small increase in the number of slow proliferating cells, but a more important effect in MM047 cells (Fig. 1D). BRM silencing had little effect in all lines. BRG1 silencing also elicited only a moderate reduction in clonogenic capacity of MM099 and MM029 cells, but had a stronger effect in MM047 cells (Fig. 1E-F).

We further assessed the impact of BRG1 and BRM silencing on senescence and apoptosis. BRG1 silencing had little effect in MM099 and MM029 cells, but induced senescence in MM047 cells, while BRM silencing had little effect in all cell types (Fig. 1G). Little apoptosis was seen upon BRG1 or BRM silencing in any of the cell lines (Fig. 1H).

As an alternative to siRNA, we infected MM099 cells with a lentiviral vector expressing shRNA against BRG1. As seen with siRNA, shBRG1 silencing led to BRM accumulation, but did not affect BAF47 expression (Fig. 2A). ShRNA-mediated BRG1 silencing had a more potent effect on cell growth with increased numbers of slow proliferating and senescent cells, but little effect on apoptosis (Fig. 2B).

To address potential redundancy, we performed siBRM silencing in the shBRG1 silenced cells. SiBRM silencing in shBRG1 cells did not further exacerbate the slow growth phenotype indicating little redundancy (Fig 2B-C) and pointing to the predominant role of BRG1 similar to what was observed in melanocytic cells^{12,16}.

We performed RNA-seq on siBRG1 and siBRM silenced MM099 and MM047 cells. Consistent with the minimal effects on cell proliferation, only 156 genes were deregulated in MM099 and 137 in MM047 cells using a standard cut-off (log₂ fold change +/- 1 and p-value >0.05) (Fig. 3A-C and Supplemental Dataset 1). With this limited set of genes only weak ontology signatures for cell adhesion and migration were seen in the down-regulated genes, with a cytokine/SASP type signature in the up-regulated genes. Nevertheless, close to 1000 de-regulated genes were identified using a less stringent cut-off (Log₂ fold change +/- 0.5 and p-value >0.01) in each cell type (Fig. 3C). Ontology analyses revealed signatures for differentiation, migration and angiogenesis in the down-regulated gene sets and inflammation and cytokine signalling in the up-regulated genes that further showed association with cell migration (Fig. 3D-E). Cellular compartment (CC-FAT) ontology analyses showed that both up and down regulated genes were predominantly associated with the membrane and the extracellular matrix. Comparison of the data sets from each cell line revealed 104 up- and 94 common down-regulated genes that showed similar ontology signatures to those of each line individually, with cell migration and cytokine signalling as represented pathways (Fig. 3F-G). In contrast, BRM silencing regulated only a very small number of genes that were not further analysed.

Together the above results showed that BRG1 silencing in 3 de-differentiated cell types had in general limited effects on cell physiology and gene expression. Even if shBRG1 silencing had a more potent effect than siRNA-mediated silencing, the impact in de-differentiated cells was much less striking than the potent proliferation arrest and senescence along with strongly de-regulated gene expression that we previously reported when BRG1 was silenced in 510Mel melanocytic cells¹².

BRG1 regulates invasion and migration of de-differentiated melanoma cells.

The ontology analyses of BRG1 regulated genes in MM099 and MM047 cells identified a potential role in cell adhesion and migration. These observations prompted us to investigate the effect

of BRG1 silencing on migration and invasion of de-differentiated cells. In a Boyden chamber assay with a matrigel barrier, siBRG1 silencing promoted increased invasion of all 3 cell lines, whereas silencing of BRM had no visible effect (Fig. 4A). Similarly, shBRG1 silencing also strongly increased invasion, that was not noticeably affected by further siBRM silencing (Fig. 4B). In a wound healing assay, siBRG1 silencing increased cell motility allowing a more rapid wound closure compared to siC or siBRM (Fig. 4C). Thus, paradoxically, BRG1 acts to negatively regulate migration and invasion of these cells that have otherwise been characterized by their high motile and invasive characteristics²⁰.

BRG1 is required for spheroid growth of de-differentiated melanoma cells.

As BRG1 did not appear to be a major regulator of cell proliferation under standard 2D growth conditions, we asked whether it may play a more important role in regulating 3D growth. Cells were transfected with appropriate siRNAs and then seeded for growth as 3D melanospheres. In all 3 lines, siBRG1 silencing efficiently inhibited melanosphere formation, while siBRM had no effect (Fig. 5A). Similarly, shBRG1 silencing potently inhibited 3D growth of MM099 cells (Fig. 5B). We also analysed the effect of BRG1 silencing on the growth of melanospheres in ultra-low attachment round bottom plates where individual spheres can be visualized and the number of cells subsequently measured. As seen with free growing spheres, BRG1 silencing led to a potent reduction in single spheroid growth of MM099 cells that was quantitated by an ATP-dependent cell quantification assay (Fig. 5C). Note that in this experiment, the siC and siBRG1 transfected cells were also incubated with control IgG antibody as described below for Fig. 14. Thus, while siBRG1 silencing had limited effect on cell proliferation in 2D, it had a potent effect on 3D spheroid formation.

Given this more potent effect, we performed RNA-seq after siBRG1 or siBRM silencing of cells grown under 3D conditions. A comparison of the siC in the 2D and 3D conditions to identify genes normally de-regulated upon the transition from monolayer to spheroid growth revealed an important re-programming of gene expression with more than 2600 and 3000 genes up or down-regulated in 3D conditions, respectively (Fig. 6A and Supplemental Dataset 2). In 3D conditions, ontology and GSEA analyses revealed a strong enrichment in genes associated with the extracellular matrix, hypoxia, TNF and inflammatory signalling and EMT, whereas genes involved in cell proliferation and DNA replication

were down-regulated (Fig. 6B-C). The 2D to 3D transition is thus associated with reduced proliferation, increased hypoxia and a major reorganisation of the cell membrane and extracellular space.

BRG1 silencing in spheroids led to reduced expression of more than 430 genes and up-regulation of 193 genes (Fig. 7A and Supplemental Dataset 2). GSEA and ontology analyses indicated up-regulation of genes associated with the interferon and inflammatory pathways and cell proliferation, whereas down-regulated genes were associated with the extracellular matrix, with reduced EMT and hypoxia signatures in agreement with the reduced 3D growth (Fig. 7B-C). Thus, many ontology terms associated with genes up-regulated upon 3D growth (EMT, hypoxia, angiogenesis) were downregulated upon BRG1 silencing (compare Figs. 6 and 7C). Strikingly, a set of more than 243 genes that are strongly induced upon 3D growth were down-regulated by siBRG1 silencing, whereas a smaller set of genes normally repressed upon 3D growth were up-regulated by 3D silencing (Fig. 7D and Supplemental Dataset 2).

The up- and down-regulation of these genes upon the 2D to 3D transition can be seen in a heatmap representation (Fig. 7E, Supplemental Dataset 3). Upon BRG1 silencing their up-regulation in 3D was strongly attenuated, whereas elevated expression was maintained for a smaller number of genes that were normally repressed upon 3D growth. The specificity of these changes was confirmed by RNA-seq of siBRM knockdown spheres where no effect on growth was observed. BRM silencing had minimal effects on gene expression (data not shown) and no appreciable effect on the genes that were induced or repressed upon the 2D to 3D transition (Fig. 7E). Thus, while BRG1 silencing impacted key genes involved in 3D growth, no comparable effects were seen following BRM silencing. Moreover, many genes associated with the locomotion and ECM signature described by Verfaillie *et al.*¹⁷ as TEAD4 targets were either induced or repressed upon 3D growth and this regulation was upset by BRG1 silencing (Fig. 7F, Supplemental Dataset 4). These data identified a set of genes that required BRG1 for their up-regulation upon transition to 3D growth. BRG1 silencing impeded their normal regulation hence inhibiting 3D growth.

Re-localization of BRG1 genomic occupancy in de-differentiated cells.

To better understand the role of BRG1 in the de-differentiated cells, we performed native BRG1 ChIP-seq in MM099 cells as previously described in 501Mel melanocytic cells¹² and ChIP-seq for H3K27ac. More than 110 000 BRG1 peaks were detected of which around 48% co-localized with H3K27ac-marked nucleosomes (Fig. 8A). Ontology analyses of the BRG1 bound promoters in each category revealed a wide range of cellular functions in agreement with the large number of bound promoters (Fig. 8B).

It has been previously shown that AP1 and TEAD factor are key determinants of the de-differentiated gene expression program^{17,18,20,21}. We integrated ChIP-seq data for FOSL2 and TEAD4 in de-differentiated type Sk-Mel-147 cells²² with the BRG1 and H3K27ac ChIP-seq data. Alignment with more than 78 000 FOSL2 bound sites revealed several clusters, where AP1 and TEAD4 were located between BRG1-bound and H3K27ac-marked nucleosomes (C1), sites where AP1 and TEAD4 were bound between H3K27ac-marked nucleosomes in absence of BRG1 (C2) and sites with AP1 and TEAD4 located between BRG1-bound nucleosomes in absence of H3K27ac (C3, Fig. 8C). Cluster C1 therefore defines a set of potentially transcriptionally active regulatory promoter and enhancer elements. Further analyses of these elements confirmed the strong enrichment of AP1 and TEAD4 DNA binding motifs at these sites, but also enrichment of motifs for SOX9 and ZEB1, additional transcription factors with important roles in de-differentiated cells and more unexpectedly, enrichment for homeodomain transcription factors, IRF1 and STAT1-STAT3. Together these data suggest that BRG1 was recruited to these sites by interactions with these different combinations of transcription factors, but principally TEAD, AP1 and ZEB1 that were the most abundant detected motifs.

We next compared BRG1 genome distribution in the MM099 and the 501Mel cells. Compared to 501Mel cells more than twice the number of BRG1 bound sites were seen in MM099 cells, although the genomic localizations were comparable (Fig. 9A). Only around 14 000 sites were commonly occupied in both cells types with a large number of cell-specific sites (Figs. 9A and B). For example, BRG1 and H3K27ac are widely distributed across the *MITF* locus in 501Mel cells, whereas H3K27ac was lost in MM099 cells and BRG1 was restricted to the promoter region of the A and B isoforms (Fig.

10A). The opposite was seen at the *SOX9* locus, with selective H3K27ac and BRG1 occupancy in MM099 cells (Fig. 10B).

Ontology analyses of the nearest genes in each cluster showed that the commonly occupied sites were associated with diverse fundamental cellular functions such as transcription, translation and intracellular transport. The MM099 specific sites were associated with more specific cellular functions like inflammatory response or angiogenesis. The 501Mel specific sites were enriched in genes involved in cell cycle, mitosis and cell division. We previously found that MITF and SOX10 actively recruited BRG1 to regulatory elements at genes associated with cell cycle and cell division. Consequently, BRG1 binding at these sites was lost in MM099 cells. Moreover, it is interesting to note that the term cell cycle appears in both the common and 501Mel specific clusters defining distinct gene sets that are regulated in both cell types or specifically only in 501Mel cells. For example, the Citron kinase (*CIT*) is a key Rho effector that functions to maintain proper structure of the mid-body during cell mitosis²³. In 501Mel cells, the *CIT* locus comprises multiple MITF binding sites, a SOX10 binding site with H3K27ac and prominent BRG1 at the promoter and intergenic regions. In MM099 cells, BRG1 occupancy was restricted to novel sites at the 3' end of the gene. *CIT* is therefore an example of mitosis function gene whose expression was BRG1 regulated under the control of MITF and SOX10 specifically in melanocytic cells.

Previously, Minnoye et al. used ATAC-seq to identify putative melanocytic or mesenchymal-specific enhancer elements based on the differential accessibility in ATAC-seq experiments¹⁸. Moreover, they performed ATAC-seq in tumours from multiple species to identify regions that showed cross species accessibility corresponding to conserved regulatory elements implicated in melanoma. Using the coordinates of these regions, we analyzed whether they were associated with BRG1 and/or H3K27ac in the 501Mel or MM099 cells. Interestingly, around 40% of the identified mesenchymal regulatory elements showed strong BRG1 occupancy at the flanking nucleosomes in MM099 cells and around 30% of these showed strong concomitant H3K27ac signal (Fig. 9D). In contrast, only a small subset showed BRG1 occupancy in 501Mel cells. In the converse comparison, more than half of the melanocytic enhancers showed BRG1 occupancy in 501Mel cells, with only a subset showing signal in MM099 cells (Fig. 9E). Moreover, it is interesting to note that while the BRG1 and H3K27ac profiles

were rather sharp at the melanocytic enhancers in the 501Mel cells they were broad and heterogeneous in the MM099 cells. This is not due to poor data quality as the profiles of the mesenchymal elements in MM099 cells was also sharp. These data showed that BRG1 selectively occupied mesenchymal- and melanocytic-defined regulatory elements in a cell specific manner. Moreover, for each cell type, the sites showing highest signal for BRG1 and H3K27ac were also those that showed the highest percentage of cross-mammalian species conserved elements (Fig. 9F). Thus, elements identified by ATAC-seq accessibility as being conserved across species were enriched amongst those with functional marks in the cell lines, whereas elements lacking appreciable BRG1 and H3K27ac signal showed the lowest presence of conserved elements.

BRG1 silencing in spheroids activates the interferon pathway

The DNA sequence motif analyses of the BRG1 bound elements in cluster C1 of Fig. 8C, defined as probable active regulatory elements, revealed the enrichment in IRF and STAT binding motifs. In addition, GSEA and ontology analyses of the RNA-seq data following BRG1 silencing in 3D spheres revealed up-regulated expression of a set of genes involved in the interferon pathway (Fig. 7C). This was confirmed by using the GSEA molecular signature for the interferon pathway where activation of a sub-set of genes of this signature was seen upon BRG1, but not BRM silencing (Fig. 11A, Supplemental dataset 6). While the fold change was overall low, the observation that many of the genes in the pathway showed coordinate regulation prompted us to look more carefully at the regulation of the pathway. Comparison of the RNA-seq data from MM099 cells in 2D and 3D conditions showed increased expression of IRF1, STAT1 and STAT4 upon BRG1 silencing mainly in 3D conditions (Fig. 11B-C). In contrast, expression of IL8 and IL1A was more affected upon BRG1 silencing in 2D conditions (Fig. 11B). We further assessed the expression of these genes over time to assess if the differential de-regulation could be accounted for by different kinetics. Comparing BRG1 silencing showed that its mRNA levels remained lower for a longer period in 3D conditions likely due to the slower dilution of siRNA by reduced cell division in the spheroids (Fig. 11D). IL8 was deregulated between 2-3 days under both 2D and 3D conditions before returning to basal levels, accounting for the fact that it was not seen as a deregulated gene in the 3D RNA-seq performed at the later times (7 days).

Elevated expression of IRF1 on the other hand was observed over a longer period and was stronger after 7 days when the 3D RNA-seq was performed. Thus, the different kinetics of BRG1 silencing led to consistent kinetics of de-regulated gene expression in 2D and 3D conditions.

Activated STAT1-STAT2 can promote IRF1 expression that in turn activates CD274, otherwise known as PD-L1, a major regulator of immune checkpoint signalling^{24,25,26}. Consistent with increased IRF1 expression by BRG1 silencing, PD-L1 expression also increased in particular under 3D conditions where it strongly increased over time (Fig. 11B-D). In contrast, no expression of the interferons in particular IFN γ the major activator of PD-L1 was seen upon BRG1 silencing. This rather suggested that BRG1 was acting directly on the IRF1 and/or PD-L1 promoters to repress their expression where upon BRG1 silencing they were upregulated even in the absence of IFN γ . Examination of the *IRF1* and *IL8A* loci, both of which are up-regulated upon BRG1 silencing, showed an extensive coverage of the upstream regions by BRG1, a phenomenon not seen in the 501Mel cells (Fig. 10C). At the PD-L1 promoter, the BRG1 coverage rather extended into the gene body (data not shown). This characteristic extended occupancy suggested that BRG1 may act to repress the expression of these genes. To test this idea, we stimulated cells with IFN γ with or without concomitant BRG1 silencing. Expression of PD-L1, IRF1 and STAT1 was stimulated by IFN γ and in most cases, was further increased upon BRG1 silencing, in particular in the MM029 cells (Fig. 11E). Thus, BRG1 was not essential for the ability of IFN γ to activate its downstream targets, but rather acted to repress their expression.

PRRX1 cooperates with BRG1 to promote spheroid growth.

Similar to what was described above, sequence motif analyses of the BRG1 bound elements in cluster C1 of Fig. 8C further revealed enrichment in homeodomain binding motifs.

Further analyses of the BRG1 silencing RNA-seq data using the EnrichR package identified several transcription factors as potential drivers of genes down-regulated by BRG1 silencing including TWIST1, and the homeodomain proteins PRRX1 and PRRX2 (Fig. 12A). Examination of the RNA-seq data showed that OSR1 was only weakly expressed in melanoma cells, PRRX2 was not expressed, whereas TWIST1 and PRRX1 expression was up-regulated in 3D conditions and down-regulated upon BRG1 silencing (Fig. 12B-C). Nevertheless, TWIST1 expression was not specific to de-differentiated

cells as it was also expressed in 501Mel cells. PRRX1 was also one of the few genes down-regulated under 2D conditions by BRG1 silencing (Figs. 3B and 12C). PRRX1 expression was also up-regulated upon siSOX10 or siMITF silencing in 501Mel cells. Examination of the *PRRX1* locus showed more extensive BRG1 occupancy mainly of intronic regions than seen in 501Mel cells (Fig. 10B). The presence of homeodomain motifs at BRG1 bound sites and its selective expression in de-differentiated cells further prompted us to investigate further a potential role for PRRX1 in 3D growth of de-differentiated cells.

We checked the levels of PRRX1 by immunoblot which was not detected in 501Mel cells, but was expressed in A375 Mel cells that have a neural-crest type state expressing SOX10, but not MITF (Fig 12D consistent with ²⁰), and in the de-differentiated cells where it was up-regulated upon 3D growth (Fig. 12B). Previous studies have shown that PRRX1 expression is activated through the BMP signaling pathway^{27,28}. Using the BMP MsigDB gene set, the down-regulation of a subset of genes of this pathway including BMP3, BPM4, BMP5, BMP7 and BMP8A was observed upon BRG1 silencing (Fig. 12E-F). These same genes were also upregulated upon 3D growth perhaps accounting for the concomitant changes in PRRX1 expression. We examined the expression of the top 200 BRG1-associated genes with PRRX1 binding motifs in 3D conditions showing that many were down-regulated upon BRG1, but not BRM silencing (Fig. 12G, Supplemental dataset 5). Surprisingly however, a smaller subset was up-regulated. Similarly, we used the iRegulon software to predict 288 PRRX1 promoter targets that were also associated with BRG1 binding. Again, expression of these genes, that largely overlap with those above, was de-regulated by BRG1 silencing, with both up-and down-regulated genes (Fig. 12H).

To address the role of PRRX1 in de-differentiated cells, we performed siRNA-mediated silencing (Fig. 13A). PRRX1 silencing led to an increased number of slow growing cells, but had little effect on senescence or apoptosis (Fig. 13B). In Boyden chamber assays, PRRX1 silencing led to reduced invasion of de-differentiated cells, but not of A375 cells (Fig. 13C). Finally, PRRX1 silencing also inhibited 3D spheroid growth (Fig 13D). Together, these data indicate that PRXX1 was found at a subset of BRG1 bound sites and regulated the expression of genes required for 3D growth.

Claudin 1 is preferentially expressed in de-differentiated melanoma and promotes spheroid growth.

The above data indicated that the transition from 2D to 3D growth involved a major remodelling of the extracellular membrane with an EMT signature that was reversed by BRG1 silencing. To investigate EMT we used the Cell Signalling EMT sampler kit that comprises a set of antibodies to proteins that should be gained or lost upon EMT including the tight junction component CLDN1, often regarded as an epithelial marker. Although melanoma cells were shown to express CLDN1^{29,30}, melanoma cells in culture do not display tight junctions. CLDN1 has also been shown to promote melanoma cell migration^{30,31}. A closer analysis of *CLDN1* mRNA expression in the single cell data of Wouters²⁰ revealed that it was low to absent in melanocytic and intermediate cells, but expressed in de-differentiated cells (Fig. 14A). Similarly, in single cell data from melanoma PDX⁶, CLDN1 expression was low at T0, but increased through the minimal residual disease phase and was stronger expressed in the kinase inhibitor resistant cells (Fig. 14B). Analyses of our own RNA-seq data indicated that CLDN1 expression was very low in melanocytic type 501Mel and MM074 cells, but was high in MM099 cells and in MM074 cells selected for resistance to the CDK7 inhibitor THZ1 that induces a melanocytic to de-differentiated phenotype switch^{20,32,33} (Fig. 14C). Examination of the *CLDN1* locus showed extensive BRG1 occupancy not seen in 501Mel cells in particular of an upstream element associated with a AP1-TEAD binding site as a potential enhancer (Fig. 10B). Immunoblot confirmed that CLDN1 was absent from melanocytic 501Mel and neural crest A375 cells, but expressed in MM099 and MM047 cells (Fig. 14D). Thus paradoxically, although CLDN1 is considered as an epithelial marker, its expression is up-regulated in mesenchymal type de-differentiated melanoma cells.

CLDN1 is known as a host entry factor for hepatitis C virus (HCV)^{34,35}. The group of Dr Thomas Baumert at the Virology Institute in Strasbourg has developed a neutralizing monoclonal antibody directed against CLDN1 that effectively blocks HCV infection^{36,37}. This antibody recognizes the extracellular domain of CLDN1 and thus can be assessed for its ability to block CLDN1 action. Given the specific expression of CLDN1 in de-differentiated melanoma cells, we assessed the effect of antibody-mediated blocking of CLDN1 on 3D spheroid growth. Melanoma cells from each of the three de-differentiated lines were incubated with 10 μ g/mL of CLDN1 antibody or control IgG of the same

isotype and then plated as individual spheres. As seen in Fig. 5C, BRG1 silencing inhibited spheroid growth, that was also inhibited by the anti-CLDN1 antibody (Fig. 14E). We next evaluated the ability of increasing doses of CLDN1 antibody to inhibit spheroid formation by de-differentiated cells or 501Mel cells that do not express CLDN1. Compared to control IgG, the CLDN1 antibody inhibited spheroid growth of MM099 cells, but not 501Mel cells when used at a dose of up to 10 μ g. At higher doses, the specific effect of the CLDN1 antibody was confounded by a general inhibitory effect of the both the CLDN1 and control IgG (Fig. 14F). Immunoblot analyses of these spheres revealed that treatment with CLDN1 antibody resulted in a mild up-regulation of CLDN1 levels (Fig 14D). These data showed that inhibition of CLDN1 function using a neutralizing antibody efficiently and selectively inhibited spheroid growth of dedifferentiated melanoma cells.

Discussion.

Here we provide new insights into understanding the role of BRG1 by showing that it specifically promotes a transcriptional program driving 3D growth of de-differentiated melanoma cells. We first studied the effects of BRG1 silencing by different 2D culture assays and showed that BRG1 silencing did not induce strong defects in proliferation and survival. This is in stark contrast with our previous studies showing the dependency of differentiated and neural crest-like melanoma on chromatin-remodeling by BRG1^{12,16}. We could confirm these cell type-specific effects by ChIP-seq in de-differentiated MM099 cells revealing that BRG1 was lost from MITF/SOX10-dependent cell cycle genes and relocated to mesenchymal-specific enhancers associated with genes involved in cell invasion, ECM organization and angiogenesis. Despite these observations, we cannot exclude potential bias resulting from cell line-specific effects, additional BRG1 ChIP-seq could be performed in other de-differentiated cell lines such as MM047 or MM029 for comparison. This would be particularly interesting as only a subset of the mesenchymal enhancers identified by Minnoye et al. are occupied by BRG1 in MM099 cells. Perhaps a distinct but overlapping set would be occupied in the other cell lines. Another point to keep in mind is that BRG1 ChIP-seq may not be fully representative of the entire SWI/SNF complex binding sites as BRM-containing complexes might have distinct genome localizations. Further ChIP-seq with additional SWI/SNF subunits such as BRM, PBAF-specific

ARID2, cBAF-specific ARID1A and ncBAF-specific BRD9 subunits might help to address that concern. Nevertheless, our findings are coherent with prior studies reporting that de-differentiated/mesenchymal cells have slower proliferation rates compared to differentiated/melanocytic cells and favor key programs implicated in cell migration, invasion and angiogenesis^{17,20}.

Next, we could confirm a more prominent effect on gene expression upon BRG1 silencing in 3D cultures of de-differentiated cells. Analysis of 2D versus 3D RNA-seq of control melanospheres demonstrated a comprehensive switch in their gene expression program with reduction of cell cycle genes and increased levels of genes involved in cell adhesion and ECM organization. One limitation of our study is the lack of BRG1 and H3K27ac ChIP-seq data in 3D-grown melanospheres, as we would expect to see a global retargeting of SWI/SNF complex towards genes essential for cell adhesion, hypoxia and 3D growth. Besides, additional ChIP-seq for RNA polymerase II or ATAC-seq experiments could improve our capacity to discriminate between active and inactive regulatory elements. Nevertheless, our analysis is in line with previous comparative studies of 2D versus 3D cultures showing that 3D cultures have lower proliferation³⁸. Our study underlines that 3D cultures are particularly pertinent to assess the functional impact of BRG1 silencing in de-differentiated cells, which can likely be explained by their highly adhesive nature.

Our BRG1 ChIP-seq data suggest that BRG1-containing SWI/SNF complexes are recruited to the genome of de-differentiated cells by a combination of colocalizing transcription factors including AP-1, TEAD, ZEB1 and the mesoderm-specific TF PRRX1 on defined active regulatory elements. This model is suggested by the colocalization of these factors at a subset of BRG1 bound elements and the high enrichment of their DNA binding motifs. Nevertheless, demonstrating an active role of these TFs in BRG1 recruitment will require additional BRG1 ChIP-seq in cells where their expression has been silenced.

PRRX1 has recently been linked to epithelial-to-mesenchymal transition (EMT) as it drives a mesenchymal program and confers migratory and invasive properties to cancer cells^{39,40}. Here we show that together with its upstream BMP regulators, PRRX1 is a direct target of BRG1 that is specific to de-differentiated cells and whose expression is further up-regulated during 3D growth. We demonstrate that PRRX1 is essential for migration, invasion and melanosphere formation of de-differentiated cells.

However, more experiments would need to be implemented to determine the extent of BRG1-PRRX1 cooperativity in these cells.

Prior reports indicated that PRRX1 might act through regulating the Wnt/B-catenin pathway⁴¹ which is also a known SWI/SNF target⁴². RNA sequencing of PRRX1-silenced 2D and 3D cultures would help understand which pathways are regulated by BRG1 and PRRX1 in a cooperative manner. Next, mapping the PRRX1 genome localizations by ChIP-seq would be useful to appreciate the quantity and ontology of sites where BRG1 and PRRX1 colocalize. Also, the question of a physical interaction between BRG1 and PRRX1 will need to be addressed in order to understand the mechanism of recruitment. A number of these approaches are hampered by the poor quality of the PRRX1 antibody that we used. We are currently assessing the quality of additional commercial antibodies.

In our previous studies, we showed that MITF and SOX10 directly interacted with BRG1 to recruit SWI/SNF complex on promoters and enhancers of the melanocytic program¹². If in a similar way, PRRX1 is necessary for the recruitment of BRG1, ChIP-seq of BRG1 following PRRX1 silencing would help define the binding sites where BRG1 occupancy requires only PRRX1. Importantly, we show that PRRX1 is repressed both by MITF and SOX10 in melanocytic-type cells. It would be interesting to map the binding sites of BRG1 in de-differentiated MM099 cells stably expressing MITF and SOX10 to see if they are able to hijack the SWI/SNF complex in order to repress the PRRX1 program and retarget BRG1 to cell cycle and pigmentation genes.

In apparent contrast with the literature⁴⁴, we found that CLDN1 is associated with the mesenchymal-like program as drug-induced phenotype switching results in its overexpression both in vitro and in vivo. However, on the one hand CLDN1 expression has been linked to the EGFR pathway in the context of HCV infection as studies show that blocking either CLDN1 or EGFR with specific antibodies inhibits HCV entry^{45,46}. On the other hand, single cell analyses established that the RTK EGFR is specifically overexpressed in de-differentiated melanoma cells as it confers drug resistance^{6,20}. Here we demonstrate that targeting CLDN1 disrupts melanosphere formation only in de-differentiated cells which express it on their membrane, thus potentially offering a novel therapeutic approach for these cell-types which contribute to drug resistance and metastatic progression^{4,6}. Our observations are in line with prior studies indicating the correlation of CLDN1 expression with poor prognosis in lung

and cervical cancers^{47,48}. Although 3D culture experiments resemble more closely *in vivo* cell environments⁴⁹, it is evident that the effects of targeting CLDN1, but also BRG1 and PRRX1 have to be tested in xenografts in nude mice.

Importantly, we showed that knocking down BRG1 or its downstream target PRRX1 and neutralizing CLDN1 all resulted in defective spheroid formation. However, CLDN1 mRNA levels were not up-regulated upon the 2D to 3D transition and we did not observe any effect of BRG1 silencing on CLDN1 mRNA levels. Intriguingly, at the protein level we observed a slight increase of CLDN1 by both BRG1 or PRRX1 knockdowns, but also in cells treated with the neutralizing CLDN1 antibody for 24hrs. This suggests that CLDN1 may perhaps be trapped by the antibody leading to accumulation on the plasma membrane. As BRG1 silencing strongly impacts the composition of the cellular membrane and ECM, these changes may also modulate CLDN1 internalization, recycling and trafficking. Further experiments will aim at determining the subcellular localization of CLDN1 in cells and melanospheres upon BRG1 knockdown or CLDN1 neutralization. Moreover, prior reports have shown that CLDN1 silencing led to decreased tumor growth and migration capacities of hepatocellular carcinoma *in vitro* and *in vivo*⁵⁰. Here we show that BRG1 silencing results in higher migration and invasion of de-differentiated cells, however we did not yet assess the effects of neutralizing CLDN1 on migration which is crucial to metastatic progression. Besides, the exact mechanism of action of CLDN1 is poorly understood and needs to be addressed. One approach would be to screen for changes in phospho-RTKs that might be involved in signal transduction downstream of CLDN1 in spheres exposed to the neutralizing antibody. Further analyses of how the eventually identified pathways are regulated by BRG1 would allow integration of the action of BRG1 and CLDN1 in 3D growth. Importantly, this might be exploited for the development of anti-CLDN1 as a novel targeted therapy, perhaps in combination with other drugs (e.g. BRAFi or MEKi) that would help ‘de-bulk’ the tumors⁵¹.

Immune checkpoint inhibitors (ICI) are often used as first-line approach in BRAF wild-type and advanced melanomas. Successful ICI is partly determined by the tumor expression of PD-L1⁵². However, numerous case reports of robust response to ICI with melanomas harboring low to no PD-L1 expression highlighted the need for better understanding of immunoregulatory mechanisms and better biomarkers for ICI response⁵³. Here we show that BRG1 seems to act as a corepressor of the interferon

gamma pathway in de-differentiated melanoma cells. In fact, BRG1 silencing resulted in increased RNA levels of several PD-L1 upstream regulators including STAT1 and IRF1 and co-treatment with IFNG revealed that BRG1 silencing could further potentiate the response. Additional experiments are required to assess if the knockdown of BRG1 has an effect on the phosphorylation of STAT1:STAT2 proteins which is a key regulator of nuclear shuttling and subsequent activation of downstream targets. Additionally, PD-L1 being only effective when exposed on the membrane, its subcellular localization upon BRG1 knockdown has to be assessed by FACS or by immunofluorescence. Although RNA levels of PD-L1 are only modestly impacted, it might well be that knocking down BRG1 induces a considerable reorganization of the plasma membrane leading to accumulation of PD-L1 in a similar manner to what we postulated for CLDN1. There is also evidence of secreted forms of PD-L1 and in melanoma exosomal PD-L1 is a marker of immune activation after ICI that predicts a clinical response to anti-PD1 therapy⁶⁴. It will be important to use our RNA-seq data to assess if BRG1 silencing alters splice isoform usage and hence localization/secretion of the protein; and further experiments to test this are on their way.

On the other hand, our ChIP-seq revealed that several PD-L1 pathway genes displayed extensive BRG1 occupancy of the upstream regions that were not associated with detectable H3K27ac, but enriched with recognition motifs for IRF family factors. The interferon-regulatory factor (IRF) family are known transcriptional regulators of immune response with 9 paralogs (IRF1 to 9) reported to this day that, despite displaying a certain degree of functional redundancy, were described to have specific functions⁵⁶. For instance, IRF2 is a potent regulator of immunosuppression as it antagonizes IRF1-mediated IFNG signaling⁵⁴. Thus, a plausible scenario would be that IRF2 cooperates with BRG1 in order to silence the IFNG pathway in de-differentiated cells. However, the extent of IRF2 and BRG1 co-localization cannot currently be appreciated as ChIP-seq data for IRF2 are lacking. Moreover, at the moment we do not understand why the kinetics of SASP cytokines are so different upon BRG1 silencing in 2D versus 3D culture. In contrast, de-regulation of interferon response can be fully appreciated only in 3D culture. One possible explanation for such results might be the existence of an ‘intratumoral heterogeneity’ in melanospheres. Remarkable single cell analyses of melanoma cell lines by Wouters et al. revealed heterogeneity within patient-derived cultures (MM029, MM047 and MM099) comprising

at least 3 subpopulations: cells expressing mitotic program, others defined by a metabolic program and a final group with a mesenchymal signature²⁰. Of note, the mesenchymal-like group of cells expressed the highest levels of immune response genes. Thus, it is possible that some cell-types such as the mesenchymal-like group survive better in 3D conditions due to their intrinsically higher expression of cell adhesion genes. Thereby, knockdown of BRG1 in 2D and 3D conditions would differ in phenotype as the 2D culture may be more favorable to groups of cells with high proliferation rate. To address this question, immunofluorescence of BRG1-silenced melanosphere sections for PD-L1 effectors would allow to better grasp the potential intra-melanosphere heterogeneity. Taken together, our data suggest that BRG1 acts in conjunction with IRF2 to silence IFNG signaling and PD-L1 expression in de-differentiated melanoma cells. Further work needs to be undertaken in order to confirm the correlation between BRG1 silencing and activation of PD-L1, which would be coherent with prior studies showing BRG1-mutated tumors to best respond to ICI in SMARCA4-deficient thoracic sarcomas as well as non-small cell lung carcinoma (NSCLC)^{55,57,58,59}. Furthermore, there are some clinical data demonstrating the correlation between mutations in SWI/SNF subunits such as PBRM1 and PD-L1 expression and immunotherapy responsiveness *in vivo*, notably in kidney (ccRCC) and ovarian tumors (SCCOHT) which bear frequent SWI/SNF mutations^{60,61,62}. However other studies have not observed this and demonstrated that RCC tumors enriched in PBRM1 mutations were associated with better anti-VEGF response, but not with anti-PD-L1 therapy⁶³. Therefore, future works may help to better understand the underlying relationship between ICI response and SWI/SNF mutations.

Altogether, this study addressed the role of BRG1 in de-differentiated/mesenchymal melanoma cells that express neither of the melanocytic master regulators MITF and SOX10. We showed that BRG1 silencing in 2D culture has only a moderate effect on cell proliferation and gene expression, in striking contrast with the major role previously described in melanocytic cells. However, we demonstrate that BRG1 is required for formation of 3D melanospheres by de-differentiated cells. Our study couples BRG1 with PRRX1 in driving a specific gene expression program essential for 3D spheroid growth. We furthermore highlighted the importance of CLDN1 as a novel potential vulnerability of these cell-types.

Methods.

Cell culture, si/shRNA silencing and anti-CLDN1 treatment

Melanoma cell lines 501Mel were grown in RPMI 1640 medium supplemented with 10% foetal calf serum (FCS). MM029, MM047 and MM099 were grown in HAM-F10 medium supplemented with 10% FCS, 5.2 mM GLUTAMAX and 25 mM HEPES.

SiRNA knockdown experiments were performed with the corresponding ON-TARGET-plus SMARTpools purchased from Dharmacon Inc. (Chicago, IL, USA). SiRNAs were transfected using Lipofectamine RNAiMax (Invitrogen, La Jolla, CA, USA) and cells were harvested after 72 hours. Lentiviral shRNA vectors were obtained from Sigma (Mission shRNA series) in the PLKO_puro vector. We used shBRG1 construct (TRCN0000015549) and lentiviral empty vector as a control and infected 1×10^6 MM099 cells.

For the CLDN1 experiments, cells were first transfected with the siRNAs for 24hr before being incubated overnight with $10 \mu\text{g/ml}$ of either humanized antibodies: IgG isotype or anti-CLDN1. For the IFNG experiments, cells were first transfected with the siRNAs for 24hr before being incubated overnight with either DMSO or 20ng/mL recombinant interferon gamma (Peprotech).

Proliferation, viability and senescence analyses by flow cytometry

To assess proliferation after siRNA treatment, cells were stained with Cell Trace Violet (Invitrogen) on the day of transfection and harvested 72hr later for FACS analysis. To assess cell viability, cells were harvested 72 hours after siRNA transfection and co-stained with Annexin-V (Biolegend) and propidium iodide following manufacturer instructions for FACS analysis. To assess senescence, cells were treated with 100nM bafilomycin A1 for 1hr followed by 2mM C12FDG (Invitrogen) for 2hr before being washed and harvested for FACS analyses. Cells were analysed on a LSRII Celesta (BD Biosciences) and data were analysed using Flowjo v6.8.

3D sphere formation and cell quantification

Antibody- or siRNA-treated cells were harvested, counted and seeded at a density of 1×10^4 in ultra-low attachment, round-bottomed 96-well plates (Corning Costar) for spheroid formation in KO-DMEM

medium. For free-floating melanospheres, harvested cells were counted and simply seeded in KO-DMEM at a density of 2×10^6 on bacteria plates without any coating. At day 7 post-siRNA, images of wells were taken with a phase-contrast microscope using a 5× objective. Melanosphere viability was assessed using the CellTiter-Glo Luminescent Cell Viability Assay (Promega, Madison, WI, USA). After addition of 100 µl of CellTiter Glo reagent to each well for 10 min with orbital rotation, luminescence was measured on a BioTek Luminescence microplate reader (using Gen5 software).

RNA preparation, quantitative PCR and RNA-seq analysis

RNA isolation was performed according to standard procedure (Qiagen kit). qRT-PCR was carried out with SYBR Green I (Roche) and SuperScript IV Reverse Transcriptase (Invitrogen) and monitored using a LightCycler 480 (Roche). The mean of ACTB, TBP, RPL13A and GAPDH gene expressions was used to normalize the results. Primer sequences for each cDNA were designed using Primer3 Software and are available upon request. RNA-seq was performed essentially as previously described (Herquel et al., 2013) Gene ontology analyses were performed with the Gene Set Enrichment Analysis software GSEA v3.0 using the hallmark gene sets of the Molecular Signatures Database v6.2 and the functional annotation clustering function of DAVID (<http://david.abcc.ncifcrf.gov/>).

Protein extraction and Western blotting

Whole cell extracts were prepared by the standard freeze-thaw technique using LSDB 500 buffer (500 mM KCl, 25 mM Tris at pH 7.9, 10% glycerol (v/v), 0.05% NP-40 (v/v), 16mM DTT, and protease inhibitor cocktail). Cell lysates were subjected to SDS–polyacrylamide gel electrophoresis (SDS-PAGE) and proteins were transferred onto a nitrocellulose membrane. Membranes were incubated with primary antibodies in 5% dry fat milk and 0.01% Tween-20 overnight at 4 °C. The membrane was then incubated with HRP-conjugated secondary antibody (Jackson ImmunoResearch) for 1h at room temperature, and visualized using the ECL detection system (GE Healthcare). Antibodies: MITF (MS-771-P, Interchim), SOX10 (ab155279, Abcam), SOX9 (82630, Cell signaling), BRG1 (ab110641, Abcam), BRM (11966, Cell signaling), BAF170 (A301-038A, Bethyl laboratories), BAF155 (sc-10756, Santa Cruz), BAF53A (ab131272; abcam), ACTB (2D7, IGBMC), BAF47 (91735, Cell signaling), NFATC2 (SC-514929X,

Santa Cruz), PRRX1 (PA518831, ThermoFisher), VCL (V4505, Sigma-Aldrich), CLDN1 (Ab211737, Abcam).

Wound healing assays

500,000 cells were seeded in 6-well collagen-coated plates before being transfected with siRNAs. 48hrs later (or when maximum confluency was obtained), a total number of 4 scratches were made in the plates using sterile 2ul tips. Pictures were captured on a phase contrast microscope at T0 and each days until cells from one condition achieved total wound healing. Quantification of cell migration was done using ImageJ with the wound healing macro.

Boyden chamber assays

siRNA-treated cells were harvested, counted and 200,000 single cells were seeded in Boyden chambers (24-well 8um inserts, Corning) in corresponding media without serum. For invasion assays, 100ul of diluted Matrigel (1:20, 356234, Corning) was added in each insert and left to dry for 2hrs at 37°C before being washed twice with PBS and seeded with the 200,000 cells. 24hrs later, migrated cells were fixed using PFA 4% for 10 min before being stained using Crystal violet for 10 min. Excess stain was washed 3 times in PBS before images were captured on contrast phase microscope. Quantification of migrated cells was done by resuspension of staining using 100mM acetic acid for 15min before luminescence was measured on a BioTek Luminescence microplate reader (using Gen5 software).

siRNA kinetics

To assess the kinetics of siBRG1, cells were plated and transfected with siRNA as mentioned above. A total number of 15 wells (10cm²) were plated: 9 wells were used for 2D cultures and 6 wells for 3D cultures. Thus, RNA from the first two days originate from 2D culture only as 3D cultures were started 48hrs post-siRNA treatment. RNA from each well were extracted every day for a total of 192hrs (9 days) using the Nucleospin RNA Plus XS kit (Macherey Nagel) according to the manufacturer guidelines. RNA was retrotranscribed and qPCR was performed as described above.

Immunoprecipitation

Whole cell extracts were prepared by the standard freeze-thaw technique using LSDB 500 buffer (500 mM KCl, 25 mM Tris at pH 7.9, 10% glycerol (v/v), 0.05% NP-40 (v/v), 16mM DTT, and protease inhibitor cocktail). Up to 1mg of whole cell extracts were diluted in LSDB without KCl to a final concentration of 150mM KCl and incubated overnight with 5ug of specific antibodies. The next day, 50ul of washed magnetic protein-A/G beads (Dynabeads, Invitrogen) were added to the extracts for 2hr. Beads were washed 3 times in LSDB 300mM KCl, twice in LSDB 150mM and immunoprecipitates were eluted in 100ul of 0.1M glycine pH 2.8 at room temperature for 15min, before addition of 10ul of Tris-HCl pH 8. For SDS-PAGE analysis, 10 to 15ul of eluted proteins were boiled in equal amount of Laemmli buffer before being loaded on the gels. Antibodies: BRG1 (ab110641, Abcam), PRRX1 (PA518831, ThermoFisher), rabbit IgG (ab171870, Abcam).

Chromatin immunoprecipitation and sequencing

BRG1 ChIP experiments were performed on native MNase-digested chromatin. 10×10^7 to 20×10^8 freshly harvested MM099 cells were resuspended in 1.5 ml ice-cold hypotonic buffer (0.3M Sucrose, 60 mM KCl, 15 mM NaCl, 5 mM MgCl₂, 0.1 mM EDTA, 15 mM Tris-HCl pH 7.5, 0.5 mM DTT, 0.1 mM PMSF, PIC) and cytoplasmic fraction was released by incubation with 1.5 ml of lysis-buffer (0.3M sucrose, 60 mM KCl, 15 mM NaCl, 5 mM MgCl₂, 0.1 mM EDTA, 15 mM Tris-HCl pH 7.5, 0.5 mM DTT, 0.1 mM PMSF, PIC, 0.5% (vol/vol) IGEPAL CA-630) for 10 min on ice. The suspension was layered onto a sucrose cushion (1.2 M sucrose, 60 mM KCl, 15 mM NaCl, 5 mM MgCl₂, 0.1 mM EDTA, 15 mM Tris-HCl [pH 7.5], 0.5 mM DTT, 0.1 mM PMSF, PIC) and centrifuged for 30 min 4°C at 4700 rpm in a swing rotor. The nuclear pellet was resuspended in digestion buffer (0.32Msucrose, 50 mM Tris-HCl [pH 7.5], 4 mM MgCl₂, 1 mM CaCl₂, 0.1 mM PMSF) and incubated with 10ul of Micrococcal Nuclease (NEB) for 7 min at 37°C. The reaction was stopped by addition of 20ul of EDTA 0.5M and suspension chilled on ice for 10 min. The suspension was cleared by centrifugation at 10,000 rpm (4°C) for 10 min and supernatant (chromatin) was used for further purposes. Chromatin was digested to around 80% of mono-nucleosomes as judged by extraction of the DNA and agarose gel electrophoresis. H3K27ac ChIP experiments were performed on 0.4% PFA-fixed chromatin isolated from MM099 cells according to standard protocols as previously described (Strub et al., 2011). ChIP-

seq libraries were prepared using MicroPlex Library Preparation kit v2 and sequenced on the Illumina Hi-seq 4000 as single-end 50-base reads (Herquel et al., 2013). Sequenced reads were mapped to the Homo sapiens genome assembly hg19 using Bowtie with the following arguments: -m 1 --strata --best -y -S -l 40 -p 2. After sequencing, peak detection was performed using the MACS software ([Zhang et al., 2008] [http:// liulab.dfci.harvard.edu/MACS/](http://liulab.dfci.harvard.edu/MACS/)). Peaks were annotated with Homer (<http://homer.salk.edu/homer/ngs/annotation.html>) using the GTF from ENSEMBL v75. Global clustering analysis and quantitative comparisons were performed using seqMINER ([Ye et al., 2011] <http://bips.u-strasbg.fr/seqminer/>) and R (<http://www.r-project.org/>).

Motif analysis

De novo motif discovery on FASTA sequences corresponding to windowed peaks was performed using MEME suite (meme-suite.org). Motif correlation matrix was calculated with in-house algorithms using JASPAR database as described in Joshi et al., 2017.

Motif analysis Searching of known TF motifs from the Jaspasr 2014 motif database at BRG1-bound sites was made using FIMO (Grant et al., 2011) within regions of 200 bp around peak summits, FIMO results were then processed by a custom Perl script which computed the frequency of occurrence of each motif. To assess the enrichment of motifs within the regions of interest, the same analysis was done 100 times on randomly selected regions of the same length as the BRG1 bound regions and the results used to compute an expected distribution of motif occurrence. The significance of the motif occurrence at the BRG1-occupied regions was estimated through the computation of a Z-score (z) with $z = (x - \mu)/\sigma$, where: x is the observed value (number of motif occurrence), μ is the mean of the number of occurrences (computed on randomly selected data), σ is the standard deviation of the number of occurrences of motifs (computed on randomly selected data). The source code is accessible at <https://github.com/slegras/motif-search-significance.git>.

Immunostaining

Cells were seeded at a density of 5×10^5 on 4-well chamber slides (Lab-Tek, ThermoFisher) and transfected with siRNAs. 72hr post-siRNA treatment, cells were first fixed in 4% PFA for 10min and then permeabilised with 3×5 min 0.1% Triton in PBS, blocked for 1 hr in 5% skim milk in PBS,

and incubated overnight in 5% milk with primary antibodies. The following antibodies were used: BRG1 (ab110641, Abcam), BRM (11966, Cell signaling) and ACTB (2D7, IGBMC). Then, cells were washed 3 × 5 min 0.1% Triton in PBS, and incubated with secondary antibodies, Cy3 mouse-anti-rabbit, and Cy5 rabbit-anti-mouse (Invitrogen) for 2 hrs. Cells were subsequently incubated with 1/2000 DAPI nuclear stain for 10 min, washed 3 × 5 min in PBS, dried and mounted with Vectashild. Visualization was done using inverted confocal microscope SP8 UV.

Analysis of public datasets

Analysis of CLDN1 expression in melanoma cell lines and PDX was performed by extracting their normalised expression levels from scRNA-seq data obtained from (Wouters et al., 2020) and (Rambow et al., 2016). Two-tailed unpaired t test was used for statistical significance (**** $p < 0,0001$, *** $p < 0.001$, ** $p < 0.01$, * $p < 0.05$, ^{ns} $p > 0,05$).

Acknowledgements

We thank Drs JC. Marine and G. Ghanem for the MM029, MM047 and MM099 primary melanoma cells, L Minnoye and S. Aerts for providing the coordinates of MES and MEL enhancers and for the statistics concerning the cross-species conserved elements, N Roehlen and T Baumert for providing the anti-CLDN1 and IgG isotype antibodies, all the staff of the IGBMC common facilities in particular cell culture, flow cytometry, confocal microscopy and biomol. This work was supported by institutional grants from the Centre National de la Recherche Scientifique, the Institut National de la Santé et de la Recherche Médicale, the Université de Strasbourg, the Association pour la Recherche contre le Cancer (CR, contract number PJA 20181208268), the Ligue Nationale contre le Cancer, the Institut National du Cancer, the ANR-10-LABX-0030-INRT French state fund through the Agence Nationale de la Recherche under the frame programme Investissements d’Avenir labelled ANR-10-IDEX-0002-02. The IGBMC high throughput sequencing facility is a member of the “France Génomique” consortium (ANR10-INBS-09-08). ID is an ‘équipe labellisée’ of the Ligue Nationale contre le Cancer. BV was supported by fellowships from the ANR and the Ligue Nationale contre le Cancer.

Author Contributions

BV, SC, AH, JG performed the experiments; GD, BV performed the bioinformatics analyses; BV, GM and ID conceived the experiments, analysed the data and wrote the paper.

References.

- 1 Cancer Genome Atlas Network. Genomic Classification of Cutaneous Melanoma. *Cell*. 2015 Jun 18;161(7):1681-96. doi: 10.1016/j.cell.2015.05.044. PMID: 26091043; PMCID: PMC4580370.
- 2 Darvin P, Toor SM, Sasidharan Nair V, Elkord E. Immune checkpoint inhibitors: recent progress and potential biomarkers. *Exp Mol Med*. 2018 Dec 13;50(12):1-11. doi: 10.1038/s12276-018-0191-1. PMID: 30546008; PMCID: PMC6292890.
- 3 Arozarena I, Wellbrock C. Phenotype plasticity as enabler of melanoma progression and therapy resistance. *Nat Rev Cancer*. 2019 Jul;19(7):377-391. doi: 10.1038/s41568-019-0154-4. Epub 2019 Jun 17. PMID: 31209265.
- 4 Rambow F, Marine JC, Goding CR. Melanoma plasticity and phenotypic diversity: therapeutic barriers and opportunities. *Genes Dev*. 2019 Oct 1;33(19-20):1295-1318. doi: 10.1101/gad.329771.119. PMID: 31575676; PMCID: PMC6771388.
- 5 Widmer DS, Hoek KS, Cheng PF, Eichhoff OM, Biedermann T, Raaijmakers MIG, Hemmi S, Dummer R, Levesque MP. Hypoxia contributes to melanoma heterogeneity by triggering HIF1 α -dependent phenotype switching. *J Invest Dermatol*. 2013 Oct;133(10):2436-2443. doi: 10.1038/jid.2013.115. Epub 2013 Mar 8. PMID: 23474946.
- 6 Rambow F, Rogiers A, Marin-Bejar O, Aibar S, Femel J, Dewaele M, Karras P, Brown D, Chang YH, Debiec-Rychter M, Adriaens C, Radaelli E, Wolter P, Bechter O, Dummer R, Levesque M, Piris A, Frederick DT, Boland G, Flaherty KT, van den Oord J, Voet T, Aerts S, Lund AW, Marine JC. Toward Minimal Residual Disease-Directed Therapy in Melanoma. *Cell*. 2018 Aug 9;174(4):843-855.e19. doi: 10.1016/j.cell.2018.06.025. Epub 2018 Jul 12. PMID: 30017245.
- 7 Tirosh I, Izar B, Prakadan SM, Wadsworth MH 2nd, Treacy D, Trombetta JJ, Rotem A, Rodman C, Lian C, Murphy G, Fallahi-Sichani M, Dutton-Regester K, Lin JR, Cohen O, Shah P, Lu D, Genshaft AS, Hughes TK, Ziegler CG, Kazer SW, Gaillard A, Kolb KE, Villani AC, Johannessen CM, Andreev AY, Van Allen EM, Bertagnolli M, Sorger PK, Sullivan RJ, Flaherty KT, Frederick DT, Jané-Valbuena J, Yoon CH, Rozenblatt-Rosen O, Shalek AK, Regev A, Garraway LA. Dissecting the multicellular ecosystem of metastatic melanoma by single-cell RNA-seq. *Science*. 2016 Apr 8;352(6282):189-96. doi: 10.1126/science.aad0501. PMID: 27124452; PMCID: PMC4944528.

- 8 Ennen M, Keime C, Kobi D, Mengus G, Lipsker D, Thibault-Carpentier C, Davidson I. Single-cell gene expression signatures reveal melanoma cell heterogeneity. *Oncogene*. 2015 Jun;34(25):3251-63. doi: 10.1038/onc.2014.262. Epub 2014 Aug 18. PMID: 25132268.
- 9 Ennen M, Keime C, Gambi G, Kieny A, Coassolo S, Thibault-Carpentier C, Margerin-Schaller F, Davidson G, Vagne C, Lipsker D, Davidson I. *MITF*-High and *MITF*-Low Cells and a Novel Subpopulation Expressing Genes of Both Cell States Contribute to Intra- and Intertumoral Heterogeneity of Primary Melanoma. *Clin Cancer Res*. 2017 Nov 15;23(22):7097-7107. doi: 10.1158/1078-0432.CCR-17-0010. Epub 2017 Aug 28. PMID: 28855355.
- 10 Fane ME, Chhabra Y, Smith AG, Sturm RA. BRN2, a POUerful driver of melanoma phenotype switching and metastasis. *Pigment Cell Melanoma Res*. 2019 Jan;32(1):9-24. doi: 10.1111/pcmr.12710. Epub 2018 Jun 5. PMID: 29781575.
- 11 Verfaillie A, Imrichova H, Atak ZK, Dewaele M, Rambow F, Hulselmans G, Christiaens V, Svetlichnyy D, Luciani F, Van den Mooter L, Claerhout S, Fiers M, Journe F, Ghanem GE, Herrmann C, Halder G, Marine JC, Aerts S. Decoding the regulatory landscape of melanoma reveals TEADS as regulators of the invasive cell state. *Nat Commun*. 2015 Apr 9;6:6683. doi: 10.1038/ncomms7683. PMID: 25865119; PMCID: PMC4403341.
- 12 Laurette P, Strub T, Koludrovic D, Keime C, Le Gras S, Seberg H, Van Otterloo E, Imrichova H, Siddaway R, Aerts S, Cornell RA, Mengus G, Davidson I. Transcription factor MITF and remodeler BRG1 define chromatin organisation at regulatory elements in melanoma cells. *Elife*. 2015 Mar 24;4:e06857. doi: 10.7554/eLife.06857. PMID: 25803486; PMCID: PMC4407272.
- 13 Leucci E, Vendramin R, Spinazzi M, Laurette P, Fiers M, Wouters J, Radaelli E, Eyckerman S, Leonelli C, Vanderheyden K, Rogiers A, Hermans E, Baatsen P, Aerts S, Amant F, Van Aelst S, van den Oord J, de Strooper B, Davidson I, Lafontaine DL, Gevaert K, Vandesompele J, Mestdagh P, Marine JC. Melanoma addiction to the long non-coding RNA SAMMSON. *Nature*. 2016 Mar 24;531(7595):518-22. doi: 10.1038/nature17161. PMID: 27008969.
- 14 Strub T, Giuliano S, Ye T, Bonet C, Keime C, Kobi D, Le Gras S, Cormont M, Ballotti R, Bertolotto C, Davidson I. Essential role of microphthalmia transcription factor for DNA replication, mitosis and genomic stability in melanoma. *Oncogene*. 2011 May 19;30(20):2319-32. doi: 10.1038/onc.2010.612. Epub 2011 Jan 24. PMID: 21258399.
- 15 Koludrovic D, Laurette P, Strub T, Keime C, Le Coz M, Coassolo S, Mengus G, Larue L, Davidson I. Chromatin-Remodelling Complex NURF Is Essential for Differentiation of Adult Melanocyte Stem Cells. *PLoS Genet*. 2015 Oct 6;11(10):e1005555. doi: 10.1371/journal.pgen.1005555. PMID: 26440048; PMCID: PMC4595011.

- 16 Laurette P, Coassolo S, Davidson G, Michel I, Gambi G, Yao W, Sohier P, Li M, Mengus G, Larue L, Davidson I. Chromatin remodellers Brg1 and Bptf are required for normal gene expression and progression of oncogenic Braf-driven mouse melanoma. *Cell Death Differ.* 2020 Jan;27(1):29-43. doi: 10.1038/s41418-019-0333-6. Epub 2019 May 7. PMID: 31065107; PMCID: PMC7205870.
- 17 Verfaillie A, Imrichova H, Atak ZK, Dewaele M, Rambow F, Hulselmans G, Christiaens V, Svetlichnyy D, Luciani F, Van den Mooter L, Claerhout S, Fiers M, Journe F, Ghanem GE, Herrmann C, Halder G, Marine JC, Aerts S. Decoding the regulatory landscape of melanoma reveals TEADS as regulators of the invasive cell state. *Nat Commun.* 2015 Apr 9;6:6683. doi: 10.1038/ncomms7683. PMID: 25865119; PMCID: PMC4403341.
- 18 Minnoye L, Taskiran II, Mauduit D, Fazio M, Van Aerschot L, Hulselmans G, Christiaens V, Makhzami S, Seltenhammer M, Karras P, Primot A, Cadieu E, van Rooijen E, Marine JC, Egidy G, Ghanem GE, Zon L, Wouters J, Aerts S. Cross-species analysis of enhancer logic using deep learning. *Genome Res.* 2020 Jul 30;gr.260844.120. doi: 10.1101/gr.260844.120. Epub ahead of print. PMID: 32732264.
- 19 Rapino F, Delaunay S, Rambow F, Zhou Z, Tharun L, De Tullio P, Sin O, Shostak K, Schmitz S, Piepers J, Ghesquière B, Karim L, Charloteaux B, Jamart D, Florin A, Lambert C, Rorive A, Jerusalem G, Leucci E, Dewaele M, Vooijs M, Leidel SA, Georges M, Voz M, Peers B, Büttner R, Marine JC, Chariot A, Close P. Codon-specific translation reprogramming promotes resistance to targeted therapy. *Nature.* 2018 Jun;558(7711):605-609. doi: 10.1038/s41586-018-0243-7. Epub 2018 Jun 20. PMID: 29925953.
- 20 Wouters J, Kalender-Atak Z, Minnoye L, Spanier KI, De Waegeneer M, Bravo González-Blas C, Mauduit D, Davie K, Hulselmans G, Najem A, Dewaele M, Pedri D, Rambow F, Makhzami S, Christiaens V, Ceyskens F, Ghanem G, Marine JC, Poovathingal S, Aerts S. Robust gene expression programs underlie recurrent cell states and phenotype switching in melanoma. *Nat Cell Biol.* 2020 Aug;22(8):986-998. doi: 10.1038/s41556-020-0547-3. Epub 2020 Aug 3. PMID: 32753671.
- 21 Riesenberger S, Groetchen A, Siddaway R, Bald T, Reinhardt J, Smorra D, Kohlmeyer J, Renn M, Phung B, Aymans P, Schmidt T, Hornung V, Davidson I, Goding CR, Jönsson G, Landsberg J, Tüting T, Hölzel M. MITF and c-Jun antagonism interconnects melanoma dedifferentiation with pro-inflammatory cytokine responsiveness and myeloid cell recruitment. *Nat Commun.* 2015 Nov 4;6:8755. doi: 10.1038/ncomms9755. PMID: 26530832; PMCID: PMC4659938.
- 22 Fontanals-Cirera B, Hasson D, Vardabasso C, Di Micco R, Agrawal P, Chowdhury A, Gantz M, de Pablos-Aragoneses A, Morgenstern A, Wu P, Filipescu D, Valle-Garcia D, Darvishian F, Roe JS, Davies MA, Vakoc CR, Hernando E, Bernstein E. Harnessing BET Inhibitor Sensitivity Reveals AMIGO2 as a Melanoma Survival Gene. *Mol Cell.* 2017 Nov 16;68(4):731-744.e9. doi: 10.1016/j.molcel.2017.11.004. PMID: 29149598; PMCID: PMC5993436.

- 23 D'Avino PP. Citron kinase - renaissance of a neglected mitotic kinase. *J Cell Sci.* 2017 May 15;130(10):1701-1708. doi: 10.1242/jcs.200253. Epub 2017 May 3. PMID: 28468989.
- 24 Garcia-Diaz A, Shin DS, Moreno BH, Saco J, Escuin-Ordinas H, Rodriguez GA, Zaretsky JM, Sun L, Hugo W, Wang X, Parisi G, Saus CP, Torrejon DY, Graeber TG, Comin-Anduix B, Hu-Lieskovan S, Damoiseaux R, Lo RS, Ribas A. Interferon Receptor Signaling Pathways Regulating PD-L1 and PD-L2 Expression. *Cell Rep.* 2017 May 9;19(6):1189-1201. doi: 10.1016/j.celrep.2017.04.031. Erratum in: *Cell Rep.* 2019 Dec 10;29(11):3766. PMID: 28494868; PMCID: PMC6420824.
- 25 Kleffel S, Posch C, Barthel SR, Mueller H, Schlapbach C, Guenova E, Elco CP, Lee N, Juneja VR, Zhan Q, Lian CG, Thomi R, Hoetzenecker W, Cozzio A, Dummer R, Mihm MC Jr, Flaherty KT, Frank MH, Murphy GF, Sharpe AH, Kupper TS, Schatton T. Melanoma Cell-Intrinsic PD-1 Receptor Functions Promote Tumor Growth. *Cell.* 2015 Sep 10;162(6):1242-56. doi: 10.1016/j.cell.2015.08.052. PMID: 26359984; PMCID: PMC4700833.
- 26 Spranger S, Bao R, Gajewski TF. Melanoma-intrinsic β -catenin signalling prevents anti-tumour immunity. *Nature.* 2015 Jul 9;523(7559):231-5. doi: 10.1038/nature14404. Epub 2015 May 11. PMID: 25970248.
- 27 Tsuji K, Cox K, Bandyopadhyay A, Harfe BD, Tabin CJ, Rosen V. BMP4 is dispensable for skeletogenesis and fracture-healing in the limb. *J Bone Joint Surg Am.* 2008 Feb;90 Suppl 1:14-8. doi: 10.2106/JBJS.G.01109. PMID: 18292351.
- 28 Bandyopadhyay A, Tsuji K, Cox K, Harfe BD, Rosen V, Tabin CJ. Genetic analysis of the roles of BMP2, BMP4, and BMP7 in limb patterning and skeletogenesis. *PLoS Genet.* 2006 Dec;2(12):e216. doi: 10.1371/journal.pgen.0020216. Epub 2006 Nov 6. PMID: 17194222; PMCID: PMC1713256.
- 29 Morita K, Morita NI, Nemoto K, Nakamura Y, Miyachi Y, Muto M. Expression of claudin in melanoma cells. *J Dermatol.* 2008 Jan;35(1):36-8. doi: 10.1111/j.1346-8138.2007.00409.x. PMID: 18181775.
- 30 Leotlela PD, Wade MS, Duray PH, Rhode MJ, Brown HF, Rosenthal DT, Dissanayake SK, Earley R, Indig FE, Nickoloff BJ, Taub DD, Kallioniemi OP, Meltzer P, Morin PJ, Weeraratna AT. Claudin-1 overexpression in melanoma is regulated by PKC and contributes to melanoma cell motility. *Oncogene.* 2007 May 31;26(26):3846-56. doi: 10.1038/sj.onc.1210155. Epub 2006 Dec 11. PMID: 17160014.
- 31 Izraely S, Sagi-Assif O, Klein A, Meshel T, Ben-Menachem S, Zaritsky A, Ehrlich M, Prieto VG, Bar-Eli M, Pirker C, Berger W, Nahmias C, Couraud PO, Hoon DS, Witz IP. The metastatic microenvironment: Claudin-1 suppresses the malignant phenotype of melanoma brain metastasis. *Int J Cancer.* 2015 Mar 15;136(6):1296-307. doi: 10.1002/ijc.29090. Epub 2014 Sep 8. PMID: 25046141.
- 32 Eliades P, Abraham BJ, Ji Z, Miller DM, Christensen CL, Kwiatkowski N, Kumar R, Njauw CN, Taylor M, Miao B, Zhang T, Wong KK, Gray NS, Young RA, Tsao H. High MITF Expression Is

Associated with Super-Enhancers and Suppressed by CDK7 Inhibition in Melanoma. *J Invest Dermatol*. 2018 Jul;138(7):1582-1590. doi: 10.1016/j.jid.2017.09.056. Epub 2018 Feb 8. PMID: 29408204; PMCID: PMC6019629.

33 Berico B, Cigrang M, Braun C, Davidson G, Sandoz J, Legras S, Peyresaubes F, Robles C, Egly JM, Compe E, Davidson I, Coin F. TFIID kinase CDK7 antagonizes phenotype switching and emergence of drug tolerance in melanoma. *BioRxiv preprint*. 2020. doi :10.1101/2020.09.24.311431

34 Bekker V, Chanock SJ, Yeager M, Hutchinson AA, von Hahn T, Chen S, Xiao N, Dotrang M, Brown M, Busch MP, Edlin BR, Rice CM, O'Brien TR. Genetic variation in CLDN1 and susceptibility to hepatitis C virus infection. *J Viral Hepat*. 2010 Mar;17(3):192-200. doi: 10.1111/j.1365-2893.2009.01166.x. Epub 2009 Aug 7. PMID: 19674288; PMCID: PMC2921226.

35 Sun S, Jin G, Kang H. CD81 and CLDN1 polymorphisms and hepatitis C virus infection susceptibility: a case control study. *Gene*. 2015 Aug 1;567(1):87-91. doi: 10.1016/j.gene.2015.04.072. Epub 2015 Apr 28. PMID: 25934191.

36 Zeisel MB, Dhawan P, Baumert TF. Tight junction proteins in gastrointestinal and liver disease. *Gut*. 2019 Mar;68(3):547-561. doi: 10.1136/gutjnl-2018-316906. Epub 2018 Oct 8. PMID: 30297438; PMCID: PMC6453741.

37 Krieger SE, Zeisel MB, Davis C, Thumann C, Harris HJ, Schnober EK, Mee C, Soulier E, Royer C, Lambotin M, Grunert F, Dao Thi VL, Dreux M, Cosset FL, McKeating JA, Schuster C, Baumert TF. Inhibition of hepatitis C virus infection by anti-claudin-1 antibodies is mediated by neutralization of E2-CD81-claudin-1 associations. *Hepatology*. 2010 Apr;51(4):1144-57. doi: 10.1002/hep.23445. PMID: 20069648.

38 Souza AG, Silva IBB, Campos-Fernandez E, Barcelos LS, Souza JB, Marangoni K, Goulart LR, Alonso-Goulart V. Comparative Assay of 2D and 3D Cell Culture Models: Proliferation, Gene Expression and Anticancer Drug Response. *Curr Pharm Des*. 2018;24(15):1689-1694. doi: 10.2174/1381612824666180404152304. PMID: 29623827.

39 Fazilaty H, Rago L, Kass Youssef K, Ocaña OH, Garcia-Asencio F, Arcas A, Galceran J, Nieto MA. A gene regulatory network to control EMT programs in development and disease. *Nat Commun*. 2019 Nov 11;10(1):5115. doi: 10.1038/s41467-019-13091-8. PMID: 31712603; PMCID: PMC6848104.

40 Jiang YP, Tang YL, Wang SS, Wu JS, Zhang M, Pang X, Wu JB, Chen Y, Tang YJ, Liang XH. PRRX1-induced epithelial-to-mesenchymal transition in salivary adenoid cystic carcinoma activates the metabolic reprogramming of free fatty acids to promote invasion and metastasis. *Cell Prolif*. 2020 Jan;53(1):e12705. doi: 10.1111/cpr.12705. Epub 2019 Oct 27. PMID: 31657086; PMCID: PMC6985691.

- 41 Guo J, Fu Z, Wei J, Lu W, Feng J, Zhang S. PRRX1 promotes epithelial-mesenchymal transition through the Wnt/ β -catenin pathway in gastric cancer. *Med Oncol*. 2015 Jan;32(1):393. doi: 10.1007/s12032-014-0393-x. Epub 2014 Nov 27. PMID: 25428393.
- 42 Li N, Kong M, Zeng S, Hao C, Li M, Li L, Xu Z, Zhu M, Xu Y. Brahma related gene 1 (Brg1) contributes to liver regeneration by epigenetically activating the Wnt/ β -catenin pathway in mice. *FASEB J*. 2019 Jan;33(1):327-338. doi: 10.1096/fj.201800197R. Epub 2018 Jul 12. PMID: 30001167.
- 43 Pope JL, Bhat AA, Sharma A, Ahmad R, Krishnan M, Washington MK, Beauchamp RD, Singh AB, Dhawan P. Claudin-1 regulates intestinal epithelial homeostasis through the modulation of Notch-signalling. *Gut*. 2014 Apr;63(4):622-34. doi: 10.1136/gutjnl-2012-304241. Epub 2013 Jun 13. PMID: 23766441; PMCID: PMC4083824.
- 44 Suh Y, Yoon CH, Kim RK, Lim EJ, Oh YS, Hwang SG, An S, Yoon G, Gye MC, Yi JM, Kim MJ, Lee SJ. Claudin-1 induces epithelial-mesenchymal transition through activation of the c-Abl-ERK signaling pathway in human liver cells. *Oncogene*. 2013 Oct 10;32(41):4873-82. doi: 10.1038/onc.2012.505. Epub 2012 Nov 19. Erratum in: *Oncogene*. 2017 Feb 23;36(8):1167-1168. PMID: 23160379.
- 45 Lupberger J, Zeisel MB, Xiao F, Thumann C, Fofana I, Zona L, Davis C, Mee CJ, Turek M, Gorke S, Royer C, Fischer B, Zahid MN, Lavillette D, Fresquet J, Cosset FL, Rothenberg SM, Pietschmann T, Patel AH, Pessaux P, Doffoël M, Raffelsberger W, Poch O, McKeating JA, Brino L, Baumert TF. EGFR and EphA2 are host factors for hepatitis C virus entry and possible targets for antiviral therapy. *Nat Med*. 2011 May;17(5):589-95. doi: 10.1038/nm.2341. Epub 2011 Apr 24. PMID: 21516087; PMCID: PMC3938446.
- 46 Diao J, Pantua H, Ngu H, Komuves L, Diehl L, Schaefer G, Kapadia SB. Hepatitis C virus induces epidermal growth factor receptor activation via CD81 binding for viral internalization and entry. *J Virol*. 2012 Oct;86(20):10935-49. doi: 10.1128/JVI.00750-12. Epub 2012 Aug 1. PMID: 22855500; PMCID: PMC3457153.
- 47 Sun BS, Yao YQ, Pei BX, Zhang ZF, Wang CL. Claudin-1 correlates with poor prognosis in lung adenocarcinoma. *Thorac Cancer*. 2016 Sep;7(5):556-563. doi: 10.1111/1759-7714.12368. Epub 2016 Jun 3. PMID: 27766775; PMCID: PMC5130200.
- 48 Zhang WN, Li W, Wang XL, Hu Z, Zhu D, Ding WC, Liu D, Li KZ, Ma D, Wang H. CLDN1 expression in cervical cancer cells is related to tumor invasion and metastasis. *Oncotarget*. 2016 Dec 27;7(52):87449-87461. doi: 10.18632/oncotarget.13871. PMID: 27974683; PMCID: PMC5350000.
- 49 Langhans SA. Three-Dimensional *in Vitro* Cell Culture Models in Drug Discovery and Drug Repositioning. *Front Pharmacol*. 2018 Jan 23;9:6. doi: 10.3389/fphar.2018.00006. PMID: 29410625; PMCID: PMC5787088.

- 50 Mahati S, Xiao L, Yang Y, Mao R, Bao Y. miR-29a suppresses growth and migration of hepatocellular carcinoma by regulating CLDN1. *Biochem Biophys Res Commun*. 2017 May 6;486(3):732-737. doi: 10.1016/j.bbrc.2017.03.110. Epub 2017 Mar 22. PMID: 28342862.
- 51 Mukherjee N, Lu Y, Almeida A, Lambert K, Shiau CW, Su JC, Luo Y, Fujita M, Robinson WA, Robinson SE, Norris DA, Shellman YG. Use of a MCL-1 inhibitor alone to de-bulk melanoma and in combination to kill melanoma initiating cells. *Oncotarget*. 2017 Jul 18;8(29):46801-46817. doi: 10.18632/oncotarget.8695. PMID: 27086916; PMCID: PMC5564524.
- 52 Mahoney KM, Freeman GJ, McDermott DF. The Next Immune-Checkpoint Inhibitors: PD-1/PD-L1 Blockade in Melanoma. *Clin Ther*. 2015 Apr 1;37(4):764-82. doi: 10.1016/j.clinthera.2015.02.018. Epub 2015 Mar 29. PMID: 25823918; PMCID: PMC4497957.
- 53 Patel SP, Kurzrock R. PD-L1 Expression as a Predictive Biomarker in Cancer Immunotherapy. *Mol Cancer Ther*. 2015 Apr;14(4):847-56. doi: 10.1158/1535-7163.MCT-14-0983. Epub 2015 Feb 18. PMID: 25695955.
- 54 Dorand RD, Nthale J, Myers JT, Barkauskas DS, Avril S, Chirieleison SM, Pareek TK, Abbott DW, Stearns DS, Letterio JJ, Huang AY, Petrosiute A. Cdk5 disruption attenuates tumor PD-L1 expression and promotes antitumor immunity. *Science*. 2016 Jul 22;353(6297):399-403. doi: 10.1126/science.aae0477. Epub 2016 Jul 21. PMID: 27463676; PMCID: PMC5051664.
- 55 Schoenfeld AJ, Bandlamudi C, Lavery JA, Montecalvo J, Namakydoust A, Rizvi H, Egger J, Concepcion CP, Paul S, Arcila ME, Daneshbod Y, Chang J, Sauter JL, Beras A, Ladanyi M, Jacks T, Rudin CM, Taylor BS, Donoghue MTA, Heller G, Hellmann MD, Rekhtman N, Riely GJ. The Genomic Landscape of *SMARCA4* Alterations and Associations with Outcomes in Patients with Lung Cancer. *Clin Cancer Res*. 2020 Jul 24. doi: 10.1158/1078-0432.CCR-20-1825. Epub ahead of print. PMID: 32709715.
- 56 Yanai H, Negishi H, Taniguchi T. The IRF family of transcription factors: Inception, impact and implications in oncogenesis. *Oncoimmunology*. 2012 Nov 1;1(8):1376-1386. doi: 10.4161/onci.22475. PMID: 23243601; PMCID: PMC3518510.
- 57 Henon C, Blay JY, Massard C, Mir O, Bahleda R, Dumont S, Postel-Vinay S, Adam J, Soria JC, Le Cesne A. Long lasting major response to pembrolizumab in a thoracic malignant rhabdoid-like *SMARCA4*-deficient tumor. *Ann Oncol*. 2019 Aug 1;30(8):1401-1403. doi: 10.1093/annonc/mdz160. PMID: 31114851.
- 58 Takada K, Sugita S, Murase K, Kikuchi T, Oomori G, Ito R, Hayasaka N, Miyanishi K, Iyama S, Ikeda H, Kobune M, Emori M, Kato J, Hasegawa T. Exceptionally rapid response to pembrolizumab in a *SMARCA4*-deficient thoracic sarcoma overexpressing PD-L1: A case report. *Thorac Cancer*. 2019

Dec;10(12):2312-2315. doi: 10.1111/1759-7714.13215. Epub 2019 Oct 16. PMID: 31617320; PMCID: PMC6885443.

59 Naito T, Umemura S, Nakamura H, Zenke Y, Udagawa H, Kirita K, Matsumoto S, Yoh K, Niho S, Motoi N, Aokage K, Tsuboi M, Ishii G, Goto K. Successful treatment with nivolumab for SMARCA4-deficient non-small cell lung carcinoma with a high tumor mutation burden: A case report. *Thorac Cancer*. 2019 May;10(5):1285-1288. doi: 10.1111/1759-7714.13070. Epub 2019 Apr 10. PMID: 30972962; PMCID: PMC6501032.

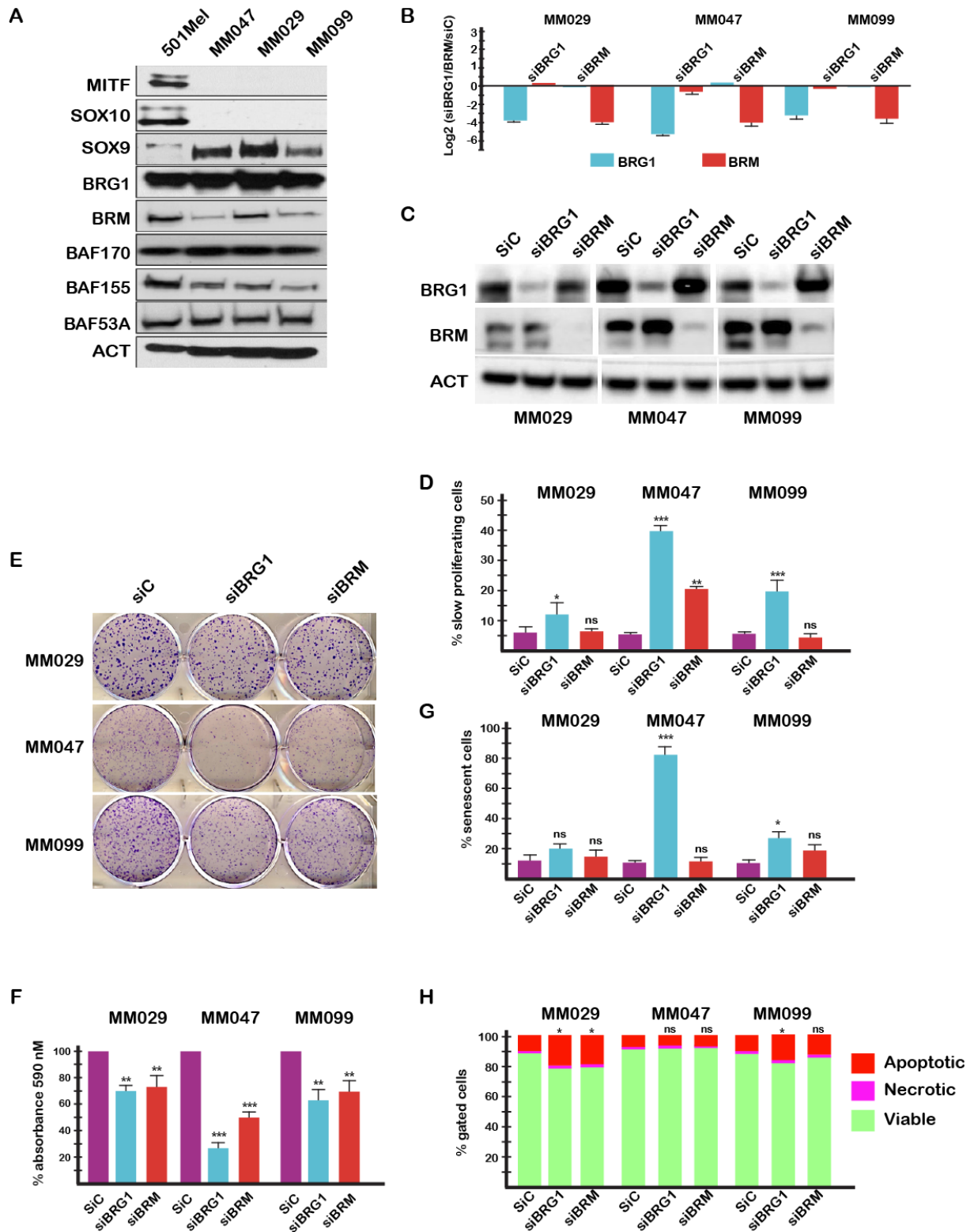
60 Miao D, Margolis CA, Gao W, Voss MH, Li W, Martini DJ, Norton C, Bossé D, Wankowicz SM, Cullen D, Horak C, Wind-Rotolo M, Tracy A, Giannakis M, Hodi FS, Drake CG, Ball MW, Allaf ME, Snyder A, Hellmann MD, Ho T, Motzer RJ, Signoretti S, Kaelin WG Jr, Choueiri TK, Van Allen EM. Genomic correlates of response to immune checkpoint therapies in clear cell renal cell carcinoma. *Science*. 2018 Feb 16;359(6377):801-806. doi: 10.1126/science.aan5951. Epub 2018 Jan 4. PMID: 29301960; PMCID: PMC6035749.

61 Jelinic P, Ricca J, Van Oudenhove E, Olvera N, Merghoub T, Levine DA, Zamarin D. Immune-Active Microenvironment in Small Cell Carcinoma of the Ovary, Hypercalcemic Type: Rationale for Immune Checkpoint Blockade. *J Natl Cancer Inst*. 2018 Jul 1;110(7):787-790. doi: 10.1093/jnci/djx277. PMID: 29365144; PMCID: PMC6037122.

62 Pan D, Kobayashi A, Jiang P, Ferrari de Andrade L, Tay RE, Luoma AM, Tsoucas D, Qiu X, Lim K, Rao P, Long HW, Yuan GC, Doench J, Brown M, Liu XS, Wucherpfennig KW. A major chromatin regulator determines resistance of tumor cells to T cell-mediated killing. *Science*. 2018 Feb 16;359(6377):770-775. doi: 10.1126/science.aao1710. Epub 2018 Jan 4. PMID: 29301958; PMCID: PMC5953516.

63 McDermott DF, Huseni MA, Atkins MB, Motzer RJ, Rini BI, Escudier B, Fong L, Joseph RW, Pal SK, Reeves JA, Sznol M, Hainsworth J, Rathmell WK, Stadler WM, Hutson T, Gore ME, Ravaud A, Bracarda S, Suárez C, Danielli R, Gruenewald V, Choueiri TK, Nickles D, Jhunjhunwala S, Piault-Louis E, Thobhani A, Qiu J, Chen DS, Hegde PS, Schiff C, Fine GD, Powles T. Clinical activity and molecular correlates of response to atezolizumab alone or in combination with bevacizumab versus sunitinib in renal cell carcinoma. *Nat Med*. 2018 Jun;24(6):749-757. doi: 10.1038/s41591-018-0053-3. Epub 2018 Jun 4. Erratum in: *Nat Med*. 2018 Dec;24(12):1941. PMID: 29867230; PMCID: PMC6721896.

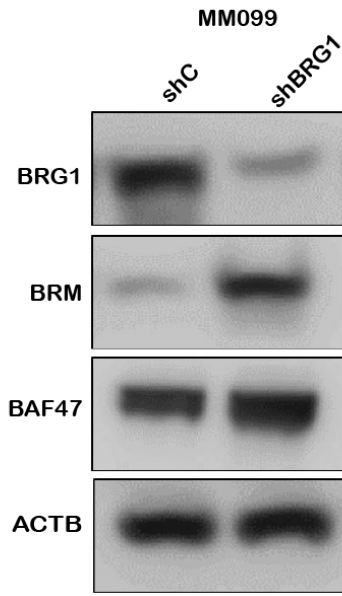
64 Daassi D, Mahoney KM, Freeman GJ. The importance of exosomal PDL1 in tumour immune evasion. *Nat Rev Immunol*. 2020 Apr;20(4):209-215. doi: 10.1038/s41577-019-0264-y. Epub 2020 Jan 21. PMID: 31965064.



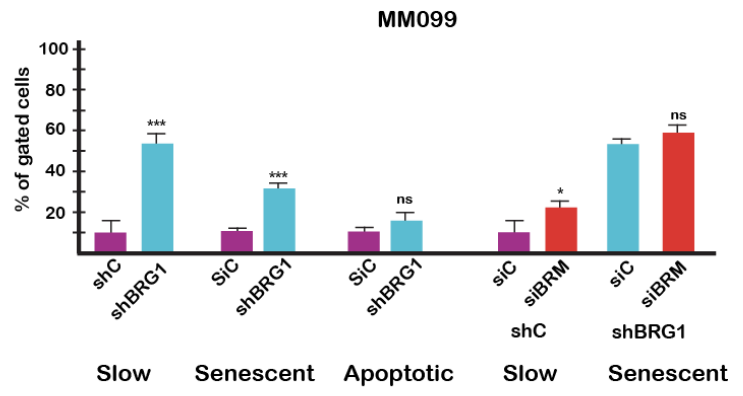
Vokshi et al., Figure 1

Figure 1. Impact of siBRG1 and siBRM silencing in de-differentiated melanoma cells. **A.** Immunoblots on cell extracts from the indicated cell lines for the indicated proteins. Note that the SOX9 antibody weakly cross reacts with SOX10 in the 501Mel cell extract. **B.** RT-qPCR analyses of BRG1 and BRM expression following silencing. Results are expressed as Log₂ fold change compared to siC. **C.** Immunoblots to assess BRG1 and BRM expression following the indicated siRNA silencing. **D.** The indicated cell lines were transfected with siRNAs and cell proliferation evaluated by cell trace violet assay. **E.** Clonogenic assays where cells are fixed and stained 7 days after the indicated transfections. **F.** Quantitation of the surviving stained cells. **G.** The indicated cell lines were transfected with siRNA and senescence detected by FACs after labelling with C₁₂FDG. **H.** The indicated cell lines were transfected with siRNA and apoptosis detected by FACs after labelling with Annexin-V. In all experiments n=3 and unpaired t-test analyses were performed by Prism 5. P-values: *= p<0,05; **= p<0,01; ***= p<0,001. Data are mean ± SEM.

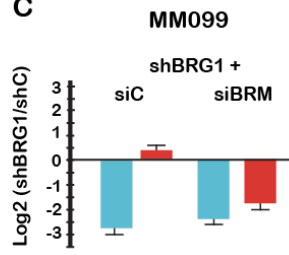
A



B

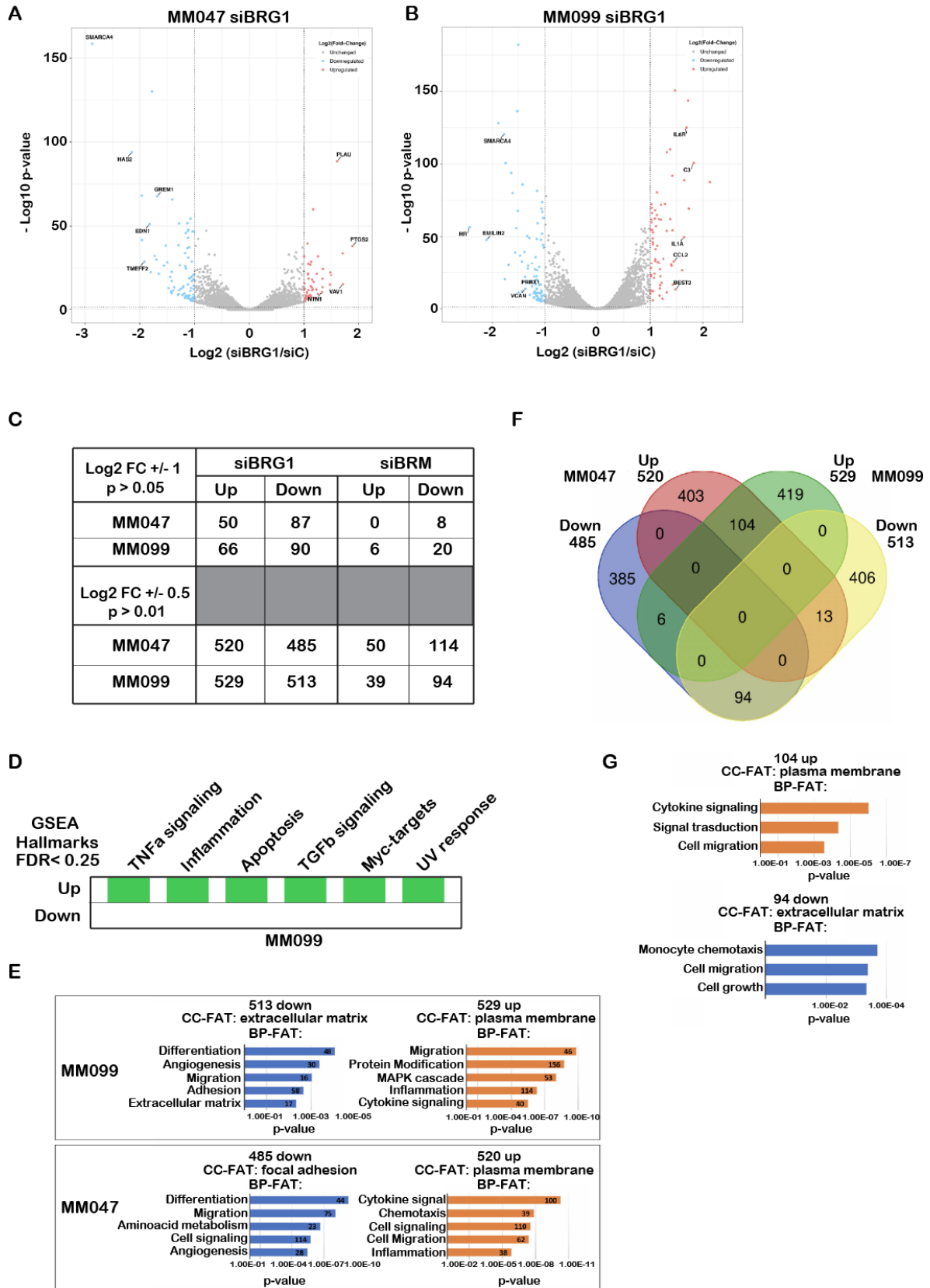


C



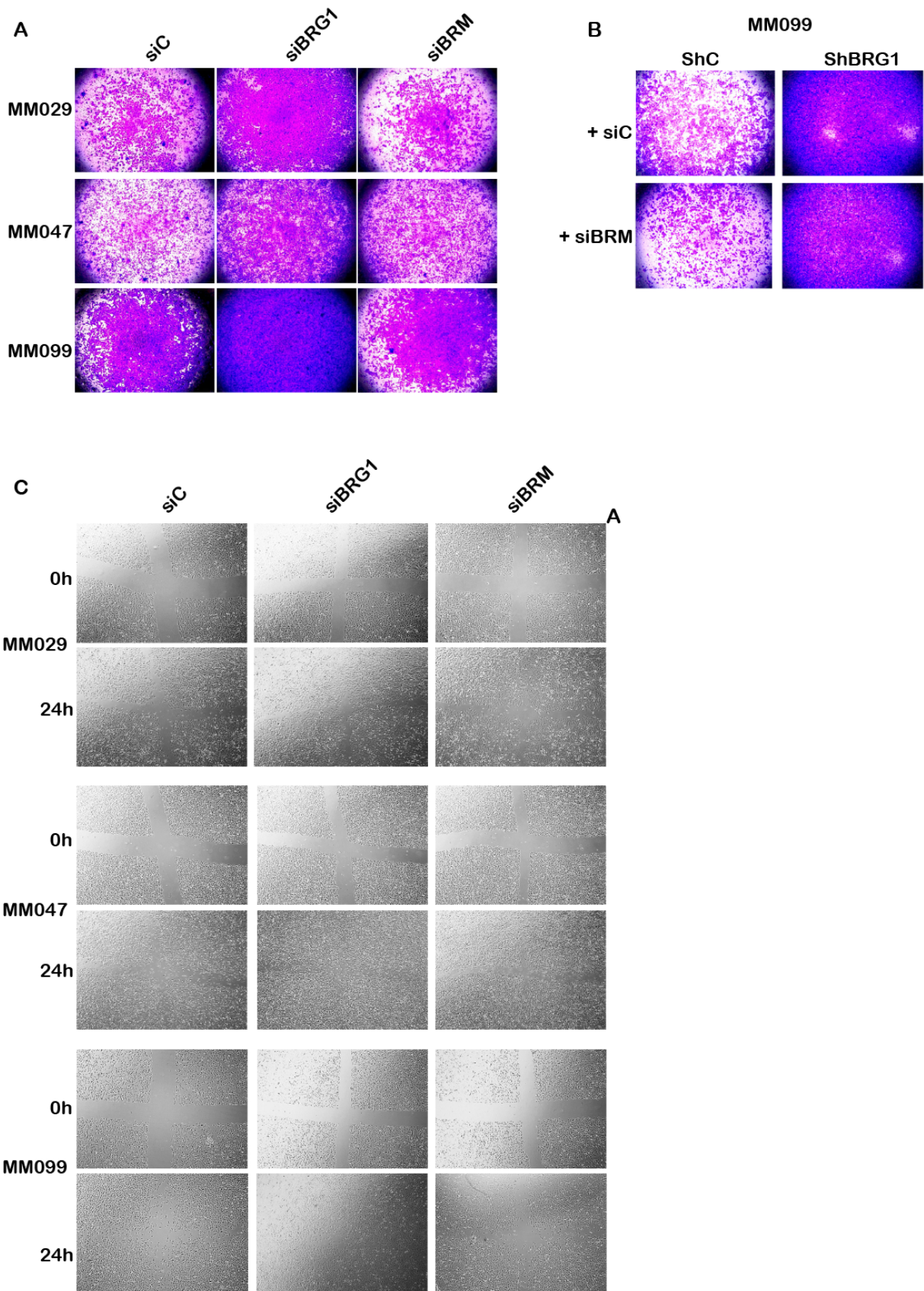
Vokshi et al., Fig. 2

Figure 2. Effects of stable BRG1 silencing. **A.** Immunoblots to assess BRG1 and BRM expression following the indicated shRNA-mediated BRG1 silencing. **B.** Cell proliferation, senescence and apoptosis were evaluated as described in Fig. 1 after shBRG1 silencing with or without concomitant siBRM silencing. **C.** RT-qPCR analyses of BRG1 and BRM expression following shBRG1 silencing with or without concomitant siBRM silencing. Results are expressed as Log₂ fold change compared to shC.



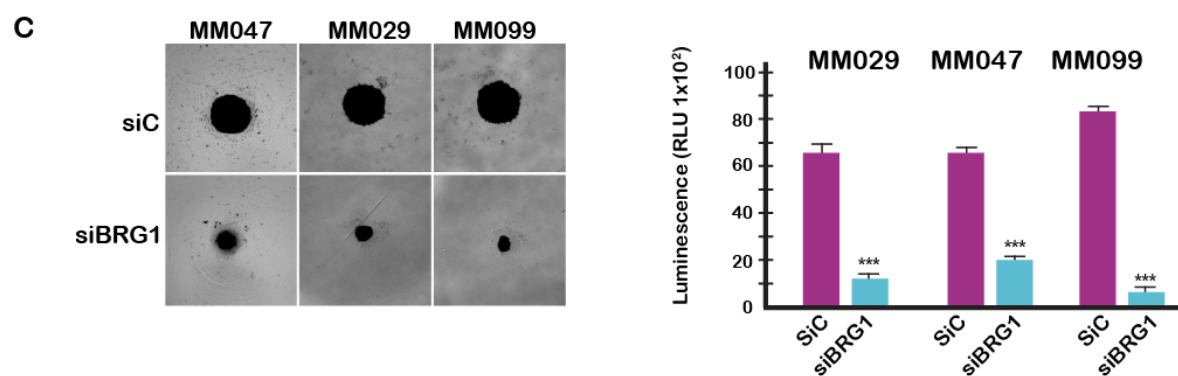
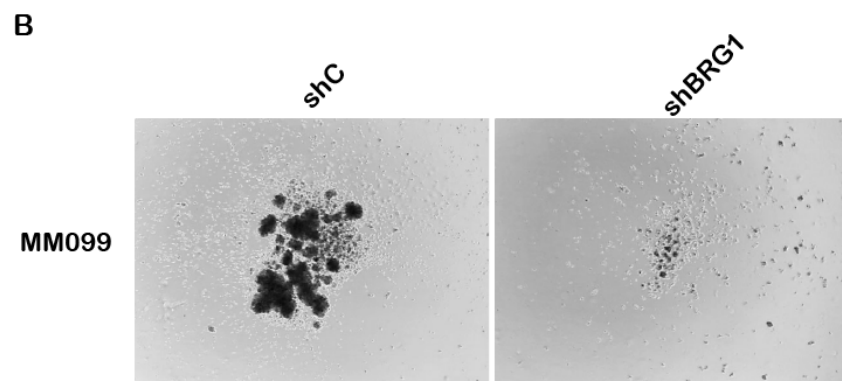
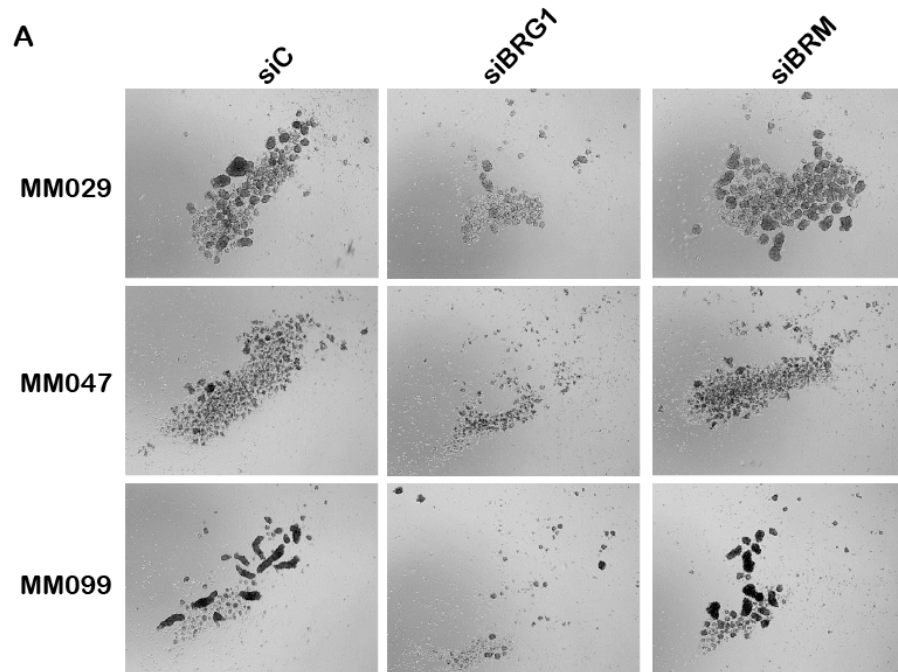
Vokshi et al., Fig. 3

Figure 3. Impact of BRG1 and BRM silencing on gene expression. **A-B.** Volcano plots showing de-regulated gene expression after BRG1 or BRM silencing in the indicated cell lines. **C.** Table showing the numbers of de-regulated genes with the indicated cut off criteria. **D.** GSEA analyses BRG1 regulated genes in MM099 cells. No significant down-regulated classes were identified. **E.** David CC-FAT and BP-FAT categories showing the number of genes and the p-values. **F.** Venn diagram showing the overlap between BRG1 regulated genes in MM047 and MM099 cells. **G.** David CC-FAT and BP-FAT analyses of the genes commonly de-regulated in MM047 and MM099 cells showing the number of genes and the p-values.



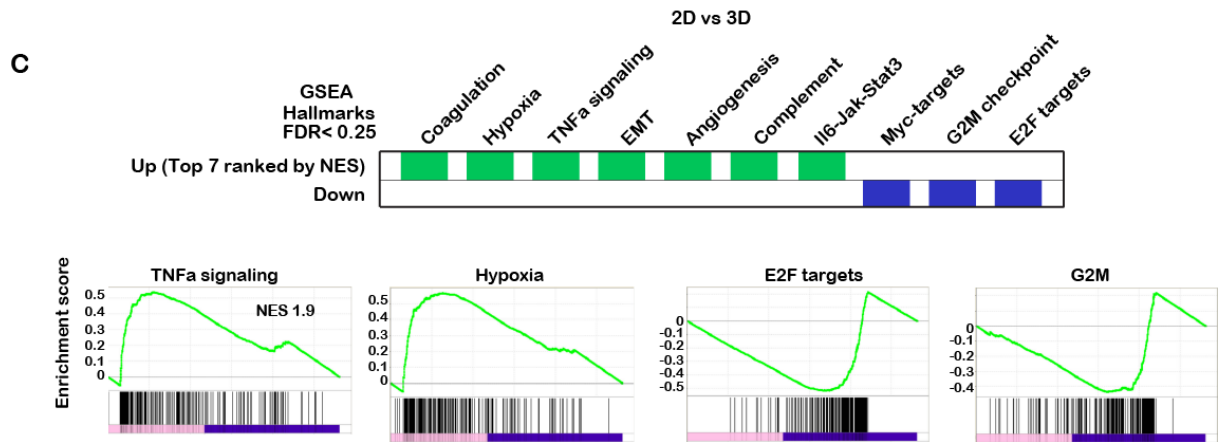
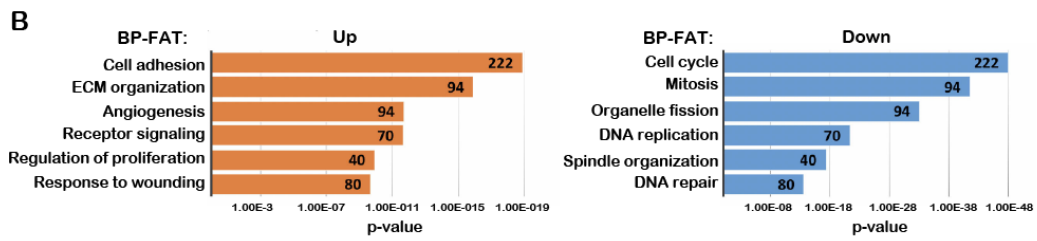
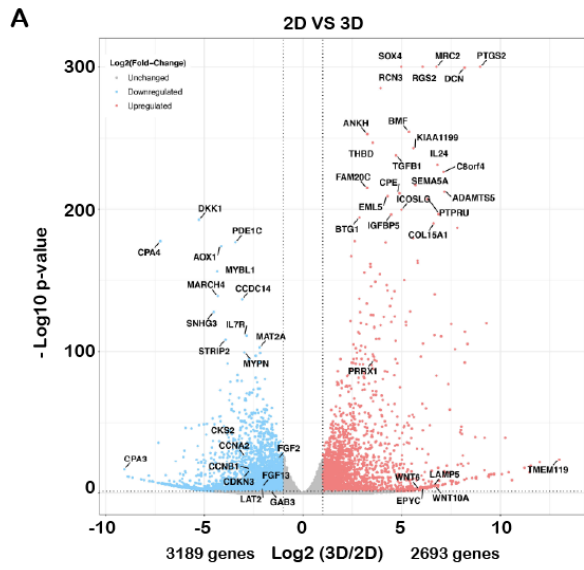
Vokshi et al., Fig. 4

Figure 4. BRG1 regulates melanoma cells motility and invasion. **A.** Boyden chamber assay showing cells that crossed the matrigel barrier after BRG1 or BRM silencing compared to control siRNA. **B.** Boyden chamber assay showing cells that crossed the matrigel barrier after shBRG1 silencing compared to control shRNA in the presence or absence of concomitant siBRM silencing. **C.** Wound healing assay illustrating increased motility of siBRG1 silenced cells. In all experiments n=3.



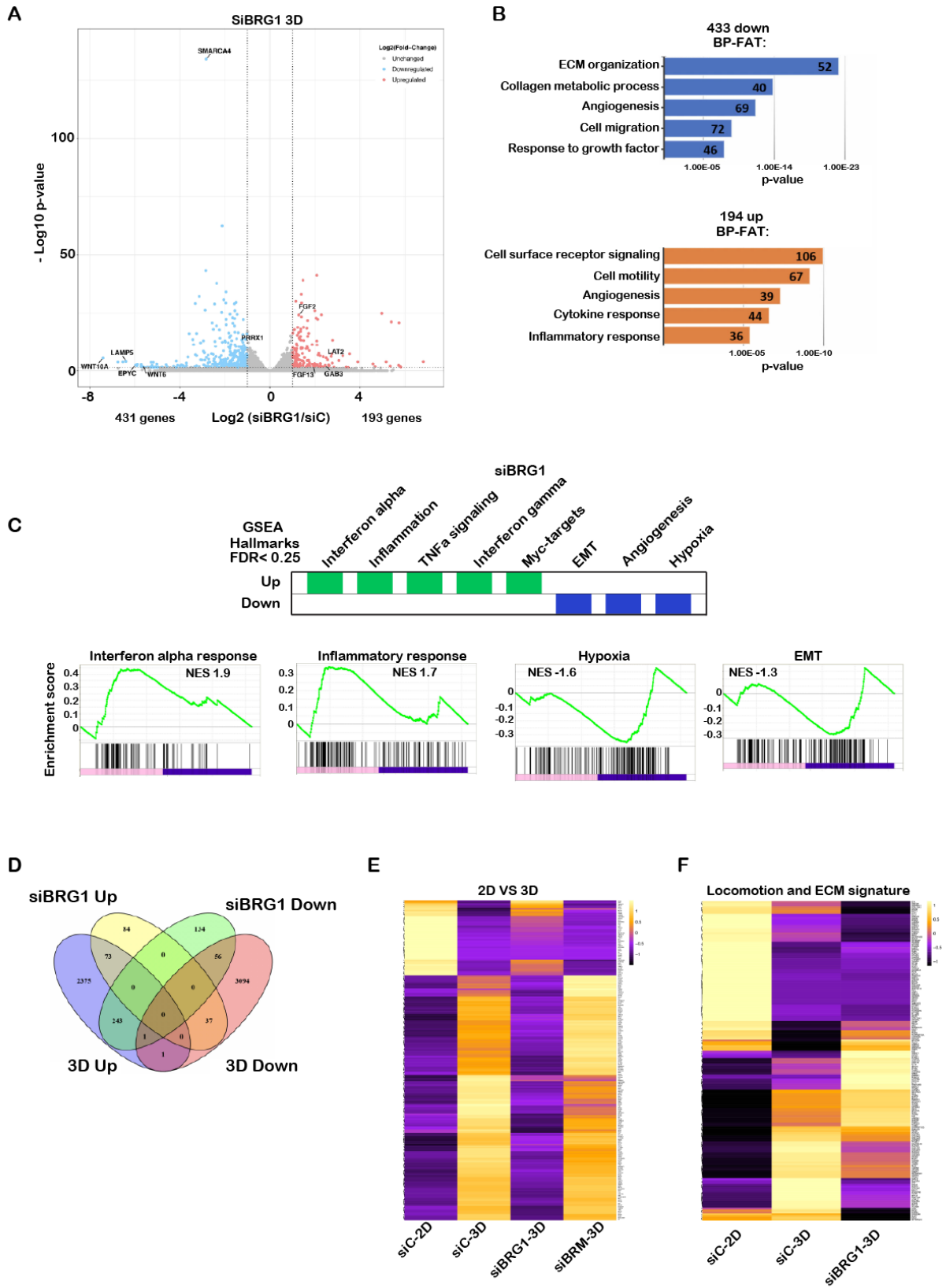
Vokshi et al., Fig. 5

Figure 5. BRG1 is required for melanoma spheroid growth. **A.** Bright field images of free growing spheroids 7 days after silencing of BRG1 or BRM compared to control siRNA. **B.** **A.** Bright field images of free growing spheroids of shBRG1 or shC cells after 7 days. **C.** Bright field images of single spheroids 7 days after silencing of BRG1 compared to control siRNA. Right panel shows quantification of ATP levels as a measure of cell number in the spheroids in the different conditions. Note that these experiments were performed in presence of 10 ug/mL of control IgG antibody as part of the experiments shown in Fig. 14. In 3D sphere experiments, n=3 with 4 technical replicates for each N. Unpaired t-test analysis were performed by Prism 5. P-values: *= p<0,05; **= p<0,01; ***= p<0,001. Data are mean ± SEM.



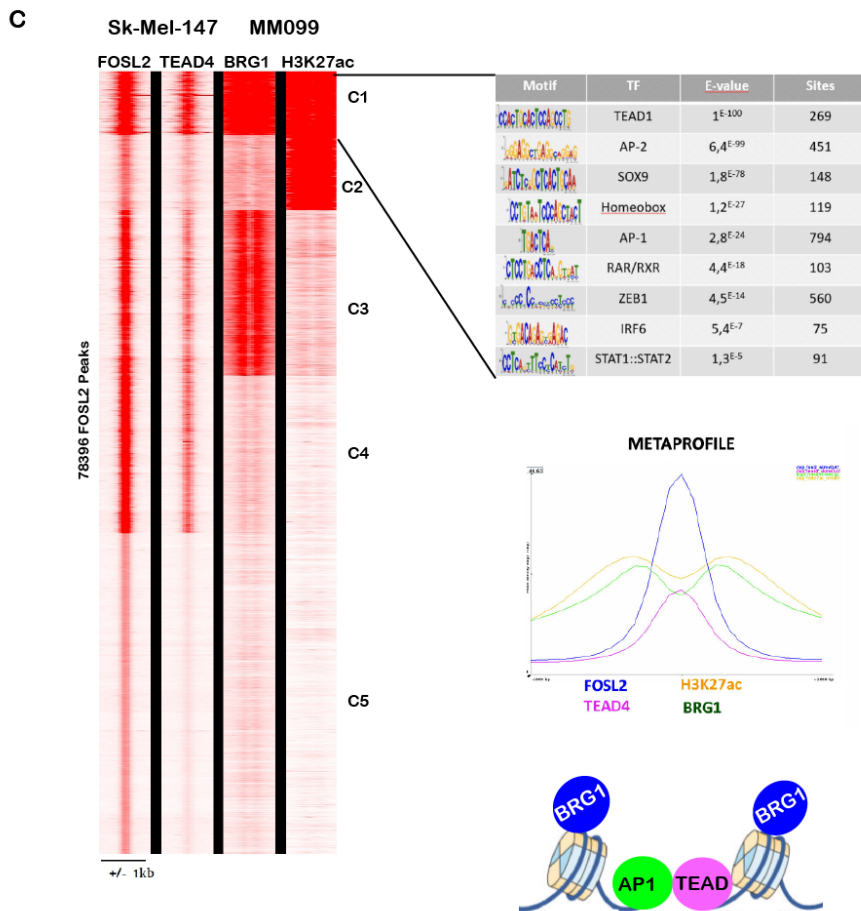
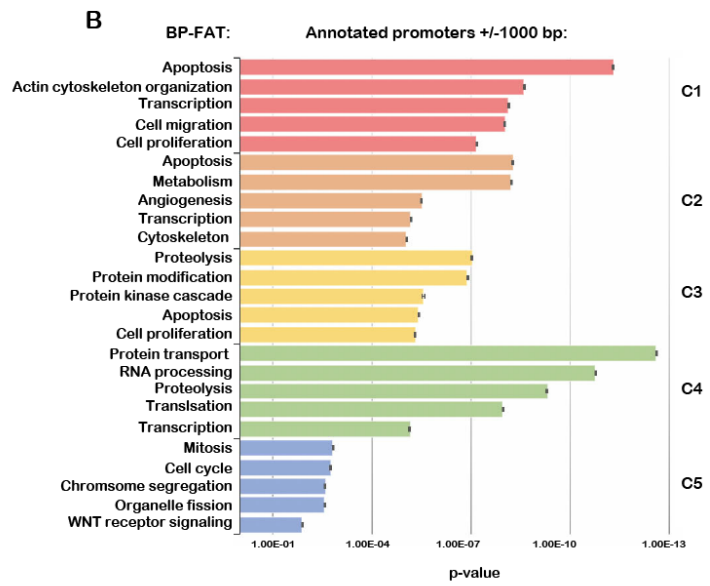
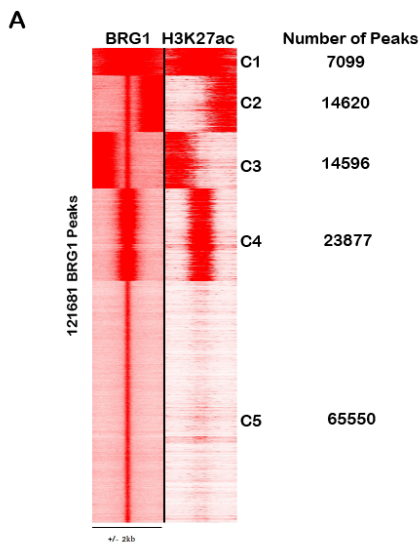
Vokshi et al., Fig. 6

Figure 6. Gene expression changes associated with transition from 2D to 3D growth. **A.** Volcano plot showing de-regulated gene expression of control silenced cells in 2D and 3D conditions. **B.** David BP-FAT categories showing the number of genes and the p-values. **C.** GSEA analyses of deregulated genes in 3D growth.



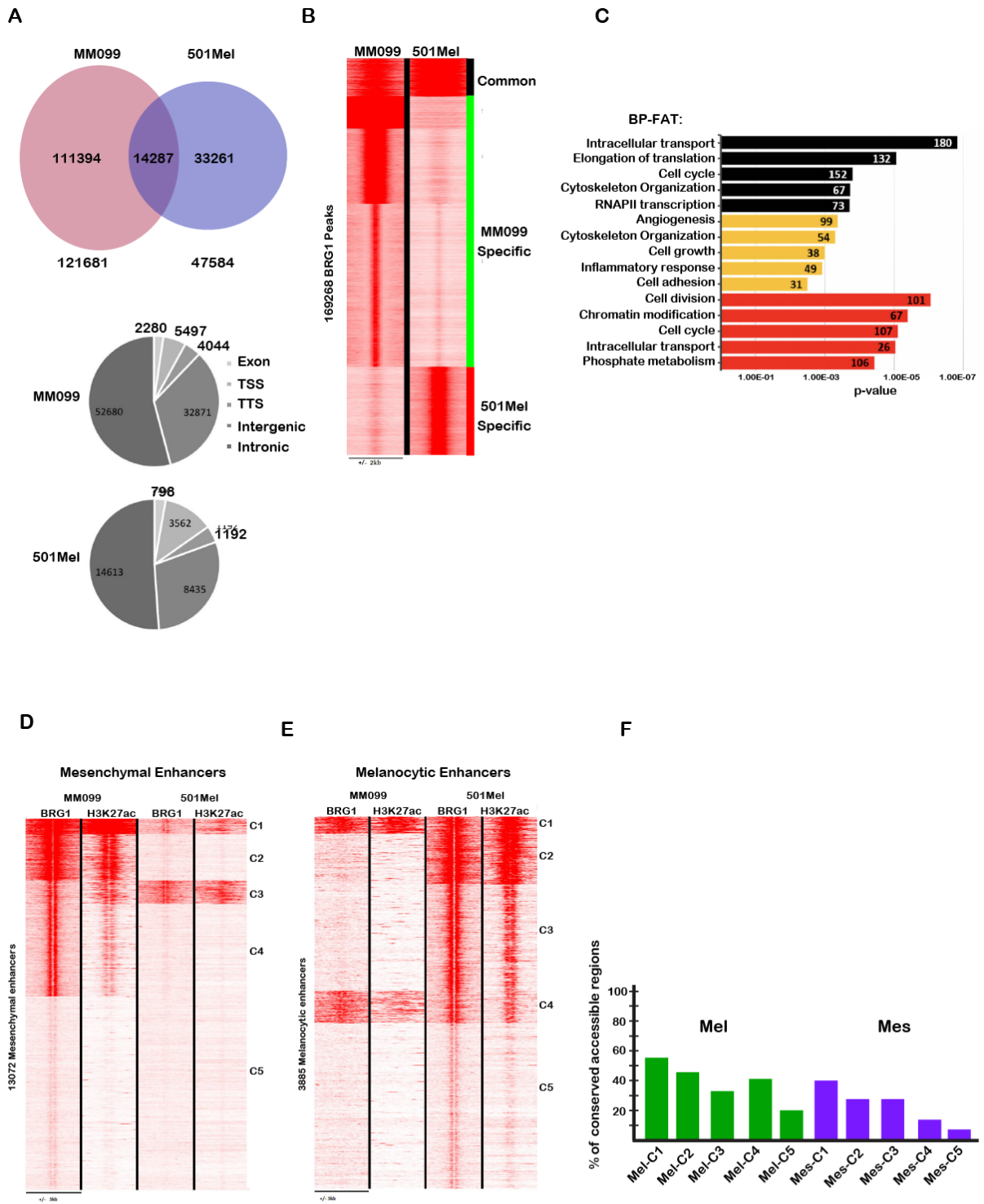
Vokshi et al., Fig. 7

Figure 7. BRG1-dependent gene expression in 3D spheroids. **A.** Volcano plot showing de-regulated gene expression in BRG1 silenced spheroids. **B.** David BP-FAT categories of BRG1 regulated genes showing the number of genes and the p-values. **C.** GSEA analyses of BRG1 regulated genes. **D.** Venn diagram showing the intersect between genes up-regulated during control 3D growth, but repressed by BRG1 silencing and genes repressed during control 3D growth whose repression was diminished by BRG1 silencing. **E.** Heatmap showing the normal and de-regulated expression of the genes identified in the Venn diagram upon the transition from 2D to 3D growth with siBRM shown as additional control. **F.** Heatmap showing the expression of the Locomotion and ECM signature genes of Verfaillie et al., upon the transition from 2D to 3D growth with or without BRG1 silencing.



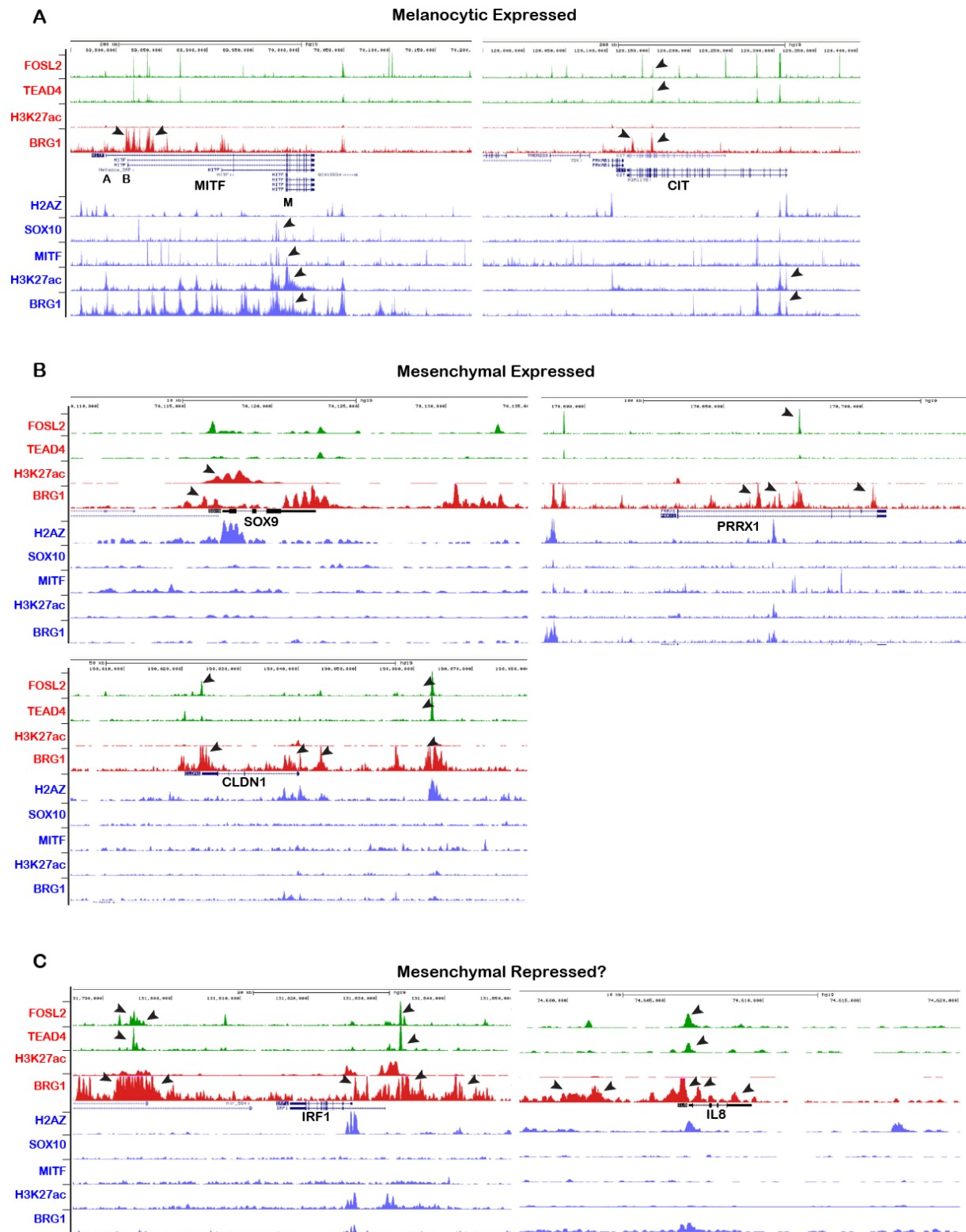
Vokshi et al., Fig. 8

Figure 8. BRG1 genome occupancy in MM099 cells. **A.** Read density map showing comparison of BRG1 bound nucleosomes and H3K27ac modified nucleosomes in MM099 cells. **B.** For each category, the BRG1 bound regions corresponding to proximal promoters were identified and their ontology determined as DAVID BP-FAT. **C.** Read density map showing comparison of FOSL2 bound sites in Sk-Mel-147 cells and TEAD4 sites in these cells with BRG1 and H3K27ac in MM099 cells. The meta-profile of cluster C1 shows that AP1 and TEAD factors bind to regulatory elements flanked by BRG1 bound and H3K27ac-marked nucleosomes. MEME de-novo sequence motif analyses of these sites showing enrichment of TEAD4 and AP1 binding motifs, but also of ZEB1 binding motifs as well those for as homeodomain and IRF factors.



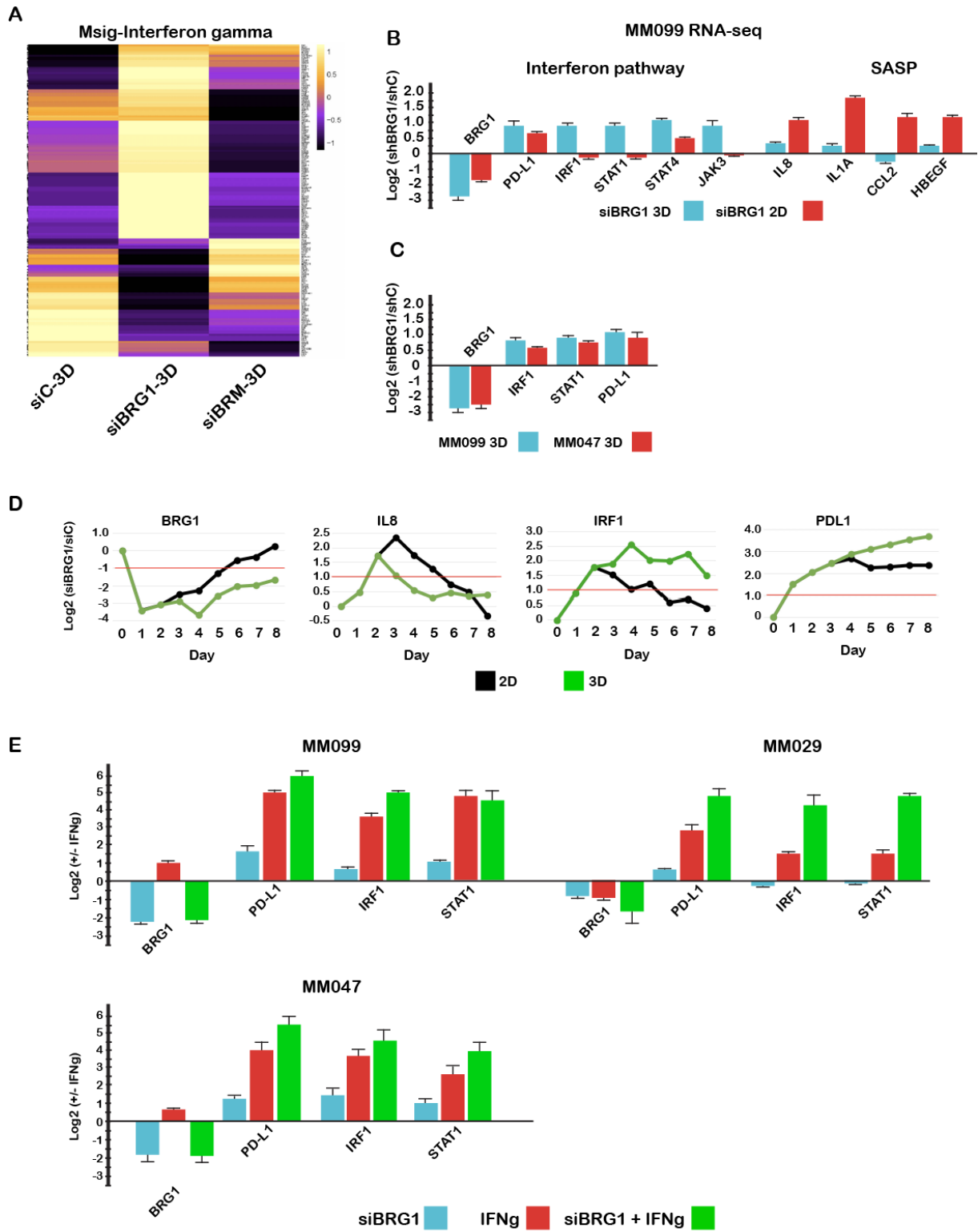
Vokshi et al., Fig. 9

Figure 9. Comparison of BRG1 genome occupancy in MM099 and 501 Mel cells. **A.** Venn diagrams showing overlap between BRG1 bound sites in 501Mel and MM099 cells (top panel) as well as pie charts illustrating the distribution of sites with respect to defined genomic regions (middle and bottom panels). **B.** Read density map showing comparison of BRG1 bound nucleosomes in MM099 and 501Mel cells. **C.** DAVID BP-FAT ontology analyses of the genes closest to the sites in each category. **D-E.** Read density maps showing BRG1 occupancy of nucleosomes surrounding the MES and MEL specific enhancers defined by Minnoye et al., in MM099 and 501Mel cells illustrating the selective occupancy of these sites in each cell type. **F.** The % of cross-species conserved accessible regions present in each of the clusters shown in the heatmaps of panels D and E.



Vokshi et al., Fig. 10

Figure 10. UCSC screenshots of specific loci showing the indicated ChIP-seq tracks in 501Mel cells in blue and MM099 cells in red. **A.** Gene loci (*MITF* and *CIT*) showing preferential BRG1 occupancy in 501Mel cells. The transcriptional start sites of the A, B and M *MITF* isoforms are indicated. Arrow heads show occupied sites around the M isoform start site in 501Mel cells absent in MM099 cells and occupied sites around the A-B isoform start sites in MM099 cells absent in 501Mel cells. At the *CIT* locus, arrow heads show occupied sites around the start site in 501Mel cells absent in MM099 cells and intronic occupied sites in MM099 cells absent in 501Mel cells. **B.** Gene loci (*SOX9*, *PRRX1* and *CLDN1*) showing preferential BRG1 occupancy in MM099 cells. Arrow heads show occupied sites in MM099 absent in 501Mel. **C.** Gene loci (*IRF1*, and *IL8A*) that show extended regions of BRG1 occupancy and whose expression is up-regulated upon BRG1 silencing. Arrow heads show regions of extended BRG1 occupancy in MM099 cells absent in 501Mel cells.

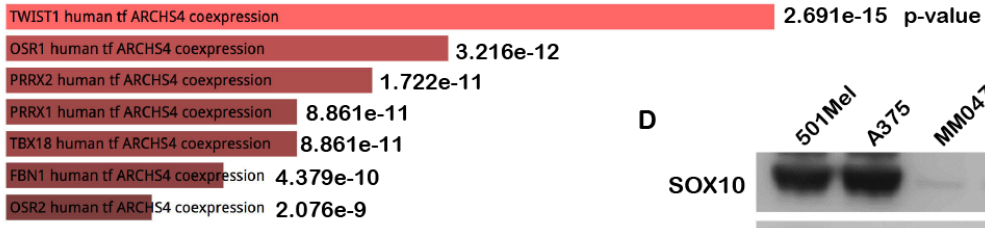


Vokshi et al., Fig. 11

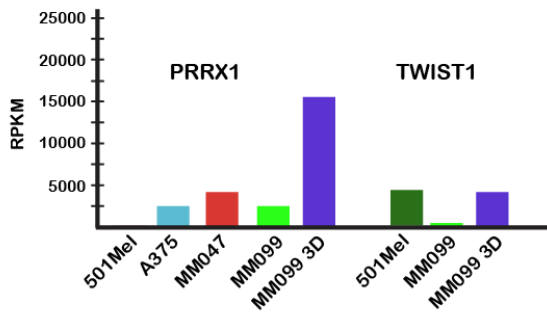
Figure 11. BRG1 represses the interferon signalling pathway. **A.** Heatmap of expression of the MsigDB interferon gamma pathway genes in 3D spheroids after BRG1 or BRM silencing. **B.** Expression of the indicated genes in the RNA-seq experiments following BRG1 silencing in 2D or 3D conditions. **C.** RT-qPCR measured changes in expression of selected genes after BRG1 silencing in MM099 and MM047 cells. **D.** RT-qPCR measured changes in expression of selected genes in 2D and 3D conditions after the indicated number of days. **E.** RT-qPCR measured changes in expression of indicated genes after IFNg treatment with or without concomitant BRG1 silencing.

A

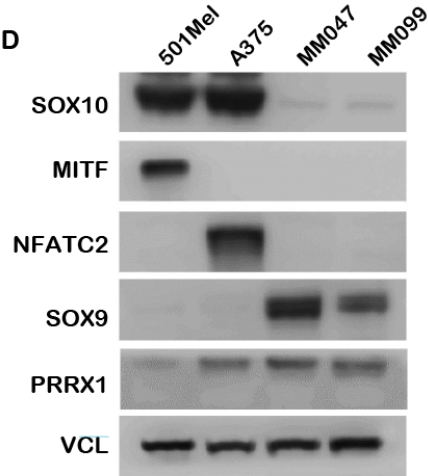
ARCHS4 TF coexpression



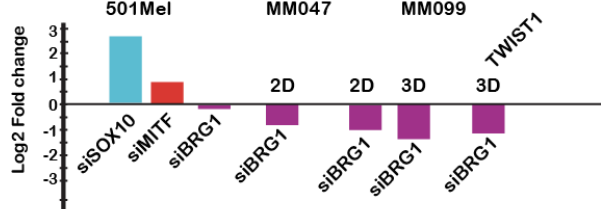
B



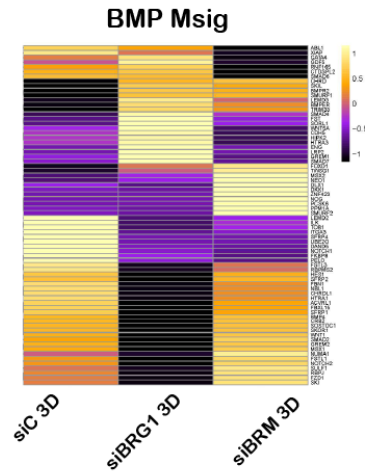
D



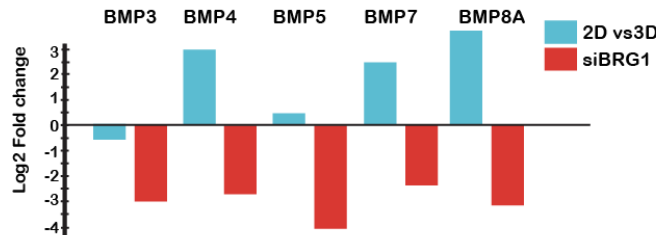
C



E

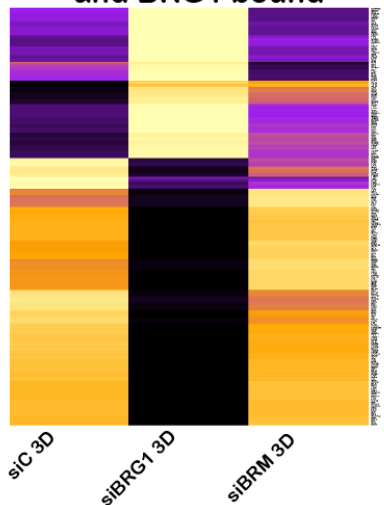


F



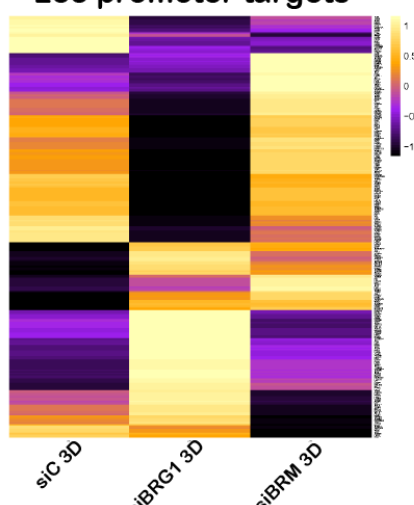
G

Top 200 PRRX1 motif containing and BRG1 bound



H

PRRX1 iRegulon and BRG1 288 promoter targets



Vokshi et al., Fig. 12

Figure 12. PRRX1 regulates gene involved in 3D growth. **A.** Genes whose expression was downregulated by BRG1 silencing in 3D spheroids were analysed using EnrichR. The ARCS4 TF co-expression category identified several transcription factors potentially involved in their regulation. **B.** PRRX1 and TWIST1 expression assessed by RNA-seq in the indicated cell lines and conditions. **C.** PRRX1 expression assessed by RNA-seq in the indicated cell lines following MITF, SOX10 or BRG1 silencing. Diminished TWIST1 expression upon BRG1 silencing is also indicated. **D.** Immunoblots showing expression of the indicated proteins in the different cell lines. **E.** Heatmap showing expression of the BMP Msig gene signature in 3D spheroids with and without BRG1 or BRM silencing. **F.** RNA-seq expression values of BMP ligands in 2D vs 3D and after BRG1 silencing. **G.** Heatmap showing expression of the top 200 BRG1-associated genes with PRRX1 binding motifs in 3D spheroids with and without BRG1 or BRM silencing. **H.** Heatmap showing expression of the 288 iRegulon predicted PRRX1 target genes additionally associated with BRG1 occupancy in 3D spheroids with and without BRG1 or BRM silencing.

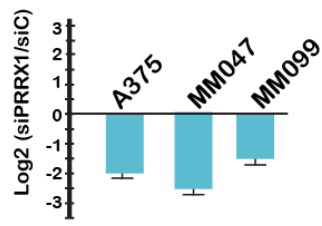
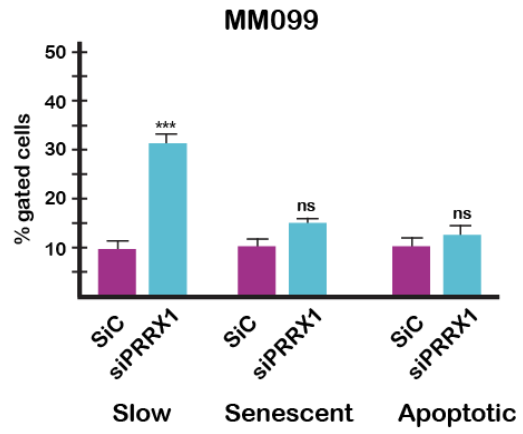
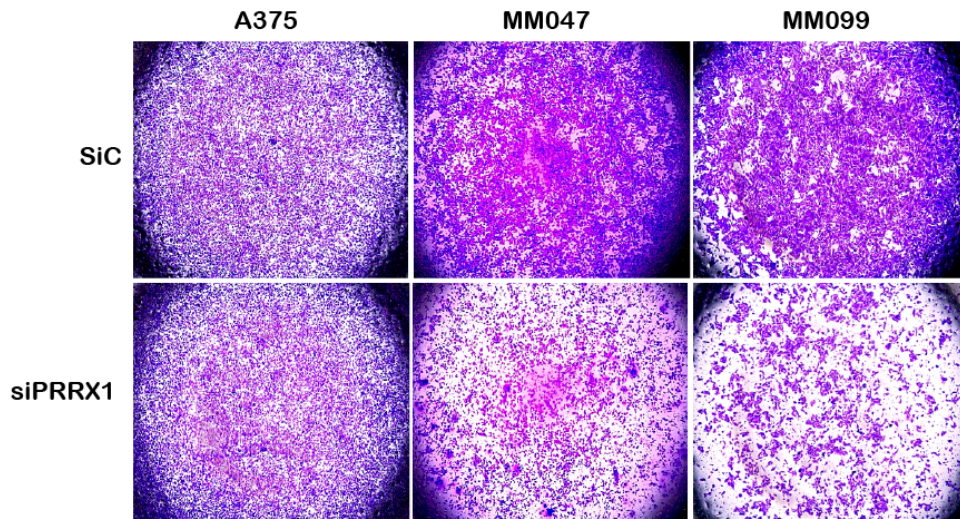
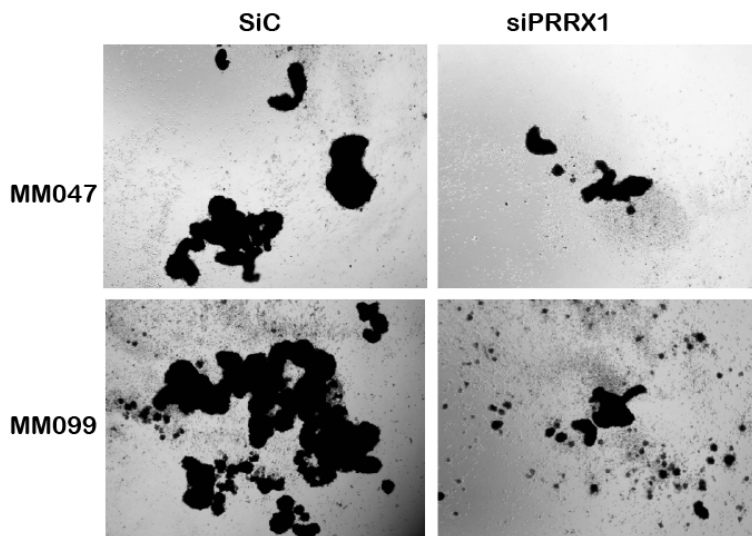
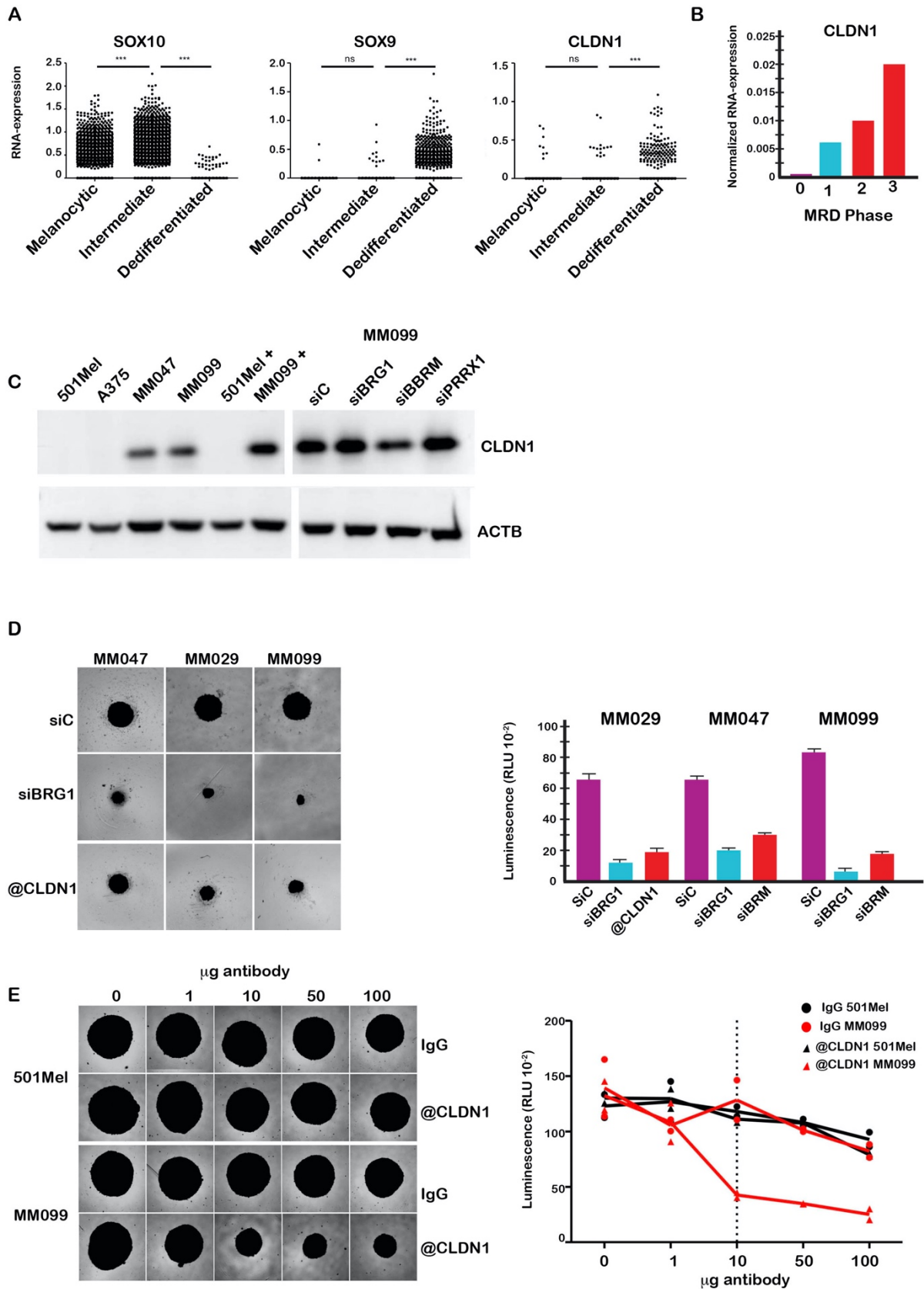
A**B****C****D**

Figure 13. PRRX1 is required for 3D spheroid growth. **A.** Silencing of PRRX1 expression in different cell lines with siRNA. **B** Proportion of slow growing senescent and apoptotic cells following PRRX1 silencing assessed as described in Fig 1. **C.** Bright field images of cells that crossed the matrigel barrier in Boyden chamber invasion assays following PRRX1 silencing. **D.** Bright field images of free growing spheroids following PRRX1 silencing.



Vokshi et al., Fig. 14

Figure 14. CLDN1 is required for 3D spheroid growth. **A.** RNA expression levels of SOX10 SOX9 and CLDN1 in scRNA-seq data from Wouters et al indicating selective CLDN1 expression in de-differentiated cells. **B.** CLDN1 expression in BRAFi et MEKi treated PDX at the stages defined by Rambow et al. MRD is minimal residual disease. **C.** CLDN1 expression in RNA-seq from 501Mel and MM099 cells as well as melanocytic type MM074 cells and THZ1 resistant MM074R cells. **D.** Immunoblots showing CLDN1 protein expression in 3D spheroids from indicated cells lines. + Indicates that the spheroids were treated with antiCLDN1 antibody as shown in panels below. Right hand section of panel shows CLDN1 expression following BRG1 or BRM silencing. **E.** Bright field images of single spheroids 7 days after silencing of BRG1 compared to control siRNA. siC and siBRG1 were performed in presence of 10 μ g of control IgG antibody to compare with the 10 μ g/mL of CLDN1 antibody. Right panel shows quantification of ATP levels as a measure of cell number in the spheroids in the different conditions. **F.** Bright field images of single spheroids after 7 days in presence of the indicated quantities of control IgG or CLDN1 antibody. Right panel shows quantification of ATP levels as a measure of cell number.

Supplementary figures.

Supplementary Dataset 1. Summary of RNA-seq results following BRG1 silencing in MM047 or MM099 cells. Shown are gene names, description, fold change, p-value and adjusted p-value. As indicated, other pages on the spreadsheet show the ontology analyses of each gene set.

Supplementary Dataset 2. Summary of RNA-seq results following BRG1 silencing in 3D-grown spheres of MM099 cells. Shown are gene names, description, fold change, p-value and adjusted p-value. As indicated, other pages on the spreadsheet show the ontology analyses of each gene set.

Supplementary Dataset 3. List of genes identified as essential to 3D growth and regulated by BRG1 in MM099 cells. Shown are gene names, description, fold change, p-value and adjusted p-value.

Supplementary Dataset 4. List of genes identified as essential to locomotion and ECM organization and regulated by TEAD factors in MM047 cells (described in Verfaillie *et al.*, 2015). Shown are gene names, description, fold change, p-value and adjusted p-value.

Supplementary Dataset 5. List of gene promoters identified as BRG1-bound and bearing PRRX1 motif in MM099 cells. Shown are gene names, description, fold change, p-value and adjusted p-value.

Supplementary Dataset 6. List of genes of the Molecular signature database (MsigDB) for interferon gamma pathway that are de-regulated by siBRG1. Shown are gene names, description, fold change, p-value and adjusted p-value.

**PART II. Role of SMARCB1 in renal
medullary carcinoma**

Chromatin remodeling subunit SMARCB1 regulates cell identity and sensitivity to ferroptosis in renal medullary carcinoma

Bujamin Vokshi¹, Guillaume Davidson¹, Alexandra Helleux¹, Marc Rippinger^{1,4}, Alexandre R. Haller¹, Justine Gantzer^{1,2}, Jonathan Thouvenin^{1,2}, Irwin Davidson^{1,7} and Gabriel Malouf^{1,2,#}.

¹ Institut de Génétique et de Biologie Moléculaire et Cellulaire. 1 rue Laurent Fries, 67404 Illkirch Cedex, Strasbourg, France

² Institut de Cancérologie Strasbourg Europe. 17 rue Albert Calmette, 67200 Strasbourg, France.

³ Université de Luxembourg.

⁴ 'Équipe Labellisée' Ligue National contre le Cancer. 89 Boulevard Auguste Blanqui, 75013 Paris, France.

To whom correspondence should be addressed

E-mail : maloufg@igbmc.fr

Tel: + 33 3 68 76 72 17

Running Title : SMARCB1 in renal medullary carcinoma

Key words : Renal medullary carcinoma, SMARCB1, TFCP2L1, MYC, ferroptosis, EMT

The authors declare no potential conflicts of interest.

Abstract.

Introduction. Renal medullary carcinoma (RMC) is a type of lethal malignant neoplasm arising from the kidney medulla region that typically afflicts young patients of African descent with sickle cell traits. RMC is a highly aggressive cancer as most patients present metastatic disease at the time of diagnosis and are resistant to all targeted therapies commonly used against other renal cell carcinomas. Characterized by a particularly low mutation burden, the transformation event of RMC is thought to be the loss of SWI/SNF subunit SMARCB1. Herein we aimed at characterizing the mechanism of tumorigenesis and the precise tumor-suppressor role of SMARCB1 in RMC.

Method. To address these questions, we used bulk and single-cell RNA-seq data of patient samples combined with *in vitro* experiments in two faithful cellular models. We established RMC cell lines stably expressing a doxycycline-inducible SMARCB1 allele and characterized the effects at both biochemical and functional levels by different approaches including : i) transcriptome analysis; ii) profiling of the epigenetic landscape and SWI/SNF genomic localisations; iii) motif enrichment analysis.

Results. First, we show that RMC tumors are heterogenous due to a gradual dedifferentiation from their cell-of-origin associated with partial EMT. We identified the putative cell-of-origin of RMC as being ascending limb cells of Henle's loop, which display a high sensitivity to ferroptosis likely driven by a SWI/SNF-TFCP2L1 axis. Second, we also demonstrate that loss of SMARCB1 induces a drastic transcriptional reprogramming resulting in the derepression of a GPX4-driven ferroptosis resistance program in RMC. Importantly, we show that the tumor-suppressor role of SMARCB1 involves a global reorganization of SWI/SNF complexes and the epigenetic landscape that leads to the induction of cell death by ferroptosis.

Conclusion. These data provide a better understanding on the essential role of SMARCB1 in suppressing RMCgenesis, by both repressing MYC/GPX4 targets and activating TFCP2L1/ASCL4 programs. Loss of SMARCB1 thus induces resistance to cell death by ferroptosis, a vulnerability that could be exploited therapeutically using GPX4 inhibitors.

Introduction.

First described in 1995¹, renal medullary carcinoma (RMC) is a form of lethal malignant neoplasm arising from the kidney medulla region. Despite being overall relatively rare, RMC is the third most common renal cancer among young adults². It typically afflicts male patients of African or Mediterranean descent with sickle cell traits at a median age of 28 years³. In fact, approximately 1 in 20,000 individuals with sickle cell trait develop RMC, yet the association is still poorly understood^{4,5}. RMC is a highly aggressive cancer as most patients present metastatic disease at the time of diagnosis and less than 5% survive longer than 36 months^{3,7}. In addition, RMC tumors are resistant to all targeted therapies commonly used against other renal cell carcinomas and the best available cytotoxic chemotherapy regimens produce a typically brief objective response in only 29% of cases^{7,8}. Alternative treatments such as anti-angiogenics, EZH2 inhibitors and immunotherapy have been tested with varying success⁷.

At the histopathological level, tumors have a predilection for the right kidney and have been reported as an ill-defined and poorly circumscribed mass of 7 cm in average size that occupies most of the renal medulla^{1,8}. The tumor tissues resemble a high-grade carcinoma exhibiting reticular or cribriform patterns and were described as ‘poorly differentiated’ by Rao *et al.* due to expression of OCT3/4 as detected by immunohistochemistry (IHC)⁹. RMC usually also stain positive for VIM, MUC1, KRT7/-8/-18, PAX8, HIF1 α and VEGF, markers that serve during the differential diagnosis^{10,8}. Importantly, other distinctive histological features of RMC are a strong desmoplastic stromal response, a prominent inflammatory infiltrate as well as the frequent presence of sickled red blood cells¹¹. The precise functions of such high infiltrates of immune cells and cancer-associated fibroblasts (CAFs) in RMC tumors remains to be elucidated.

The hallmark of RMC tumors is the loss of SMARCB1 expression¹², a core subunit of the SWItch/Sucrose Non-Fermentable (SWI/SNF) complex which hydrolyzes ATP to remodel chromatin structure. The *SMARCB1* gene maps to the long arm of chromosome 22 (22q11.23) and several mechanisms have been associated with its loss in RMC including deletions, point mutations, inactivating translocations and loss-of-heterozygosity⁷. Besides RMC tumors, loss of SMARCB1 occurs in the

majority of malignant rhabdoid tumors (MRTs), atypical teratoid/rhabdoid tumors (ATRTs) and epithelioid sarcomas (ESs). Historically, SMARCB1 was first described in MRT which is an extremely aggressive malignancy affecting children¹⁷. MRT and RMC share common features such as their renal origin and their particularly low mutation burden⁷. Most of what is known about SMARCB1 comes from studies done with MRT tumors where it was shown to be a potent tumor-suppressor gene^{13,18,19}. Mechanistically, the inactivation of SMARCB1 in MRT results in deregulated targeting of SWI/SNF complex leading to uncontrolled progression through the cell cycle¹⁴. In RMC, SMARCB1 rescue experiments by Hong et al. indicated a significant decrease in cell counts and a senescence phenotype²⁰. While these studies demonstrated the tumor-suppressor role of SMARCB1, the mechanism of action remains elusive.

More recently, a multi-omic study by Msaouel *et al.* shed light on several molecular characteristics of RMC with notably a chromosome 8q gain associated with an amplification of MYC⁷. They found that the loss of SMARCB1 activates the c-MYC pathway resulting in a strong increase of DNA replication stress and DNA damage response, that could potentially be targeted therapeutically. Historically, RMC are thought to arise from the distal region of the nephron, however to this day the evidence has been limited to correlation inference using bulk RNA-seq data from 8 nephron biopsies with identified renal cell populations^{21,7}.

Thus, several questions remain opened in the field. First, the cell-of-origin of RMC is of importance as it would help to better understand the fundamental basis of oncogenic transformation. The second and related question concerns the mechanism of action of SMARCB1 tumor-suppressor role as it is still unclear whether it induces cell death or senescence and how exactly it perturbs SWI/SNF function in RMC. Finally, RMC tumors are known for their high desmoplasia and immune infiltration, yet the underlying mechanisms remain poorly understood. Due to the rarity of the disease, our understanding of the intra-tumoral heterogeneity, that is common in other types of cancers²¹, has also been limited.

To address these interrogations, we developed a translational approach using single-cell RNA sequencing, bulk transcriptomic data from RMC cohorts and *in vitro* experiments using faithful cellular models. Using our single-cell data, we characterized signatures of several renal tubule populations and

identified the putative cell-of-origin of RMC as being tubule cells from the thick ascending loop of Henle (TAL). We highlight key features of RMC tumors which seem to partly retain their original identity while displaying a partial EMT phenotype. For the first time, we describe that RMC are heterogenous tumors composed of two subpopulations that are characterized by either an ‘epithelial-like’ or a ‘mesenchymal-like’ phenotype. Using specific signatures for each cluster, we confirmed that both are found *in vivo* to varying degrees and allow classification of RMC cohorts in two groups with distinct fibroblast and immune infiltrates. Importantly, we show that malignant transformation to RMC may involve a transcriptional switch that results in increased GPX4 expression and resistance to ferroptotic cell death, which could be exploited therapeutically. We confirmed these data using our cellular models and demonstrated that RMC sensitivity to ferroptosis is regulated by SMARCB1. Finally, we identified a novel SWI/SNF target TFCEP2L1 as a master regulator of TAL cell identity that is lost in RMC tumors and might be involved in SMARCB1 tumor-suppressor program.

Results.

1. Key features of RMC and putative cell-of-origin

To identify features and ontogeny of RMC, single-cell RNA sequencing (scRNA-seq) was performed separately on a RMC biopsy and its adjacent normal renal tissue (NAT). Upon resection, the samples were independently validated by IHC confirming tumor cells, with rhabdoid morphology, negative for SMARCB1 and positive for cytokeratin 7 and vimentin. A total of 1600 cells for the NAT sample and 900 cells for the tumor sample passed the quality control check and were subsequently aggregated and analyzed. Seurat UMAP clustering revealed 14 distinct populations amongst which were 7 renal epithelial clusters, 5 renal glomerular clusters and 2 fibroblastic clusters (Figure 1A). Analyses of epithelial clusters allowed identification of 3 groups of proximal tubule cells and 3 groups of distal tubule cells and 1 group of collecting duct cells with expression of specific markers (Figure 1B). Amongst these groups, we were also able to identify thick ascending tubule cells of Henle’s loop (TAL) with specific expression of SLC12A1, MUC1 and CLDN10 but also epithelial markers, such as EPCAM, PAX2 and keratins, consistent with previous renal scRNA-seq data^{23,24}.

Analysis of sample distribution showed TALs and all renal epithelial groups to be highly enriched in the normal sample. In fact, only 3 specific populations were enriched in the tumor sample: an immune group expressing macrophage markers and 2 other groups expressing known fibroblastic markers FN1, VIM, CDH2 (Fig. 1B, S1A). Subsequent AUCell analysis of these 2 clusters revealed that they both expressed a high EMT signature (183 genes); however, only one cluster also expressed a cytokeratin signature (25 genes), which suggested that it might be the RMC cluster (Fig. S1B). Specific markers of these cells were identified to be SFRP2, CLDN1 and MMP7 by Seurat (Fig. 1B), genes whose expression was also found to be higher in bulk RNA-seq of the RMC cohort published by Msaouel *et al.*⁷ (Fig. S1C). Given their EMT signature and their enrichment in the tumor sample, we reasoned that the remaining cytokeratin-negative cluster was composed of cancer-associated fibroblasts as they also express known CAF markers such as ACTA2 (α -smooth muscle actin), POSTN and MMP11^{25,26}. We further analyzed the EMT genes of RMC versus CAF groups and were able to identify specific signatures for both, suggesting tumor cells and CAFs use alternative EMT pathways (Fig. S1D).

We then validated two bulk RNA-seq of RMC cohorts by in-house deconvolution of their mean upregulated signatures on our single-cell dataset, which showed that biopsies have high expression of RMC and CAF genes in both cohorts (Fig. 1C) with a high immune infiltration in the US cohorts in line with top gene ontology terms (Fig. S1E). Additionally, we individually deconvoluted the NAT upregulated signatures of the US cohort which, as expected, were enriched in renal epithelial cells, mostly PCT and DCT cells (Fig. S1F). To validate our findings with an independent method of deconvolution, we used the CIBERTSORTX deep learning algorithm which used our single-cell data to dissect the US cohort bulk RNA-seq (Fig. S2A). The results essentially recapitulated that the US tumor biopsies were mostly composed of varying proportions of RMC cells, macrophages and fibroblasts, whereas these cells were virtually not found in the NAT biopsies. Next, we analyzed the US biopsies using MCP-counter which allows definition of the immune cell types in bulk RNA-seq data (Fig. S2B). The analysis revealed that macrophages (monocytic lineage) are the predominant immune population in RMC tumors, which may explain why they were the only captured immune cells in our single-cell analysis. For validation, we used the classical CIBERSORT algorithm which confirmed that up to 80%

of immune cells in the RMC tumors were either CD4⁺ T cells or macrophages, particularly of the M2 type (Fig. S2C). Thus, besides validating our single-cell dataset using existing bulk RNA-seq from RMC cohorts, we confirmed RMC tumors to be highly infiltrated by both CAFs and macrophages.

RMC are believed to be derived from transformed distal tubule cells, however the evidence has been limited to correlative inference using bulk RNA-seq data⁷. Here we interrogated all renal epithelial populations with the RMC markers. We found that RMC cells correlate well with distal tubule cells generally, however we see the best correlation with TAL cells which are located in the kidney medulla (Fig. 1D). Differential gene expression analysis of RMC versus CAF identified about 100 signature genes for RMC and 50 genes for CAF. Surprisingly, whilst RMC cells indeed have their specific oncogenic program, they still share many genes with TAL cells, genes that we identified as being associated with TAL and more broadly epithelial identities (Fig. 1E). Of note, RMC and CAF cells have in common the expression of EMT genes such as vimentin, in contrast with TAL cells. Altogether, these observations suggest that Henle's loop TAL cells may be the cell-of-origin of RMC.

We then investigated the oncogenic program of RMC cells by analyzing their signature genes. DAVID 6.8 gene ontology revealed key features of RMC with high proliferation and cell survival (Fig. 1F). Intriguingly, the analysis suggested that these cells significantly express inhibitors of cell death, response to reactive oxygen species and regulators of ferroptosis *in vivo*. By comparing expression of ferroptosis genes in RMC and TAL, we showed the specific upregulation of a number of well-known anti-ferroptotic genes such as NFE2L2 and GPX4 (Fig. 1G). Moreover, the data highlighted the physiological ferroptotic sensitivity of TAL cells as high expression of pro-ferroptotic genes such as ACSL4 and LPCATs was detected only in these cells. Importantly, this suggest a transcriptional switch from ferroptosis-sensitive TAL cells to ferroptosis-resistant RMC. Of note, some anti-ferroptotic genes were shared with CAF cells. Nevertheless, RMC cells express a specific anti-ferroptotic program consisting of GPX4 and NFE2L2.

To determine if the activity of NFE2L2 was indeed specifically detected in RMC cells, we performed SCENIC regulome analysis²⁷ which identified top regulators of each population. Of note, we identified TP53 and TBL1XR1 as specific TFs for our CAF cells, whereas IRF7 and MAFG targets were highly activated in macrophages (Fig. S3A). Next, we revealed master regulators of RMC and

TAL cells through unsupervised clustering (Fig. 1H, S2B). As previously described, we observed high MYC and HIF1A activities consistent with the hypoxic nature of these tumors²⁸ and the recurrent amplification of MYC locus⁷. We also confirmed high JUND, YY1 and finally NFE2L2 activity which is consistent with resistance to ferroptosis. In contrast, all these TFs have low or no activity in TAL cells where we found high levels of TFCP2L1, ESRRA, MITF, HOXB9 and SMARCA4 activities. The activity of SMARCA4 seems to be lost in RMC cells in keeping with SMARCB1 inactivation.

Taken together, we identified the key features of RMC cells and their putative cell-of-origin as being the thick ascending limb cells. The data seems to suggest that RMC transform from TAL cells via acquisition of a mesenchymal phenotype and inhibition of their sensitivity to cell death by ferroptosis.

2. RMC intratumoral heterogeneity and partial EMT in vivo

Recent developments of single-cell technology have allowed tremendous advances in understanding intra-tumoral heterogeneity^{22,29}. To test this in RMC, we extracted our tumor cells and sub-clustered them separately using Seurat which identified 2 distinct populations (Fig. 2A) that we termed cluster 0 ('RMC0') and cluster 1 ('RMC1'). DAVID GO terms analysis revealed RMC0 to express genes associated with oxidative phosphorylation and metabolism, while RMC1 favors resistance to cell death, angiogenesis and cell growth as well as extracellular matrix organization (Fig. 2B). We obtained essentially the same results using Gene Set Enrichment Analysis (GSEA), suggesting that EMT genes were more enriched in RMC1 (Fig. 2C). Importantly, ontogeny analysis using RMC0 and RMC1 specific signatures revealed that whilst RMC0 highly correlated with TAL cells, this was much less the case for RMC1 suggesting these cells lost their TAL identity program (Fig. 2D). These observations were independently confirmed by monocle3 trajectory analysis which show a clear line of differentiation going from RMC1 to TAL passing through RMC0 (Fig. 2E). Intriguingly, there seems to be two distinct trajectories involving RMC0 cells: a first one going to RMC1, and a second one segregating within the RMC0 cluster but closer to TAL cells. Thus, we performed SWNE analysis which identified two pathways starting from normal TAL cells: one leading to dedifferentiation and overexpression of mesenchymal markers such as SFRP2, CDH2 and FN1 through partial EMT (Fig. 2F). However, some RMC0 cells seem to separate into a 'stressed' epithelial-like phenotype with higher levels of cytokines

(IL8, LCN2), keratins and epithelial markers such as CDH1, CLDN1. Thus, the RMC tumor seemed to be heterogeneous and comprised at least two subtypes with distinctive features.

Next, we sought to validate that this intra-tumoral heterogeneity can be seen in other RMC tumors. Since RMC1 seem to have a mesenchymal-like program, we crossed its signature genes with our CAF signature in order to eliminate genes that might aspecifically point out the presence of fibroblasts (Fig. 2G). Next, we applied the highly specific RMC0 and RMC1 signatures on the US RMC cohort and were able to detect the heterogeneity by unsupervised clustering. Among the 11 US RMC biopsies that were analyzed, we could divide the tumors in 3 groups: a first with high RMC1 signature, a second with high RMC0 signature and a third one with mixed signatures (Fig. 2H). Higher RMC1 signature expression suggests higher proportions of mesenchymal-like cells in those 3 tumors, while higher RMC0 signature should be associated with a higher percentage of epithelial-like cells. We also analyzed an independent French RMC cohort which revealed that the tumors were predominantly epithelial-like or mixed (Fig. S3C). More importantly, among the 11 biopsies included in the US cohort, 4 were duplicates from the same tumor tissue namely RMCr30T7/RMCr30T8 and RMCr31T13/RMCr31T19. Surprisingly, we found that these 4 tumors divided differently in our clustering: RMCr31T13 highly expressed mesenchymal-like genes whereas RMCr31T19 had equal amounts of epithelial-like and mesenchymal-like. In contrast RMCr30T7 was predominantly epithelial-like, however RMCr30T8 was mixed. We validated these observations using CIBERSORTX which revealed the relative proportions of both RMC subtypes in each RMC biopsy (Fig. S2D). Thus, this suggested that not only we were able to divide tumors according to predominant subtypes, we could also detect spatial heterogeneity within the same tumor samples by analyzing different sections using our specific signatures. Integration of these data with the aforementioned MCP-counter results showed a tendency towards higher immune infiltration in tumors containing mesenchymal-like cells, in contrast to epithelial-like only biopsies (Fig. 2I).

Next, we sought to identify specific regulators of these 2 RMC subtypes by analyzing the regulons provided by SCENIC. First, we were able to show that whilst some regulons are maintained during the dedifferentiation from TAL to RMC1 namely RAD21 and SOX9, we observed a stepwise loss of TAL specific regulons (Fig. 2J). Indeed, master regulator TFCP2L1 but also MITF, PAX2,

SOX6, PPARGC1A and HOXB9 activities decrease in epithelial-like RMC cells and are lost in mesenchymal-like RMC cells. The latter is accompanied by a complete loss of SWI/SNF activity (SMARCA4 and SMARCC1) and TGF- β inhibitory factor TGIF1. We then analyzed subtype specific TFs and found that RMC regulators, previously described in Fig. 1H, namely MYC, HIF1A, NFE2L2, YY1 and JUND but also NFKB1 and MAZ to be common to both RMC subtypes, suggesting a global RMC oncogenic program. However, we were also able to identify specific regulators such as TRPS1 for epithelial-like RMC0 subtype (Fig. 2K). TRPS1 is a known repressor of GATA-regulated genes which was found as a driver of multidrug resistance in lung cancer via regulation of MGMT³⁰. This would be coherent with the high metabolic/OXPHOS signature of this cluster (Fig. 2B) as metabolic reprogramming has widely been described as a mechanism of drug resistance^{31,32}. We additionally identified stress and cytokines regulators FOSL2 and MAFF, as well as pluripotency factor KLF5 for which the role in cancer has been well-studied^{33,34,35}. Finally, we observe specific activation of BCL3, HOXB2 and ATF7 activities in the RMC1 mesenchymal-like subtype, whose involvement in lymphoma, cervical cancer and melanoma has previously been characterized^{36,37,38}. Importantly, we saw a progressive elevation of HES1 activity during the RMC dedifferentiation from TAL. HES1 is a known oncogene specifically involved in EMT, cancer stemness and metastasis³⁹. Interestingly, it has been shown that upon induction by the Sonic hedgehog pathway, HES1 activates mesenchymal cell proliferation through suppression of CDKN1B and also inhibits SOX6 expression⁴⁰. Of note we found SOX6 to be a TAL-specific regulator (Fig. 2J), therefore HES1 could be one of the possible inducers of the pEMT we observed in the RMC1 group.

Altogether, we were able for the first time to show that RMC are heterogeneous tumors containing cells with a partial-EMT phenotype. We studied the master regulators underlying this transition and revealed the gradual loss of TAL programs in RMC0 and RMC1 cells. These 2 subclusters have distinct features with RMC0 remaining epithelial but with a TRPS1 metabolic signature, while RMC1 becomes dedifferentiated and expressing HES1 mesenchymal signature. More importantly, we demonstrate that specific signatures of the 2 subclusters can classify RMC tumors in different groups and are also able to detect spatial intra-tumoral heterogeneity.

3. SMARCB1 re-expression and global reorganization of SWI/SNF architecture

The data presented above suggested that the putative cell-of-origin of RMC to be transcriptionally dependent on a SWI/SNF-TFCP2L1-driven program, likely to specify and maintain TAL cell identity. In RMC, the loss of SWI/SNF activity may be induced by biallelic SMARCB1 inactivation. In the past, several studies attempted to investigate the precise role of SMARCB1 within SWI/SNF complex. Some found SMARCB1 to be essential for the structure of the complex⁴¹, whilst Nakayama and colleagues claim that SMARCB1 has no role in SWI/SNF architecture but rather on genome targeting⁴². In order to better understand the role of SMARCB1 as a driver of RMC, we first investigated SWI/SNF subunit expression in the RMC cohorts. Unsupervised clustering of the 11 US tumors vs their 6 NAT counterparts based on the SWI/SNF genes clearly separated tumors from NATs (Fig. 3A). As expected, we observe a global loss of SMARCB1 expression in tumors, however we also detect a significant and concomitant downregulation of the ATPase subunit SMARCA2 and the PHD-containing DPF3 (Fig. 3B). Similar results were obtained from unsupervised clustering of the French cohort (Fig. S3D), suggesting this mechanism to be conserved in RMC tumors. This is of great importance, as loss of SMARCA2 expression leads to destabilization of all SMARCA2-dependent SWI/SNF complexes, which might contribute to aberrant oncogenic functions as described by others^{43,44}.

We sought to investigate the causal link between the concomitant loss of SMARCB1 and SMARCA2 by assessing SWI/SNF subunit expression in a cellular model of RMC (RMC2C) and other known SMARCB1-deficient cell lines, taking HEK293T cells for reference (Fig. 3C). As expected, we could not detect SMARCB1 in all 4 cell lines and neither SMARCA4 nor SMARCA2 were expressed by the ATRT model which are known to lose both SWI/SNF ATPases⁴⁵. We were able to confirm the specific concomitant loss of SMARCA2 and DPF3 in RMC2C cells, in line with the RNA-seq data from both cohorts. Overall, RMC2C cells presented strongest perturbation of SWI/SNF subunit expression as we observed a loss or downregulation of SMARCC1, SMARCD2, SMARCD3, ARID1A/B, ARID2, PBRM1 and BRD7 compared to the other tested cell lines. This suggests that loss of SMARCB1 may specifically be critical for SWI/SNF integrity in RMC. To test if SMARCB1 re-expression restored the expression of the lost subunits, we established a RMC2C cell line stably expressing a doxycycline (Dox)-inducible allele of SMARCB1. Following Dox-induction, SMARCB1 was expressed at a level

comparable to that seen in HEK293T cells (Fig. 3D), and its nuclear localization was confirmed independently by immunofluorescence and by cell compartment fractionation (Fig. S3E).

Upon re-expression of SMARCB1 in RMC2C cells, we observed a significant increase in several SWI/SNF proteins namely SMARCA2, PBRM1, SMARCC2, SMARCD3, DPF1, DPF2, DPF3 and BCL7B (Fig. 3D). We asked if this could be explained by decreased proteasome degradation due to increased stability by interaction with SMARCB1. However, the analysis of several SWI/SNF subunits upon MG132 treatment revealed that only DPF1 seem to be stabilized by SMARCB1 re-expression (data not shown). Rather, the reduction of SMARCA2 and DPF3 correlates with aforementioned observations of reduced mRNA expression in RMC cohorts. To confirm these observations, we established a second RMC cell line (RMC219) with Dox-inducible SMARCB1 expression and showed by immunoblot that SMARCA2 and DPF3 were lost in wild type RMC219 cells but recovered upon SMARCB1 re-expression (Fig. S3F). Importantly, 1 week after doxycycline washout, we observed a dramatic decrease of SMARCB1 levels in RMC219 cells which was accompanied by a concomitant down-regulation of SMARCA2 and DPF3, highlighting that at least the expression of these 2 SWI/SNF subunits is dependent on SMARCB1 in RMC.

Next, in order to assess the effects of SMARCB1 re-expression, we performed co-immunoprecipitations of SWI/SNF complexes using SMARCA4 as bait, since its expression was not influenced by SMARCB1. As expected, we confirmed the re-incorporation of SMARCB1 into SWI/SNF complexes upon 48hrs of doxycycline treatment (Fig. 3E). Also expected and despite its up-regulation, SMARCA2 was not co-precipitated by SMARCA4 as they are mutually exclusive in SWI/SNF complexes. We confirmed higher integration of pBAF-specific subunit PBRM1, SMARCD3, and all DPF paralogs. However, some subunits were less abundant in SMARCA4-containing complexes namely SMARCD1, ACTL6A and SMARCC2 suggesting they may preferentially integrate the SMARCA2-containing SWI/SNF complexes.

Overall, our data revealed that RMC tumors are characterized by lost expression of additional SWI/SNF subunits other than SMARCB1 itself some of which are not seen in MRT lines. SMARCB1 appears to be instrumental in maintaining the physiological architecture of SWI/SNF complexes,

especially those that depend on the ATPase SMARCA2. Loss of SMARCB1 induces a global reorganization of SWI/SNF complexes which might be one of the oncogenic triggers.

4. Global tumor suppressor program and kinetics of cell death

To investigate the consequences of SMARCB1 induction in our RMC cell lines, we performed several functional assays. Upon SMARCB1 re-expression in both RMC cell lines, the first striking phenotype we observed was a strong decrease of cell survival that was more rapid and complete in RMC219 cells compared to RMC2C cells (Fig. 4A). By analyzing the kinetics of cell death using a FACS-based annexin-V assay, we found that SMARCB1 re-expression gradually increased the number of dying cells over time (Fig. 4B). In addition, in the RMC2C cells we observed a change of cell morphology associated with cytoskeleton reorganization and evident cytoplasmic protrusions visible by anti-TUBB immunofluorescence (Fig. S4A). Since cell protrusions were shown to participate to ‘migration-by-tethering’ following EMT reprogramming in other cancers^{46,47}, we checked the effects of SMARCB1 re-expression on EMT markers and found a marked reduction of vimentin but also a downregulation of EMT inducers SLUG and ZEB1. We also observed a reduction of CLDN1 that is commonly viewed as an epithelial marker, however it appears as a RMC marker in our single-cell analysis and was shown to be overexpressed in RCCs and associated with unfavorable prognosis⁴⁸.

To identify the molecular mechanisms regulated by SMARCB1, we analyzed transcriptomic changes by total RNA sequencing upon Dox treatment of both RMC cell lines. Importantly, we sought to distinguish early targets of SMARCB1 reintroduction from late and possible indirect effects by analyzing two different time-points. Indeed, whilst SMARCB1 was already expressed at 12 hours, its targets such as aforementioned DPF1 were fully induced only at 48 hours (Fig. S4B). A total of 2302 and 1476 genes were deregulated respectively at 12 and 48 hours in the RMC2C cell line. Gene set enrichment analysis (GSEA) of the 12 hour transcriptome revealed the top ranked up-regulated ontologies to be MYC and E2F targets, cell cycle and DNA repair genes, meanwhile interferon response alpha and gamma were down-regulated (Fig. 4C). Surprisingly, we observed a switch in transcriptional regulation at 48 hours with formerly upregulated MYC and E2F targets and cell cycle being repressed while interferon response increased along with KRAS signaling, estrogen response, heme metabolism

and apical junction (Fig. 4D). Next, we applied GSEA on our two RMC cohorts and found an anti-correlation between RMC2C when SMARCB1 was re-expressed and both cohorts where SMARCB1 is inactivated for cell cycle, DNA repair and mTOR pathway, in line with prior reports⁷. Additionally, we observed an anti-correlation for apical junction and heme metabolism (Fig. S4C). We were intrigued by the latter and used DAVID to identify the ontology of the 89 genes involved in the ‘heme metabolism’ hallmark which revealed their implication in iron transport, metabolism and cell death due to defective iron homeostasis, also known as ‘ferroptosis’ (Fig. S4D).

In the RMC219 cell line, the number of deregulated genes was more modest with only a dozen genes upregulated at 12 hours. However, overlap with RMC2C data showed TFRC the transferrin receptor involved in iron transport to be commonly upregulated (Fig. 4E). Moreover, analysis of late transcriptomic changes at 48 hours showed that SMARCB1 regulates similar networks in both cell lines namely it represses MYC targets and up-regulates cell adhesion (Fig. 4F; S4E; S5A). In addition, we checked the effects of SMARCB1 re-expression on SWI/SNF subunits and confirmed that the aforementioned up-regulation of SMARCA2 and DPF3 subunits could be explained by transcriptional regulation (Fig. S5B).

Taken together, we showed that SMARCB1 re-expression led to dynamic changes in the organization of SWI/SNF complexes and on key gene networks regulating cell proliferation and adhesion and iron homeostasis that could explain the EMT phenotype and the strong induction of cell death.

5. Transcriptional reprogramming and stepwise induction of ferroptosis

To investigate the question whether SMARCB1 has any role in cell death due to defective iron homeostasis, we made an in-depth analysis of the RNA-seq data from both cell lines. Taking KEGG Ferroptosis genes, we observed a shared modulation of ferroptosis genes in both lines (Fig. 5A). First, at 12 hours we saw an acute induction of TFRC and its ligand transferrin which is accompanied by a down-regulation of GPX4, a gene well-characterized as a crucial inhibitor of lipid peroxidation⁴⁹. Following these acute events, we observed at 48 hours increased expression of a subset of genes involved in lipid peroxidation namely ACSL4, LOX, LPCAT paralogs and DPP4. Analysis of their

regulatory elements revealed that several harbor iron-responsive elements (IREs) in their promoters (data not shown). This data were consistent with a working model where induction of lipid peroxidation following acute iron uptake leads to ferroptosis, in line with the observed cell death upon SMARCB1 re-expression.

To test the above idea, we performed two additional *in vitro* assays to assess if cells were indeed undergoing ferroptotic death. Firstly, we examined if SMARCB1 re-expression in RMC2C cells resulted in activation of the Caspase pathway using a standard FACS-based Caspase-3 assay (Fig. 5B). Whilst we measured a significant increase of Caspase-3 using camptothecin as a positive control, we did not detect induction of Caspase-3 neither early at 12 hours nor late at 72 hours, indicating SMARCB1-induced cell death was likely not mediated by a programmed apoptotic cell death via caspases. Secondly, we verified if the altered expression of the lipid peroxidation genes translated into an elevation of lipid ROS as assessed using FACS-based BODIPY-C11 (Fig. 5C). Re-expression of SMARCB1 in RMC2C cells indeed induced a striking increase of lipid ROS not seen after Dox treatment of the mCherry negative control cell line. Importantly, the specific induction of lipid ROS by SMARCB1 was abolished by adding ferrostatin-1, a known ferroptosis inhibitor that also led to a net decrease of cell death using Annexin-V assay (Fig. 5D). Altogether, these functional assays confirmed that the cell death phenotype we observed was likely due to ferroptosis.

Next, we sought to determine how SMARCB1 expression affected expression of ferroptosis and known EMT effector proteins. Since the RMC2C cells were dying slower than RMC219, we used them to study the kinetics by immunoblot at 4 time-points until 72 hours post-Dox treatment, when the peak of cell death was detected (Fig. 4B). As already mentioned, 12 hours after Dox addition, we detected a high level of SMARCB1 or mCherry in the control line that was stably maintained until 72 hours (Fig. 5E). Additionally, we tested SMARCA2 and DPF3 to validate that indeed the SMARCB1 activity was progressively increasing. Then we measured the levels of 3 ferroptosis regulators and detected a striking induction of the lipid ROS inducer ACSL4 and a decrease of ferroptosis inhibitors NFE2L2 and its transcriptional target GPX4⁵⁰. These results indicated that SMARCB1 has an instrumental role in maintaining the ACSL4/GPX4 antagonistic equilibrium in RMC2C cells thus regulating their ferroptosis. Next, we showed that induction of SMARCB1 increased expression of E-cadherin (CDH1)

and MITF, while vimentin and fibronectin were notably reduced starting at 48 hours. These dynamic molecular changes suggested that upon SMARCB1 expression, RMC cells undergo a profound transcriptional reprogramming involving repression of mesenchymal genes and activation of epithelial markers, consistent with the top ontology term being ‘apical junction’ at 48hrs (Fig. 4F).

Finally, we also confirmed by immunoblot a gradual repression of MYC upon SMARCB1 expression in RMC2C cells in line with previous studies⁷. RMC tumors were shown to be globally associated with an induction of MYC and its targets. To determine if SMARCB1 directly antagonized MYC activity, we performed crosslinked ChIP-qPCR of both MYC and MAX heterodimeric partners in RMC2C cells treated with DMSO or Dox. Whilst our negative control PRM6 did not enrich at all, we found specific enrichments of both MYC and MAX at the TSS of several known MYC targets such as CDK4, AT4, NRAS and METTL1 in control DMSO treated RMC2C cells. Upon Dox treatment, reduced binding of MYC and MAX to these sites was observed (Fig. 5F), consistent with prior reports in other cell lines⁵¹. These observations demonstrated two potentially distinct effects of SMARCB1 expression, a repression of MYC expression and a direct antagonism of MYC genome occupancy, the net result being the reduced activity of this master RMC regulator.

Overall, these observations demonstrate the tumor-suppressor role of SMARCB1 in RMC cells through transcription regulation of EMT and ferroptotic cell death as well as antagonizing the MYC-regulated oncogenic program linked to both ferroptosis^{52,53} and cell reprogramming^{54,55}.

6. SMARCB1-TFCP2L1 axis and reorganization of the epigenetic landscape

Previous reports documented the role of SMARCB1 in regulation of enhancers and bivalent promoters in MRT cells^{41,42}. We sought to analyze the H3K27ac landscape of RMC2C and compare it to RCC4 cells, a model for clear cell RCC, the most common form of RCC. Unsupervised clustering of H3K27ac from both lines showed specific regions associated with each cell type (Fig. S5C). Since MYC overexpression in cancer has been associated with super-enhancer activity⁵⁶, we sought to analyze the super-enhancers of RMC2C cells using the ROSE algorithm (Fig. 6A, S5C). A total of 1921 and 386 super-enhancers were found in RCC4 and RMC2C cells respectively, with 204 being shared. As expected, GREAT ontology analysis of the associated genes revealed RCC4 super-enhancers to be

involved in VEGF signaling, in line with what is known about these renal tumors⁵⁷. In contrast, RMC2C cells have specific super-enhancers related to negative regulation of cell death, positive regulation of cell migration as well as HGF/MET signaling, pathways implicated in both EMT and its reversal⁵⁸. We then analyzed the super-enhancers with respect to our scRNA-seq data which revealed that the top markers of RMC cells are widely found to be associated with super-enhancers, namely MYC, NFE2L2, VIM, NNMT, CLDN1, FOSL1 and MET (Fig. 6B).

Next, we sought to analyze the effect of SMARCB1 re-expression on SWI/SNF targeting by profiling SMARCA4 genomic occupancy in DMSO or Dox-treated RMC2C cells by native ChIP-seq. More than 100,000 SMARCA4-occupied sites per condition were identified (Fig. S5D). Unsupervised clustering by SeqMINER using the merged set of non-redundant sites revealed a specific gain of SWI/SNF binding sites after SMARCB1 expression (Fig. 6C). Subsequent analysis of TSS-proximal and TSS-distal binding sites clearly showed that the gained peaks were not located in gene promoters, but rather in TSS-distal regions (> 30,000bp). This result showed that SMARCB1 re-expression induced a gain of function of SWI/SNF complexes in RMC, consistent with prior studies in MRT⁴¹. GREAT ontology analysis of the TSS-distal gained SMARCA4 binding sites (Cluster 2) revealed the associated genes to be involved in angiogenesis, regulation of cell differentiation and adhesion, as well as the TGF-beta pathway, in line with cell adhesion being the top commonly up-regulated hallmark upon induction of SMARCB1 in RMC cells. Next, we interrogated the motifs found in cluster 2 to identify associated transcription factors potentially responsible for SWI/SNF recruitment. We found top 5 motifs to be that of Grainyhead family (TFCP2L1), the Paired-box family factor (PAX2), the Homeobox (TGIF2), the HMG domain (SOX6) and the ER-like domain (ESRRA). The latter could explain the ‘estrogen response’ hallmark we found in our GSEA analysis of RMC2C up-regulated genes upon SMARCB1 induction. All of these factors were associated with TAL cell identity in our scRNA-seq, and some are known renal developmental regulators whose deregulation can lead disease and cancer^{59,60,61}.

The above data prompted us to check if any of these TAL TFs are lost in RMC tumors from our cohorts. Thus, we overlapped the list of RMC2C up-regulated genes at 12 and 48 hours as well as the down-regulated genes sets from the RNA-seq of the US and French cohorts. We reasoned that if

SMARCB1/SWI/SNF acted as a cofactor for a given TF, the TF and/or its target genes would be induced by SMARCB1 cell lines while being lost in patients. We found 19 genes down-regulated in both cohorts and up-regulated at both time-points in RMC2C cells (Fig. 6D, Fig. S5E) amongst which 3 were known tumor-suppressors namely FRIMD3, MTUS1 and TFCP2L1. While we already identified TFCP2L1 as highly expressed in TAL and distal tubule cells, the other two TFs were either not expressed or not captured in the scRNA-seq. TFCP2L1 is significantly down-regulated in RMC tumors (Fig. 6D), an event that correlated with lowered epithelial markers EPCAM and CDH1 and anti-correlated with mesenchymal markers VIM and ZEB1 in a collection of cancer cell lines (CCLE, TGCA; Fig. S5F). Immunoblot showed that TFCP2L1 expression was undetectable in absence of SMARCB1, but induced upon Dox treatment (Fig. 6E). TFCP2L1 was therefore a direct target of SMARCB1-containing SWI/SNF complexes.

We next analyzed the SMARCA4 ChIP-seq data to identify all SMARCA4 binding sites that contain a TFCP2L1 motif using the FIMO algorithm. Unsupervised clustering of these selected peaks revealed a specific gain of TFCP2L1 motif-containing binding sites following SMARCB1 induction (Fig. 6F; Cluster 5). These sites were devoid of H3K27ac in non-treated RMC2C cells suggesting the associated genes were not transcribed in absence of TFCP2L1 and its cofactor SMARCB1. GREAT analysis of the associated cluster of genes revealed their implication in regulating cell adhesion and differentiation as well as kidney development. These ontologies correlated well with those found in TSS-distal gain sites upon SMARCB1 (Fig. 6C), suggesting TFCP2L1 re-expression may be responsible for a large fraction of the gained SMARCA4 occupied sites.

Taken altogether, these data converge towards a mechanism whereby the tumor-suppressive role of SMARCB1 in RMC relies on maintaining the crucial balance between two opposing programs both by actively keeping the MYC program in check through direct antagonism and by directly activating TFCP2L1 expression allowing it to regulate its down-stream program of cell adhesion and differentiation in normal TAL cells (Fig. 7).

Discussion.

Here we provide novel insights into understanding the tumor-suppressor function of *SMARCB1* showing that it safeguards the cell identity of RMC cell-of-origin which we identified as being the thick ascending limb cells (TAL) of Henle's loop. Historically RMC was suggested to arise from cells of the kidney medulla due to the localization of the primary tumors. The kidney medulla is thought to be the most hypoxic micro-environment in the organism for many physiological reasons⁶². According to the current model of RMC pathogenesis²⁸, the extreme conditions in the medulla induce sickling of erythrocytes in patients presenting a sickle cell trait which results in recurrent local ischemia and microinfarctions. Then, chronic kidney injury leads to activation of error-prone DNA repair pathways (NHEJ) which likely favour translocations and deletions, particularly in fragile regions such as chromosome 22q where the *SMARCB1* locus is located. Due to its central role in urine concentration, the loop of Henle is characterized by an increasing osmolarity which reaches its highest point in the TAL region, where hypoxia is at its peak. Thus, we propose that RMC could arise from the initial transformation of a TAL cell. Naturally, a definitive answer on RMC ontogeny could only be given by direct transformation of TAL cells, similarly to established mouse model for MRTs⁶⁵. To achieve this, TAL-specific conditional knockout of *SMARCB1* would be necessary in mice, if possibly engineered to bear sickle cell traits^{63,64}.

Nevertheless, we show herein that while TAL and RMC cells share a common background, tumor cells activate a specific oncogenic program associated with activation of cell cycle, EMT and negative regulation of cell death. Intriguingly, we found that the malignant transformation results in a transcriptional switch from ferroptosis-sensitive TAL cells to ferroptosis-resistant RMC cells. Ferroptosis is a new mechanism of death associated with iron overload and accumulation of intracellular toxic lipid peroxides⁶⁶. We showed that TAL cells express high levels of lipid peroxidation enzymes *in vivo* which renders them sensitive to iron-dependent death. Given that an estimated 25% of the cardiac output goes to the kidney where the iron-rich plasma is filtered, it makes sense that renal tubule cells have developed specialized adaptations to manage the influx of iron⁶⁷. Recent *in vivo* studies have reported that the majority of iron is reabsorbed along the loop of Henle and collecting ducts, where it

competes with other divalent metals such as copper and manganese⁶⁸. Due to its ability to donate electrons and reduce oxygen, iron is key for heme metabolism but may also generate reactive oxygen species (ROS). Hence, it was reported that ferroptosis may be a central player in acute kidney injury as renal tubular cells undergo sequential death after ischemic injury⁶⁹. The kidney is also a known positive regulator of hematopoiesis through the secretion of erythropoietin by specialized renal cells that are able to detect anemic or hypoxic conditions⁷⁰.

Taking all this information into account, we propose a model in which sickle cell trait induces chronic ischemia particularly in the kidney medulla. The extreme hypoxic conditions may result in an increased production of erythrocytes, due to positive feedback via renal erythropoietin, in order to compensate the lowering of oxygen availability in the medulla. In turn, this could lead to increased iron influx, with the resulting overload triggering TAL cells to suicide by ferroptotic death. Such a tumor-suppressor mechanism might be regulated by SMARCB1 *in vivo*, consistent with our SCENIC analysis showing the activity of SWI/SNF complex (SMARCA4 and SMARCC1 targets) to be the highest in TAL cells. However, loss of SMARCB1 induced by chromosome rearrangements would inactivate this mechanism thus giving a selective advantage to the initially transformed cell. Subsequent activation of MYC program would lead to uncontrolled cell division and tumorigenesis. Thus, our model extends prior understanding of the genesis of RMC by linking the sickle cell trait observed in all patients to ferroptosis-resistance induced by SMARCB1 loss. Our *in vitro* experiments demonstrated that SMARCB1 re-expression induces ferroptosis in RMC cells and further supported by *in vivo* patient cohort data showing a transcriptional reprogramming associated with a loss of pro-ferroptotic signals (ACSL4, LPCATs) and an overexpression of anti-ferroptotic signals (NFE2L2, GPX4) in RMC.

SCENIC regulome analysis clearly corroborates the specific increase in activity of NFE2L2, a TF known for regulating antioxidant response element (ARE)-pathway and reported to regulate notably GPX4, an enzyme responsible for converting toxic lipid ROS into inoffensive lipid alcohols via the glutathione system⁷¹. An analogous transcriptional switch targeting ferroptosis has been described notably in melanoma where it is regulated in part by the melanocyte master regulator MITF-M⁷². Our SCENIC analysis also revealed that MITF activity was detected specifically in TAL cells and was essentially lost in RMC, together with SMARCA4. The renal-specific isoform, MITF-A, was shown to

be essential for kidney development⁷³, and MITF has been linked to both melanoma and kidney cancers through different mechanisms including translocations⁷⁴ and sumoylation⁷⁵. In RMC, we observed an up-regulation of MITF after SMARCB1 expression, however we do not know yet if MITF plays a role in ferroptosis. Further experiments would need to be undertaken to decipher the exact contribution of MITF as well as NFE2L2. Additional ChIP-seq for MITF and NFE2L2 in RMC2C-mCherry and RMC2C-SMARCB1 cells would give important insights on the targets of each TFs. Moreover, knockdown experiments of MITF and NFE2L2 would demonstrate the causal links between these factors and ferroptosis. We could verify on one hand if SMARCB1 can induce ferroptosis without MITF; and on another hand if knocking down NFE2L2 in native RMC cells makes the cells more prone ferroptosis.

In their study, Hong et al. showed that reintroduction of SMARCB1 in their RMC cell line induced both senescence and death which lead them to propose a model by which G2/M cell cycle arrest caused apoptosis, as assessed by AnnexinV assay²⁰. In our case, we observed only marginal senescence upon SMARCB1 re-expression (<10% of cells, data not shown) as assessed by FACS-based β -galactosidase assay. However, we could confirm a striking increase of Annexin V-positive cells. Historically Annexin V was shown to specifically bind phosphatidylserines (PS), hence it is often considered a hallmark of apoptosis, a type of cell death associated with PS externalization. However recent studies revealed that PS are also externalized during necrosis and ferroptosis, thus Annexin V-based assays should be viewed as indicator of general cell death⁷⁶. Herein, we could demonstrate that RMC were dying in a manner that could be inhibited by ferrostatin-1 and without induction of the Caspase pathways. Experiments using iron chelators in RMC would further validate the ferroptosis phenotype. Ferroptosis is also associated with a global deregulation of mitochondrial function which will need to be addressed in the future⁷⁷. Moreover, to verify that these observations are not cell line-specific, all ferroptosis assays will need to be conducted in RMC219 cells. Of note, renal cell carcinomas were found to be the most sensitive to GPX4 inhibitors in early drug-sensitivity screens of 177 cell lines of various cancer types⁷⁸, in line with the aforementioned physiological role of kidney cells in regulating iron homeostasis. Here we showed that SMARCB1 represses both GPX4 and NFE2L2 protein levels in

RMC cells, which in principle mimics the effect of GPX4 inhibitors such as RLS3. Further SMARCB1 re-expression experiments in other non-RMC rhabdoid cell lines are on-going and will determine if ferroptosis resistance is specific to RMC or if it may be a widely conserved mechanism in SMARCB1-deficient tumors. In addition, it is evident that the effects of GPX4 inhibitors will need to be tested in xenografts in nude mice as 3D-growing tumors may result in different outputs.

In concordance with the study by Msaouel et al.⁷, we found that RMC cells overexpress MYC targets as supported by RNA-seq from RMC cell lines as well as by our scRNA-seq results. *In vitro*, we validated that SMARCB1 represses MYC thus antagonizing its binding to the genome, however the genome-wide targets of MYC in RMC have yet to be characterized. On-going sequencing of MYC and MAX ChIP-seq in RMC-mCherry and RMC-SMARCB1 cells will address this issue. Intriguingly, RNA-seq from RMC2C cells revealed that at 12 hours SMARCB1 induces at first an increase of MYC targets, before repressing them at the 48 hours. Hence, we cannot exclude that MYC repression could be due to indirect effects, such as the reorganization of SWI/SNF complexes. Of note, we could not see such dynamics in the RMC219 cell line, however this might be a technical issue as this particular cell line had distinct dynamics and seemed to be more sensitive to death than RMC2C cells for a reason yet to be identified. To our knowledge, there is yet no report of such dynamics between SWI/SNF and MYC. Of note, the transferrin receptor TFRC, which regulates iron uptake, has been described as MYC target⁷⁹. Thus, it is possible that MYC inhibits TFRC while SMARCB1 activates it, as they have been reported to have antagonistic functions on their overlapping targets^{80,81}. While our work is consistent with studies reporting that SMARCB1 re-expression in MRT cells mimics a ‘MYC inhibition’ phenotype⁵¹, it remains unclear if the tumor-suppressor role of SMARCB1 can be reduced to solely repressing MYC in RMC.

Our analysis of H3K27ac ChIP-seq from RMC2C cells identified MYC as being associated with a super-enhancer (SE). A recent study in human embryonic stem cells showed that SMARCB1 expression is essential for repressing super-enhancers found at pluripotency genes⁸². Given that MYC is one of the Yamanaka factors, it might be relevant to check if re-expressing SMARCB1 has any effect on the oncogenic super-enhancer landscape in RMC, especially at the MYC locus. Additionally, our SMARCA4 ChIP-seq revealed that SMARCB1 alters SWI/SNF targeting to the genome resulting in a

gain of 7000 novel peaks at genes associated with cell differentiation and apical junction. Although this finding is in line with several studies in MRT^{41,42}, we noted that SMARCB1 induced a lesser gain in RMC2C, as compared to G401 cells. This might either be biologically representative or due to a technical issue as we performed our first ChIP-seq in suboptimal conditions. The control consisted in RMC2C cells bearing the Dox-inducible SMARCB1 transgene but treated DMSO, and it is probable that a residual amount of SMARCB1 is expressed in our control cells due to leakage. Hence, all future ChIP-seq will be performed in RMC cells stably expressing either a Dox-inducible mCherry or SMARCB1 transgenes. Moreover, although the gained peaks were localized more than 30kb from the TSS, we currently cannot be certain that they correspond to enhancers. Thus, on-going H3K27ac ChIP-seq in RMC-mCherry and RMC-SMARCB1 cells as well as functional enhancer assays will better characterize the properties of these elements and hence the role of SMARCB1 in regulating both enhancers and super-enhancers.

Despite agreeing on its role in regulating enhancers, aforementioned studies by Nakayama *et al.* and Wang *et al.* showed conflicting results on the role of SMARCB1 for SWI/SNF complex integrity. While the former concluded that SMARCB1 loss has no effect on SWI/SNF integrity, the latter showed that SMARCB1 was required for SWI/SNF integrity by co-immunoprecipitating different components of the complex, namely SMARCC1, SMARCA4 and ARID1A^{41,42}. Of note, both studies were performed with the same widely-used MRT cell line G401. Our results clearly favor a model where SMARCB1 is not only required for stabilizing the complex, but it also directly regulates several subunits, notably SMARCA2 and DPF3. This is important as SMARCA2 is the paralog of SMARCA4 and they compete for incorporation within SWI/SNF complexes. By clustering RMC biopsies by their expression of SWI/SNF subunits, we show that SMARCA2 is specifically lost in RMC. Further experiments are necessary to understand the role of SMARCA2 in RMC cells. First, additional ChIP-seq of SMARCA2 in RMC-mCherry and RMC-SMARCB1 cells will allow identify the extent of overlap of genome occupancy between SMARCA2- versus SMARCA4-containing complexes. As mentioned previously, MYC seems to first increase upon SMARCB1 expression. Perhaps this is due to a stabilizing effect of SMARCB1 on SMARCA4-containing complexes which could positively regulate MYC targets. At 48 hours, SMARCA2 is expressed through activation by SMARCB1, thus SMARCA2-containing

complexes may be responsible for MYC repression. Therefore, we have established cell lines stably expressing an inducible allele of SMARCA2 and further RNA-seq and functional analyses may decipher the precise contribution of SMARCA2 in the presence or absence of SMARCB1.

Our study identified TFCP2L1 as a novel direct target of SMARCB1 down-regulated in both RMC cohorts. TFCP2L1 is a member of the Grainyhead family of TFs previously reported to be required for kidney development and specification of collecting ducts and distal tubule cells in mice^{83,84,85}. Our scRNA-seq data clearly showed that TFCP2L1 activity is highest in TAL cells, the putative cell-of-origin of RMC, while it was undetectable in RMC cells. As mentioned above, SMARCB1 induced a retargeting of SWI/SNF complex to 7000 new sites for which the best enriched motif is that of TFCP2L1. Altogether, these data suggest that TFCP2L1 might contribute to SMARCB1 tumor-suppressor function perhaps by recruiting SWI/SNF to cell differentiation and adhesion genes. In the future, we will investigate its role by establishing stable RMC lines expressing inducible TFCP2L1 in order to identify its specific targets by RNA-seq and ChIP-seq. To demonstrate that the TF has an active role in recruiting SWI/SNF complexes, additional SMARCA4 or SMARCA2 ChIP-seq will be required in RMC cells re-expressing SMARCB1 but where TFCP2L1 expression has been silenced. Furthermore, given that TFCP2L1 has been reported to regulate pluripotency genes through recruitment of TET2⁹¹, on-going experiments are investigating the potential effects of SMARCB1 re-expression on DNA methylation in RMC cells. All these approaches will determine if TFCP2L1 loss is a key step in loss of epithelial identity and induction of EMT in RMC.

The data that we present here suggest a model (see Fig. 7) where in TAL cells, TFCP2L1 perhaps through direct interactions with SMARCB1 recruits SWI/SNF to activate genes conferring sensitivity to ferroptosis, TAL cell identity and associated cell adhesion and epithelial phenotype either directly and/or through the subordinate action of MITF, HOXB9 or other TFs. The presence of SMARCB1 in these cells also acts to antagonize any basal level of MYC activity. Upon SMARCB1 inactivation, TFCP2L1 expression is lost, and the residual SWI/SNF complex is hijacked by MYC to drive cell proliferation, EMT and resistance to ferroptosis, again either directly and/or in collaboration with HIF1A, NFE2L2 and other TFs. SMARCB1 re-expression antagonizes MYC blocking its activation of target genes and likely repressing expression of MYC itself through inhibition of a positive feedback

loop by which MYC activates and sustains its own expression. SMARCB1 reactivates TFCP2L1 by an as yet undefined mechanism the recruits SMARCB1-containing SWI/SNF to its target genes thereby re-establishing, at least in part, the TAL-identity program and sensitivity to ferroptosis. An interesting hypothesis is that, like MYC, TFCP2L1 activates and maintains its own expression by a positive SMARCB1-dependent manner account for the loss and gain of its expression upon SMARCB1 (in)activation. If this were the case a large part of the oncogenic mechanism may be based on the SMARCB1-modulated regulation of positive feedback loops of two master regulators TFCP2L1 and MYC. In the future, it will be interesting test this model by assessing the effect of MYC silencing or forced TFCP2L1 expression in RMC cells or forced MYC expression or TFCP2L1 silencing in the Dox-treated RMC cells.

Furthermore, our single-cell analysis revealed for the first time the intra-tumoral heterogeneity found in RMC. Our data suggest that transformation involves a loss activity of TAL-specific TFs and an acquisition of known EMT-TFs. It is important to note that this transition is rather progressive which results in two co-existing RMC subpopulations that we termed epithelial- and mesenchymal-like due to their preferential expression of EMT markers. Although our scRNA-seq represents only one case, we were able to show that our specific signatures were reproduced in patient cohorts *in vivo* and allowing their clustering in two groups that present distinct immune infiltration. SCENIC analysis of the macrophages revealed that their high activity of IRF7, a positive regulator of M2 polarization^{86,87,89}, suggesting that these macrophages displayed a immunosuppressive activity. As we observed higher immune infiltrates in biopsies that present mesenchymal-like RMC cells, it might be important to further investigate this question for prognosis. By their presence, mesenchymal-like tumor cells might either signal the recruitment of tumor-supportive M2 macrophages, or promote the conversion of tumoricidal M1 into pro-tumoral M2 macrophages. It will also be important to address the interplay between RMC and stromal cells, as these tumors are well known for their high desmoplasia. In our scRNA-seq, we found that cancer-associated fibroblasts had high p53 activity which was recently reported to promote lung tumor growth *in vivo* as well as cancer cell migration and invasion via the production of periostin and matrix metalloproteinases (MMPs)⁸⁹. Accordingly, periostin, decorin and MMP11 were among top

markers of CAF cells in our scRNA-seq data. Of note, RMC cells highly expressed SFRP2, CLDN1 and MMP7 which were all separately reported to drive metastatic progression and drug resistance^{90,92,93}.

Recently, multiplexed scRNA sequencing of 198 cell lines from 22 tumor types have highlighted the heterogeneous cellular states found within cell lines with at least two co-existing populations displaying distinct proliferation rates and drug sensitivity patterns⁹⁴. Given that RMC tumors seem to be heterogenous, it is possible that the patient-derived cellular models we use also display some degree of heterogeneity. By light microscopy, visible heterogeneity in cell morphologies can already be spotted in RMC219 cells; with at least two populations: one being flat and very adherent, another displaying a more round-shaped. Importantly, long-term culture of both RMC cell lines in presence of Dox led to the development of a resistant subpopulation which survived despite SMARCB1 expression. Therefore, FACS and scRNA-seq experiments would reveal if indeed RMC cell lines comprise populations of cells with distinct EMT phenotypes. One possible approach would be to stain the cells with distinct epithelial/mesenchymal markers in order to estimate the proportions of each subpopulations. Further FACS sorting of these two populations will allow Boyden chamber migration and invasion assays as well as ferroptosis experiments. It would be particularly pertinent to connect a given RMC phenotype with ferroptosis resistance. In melanoma, cells with mesenchymal-like phenotype display higher GPX4 levels and resistance to ferroptosis⁷². However, it is still unclear if this is also the case for RMC. In addition to these experiments, future directions should include the generation of patient-derived xenografts (PDX), which would constitute the ideal model for studying RMC heterogeneity.

Altogether, this study addressed the tumor-suppressor role of SMARCB1 in renal medullary carcinoma. By integrating *in vitro* and *in vivo* approaches, we shed light on two novel features of RMC tumors. First, we show that RMC tumors are heterogenous due to a gradual dedifferentiation from their cell-of-origin associated with partial EMT. We identified the putative cell-of-origin of RMC as being cells of Henle's ascending loop that display a high sensitivity to ferroptosis likely driven by a SWI/SNF-TFCP2L1 axis. Second, we also demonstrate that loss of SMARCB1 induces a transcriptional reprogramming resulting in loss of TFCP2L1, gain of MYC and the derepression of a GPX4-driven ferroptosis resistance program in RMC. Importantly, we show that the tumor-suppressor role of

SMARCB1 involves the induction of cell death by ferroptosis, a vulnerability that could be exploited therapeutically using GPX4 inhibitors.

References.

- 1 Davis CJ Jr, Mostofi FK, Sesterhenn IA. Renal medullary carcinoma. The seventh sickle cell nephropathy. *Am J Surg Pathol.* 1995 Jan;19(1):1-11. doi: 10.1097/0000478-199501000-00001. PMID: 7528470.
- 2 Cajaiba MM, Dyer LM, Geller JI, Jennings LJ, George D, Kirschmann D, Rohan SM, Cost NG, Khanna G, Mullen EA, Dome JS, Fernandez CV, Perlman EJ. The classification of pediatric and young adult renal cell carcinomas registered on the children's oncology group (COG) protocol AREN03B2 after focused genetic testing. *Cancer.* 2018 Aug;124(16):3381-3389. doi: 10.1002/ncr.31578. Epub 2018 Jun 15. PMID: 29905933; PMCID: PMC6108909.
- 3 Msaouel P, Carugo A, Genovese G. Targeting proteostasis and autophagy in SMARCB1-deficient malignancies: where next?. *Oncotarget.* 2019;10(40):3979-3981. Published 2019 Jun 18. doi:10.18632/oncotarget.26970
- 4 Alvarez O, Rodriguez MM, Jordan L, Sarnaik S. Renal medullary carcinoma and sickle cell trait: A systematic review. *Pediatr Blood Cancer.* 2015 Oct;62(10):1694-9. doi: 10.1002/pbc.25592. Epub 2015 Jun 5. PMID: 26053587.
- 5 Msaouel P, Hong AL, Mullen EA, Atkins MB, Walker CL, Lee CH, Carden MA, Genovese G, Linehan WM, Rao P, Merino MJ, Grodman H, Dome JS, Fernandez CV, Geller JI, Apolo AB, Daw NC, Hodges HC, Moxey-Mims M, Wei D, Bottaro DP, Staehler M, Karam JA, Rathmell WK, Tannir NM. Updated Recommendations on the Diagnosis, Management, and Clinical Trial Eligibility Criteria for Patients With Renal Medullary Carcinoma. *Clin Genitourin Cancer.* 2019 Feb;17(1):1-6. doi: 10.1016/j.clgc.2018.09.005. Epub 2018 Sep 12. PMID: 30287223; PMCID: PMC6348017.
- 6 Shah AY, Karam JA, Malouf GG, Rao P, Lim ZD, Jonasch E, Xiao L, Gao J, Vaishampayan UN, Heng DY, Plimack ER, Guancial EA, Fung C, Lowas SR, Tamboli P, Sircar K, Matin SF, Kimryn Rathmell W, Wood CG, Tannir NM. Management and outcomes of patients with renal medullary carcinoma: a multicentre collaborative study. *BJU Int.* 2017 Dec;120(6):782-792. doi: 10.1111/bju.13705. Epub 2016 Dec 9. PMID: 27860149; PMCID: PMC6857178.
- 7 Msaouel P, Malouf GG, Su X, Yao H, Tripathi DN, Soeung M, Gao J, Rao P, Coarfa C, Creighton CJ, Bertocchio JP, Kunnimalaiyaan S, Multani AS, Blando J, He R, Shapiro DD, Perelli L, Srinivasan S, Carbone F, Pilié PG, Karki M, Seervai RNH, Vokshi BH, Lopez-Terrada D, Cheng EH, Tang X, Lu W, Wistuba II, Thompson TC, Davidson I, Giuliani V, Schlacher K, Carugo A, Heffernan TP, Sharma P, Karam JA, Wood CG, Walker CL, Genovese G, Tannir NM. Comprehensive Molecular Characterization Identifies Distinct Genomic and Immune Hallmarks of Renal Medullary Carcinoma. *Cancer Cell.* 2020 May 11;37(5):720-734.e13. doi: 10.1016/j.ccell.2020.04.002. Epub 2020 Apr 30. PMID: 32359397; PMCID: PMC7288373.
- 8 Swartz MA, Karth J, Schneider DT, Rodriguez R, Beckwith JB, Perlman EJ. Renal medullary carcinoma: clinical, pathologic, immunohistochemical, and genetic analysis with pathogenetic implications. *Urology.* 2002 Dec;60(6):1083-9. doi: 10.1016/s0090-4295(02)02154-4. PMID: 12475675.
- 9 Rao P, Tannir NM, Tamboli P. Expression of OCT3/4 in renal medullary carcinoma represents a potential diagnostic pitfall. *Am J Surg Pathol.* 2012 Apr;36(4):583-8. doi: 10.1097/PAS.0b013e3182417d78. PMID: 22301499.
- 10 Gupta R, Billis A, Shah RB, Moch H, Osunkoya AO, Jochum W, Hes O, Bacchi CE, de Castro MG, Hansel DE, Zhou M, Vankalakunti M, Salles PG, Cabrera RA, Gown AM, Amin MB. Carcinoma of the collecting ducts of Bellini and renal medullary carcinoma: clinicopathologic analysis of 52 cases of rare

- aggressive subtypes of renal cell carcinoma with a focus on their interrelationship. *Am J Surg Pathol*. 2012 Sep;36(9):1265-78. doi: 10.1097/PAS.0b013e3182635954. PMID: 22895263.
- 11 Dimashkieh H, Choe J, Mutema G. Renal medullary carcinoma: a report of 2 cases and review of the literature. *Arch Pathol Lab Med*. 2003 Mar;127(3):e135-8. doi: 10.1043/0003-9985(2003)1272.0.CO;2. PMID: 12653601.
- 12 Elliott A, Bruner E. Renal Medullary Carcinoma. *Arch Pathol Lab Med*. 2019 Dec;143(12):1556-1561. doi: 10.5858/arpa.2017-0492-RS. Epub 2019 Mar 11. PMID: 30855171.
- 13 Kadoch C, Crabtree GR. Reversible disruption of mSWI/SNF (BAF) complexes by the SS18-SSX oncogenic fusion in synovial sarcoma. *Cell*. 2013 Mar 28;153(1):71-85. doi: 10.1016/j.cell.2013.02.036. PMID: 23540691; PMCID: PMC3655887.
- 14 Seo AN, Yoon G, Ro JY. Clinicopathologic and Molecular Pathology of Collecting Duct Carcinoma and Related Renal Cell Carcinomas. *Adv Anat Pathol*. 2017 Mar;24(2):65-77. doi: 10.1097/PAP.000000000000138. PMID: 28181950.
- 15 Nakayama RT, Pulice JL, Valencia AM, McBride MJ, McKenzie ZM, Gillespie MA, Ku WL, Teng M, Cui K, Williams RT, Cassel SH, Qing H, Widmer CJ, Demetri GD, Irizarry RA, Zhao K, Ranish JA, Kadoch C. SMARCB1 is required for widespread BAF complex-mediated activation of enhancers and bivalent promoters. *Nat Genet*. 2017 Nov;49(11):1613-1623. doi: 10.1038/ng.3958. Epub 2017 Sep 25. PMID: 28945250; PMCID: PMC5803080.
- 16 Nakayama RT, Pulice JL, Valencia AM, McBride MJ, McKenzie ZM, Gillespie MA, Ku WL, Teng M, Cui K, Williams RT, Cassel SH, Qing H, Widmer CJ, Demetri GD, Irizarry RA, Zhao K, Ranish JA, Kadoch C. SMARCB1 is required for widespread BAF complex-mediated activation of enhancers and bivalent promoters. *Nat Genet*. 2017 Nov;49(11):1613-1623. doi: 10.1038/ng.3958. Epub 2017 Sep 25. PMID: 28945250; PMCID: PMC5803080.
- 17 Versteeg I, Sévenet N, Lange J, Rousseau-Merck MF, Ambros P, Handgretinger R, Aurias A, Delattre O. Truncating mutations of hSNF5/INI1 in aggressive paediatric cancer. *Nature*. 1998 Jul 9;394(6689):203-6. doi: 10.1038/28212. PMID: 9671307.
- 18 Kalimuthu SN, Chetty R. Gene of the month: SMARCB1. *J Clin Pathol*. 2016;69(6):484-489. doi:10.1136/jclinpath-2016-203650
- 19 Betz BL, Strobeck MW, Reisman DN, Knudsen ES, Weissman BE. Re-expression of hSNF5/INI1/BAF47 in pediatric tumor cells leads to G1 arrest associated with induction of p16ink4a and activation of RB. *Oncogene*. 2002 Aug 8;21(34):5193-203. doi: 10.1038/sj.onc.1205706. PMID: 12149641.
- 20 Hong AL, Tseng YY, Wala JA, Kim WJ, Kynnap BD, Doshi MB, Kugener G, Sandoval GJ, Howard TP, Li J, Yang X, Tillgren M, Ghandi M, Sayeed A, Deasy R, Ward A, McSteen B, Labella KM, Keskula P, Tracy A, Connor C, Clinton CM, Church AJ, Crompton BD, Janeway KA, Van Hare B, Sandak D, Gjoerup O, Bandopadhyay P, Clemons PA, Schreiber SL, Root DE, Gokhale PC, Chi SN, Mullen EA, Roberts CW, Kadoch C, Beroukhi R, Ligon KL, Boehm JS, Hahn WC. Renal medullary carcinomas depend upon SMARCB1 loss and are sensitive to proteasome inhibition. *Elife*. 2019 Mar 12;8:e44161. doi: 10.7554/eLife.44161. PMID: 30860482; PMCID: PMC6436895.
- 21 Cheval L, Pierrat F, Rajerison R, Piquemal D, Doucet A. Of mice and men: divergence of gene expression patterns in kidney. *PLoS One*. 2012;7(10):e46876. doi: 10.1371/journal.pone.0046876. Epub 2012 Oct 3. PMID: 23056504; PMCID: PMC3463552.
- 22 Tirosh I, Izar B, Prakadan SM, Wadsworth MH 2nd, Treacy D, Trombetta JJ, Rotem A, Rodman C, Lian C, Murphy G, Fallahi-Sichani M, Dutton-Regester K, Lin JR, Cohen O, Shah P, Lu D, Genshaft AS, Hughes TK, Ziegler CG, Kazer SW, Gaillard A, Kolb KE, Villani AC, Johannessen CM, Andreev AY, Van Allen EM, Bertagnolli M, Sorger PK, Sullivan RJ, Flaherty KT, Frederick DT, Jané-Valbuena J, Yoon CH, Rozenblatt-Rosen O, Shalek AK, Regev A, Garraway LA. Dissecting the multicellular ecosystem of metastatic melanoma by single-cell RNA-seq. *Science*. 2016 Apr 8;352(6282):189-96. doi: 10.1126/science.aad0501. PMID: 27124452; PMCID: PMC4944528.

- 23 Lake BB, Chen S, Hoshi M, Plongthongkum N, Salamon D, Knoten A, Vijayan A, Venkatesh R, Kim EH, Gao D, Gaut J, Zhang K, Jain S. A single-nucleus RNA-sequencing pipeline to decipher the molecular anatomy and pathophysiology of human kidneys. *Nat Commun.* 2019 Jun 27;10(1):2832. doi: 10.1038/s41467-019-10861-2. PMID: 31249312; PMCID: PMC6597610.
- 24 Young MD, Mitchell TJ, Vieira Braga FA, Tran MGB, Stewart BJ, Ferdinand JR, Collord G, Botting RA, Popescu DM, Loudon KW, Vento-Tormo R, Stephenson E, Cagan A, Farndon SJ, Del Castillo Velasco-Herrera M, Guzzo C, Richoz N, Mamanova L, Aho T, Armitage JN, Riddick ACP, Mushtaq I, Farrell S, Rampling D, Nicholson J, Filby A, Burge J, Lisgo S, Maxwell PH, Lindsay S, Warren AY, Stewart GD, Sebire N, Coleman N, Haniffa M, Teichmann SA, Clatworthy M, Behjati S. Single-cell transcriptomes from human kidneys reveal the cellular identity of renal tumors. *Science.* 2018 Aug 10;361(6402):594-599. doi: 10.1126/science.aat1699. PMID: 30093597; PMCID: PMC6104812.
- 25 Sebastian A, Hum NR, Martin KA, et al. Single-Cell Transcriptomic Analysis of Tumor-Derived Fibroblasts and Normal Tissue-Resident Fibroblasts Reveals Fibroblast Heterogeneity in Breast Cancer. *Cancers (Basel).* 2020;12(5):1307. Published 2020 May 21. doi:10.3390/cancers12051307
- 26 Lin W, Noel P, Borazanci EH, Lee J, Amini A, Han IW, Heo JS, Jameson GS, Fraser C, Steinbach M, Woo Y, Fong Y, Cridebring D, Von Hoff DD, Park JO, Han H. Single-cell transcriptome analysis of tumor and stromal compartments of pancreatic ductal adenocarcinoma primary tumors and metastatic lesions. *Genome Med.* 2020 Sep 29;12(1):80. doi: 10.1186/s13073-020-00776-9. PMID: 32988401; PMCID: PMC7523332.
- 27 Aibar S, González-Blas CB, Moerman T, Huynh-Thu VA, Imrichova H, Hulselmans G, Rambow F, Marine JC, Geurts P, Aerts J, van den Oord J, Atak ZK, Wouters J, Aerts S. SCENIC: single-cell regulatory network inference and clustering. *Nat Methods.* 2017 Nov;14(11):1083-1086. doi: 10.1038/nmeth.4463. Epub 2017 Oct 9. PMID: 28991892; PMCID: PMC5937676.
- 28 Msaouel P, Tannir NM, Walker CL. A Model Linking Sick Cell Hemoglobinopathies and SMARCB1 Loss in Renal Medullary Carcinoma. *Clin Cancer Res.* 2018 May 1;24(9):2044-2049. doi: 10.1158/1078-0432.CCR-17-3296. Epub 2018 Feb 12. PMID: 29440190.
- 29 Hu J, Chen Z, Bao L, Zhou L, Hou Y, Liu L, Xiong M, Zhang Y, Wang B, Tao Z, Chen K. Single-Cell Transcriptome Analysis Reveals Intratumoral Heterogeneity in ccRCC, which Results in Different Clinical Outcomes. *Mol Ther.* 2020 Jul 8;28(7):1658-1672. doi: 10.1016/j.ymthe.2020.04.023. Epub 2020 Apr 29. PMID: 32396851; PMCID: PMC7335756.
- 30 Liu H, Liao Y, Tang M, Wu T, Tan D, Zhang S, Wang H. Trps1 is associated with the multidrug resistance of lung cancer cell by regulating MGMT gene expression. *Cancer Med.* 2018 May;7(5):1921-1932. doi: 10.1002/cam4.1421. Epub 2018 Mar 30. PMID: 29601666; PMCID: PMC5943538.
- 31 Hirpara J, Eu JQ, Tan JKM, Wong AL, Clement MV, Kong LR, Ohi N, Tsunoda T, Qu J, Goh BC, Pervaiz S. Metabolic reprogramming of oncogene-addicted cancer cells to OXPHOS as a mechanism of drug resistance. *Redox Biol.* 2019 Jul;25:101076. doi: 10.1016/j.redox.2018.101076. Epub 2018 Dec 17. PMID: 30642723; PMCID: PMC6859574.
- 32 Salunkhe S, Mishra SV, Ghorai A, Hole A, Chandrani P, Dutt A, Chilakapati M, Dutt S. Metabolic rewiring in drug resistant cells exhibit higher OXPHOS and fatty acids as preferred major source to cellular energetics. *Biochim Biophys Acta Bioenerg.* 2020 Dec 1;1861(12):148300. doi: 10.1016/j.bbabi.2020.148300. Epub 2020 Aug 25. PMID: 32858000.
- 33 Farrugia MK, Vanderbilt DB, Salkeni MA, Ruppert JM. Kruppel-like Pluripotency Factors as Modulators of Cancer Cell Therapeutic Responses. *Cancer Res.* 2016 Apr 1;76(7):1677-82. doi: 10.1158/0008-5472.CAN-15-1806. Epub 2016 Mar 10. PMID: 26964625; PMCID: PMC4873413.
- 34 Ma D, Chang LY, Zhao S, Zhao JJ, Xiong YJ, Cao FY, Yuan L, Zhang Q, Wang XY, Geng ML, Zheng HY, Li O. KLF5 promotes cervical cancer proliferation, migration and invasion in a manner partly dependent on TNFRSF11a expression. *Sci Rep.* 2017 Nov 16;7(1):15683. doi: 10.1038/s41598-017-15979-1. PMID: 29146991; PMCID: PMC5691198.
- 35 Ma Y, Wang Q, Liu F, Ma X, Wu L, Guo F, Zhao S, Huang F, Qin G. KLF5 promotes the

tumorigenesis and metastatic potential of thyroid cancer cells through the NF- κ B signaling pathway. *Oncol Rep.* 2018 Nov;40(5):2608-2618. doi: 10.3892/or.2018.6687. Epub 2018 Sep 6. PMID: 30226614; PMCID: PMC6151893.

36 Chang TP, Vancurova I. Bcl3 regulates pro-survival and pro-inflammatory gene expression in cutaneous T-cell lymphoma. *Biochim Biophys Acta.* 2014 Nov;1843(11):2620-30. doi: 10.1016/j.bbamcr.2014.07.012. Epub 2014 Jul 30. PMID: 25089799; PMCID: PMC4158825.

37 López R, Garrido E, Piña P, Hidalgo A, Lazos M, Ochoa R, Salcedo M. HOXB homeobox gene expression in cervical carcinoma. *Int J Gynecol Cancer.* 2006 Jan-Feb;16(1):329-35. doi: 10.1111/j.1525-1438.2006.00350.x. PMID: 16445654.

38 Wouters J, Stas M, Govaere O, Van den Eynde K, Vankelecom H, van den Oord JJ. Gene expression changes in melanoma metastases in response to high-dose chemotherapy during isolated limb perfusion. *Pigment Cell Melanoma Res.* 2012 Jul;25(4):454-65. doi: 10.1111/j.1755-148X.2012.01004.x. Epub 2012 May 3. PMID: 22486811.

39 Liu ZH, Dai XM, Du B. Hes1: a key role in stemness, metastasis and multidrug resistance. *Cancer Biol Ther.* 2015;16(3):353-9. doi: 10.1080/15384047.2015.1016662. PMID: 25781910; PMCID: PMC4622741.

40 Sharma D, Mirando AJ, Leinroth A, Long JT, Karner CM, Hilton MJ. HES1 is a Critical Mediator of the SHH-GLI3 Axis in Regulating Digit Number. *bioRxiv [Internet].* 2020 Jan 1;2020.06.17.158501. Available from: <http://biorxiv.org/content/early/2020/06/18/2020.06.17.158501.abstract>

41 Wang X, Lee RS, Alver BH, Haswell JR, Wang S, Mieczkowski J, Drier Y, Gillespie SM, Archer TC, Wu JN, Tzvetkov EP, Troisi EC, Pomeroy SL, Biegel JA, Tolstorukov MY, Bernstein BE, Park PJ, Roberts CW. SMARCB1-mediated SWI/SNF complex function is essential for enhancer regulation. *Nat Genet.* 2017 Feb;49(2):289-295. doi: 10.1038/ng.3746. Epub 2016 Dec 12. PMID: 27941797; PMCID: PMC5285474.

42 Nakayama RT, Pulice JL, Valencia AM, McBride MJ, McKenzie ZM, Gillespie MA, Ku WL, Teng M, Cui K, Williams RT, Cassel SH, Qing H, Widmer CJ, Demetri GD, Irizarry RA, Zhao K, Ranish JA, Kadoch C. SMARCB1 is required for widespread BAF complex-mediated activation of enhancers and bivalent promoters. *Nat Genet.* 2017 Nov;49(11):1613-1623. doi: 10.1038/ng.3958. Epub 2017 Sep 25. PMID: 28945250; PMCID: PMC5803080.

43 Hohmann AF, Vakoc CR. A rationale to target the SWI/SNF complex for cancer therapy. *Trends Genet.* 2014 Aug;30(8):356-63. doi: 10.1016/j.tig.2014.05.001. Epub 2014 Jun 3. PMID: 24932742; PMCID: PMC4112150.

44 Sen P, Luo J, Hada A, Hailu SG, Dechassa ML, Persinger J, Brahma S, Paul S, Ranish J, Bartholomew B. Loss of Snf5 Induces Formation of an Aberrant SWI/SNF Complex. *Cell Rep.* 2017 Feb 28;18(9):2135-2147. doi: 10.1016/j.celrep.2017.02.017. PMID: 28249160; PMCID: PMC5424545.

45 Johann PD, Erkek S, Zapatka M, Kerl K, Buchhalter I, Hovestadt V, Jones DTW, Sturm D, Hermann C, Segura Wang M, Korshunov A, Rhyzova M, Gröbner S, Brabetz S, Chavez L, Bens S, Gröschel S, Kratochwil F, Wittmann A, Sieber L, Geörg C, Wolf S, Beck K, Oyen F, Capper D, van Sluis P, Volckmann R, Koster J, Versteeg R, von Deimling A, Milde T, Witt O, Kulozik AE, Ebinger M, Shalaby T, Grotzer M, Sumerauer D, Zamecnik J, Mora J, Jabado N, Taylor MD, Huang A, Aronica E, Bertoni A, Radlwimmer B, Pietsch T, Schüller U, Schneppenheim R, Northcott PA, Korbel JO, Siebert R, Frühwald MC, Lichter P, Eils R, Gajjar A, Hasselblatt M, Pfister SM, Kool M. Atypical Teratoid/Rhabdoid Tumors Are Comprised of Three Epigenetic Subgroups with Distinct Enhancer Landscapes. *Cancer Cell.* 2016 Mar 14;29(3):379-393. doi: 10.1016/j.ccell.2016.02.001. Epub 2016 Feb 25. PMID: 26923874.

46 Muscarella AM, Dai W, Mitchell PG, Zhang W, Wang H, Jia L, Stossi F, Mancini MA, Chiu W, Zhang XH. Unique cellular protrusions mediate breast cancer cell migration by tethering to osteogenic cells. *NPJ Breast Cancer.* 2020 Sep 7;6:42. doi: 10.1038/s41523-020-00183-8. PMID: 32964116; PMCID: PMC7477119.

- 47 Yamaguchi H, Condeelis J. Regulation of the actin cytoskeleton in cancer cell migration and invasion. *Biochim Biophys Acta*. 2007 May;1773(5):642-52. doi: 10.1016/j.bbamcr.2006.07.001. Epub 2006 Jul 14. PMID: 16926057; PMCID: PMC4266238.
- 48 Fritzsche FR, Oelrich B, Johannsen M, Kristiansen I, Moch H, Jung K, Kristiansen G. Claudin-1 protein expression is a prognostic marker of patient survival in renal cell carcinomas. *Clin Cancer Res*. 2008 Nov 1;14(21):7035-42. doi: 10.1158/1078-0432.CCR-08-0855. PMID: 18981000.
- 49 Seibt TM, Proneth B, Conrad M. Role of GPX4 in ferroptosis and its pharmacological implication. *Free Radic Biol Med*. 2019 Mar;133:144-152. doi: 10.1016/j.freeradbiomed.2018.09.014. Epub 2018 Sep 13. PMID: 30219704.
- 50 Dai C, Chen X, Li J, Comish P, Kang R, Tang D. Transcription factors in ferroptotic cell death. *Cancer Gene Ther*. 2020 Sep;27(9):645-656. doi: 10.1038/s41417-020-0170-2. Epub 2020 Mar 3. PMID: 32123318.
- 51 Weissmiller AM, Wang J, Lorey SL, Howard GC, Martinez E, Liu Q, Tansey WP. Inhibition of MYC by the SMARCB1 tumor suppressor. *Nat Commun*. 2019 May 1;10(1):2014. doi: 10.1038/s41467-019-10022-5. PMID: 31043611; PMCID: PMC6494882.
- 52 Jiang Y, Mao C, Yang R, Yan B, Shi Y, Liu X, Lai W, Liu Y, Wang X, Xiao D, Zhou H, Cheng Y, Yu F, Cao Y, Liu S, Yan Q, Tao Y. EGLN1/c-Myc Induced Lymphoid-Specific Helicase Inhibits Ferroptosis through Lipid Metabolic Gene Expression Changes. *Theranostics*. 2017 Jul 23;7(13):3293-3305. doi: 10.7150/thno.19988. PMID: 28900510; PMCID: PMC5595132.
- 53 Li D, Li Y. The interaction between ferroptosis and lipid metabolism in cancer. *Signal Transduct Target Ther*. 2020 Jun 30;5(1):108. doi: 10.1038/s41392-020-00216-5. PMID: 32606298; PMCID: PMC7327075.
- 54 Cho KB, Cho MK, Lee WY, Kang KW. Overexpression of c-myc induces epithelial mesenchymal transition in mammary epithelial cells. *Cancer Lett*. 2010 Jul 28;293(2):230-9. doi: 10.1016/j.canlet.2010.01.013. Epub 2010 Feb 9. PMID: 20144848.
- 55 Wang XN, Su XX, Cheng SQ, Sun ZY, Huang ZS, Ou TM. MYC modulators in cancer: a patent review. *Expert Opin Ther Pat*. 2019 May;29(5):353-367. doi: 10.1080/13543776.2019.1612878. Epub 2019 May 8. PMID: 31068032.
- 56 Jia Y, Chng WJ, Zhou J. Super-enhancers: critical roles and therapeutic targets in hematologic malignancies. *J Hematol Oncol*. 2019 Jul 16;12(1):77. doi: 10.1186/s13045-019-0757-y. PMID: 31311566; PMCID: PMC6636097.
- 57 Hsieh JJ, Purdue MP, Signoretti S, Swanton C, Albiges L, Schmidinger M, Heng DY, Larkin J, Ficarra V. Renal cell carcinoma. *Nat Rev Dis Primers*. 2017 Mar 9;3:17009. doi: 10.1038/nrdp.2017.9. PMID: 28276433; PMCID: PMC5936048.
- 58 Jeon HM, Lee J. MET: roles in epithelial-mesenchymal transition and cancer stemness. *Ann Transl Med*. 2017 Jan;5(1):5. doi: 10.21037/atm.2016.12.67. PMID: 28164090; PMCID: PMC5253283.
- 59 Werth M, Schmidt-Ott KM, Leete T, Qiu A, Hinze C, Viltard M, Paragas N, Shawber CJ, Yu W, Lee P, Chen X, Sarkar A, Mu W, Rittenberg A, Lin CS, Kitajewski J, Al-Awqati Q, Barasch J. Transcription factor *TFCP2L1* patterns cells in the mouse kidney collecting ducts. *Elife*. 2017 Jun 3;6:e24265. doi: 10.7554/eLife.24265. PMID: 28577314; PMCID: PMC5484618.
- 60 Ráduly G, Pap Z, Dénes L, Szántó A, Sipos TC, Pávai Z. The immunoexpression of aquaporin 1, PAX2, PAX8, connexin 36, connexin 43 in human fetal kidney. *Rom J Morphol Embryol*. 2019;60(2):437-444. PMID: 31658316.
- 61 Saleem M, Hodgkinson CP, Xiao L, Gimenez-Bastida JA, Rasmussen ML, Foss J, Payne AJ, Mirotsoy M, Gama V, Dzau VJ, Gomez JA. Sox6 as a new modulator of renin expression in the kidney. *Am J Physiol Renal Physiol*. 2020 Feb 1;318(2):F285-F297. doi: 10.1152/ajprenal.00095.2019. Epub 2019 Nov 25. PMID: 31760770; PMCID: PMC7052657.

- 62 Evans RG, Smith DW, Lee CJ, Ngo JP, Gardiner BS. What Makes the Kidney Susceptible to Hypoxia? *Anat Rec (Hoboken)*. 2019 Sep 30. doi: 10.1002/ar.24260. Epub ahead of print. PMID: 31566903.
- 63 Noguchi CT, Gladwin M, Diwan B, Merciris P, Smith R, Yu X, Buzard G, Fitzhugh A, Keefer LK, Schechter AN, Mohandas N. Pathophysiology of a sickle cell trait mouse model: human alpha(beta)(S) transgenes with one mouse beta-globin allele. *Blood Cells Mol Dis*. 2001 Nov-Dec;27(6):971-7. doi: 10.1006/bcmd.2001.0469. PMID: 11831863.
- 64 Beuzard Y. Mouse models of sickle cell disease. *Transfus Clin Biol*. 2008 Feb-Mar;15(1-2):7-11. doi: 10.1016/j.tracli.2008.04.001. Epub 2008 May 27. PMID: 18502677.
- 65 Carugo A, Minelli R, Sapio L, Soeung M, Carbone F, Robinson FS, Tepper J, Chen Z, Lovisa S, Svelto M, Amin S, Srinivasan S, Del Poggetto E, Loponte S, Puca F, Dey P, Malouf GG, Su X, Li L, Lopez-Terrada D, Rakheja D, Lazar AJ, Netto GJ, Rao P, Sgambato A, Maitra A, Tripathi DN, Walker CL, Karam JA, Heffernan TP, Viale A, Roberts CWM, Msaouel P, Tannir NM, Draetta GF, Genovese G. p53 Is a Master Regulator of Proteostasis in SMARCB1-Deficient Malignant Rhabdoid Tumors. *Cancer Cell*. 2019 Feb 11;35(2):204-220.e9. doi: 10.1016/j.ccell.2019.01.006. PMID: 30753823.
- 66 Li J, Cao F, Yin HL, Huang ZJ, Lin ZT, Mao N, Sun B, Wang G. Ferroptosis: past, present and future. *Cell Death Dis*. 2020 Feb 3;11(2):88. doi: 10.1038/s41419-020-2298-2. PMID: 32015325; PMCID: PMC6997353.
- 67 Scindia PhD Y, Leeds Md J, Swaminathan Md S. Iron Homeostasis in Healthy Kidney and its Role in Acute Kidney Injury. *Semin Nephrol*. 2019 Jan;39(1):76-84. doi: 10.1016/j.semnephrol.2018.10.006. PMID: 30606409.
- 68 Wareing M, Ferguson CJ, Green R, Riccardi D, Smith CP. In vivo characterization of renal iron transport in the anaesthetized rat. *J Physiol*. 2000 Apr 15;524 Pt 2(Pt 2):581-6. doi: 10.1111/j.1469-7793.2000.00581.x. PMID: 10766935; PMCID: PMC2269874.
- 69 Linkermann A, Bräsen JH, Darding M, Jin MK, Sanz AB, Heller JO, De Zen F, Weinlich R, Ortiz A, Walczak H, Weinberg JM, Green DR, Kunzendorf U, Krautwald S. Two independent pathways of regulated necrosis mediate ischemia-reperfusion injury. *Proc Natl Acad Sci U S A*. 2013 Jul 16;110(29):12024-9. doi: 10.1073/pnas.1305538110. Epub 2013 Jul 1. PMID: 23818611; PMCID: PMC3718149.
- 70 Souma T, Suzuki N, Yamamoto M. Renal erythropoietin-producing cells in health and disease. *Front Physiol*. 2015 Jun 3;6:167. doi: 10.3389/fphys.2015.00167. PMID: 26089800; PMCID: PMC4452800.
- 71 Abdalkader M, Lampinen R, Kanninen KM, Malm TM, Liddell JR. Targeting Nrf2 to Suppress Ferroptosis and Mitochondrial Dysfunction in Neurodegeneration. *Front Neurosci*. 2018 Jul 10;12:466. doi: 10.3389/fnins.2018.00466. PMID: 30042655; PMCID: PMC6048292.
- 72 Tsoi J, Robert L, Paraiso K, Galvan C, Sheu KM, Lay J, Wong DJL, Atefi M, Shirazi R, Wang X, Braas D, Grasso CS, Palaskas N, Ribas A, Graeber TG. Multi-stage Differentiation Defines Melanoma Subtypes with Differential Vulnerability to Drug-Induced Iron-Dependent Oxidative Stress. *Cancer Cell*. 2018 May 14;33(5):890-904.e5. doi: 10.1016/j.ccell.2018.03.017. Epub 2018 Apr 12. PMID: 29657129; PMCID: PMC5953834.
- 73 Phelep A, Laouari D, Bharti K, Burtin M, Tammaccaro S, Garbay S, Nguyen C, Vasseur F, Blanc T, Berissi S, Langa-Vives F, Fischer E, Druilhe A, Arnheiter H, Friedlander G, Pontoglio M, Terzi F. MITF - A controls branching morphogenesis and nephron endowment. *PLoS Genet*. 2017 Dec 14;13(12):e1007093. doi: 10.1371/journal.pgen.1007093. PMID: 29240767; PMCID: PMC5746285.
- 74 Argani P. MiT family translocation renal cell carcinoma. *Semin Diagn Pathol*. 2015 Mar;32(2):103-13. doi: 10.1053/j.semdp.2015.02.003. Epub 2015 Feb 4. PMID: 25758327.
- 75 Bertolotto C, Lesueur F, Giuliano S, Strub T, de Lichy M, Bille K, Dessen P, d'Hayer B, Mohamdi H, Remenieras A, Maubec E, de la Fouchardière A, Molinié V, Vabres P, Dalle S, Poulalhon N, Martin-Denavit T, Thomas L, Andry-Benzaquen P, Dupin N, Boitier F, Rossi A, Perrot JL, Labeille B, Robert

- C, Escudier B, Caron O, Brugières L, Saule S, Gardie B, Gad S, Richard S, Couturier J, Teh BT, Ghiorzo P, Pastorino L, Puig S, Badenas C, Olsson H, Ingvar C, Rouleau E, Lidereau R, Bahadoran P, Vielh P, Corda E, Blanché H, Zelenika D, Galan P; French Familial Melanoma Study Group, Aubin F, Bachollet B, Becuwe C, Berthet P, Bignon YJ, Bonadona V, Bonafe JL, Bonnet-Dupeyron MN, Cambazard F, Chevrant-Breton J, Coupier I, Dalac S, Demange L, d'Incan M, Dugast C, Faivre L, Vincent-Fétita L, Gauthier-Villars M, Gilbert B, Grange F, Grob JJ, Humbert P, Janin N, Joly P, Kerob D, Lasset C, Leroux D, Levang J, Limacher JM, Livideanu C, Longy M, Lortholary A, Stoppa-Lyonnet D, Mansard S, Mansuy L, Marrou K, Matéus C, Maugard C, Meyer N, Nogues C, Souteyrand P, Venat-Bouvet L, Zattara H, Chaudru V, Lenoir GM, Lathrop M, Davidson I, Avril MF, Demenais F, Ballotti R, Bressac-de Paillerets B. A SUMOylation-defective MITF germline mutation predisposes to melanoma and renal carcinoma. *Nature*. 2011 Oct 19;480(7375):94-8. doi: 10.1038/nature10539. Erratum in: *Nature*. 2016 Mar 3;531(7592):126. PMID: 22012259.
- 76 Klöditz K, Fadeel B. Three cell deaths and a funeral: macrophage clearance of cells undergoing distinct modes of cell death. *Cell Death Discov*. 2019 Feb 8;5:65. doi: 10.1038/s41420-019-0146-x. PMID: 30774993; PMCID: PMC6368547.
- 77 Dixon SJ, Lemberg KM, Lamprecht MR, Skouta R, Zaitsev EM, Gleason CE, Patel DN, Bauer AJ, Cantley AM, Yang WS, Morrison B 3rd, Stockwell BR. Ferroptosis: an iron-dependent form of nonapoptotic cell death. *Cell*. 2012 May 25;149(5):1060-72. doi: 10.1016/j.cell.2012.03.042. PMID: 22632970; PMCID: PMC3367386.
- 78 Yang WS, SriRamaratnam R, Welsch ME, Shimada K, Skouta R, Viswanathan VS, Cheah JH, Clemons PA, Shamji AF, Clish CB, Brown LM, Girotti AW, Cornish VW, Schreiber SL, Stockwell BR. Regulation of ferroptotic cancer cell death by GPX4. *Cell*. 2014 Jan 16;156(1-2):317-331. doi: 10.1016/j.cell.2013.12.010. PMID: 24439385; PMCID: PMC4076414.
- 79 O'Donnell KA, Yu D, Zeller KI, Kim JW, Racke F, Thomas-Tikhonenko A, Dang CV. Activation of transferrin receptor 1 by c-Myc enhances cellular proliferation and tumorigenesis. *Mol Cell Biol*. 2006 Mar;26(6):2373-86. doi: 10.1128/MCB.26.6.2373-2386.2006. PMID: 16508012; PMCID: PMC1430295.
- 80 Stojanova A, Tu WB, Ponzielli R, Kotlyar M, Chan PK, Boutros PC, Khosravi F, Jurisica I, Raught B, Penn LZ. MYC interaction with the tumor suppressive SWI/SNF complex member INI1 regulates transcription and cellular transformation. *Cell Cycle*. 2016 Jul 2;15(13):1693-705. doi: 10.1080/15384101.2016.1146836. Epub 2016 Jun 7. PMID: 27267444; PMCID: PMC4957596.
- 81 Willis MS, Holley DW, Wang Z, Chen X, Quintana M, Jensen BC, Tannu M, Parker J, Jeyaraj D, Jain MK, Wolfram JA, Lee HG, Bultman SJ. BRG1 and BRM function antagonistically with c-MYC in adult cardiomyocytes to regulate conduction and contractility. *J Mol Cell Cardiol*. 2017 Apr;105:99-109. doi: 10.1016/j.yjmcc.2017.02.003. Epub 2017 Feb 21. PMID: 28232072; PMCID: PMC5415084.
- 82 Langer LF, Ward JM, Archer TK. Tumor suppressor SMARCB1 suppresses super-enhancers to govern hESC lineage determination. *Elife*. 2019 Apr 29;8:e45672. doi: 10.7554/eLife.45672. PMID: 31033435; PMCID: PMC6538374.
- 83 Klämbt V, Werth M, Onuchic-Whitford AC, Getwan M, Kitzler TM, Buerger F, Mao Y, Deutsch K, Mann N, Majmundar AJ, Kaminski MM, Shen T, Schmidt-Ott KM, Shalaby M, El Desoky S, Kari JA, Shril S, Lienkamp SS, Barasch J, Hildebrandt F. Mutations in transcription factor CP2-like 1 may cause a novel syndrome with distal renal tubulopathy in humans. *Nephrol Dial Transplant*. 2020 Oct 23:gfaa215. doi: 10.1093/ndt/gfaa215. Epub ahead of print. PMID: 33097957.
- 84 Aguilar A. Development: Tfcpl21 drives Notch signalling and epithelial diversity in the collecting duct. *Nat Rev Nephrol*. 2017 Aug;13(8):445. doi: 10.1038/nrneph.2017.93. Epub 2017 Jun 19. PMID: 28626223.
- 85 Werth M, Schmidt-Ott KM, Leete T, Qiu A, Hinze C, Viltard M, Paragas N, Shawber CJ, Yu W, Lee P, Chen X, Sarkar A, Mu W, Rittenberg A, Lin CS, Kitajewski J, Al-Awqati Q, Barasch J. Transcription factor *TFCPL2L1* patterns cells in the mouse kidney collecting ducts. *Elife*. 2017 Jun 3;6:e24265. doi: 10.7554/eLife.24265. PMID: 28577314; PMCID: PMC5484618.

- 86 Hagemeyer N, Prinz M. Burning down the house: IRF7 makes the difference for microglia. *EMBO J.* 2014 Dec 17;33(24):2885-6. doi: 10.15252/embj.201490345. Epub 2014 Nov 13. PMID: 25394636; PMCID: PMC4282636.
- 87 Cohen M, Matcovitch O, David E, Barnett-Itzhaki Z, Keren-Shaul H, Blecher-Gonen R, Jaitin DA, Sica A, Amit I, Schwartz M. Chronic exposure to TGF β 1 regulates myeloid cell inflammatory response in an IRF7-dependent manner. *EMBO J.* 2014 Dec 17;33(24):2906-21. doi: 10.15252/embj.201489293. Epub 2014 Nov 10. PMID: 25385836; PMCID: PMC4282639.
- 88 Huang B, Han W, Sheng ZF, Shen GL. Identification of immune-related biomarkers associated with tumorigenesis and prognosis in cutaneous melanoma patients. *Cancer Cell Int.* 2020 May 25;20:195. doi: 10.1186/s12935-020-01271-2. PMID: 32508531; PMCID: PMC7249670.
- 89 Arandkar S, Furth N, Elisha Y, Nataraj NB, van der Kuip H, Yarden Y, Aulitzky W, Ulitsky I, Geiger B, Oren M. Altered p53 functionality in cancer-associated fibroblasts contributes to their cancer-supporting features. *Proc Natl Acad Sci U S A.* 2018 Jun 19;115(25):6410-6415. doi: 10.1073/pnas.1719076115. Epub 2018 Jun 4. PMID: 29866855; PMCID: PMC6016816.
- 90 Kaur A, Webster MR, Marchbank K, Behera R, Ndoye A, Kugel CH 3rd, Dang VM, Appleton J, O'Connell MP, Cheng P, Valiga AA, Morissette R, McDonnell NB, Ferrucci L, Kossenkov AV, Meeth K, Tang HY, Yin X, Wood WH 3rd, Lehrmann E, Becker KG, Flaherty KT, Frederick DT, Wargo JA, Cooper ZA, Tetzlaff MT, Hudgens C, Aird KM, Zhang R, Xu X, Liu Q, Bartlett E, Karakousis G, Eroglu Z, Lo RS, Chan M, Menzies AM, Long GV, Johnson DB, Sosman J, Schilling B, Schadendorf D, Speicher DW, Bosenberg M, Ribas A, Weeraratna AT. sFRP2 in the aged microenvironment drives melanoma metastasis and therapy resistance. *Nature.* 2016 Apr 14;532(7598):250-4. doi: 10.1038/nature17392. Epub 2016 Apr 4. PMID: 27042933; PMCID: PMC4833579.
- 91 Sardina JL, Collombet S, Tian TV, Gómez A, Di Stefano B, Berenguer C, Brumbaugh J, Stadhouders R, Segura-Morales C, Gut M, Gut IG, Heath S, Aranda S, Di Croce L, Hochedlinger K, Thieffry D, Graf T. Transcription Factors Drive Tet2-Mediated Enhancer Demethylation to Reprogram Cell Fate. *Cell Stem Cell.* 2018 Dec 6;23(6):905-906. doi: 10.1016/j.stem.2018.11.001. Erratum for: *Cell Stem Cell.* 2018 Nov 1;23(5):727-741.e9. PMID: 30526885; PMCID: PMC6292969.
- 92 Zhang WN, Li W, Wang XL, Hu Z, Zhu D, Ding WC, Liu D, Li KZ, Ma D, Wang H. CLDN1 expression in cervical cancer cells is related to tumor invasion and metastasis. *Oncotarget.* 2016 Dec 27;7(52):87449-87461. doi: 10.18632/oncotarget.13871. PMID: 27974683; PMCID: PMC5350000.
- 93 Niu J, Li XM, Wang X, Liang C, Zhang YD, Li HY, Liu FY, Sun H, Xie SQ, Fang D. DKK1 inhibits breast cancer cell migration and invasion through suppression of β -catenin/MMP7 signaling pathway. *Cancer Cell Int.* 2019 Jun 24;19:168. doi: 10.1186/s12935-019-0883-1. PMID: 31285694; PMCID: PMC6591985.
- 94 Kinker GS, Greenwald AC, Tal R, Orlova Z, Cuoco MS, McFarland JM, Warren A, Rodman C, Roth JA, Bender SA, Kumar B, Rocco JW, Fernandes PACM, Mader CC, Keren-Shaul H, Plotnikov A, Barr H, Tsherniak A, Rozenblatt-Rosen O, Krizhanovsky V, Puram SV, Regev A, Tirosh I. Pan-cancer single-cell RNA-seq identifies recurring programs of cellular heterogeneity. *Nat Genet.* 2020 Nov;52(11):1208-1218. doi: 10.1038/s41588-020-00726-6. Epub 2020 Oct 30. PMID: 33128048.

Material and methods.

Origin of patient sample and ethical committee approval

These samples were collected as part of the UNICELL protocol, study approved by the local ethics committee at the University Hospital of Strasbourg. The patient signed an informed consent.

Single-cell sample preparation and RNA-seq

Following resection, samples from the tumor and adjacent non-malignant tissue were each conserved at 4°C in 1mL of MACS Tissue Storage Solution (Miltenyi Biotech). Single cell suspensions were prepared using gentleMACS™ dissociator and human tumor kit dissociation (Miltenyi Biotech) following kit instructions. Briefly, samples were rinsed with PBS, transferred to C tubes (Miltenyi Biotech) containing 4,7mL pre-warmed DMEM and minced to pieces of <math><5\text{mm}^3</math>. 200μL enzyme H, 100μL enzyme R and 25μL enzyme A were added to each C tubes, tubes were loaded on the dissociator and program h_tumor_01 was run. C tubes were detached and incubated for 30 minutes at 120rpm, 37°C. Tubes were loaded again on the dissociator, program h_tumor_02 was run and tubes were incubated for another 30 minutes. Finally, the program h_tumor_03 was run. Samples were applied to a MACS SmartStrainer 70μm (Miltenyi Biotech) placed on a 15mL Falcon tube and 10mL DMEM were used to wash C tube and SmartStrainer. Following centrifugation at 300g and 4°C for 10min, cells were sorted using CD45 (TIL) Microbeads (Miltenyi Biotech). Cells were resuspended in 80μL of buffer (PBS (pH7.2), 0,5% BSA, 2mmM EDTA) and 20μL CD45 (TIL) microbeads per 10^7 cells and incubated for 15 minutes at 4°C. Buffer was added to a final volume of 500μL for up to $5 \cdot 10^7$ cells and cell suspension was applied to prepared LS column placed in magnetic field. The column was washed twice with 1mL of buffer and unlabelled cells were collected on ice (CD45- fraction). The column was removed from the separator and placed on a Falcon15 tube in ice. 3mL of buffer were pipetted onto the column and magnetically labelled cells were immediately flushed out using a plunger into the column (CD45+ fraction). All fractions were centrifuged (300g, 10min, 4°C) and dead cells were removed using Dead cell removal kit (Miltenyi Biotech). Briefly, cells were resuspended in dead cell removal microbeads, incubated for 15 minutes at room temperature and applied to a prepared LS column placed in separator in magnetic field. Column was rinsed with binding buffer and unlabelled cells were

collected in ice as live cell fraction. CD45⁻ and CD45⁺ were mixed in 1 to 4 ratio. Cell viability and concentration were assessed mixing cells with trypan blue (1:1 ratio) and using a Malassez counting chamber. 3'-mRNA single-cell libraries were prepared using the Chromium (10x Genomics) following the instructions. Libraries were sequenced 2x100bp on HiSeq4000 sequencer.

Single cell RNA-seq analysis

After sequencing, raw reads were processed using Cell Ranger (v 3.1) to align on the hg19 human genome, remove unexpressed genes and quantify barcodes and UMIs. Data were then analyzed in R (v4.0.2). Tumor and NAT samples were aggregated with the cellranger 'aggr' command. The resulting aggregation was analyzed with Seurat v3.2.0 following the recommended workflow. Cells were filtered for feature count ranging from 120 to 2000 and percentage of mitochondrial reads <15%. Counts were normalized with the "LogNormalize" method and data scaled to remove unwanted sources of variation (UMI count and mitochondrial reads). The number of principal components to use was determined from the Jackstraw plots. Clustering was performed on variable features using the 25 most significant principal components and a resolution of 1.15. Regulome analyses of active transcription factors were performed using the SCENIC v1.1.2.2 package. Transcription factor activities were visualized on the UMAP using AUCell or as heatmaps using the R-package pheatmap. Trajectory on the UMAP projection was resolved by monocle3 v0.2.0. Correlation of the RMC gene signature with the different renal tubule clusters was computed by clustifyr v1.0.0. TAL to RMC differentiation trajectory was plotted and visualized using Similarity Weighted Nonnegative Embedding.

Cell culture, establishment of RMC lines stably expressing SMARCB1

RMC219 cells were grown in HAM-F12/D-MEM (1:1) medium supplemented with 10% foetal calf serum (FCS) and AANE. RMC-2C cells were grown in MEM medium with 10% FCS, AANE and 50ng/mL EGF. RMC cells infected with lentiviral constructs were grown in respective media with G418 (300ug/mL). When inducing the lentiviral construct, stable cell lines were treated with either DMSO or 2uM of doxycycline.

Lentiviral vectors pInducer20 were obtained from Addgene and the cDNA of either SMARCB1 or mCherry was cloned into the vector by Gateway. We then used pInducer20-mCherry or -SMARCB1

containing lentiviruses and infected 1×10^6 RMC2C or RMC219 cells. Cells were selected using 500ug/mL G418 for a week.

For the ferroptosis experiments, cells were either treated with DMSO or 2uM doxycycline alone or co-treated with 2uM doxycycline and 1uM ferrostatin-1 for at least 48hrs before functional assays. For the Caspase-3 assay, cells were either treated with camptothecin 5uM for 4hr, DMSO or 2uM doxycycline for at least 24hrs before functional assays.

Cell viability, caspase-3 and lipid peroxidation analyses by flow cytometry

To assess cell death, cells were harvested 72 hours after siRNA transfection and co-stained with Annexin-V (Biolegend) and propidium iodide following manufacturer instructions for FACS analysis. To assess active Caspase-3, cells were fixed and permeabilized before incubation with the FITC-conjugated caspase-3 antibody following manufacturer instructions for subsequent FACS analysis. To assess membrane lipid peroxidation, cells were stained using Bodipy 581/591 C11 (ThermoFisher) following manufacturer instructions for subsequent FACS analysis. To assess senescence, cells were treated with 100nM bafilomycin A1 for 1hr followed by 2mM C12FDG (Invitrogen) for 2hr before being washed and harvested for FACS analyses. All functional assays were analysed on a LSRII Fortessa (BD Biosciences) and data were analysed using Flowjo v6.8.

RNA preparation and quantitative PCR

RNA isolation was performed according to standard procedure (Qiagen kit). qRT-PCR was carried out with SYBR Green I (Roche) and SuperScript IV Reverse Transcriptase (Invitrogen) and monitored using a LightCycler 480 (Roche). The mean of ACTB, TBP, RPL13A and GAPDH gene expressions was used to normalize the results. Primer sequences for each cDNA were designed using Primer3 Software and are available upon request.

Bulk RNA-seq analysis

For cell lines, after sequencing raw reads were preprocessed in order to remove adapter and low-quality sequences (Phred quality score below 20). After this preprocessing, reads shorter than 40 bases were discarded for further analysis. These preprocessing steps were performed using cutadapt version 1.10.

Reads were mapped to rRNA sequences using bowtie version 2.2.8, and reads mapping to rRNA sequences were removed for further analysis. Reads were mapped onto the hg19 assembly of Homo sapiens genome using STAR version 2.5.3a. Gene expression quantification was performed from uniquely aligned reads using htseq-count version 0.6.1p1, with annotations from Ensembl version 75 and “union” mode. Only non-ambiguously assigned reads have been retained for further analyses. Read counts have been normalized across samples with the median-of-ratios method proposed by Anders and Huber (2010), to make these counts comparable between samples. Comparisons of interest were performed using the Wald test for differential expression proposed by Love et al. and implemented in the Bioconductor package DESeq2 version 1.16.1. Genes with high Cook’s distance were filtered out and independent filtering based on the mean of normalized counts was performed. P-values were adjusted for multiple testing using the Benjamini and Hochberg method. Deregulated genes were defined as genes with $\log_2(\text{foldchange}) > 1$ or < -1 and adjusted p-value < 0.05 . Heatmaps were generated with R-package pheatmap v1.0.12 and volcano plots with ggplot2 v3.3.2. Gene set enrichment analyses were done with the GSEA software v3.0 using the hallmark gene sets of Molecular Signature Database v6.2 and the functional annotation clustering function of DAVID (<http://david.abcc.ncifcrf.gov/>). Gene list intersections and Venn diagrams were performed by Venny.

For RMC cohorts, data were retrieved in excel format with already normalized TPM counts and analyzed in R. RMC heterogeneity was inferred using the geometric mean expression of RMC0 and RMC1 signature genes determined from single-cell data. Samples were clustered using an unsupervised clustering with “ward.D2” linkage function from hclust and visualized as heatmaps using pheatmap package v1.0.12. The tumor micro-environment composition of each sample was assessed using MCP-counter v1.2.0 and CIBERSORT with the LM22 gene matrix for immune cells. The sample compositions were inferred from our in-house single-cell signatures using CIBERSORTx.

Protein extraction and Western blotting

Whole cell extracts were prepared by the standard freeze-thaw technique using LSDB 500 buffer (500 mM KCl, 25 mM Tris at pH 7.9, 10% glycerol (v/v), 0.05% NP-40 (v/v), 16mM DTT, and protease inhibitor cocktail). Cell lysates were subjected to SDS–polyacrylamide gel electrophoresis (SDS-PAGE)

and proteins were transferred onto a nitrocellulose membrane. Membranes were incubated with primary antibodies in 5% dry fat milk and 0.01% Tween-20 overnight at 4 °C. The membrane was then incubated with HRP-conjugated secondary antibody (Jackson ImmunoResearch) for 1h at room temperature, and visualized using the ECL detection system (GE Healthcare). Antibodies: SMARCB1 (91735, Cell signaling), SMARCA4 (ab110641, Abcam), SMARCA2 (11966, Cell signaling), SMARCC1 (A301-038A, Bethyl laboratories), SMARCC2 (sc-10756, Santa Cruz), SMARCD1 (611728, BD Transduction Labs), SMARCD2 (ab166622, Abcam), SMARCD3 (622665, CST), SMARCE1 (), BAF53A (ab131272; abcam), ACTB (2D7, IGBMC), BCL7A (PA5-27123, Invitrogen), BCL7B (sc-134278), ARID1A (12354, CST), ARID1B (92964, CST), PBRM1 (ABE70, Merck), ARID2 (ab166850, Abcam), BRD7 (ab56036, Abcam), DPF1 (PA5-61895, ThermoFisher), DPF2 (ab134942, Abcam), DPF3 (PA5-38011, ThermoFisher), VCL (V4505, Sigma-Aldrich), VIM (5741, CST), FN1 (F3648, Sigma Aldrich), CDH1 (3195, CST), MYC (sc-40, SCT), NFE2L2 (ab62352, Abcam), GPX4 (MAB5457-SP, R&D Bio-Techne), ASCL4 (PA5-89830, ThermoFisher), HA (H6908, Sigma Aldrich), MITF (MS-771-P, Interchim), TFCP2L1 (HPA029708, Sigma Aldrich), SLUG (9585, CST), ZEB1 (3396, CST), CLDN1 (13255, CST).

Immunoprecipitation

Whole cell extracts were prepared by the standard freeze-thaw technique using LSDB 500 buffer (500 mM KCl, 25 mM Tris at pH 7.9, 10% glycerol (v/v), 0.05% NP-40 (v/v), 16mM DTT, and protease inhibitor cocktail). Up to 1mg of whole cell extracts were diluted in LSDB without KCl to a final concentration of 150mM KCl and incubated overnight with 5ug of specific antibodies. The next day, 50ul of washed magnetic protein-A/G beads (Dynabeads, Invitrogen) were added to the extracts for 2hr. Beads were washed 3 times in LSDB 300mM KCl, twice in LSDB 150mM and immunoprecipitates were eluted in 100ul of 0.1M glycine pH 2.8 at room temperature for 15min, before addition of 10ul of Tris-HCl pH 8. For SDS-PAGE analysis, 10 to 15ul of eluted proteins were boiled in equal amount of Laemmli buffer before being loaded on the gels. Antibodies : BRG1 (ab110641, Abcam), rabbit IgG (ab171870, Abcam).

Chromatin immunoprecipitation and sequencing

BRG1 ChIP experiments were performed on native MNase-digested chromatin. 10×10^7 to 20×10^8 freshly harvested RMC2C-SMARCB1 cells treated with either DMSO or 2 μ M doxycycline for 72hrs were resuspended in 1.5 ml ice-cold hypotonic buffer (0.3M Sucrose, 60 mM KCl, 15 mM NaCl, 5 mM MgCl₂, 0.1 mM EDTA, 15 mM Tris-HCl pH 7.5, 0.5 mM DTT, 0.1 mM PMSF, PIC) and cytoplasmic fraction was released by incubation with 1.5 ml of lysis-buffer (0.3M sucrose, 60 mM KCl, 15 mM NaCl, 5 mM MgCl₂, 0.1 mM EDTA, 15 mM Tris-HCl pH 7.5, 0.5 mM DTT, 0.1 mM PMSF, PIC, 0.5% (vol/vol) IGEPAL CA-630) for 10 min on ice. The suspension was layered onto a sucrose cushion (1.2 M sucrose, 60 mM KCl, 15 mM NaCl, 5 mM MgCl₂, 0.1 mM EDTA, 15 mM Tris-HCl [pH 7.5], 0.5 mM DTT, 0.1 mM PMSF, PIC) and centrifuged for 30 min 4°C at 4700 rpm in a swing rotor. The nuclear pellet was resuspended in digestion buffer (0.32M sucrose, 50 mM Tris-HCl [pH 7.5], 4 mM MgCl₂, 1 mM CaCl₂, 0.1 mM PMSF) and incubated with 10 μ l of Micrococcal Nuclease (NEB) for 7 min at 37°C. The reaction was stopped by addition of 20 μ l of EDTA 0.5M and suspension chilled on ice for 10 min. The suspension was cleared by centrifugation at 10,000 rpm (4°C) for 10 min and supernatant (chromatin) was used for further purposes. Chromatin was digested to around 80% of mono-nucleosomes as judged by extraction of the DNA and agarose gel electrophoresis. H3K27ac, MYC and MAX ChIP experiments were performed on 0.4% PFA-fixed chromatin isolated from RMC2C-SMARCB1 cells treated with either DMSO or 2 μ M doxycycline for 72hrs according to standard protocols as previously described (Strub et al., 2011). ChIP-seq libraries were prepared using MicroPlex Library Preparation kit v2 and sequenced on the Illumina Hi-seq 4000 as single-end 50-base reads (Herquel et al., 2013). Sequenced reads were mapped to the Homo sapiens genome assembly hg19 using Bowtie with the following arguments: -m 1 --strata --best -y -S -l 40 -p 2. After sequencing, peak detection was performed using the MACS software ([Zhang et al., 2008] <http://liulab.dfci.harvard.edu/MACS/>). Peaks were annotated with Homer (<http://homer.salk.edu/homer/ngs/annotation.html>) using the GTF from ENSEMBL v75. Global clustering analysis and quantitative comparisons were performed using seqMINER ([Ye et al., 2011] <http://bips.u-strasbg.fr/seqminer/>) and R (<http://www.r-project.org/>).

Motif analysis

De novo motif discovery on FASTA sequences corresponding to windowed peaks was performed using MEME suite (meme-suite.org). Motif correlation matrix was calculated with in-house algorithms using JASPAR database as described in Joshi et al., 2017.

Motif analysis Searching of known TF motifs from the Jaspas 2014 motif database at BRG1-bound sites was made using FIMO (Grant et al., 2011) within regions of 200 bp around peak summits, FIMO results were then processed by a custom Perl script which computed the frequency of occurrence of each motif. To assess the enrichment of motifs within the regions of interest, the same analysis was done 100 times on randomly selected regions of the same length as the BRG1 bound regions and the results used to compute an expected distribution of motif occurrence. The significance of the motif occurrence at the BRG1-occupied regions was estimated through the computation of a Z-score (z) with $z = (x - \mu)/\sigma$, where: x is the observed value (number of motif occurrence), μ is the mean of the number of occurrences (computed on randomly selected data), σ is the standard deviation of the number of occurrences of motifs (computed on randomly selected data). The source code is accessible at <https://github.com/slegras/motif-search-significance.git>.

Immunostaining

Cells were seeded at a density of 5×10^5 on 4-well chamber slides (Lab-Tek, ThermoFisher) and treated with either DMSO or 2 μ M doxycycline. 72hr post-treatment, cells were first fixed in 4% PFA for 10min and then permeabilised with 3×5 min 0.1% Triton in PBS, blocked for 1 hr in 5% skim milk in PBS, and incubated overnight in 5% milk with primary antibodies. The following antibodies were used: BRG1 (ab110641, Abcam), BRM (11966, Cell signaling), BAF47 (91735, Cell signaling), DPF3 (PA5-31963, ThermoFisher) and ACTB (2D7, IGBMC). Then, cells were washed 3×5 min 0.1% Triton in PBS, and incubated with secondary antibodies, Cy3 mouse-anti-rabbit, and Cy5 rabbit-anti-mouse (Invitrogen) for 2 hrs. Cells were subsequently incubated with 1/2000 DAPI nuclear stain for 10 min, washed 3×5 min in PBS, dried and mounted with Vectashild. Visualization was done using inverted confocal microscope SP8 UV.

Statistics

All experiments were performed in biological triplicates, unless stated otherwise in the figure legends. All tests used for statistical significance were calculated using Prism5 and are directly indicated in the figure legends (**** $p < 0.0001$, *** $p < 0.001$, ** $p < 0.01$, * $p < 0.05$, ^{ns} $p > 0.05$).

Acknowledgements

We thank Drs P. Msaouel and N. Tannir for the RMC219, RMC-2C primary RMC cells, all the staff of the IGBMC common facilities in particular cell culture, flow cytometry, confocal microscopy and biomol. This work was supported by institutional grants from the Centre National de la Recherche Scientifique, the Institut National de la Santé et de la Recherche Médicale, the Université de Strasbourg, the Association pour la Recherche contre le Cancer (CR, contract number PJA 20181208268), the Ligue Nationale contre le Cancer, the Institut National du Cancer, the ANR-10-LABX-0030-INRT French state fund through the Agence Nationale de la Recherche under the frame programme Investissements d'Avenir labelled ANR-10-IDEX-0002-02. The IGBMC high throughput sequencing facility is a member of the "France Génomique" consortium (ANR10-INBS-09-08). ID is an 'équipe labellisée' of the Ligue Nationale contre le Cancer. BV was supported by fellowships from the ANR and the Ligue Nationale contre le Cancer.

Author Contributions

BV, MR, AH, ARH, JG, JT performed the experiments; GD, BV performed the bioinformatics analyses; BV, ID and GM conceived the experiments, analysed the data and wrote the paper.

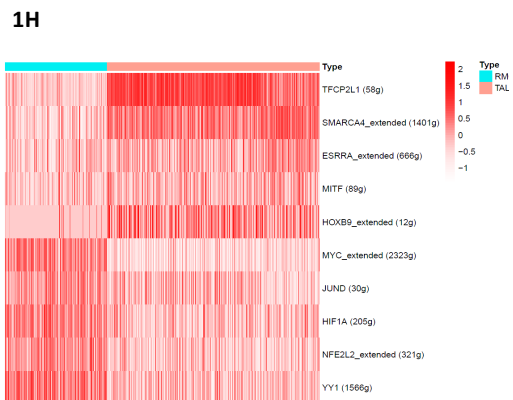
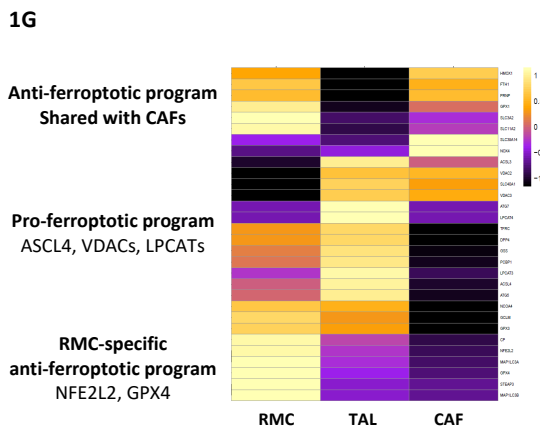
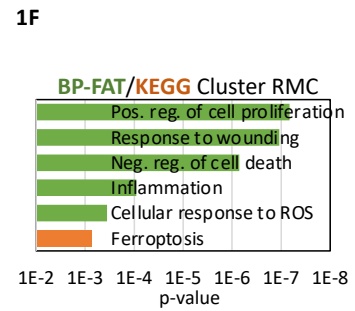
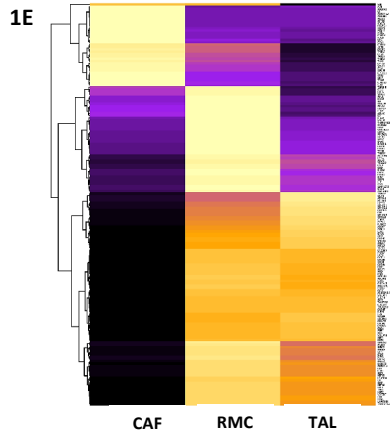
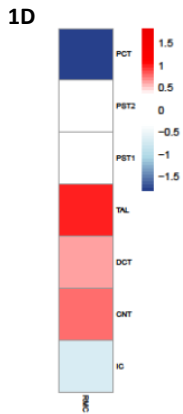
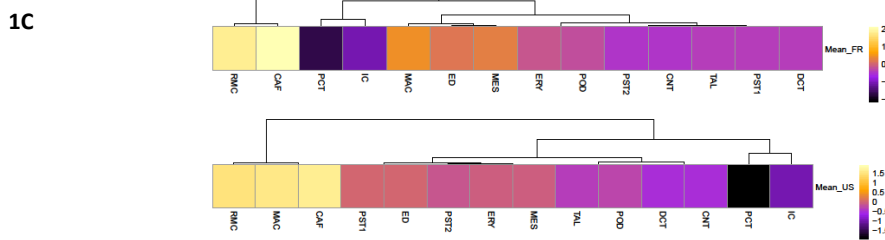
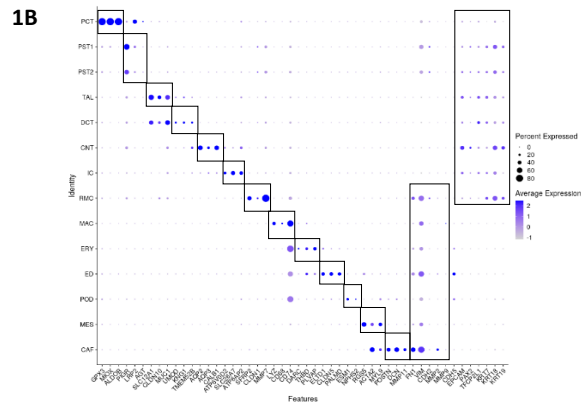
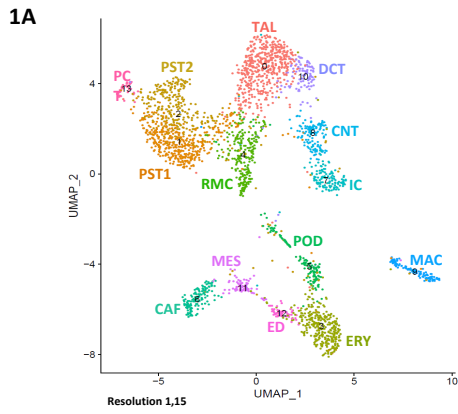
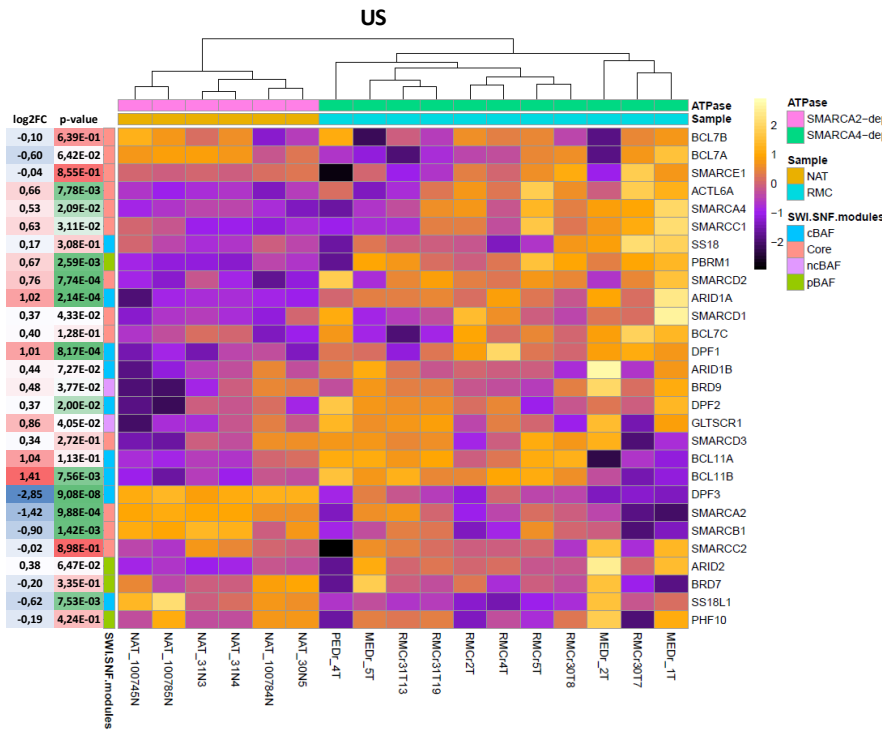


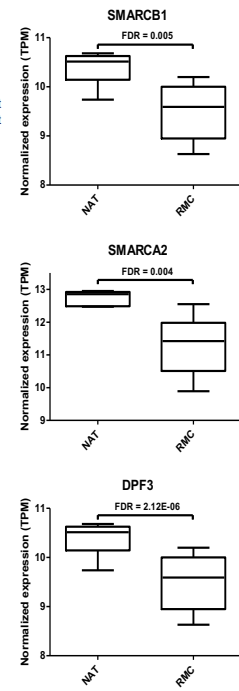
Figure 1. Single-cell RNA sequencing analysis of renal medullary carcinoma and normal adjacent tissue. **A.** Aggregated UMAP representing the clusters identified by Seurat using a resolution of 1.15. Note that proximity of clusters indicate transcriptomic similarities. PC: Proximal convoluted tubule cells; PST1/2: Proximal straight tubule cells; RMC: Renal medullary carcinoma; TAL: thick ascending tubule cells of Henle's loop; DCT: distal convoluted tubule cells; CNT: connecting tubule cells; IC: intercalated collecting duct cells; CAF: cancer-associated fibroblasts; MES: mesangial cells; ED: endothelial cells; ERY: circulating blood cells; POD: podocytes; MAC: macrophages. **B.** Bubble plot representing top 3 markers per identified clusters which are highlighted by small squares. Big rectangles regroup clusters in either mesenchymal or epithelial markers. **C.** Digital deconvolution of bulk RNA-seq from two independent cohorts (US and FR) showing the enrichment of tumour-associated clusters. **D.** Ontogeny correlation matrix showing the transcriptomic proximity of RMC with renal epithelial tubule clusters. **E.** Heatmap representation of RMC versus CAF specific-genes using CAF, RMC and TAL clusters as a matrix. **F.** DAVID 6.8 analysis of RMC-specific genes as analysed in E. Note that the plot represents ontologies of BP-FAT and KEGG pathways together ranked by Benjamini p-values. **G.** Heatmap representation of KEGG Ferroptosis signature (30 genes) using RMC, TAL and CAF clusters as matrix. **H.** SCENIC supervised clustering showing calculated AUCell values of most represented regulons (genes targeted by specific TFs).

Figure 2. Dissection of the intratumoral heterogeneity of renal medullary carcinoma. **A.** UMAP representing the clusters identified by Seurat using a standard resolution of 1. C0: RMC cluster 0; C1: RMC cluster 1. **B.** DAVID 6.8 ontology analysis of RMC0 (right) and RMC1 (left) signature genes ranked Benjamini p-values. **C.** GSEA ontology analysis of RMC1- versus RMC0-specific genes using the Hallmarks gene set of MsigDB. **D.** Ontogeny correlation matrix representing the transcriptomic proximity between RMC0 and RMC1 with each renal epithelial tubule clusters. **E.** Monocle3 trajectory analysis represented on the UMAP as calculated by Seurat. Note that the black line indicate which clusters could potentially transition into one another. **F.** SWNE analysis which indicates the possible trajectories between TAL, RMC0 and RMC1 with associated markers. **G.** Venn diagram showing the overlap between RMC0, RMC1 and CAF most expressed genes. Cut-off used : \log_2 fold change > 1 and p-value $< 0,05$. **H.** Unsupervised clustering representing the mean expression of RMC0 versus RMC1 signatures in US RMC cohort (n=11). **I.** Unsupervised clustering of immune infiltration rates as calculated by MCP-counter in US RMC cohort. Note that we kept the epithelial/mesenchymal/mixed labels that were obtained from analysis in figure 2H. **J-K.** SCENIC heatmap representation comparing the average activity values per cluster of a selection of TFs.

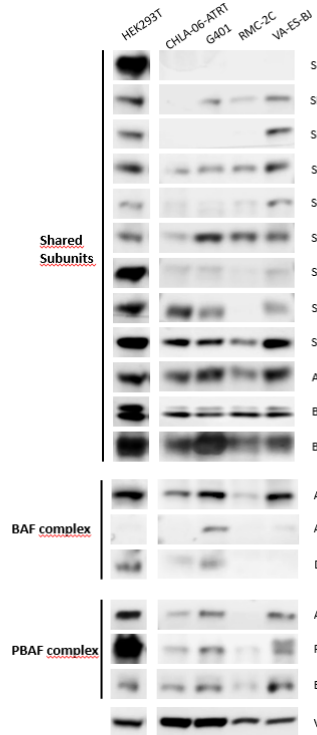
3A



3B



3C



3D



3E

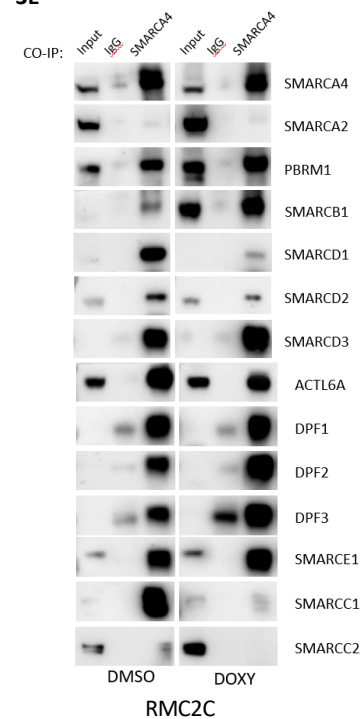


Figure 3. SMARCB1 loss induces a global reorganization of SWI/SNF complexes in renal medullary carcinoma. **A.** Unsupervised clustering representing the average expression of SWI/SNF genes in 11 RMC tumors (US cohort) and 6 matched normal adjacent tissues (NAT). Associated log₂ fold changes and p-values were calculated using Deseq2 comparing all tumors versus all NAT. Note that : 1) the ‘SWI/SNF modules’ tag is based on (Mashtalir et al., 2018); 2) the ‘SMARCA2- and SMARCA4-dependent’ tag is based on the relative expression of the obligatory ATPase subunit of SWI/SNF. **B.** Box plots showing the expression of a selection of SWI/SNF genes in RMC and in NAT, with associated FDR value for statistical significance. **C.** Immunoblot for a selection of SWI/SNF proteins in 4 SMARCB1-deficient cell lines and HEK293T cells for reference. HEK293T : immortalized human embryonic kidney cells; CHLA-06-ATRT: atypical teratoid/rhabdoid tumor cell line; G401: malignant rhabdoid tumor cell line; RMC-2C: RMC cell line; VA-ES-BJ: epithelioid sarcoma cell line. Loading normalisation : VCL. **D.** Immunoblot for a selection of SWI/SNF proteins in HEK293 and RMC-2C cells stably expressing an inducible allele of SMARCB1, treated with DMSO or doxycycline. Loading normalisation : ACTB. **E.** Immunoblot for a selection of SWI/SNF proteins of SMARCA4 co-immunoprecipitation (co-IP) in RMC2C-SMARCB1 cells treated with DMSO or doxycycline. Note that the input serves as a reference and IgG co-IP as a negative control.

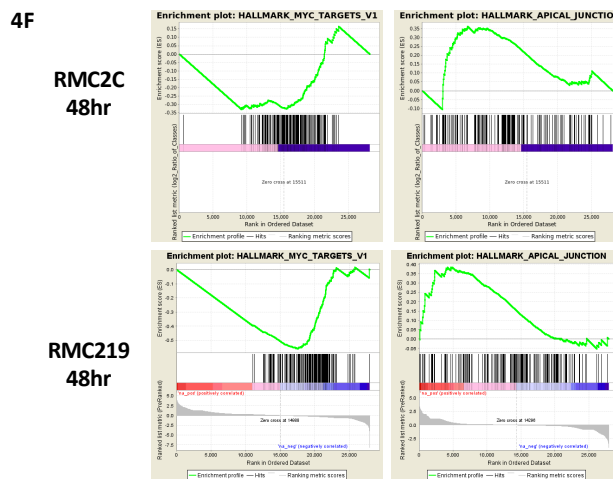
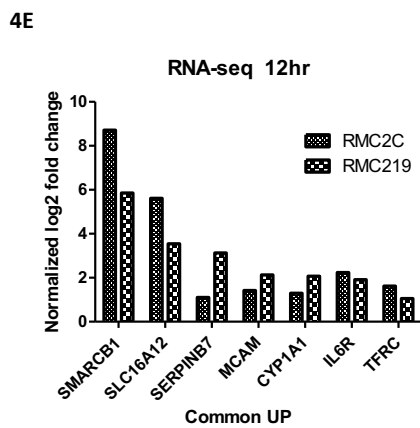
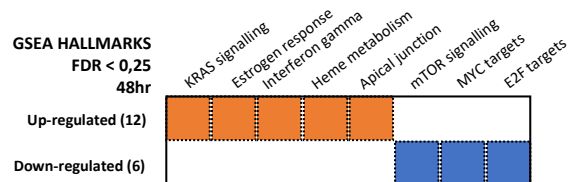
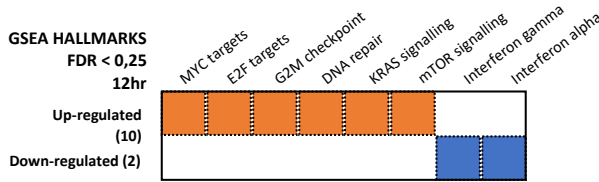
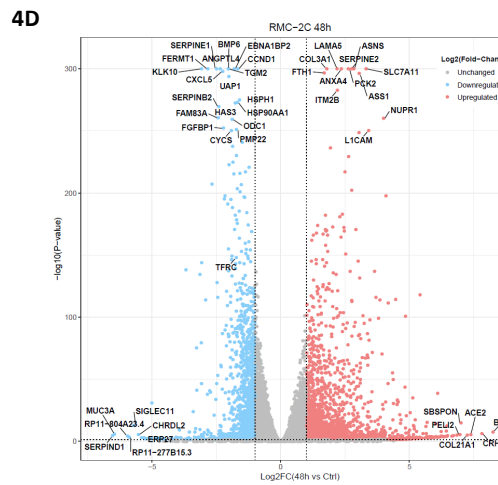
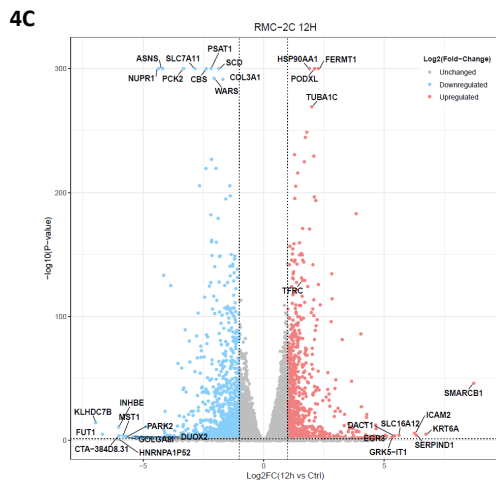
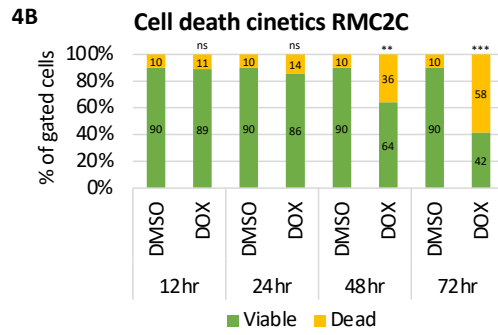
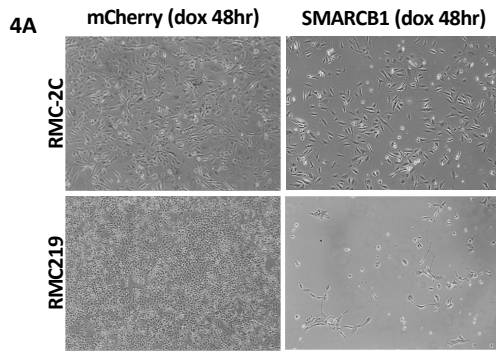


Figure 4. Tumor-suppressor role of SMARCB1. **A.** Phase contrast microscopy pictures of two RMC cell lines stably expressing a doxycycline-inducible allele of mCherry of SMARCB1 that were treated with doxycycline for 48hrs. Note the visually striking decrease in cell numbers. **B.** Bar plot representing the kinetics of cell death after doxycycline treatment as assessed by FACS. Note that the % of cells that stained for either Annexin-V or propidium iodide were tagged 'dead'. The remaining unstained cells were tagged 'viable'. Represented values are the mean of three biological replicates and unpaired t-test analyses were performed by Prism 5 by comparing matched time-points. P-values: ns= $p>0,05$; *= $p<0,05$; **= $p<0,01$; ***= $p<0,001$ and ****= $p<0,0001$. **C-D.** Volcano plot showing the genes were down- (blue) and up-regulated (red) 12hrs (left panel) or 48hrs (right panel) upon treatment with doxycycline, as assessed by RMC2C RNA-seq, with associated GSEA analysis showing the ontology of the de-regulated genes. **E.** Bar plot showing the normalized log₂ fold change of a selection of genes that were commonly up-regulated in RMC2C and RMC219 cells. **F.** GSEA enrichment plots for MYC targets and apical junction hallmarks in both RMC cell lines, at 48hrs post-doxycycline treatment.

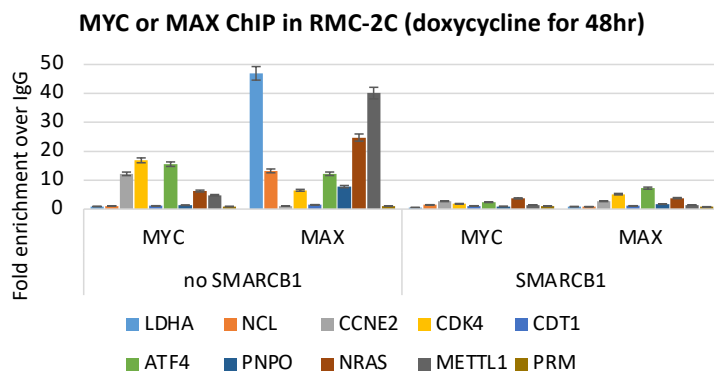
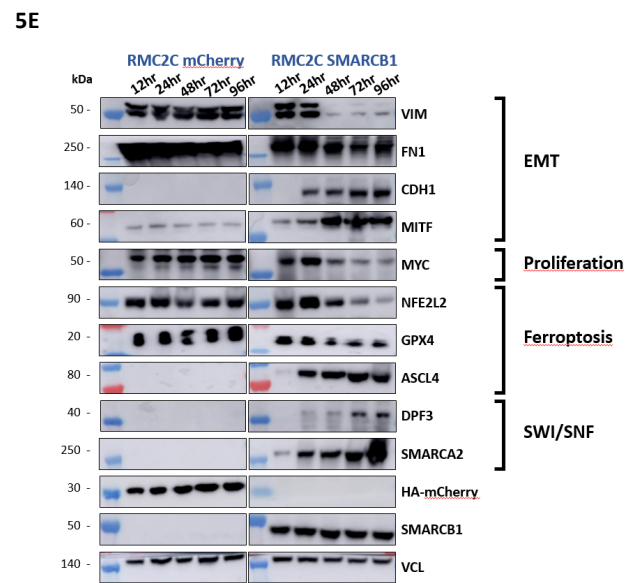
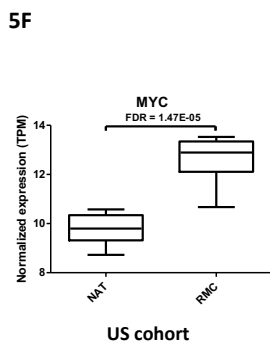
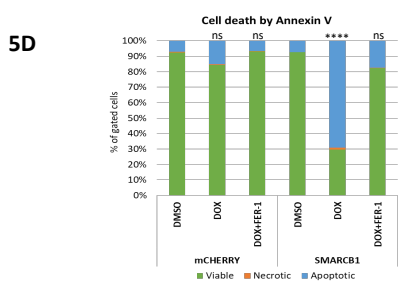
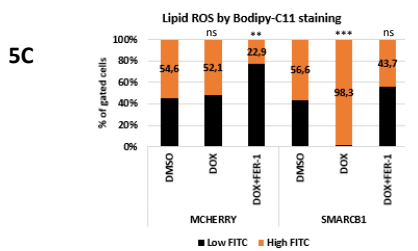
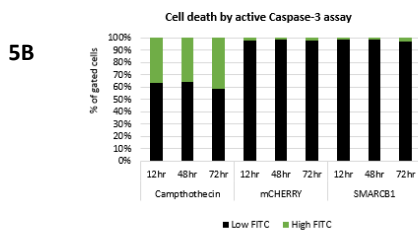
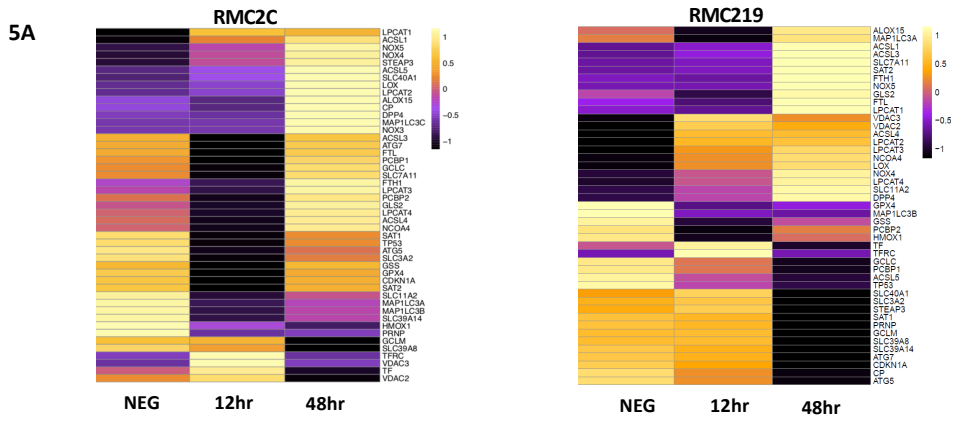
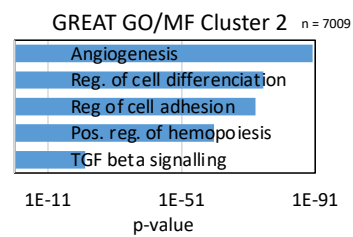
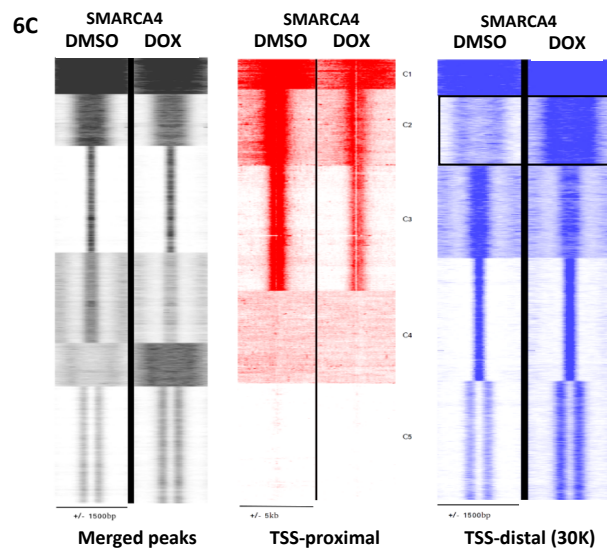
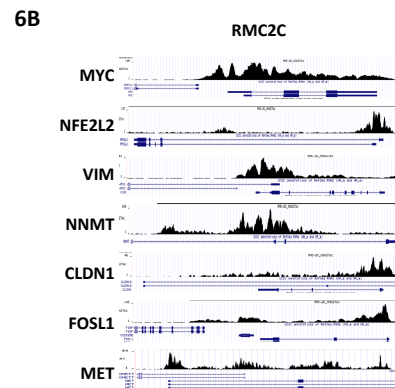
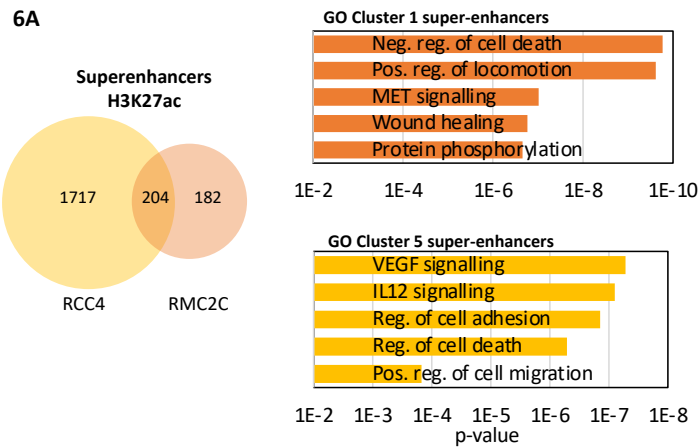


Figure 5. SMARCB1 induces ferroptosis in RMC cells. **A.** Heatmap showing the expression kinetics of KEGG ferroptosis genes (30 genes), as assessed by RNA-seq of RMC2C (left) and RMC219 (right) cells. Note that expression corresponds to the RPKM values here. **B.** Bar plot representing assessed Caspase-3 activation after doxycycline treatment as assessed by FACS, using camptothecin as a positive control and RMC2C-mCherry as negative control. **C.** Bar plot representing assessed lipid peroxidation after doxycycline treatment as assessed with Bodipy-C11 staining by FACS. Represented values are the mean of three biological replicates and unpaired t-test analyses were performed with Prism5 by comparing conditions to matched DMSO. P-values: ns= $p > 0,05$; * = $p < 0,05$; ** = $p < 0,01$; *** = $p < 0,001$ and **** = $p < 0,0001$. **D.** Bar plot representing the kinetics of cell death after doxycycline treatment as assessed by FACS. Represented values are the mean of three biological replicates and unpaired t-test analyses were performed with Prism5 by comparing conditions to matched DMSO. P-values: ns= $p > 0,05$; * = $p < 0,05$; ** = $p < 0,01$; *** = $p < 0,001$ and **** = $p < 0,0001$. **E.** Immunoblot showing the kinetics of expression for a selection of genes in RMC2C-mCherry and RMC2C-SMARCB1 after doxycycline treatment. VCL was used as loading normalisation. **F.** (left panel) Box plots showing the expression of MYC in RMC and in NAT, with associated FDR value for statistical significance. (right panel) Anti-MYC and anti-MAX ChIP-qPCR in RMC2C, treated with DMSO or doxycycline, showing fold enrichment over control anti-IgG for several documented MYC targets or PRM6, a spermatogenesis-specific gene not targeted by MYC, used as a negative control. Represented values are the mean of three technical replicates.



Top 5 Cluster 2 specific motifs

Sequence	Motif	TF	E-value	Sites
	Grainyhead	TFCP2L1	4,2E-062	543
	Paired box	PAX2	6,2E-054	421
	Homeobox	TGIF2	5,9E-055	432
	ER-like	ESRRA	6,0E-043	457
	HMG	SOX6	2,5E-039	479

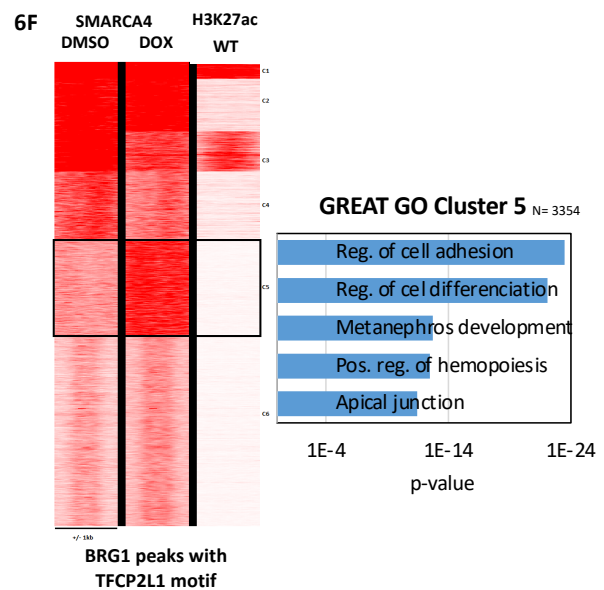
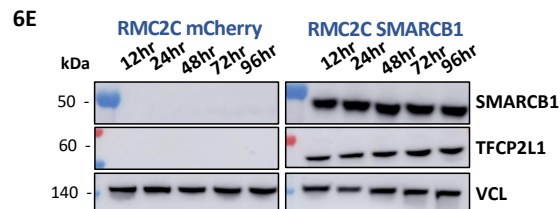
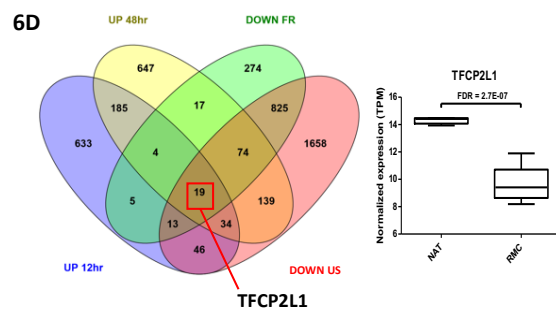


Figure 6. Identification of putative tumor-suppressor TFCP2L1 as a novel SMARCB1 target. A. Venn diagram of H3K27ac super-enhancers from RCC4 and RMC2C cells (left panel); and associated GREAT ontology analysis for specific super-enhancers ranked by p-value. Clusters 1 and 5 refer to RMC2C-specific and RCC4-specific enhancers respectively in the SeqMINER clustering presented in Figure S5C **B.** UCSC snapshots of indicated gene loci showing RMC2C H3K27ac tracks. **C.** SeqMINER read density mapping of all merged, TSS-proximal and TSS-distal (30kb) SMARCA4 peaks in RMC2C cells treated with DMSO or doxycycline (left panel). GREAT ontology analysis for cluster 2 of TSS-distal SMARCA4 peaks (gained in doxycycline condition) ranked by p-value (right panel, up). MEME motif enrichment analysis showing top 5 motifs of cluster 2 (TSS-distal peaks) with associated TFs, p-value and number of sites (right panel, down). **D.** Venn diagram of genes up-regulated at 12 and 48hrs upon SMARCB1 reexpression in RMC2C and genes down-regulated in both US and FR RMC cohorts (left) and box plot representing the expression of TFCP2L1 in US RMC and NAT samples with associated FDR value (right). **E.** Immunoblot showing the kinetics of expression for a selection of genes in RMC2C-mCherry and RMC2C-SMARCB1 after doxycycline treatment. VCL was used as loading normalisation. **F.** SeqMINER read density mapping of all SMARCA4 peaks bearing a TFCP2L1 motif, as assessed by FIMO, in RMC2C treated with DMSO or doxycycline and H3K27ac from RMC2C wildtype cells (left); and associated GREAT ontology analysis showing the top terms for cluster 5 TFCP2L1 motif containing SMARCA4 peaks, ranked by p-value.

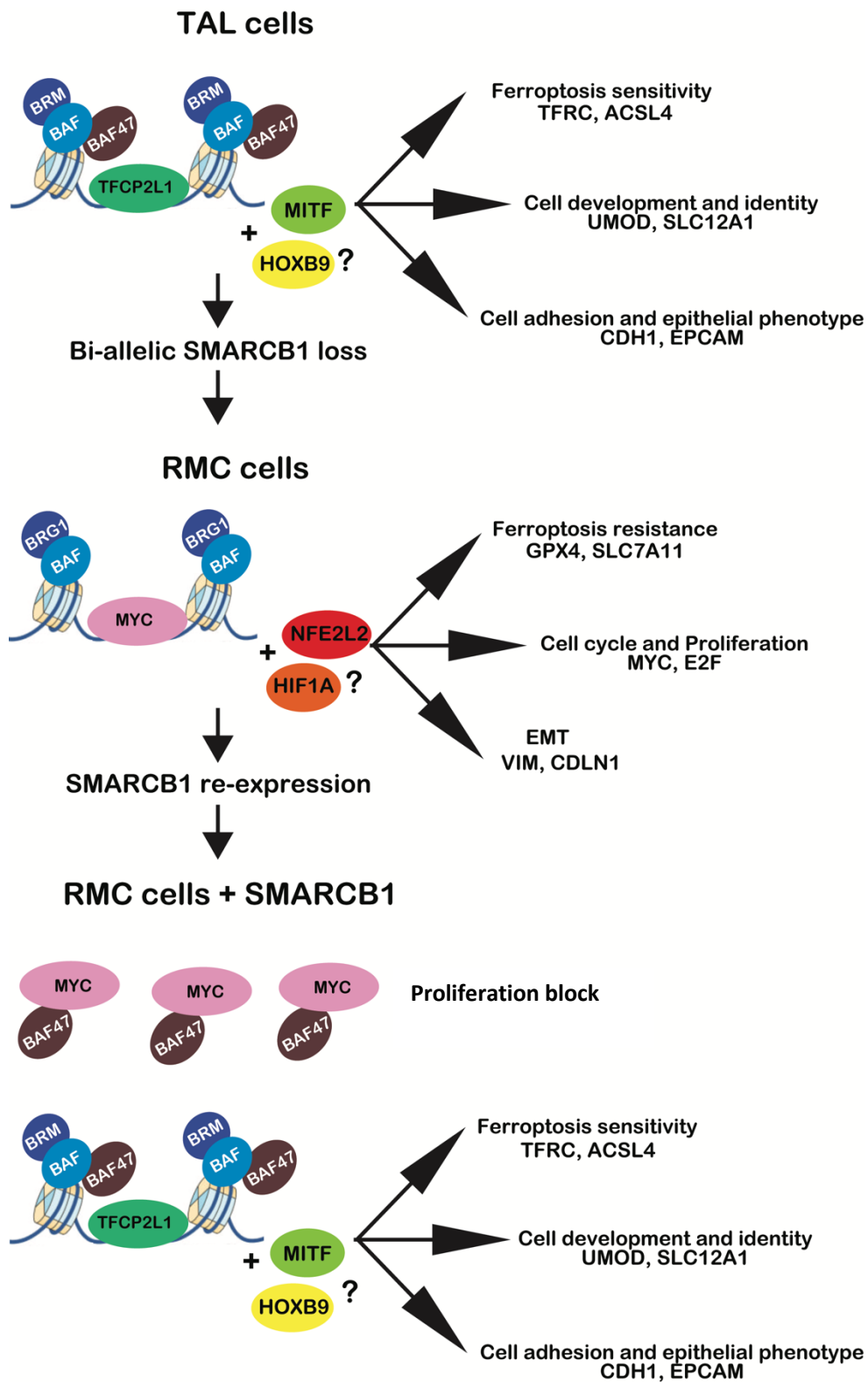
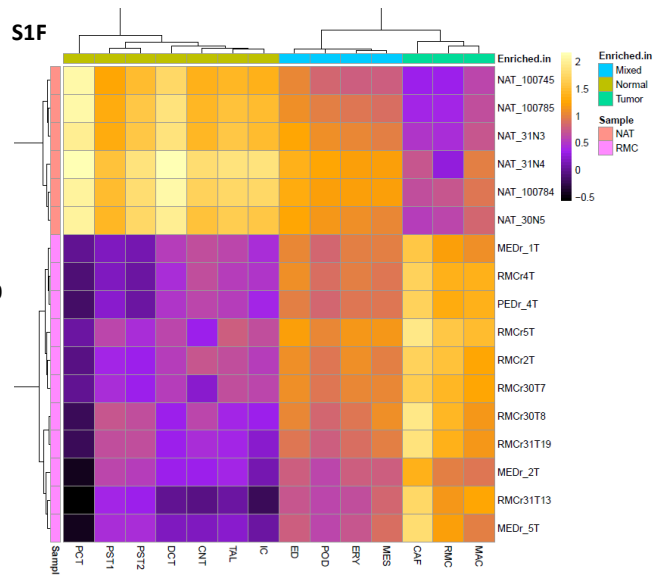
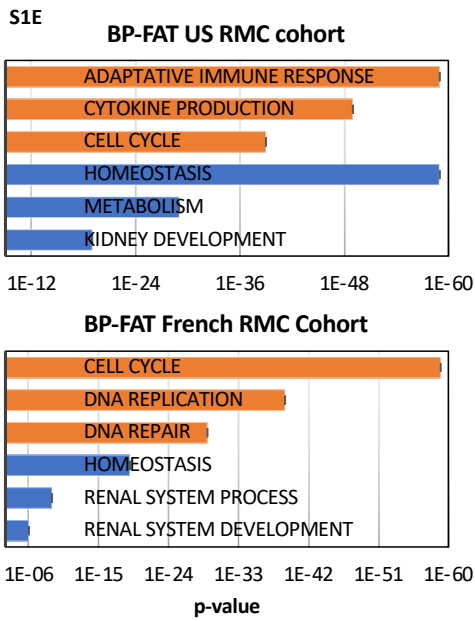
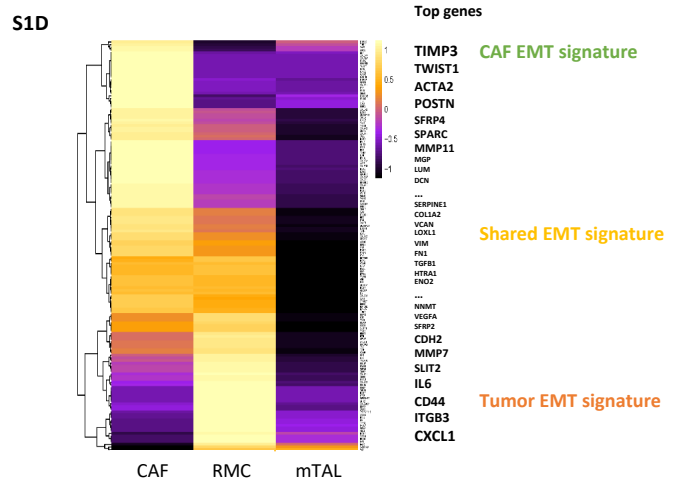
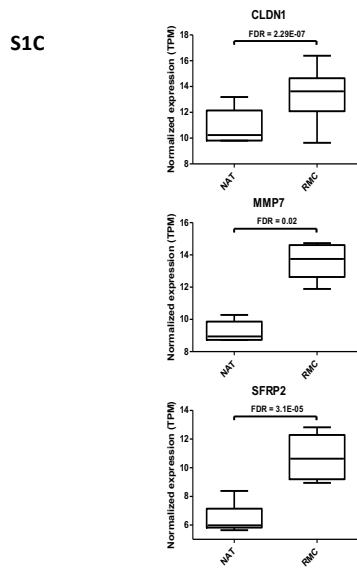
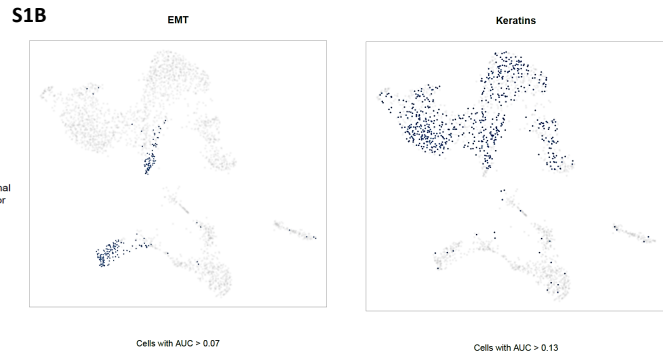
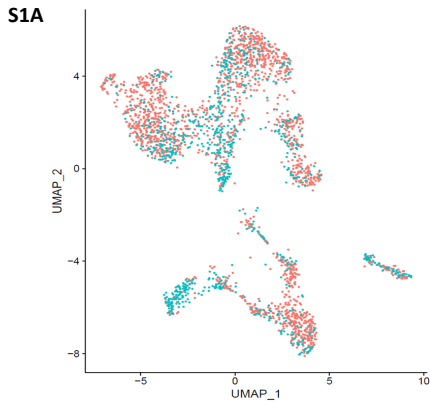


Figure 7. A model of the tumor-suppressor role of SMARCB1 in RMC.

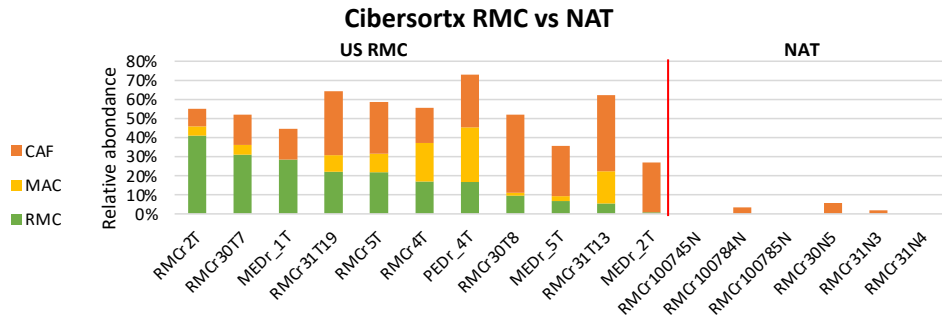
Supplementary Figure 1.



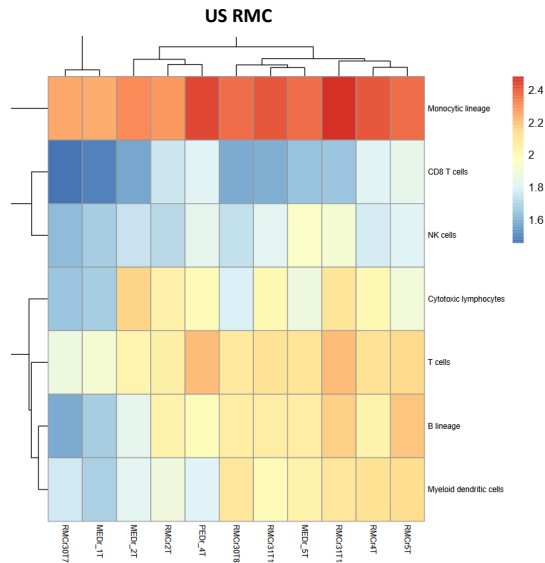
Supplementary Figure 1. A. Seurat UMAP showing the Tumor sample versus NAT sample origin of cells in the aggregated clustering. Note that there is an enrichment of Tumor origin in the cluster corresponding to RMC, CAF and macrophage clusters (compare with Fig. 1A). **B.** AUCell analysis using epithelial-to-mesenchymal transition (180 genes) and cytokeratins (30 genes) MsigDB signatures represented spatially on the UMAP clustering with the indicated cut-off. Note that cells expressing significantly the signature will be colored in blue. **C.** Box plots revealing the expression of a selection of RMC markers from our scRNA-seq data in RMC and in NAT from the US cohort, with associated FDR value. **D.** Heatmap representation of the relative expression of the EMT signature (MsigDB) taking CAF, RMC and TAL clusters as a matrix. Order and font size of genes indicate their respective higher expression in CAF versus RMC. Note that contrary to CAF cells, tumor cells do not express high levels of TWIST, suggesting a partial-EMT phenotype. **E.** DAVID v6.8 ontology terms in the US and FR RMC cohorts and ranked by p-value. **F.** Heatmap representing the relative expression of most up-regulated genes in each individual biopsy from the US cohort. Note that while virtually all biopsies highly expressed genes found in our RMC, CAF and macrophage clusters, very few are expressed in the NAT indicating the specificity of our clustering. In contrast, we found that NAT biopsies highly expressed genes that correlate with PCT and DCT cells, in line with their localization being in the kidney cortex. We also found that glomerular populations such as podocytes, mesangium, endothelium and blood cells are essentially found in both RMC and NAT biopsies.

Supplementary Figure 2.

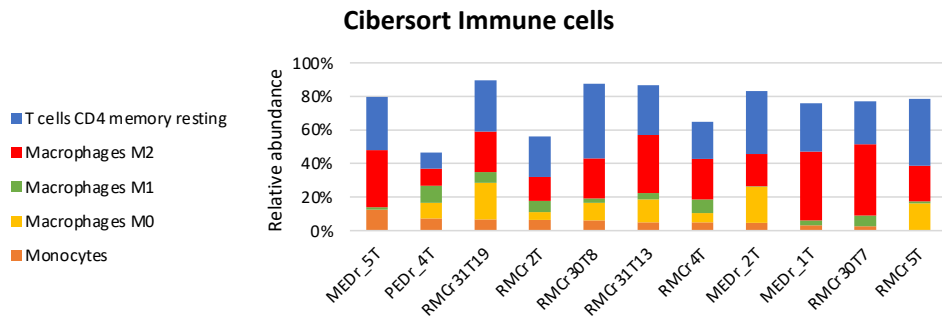
S2A



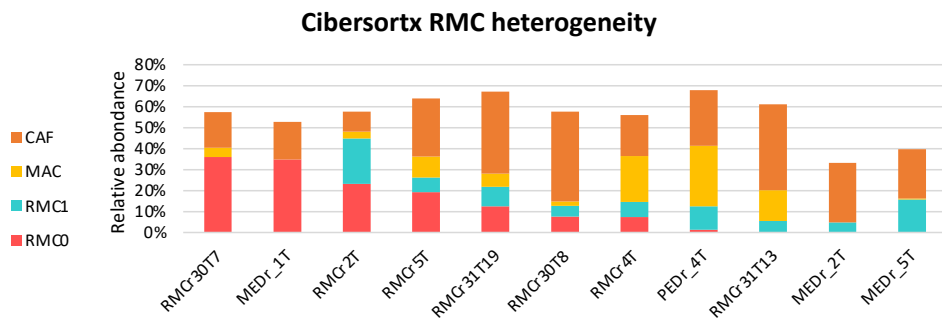
S2B



S2C

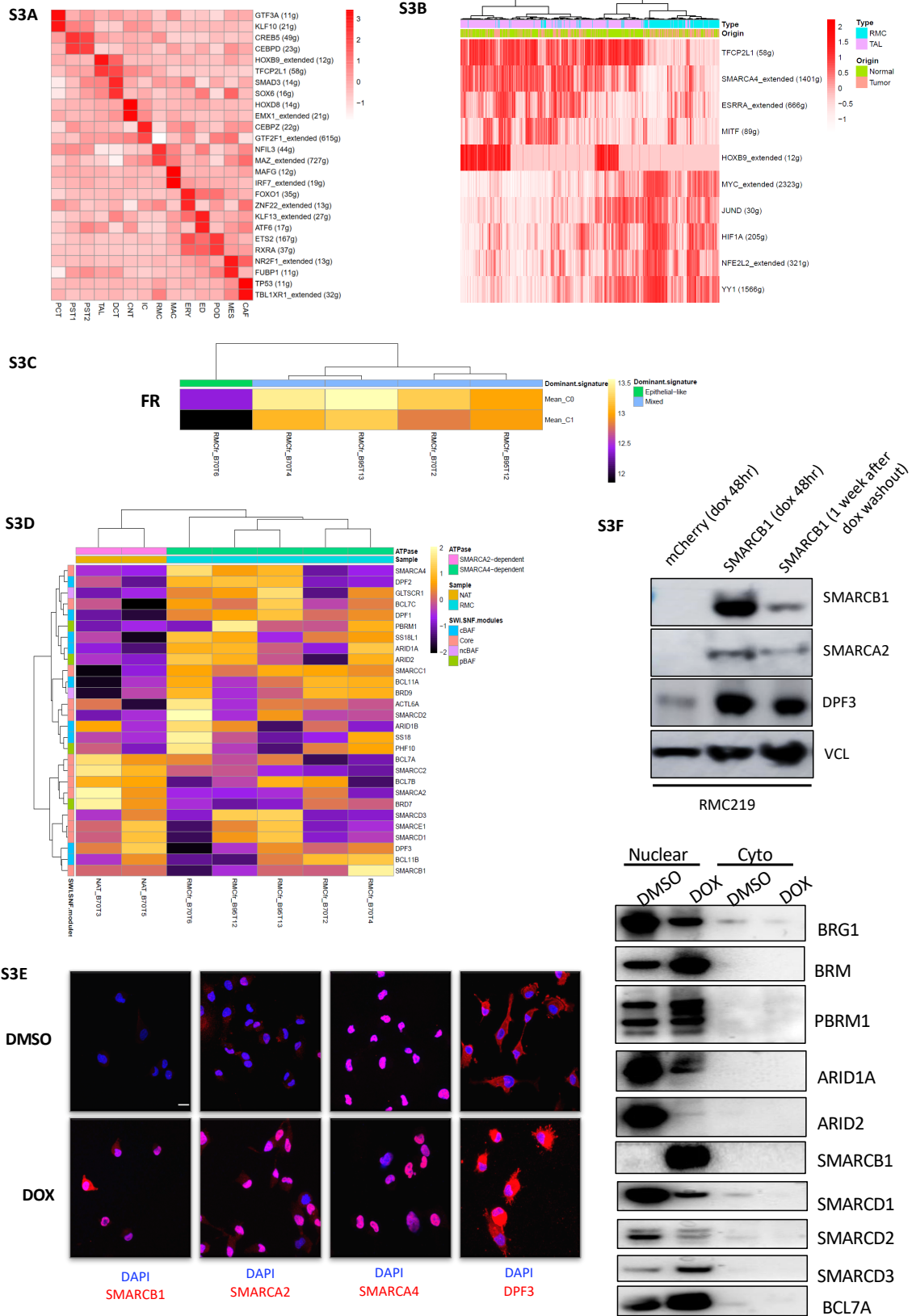


S2D



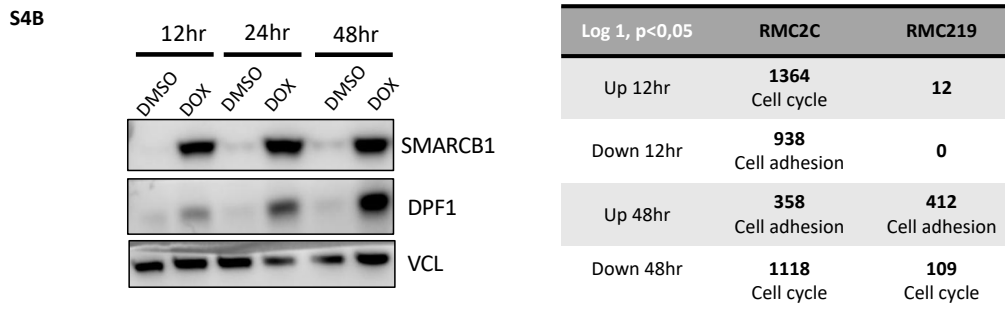
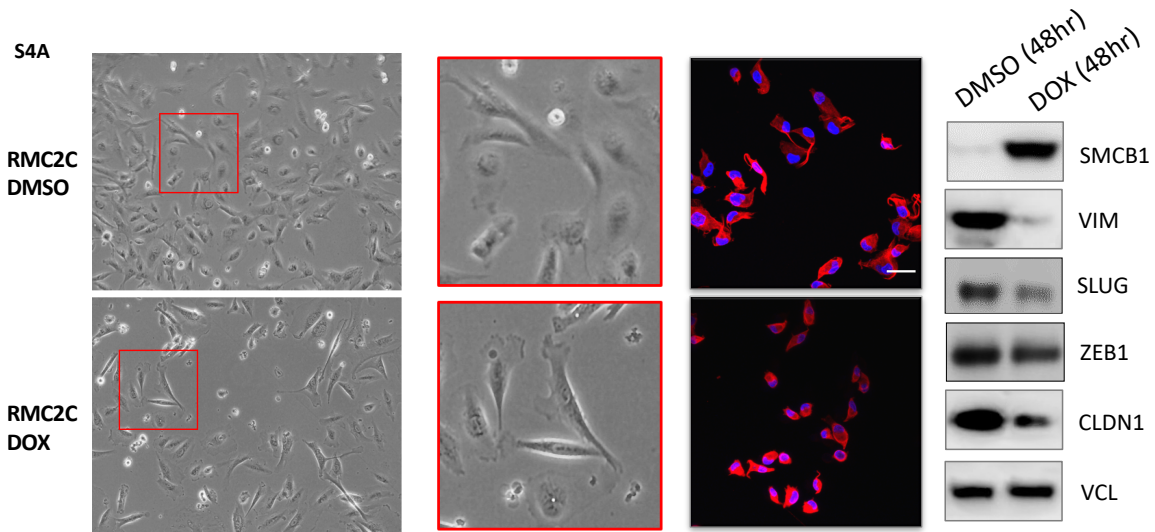
Supplementary Figure 2. A. Bar plot representing the relative proportions (in %) of RMC, CAF and MAC cells in US RMC biopsies versus NATs, as assessed by CIBERSORTX deep-learning analysis of our scRNA-seq data. We found that essentially most tumor biopsies were composed by varying amounts of all three populations, whereas only weak proportions of fibroblasts were found in NATs. Note that here the other clusters of our scRNA-seq data were not represented. **B.** MCP-counter analysis of immune infiltration in US RMC biopsies. **C.** CIBERSORT analysis using built-in 22 immune signatures representing the relative proportions of each immune cell-types. **D.** CIBERSORTX analysis dissecting the relative proportions of CAF, MAC and our two RMC subtypes in the US RMC cohort.

Supplementary Figure 3.



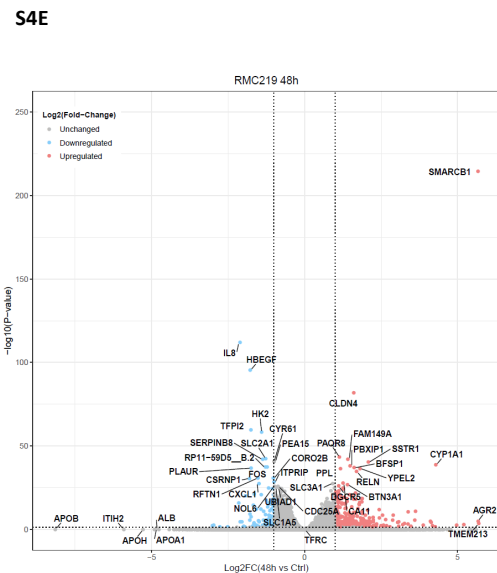
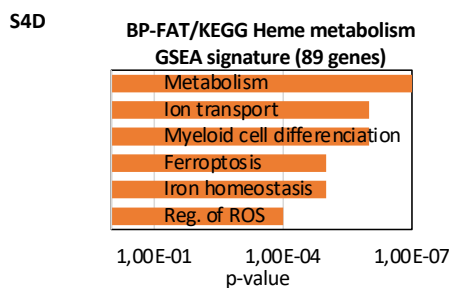
Supplementary Figure 3. A. SCENIC heatmap representing top 2 transcription factors which activity is significantly high per each cluster. **B.** SCENIC unsupervised clustering showing calculated AUCell values of most represented TFs in RMC versus TAL clusters. Note that clustering of these TFs was sufficient to well separate RMC cells from TAL cells, but also tumor sample from NAT sample. **C.** Unsupervised clustering representing the mean expression of RMC0 versus RMC1 signatures in FR RMC biopsies (n=5). **D.** Unsupervised clustering representing the average expression of SWI/SNF genes in 6 RMC tumors (FR cohort) and 2 matched normal adjacent tissues (NAT). Note that : 1) the ‘SWI/SNF modules’ tag is based on (Mashtalir et al., 2018); 2) the ‘SMARCA2- and SMARCA4-dependent’ tag is based on the relative expression of the obligatory ATPase subunit of SWI/SNF. **E.** Confocal microscopy pictures of immunofluorescence using DAPI for nuclear staining and indicated antibodies in RMC2C-SMARCB1 cells treated either with DMSO or doxycycline (left panel). Immunoblot for a selection of SWI/SNF proteins using extracts from subcellular fractionation of RMC2C cells treated either with DMSO or doxycycline. Note that the nuclear-cytoplasmic separation was validated using histone H3 and TUBB (data not shown). **F.** Immunoblot for indicated proteins using VCL as loading control in RMC219 cells stably expressing either mcherry or SMARCB1 for the indicated amount of time.

Supplementary Figure 4.



S4C

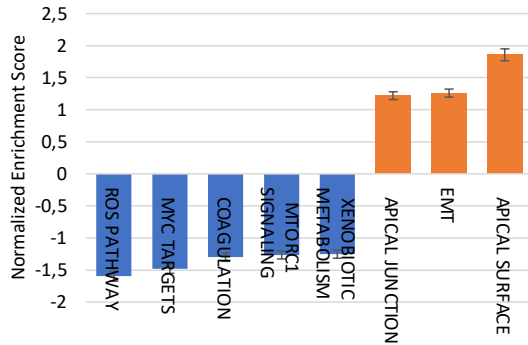
Anti-correlation	GSEA Down	GSEA Up
RMC2C 48hr	Cell cycle, DNA repair MTORC1 pathway	Cell adhesion Heme metabolism
Cohort US	Cell adhesion Heme metabolism	Cell cycle, DNA repair MTORC1 pathway
Cohort FR	Cell adhesion Heme metabolism	Cell cycle, DNA repair MTORC1 pathway



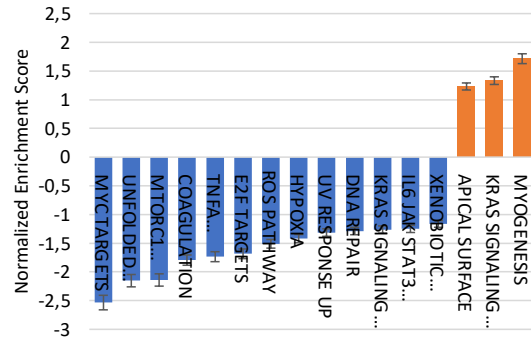
Supplementary Figure 4. A. Phase contrast and confocal microscopy pictures of RMC2C cells treated with either DMSO or doxycycline (left); and immunoblot of associated extracts for the indicated EMT markers (right). Note that VIM, SLUG and ZEB1 are known EMT inducers, while CLDN1 is generally found to be overexpressed in kidney cancers. **B.** Immunoblot of the kinetics of SMARCB1 reexpression and its target DPF1, using VCL as a loading control (left); table summarizing the RNA-seq results from RMC2C and RMC219 cells at 12 and 48hrs upon SMARCB1 reexpression (right). **C.** Table recapitulating the anti-correlation between ontologies found in vitro and in vivo as assessed by GSEA. Note that RMC2C are reexpressing SMARCB1, while cohorts are defined by its loss. **D.** DAVID v6.8 ontology analysis of the GSEA ‘Heme metabolism’ hallmark, ranked by Benjamini p-value. **E.** Volcano plot showing the down- (blue) and up-regulated (red) genes in RMC219 upon reexpression of SMARCB1.

Supplementary Figure 5.

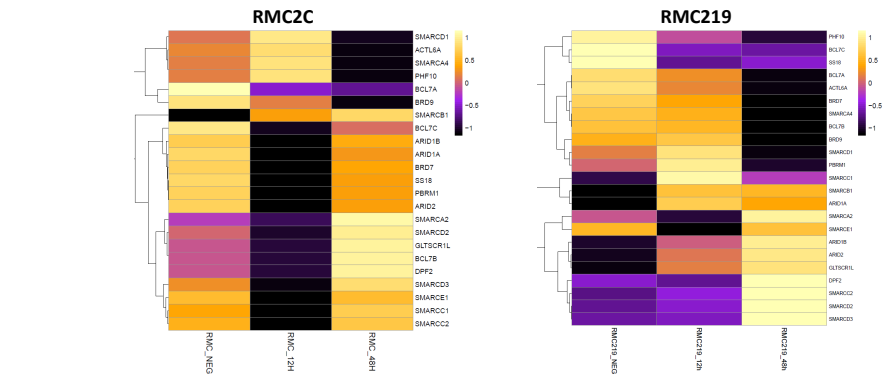
S5A GSEA RMC219 12hr (FDR < 0,25)



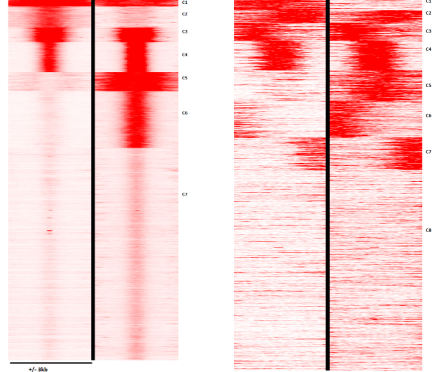
GSEA RMC219 48hr (FDR < 0,25)



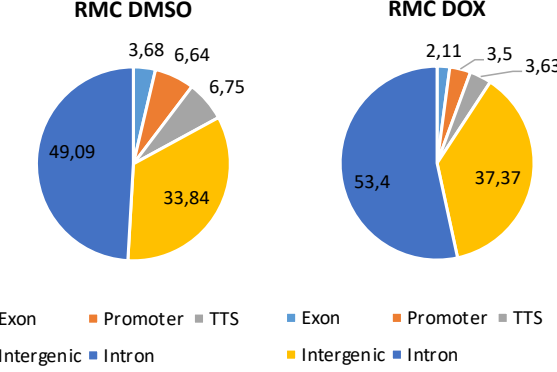
S5B



S5C



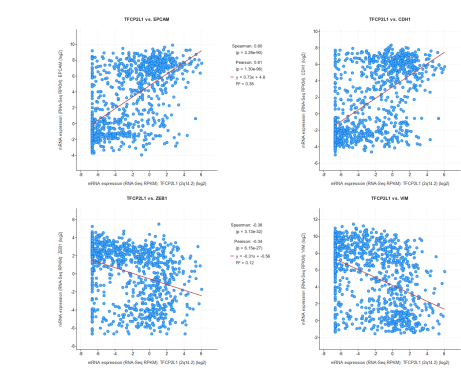
S5D



S5E

19 common	Name
SLC16A12	Monocarboxylate transporter 12
ACOX2	Peroxisomal acyl-coenzyme A oxidase 2
TNS1	Tensin-1
FRMD3	FERM domain-containing protein 3
ABCG2	substrate specificity ATP-binding cassette transport
PLAT	Tissue-type plasminogen activator
SAMD5	Sterile alpha motif domain-containing protein 5
AQP3	Aquaporin-3
CAPN5	Calpain-5
MTUS1	Microtubule-associated tumor suppressor 1
CA2	Carbonic anhydrase 2
PDE2A	cGMP-dependent 3',5'-cyclic phosphodiesterase
CA12	Carbonic anhydrase 12
TFCP2L1	Transcription factor CP2-like protein 1
ABCC4	Multidrug resistance-associated protein 4
NEDD4L	E3 ubiquitin-protein ligase NEDD4-like
MYO5B	Unconventional myosin-Vb
SMPD1	Sphingomyelin phosphodiesterase
AIF1L	Allograft inflammatory factor 1-like

S5F



Supplementary Figure 5. A. GSEA ontology analysis of RMC219 cells 12 and 48hrs after doxycycline treatment, ranked by normalized enrichment score. **B.** Heatmaps representing the kinetics of SWI/SNF genes relative expression at 12 and 48hrs in both RMC cell lines. Note that in both cases, SMARCB1, SMARCA2 and DPF are strongly activated at 48hrs. **C.** SeqMINER read density mapping of H3K27ac enhancers (left) and super-enhancers (right) from RCC4 and RMC2C cell lines. **D.** Pie chart of the distribution of SMARCA4 on the genome as assessed by ChIP-seq and HOMER annotation of the peaks in RMC2C cells treated with either DMSO or doxycycline. **E.** List and expression analysis of the 19 genes that are up-regulated at 12 and 48hrs post-SMARCB1 reexpression and are found lost in both RMC cohorts. Note that each colored dot represent a cell in our UMAP that expresses the indicated genes. **F.** Spearman correlation analysis between TFCEP2L1 and indicated genes using TGCA data from Cancer Cell Line Encyclopedia (CCLE). Note that EPCAM and CDH1 are known epithelial markers, while VIM and ZEB1 are associated with a mesenchymal program and EMT.

GENERAL CONCLUSIONS AND PERSPECTIVES

General conclusions and perspectives

1 – SWI/SNF: important but distinct roles in oncogenesis.

Our results demonstrate that both SMARCA4 and SMARCB1 are important regulators of tumorigenesis, despite displaying distinct functions.

On one hand, we show that BRG1 activates and acts in conjunction with the mesenchymal-specific transcription factor PRRX1 to regulate cell migration and invasion, extracellular matrix remodeling and to promote, in concert with CLDN1, the 3D spheroid growth of dedifferentiated melanoma cells. Furthermore we show that blocking CLDN1 with a targeted antibody mimics the effects of BRG1 and PRRX1 knockdowns in this type of drug-resistant and highly invasive melanoma cells, which could lead to potential novel therapeutic strategies.

On the other hand, we revealed that SMARCB1 acts as a tumor-suppressor in renal medullary carcinoma by antagonizing MYC and actively cooperates with a TAL-specific transcription factor TFCP2L1 to induce cell death by ferroptosis and mesenchymal-to-epithelial transition (MET). Furthermore we provide insights into a novel mechanism of pathogenesis that links sickle cell anemia to loss of SMARCB1 in TAL cells which seem to be sensitive to ferroptosis by nature. Moreover, SMARCB1 tumor-suppressor role mimics a GPX4 inhibition phenotype and this mechanism could potentially be exploited to develop novel targeted therapies for RMC, a lethal disease for which effective treatments are urgently needed.

2 – Melanoma addiction to chromatin-remodeling by SWI/SNF

My host laboratory dedicated a decade worth of projects focused on the role of the oncogene MITF in melanoma. While these works established unequivocally that MITF depends on chromatin-remodelers such as BRG1 and BPTF, the MITF-independent role of BRG1 was not further investigated until now.

Here we provide novel insights into the tumor-promoting role of BRG1 in a type of melanoma cells that does not express neither MITF, nor SOX10. Intriguingly, our results suggest that upon loss of MITF and SOX10, melanoma cells de-repress PRRX1 which hijacks BRG1-containing SWI/SNF

complexes and likely recruits them to genes regulating cell adhesion and 3D growth such as CLDN1. These findings are corroborated by our ChIP-seq data which show a retargeting of BRG1 towards specific loci required for the identity, survival and growth of dedifferentiated melanoma cells.

Thus, despite BRG1 being a major regulator of MITF, we show that it encompasses MITF-independent roles that promote tumor-growth of drug-resistant mesenchymal-like melanoma cells. Importantly, this also demonstrate that melanoma in general is very dependent on chromatin-remodeling, consistent with BRG1 being expressed in all melanoma cell types and past publications of our lab showing the role of BRG1 in melanocytic and neural-crestic melanoma cells.

3 – EMT and ferroptosis : a new paradigm ?

By combining in vitro and patient samples data, we were able to demonstrate that SMARCB1 regulates both EMT and ferroptosis in renal medullary carcinoma. But how can a cell die and change phenotype at the same time? Although it may seem paradoxical at first, we show that SMARCB1 links both ferroptosis and cell identity through its structural domains.

First, SMARCB1 contains a MYC-binding domain at its C-terminus which allows it to directly bind to and therefore block MYC from binding to its own targets and arresting the uncontrolled proliferation of RMC cells. Second, SMARCB1 contains two C-terminal RPT1/2 domains which are important for interactions with other SWI/SNF core subunits. Upon doxycycline induction, SMARCB1 stabilizes SWI/SNF complexes which are hijacked by TFCP2L1 that is re-expressed and brings SMARCB1-containing SWI/SNF complexes to genes essential for mesenchymal-to-epithelial transition (MET), thereby switching from anti-ferroptotic to pro-ferroptotic signals.

Given that in melanoma, dedifferentiated cells acquire resistance to ferroptosis, it may well be that the resistance to ferroptosis in RMC might be due to EMT-TFs. This could have implications for a broader spectrum of cancers that feature EMT, as anti-GPX4 could be used as a targeted therapy to specifically kill those drug-resistant cells.

4 – Role of SWI/SNF : the global and the tissue-specific

Another important point that is revealed by our work on both melanoma and RMC is that SWI/SNF may have a global role in cancer which is to regulate MITF and its targets. In melanoma and

in RMC, dedifferentiation requires the inhibition of MITF activity. In both cases, the loss of MITF seems to be associated with an induction of ferroptosis-resistance. Thus it is possible that MITF represses GPX4 through a mechanism yet to be determined, probably through direct transcriptional regulation. Future experiments will determine the potential role of MITF in regulating ferroptosis in RMC and melanoma.

Intriguingly, when we compared the binding sites of BRG1 in dedifferentiated MM099 cells and RMC-2C cells (DMSO), most peaks were overlapping in both cell-types (data available upon request). This was unexpected as these are cancers from totally different embryonic- and tissue-origins. Furthermore, it might be that SMARCB1 regulates enhancers in both melanoma and RMC, as it also was shown in other SMARCB1-deficient tumors and embryonic stem cells. Therefore, SWI/SNF might have global functions that are conserved in tumors from distinct tissue-types.

In the future we will perhaps be able to decipher the ‘pan-cancer’ role of SWI/SNF, for instance in regulating ferroptosis, immune response or EMT. Nevertheless, our study also showed that SWI/SNF depends a lot on the recruitment by tissue-specific factors such as PRRX1 and TFCP2L1, perhaps even tissue-specific non-coding RNAs.

5 – SWI/SNF as a tool to identify tumor vulnerabilities

As SWI/SNF is an essential co-factor of so many tissue-specific TFs, studying SWI/SNF in cancer could be used as a tool to discover intrinsic vulnerabilities. Here our works identified novel tumor-intrinsic vulnerabilities, namely CLDN1 in dedifferentiated melanoma and GPX4 in renal medullary carcinoma.

Regardless of the high SWI/SNF mutations found in human tumors, chromatin-remodeling by SWI/SNF appears to be an essential tool that is often hijacked by oncogenes to promote the expression of their tumor-promoting targets. Thus SWI/SNF is often upstream of important pathways involved in cancer, which means that knockdown and overexpression experiments can help to better understand underlying oncogenic mechanisms.

While SMARCB1 is mutated in 100% of RMC, SMARCA4 is mutated in only 10% of melanoma, however it is required at all stages of melanoma development for maintaining

MITF/SOX10/TFAP2A as well as AP1/TEAD/PRRX1 programs. Therefore, SWI/SNF is important in both genetically- and epigenetically-altered tumors, and constitute an ideal tool for studying cancer.

6 – On the importance of 3D sphere experiments

Lastly, our work on dedifferentiated melanoma cells demonstrated that 2D and 3D conditions display major differences with respect to cell proliferation and adhesion functions. It is important to note that while it might not be relevant to study the role of BRG1 in melanocytic melanoma cells that are highly proliferative, the dedifferentiated cells divide much slower and are more adhesive.

Besides, if melanoma dedifferentiation is induced by hypoxia and starvation (as is currently believed), then differentiated cells might truly represent their ‘in vivo’ state only in 3D-growing tumors where hypoxia and nutrient deprivation is increased in the center of the tumorspheres. Therefore, growing dedifferentiated cells in 2D might ‘denature’ their original properties and using 3D cultures might be the best strategy to study the effects of BRG1 silencing in dedifferentiated cells.

Evidently, if studying the role of a protein of interest in cell cycle makes sense in 2D cultures, the effects on cell adhesion should be assessed in 3D conditions to be more representative. Also, the choice of using 2D or 3D conditions should be made taking into account the intrinsic nature of studied cells (proliferative/differentiated or invasive/dedifferentiated). The study in 3D conditions has the added benefit of representing more closely *in vivo* effects.

Publications

1). Msaouel P, Malouf GG, Su X, Vokshi B et al. Comprehensive Molecular Characterization Identifies Distinct Genomic and Immune Hallmarks of Renal Medullary Carcinoma. *Cancer Cell*. 2020;37(5):720-734.e13. doi:10.1016/j.ccell.2020.04.002

2). Vokshi B, Davidson G, Coassolo S, Haller AR, Gantzer J, Malouf G and Davidson I. Essential role of the chromatin remodeler BRG1 for formation of tumour spheroids by dedifferentiated melanoma cells. (Manuscript in preparation)

3). Vokshi B, Davidson G, Helleux A, Rippinger M, Haller AR, Gantzer J, Thouvenin J, Davidson I and Malouf G. Chromatin remodeling subunit SMARCB1 regulates cell identity and sensitivity to ferroptosis in renal medullary carcinoma. (Manuscript in preparation)

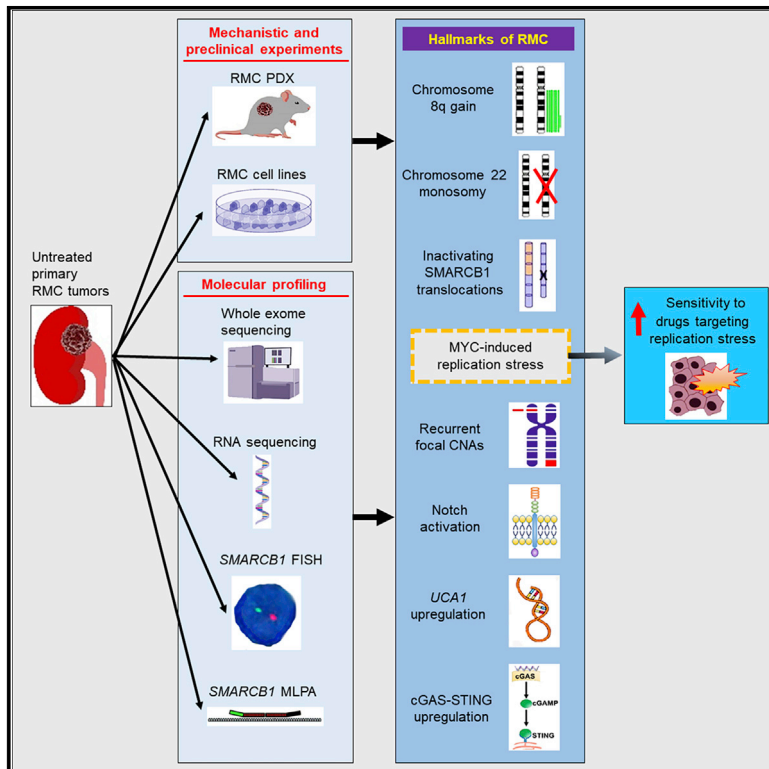
Communications

Poster : Vokshi B, Davidson G, Coassolo S and Davidson I. The Chromatin-Remodeler BRG1 regulates mesenchymal cell invasion, tumor 3D growth and immune response. Présentation à la conférence ESPCR en septembre 2019 à Bruxelles, Belgique.

ANNEXES

Comprehensive Molecular Characterization Identifies Distinct Genomic and Immune Hallmarks of Renal Medullary Carcinoma

Graphical Abstract



Authors

Pavlos Msaouel, Gabriel G. Malouf, Xiaoping Su, ..., Cheryl L. Walker, Giannicola Genovese, Nizar M. Tannir

Correspondence

pmsaouel@mdanderson.org (P.M.), cheryl.walker@bcm.edu (C.L.W.), ggenovese@mdanderson.org (G.G.), ntannir@mdanderson.org (N.M.T.)

In Brief

Msaouel et al. describe the molecular landscape of renal medullary carcinomas (RMC). These tumors harbor SMARCB1 mutations leading to high MYC expression and replicative stress that sensitize RMC cells to PARP inhibitors. cGAS-STING activation in RMCs warrants exploration of immunotherapy for these patients.

Highlights

- The molecular profile of RMC distinguishes it from other renal malignancies
- RMC harbors a high number of focal chromosomal alterations
- RMC has a distinct immune profile characterized by upregulation of cGAS-STING
- DNA replication stress is a hallmark of RMC that can be therapeutically targeted



Article

Comprehensive Molecular Characterization Identifies Distinct Genomic and Immune Hallmarks of Renal Medullary Carcinoma

Pavlos Msaouel,^{1,2,22,*} Gabriel G. Malouf,^{3,4} Xiaoping Su,⁵ Hui Yao,⁵ Durga N. Tripathi,² Melinda Soeung,⁶ Jianjun Gao,¹ Priya Rao,⁷ Cristian Coarfa,⁸ Chad J. Creighton,^{5,8} Jean-Philippe Bertocchio,^{1,2} Selvi Kunnimalaiyaan,⁹ Asha S. Multani,¹⁰ Jorge Blando,¹¹ Rong He,¹ Daniel D. Shapiro,¹² Luigi Perelli,¹ Sanjana Srinivasan,^{6,13} Federica Carbone,¹ Patrick G. Pilié,¹ Menuka Karki,² Riyad N.H. Seervai,^{2,14} Bujamin H. Vokshi,^{3,4} Dolores Lopez-Terrada,¹⁵ Emily H. Cheng,¹⁶ Ximing Tang,¹⁷ Wei Lu,¹⁷ Ignacio I. Wistuba,¹⁷ Timothy C. Thompson,¹ Irwin Davidson,⁴ Virginia Giuliani,^{13,18} Katharina Schlacher,⁹ Alessandro Carugo,^{13,18} Timothy P. Heffernan,^{13,18} Padmanee Sharma,^{1,11} Jose A. Karam,^{12,17} Christopher G. Wood,¹² Cheryl L. Walker,^{2,19,20,21,*} Giannicola Genovese,^{1,6,*} and Nizar M. Tannir^{1,*}

¹Department of Genitourinary Medical Oncology, Unit 1374, The University of Texas MD Anderson Cancer Center, 1155 Pressler Street, Houston, TX 77030-3721, USA

²Center for Precision Environmental Health, Baylor College of Medicine, Houston, Texas, USA

³Department of Hematology and Oncology, Strasbourg University Hospitals, Strasbourg University, Strasbourg, France

⁴Department of Functional Genomics and Cancer, Institut de Génétique et de Biologie Moléculaire et Cellulaire, CNRS/INSERM/UNISTRA, Illkirch Cedex, France

⁵Department of Bioinformatics and Computational Biology, The University of Texas MD Anderson Cancer Center, Houston, TX 77030, USA

⁶Department of Genomic Medicine, The University of Texas M.D. Anderson Cancer Center, Houston, TX 77030, USA

⁷Department of Pathology, The University of Texas M.D. Anderson Cancer Center, Houston, TX 77030, USA

⁸Department of Medicine and Dan L. Duncan Cancer Center, Baylor College of Medicine, Houston, TX 77030, USA

⁹Department of Cancer Biology, University of Texas MD Anderson Cancer Center, Houston, TX 77030, USA

¹⁰Department of Genetics, The University of Texas M.D. Anderson Cancer Center, Houston, TX 77030, USA

¹¹Department of Immunology, The University of Texas M.D. Anderson Cancer Center, Houston, TX 77030, USA

¹²Department of Urology, The University of Texas M.D. Anderson Cancer Center, Houston, TX 77030, USA

¹³Institute for Applied Cancer Science, The University of Texas MD Anderson Cancer Center, Houston, TX 77030, USA

¹⁴Molecular & Cellular Biology Graduate Program, Medical Scientist Training Program, Baylor College of Medicine, Houston, TX 77030, USA

¹⁵Department of Pathology, Texas Children's Hospital, Houston, TX 77030, USA

¹⁶Human Oncology & Pathogenesis Program and Department of Pathology, Memorial Sloan Kettering Cancer Institute, New York City, NY 10065, USA

¹⁷Department of Translational Molecular Pathology, The University of Texas M.D. Anderson Cancer Center, Houston, TX 77030, USA

¹⁸Translational Research to Advance Therapeutics and Innovation in Oncology (TRACTION), The University of Texas MD Anderson Cancer Center, Houston, TX 77030, USA

¹⁹Department of Molecular and Cellular Biology, Baylor College of Medicine, Houston, Texas, USA

²⁰Department of Medicine, Baylor College of Medicine, Houston, Texas, USA

²¹Department of Molecular and Human Genetics, Baylor College of Medicine, Houston, Texas, USA

²²Lead Contact

*Correspondence: pmsaouel@mdanderson.org (P.M.), cheryl.walker@bcm.edu (C.L.W.), ggenovese@mdanderson.org (G.G.), ntannir@mdanderson.org (N.M.T.)

<https://doi.org/10.1016/j.ccell.2020.04.002>

SUMMARY

Renal medullary carcinoma (RMC) is a highly lethal malignancy that mainly afflicts young individuals of African descent and is resistant to all targeted agents used to treat other renal cell carcinomas. Comprehensive genomic and transcriptomic profiling of untreated primary RMC tissues was performed to elucidate the molecular landscape of these tumors. We found that RMC was characterized by high replication stress and an abundance of focal copy-number alterations associated with activation of the stimulator of the cyclic GMP-AMP synthase interferon genes (cGAS-STING) innate immune pathway. Replication stress conferred a therapeutic vulnerability to drugs targeting DNA-damage repair pathways. Elucidation of these previously unknown RMC hallmarks paves the way to new clinical trials for this rare but highly lethal malignancy.

Significance

Renal medullary carcinoma (RMC) is a highly aggressive malignancy with poor prognosis that predominantly afflicts young people of African descent. Effective treatment strategies are needed for RMC, as less than 5% of patients survive beyond 3 years despite best available therapies. We comprehensively profiled a multi-institutional patient cohort of previously untreated primary RMC tumor samples and identified molecular and immune hallmarks that distinguish RMC from other closely related malignancies and can be therapeutically exploited. Our results provide insights into RMC biology and pave the way to clinical trials for this lethal disease.



INTRODUCTION

Although relatively rare, renal medullary carcinoma (RMC) is the third most common kidney malignancy among adolescents and young adults (Cajaiba et al., 2018). It is uniformly associated with sickle hemoglobinopathies (Msaouel et al., 2018) and most frequently occurs in young males of African descent at a median age of 28 years old (Msaouel et al., 2019; Shah et al., 2017). RMC is resistant to all targeted therapies commonly used against other renal cell carcinomas and is highly aggressive, with <5% of patients surviving longer than 36 months (Msaouel et al., 2019). In addition, the best available cytotoxic chemotherapy regimens produce a, typically brief, objective response in only 29% of RMC cases (Msaouel et al., 2019; Shah et al., 2017). Consequently, effective treatment strategies are urgently needed for this lethal disease—a need that is difficult to address given the dearth of knowledge regarding the molecular landscape of this rare malignancy.

All RMC tumors are characterized by loss, as determined by immunohistochemistry (IHC), of the potent tumor suppressor SMARCB1, alternatively known as INI1, hSNF5, or BAF47. SMARCB1 is a subunit of the SWI/SNF complex, which hydrolyzes ATP to remodel chromatin structure. Inactivation of SMARCB1 deregulates the activity of SWI/SNF, resulting in aggressive tumors (Kadoch and Crabtree, 2015). In addition to RMC, inactivation of SMARCB1 occurs in the majority of malignant rhabdoid tumors (MRTs), atypical teratoid/rhabdoid tumors (ATRTs), and epithelioid sarcomas (ESs) (Fuller, 2016).

RMC occurs in approximately 1 in 20,000 individuals with sickle cell trait (Alvarez et al., 2015; Msaouel et al., 2018). To meet the need for new therapies for this disease, we established and molecularly profiled a multi-institutional patient cohort of previously untreated primary RMC tumor samples.

RESULTS

The Mutational Landscape of RMC Distinguishes It from Other Renal Cell Carcinomas

As is typical of RMC (Alvarez et al., 2015; Shah et al., 2017), the majority of our cases (68.4%) arose from the right kidney, the median age at diagnosis was 28 years old, 73.7% of patients were men, 65.8% had metastatic stage IV disease at diagnosis, and only 34.2% had an objective, albeit temporary, response to cytotoxic chemotherapy (Figure 1). All RMC samples were confirmed to be SMARCB1 negative by IHC (Figure S1A). Overall, rates of single-nucleotide variants (SNVs) and insertion and deletion mutations (inDels) were very low for RMC. Whole-exome sequencing (WES) landscapes for 31 untreated primary tumor samples and 15 matched normal samples were used to determine SNVs and inDels, with an average mean target sequencing coverage of 73-fold for tumor tissue and 60-fold for matched normal tissue, and a mean estimated tumor purity of 49.1% (range, 24%–98%). A total of 1,332 SNVs and inDels in 1,165 genes were identified by WES, with a median of 24 per patient (Figure 1 and Table S1). Clinical targeted next-generation sequencing of 5 of 31 untreated primary tumor samples (Figure 1) did not detect additional SNVs and inDels. In two additional patient samples (RMC20T and RMC27T) for which no tissue was available to reliably perform WES, targeted next-generation

sequencing by FoundationOne CDx did not detect any mutations. The low non-synonymous mutation load of RMC was similar to that of MRT (which is also characterized by loss of SMARCB1) and lower than most of the tumors sequenced by The Cancer Genome Atlas, including other renal cell carcinomas (Figure 2A).

Of the 1,165 genes mutated in untreated primary RMC tumors from a total of 31 patients, only 22 were known tumor suppressors or oncogenes listed in the Catalog of Somatic Mutations in Cancer (COSMIC) database (Forbes et al., 2017) (Figure S1B and Table S1). An additional ten genes were previously identified as splicing factors linked to other cancer types (Seiler et al., 2018) (Figure S1B and Table S1). Figure S1C shows the mutational signature patterns of RMC samples compared with matched normal samples. The protein classes encoded by the 1,165 genes were determined using the PANTHER classification system (Mi et al., 2013) (Figure S1D and Table S1). *SETD2* was mutated in 2 of 31 (6.5%) RMC tumors and was the only established gene driver of other renal cell carcinomas (Brugarolas, 2014) to be altered in RMC (Figure 1 and Table S1).

RMC Is Characterized by 8q Gain and Focal Chromosomal Alterations

SMARCB1 is located on chromosome 22, which was lost in 40% of RMC tumors (Figure 2B). Whereas other SMARCB1-deficient malignancies, such as the rhabdoid tumors MRT and ATRT, harbor a simple genome with very few CNAs other than 22q11.23 loss (Chun et al., 2016; Hasselblatt et al., 2013; Lee et al., 2012) (Figure S1E), RMC had recurrent focal chromosomal amplifications and deletions in addition to 22q11.23 loss (Figures 2C, 2D, and S2). Our analysis of previously published WES from MRT and ATRT samples (Lee et al., 2012) revealed a much lower number of focal CNAs (Figure 2E) compared with RMC (Figure 2D). Chromosome 8q gain was noted in 46.7% of RMC tumors, and 21.1% of genes in that chromosome arm were significantly upregulated (false discovery rate [FDR] < 0.1) upon RNA sequencing (RNA-seq) in RMC tumors compared with adjacent normal kidney (Table S2). None of the MRTs and ATRTs harbored an 8q gain (Figure S1E). The genome plots of all seven RMC samples harboring 8q gain are shown in Figure S2. No other recurrent whole or arm-level chromosome gains or losses were found, and approximately half of all RMC tumors (46.2%) were diploid (Figures 2C and S2). Significant focal copy-number changes as quantified by GISTIC analysis are shown in Figure 2D, including recurrent deletions in and around the *SMARCB1* locus (22q11.23). Using previously published genomic coordinates (Durkin and Glover, 2007; Kumar et al., 2019), we found that 32.5% of recurrent CNAs in RMC tissues were in chromosomal fragile sites (Table S2), suggesting that these alterations are not randomly distributed across the genome. To investigate the biological role of the recurrent focal CNAs found in RMC (Table S2), we performed gene ontology (GO) analysis, which revealed that genes within the recurrent focal CNAs were enriched for GO terms (Figure 2F) related to histone deacetylation ($p < 0.001$), lipid metabolism and biosynthesis ($p = 0.024$), response to ammonium ions and acetylcholine ($p = 0.024$), DNA transcription ($p = 0.028$), and cytoskeleton-dependent cytokinesis ($p = 0.031$).

The most common focal deletion in both RMC and rhabdoid tumors was in the *SMARCB1* locus 22q11.23 found in 9 of 15

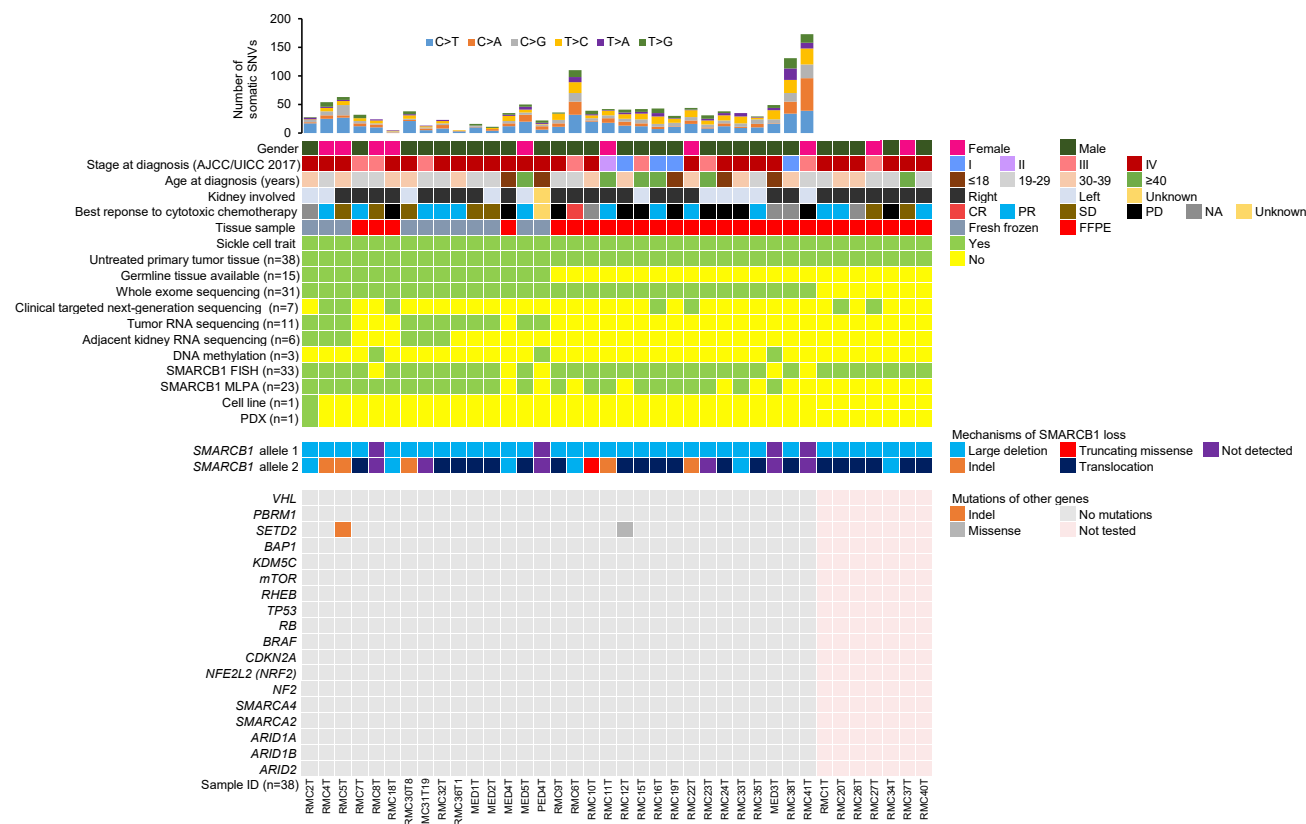


Figure 1. Somatic Genomic Alterations in RMC

Oncoplot showing the clinical characteristics, assays used, and the number and types of somatic single-nucleotide variations (SNVs), as well as selected genomic alterations detected in renal medullary carcinoma (RMC) samples. Each column represents a different patient. CR, complete response with long-term remission following perioperative chemotherapy and nephrectomy; FFPE, formalin-fixed, paraffin-embedded; PR, partial response by the Response Evaluation Criteria in Solid Tumors (RECIST) 1.1; SD, stable disease by RECIST 1.1; PD, progressive disease by RECIST 1.1; PDX, patient-derived xenograft. See also Figure S1 and Table S1.

(60%) RMC tumors and in 28 of 35 (80%) rhabdoid tumors. In contrast to RMC, focal amplifications were rare in rhabdoid tumors (Figure 2E) and none were found in more than 15% of rhabdoid tumors. The most common focal amplification, found in 15 (60%) RMC tumors, was in the 11q14.3 region (Table S2). Furthermore, we found amplification of *NOTCH2* in 6 of 15 (40%) RMC tumors, with 4 of 15 (26.7%) demonstrating concurrent deletion of *NOTCH1* and *NOTCH3* and amplification of *NOTCH2*, a distinct pattern also found in the basal subtype of bladder urothelial carcinoma (BLCA) and associated with increased cell-cycle progression and epithelial-mesenchymal transition (EMT) (Hayashi et al., 2016). Our transcriptomic analysis (see below) further revealed significant upregulation of genes associated with the Notch pathway in RMC compared with adjacent normal kidney (Figure S3A) and kidney MRT (Figure S3B). By integrating our genomic and RNA-seq data, we identified 341 genes (Table S2) in areas of recurrent focal copy-number gain or loss that were significantly ($FDR < 0.1$) upregulated or downregulated, respectively, in RMC tumors compared with adjacent normal kidney. The reliability of our CNA analyses of WES data was confirmed in sample MED1T by array CGH (Figure 3A), which detected the presence of the

focal amplification on chromosome 2p, large amplification of chromosome 8, monosomy of chromosomes 4 and 22, large deletions of chromosomes 15 and 16, and a focal deletion of chromosome 17p13.1 (*TP53* gene region), which were also found by WES (Figure S2).

Structural alterations such as recurrent loss of chromosome 22 (Figure 2B) and focal deletions of the *SMARCB1* locus 22q11.23 (Figure 2D) were far more common than *SMARCB1* SNVs (Figure 1). To further elucidate the molecular events leading to *SMARCB1* loss in RMC, we employed a combination of fluorescence *in situ* hybridization (FISH), exome DNA sequencing (WES and targeted sequencing), and multiplex ligation-dependent probe amplification (MLPA) in untreated primary RMC tumor samples (Figures 1, 3B, 3C, and 3D; Table S3). Using this comprehensive approach, we identified a genetic *SMARCB1* loss in 32 of 38 (84.2%) patients with RMC (Figure 1). The most common molecular alteration, noted in 20 of 38 cases (52.6%), was inactivating translocation of one *SMARCB1* allele and deletion of the second allele. Less frequent were deletion of both *SMARCB1* alleles (6 of 38 patients; 15.8%), deletion of one *SMARCB1* allele and inDel of the second *SMARCB1* allele (5 of 38 patients; 13.2%), and deletion of one *SMARCB1* allele

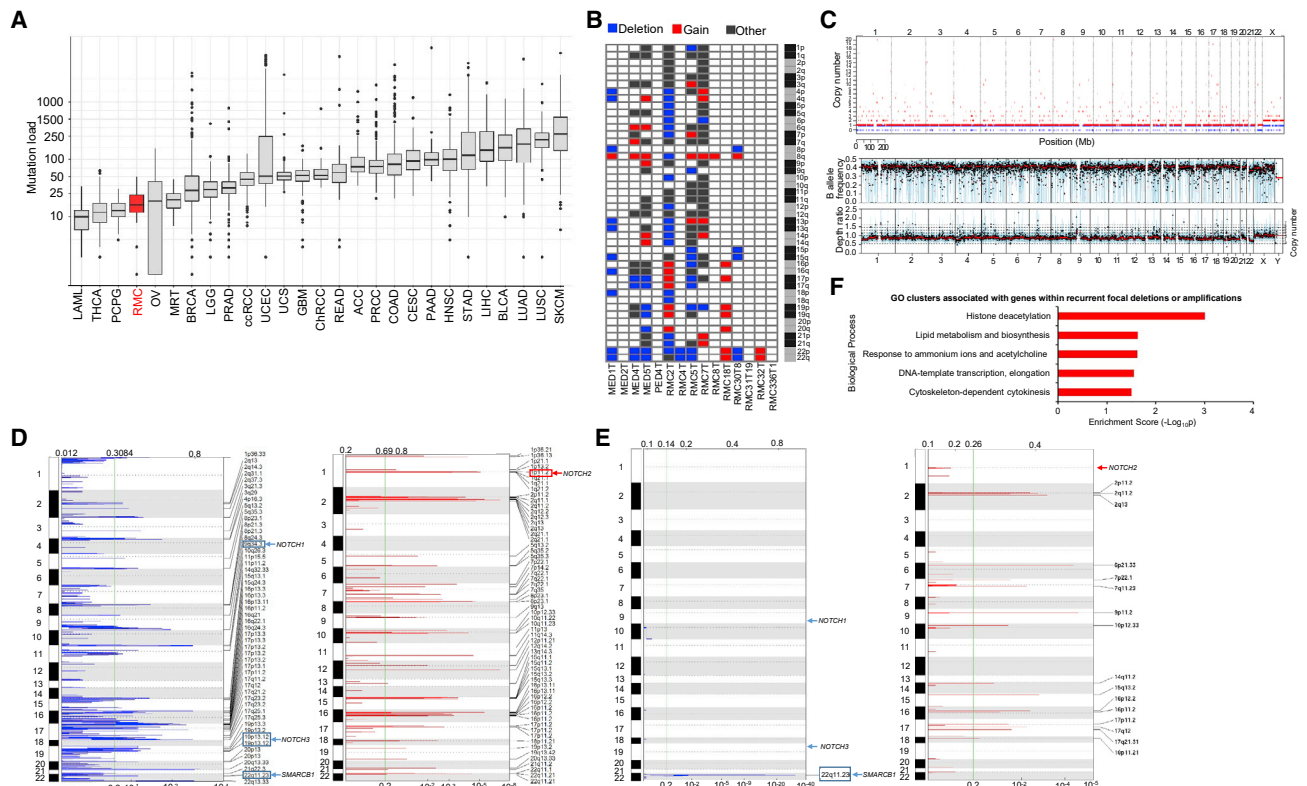


Figure 2. Mutational and Copy-Number Landscape of RMC

(A) Tukey box plots of non-synonymous mutation load per genome for different tumor types. Tumor types are ordered by their median mutation load. RMC samples are highlighted in red. For each box plot, the central rectangle spans the interquartile range (IQR), the segment within the rectangle shows the median, and the upper and lower whiskers respectively extend the upper and lower hinges of the rectangle by $1.5 \times$ IQR. Black dots represent outliers outside $1.5 \times$ IQR from each hinge. Abbreviations are detailed in STAR Methods.

(B) Arm-level copy-number alterations in untreated primary RMC tumors. Blue corresponds to loss of one copy, red corresponds to a gain, and dark gray corresponds to more complex alterations shown in detail in Figure S2.

(C) Genome plot of RMC4T. In the bottom two panels, the thick black line indicates the median value, blue bars indicate the IQR, and red lines indicate segmented values. Loss of heterozygosity is noted on chromosome 22 encompassing the *SMARCB1* locus.

(D and E) Regions of focal deletion (left) and amplification (right) identified by GISTIC analysis in untreated primary RMC (D) and rhabdoid (E) tumors. G scores (top x axis) and q values (bottom x axis) are shown. Regions with q values of less than 0.20 (as delineated by the vertical green line) are considered to be significantly aberrant. Only focal copy-number alterations (shorter than half the length of a chromosome arm) are shown.

(F) Gene ontology (GO) analysis of genes within regions of recurrent copy-number alterations in RMC.

See also Figures S1–S3 and Table S2.

and truncating nonsense mutation of the second *SMARCB1* allele (1 of 38 patients; 2.6%). These results are consistent with two previous studies in a total of 25 patients with RMC that found *SMARCB1* to be inactivated via translocation combined with hemizygous deletion in 15 of 25 (60%) cases and by homozygous deletions in 7 of 25 (28%) cases (Calderaro et al., 2016; Carlo et al., 2017; Jia et al., 2019). In addition, we determined that this pattern for *SMARCB1* inactivation (inactivating translocation combined with hemizygous deletion) occurred not only in primary tumors but also in lymph node and liver metastases of patients RMC38 and RMC32, respectively. Sanger sequencing confirmed that both the primary kidney tumor and the liver metastasis of patient RMC32 harbored the same translocation between the *SMARCB1* and *MYOM1* genes (Figures 3E and 3F). We performed DNA methylation analysis in three out of the four RMC samples that had no detectable genetic *SMARCB1*

loss (Figure 1) and found no evidence of increased methylation in and around the *SMARCB1* promoter (Table S3). Of note, due to lack of available tissue, these four RMC samples did not undergo multiplatform interrogation by all three assays (WES, FISH, and MLPA), and a potential genetic cause of *SMARCB1* loss may thus have been missed.

RNA-seq (see below) of five samples (RMC32T, RMC36T1, MED1T, MED2T, and MED5T) that harbored inactivating translocations identified *SMARCB1* fusion transcripts in two of the five cases (RMC32T and MED1T) as shown in Figure 3E. Both of the *SMARCB1* fusion products are predicted to be functionally inactive, as they lack all of the known protein interaction domains of this member of the SWI/SNF complex (Figure 3G). Additionally, we interrogated our RNA-seq data for evidence of infection by oncogenic human viruses (for a complete list, see STAR Methods) and detected no viral genomes in any RMC samples,

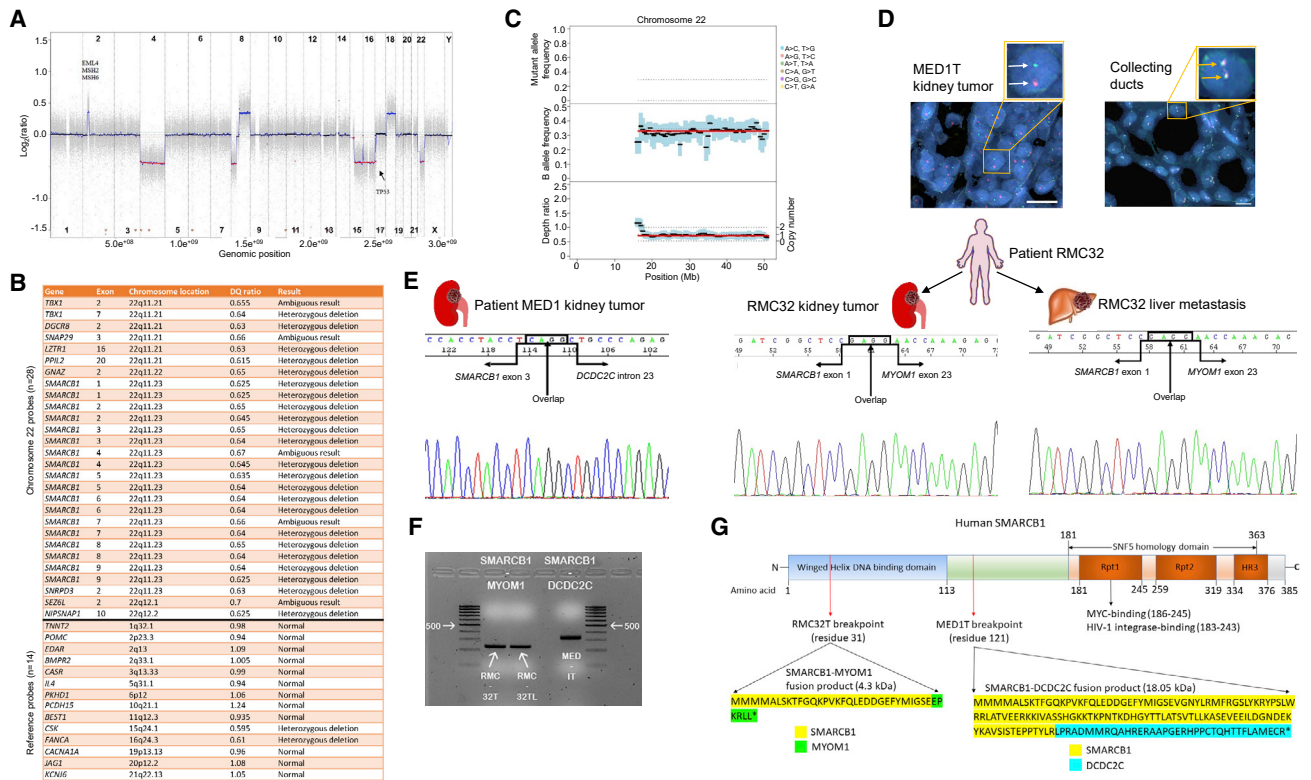


Figure 3. Integrative Characterization of the Mechanisms of SMARCB1 Loss

(A) Array CGH profile of MED1T.
 (B) MLPA analysis of MED1T confirmed the heterozygous deletion present around the *SMARCB1* locus. The heterozygous deletions noted on chromosomes 15 and 16 (CSK and *FANCA* probes, respectively) were also detected in the WES analysis (Figure S2).
 (C) WES chromosome 22 monosomy plot showing chromosome 22 monosomy in sample MED1T. In the bottom two panels, the thick black line indicates the median value, blue bars indicate the IQR, and red lines indicate segmented values.
 (D) Break-apart FISH of MED1T confirmed the presence of chromosome 22 monosomy and revealed the presence of a disruptive translocation around the *SMARCB1* locus as shown by the separation of the green and orange probes (white arrows) seen inside RMC tumor cells (left image). Two yellow fusion signals (yellow arrows) representing two intact *SMARCB1* alleles are noted within the nuclei of normal kidney cells (right image). Scale bars, 10 μ m.
 (E) Sanger sequencing confirmation of the fusion RNA product between exon 3 of *SMARCB1* and intron 23 of *DCDC2* in the MED1T sample (untreated primary tumor) and of the fusion RNA product exon 1 of *SMARCB1* and exon 23 of *MYOM1* on both untreated primary tumor (RMC32T) and untreated liver metastasis (RMC32TL) from patient RMC32.
 (F) Agarose gel electrophoresis of the *SMARCB1* fusion products using cDNA from samples RMC32T, RMC32TL, and MED1T.
 (G) Predicted amino acid sequences of the *SMARCB1*-*DCDC2C* fusion product in patient MED1 and of the *SMARCB1*-*MYOM1* fusion product in patient RMC32. See also Table S3.

indicating that viral genomic integration did not contribute to RMC pathogenesis.

Transcriptomic Signature Distinguishes RMC from Other Renal Malignancies

We compared the protein-coding and long non-coding RNA (lncRNA) gene expression profiles of 11 untreated primary RMC tumors with those of other malignancies arising in or near the renal medulla: collecting duct carcinoma (CDC) and upper tract urothelial carcinoma (UTUC). As shown in the heatmap in Figure 4A, RMC harbored a distinct signature that clustered more closely to CDC than to UTUC (Figures 4A and S3C). The RMC36T1 sample that clustered within the CDC samples in our unsupervised analysis of protein-coding gene expression (Figure 4A) was confirmed to be RMC, as the patient had sickle cell trait by hemoglobin electrophoresis (Figure 1) and the tumor

was negative for *SMARCB1* by IHC (Figure S1A). Additional comparisons with other cancers arising from the kidney (Figures 4B and S3D) again confirmed that RMC is most closely related to CDC and is clearly distinct from kidney MRT, the second most common *SMARCB1*-deficient malignancy arising from the kidney. Notably, all five renal cell carcinomas formed a separate cluster from kidney MRT (Figures 4B and S3D), consistent with the distinct morphological appearance of kidney MRT from carcinomas (Pawel, 2018).

The distinct gene expression profiles of RMC compared with kidney MRT, despite their common renal origin and shared etiology of *SMARCB1* inactivation, led us to explore the nephron site of origin of these malignancies. Using an external gene expression dataset of normal tissue microdissected from various nephron regions (Cheval et al., 2012), the gene expression profiles of RMC, CDC, clear cell renal cell carcinoma (ccRCC),

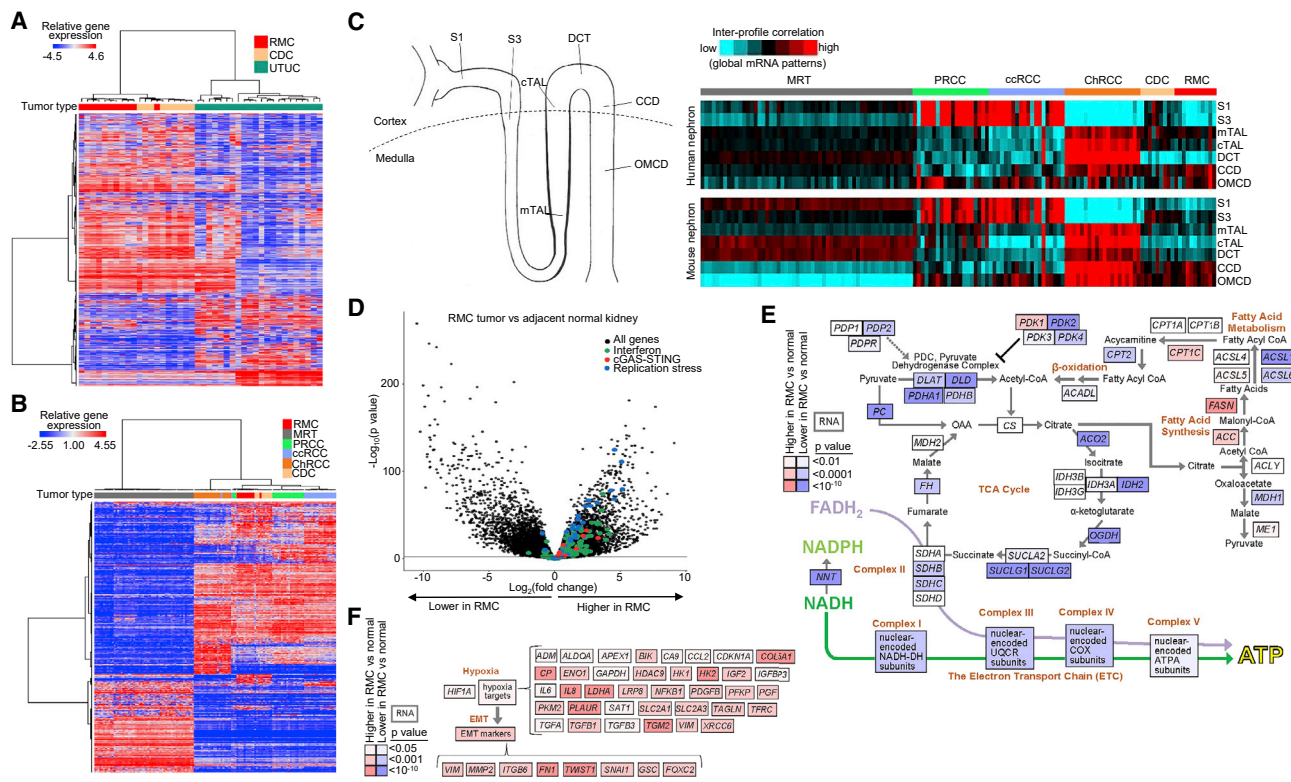


Figure 4. Transcriptomic Signature Distinguishes RMC from Other Renal Malignancies

(A) Unsupervised hierarchical clustering of protein-coding gene expression from RMC, CDC, and UTUC. (B) Unsupervised hierarchical clustering of protein-coding gene expression from kidney malignancies. (C) A cartoon of the nephron regions (left; the dashed line separates the renal cortex from the medulla) and heatmaps (right) showing intersample correlations (Pearson's r) between expression profiles of kidney malignancies (arranged by subtype) and expression profiles of kidney nephron sites. S1 and S3, initial and terminal portions of the proximal tubule; mTAL, medullary thick ascending limb of Henle's loop; cTAL, cortical thick ascending limb of Henle's loop; DCT, distal convoluted tubule; CCD, cortical collecting duct; OMCD, outer medullary collecting duct. (D) Volcano plot showing the differential expression of genes involved in replication stress and innate immunity (interferon signaling and cGAS-STING pathways). The secondary horizontal line corresponds to a p value of 0.01. (E and F) Pathway diagrams representing differential expression patterns in core metabolic pathways (E) as well as hypoxia-induced genes and EMT (F) between RMC tissues and adjacent normal kidney. See also [Figures S3 and S4](#); [Tables S2 and S4](#).

papillary renal cell carcinoma (PRCC), chromophobe renal cell carcinoma (ChRCC), and kidney MRT were globally compared by supervised analysis with that of each sample in the nephron atlas ([Figure 4C](#)). RMC mRNA expression demonstrates a high degree of correlation with the collecting duct, which is also the putative site of origin for CDC, whereas there was no correlation between the transcriptome of kidney MRT and the collecting duct, suggesting that RMC and kidney MRT have a different origin in the nephron ([Figure 4C](#)). As expected ([Young et al., 2018](#)), the transcriptomes of ccRCC and PRCC indicate an origin from more proximal (cortical) regions of the nephron.

[Table S4](#) lists the protein-coding genes differentially expressed between untreated primary RMC tumor samples ($n = 11$ cases) and adjacent control kidney ($n = 6$ cases). We noted that genes associated with replication stress and innate immune responses were predominantly upregulated in RMC compared with normal kidney ([Figure 4D](#)). This was confirmed by GSEA analysis, which revealed that biological pathways upregulated in untreated primary RMC compared with adjacent normal kid-

ney were enriched for genes involved in inflammatory/immune responses, DNA repair, and c-MYC signaling ([Figure S3E](#)). Several metabolic pathways were downregulated in RMC ([Figure S3E](#)), and [Figure 4E](#) shows a metabolic pathway diagram of the individual genes altered in RMC compared with adjacent normal kidney. Genes related to the tricarboxylic acid (TCA) cycle and oxidative phosphorylation were decreased in RMC, whereas genes involved in fatty acid synthesis were increased. Interestingly, given the hypoxic nature of the renal medulla, RMC displayed increased expression of genes associated with hypoxia and hypoxia-induced EMT ([Figure 4F](#)). RMC and CDC demonstrated similar core metabolic and hypoxia-associated gene expression patterns ([Figures S4A and S4B](#)). Conversely, when comparing RMC with MRT, genes related to the TCA cycle and fatty acid synthesis were upregulated in RMC, whereas genes involved in oxidative phosphorylation were downregulated in RMC ([Figures S4C and S4D](#)).

In addition to protein-coding genes, we identified lncRNAs differentially expressed between RMC and normal kidney

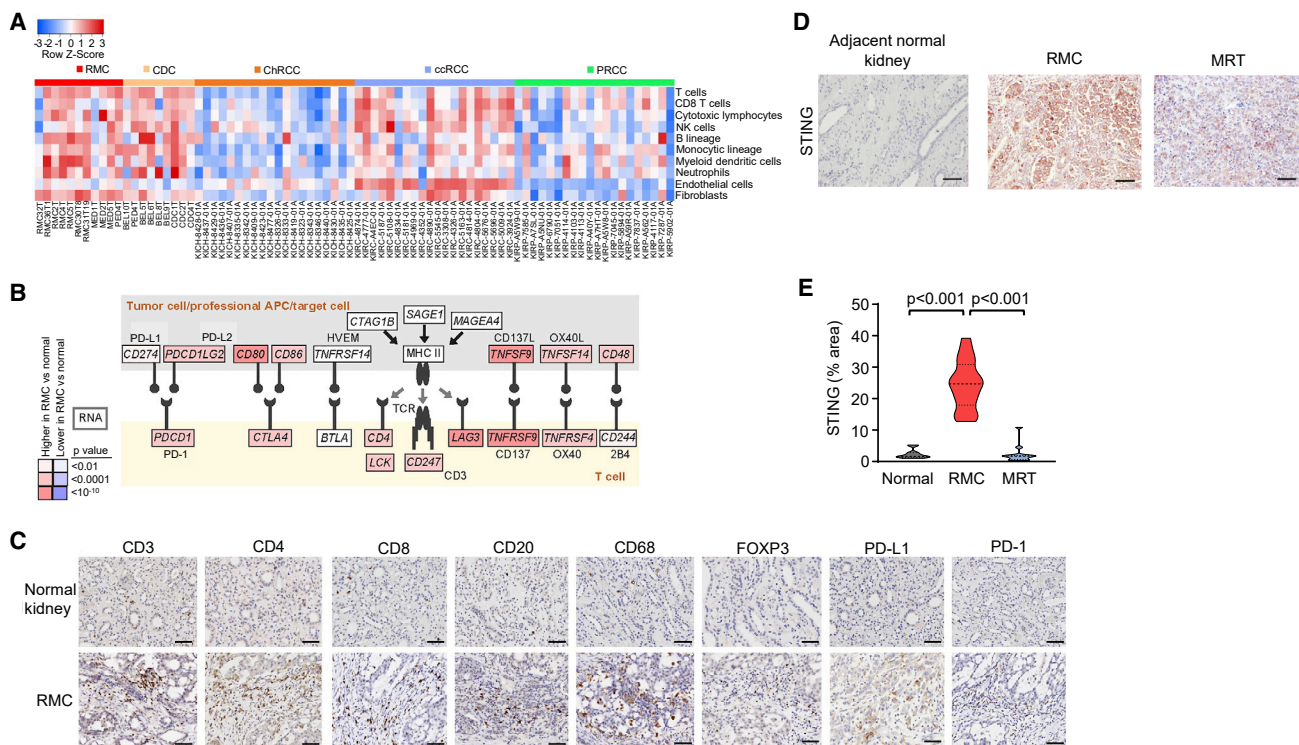


Figure 5. RMC Has a Distinct Immune Profile

(A) MCP counter estimates of infiltrating immune and stromal cells in RMC compared with other carcinomas of the kidney. (B) Immune checkpoint pathway diagram showcasing the interactions of T cells with tumor cells and professional antigen-presenting cells based on the differential RNA expression patterns between RMC tumors and adjacent normal kidney tissues. (C) Representative immunohistochemistry (IHC) microphotographs for CD3, CD4, CD8, CD20, CD68, FOXP3, PD-L1, and PD-1 in RMC tumor tissues and adjacent normal collecting tubules. Scale bars, 50 μ m. (D) Representative IHC microphotographs for STING in RMC tumor tissues, adjacent normal collecting tubules, and MRT tumor tissues. Scale bars, 50 μ m. (E) Violin plots of the IHC quantification levels for STING in RMC tumor tissues (n = 20), adjacent normal kidney (n = 12), and MRT tumor tissues (n = 12). The width of each violin plot is proportional to the density of observed data points in each region. Dashed and dotted lines correspond to the median and interquartile values, respectively. The upper and lower lines correspond to the highest and lowest observed values, respectively. See also [Figure S5](#); [Tables S4](#) and [S5](#).

([Figure S4E](#) and [Table S4](#)). The highest upregulated lncRNA was *urothelial cancer associated 1 (UCA1)*, which showed a 305-fold increase in RMC tumors. *UCA1* is also dramatically upregulated in urothelial carcinoma and was previously considered to be highly specific for urothelial carcinoma ([Wang et al., 2006](#)). *UCA1* levels in RMC tumors were similar to those in UTUC and significantly higher than in CDC or other carcinomas of the kidney ([Figure S4F](#)). Four other lncRNAs previously shown to be associated with cancer ([Arun et al., 2018](#)) were upregulated in RMC: *GAS5*, *HOTAIR*, *PVT1*, and *H19*. There was no copy-number gain noted at the genomic loci of the five cancer-associated lncRNAs upregulated in RMC ([Table S2](#)).

RMC Has a Distinct Immune Profile

The inflammatory/immune response gene expression signature of RMC led us to next characterize the immune cell infiltration of these tumors. Deconvolution of tissue-infiltrating immune and stromal populations revealed that RMC harbored an abundance of fibroblasts ([Figure 5A](#) and [Table S5](#)), consistent with the prominent stromal desmoplasia that is characteristic of this tumor ([Gupta et al., 2012](#)). Notably, the abundance of stromal

cells in the tumor microenvironment of RMC was similar to that of CDC and very distinct from kidney MRT ([Figure S5A](#)). RMC had a paucity of endothelial cells relative to ccRCC ([Figure 5A](#)), consistent with the prominent angiogenesis induced by von Hippel-Lindau loss in ccRCC ([Choueiri and Motzer, 2017](#)).

RMC contains a similarly high number of T cells and cytotoxic lymphocytes compared with those of ccRCC ([Figure 5A](#)), a kidney malignancy known to be susceptible to immune-checkpoint therapies ([Choueiri and Motzer, 2017](#)). However, in contrast to ccRCC, RMC tumors harbor an abundance of myeloid dendritic cells, neutrophils, and B lineage cells ([Figure 5A](#)). Immune suppression can involve multiple immune checkpoints, many of which were found to be upregulated in RMC tissues, which showed increased expression of immune-checkpoint receptors such as PD-1, CTLA-4, and LAG3 ([Figure 5B](#)). We validated these transcriptomic findings by IHC, which confirmed that RMC tissues contain high levels of CD3⁺ T cell lymphocytes, CD4⁺ helper T cells, CD8⁺ cytotoxic T cells, FOXP3⁺ regulatory T cells, CD68⁺ macrophages, CD20⁺ B cell lymphocytes, and the PD-1 immune checkpoint, whereas the staining pattern of the PD-L1 immune checkpoint was heterogeneous with some

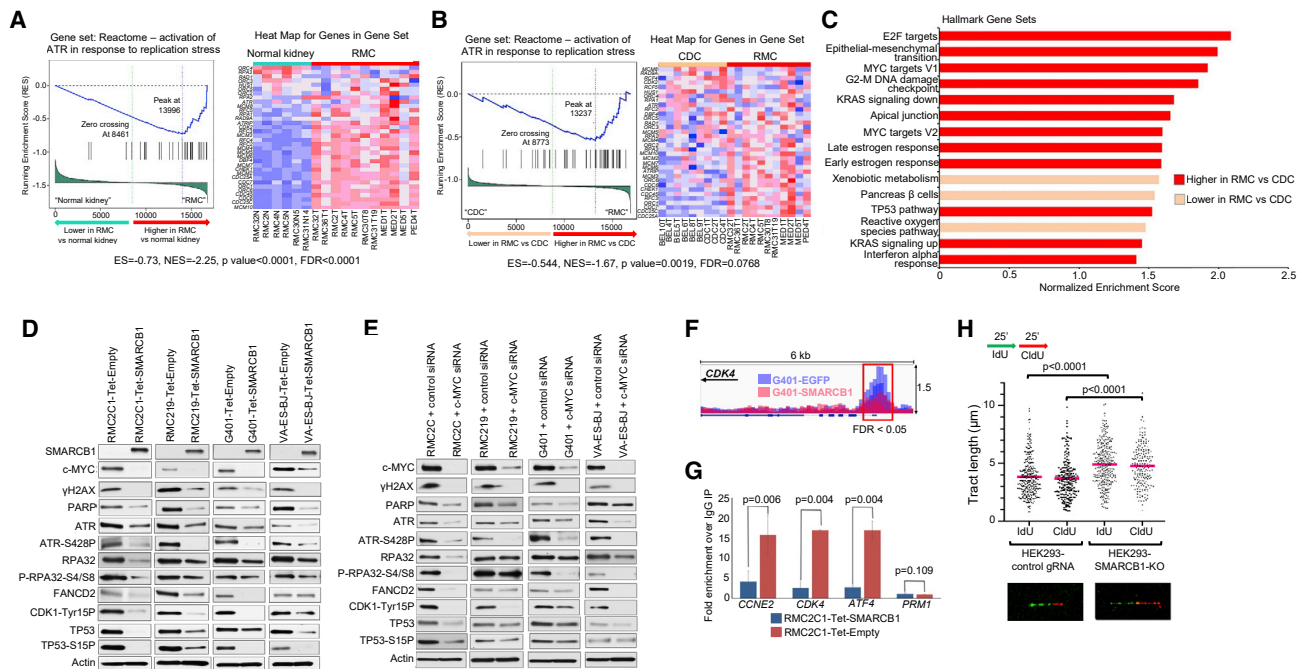


Figure 6. SMARCB1 Loss Promotes MYC-Induced Replication Stress

(A and B) GSEA revealed a significant enrichment for the ATR DNA-damage repair pathway in response to replication stress in RMC compared with (A) adjacent normal kidney tissues or (B) CDC. ES, enrichment score; NES, normalized enrichment score; FDR, false discovery rate.

(C) Hallmark pathways significantly altered (FDR < 0.1) between RMC and CDC by GSEA analysis.

(D and E) Western blots of replication stress and DNA-damage response pathways following SMARCB1 rescue (D) or direct small interfering RNA (siRNA) inhibition of c-MYC (E) in RMC2C, RMC219, and other SMARCB1-negative cell lines (G401 and VA-ES-BJ).

(F) c-MYC peak differences on the promoter site (boxed in red) of the *CDK4* gene in G401 MRT cells re-expressing SMARCB1 or EGFP control. The y axis represents ChIP-seq read counts normalized to 1 million mapped reads.

(G) Fold enrichment in c-MYC relative to negative control (normal rabbit immunoglobulin G) and normalized with input DNA in RMC2C cells following re-expression of SMARCB1 or empty vector control. *CCNE2*, *CDK4*, and *ATF4* are established c-MYC transcriptional targets, whereas *PRM1* is a spermatogenesis-specific gene that is not regulated by c-MYC and serves as negative control. The values are expressed as mean fold change \pm SEM from triplicates.

(H) Dot plot of DNA fiber tract lengths indicating a replication speed of \sim 0.39 kb/min in HEK293-control guide RNA cells compared with \sim 0.51 kb/min in SMARCB1 knockout cells. Bars (pink) represent the mean of replication tracts (n = 187–291, from biological replicates). Top: experimental labeling scheme. Bottom: representative fibers (original magnification \times 40).

See also Figures S6 and S7; Tables S4 and S6.

RMC tumors demonstrating increased PD-L1 expression on both tumor cells and surrounding immune cells (Figures 5C, S5B, S5C, and S5D; Table S5).

Focal CNAs such as deletions, duplications, and translocations are associated with increased cytosolic DNA leakage, leading to upregulation of the cyclic GMP-AMP synthase stimulator of interferon genes (cGAS-STING) cytosolic double-stranded DNA-sensing antiviral innate immune pathway (Bakhom et al., 2018; Tijhuis et al., 2019). Accordingly, in regard to the differential gene expression between RMC and normal kidney (Table S4), we noted upregulation of the *MB21D1* gene encoding cGAS (8.84-fold increase, FDR < 0.001) and the *TMEM173* gene encoding STING (3.2-fold increase, FDR < 0.001), with associated enrichment for pathways related to cytosolic DNA sensing and innate immunity (Figures S5E and S5F). CDC also harbors multiple recurrent CNAs (Becker et al., 2013) and demonstrated similar levels of cGAS and STING gene expression (Table S4). Furthermore, when compared with kidney MRT, a much more chromosomally stable disease (Figures 2E and S1E), RMC expressed significantly higher STING mRNA

levels (4.2-fold increase, FDR < 0.001) and enrichment for cytosolic DNA sensing and innate immune pathways (Figures S5E and S5F). IHC confirmed the substantially higher presence of cytoplasmic STING in RMC compared with adjacent normal kidney and kidney MRT tissues (Figures 5D and 5E).

DNA Replication Stress Is a Hallmark of RMC

SMARCB1 in the SWI/SNF complex is known to antagonize c-MYC function by directly interacting with c-MYC target gene promoters (Stojanova et al., 2016; Weissmiller et al., 2019). Our GSEA analysis (Figure S3E) revealed that SMARCB1-deficient RMC tissues showed enrichment for multiple hallmark pathways associated with cell-cycle progression and DNA replication and repair, including the G2-M checkpoint, c-MYC and E2F target genes, and TP53 and DNA repair pathways, consistent with these tumors having a replication stress phenotype (Zhang et al., 2016). Furthermore, RMC tumors exhibited enrichment for expression of genes upregulated in response to activation of the ATR (ataxia telangiectasia- and Rad3-related) DNA-damage repair pathway triggered by replication stress (Figure 6A).

Kidney MRT tumors demonstrate a similar signature for MYC-induced replication stress and DNA-damage repair (Figures S6A–S6C). Furthermore, we found that gene sets associated with MYC-induced replication stress were upregulated in RMC (SMARCB1-negative) compared with CDC (SMARCB1-positive) tumors (Table S4; Figures 6B, 6C, and S6D). The c-MYC gene is located on chromosome 8q, which we found to be gained in almost half of RMC tumors (Figures 2B and S2), with associated upregulation of MYC and other established regulators of the oncogenic MYC network such as PVT1 (Tseng et al., 2014) and ATAD2 (Ciro et al., 2009) (Table S2).

In the mutational landscape of RMC, we noted that the most common substitutions in most RMC tumors were C>T transitions (Figure 1), which are linked to the process of cytosine deamination often associated with age or DNA replication stress (Cescon and Haibe-Kains, 2016). However, patient age did not strongly correlate with the number of C>T mutations (Spearman rank correlation = 0.395, $p = 0.145$), suggesting that they are instead caused by replication stress in the setting of high cell turnover. Furthermore, the predominant mutational signature pattern in RMC tumors was Signature 1 (Figure S1C), which consists mainly of C>T transitions at CpG dinucleotide motifs and is known to be associated with age and/or high number of mitoses (Alexandrov et al., 2015). Again, however, there was no correlation between patient age and Signature 1 in our RMC samples (Spearman rank correlation = 0.167, $p = 0.568$). Thus, the genomic profile of RMC demonstrates mutational patterns compatible with replication stress.

SMARCB1 Loss Promotes MYC-Induced Replication Stress

To perform *in vitro* functional experiments, we generated a new cell line (RMC2C) from the untreated primary tumor sample (RMC2T) of a male patient with RMC. The cell line grew in adherent monoculture (Figure S6E) with a doubling time of 32 h for >40 passages. Spectral karyotyping (SKY) for this cell line revealed multiple CNAs as shown in Figure S6F. The near-tetraploid karyotype of RMC2C was not observed in the original RMC2T tumor (Figure S2). FISH demonstrated that both RMC2C and RMC2T harbored centromeric deletions of both SMARCB1 alleles and no inactivating translocations (Table S3). MLPA confirmed the absence of the SMARCB1 gene in RMC2C cells (Figure S6G). We additionally used a previously established RMC cell line (RMC219) (Dong et al., 2017), which is also negative for inactivating SMARCB1 translocations and harbors centromeric deletions of both SMARCB1 alleles (Table S3 and Figure S6H). Karyotyping revealed loss of one copy of chromosome 22 and gain of one copy of chromosome 8, as well as gain of two more 8q copies via two der(7)t(7q; 8q) derivative chromosomes (Figure S6I). Table S6 lists all RMC2C and RMC219 mutations detected by WES. From these cell lines, we also generated tet-inducible rescue lines capable of re-expressing SMARCB1 at near-endogenous levels (Figure S6J) and showed that exogenous SMARCB1 was incorporated into SWI/SNF complexes (Figure S7A).

As shown using our two RMC cell lines and two other SMARCB1-negative cell lines (MRT line G401 and epithelioid sarcoma line VA-ES-BJ) in Figure 6D, high c-MYC levels correlated with expression of the DNA-damage marker γ H2AX,

expression of DNA-damage repair enzymes poly(ADP-ribose) polymerase (PARP) and ATR, ATR activation via phosphorylation at serine 428, upregulation and phosphorylation at serines 4 and 8 of the RPA32 subunit of human replication protein A (a marker of DNA-damage response [DDR]), upregulation of FANCD2 (which protects cells from replication stress), and phosphorylation of CDK1 at tyrosine 15 (which regulates the G2-M checkpoint), as well as phosphorylation of TP53 at serine 15, a marker specific to DDR and not to other stimuli such as hyperproliferation (Loughery et al., 2014). Re-expression of SMARCB1 in all four lines decreased c-MYC activity and the resulting replication stress (Figure 6D). Similarly to rescue of SMARCB1, direct inhibition of c-MYC also reversed the replication stress cascade in these cells (Figure 6E). Conversely, SMARCB1 knockout by CRISPR/Cas9 in human embryonic kidney (HEK-293FT) cells increased c-MYC and the resulting replication stress (Figures S7B and S7C). Figure S7D demonstrates the significant downregulation of γ H2AX in the nuclei of RMC2C and RMC219 cells following rescue of SMARCB1.

We interrogated previously published chromatin immunoprecipitation sequencing (ChIP-seq) data of c-MYC (Weissmiller et al., 2019) and found that tet-inducible re-expression of SMARCB1 in G401 MRT cells resulted in a significant decrease (FDR < 0.05) of peaks at the promoter regions of genes associated with replication stress (Figures 6F and S7E). SMARCB1-negative G401 cells showed c-MYC enrichment at the promoter regions of genes associated with multiple hallmark pathways related to cell-cycle progression and DNA replication and repair (Figure S7F). Similarly, we found that SMARCB1 re-expression in our RMC2C cells resulted in significant decrease of c-MYC enrichment at the promoters of genes associated with cell-cycle progression and DNA replication (Figure 6G). We performed DNA fiber assays to directly explore the effect of SMARCB1 loss on DNA replication fork dynamics. SMARCB1 knockout significantly accelerated replication fork progression (Figure 6H), an established general mechanism of replication stress and associated DDR (Maya-Mendoza et al., 2018). Collectively, our findings suggest that SMARCB1 loss increases c-MYC binding to the promoters of downstream genes associated with DNA replication and cell-cycle progression, and induces replication stress by increasing the speed of replication fork progression with resultant upregulation of DDR pathways.

RMC Is Vulnerable to Drugs Targeting Replication Stress *In Vitro* and *In Vivo*

Tumors with high levels of replication stress depend on intact DDR pathways for survival (Zhang et al., 2016). We reasoned that as a result of this dependence, SMARCB1-negative tumors such as RMC would be vulnerable to direct targeting of DDR pathways such as the PARP and ATR pathways, or to targeting of cell-cycle regulators such as the WEE1 kinase, which suppresses replication stress (Beck et al., 2010). We first queried the Genomics of Drug Sensitivity in Cancer database (release 7.0) (Yang et al., 2013) and found that the PARP inhibitor olaparib, clinically approved for use in breast and ovarian cancer, induces a more potent antiproliferative response in the SMARCB1-negative MRT cell line G401 than that seen in BRCA1-mutant cell lines such as HCC1395 and HCC1937 or most other breast and ovarian cancer cell lines (Table S7).

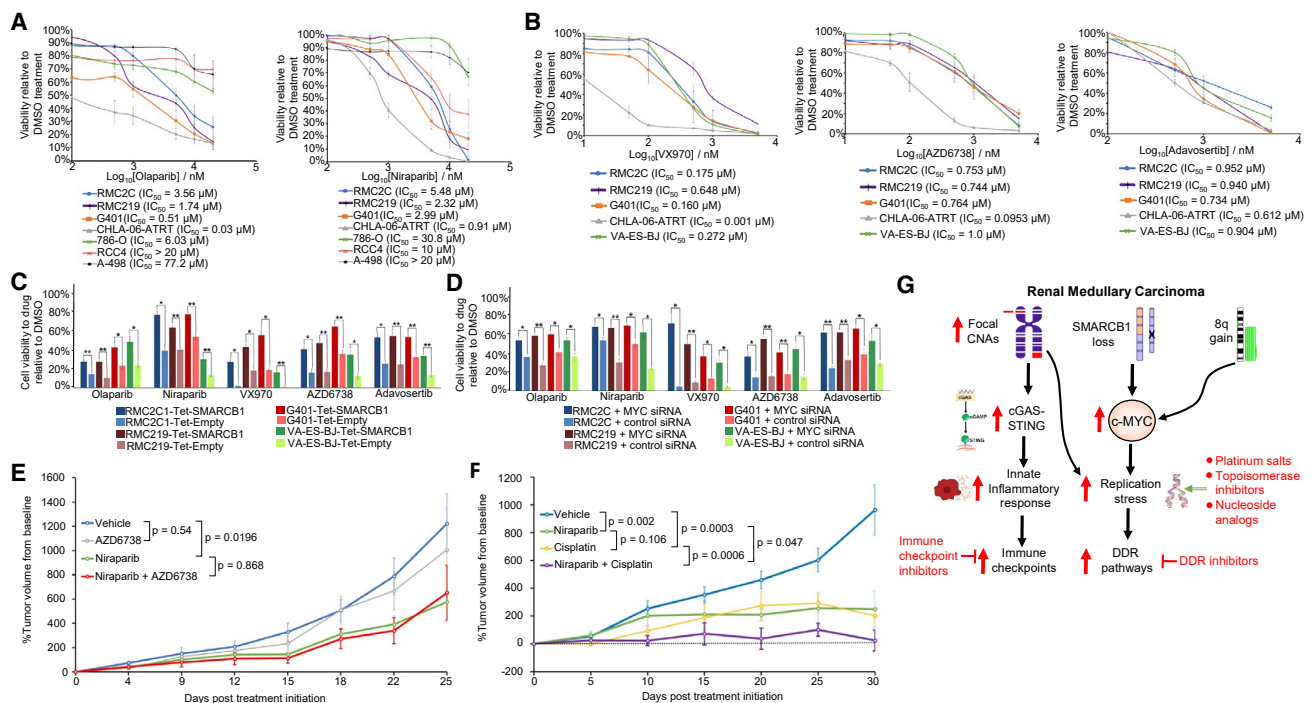


Figure 7. RMC is Vulnerable to Drugs Targeting Replication Stress *In Vitro* and *In Vivo*
 (A) Viability curves and half-maximal inhibitory concentrations (IC_{50}) of SMARCB1-negative (RMC2C, RMC219, G401, CHLA-06-ATRT) and SMARCB1-positive (786-O, RCC4, A-498) cell lines after 120-h exposure to the PARP inhibitors olaparib and niraparib.
 (B) Viability curves and IC_{50} of SMARCB1-negative cell lines after exposure to the ATR inhibitors VX970 and AZD6738 and to the WEE1 inhibitor adavosertib.
 (C and D) Viability of RMC2C, RMC219, G401, and VA-ES-BJ cells expressing doxycycline-induced SMARCB1 or empty vector control (C) or treated with siRNA against c-MYC or sham control (D) followed by 120-h exposure to olaparib (10 μ M), niraparib (10 μ M), VX970 (1 μ M), AZD6738 (1 μ M), or adavosertib (1 μ M). * $p < 0.05$, ** $p < 0.01$ by unpaired two-tailed Welch's t test.
 (E) *In vivo* antitumor effect of niraparib, AZD6738, and their combination in the RMC2X PDX mouse model ($n = 5$ mice/group). Plots represent mean percentage tumor volume change from baseline \pm SEM.
 (F) *In vivo* antitumor effect of cisplatin alone or in combination with niraparib in RMC tumors ($n = 10$ mice/group). Plots represent mean percentage tumor volume change from baseline \pm SEM.
 (G) Schematic model of the interplay between SMARCB1 loss and CNAs in inducing replication stress and inflammatory responses in RMC. Loss of SMARCB1 and gain of 8q promote MYC-induced replication stress, which renders RMC cells susceptible to DNA-damaging agents such as platinum salts, topoisomerase inhibitors, and nucleoside analogs. DNA-damage repair (DDR) pathways induced by replication stress can be directly targeted by DDR inhibitors. The inflammatory responses activated via cGAS-STING signaling in RMC upregulate immune checkpoints that can be therapeutically targeted.
 All results in (A) to (D) are presented as means \pm SEM from triplicates. See also Figure S7 and Table S7.

Subsequently, we confirmed *in vitro* using two separate PARP inhibitors (olaparib and niraparib) that, compared with three SMARCB1-positive renal cell carcinoma cell lines, SMARCB1-negative cell lines are sensitive to targeting of the PARP pathway (Figure 7A). We also found that SMARCB1-negative cell lines are sensitive to the ATR inhibitors VX970 and AZD6738 and to the WEE1 inhibitor adavosertib (Figure 7B). Rescuing of SMARCB1 or directly inhibiting c-MYC reversed the sensitivity of SMARCB1-negative cells to PARP, ATR, and WEE1 inhibitors (Figures 7C and 7D). Collectively, these data demonstrate that SMARCB1 loss sensitizes cancer cells to pharmacologic perturbation of the DDR and cell-cycle checkpoint pathways. Sensitivity to platinum salts such as cisplatin and carboplatin, DNA synthesis inhibitors such as gemcitabine, and topoisomerase inhibitors such as doxorubicin represent a hallmark of tumors with high levels of replication stress because these drugs can induce or augment DNA damage, which can overwhelm DDR pathways and thus lead to insurmountable genomic instability and cell

death (Zhang et al., 2016). We accordingly found that the sensitivity of RMC cell lines to these agents is significantly reduced by either rescuing of SMARCB1 or direct inhibition of c-MYC (Figures S7G and S7H).

To investigate the *in vivo* antitumor effect of targeting DDR pathways in RMC, we used a subcutaneous patient-derived xenograft (PDX) model (RMC2X) generated from the untreated primary tumor sample (RMC2T) of a male patient with RMC. Mice harboring RMC2X tumors ($n = 5$ per group; average tumor volume of 158 mm^3 at treatment initiation) were randomly assigned to receive niraparib, AZD6738, the combination of niraparib with AZD6738, or vehicle control for a total of 25 days. One mouse in the control group died on day 8 after treatment initiation, whereas all mice in the three treatment groups were alive by the end of treatment. As shown in Figure 7E, treatment with niraparib led to significantly lower tumor volume compared with vehicle control ($p = 0.0196$). Conversely, treatment with AZD6738 did not significantly reduce tumor volume compared

with vehicle control ($p = 0.54$), and its combination with niraparib did not produce a stronger antitumor effect compared with niraparib alone ($p = 0.868$). The treatments were well tolerated, with no significant reduction in animal body weight compared with vehicle control (Figure S7). The addition of niraparib to cisplatin produced higher antitumor efficacy than either agent alone (Figure 7F). These findings suggest the potential therapeutic value of targeting the PARP pathway alone or in combination with platinum chemotherapy in RMC.

DISCUSSION

In contrast to the low number of focal CNAs found in MRT and ATRT (Chun et al., 2016; Hasselblatt et al., 2013; Takita et al., 2014), we found that RMC harbors a much more complex genome with high levels of focal CNAs with approximately one-third mapped to chromosomal fragile sites. This is consistent with our previously hypothesized model of RMC pathogenesis whereby red blood cell sickling in individuals with sickle cell trait induces chromosomal structural alterations in renal medullary cells, particularly in hotspots for chromosomal rearrangements (Msaouel et al., 2018). We found that one copy of chromosome 22, which harbors SMARCB1, is lost in over one-third of RMC tumors. The only other recurrent arm-level CNA, observed in approximately half of RMC tissues, was 8q gain where the *c-MYC* gene is located. In addition, we found that RMC tumors contain recurrent focal CNAs in regions of genes related to cell proliferation, including a distinct CNA pattern that results in Notch pathway activation and is also found in the basal subtype of BLCA (Hayashi et al., 2016).

We found that a notable distinction between RMC and CDC is that SMARCB1 loss in RMC activates the *c-MYC* pathway and subsequently induces high levels of DNA replication stress, resulting in the upregulation of DDR and cell-cycle checkpoint pathways compared with CDC. CNAs in chromosomal fragile sites such as those noted in RMC can be both a source and a consequence of DNA replication stress in cancer cells (Zeman and Cimprich, 2014). Therefore, the abundance of chromosomal alterations in RMC may confer a higher sensitivity to therapies that harness replication stress compared with SMARCB1-negative malignancies with more simple genomes such as MRT and ATRT. Platinum-based chemotherapy is currently the recommended standard of care for RMC (Msaouel et al., 2019). Furthermore, the combination of gemcitabine with doxorubicin, targeting replication stress, is one of the most clinically active cytotoxic chemotherapy regimens used for the treatment of RMC (Shah et al., 2017). Aberrant *c-MYC* activity in the setting of SMARCB1 loss also upregulates the unfolded protein response, thus making cells susceptible to agents that induce proteotoxic stress such as ixazomib (Carugo et al., 2019; Genova et al., 2017). We have accordingly activated an ongoing clinical trial (NCT03587662 at clinicaltrials.gov) testing the efficacy of ixazomib in combination with gemcitabine and doxorubicin in patients with RMC. We further identified and demonstrated both *in vitro* and *in vivo* that RMC is vulnerable to direct targeting of DDR pathways. Of note, the combination of niraparib and platinum produced significantly better *in vivo* antitumor responses. PARP inhibitors such as olaparib, niraparib, and rucaparib have now been clinically approved for the treatment of mul-

tip malignancies as single-agent therapies or in sequence with cytotoxic chemotherapy (Cook and Tinker, 2019). The extensive clinical experience with these agents and the efficacy shown in our preclinical models makes clinical testing of PARP inhibitors in patients with RMC a logical next step.

SMARCB1 loss was recently shown to induce interferon-mediated immunogenicity in rhabdoid tumors (Leruste et al., 2019). The highly inflamed phenotype of RMC in the setting of low tumor mutational burden and high number of focal CNAs and replication stress led us to identify the cGAS-STING pathway as a distinct source of pro-inflammatory signaling in this malignancy. We have activated an ongoing biopsy-driven clinical trial (NCT03274258 at clinicaltrials.gov) to better delineate how the distinct immune profile of RMC affects the efficacy of currently approved immune-checkpoint therapies. Figure 7G depicts our schematic model of the inflammatory responses and replication stress induced by the crosstalk between SMARCB1 loss and CNAs in RMC. It should be noted that our genomic sequencing lacked the sensitivity to detect rare subclonal alterations, and further studies will be needed to delineate the intratumoral mutational and copy-number heterogeneity of RMC.

In summary, our study has revealed several insights into the molecular foundations of RMC. We found that RMC is defined by a high number of focal CNAs and harbors a distinct immune microenvironment compared with other renal cell carcinomas, paving the way for future studies assessing the role of the cGAS-STING pathway in the immunotherapy of RMC. Furthermore, we identified the importance of SMARCB1 loss as a major recurrent genetic alteration in RMC and found that it confers replication stress-induced vulnerabilities that can be therapeutically targeted. These results highlight a potential opportunity to utilize agents targeting replication stress pathways alone or in combination with other therapies to yield deep and durable therapeutic responses.

STAR★METHODS

Detailed methods are provided in the online version of this paper and include the following:

- KEY RESOURCES TABLE
- LEAD CONTACT AND MATERIALS AVAILABILITY
- EXPERIMENTAL MODELS AND SUBJECT DETAILS
 - Tumor Samples
 - Generation and Authentication of New RMC Cell Line
 - Commercial and Other Cell Lines
 - Generation of RMC PDX Model
 - Mouse Studies
- METHOD DETAILS
 - WES and Targeted DNA Sequencing
 - Somatic Mutation Detection from Whole Exome Sequencing
 - Identification of Copy Number Alterations
 - RNA Sequencing
 - Virus Integration Analyses
 - Analysis of Kidney Nephron Atlas Expression Data
 - Gene Set Enrichment Analysis (GSEA)
 - Deconvolution of Tissue-Infiltrating Immune and Stromal Cell Populations
 - DNA Methylation Analysis

- Fluorescence In Situ Hybridization (FISH)
- Multiplex Ligation-Dependent Probe Amplification (MLPA)
- Spectral Karyotyping and G-banding
- SMARCB1 Re-expression Experiments
- Western Blot Analyses
- Co-immunoprecipitation Experiments
- Immunohistochemistry
- Small Interfering RNA (siRNA) Knockdown
- CRISPR/Cas9 Knockout
- Immunofluorescence Staining
- Chromatin Immunoprecipitation Sequencing (ChIP)
- Chemical Compounds
- Cell Viability Experiments
- DNA Fiber Assay
- *In Vivo* Treatments
- **QUANTIFICATION AND STATISTICAL ANALYSIS**
- **DATA AND CODE AVAILABILITY**

SUPPLEMENTAL INFORMATION

Supplemental Information can be found online at <https://doi.org/10.1016/j.ccell.2020.04.002>.

ACKNOWLEDGMENTS

We thank Dr. Waun Ki Hong for discussions and suggestions. We thank Dr. Bernard E. Weissman for discussions and reagents. We thank Dr. Bora Lim for creative assistance with illustrations. We thank the UTMACC Advanced Technology Genomics Core (ATGC) and the Cytogenetics and Cell Authentication Core. We thank Thomas Huynh and the UTMACC Department of Veterinary Medicine & Surgery Anatomic Pathology Laboratory. This work was supported in part by the Cancer Center support grant to MDACC (grant number P30 CA016672) from the National Cancer Institute of the National Institutes of Health, and by philanthropic donations from the Chris “CJ” Johnson Foundation Inc and RMC Inc. P.M. was supported by a Conquer Cancer Foundation Young Investigator award, a Kidney Cancer Association Young Investigator award, a United States Department of Defense Concept award, and the National Institutes of Health grant T32 CA009666. J.-P.B. and B.H.V. were funded by La Ligue Nationale Contre le Cancer. J.-P.B. was also supported by the Philip Foundation. I.D. is an ‘équipe labélisée’ of the Ligue Nationale contre le Cancer. S.S. was supported by the CPRIT research training grant RP170067. C.C. and C.J.C. were supported by the NIH grant CA125123. F.C. is supported by the Italian Association for Cancer Research AIRC for abroad fellowship. R.N.H.S. is supported by an American Heart Association predoctoral fellowship 19PRE34430069. K.S. is supported by grants NIH 1R01ES029680, CPRIT RP180813, and RP180463, and is a Rita Allen Fellow and a CPRIT Scholar in Cancer Biology.

AUTHOR CONTRIBUTIONS

Conceptualization, P.M., G.G.M., C.L.W., G.G., and N.M.T.; Methodology, P.M., G.G.M., X.S., H.Y., D.N.T., J.J.G., C.C., C.J.C., P.G.P., M.S., S.S., J.-P.B., D.D.S., R.N.H.S., S.K., K.S., B.H.V., C.L.W., G.G., and N.M.T.; Formal Analysis, P.M., G.G.M., X.S., H.Y., D.N.T., C.C., C.J.C., M.S., S.S., J.-P.B., D.D.S., R.N.H.S., S.K., and K.S.; Investigation, P.M., G.G.M., D.N.T., P.R., A.S.M., X.T., I.I.W., R.H., M.S., L.P., J.-P.B., D.D.S., M.K., R.N.H.S., B.H.V., D.L.-T., W.L., V.G., A.C., T.P.H., P.S., J.A.K., C.G.W., C.L.W., G.G., and N.M.T.; Writing – Original Draft, P.M., G.G., and C.L.W.; Writing – Review and Editing, P.M., G.G.M., X.S., H.Y., D.N.T., J.J.G., P.R., C.C., C.J.C., A.S.M., J.B., D.D.S., M.S., L.P., S.S., J.-P.B., P.G.P., R.N.H.S., D.L.-T., I.I.W., V.G., A.C., T.P.H., P.S., J.A.K., C.G.W., C.L.W., G.G., and N.M.T.; Resources, P.M., G.G.M., X.S., H.Y., D.N.T., C.C., C.J.C., A.S.M., J.B., R.H., M.S., L.P., J.-P.B., D.D.S., F.C., M.K., R.N.H.S., D.L.-T., E.H.C., X.T., W.L., I.I.W., T.C.T., I.D., V.G., A.C., T.P.H., P.S., C.L.W., G.G., and N.M.T.; Supervision,

P.M., C.L.W., G.G., and N.M.T.; Funding Acquisition, P.M., C.L.W., G.G., and N.M.T.

DECLARATION OF INTERESTS

The authors declare no competing interests.

Received: September 4, 2019

Revised: February 2, 2020

Accepted: April 1, 2020

Published: April 30, 2020

REFERENCES

Alexandrov, L.B., Jones, P.H., Wedge, D.C., Sale, J.E., Campbell, P.J., Nik-Zainal, S., and Stratton, M.R. (2015). Clock-like mutational processes in human somatic cells. *Nat. Genet.* *47*, 1402–1407.

Alexandrov, L.B., Nik-Zainal, S., Wedge, D.C., Aparicio, S.A., Behjati, S., Biankin, A.V., Bignell, G.R., Bolli, N., Borg, A., Borresen-Dale, A.L., et al. (2013). Signatures of mutational processes in human cancer. *Nature* *500*, 415–421.

Alvarez, O., Rodriguez, M.M., Jordan, L., and Sarnaik, S. (2015). Renal medullary carcinoma and sickle cell trait: a systematic review. *Pediatr. Blood Cancer* *62*, 1694–1699.

Anders, S., Pyl, P.T., and Huber, W. (2015). HTSeq—a Python framework to work with high-throughput sequencing data. *Bioinformatics* *31*, 166–169.

Andrews, S. (2014). FastQC: A Quality Control Tool for High Throughput Sequence Data. <https://www.bioinformatics.babraham.ac.uk/projects/fastqc/>.

Arun, G., Diermeier, S.D., and Spector, D.L. (2018). Therapeutic targeting of long non-coding RNAs in cancer. *Trends Mol. Med.* *24*, 257–277.

Aryee, M.J., Jaffe, A.E., Corrada-Bravo, H., Ladd-Acosta, C., Feinberg, A.P., Hansen, K.D., and Irizarry, R.A. (2014). Minfi: a flexible and comprehensive Bioconductor package for the analysis of Infinium DNA methylation microarrays. *Bioinformatics* *30*, 1363–1369.

Bakhom, S.F., Ngo, B., Laughney, A.M., Cavallo, J.A., Murphy, C.J., Ly, P., Shah, P., Sriram, R.K., Watkins, T.B.K., Taunk, N.K., et al. (2018). Chromosomal instability drives metastasis through a cytosolic DNA response. *Nature* *553*, 467–472.

Becht, E., Giraldo, N.A., Lacroix, L., Buttard, B., Elarouci, N., Petitprez, F., Selves, J., Laurent-Puig, P., Sautes-Fridman, C., Fridman, W.H., and de Reynies, A. (2016). Estimating the population abundance of tissue-infiltrating immune and stromal cell populations using gene expression. *Genome Biol.* *17*, 218.

Beck, H., Nahse, V., Larsen, M.S., Groth, P., Clancy, T., Lees, M., Jorgensen, M., Helleday, T., Syljuasen, R.G., and Sorensen, C.S. (2010). Regulators of cyclin-dependent kinases are crucial for maintaining genome integrity in S phase. *J. Cell Biol.* *188*, 629–638.

Becker, F., Junker, K., Parr, M., Hartmann, A., Fussel, S., Toma, M., Grobholz, R., Pflugmann, T., Wullich, B., Strauss, A., et al. (2013). Collecting duct carcinomas represent a unique tumor entity based on genetic alterations. *PLoS One* *8*, e78137.

Beroukhi, R., Mermel, C.H., Porter, D., Wei, G., Raychaudhuri, S., Donovan, J., Barretina, J., Boehm, J.S., Dobson, J., Urashima, M., et al. (2010). The landscape of somatic copy-number alteration across human cancers. *Nature* *463*, 899–905.

Brugarolas, J. (2014). Molecular genetics of clear-cell renal cell carcinoma. *J. Clin. Oncol.* *32*, 1968–1976.

Cajaiba, M.M., Dyer, L.M., Geller, J.I., Jennings, L.J., George, D., Kirschmann, D., Rohan, S.M., Cost, N.G., Khanna, G., Mullen, E.A., et al. (2018). The classification of pediatric and young adult renal cell carcinomas focused on the Children’s Oncology Group (COG) protocol AREN03B2 after focused genetic testing. *Cancer* *124*, 3381–3389.

Calderaro, J., Masliah-Planchon, J., Richer, W., Maillot, L., Maille, P., Mansuy, L., Bastien, C., de la Taille, A., Bousson, H., Charpy, C., et al. (2016). Balanced

- translocations disrupting SMARCB1 are hallmark recurrent genetic alterations in renal medullary carcinomas. *Eur. Urol.* 69, 1055–1061.
- Campan, M., Weisenberger, D.J., Trinh, B., and Laird, P.W. (2009). MethyLight. *Methods Mol. Biol.* 507, 325–337.
- Cancer Genome Atlas Research Network (2013). Comprehensive molecular characterization of clear cell renal cell carcinoma. *Nature* 499, 43–49.
- Cancer Genome Atlas Research Network, Linehan, W.M., Spellman, P.T., Ricketts, C.J., Creighton, C.J., Fei, S.S., Davis, C., Wheeler, D.A., Murray, B.A., Schmidt, L., et al. (2016). Comprehensive molecular characterization of papillary renal-cell carcinoma. *N. Engl. J. Med.* 374, 135–145.
- Carlo, M.I., Chaim, J., Patil, S., Kemel, Y., Schram, A.M., Woo, K., Coskey, D., Nanjangud, G.J., Voss, M.H., Feldman, D.R., et al. (2017). Genomic characterization of renal medullary carcinoma and treatment outcomes. *Clin. Genitourin Cancer* 15, e987–e994.
- Carugo, A., Minelli, R., Sapio, L., Soeung, M., Carbone, F., Robinson, F.S., Tepper, J., Chen, Z., Lovisa, S., Svelto, M., et al. (2019). p53 is a master regulator of proteostasis in SMARCB1-deficient malignant rhabdoid tumors. *Cancer Cell* 35, 204–220.e9.
- Cescon, D.W., and Haibe-Kains, B. (2016). DNA replication stress: a source of APOBEC3B expression in breast cancer. *Genome Biol.* 17, 202.
- Chen, F., Zhang, Y., Gibbons, D.L., Deneen, B., Kwiatkowski, D.J., Ittmann, M., and Creighton, C.J. (2018). Pan-cancer molecular classes transcending tumor lineage across 32 cancer types, multiple data platforms, and over 10,000 cases. *Clin. Cancer Res.* 24, 2182–2193.
- Chen, P.L., Roh, W., Reuben, A., Cooper, Z.A., Spencer, C.N., Prieto, P.A., Miller, J.P., Bassett, R.L., Gopalakrishnan, V., Wani, K., et al. (2016). Analysis of immune signatures in longitudinal tumor samples yields insight into biomarkers of response and mechanisms of resistance to immune checkpoint blockade. *Cancer Discov.* 6, 827–837.
- Chen, Y., Yao, H., Thompson, E.J., Tannir, N.M., Weinstein, J.N., and Su, X. (2013). VirusSeq: software to identify viruses and their integration sites using next-generation sequencing of human cancer tissue. *Bioinformatics* 29, 266–267.
- Cheval, L., Pierrat, F., Rajerison, R., Piquemal, D., and Doucet, A. (2012). Of mice and men: divergence of gene expression patterns in kidney. *PLoS One* 7, e46876.
- Choueiri, T.K., and Motzer, R.J. (2017). Systemic therapy for metastatic renal-cell carcinoma. *N. Engl. J. Med.* 376, 354–366.
- Chun, H.E., Lim, E.L., Heravi-Moussavi, A., Saberi, S., Mungall, K.L., Bilenky, M., Carles, A., Tse, K., Shlafman, I., Zhu, K., et al. (2016). Genome-wide profiles of extra-cranial malignant rhabdoid tumors reveal heterogeneity and dysregulated developmental pathways. *Cancer Cell* 29, 394–406.
- Cibulskis, K., Lawrence, M.S., Carter, S.L., Sivachenko, A., Jaffe, D., Sougnez, C., Gabriel, S., Meyerson, M., Lander, E.S., and Getz, G. (2013). Sensitive detection of somatic point mutations in impure and heterogeneous cancer samples. *Nat. Biotechnol.* 31, 213–219.
- Ciccolini, J., Serdjebi, C., Peters, G.J., and Giovannetti, E. (2016). Pharmacokinetics and pharmacogenetics of gemcitabine as a mainstay in adult and pediatric oncology: an EORTC-PAMM perspective. *Cancer Chemother. Pharmacol.* 78, 1–12.
- Ciro, M., Prosperini, E., Quarto, M., Grazini, U., Walfridsson, J., McBlane, F., Nucifero, P., Pacchiana, G., Capra, M., Christensen, J., and Helin, K. (2009). ATAD2 is a novel cofactor for MYC, overexpressed and amplified in aggressive tumors. *Cancer Res.* 69, 8491–8498.
- Cook, S.A., and Tinker, A.V. (2019). PARP inhibitors and the evolving landscape of ovarian cancer management: a review. *BioDrugs* 33, 255–273.
- Davis, C.F., Ricketts, C.J., Wang, M., Yang, L., Cherniack, A.D., Shen, H., Buhay, C., Kang, H., Kim, S.C., Fahey, C.C., et al. (2014). The somatic genomic landscape of chromophobe renal cell carcinoma. *Cancer Cell* 26, 319–330.
- Di Veroli, G.Y., Fomari, C., Goldlust, I., Mills, G., Koh, S.B., Bramhall, J.L., Richards, F.M., and Jodrell, D.I. (2015). An automated fitting procedure and software for dose-response curves with multiphasic features. *Sci. Rep.* 5, 14701.
- Do, H., and Dobrovic, A. (2015). Sequence artifacts in DNA from formalin-fixed tissues: causes and strategies for minimization. *Clin. Chem.* 61, 64–71.
- Doench, J.G., Fusi, N., Sullender, M., Hegde, M., Vaimberg, E.W., Donovan, K.F., Smith, I., Tothova, Z., Wilen, C., Orchard, R., et al. (2016). Optimized sgRNA design to maximize activity and minimize off-target effects of CRISPR-Cas9. *Nat. Biotechnol.* 34, 184–191.
- Dong, Y., Manley, B.J., Becerra, M.F., Redzematovic, A., Casuscelli, J., Tennenbaum, D.M., Reznik, E., Han, S., Benfante, N., Chen, Y.B., et al. (2017). Tumor xenografts of human clear cell renal cell carcinoma but not corresponding cell lines recapitulate clinical response to sunitinib: feasibility of using biopsy samples. *Eur. Urol. Focus* 3, 590–598.
- Durkin, S.G., and Glover, T.W. (2007). Chromosome fragile sites. *Annu. Rev. Genet.* 41, 169–192.
- Fabregat, A., Jupe, S., Matthews, L., Sidiropoulos, K., Gillespie, M., Garapati, P., Haw, R., Jassal, B., Korninger, F., May, B., et al. (2018). The reactome pathway knowledgebase. *Nucleic Acids Res.* 46, D649–D655.
- Favero, F., Joshi, T., Marquard, A.M., Birkbak, N.J., Krzystanek, M., Li, Q., Szallasi, Z., and Eklund, A.C. (2015). Sequenza: allele-specific copy number and mutation profiles from tumor sequencing data. *Ann. Oncol.* 26, 64–70.
- Forbes, S.A., Beare, D., Boutselakis, H., Bamford, S., Bindal, N., Tate, J., Cole, C.G., Ward, S., Dawson, E., Ponting, L., et al. (2017). COSMIC: somatic cancer genetics at high-resolution. *Nucleic Acids Res.* 45, D777–D783.
- Frampton, G.M., Fichtenholtz, A., Otto, G.A., Wang, K., Downing, S.R., He, J., Schnall-Levin, M., White, J., Sanford, E.M., An, P., et al. (2013). Development and validation of a clinical cancer genomic profiling test based on massively parallel DNA sequencing. *Nat. Biotechnol.* 31, 1023–1031.
- Fuller, C.E. (2016). All things rhabdoid and SMARC: an enigmatic exploration with Dr. Louis P. Dehner. *Semin. Diagn. Pathol.* 33, 427–440.
- Genovese, G., Carugo, A., Tepper, J., Robinson, F.S., Li, L., Svelto, M., Nezi, L., Corti, D., Minelli, R., Pettazzoni, P., et al. (2017). Synthetic vulnerabilities of mesenchymal subpopulations in pancreatic cancer. *Nature* 542, 362–366.
- Gupta, R., Billis, A., Shah, R.B., Moch, H., Osunkoya, A.O., Jochum, W., Hes, O., Bacchi, C.E., de Castro, M.G., Hansel, D.E., et al. (2012). Carcinoma of the collecting ducts of Bellini and renal medullary carcinoma: clinicopathologic analysis of 52 cases of rare aggressive subtypes of renal cell carcinoma with a focus on their interrelationship. *Am. J. Surg. Pathol.* 36, 1265–1278.
- Ha, G., Roth, A., Lai, D., Bashashati, A., Ding, J., Goya, R., Giuliani, R., Rosner, J., Oloumi, A., Shumansky, K., et al. (2012). Integrative analysis of genome-wide loss of heterozygosity and monoallelic expression at nucleotide resolution reveals disrupted pathways in triple-negative breast cancer. *Genome Res.* 22, 1995–2007.
- Harrell, F.E.J. (2015). *Regression Modeling Strategies, Second Edition* (Springer-Verlag).
- Harrow, J., Frankish, A., Gonzalez, J.M., Tapanari, E., Diekhans, M., Kokocinski, F., Aken, B.L., Barrell, D., Zadissa, A., Searle, S., et al. (2012). GENCODE: the reference human genome annotation for the ENCODE Project. *Genome Res.* 22, 1760–1774.
- Hasselblatt, M., Isken, S., Linge, A., Eikmeier, K., Jeibmann, A., Oyen, F., Nagel, I., Richter, J., Bartelheim, K., Kordes, U., et al. (2013). High-resolution genomic analysis suggests the absence of recurrent genomic alterations other than SMARCB1 aberrations in atypical teratoid/rhabdoid tumors. *Genes Chromosomes Cancer* 52, 185–190.
- Hayashi, T., Gust, K.M., Wyatt, A.W., Goriki, A., Jager, W., Awrey, S., Li, N., Oo, H.Z., Altamirano-Dimas, M., Buttyan, R., et al. (2016). Not all NOTCH is created equal: the oncogenic role of NOTCH2 in bladder cancer and its implications for targeted therapy. *Clin. Cancer Res.* 22, 2981–2992.
- Herbert, A.D., Carr, A.M., and Hoffmann, E. (2014). FindFoci: a focus detection algorithm with automated parameter training that closely matches human assignments, reduces human inconsistencies and increases speed of analysis. *PLoS One* 9, e114749.
- Herbst, R.S., Soria, J.C., Kowanetz, M., Fine, G.D., Hamid, O., Gordon, M.S., Sosman, J.A., McDermott, D.F., Powderly, J.D., Gettinger, S.N., et al. (2014). Predictive correlates of response to the anti-PD-L1 antibody MPDL3280A in cancer patients. *Nature* 515, 563–567.

- Huang da, W., Sherman, B.T., and Lempicki, R.A. (2009a). Bioinformatics enrichment tools: paths toward the comprehensive functional analysis of large gene lists. *Nucleic Acids Res.* **37**, 1–13.
- Huang da, W., Sherman, B.T., and Lempicki, R.A. (2009b). Systematic and integrative analysis of large gene lists using DAVID bioinformatics resources. *Nat. Protoc.* **4**, 44–57.
- Jackson, D.A., and Pombo, A. (1998). Replicon clusters are stable units of chromosome structure: evidence that nuclear organization contributes to the efficient activation and propagation of S phase in human cells. *J. Cell Biol.* **140**, 1285–1295.
- Jalali, G.R., Vorstman, J.A., Errami, A., Vijzelaar, R., Biegel, J., Shaikh, T., and Emanuel, B.S. (2008). Detailed analysis of 22q11.2 with a high density MLPA probe set. *Hum. Mutat.* **29**, 433–440.
- Jia, L., Carlo, M.I., Khan, H., Nanjangud, G.J., Rana, S., Cimer, R., Zhang, Y., Hakimi, A.A., Verma, A.K., Al-Ahmadie, H.A., et al. (2019). Distinctive mechanisms underlie the loss of SMARCB1 protein expression in renal medullary carcinoma: morphologic and molecular analysis of 20 cases. *Mod. Pathol.* **32**, 1329–1343.
- Kadoch, C., and Crabtree, G.R. (2015). Mammalian SWI/SNF chromatin remodeling complexes and cancer: mechanistic insights gained from human genomics. *Sci. Adv.* **1**, e1500447.
- Karam, J.A., Zhang, X.Y., Tamboli, P., Margulis, V., Wang, H., Abel, E.J., Culp, S.H., and Wood, C.G. (2011). Development and characterization of clinically relevant tumor models from patients with renal cell carcinoma. *Eur. Urol.* **59**, 619–628.
- Kerrigan, L., and Nims, R.W. (2011). Authentication of human cell-based products: the role of a new consensus standard. *Regen. Med.* **6**, 255–260.
- Kim, M.P., Evans, D.B., Wang, H., Abbruzzese, J.L., Fleming, J.B., and Gallick, G.E. (2009). Generation of orthotopic and heterotopic human pancreatic cancer xenografts in immunodeficient mice. *Nat. Protoc.* **4**, 1670–1680.
- Kumar, R., Nagpal, G., Kumar, V., Usmani, S.S., Agrawal, P., and Raghava, G.P.S. (2019). HumCFS: a database of fragile sites in human chromosomes. *BMC Genomics* **19**, 985.
- Langmead, B., and Salzberg, S.L. (2012). Fast gapped-read alignment with Bowtie 2. *Nat. Methods* **9**, 357–359.
- Lee, R.S., Stewart, C., Carter, S.L., Ambrogio, L., Cibulskis, K., Sougnez, C., Lawrence, M.S., Auclair, D., Mora, J., Golub, T.R., et al. (2012). A remarkably simple genome underlies highly malignant pediatric rhabdoid cancers. *J. Clin. Invest.* **122**, 2983–2988.
- Lee, W.P., Stromberg, M.P., Ward, A., Stewart, C., Garrison, E.P., and Marth, G.T. (2014). MOSAIK: a hash-based algorithm for accurate next-generation sequencing short-read mapping. *PLoS One* **9**, e90581.
- Leruste, A., Tosello, J., Ramos, R.N., Tauziède-Espariat, A., Brohard, S., Han, Z.Y., Beccaria, K., Andriantaranagna, M., Caudana, P., Nikolic, J., et al. (2019). Clonally expanded T cells reveal immunogenicity of rhabdoid tumors. *Cancer Cell* **36**, 597–612.e8.
- Liberzon, A., Birger, C., Thorvaldsdottir, H., Ghandi, M., Mesirov, J.P., and Tamayo, P. (2015). The Molecular Signatures Database (MSigDB) hallmark gene set collection. *Cell Syst.* **1**, 417–425.
- Loughery, J., Cox, M., Smith, L.M., and Meek, D.W. (2014). Critical role for p53-serine 15 phosphorylation in stimulating transactivation at p53-responsive promoters. *Nucleic Acids Res.* **42**, 7666–7680.
- Love, M.I., Huber, W., and Anders, S. (2014). Moderated estimation of fold change and dispersion for RNA-seq data with DESeq2. *Genome Biol.* **15**, 550.
- Luthra, R., Patel, K.P., Routbort, M.J., Broaddus, R.R., Yau, J., Simien, C., Chen, W., Hatfield, D.Z., Medeiros, L.J., and Singh, R.R. (2017). A targeted high-throughput next-generation sequencing panel for clinical screening of mutations, gene amplifications, and fusions in solid tumors. *J. Mol. Diagn.* **19**, 255–264.
- Marth, G.T., Korf, I., Yandell, M.D., Yeh, R.T., Gu, Z., Zakeri, H., Stitzel, N.O., Hillier, L., Kwok, P.Y., and Gish, W.R. (1999). A general approach to single-nucleotide polymorphism discovery. *Nat. Genet.* **23**, 452–456.
- Maya-Mendoza, A., Moudry, P., Merchut-Maya, J.M., Lee, M., Strauss, R., and Bartek, J. (2018). High speed of fork progression induces DNA replication stress and genomic instability. *Nature* **559**, 279–284.
- Meerbrey, K.L., Hu, G., Kessler, J.D., Roarty, K., Li, M.Z., Fang, J.E., Herschkowitz, J.I., Burrows, A.E., Ciccia, A., Sun, T., et al. (2011). The pINDUCER lentiviral toolkit for inducible RNA interference in vitro and in vivo. *Proc. Natl. Acad. Sci. U S A* **108**, 3665–3670.
- Mermel, C.H., Schumacher, S.E., Hill, B., Meyerson, M.L., Beroukhi, R., and Getz, G. (2011). GISTIC2.0 facilitates sensitive and confident localization of the targets of focal somatic copy-number alteration in human cancers. *Genome Biol.* **12**, R41.
- Mi, H., Muruganujan, A., and Thomas, P.D. (2013). PANTHER in 2013: modeling the evolution of gene function, and other gene attributes, in the context of phylogenetic trees. *Nucleic Acids Res.* **41**, D377–D386.
- Msaouel, P., Hong, A.L., Mullen, E.A., Atkins, M.B., Walker, C.L., Lee, C.H., Carden, M.A., Genovese, G., Linehan, W.M., Rao, P., et al. (2019). Updated recommendations on the diagnosis, management, and clinical trial eligibility criteria for patients with renal medullary carcinoma. *Clin. Genitourin Cancer* **17**, 1–6.
- Msaouel, P., Tannir, N.M., and Walker, C.L. (2018). A model linking sickle cell hemoglobinopathies and SMARCB1 loss in renal medullary carcinoma. *Clin. Cancer Res.* **24**, 2044–2049.
- Olshen, A.B., Venkatraman, E.S., Lucito, R., and Wigler, M. (2004). Circular binary segmentation for the analysis of array-based DNA copy number data. *Biostatistics* **5**, 557–572.
- Parra, E.R., Behrens, C., Rodriguez-Canales, J., Lin, H., Mino, B., Blando, J., Zhang, J., Gibbons, D.L., Heymach, J.V., Sepesi, B., et al. (2016). Image analysis-based assessment of PD-L1 and tumor-associated immune cells density supports distinct intratumoral microenvironment groups in non-small cell lung carcinoma patients. *Clin. Cancer Res.* **22**, 6278–6289.
- Pavlik, E.J., van Nagell, J.R., Jr., Hanson, M.B., Donaldson, E.S., Powell, D.E., and Kenady, D.E. (1982). Sensitivity to anticancer agents in vitro: standardizing the cytotoxic response and characterizing the sensitivities of a reference cell line. *Gynecol. Oncol.* **14**, 243–261.
- Pawel, B.R. (2018). SMARCB1-deficient tumors of childhood: a practical guide. *Pediatr. Dev. Pathol.* **21**, 6–28.
- Quinlan, A.R., and Hall, I.M. (2010). BEDTools: a flexible suite of utilities for comparing genomic features. *Bioinformatics* **26**, 841–842.
- R Core Team (2019). R: A Language and Environment for Statistical Computing (R Foundation for Statistical Computing).
- Schlacher, K., Christ, N., Siaud, N., Egashira, A., Wu, H., and Jasin, M. (2011). Double-strand break repair-independent role for BRCA2 in blocking stalled replication fork degradation by MRE11. *Cell* **145**, 529–542.
- Schneider, C.A., Rasband, W.S., and Eliceiri, K.W. (2012). NIH Image to ImageJ: 25 years of image analysis. *Nat. Methods* **9**, 671–675.
- Seiler, M., Peng, S., Agrawal, A.A., Palacino, J., Teng, T., Zhu, P., Smith, P.G., Cancer Genome Atlas Research Network, Buonomici, S., and Yu, L. (2018). Somatic mutational landscape of splicing factor genes and their functional consequences across 33 cancer types. *Cell Rep.* **23**, 282–296.e4.
- Shah, A.Y., Karam, J.A., Malouf, G.G., Rao, P., Lim, Z.D., Jonasch, E., Xiao, L., Gao, J., Vaishampayan, U.N., Heng, D.Y., et al. (2017). Management and outcomes of patients with renal medullary carcinoma: a multicentre collaborative study. *BJU Int.* **120**, 782–792.
- Stojano,va, A., Tu, W.B., Ponzelli, R., Kotlyar, M., Chan, P.K., Boutros, P.C., Khosravi, F., Jurisica, I., Raught, B., and Penn, L.Z. (2016). MYC interaction with the tumor suppressive SWI/SNF complex member INI1 regulates transcription and cellular transformation. *Cell Cycle* **15**, 1693–1705.
- Subramanian, A., Tamayo, P., Mootha, V.K., Mukherjee, S., Ebert, B.L., Gillette, M.A., Paulovich, A., Pomeroy, S.L., Golub, T.R., Lander, E.S., and Mesirov, J.P. (2005). Gene set enrichment analysis: a knowledge-based approach for interpreting genome-wide expression profiles. *Proc. Natl. Acad. Sci. U S A* **102**, 15545–15550.

- Swift, L.H., and Golsteyn, R.M. (2014). Genotoxic anti-cancer agents and their relationship to DNA damage, mitosis, and checkpoint adaptation in proliferating cancer cells. *Int. J. Mol. Sci.* *15*, 3403–3431.
- Takita, J., Chen, Y., Kato, M., Ohki, K., Sato, Y., Ohta, S., Sugita, K., Nishimura, R., Hoshino, N., Seki, M., et al. (2014). Genome-wide approach to identify second gene targets for malignant rhabdoid tumors using high-density oligonucleotide microarrays. *Cancer Sci.* *105*, 258–264.
- The Bioconductor Dev Team (2014). BSgenome.Hsapiens.UCSC.hg19: Full Genome Sequences for Homo sapiens (UCSC Version hg19). R package version 1.4.0. <https://bioconductor.org/packages/release/data/annotation/html/BSgenome.Hsapiens.UCSC.hg19.html>.
- Thorvaldsdottir, H., Robinson, J.T., and Mesirov, J.P. (2013). Integrative Genomics Viewer (IGV): high-performance genomics data visualization and exploration. *Brief Bioinform.* *14*, 178–192.
- Tijhuis, A.E., Johnson, S.C., and McClelland, S.E. (2019). The emerging links between chromosomal instability (CIN), metastasis, inflammation and tumour immunity. *Mol. Cytogenet.* *12*, 17.
- Triche, T.J., Jr., Weisenberger, D.J., Van Den Berg, D., Laird, P.W., and Siegmund, K.D. (2013). Low-level processing of Illumina Infinium DNA methylation BeadArrays. *Nucleic Acids Res.* *41*, e90.
- Tseng, Y.-Y., Moriarity, B.S., Gong, W., Akiyama, R., Tiwari, A., Kawakami, H., Ronning, P., Reuland, B., Guenther, K., Beadnell, T.C., et al. (2014). PVT1 dependence in cancer with MYC copy-number increase. *Nature* *512*, 82–86.
- Tumeh, P.C., Harview, C.L., Yearley, J.H., Shintaku, I.P., Taylor, E.J., Robert, L., Chmielowski, B., Spasic, M., Henry, G., Ciobanu, V., et al. (2014). PD-1 blockade induces responses by inhibiting adaptive immune resistance. *Nature* *515*, 568–571.
- Twyman-Saint Victor, C., Rech, A.J., Maity, A., Rengan, R., Pauken, K.E., Stelekati, E., Benci, J.L., Xu, B., Dada, H., Odorizzi, P.M., et al. (2015). Radiation and dual checkpoint blockade activate non-redundant immune mechanisms in cancer. *Nature* *520*, 373–377.
- Vaser, R., Adusumalli, S., Leng, S.N., Sikic, M., and Ng, P.C. (2016). SIFT missense predictions for genomes. *Nat. Protoc.* *11*, 1–9.
- Von Hoff, D.D., Clark, G.M., Weiss, G.R., Marshall, M.H., Buchok, J.B., Knight, W.A., 3rd, and LeMaistre, C.F. (1986). Use of in vitro dose response effects to select antineoplastics for high-dose or regional administration regimens. *J. Clin. Oncol.* *4*, 1827–1834.
- Wang, X.S., Zhang, Z., Wang, H.C., Cai, J.L., Xu, Q.W., Li, M.Q., Chen, Y.C., Qian, X.P., Lu, T.J., Yu, L.Z., et al. (2006). Rapid identification of UCA1 as a very sensitive and specific unique marker for human bladder carcinoma. *Clin. Cancer Res.* *12*, 4851–4858.
- Wei, D., Goldfarb, D., Song, S., Cannon, C., Yan, F., Sakellariou-Thompson, D., Emanuele, M., Major, M.B., Weissman, B.E., and Kuwahara, Y. (2014). SNF5/INI1 deficiency redefines chromatin remodeling complex composition during tumor development. *Mol. Cancer Res.* *12*, 1574–1585.
- Weissmiller, A.M., Wang, J., Lorey, S.L., Howard, G.C., Martinez, E., Liu, Q., and Tansey, W.P. (2019). Inhibition of MYC by the SMARCB1 tumor suppressor. *Nat. Commun.* *10*, 2014.
- Xu, K., Ma, H., McCown, T.J., Verma, I.M., and Kafri, T. (2001). Generation of a stable cell line producing high-titer self-inactivating lentiviral vectors. *Mol. Ther.* *3*, 97–104.
- Yang, W., Soares, J., Greninger, P., Edelman, E.J., Lightfoot, H., Forbes, S., Bindal, N., Beare, D., Smith, J.A., Thompson, I.R., et al. (2013). Genomics of Drug Sensitivity in Cancer (GDSC): a resource for therapeutic biomarker discovery in cancer cells. *Nucleic Acids Res.* *41*, D955–D961.
- Young, M.D., Mitchell, T.J., Vieira Braga, F.A., Tran, M.G.B., Stewart, B.J., Ferdinand, J.R., Collord, G., Botting, R.A., Popescu, D.M., Loudon, K.W., et al. (2018). Single-cell transcriptomes from human kidneys reveal the cellular identity of renal tumors. *Science* *361*, 594–599.
- Zeman, M.K., and Cimprich, K.A. (2014). Causes and consequences of replication stress. *Nat. Cell Biol.* *16*, 2–9.
- Zhang, J., Dai, Q., Park, D., and Deng, X. (2016). Targeting DNA replication stress for cancer therapy. *Genes (Basel)* *7*, <https://doi.org/10.3390/genes7080051>.
- Zhang, J., Fujimoto, J., Zhang, J., Wedge, D.C., Song, X., Zhang, J., Seth, S., Chow, C.W., Cao, Y., Gumbs, C., et al. (2014). Intratumor heterogeneity in localized lung adenocarcinomas delineated by multiregion sequencing. *Science* *346*, 256–259.
- Zhang, Y., Liu, T., Meyer, C.A., Eeckhoute, J., Johnson, D.S., Bernstein, B.E., Nussbaum, C., Myers, R.M., Brown, M., Li, W., and Liu, X.S. (2008). Model-based analysis of ChIP-seq (MACS). *Genome Biol.* *9*, R137.

STAR★METHODS

KEY RESOURCES TABLE

REAGENT or RESOURCE	SOURCE	IDENTIFIER
Antibodies		
Mouse monoclonal anti-BAF47 (anti-SMARCB1) Clone 25	BD Biosciences	Cat# 612111; RRID: AB_2191717
Mouse monoclonal anti-INI1/SNF5 (anti-SMARCB1) antibody clone 2C2	Sigma-Aldrich	Cat# SAB4200202; RRID: AB_10697389
Rabbit polyclonal anti-phospho-Histone H2A.X at serine 139	Cell Signaling Technology	Cat# 2577; RRID: AB_2118010
Mouse monoclonal anti-c-MYC antibody 9E10	Santa Cruz Biotechnology	Cat# sc-40; RRID: AB_627268
Rabbit polyclonal anti-PARP	Cell Signaling Technology	Cat# 9542; RRID: AB_2160739
Goat polyclonal anti-ATR	Santa Cruz Biotechnology	Cat# sc-1887; RRID: AB_630893
Rabbit polyclonal anti-phospho-ATR at serine 428	Cell Signaling Technology	Cat# 2853; RRID: AB_2290281
Mouse monoclonal anti-TP53	Santa Cruz Biotechnology	Cat# sc-126; RRID: AB_628082
Rabbit polyclonal anti-phospho-TP53 at serine 15	Cell Signaling Technology	Cat# 9284; RRID: AB_331464
Mouse monoclonal anti-actin	Santa Cruz Biotechnology	Cat# sc-47778 HRP; RRID: AB_2714189
Rabbit polyclonal anti-phospho-CDK1 at tyrosine 15	Cell Signaling Technology	Cat# 9111; RRID: AB_331460
Mouse monoclonal anti-RPA 32 kDa subunit 9H8	Santa Cruz Biotechnology	Cat# sc-56770; RRID: AB_785534
Rabbit polyclonal anti-phospho-RPA32 at serines 4 and 8	Bethyl	Cat# A300-245A; RRID: AB_210547
Mouse monoclonal anti-FANCD2	Santa Cruz Biotechnology	Cat# sc-20022; RRID: AB_2278211
Rabbit polyclonal anti-PBRM1	Bethyl	Cat# A301-591A; RRID: AB_1078808
Rabbit monoclonal anti-BRG1 (anti-SMARCA4)	Abcam	Cat# ab110641; RRID: AB_10861578
Mouse monoclonal anti-BAF250a (anti-ARID1A)	Santa Cruz Biotechnology	Cat# sc-32761; RRID: AB_673396
Anti-rabbit IgG-HRP	Rockland	Cat# 88-8886-31; RRID: AB_2614893
Anti-mouse IgG-HRP	Rockland	Cat# 18-8817-30; RRID: AB_2610849
Rabbit monoclonal anti-STING	Cell Signaling Technology	Cat# 13647; RRID: AB_2732796
Rabbit polyclonal anti-CD3	Agilent	Cat# A0452; RRID: AB_2335677
Mouse monoclonal anti-CD4	Leica Biosystems	Cat# NCL-L-CD4-368; RRID: AB_563559
Mouse monoclonal anti-CD8	Thermo Fisher Scientific	Cat# MS-457-S; RRID: AB_61027
Mouse monoclonal anti-FOXP3	BioLegend	Cat# 320102; RRID: AB_430881
Mouse monoclonal anti-CD20	Agilent	Cat# M0755; RRID: AB_2282030
Mouse monoclonal anti-CD68	Agilent	Cat# M0876; RRID: AB_2074844
Rabbit monoclonal anti-PD-L1	Cell Signaling Technology	Cat# 13684; RRID: AB_2687655
Rabbit monoclonal anti-PD-1	Abcam	Cat# AB201825; RRID: AB_2728811
Rabbit polyclonal anti-c-MYC	Santa Cruz Biotechnology	Cat# sc-764; RRID: AB_631276
Rabbit Normal IgG Control Antibody	Cell Signaling Technology	Cat# 2729; RRID: AB_1031062
Mouse monoclonal anti-IdU / anti-BrdU clone B44	BD Biosciences	Cat# B44; RRID: AB_2313824
Rat monoclonal anti-CldU / anti-BrdU (BU1/75 ICR1)	Santa Cruz Biotechnology	Cat# sc-56258; RRID: AB_781696
Goat polyclonal anti-mouse Alexa Fluor 488	Thermo Fisher Scientific	Cat# A-11001; RRID: AB_2534069

(Continued on next page)

Continued

REAGENT or RESOURCE	SOURCE	IDENTIFIER
Goat polyclonal anti-rat Alexa Fluor 555	Thermo Fisher Scientific	Cat# A-21434; RRID: AB_2535855
Bacterial and Virus Strains		
<i>E.coli</i> DH5 α	Invitrogen	Cat#18265017
Biological Samples		
Renal medullary carcinoma tumor samples	UTMDACC Department of Genitourinary Medical Oncology	N/A
Normal adjacent kidney	UTMDACC Department of Genitourinary Medical Oncology	N/A
Collecting duct carcinoma tumor samples	UTMDACC Department of Genitourinary Medical Oncology	N/A
Upper tract urothelial carcinoma tumor samples	UTMDACC Department of Genitourinary Medical Oncology	N/A
Malignant rhabdoid tumor FFPE slides	Dolores Lopez-Terrada (dherrad@texaschildrenshospital.org)	N/A
Chemicals, Peptides, and Recombinant Proteins		
Doxycycline	Thermo Fisher Scientific	Cat# BP26531; CAS: 10592-13-9
Olaparib (AZD2281)	Selleckchem	Cat# S1060; CAS: 763113-22-0
Niraparib (MK-4827)	Selleckchem	Cat# S2741; CAS: 1038915-60-4
Berzosertib (VX970)	Selleckchem	Cat# S7102; CAS: 1232416-25-9
Ceralasertib (AZD6738)	Selleckchem	Cat# S7693; CAS: 1352226-88-0
Adavosertib (MK-1775)	Selleckchem	Cat# S1525; CAS: 955365-80-7
Doxorubicin	UTMDACC Department of Pharmacy	CAS: 23214-92-8
Gemcitabine	UTMDACC Department of Pharmacy	CAS: 95058-81-4
Carboplatin	UTMDACC Department of Pharmacy	CAS: 41575-94-4
Cisplatin	UTMDACC Department of Pharmacy	CAS: 15663-27-1
Paclitaxel	UTMDACC Department of Pharmacy	CAS: 33069-62-4
Critical Commercial Assays		
Universal Mycoplasma Detection Kit	ATCC	Cat#30-1012K
QIAamp DNA FFPE Tissue Kit (50)	Qiagen	Cat#56404
AllPrep DNA/RNA Mini Kit (50)	Qiagen	Cat#80204
SureSelectXT Reagent Kit	Agilent	Cat#G9612B
4200 TapeStation High Sensitivity D1000 ScreenTape	Agilent	Cat#5067-5584
Qubit dsDNA HS Assay Kit	Thermo Fisher Scientific	Cat#Q32851
KAPA Library Quantification Kit	Roche	Cat#KK4824
FoundationOne CDx	Foundation Medicine	F1CDX
Oligonucleotide Array-Based CGH for Genomic DNA Analysis	Agilent	Protocol # G4410-90010
RNeasy Mini Kit (250)	Qiagen	Cat#74106
Infinium HumanMethylation450 (HM450) BeadChip array	Illumina	Cat#WG-314-1002
EZ DNA methylation kit	Zymo Research	Cat#D5001
SMARCB1BA-20-GROR Break Apart FISH Probe	Empire Genomics	Cat#SMARCB1BA-20-GROR
SALSA MLPA P258 (SMARCB1) kit	MRC-Holland	Cat#P258-050R
HiSKY Probe Kit	Applied Spectral Imaging	Cat#FPRPR0028
siGENOME Human MYC siRNA SMARTpool	Horizon Discovery	Cat#M-003282-07-0010
siGENOME Non-targetin siRNA control pool	Horizon Discovery	Cat# D-001206-13-20
Cell Proliferation Kit I (MTT)	Sigma-Aldrich	Cat#11 465 007 001

(Continued on next page)

REAGENT or RESOURCE	SOURCE	IDENTIFIER
Continued		
Deposited Data		
Raw RMC sequencing data	This paper	NCBI Sequence Read Archive (SRA) accession: PRJNA605003 ; https://www.ncbi.nlm.nih.gov/sra/PRJNA605003
Clear cell renal cell carcinoma sequencing data	TCGA; Cancer Genome Atlas Research Network, 2013	https://portal.gdc.cancer.gov/projects/TCGA-KIRC
Papillary renal cell carcinoma sequencing data	TCGA; Cancer Genome Atlas Research Network et al., 2016	https://portal.gdc.cancer.gov/projects/TCGA-KIRP
Chromophobe renal cell carcinoma sequencing data	TCGA; Davis et al., 2014	https://portal.gdc.cancer.gov/projects/TCGA-KICH
Kidney MRT sequencing data	Chun et al., 2016	http://target.nci.nih.gov/dataMatrix/TARGET_DataMatrix.html
MRT and ATRT sequencing data	Lee et al., 2012	dbGaP accession no. phs000508
G401 c-MYC ChIP-seq data	Weissmiller et al., 2019	GEO: GSE109310
Experimental Models: Cell Lines		
HEK-293FT	Thermo Fisher Scientific	Cat# R70007, RRID: CVCL_6911
G401	ATCC	Cat#CRL-1441, RRID: CVCL_0270
CHLA-06-ATRT	ATCC	Cat#CRL-3038, RRID: CVCL_AQ42
VA-ES-BJ	ATCC	Cat#CRL-2138, RRID: CVCL_1785
A-498	ATCC	Cat#CRL-7908, RRID: CVCL_1056
786-O	ATCC	Cat#CRL-1932, RRID: CVCL_1051
RCC4	ECACC	Cat#03112702, RRID: CVCL_UY81
RMC2C	This paper	N/A
RMC219 (JHRCC219)	Dong et al., 2017 Emily H. Cheng (ChengE1@mskcc.org)	N/A
RMC2C1-Tet-Empty	This paper	N/A
RMC2C1-Tet-SMARCB1	This paper	N/A
RMC219-Tet-Empty	This paper	N/A
RMC219-Tet-SMARCB1	This paper	N/A
G401-Tet-Empty	This paper	N/A
G401-Tet-SMARCB1	This paper	N/A
VA-ES-BJ-Tet-Empty	This paper	N/A
VA-ES-BJ-Tet-SMARCB1	This paper	N/A
HEK293-control gRNA	This paper	N/A
HEK293-SMARCB1-KO	This paper	N/A
Experimental Models: Organisms/Strains		
Mouse: CB17/lcr-Prk ^{scid} /lcrIcoCrl	Charles River	Cat#236; RRID: IMSR_CRL:561
Mouse: RMC2X patient-derived xenograft	This paper; Jose A. Karam (JAKaram@mdanderson.org) and Christopher G. Wood (cgwood@mdanderson.org)	N/A
Oligonucleotides		
SMARCB1 gRNA (1): TGAGAACGCATCTCAGCCCG	GenScript	https://www.genscript.com/gRNA-detail/6598/SMARCB1-CRISPR-guide-RNA.html
SMARCB1 gRNA (2): CATCGATCTCCATGTCCAGC	GenScript	https://www.genscript.com/gRNA-detail/6598/SMARCB1-CRISPR-guide-RNA.html
Non-targeting control gRNA sequence: GGGACGCGAAAGAAACCAGT	John Doench & David Root	Addgene plasmid # 80196; RRID: Addgene_80196
CCNE2 TSS primer forward: CAGCACAAACGTGGAGTGG	This paper	N/A

(Continued on next page)

Continued

REAGENT or RESOURCE	SOURCE	IDENTIFIER
CCNE2 TSS primer reverse: AGAGCAGAGCCGCACTTG	This paper	N/A
CDK4 TSS primer forward: ATGTGACCAGCTGCCAAAG	This paper	N/A
CDK4 TSS primer reverse: TTACACTCTTCGCCCTCCTC	This paper	N/A
ATF4 TSS primer forward: CGAAGGAAAGAACGGACTCTG	This paper	N/A
ATF4 TSS primer reverse: TTATGGCCTCACGAAAGGAG	This paper	N/A
PRM1 TSS primer forward: ACAGAGCGACACCCTGTCAT	This paper	N/A
PRM1 TSS primer reverse: AGGCGGTGGTTACACAACAT	This paper	N/A
Recombinant DNA		
pIND20-fSNF5-HA vector	Bernard E. Weissman; Wei et al., 2014	N/A
pInducer20 empty backbone	Stephen Elledge	Addgene plasmid # 44012; RRID: Addgene_44012
pLentiCRISPR v2 anti-SMARCB1 gRNA	GenScript	https://www.genscript.com/gRNA-detail/6598/SMARCB1-CRISPR-guide-RNA.html
psPAX2	Didier Trono	Addgene plasmid # 12260; RRID: Addgene_12260
pMD2.G	Didier Trono	Addgene plasmid # 12259; RRID: Addgene_12259
pLentiCRISPR v2 non-targeting control gRNA	John Doench & David Root	Addgene plasmid # 80196; RRID: Addgene_80196
Software and Algorithms		
R statistical package	R Core Team, 2019	http://www.r-project.org/
Rms	Harrell, 2015	https://github.com/harrelfe/rms
Hmisc	Harrell, 2015	https://github.com/harrelfe/Hmisc
DAVID Bioinformatics resources database (v6.8)	Huang da et al., 2009a ; Huang da et al., 2009b	https://david.ncifcrf.gov/
Gene set enrichment Analysis	Subramanian et al., 2005	http://software.broadinstitute.org/gsea/index.jsp
MOSAIC alignment software	Lee et al., 2014	https://github.com/wanplinglee/MOSAIC
GigaBayes/FreeBayes	Marth et al., 1999	https://github.com/ekg/freebayes
SIFT	Vaser et al., 2016	http://sift-dna.org/sift4g
Mutational signature database	Sanger Institute Alexandrov et al., 2013	https://cancer.sanger.ac.uk/cosmic/signatures
BSgenome.Hsapiens.UCSC.hg19 (version:1.4.0)	The Bioconductor Dev Team, 2014	http://bioconductor.org/packages/release/data/annotation/html/BSgenome.Hsapiens.UCSC.hg19.html
VirusSeq	Chen et al., 2013	http://odin.mdacc.tmc.edu/~xsu1/VirusSeq.html
ExomeCN	Zhang et al., 2014	MD Anderson Cancer Cent in-house software
Sequenza	Favero et al., 2015	https://github.com/cran/sequenza
GISTIC2.0	Mermel et al., 2011 ; Beroukhim et al., 2010	http://portals.broadinstitute.org/cgi-bin/cancer/publications/pub_paper.cgi?mode=view&paper_id=216&p=t
hg19 cytoband coordinates	Genome Reference Consortium	http://hgdownload.cse.ucsc.edu/goldenpath/hg19/database

(Continued on next page)

Continued

REAGENT or RESOURCE	SOURCE	IDENTIFIER
Feature-Extraction V9.1.3	Agilent	https://www.agilent.com/en/promotions/release-note-feature-extraction-software-version-9-1-3
GENCODE annotation	Harrow et al., 2012	https://www.gencodegenes.org/
HTSeq	Anders et al., 2015	https://github.com/simon-anders/htseq
DESeq2	Love et al., 2014	https://github.com/mikelove/DESeq2
Molecular Signatures Database (MSigDB)	Subramanian et al., 2005 ; Liberzon et al., 2015	http://software.broadinstitute.org/gsea/msigdb/collections.jsp
MCP-counter 1.1.0	Becht et al., 2016	https://omictools.com/mcp-counter-tool
Minfi	Aryee et al., 2014	https://github.com/hansenlab/minfi
HiBand	Applied Spectral Imaging	https://spectral-imaging.com/products/hiband/
ImageJ	NIH Schneider et al., 2012	https://imagej.nih.gov/ij/
FindFoci	Herbert et al., 2014	https://github.com/aherbert/gdsc
bowtie2	Langmead and Salzberg, 2012	https://github.com/BenLangmead/bowtie2
Integrative Genome Viewer	Thorvaldsdottir et al., 2013	https://software.broadinstitute.org/software/igv/
MACS2	Zhang et al., 2008	https://github.com/taoliu/MACS
BEDTOOLS	Quinlan and Hall, 2010	https://github.com/ryanlayer/bedtools
Hallmark pathways	Liberzon et al., 2015	https://www.gsea-msigdb.org/gsea/msigdb/collections.jsp
REACTOME pathways	Fabregat et al., 2018	https://www.gsea-msigdb.org/gsea/msigdb/collections.jsp
Dr Fit	Di Veroli et al., 2015	https://sourceforge.net/projects/drfit/
Other		
Sensitivity of human cell lines to olaparib	Genomics of Drug Sensitivity in Cancer database	https://www.cancerrxgene.org/translation/Drug

LEAD CONTACT AND MATERIALS AVAILABILITY

Further information and requests for resources and reagents should be directed to and will be fulfilled by the Lead Contact, Pavlos Msaouel (pmsaouel@mdanderson.org).

EXPERIMENTAL MODELS AND SUBJECT DETAILS

Tumor Samples

Tumor samples were obtained from 38 patients with RMC, 9 patients with CDC, and 22 patients with UTUC using endoscopic biopsy or surgical resection. Histology slides were reviewed by a genitourinary pathology expert (Priya Rao) and the RMC samples were all confirmed to be SMARCB1 negative by immunohistochemistry using purified mouse anti-BAF47 Clone 25/BAF47 (BD Biosciences) as shown in [Figure S1A](#). CDC samples were all SMARCB1 positive by the same immunohistochemical assay and were derived from untreated primary tumors. Sick cell status was determined by hemoglobin electrophoresis. [Figure 1](#) lists patient characteristics and also provides RMC sample annotation, clinical details, and the assays performed on each sample. This study was performed under Institutional Review Board–approved protocols (PA11-1045 and PA19-0250) and conducted in accordance with the principles of the Declaration of Helsinki.

Generation and Authentication of New RMC Cell Line

The new RMC cell line RMC2C was derived from the untreated primary nephrectomy specimen (corresponding to the RMC2T tumor sample) of a 35-year-old African American male patient with sickle cell trait using previously reported methodology ([Karam et al., 2011](#)). Cell line authentication was performed by short tandem repeat (STR) DNA profiling ([Kerrigan and Nims, 2011](#)) in direct comparison with the primary patient-derived tissue. RMC2C was cultured at 37°C in minimum essential medium (MEM) supplemented with MEM non-essential amino acids, EGF (5 µg/mL), 100 U/mL penicillin-streptomycin, and 10% heat-inactivated fetal bovine serum. Cell line doubling time was calculated as: duration of culture * ln(2) / ln(final cell number - initial cell number).

Commercial and Other Cell Lines

G401, CHLA-06-ATRT, VA-ES-BJ, A-498, and 786-O were purchased from American Type Culture Collection (ATCC, Manassas, VA). HEK-293FT were purchased from Thermo Fisher Scientific (Waltham, MA). All cell lines were grown at 37°C in media recommended by ATCC in a humidified atmosphere of 5% CO₂. The RCC4 cell line was purchased from the European Collection of Authenticated Cell Cultures (ECACC, Porton Down, Salisbury, United Kingdom) and was grown at 37 °C in the medium recommended by ECACC in a humidified atmosphere of 5% CO₂. The RMC219 cell line (also designated as JHRCC219) was established from a previously described patient-derived xenograft (Dong et al., 2017) derived from the bone metastasis of a 39 year old African American male patient with sickle cell trait who was previously treated with 5 cycles of gemcitabine and carboplatin for metastatic RMC. RMC219 was cultured at 37°C in Ham's F-12 medium supplemented with 1% essential amino acids, 1% sodium pyruvate, and 1% L-glutamine. All media contained 100 U/mL penicillin-streptomycin and were supplemented with 10% heat-inactivated fetal bovine serum. We monitored all cell lines for mycoplasma every 3 months using the Universal Mycoplasma Detection Kit by ATCC (Manassas, VA). All cell lines were refreshed from frozen early-passage stock after approximately 20 passages.

Generation of RMC PDX Model

The new RMC2X PDX model was derived from the untreated primary nephrectomy specimen (corresponding to the RMC2T tumor sample) of a 35-year-old African American male patient with sickle cell trait. The banked RMC2X tumor was implanted into the subcutaneous tissue of immunodeficient female CB17/lcr-Prkd^{scid}/lcrIcoCrl mice aged 6-9 weeks old using previously reported methodology (Kim et al., 2009). PDX authentication was performed by short tandem repeat (STR) DNA profiling (Kerrigan and Nims, 2011) in direct comparison with the primary patient-derived tissue.

Mouse Studies

Female CB17/lcr-Prkd^{scid}/lcrIcoCrl mice were obtained by Charles River. Mice aged 6-9 weeks old were used for all PDX transplantation studies. All animal studies and procedures were approved by the UTMDACC Institutional Animal Care and Use Committee (protocols 00001200 and 00000884). All experiments conformed to the relevant regulatory standards and overseen by the institutional review board.

METHOD DETAILS

WES and Targeted DNA Sequencing

Genomic DNA was isolated from formalin-fixed paraffin-embedded (FFPE) samples using QIAamp DNA FFPE Tissue kit (Qiagen) and from fresh frozen tissue using the AllPrep DNA/RNA Mini Kit (Qiagen). Figure 1 lists the patient samples where fresh frozen tissue (tumor and, where available, adjacent normal kidney) was available for WES. Illumina-compatible exome libraries were prepared from 200 ng of Bioruter Ultrasonicator (Diagenode) sheared RNase treated gDNA using the Agilent SureSelectXT Reagent Kit (Agilent Technologies). Libraries were uniquely indexed and prepared for capture with 8 to 11 cycles of PCR amplification, then assessed for size distribution on 4200 TapeStation High Sensitivity D1000 ScreenTape (Agilent Technologies) and quantified using the Qubit dsDNA HS Assay Kit (ThermoFisher Scientific). Exon target capture was performed using the Agilent SureSelectXT Human All Exon V7 Target Enrichment Baits. Following capture, the exon-enriched libraries were amplified using nine cycles of PCR, then assessed for size distribution using the Agilent TapesStation and quantified using the Qubit dsDNA HS Assay Kit. Libraries were multiplexed with eight samples per pool and the pools were quantified by qPCR using the KAPA Library Quantification Kit (Roche). The pool was sequenced in one lane of the HiSeq 4000 sequencer using the paired-end format.

To minimize sequence artifacts from FFPE-derived DNA, all tissue samples were less than one year old and were first reviewed by a genitourinary pathology expert (Priya Rao) to identify tumor-rich areas (or adjacent normal kidney where applicable) prior to proceeding with DNA isolation. We removed formaldehyde-induced crosslinks using a heat treatment step prior to sequencing as described in the QIAamp DNA FFPE Tissue kit (Qiagen). We followed rigorous quality control methods and used a high-fidelity capture-based sequencing approach using the Agilent SureSelectXT Human All Exon V7 Target Enrichment Baits known to perform well with FFPE samples (Do and Dobrovic, 2015). Baseline noise during sequencing of FFPE samples is in large part due to cytosine deamination. This usually occurs in one strand and not both DNA strands (Do and Dobrovic, 2015). Thus, we required that each specific mutant allele had to be detected in both strands in order to be called positive. This restriction allowed us to reliably distinguish true mutations from sequence artifacts.

The average mean target WES coverage was 73-fold for RMC tumor tissues and 60-fold for matched normal tissue, with a mean estimated tumor purity of 49.1% (range, 24%–98%). Previous benchmarking (Cibulskis et al., 2013) has demonstrated that our approximately 70-fold mean WES depth provided a >97% sensitivity to detect somatic mutations present in as low as 20% of sequenced cells, representing an expected mutation allele fraction of 0.1 (assuming that heterozygous mutations are present in a diploid region). However, more rare somatic mutations such as those present in 8% of sequenced cells would be detected with a sensitivity of approximately 53%. Thus, although our WES had high sensitivity to detect dominant clonal or subclonal RMC tumor mutations, it would be less likely to detect more rare subclonal alterations.

Confirmatory Sanger sequencing was performed at the MD Anderson Cancer Center Sequencing and Microarray Facility using Big Dye terminator cycle sequencing chemistry. We additionally performed hybrid capture-based targeted DNA sequencing in FFPE samples using FoundationOne CDx (Frampton et al., 2013) for untreated primary tumor samples from patients RMC5, RMC18,

RMC20, and RMC27, as well as PCR-amplicon-based target capture using OncoPrint (Luthra et al., 2017) for samples RMC4, RMC16, and RMC22. Gene Ontology analysis was carried out using DAVID release 6.8 with default parameters for biological processes (GOTERM_BP_FAT) (Huang da et al., 2009a; Huang da et al., 2009b).

Somatic Mutation Detection from Whole Exome Sequencing

The raw paired-end (PE) reads in FASTQ format were aligned to the human reference genome (hg19), using the MOSAIK alignment software (Lee et al., 2014). We then analyzed the resulting alignments with PCR duplicate removal using the Bayesian model-based software GigaBayes/FreeBayes (Marth et al., 1999), which enables efficient analysis of billions of aligned short-read sequences. The program evaluates each aligned base and its base quality value at each position to indicate putative single-nucleotide variations (SNVs) and short insertions/deletions (inDels), and their corresponding SNV probability value (P_{SNV}). Base quality values are converted to base probabilities corresponding to every one of the four possible nucleotides. Using a Bayesian formulation, a P_{SNV} (or inDel probability value, as appropriate) is calculated as the likelihood that multiple different alleles are present between the reference genome sequence and the reads aligned at that position. If the probability value exceeds a pre-specified threshold, the SNV or inDel candidate is reported in the output. We used a P_{SNV} cutoff value of 0.9 to define a high-confidence SNV or short inDel candidate. We also filtered out all known SNVs/inDels in UCSC dbSNP 142 (human). Furthermore, we required that a specific mutant allele had to be detected at least 6 times, and in both strands at least once, in order to be considered an SNV or inDel candidate. We then determined the somatic status of each SNV (or inDel) by comparing the genotypes and their likelihood in matched tumor and germline samples when available. The somatic status of a specific SNV/inDel was reported once the matched germline had wild allele-based homozygous genotype and the tumor had heterozygous or mutant allele-based homozygous genotype with a certain cutoff of genotype likelihood/p value of 0.99. Each somatic mutation or inDel was annotated with functional effect by SIFT (Vaser et al., 2016) to determine if a mutation candidate was synonymous or non-synonymous.

To maximize specificity in mutational signature analysis, we only used the 15 RMC samples with available germline tissue to calculate mutational signature weights. Sample RMC36T1 was excluded from further analysis because it lacked SNVs. All SNVs in a sample can be allocated to one of 96 “bins” according to the “before/after” status of the initial pyrimidine and the nucleotides on either side. The final vector of 96 bin counts defines a “mutational context histogram” (MCH) characterizing that sample. Particularly common MCH patterns can be used to define mutational “signatures” which may be indicative of modes of mutagenesis. The Sanger institute maintains a canonical set of 30 mutational signatures (<http://cancer.sanger.ac.uk/cosmic/signatures>) identified by applying non-negative matrix factorization (NMF) to the MCHs of thousands of tumors (Alexandrov et al., 2013). Taking these signatures as given, we can “score” the MCH of a new sample for the relative contributions of each signature using quadratic programming. We obtained the neighboring bases of each SNV using the R package, BSgenome.Hsapiens.UCSC.hg19 (version:1.4.0) (The Bioconductor Dev Team, 2014).

Comparison of non-synonymous mutation load per genome for different tumor types (shown in Figure 2A) was performed using our sequencing data from RMC as well as previously published DNA sequencing data (Chun et al., 2016) from 34 patients with MRT originating from the kidney, as well as tumors sequenced by The Cancer Genome Atlas (TCGA; <http://cancergenome.nih.gov/>). Tumors were abbreviated as per the following: ACC, adrenocortical carcinoma; BLCA, bladder urothelial carcinoma; BRCA, breast invasive carcinoma; ccRCC, clear cell renal cell carcinoma; CESC, cervical squamous cell carcinoma & endocervical adenocarcinoma; ChRCC, chromophobe renal cell carcinoma; COAD, colon adenocarcinoma; GBM, glioblastoma; HNSC, head & neck squamous cell carcinoma; LAML, acute myeloid leukemia; LGG, low grade glioma; LIHC, hepatocellular carcinoma; LUAD, lung adenocarcinoma; LUSC, lung squamous cell carcinoma; MRT, malignant rhabdoid tumor of the kidney; OV, ovarian serous cystadenocarcinoma; PAAD, pancreatic adenocarcinoma; PCPG, pheochromocytoma & paraganglioma; PRAD, prostate adenocarcinoma; PRCC, papillary renal cell carcinoma; READ, rectal adenocarcinoma; RMC, renal medullary carcinoma; SKCM, skin cutaneous melanoma; STAD, stomach adenocarcinoma; THCA, papillary thyroid carcinoma; UCEC, uterine corpus endometrial carcinoma; UCS, uterine carcinosarcoma.

Identification of Copy Number Alterations

Copy number analyses were performed on WES data of the 15 RMC samples with available germline tissue to improve the specificity of our results. The aligned reads were processed by our inhouse R package, ExomeCN (Zhang et al., 2014), followed by Circular Binary Segmentation (Olshen et al., 2004). ExomeCN is a modified version of HMMcopy (Ha et al., 2012) tuned for our data. Sequenza (Favero et al., 2015) with default parameters was used to estimate cellularity and ploidy and to identify and visualize copy number alterations (CNAs) per sample. Recurrent focal somatic CNAs were detected and localized using GISTIC2.0 (Mermel et al., 2011) (Beroukhi et al., 2010) with the thresholds of copy number amplifications/deletions being equal to ± 0.15 and q-value threshold being equal to 0.2. For comparison, we performed GISTIC2 analyses using the same parameters in previously published WES results from 35 patients with MRT and ATRT (Lee et al., 2012), comprised of 22 cases of ATRT, 4 cases of kidney MRT, and 9 cases of MRT arising from other soft tissues. Arm-level copy number alterations are defined by GISTIC as those exceeding half the length of a chromosome arm, whereas focal copy number alterations are those shorter than half the length of a chromosome arm. Using cytoband data from hg19 (<http://hgdownload.cse.ucsc.edu/goldenpath/hg19/database/>), we defined 8q gain as a gain in the following genome coordinates of chromosome 8: 45,600,000 to 146,364,022. Using these coordinates, a total of 376 protein-coding genes and 334 lncRNA genes from our RNA-seq profiling were mapped to the chromosome 8q arm.

Validation of WES copy number findings was performed using high-resolution oligonucleotide comparative genomic hybridization (CGH) arrays using standard operating procedures from Agilent Technologies (Agilent Oligonucleotide Array-Based CGH for Genomic DNA Analysis G4410-90010). Double enzymatic digestion (Alu I + Rsa I) was used to fragment 500 ng of DNA which was then evaluated with LabOnChip (2100 Bioanalyzer System; Agilent Technologies) prior to labeling and hybridization. Control DNA was used from Promega (Human Genomic DNA Female N 30742202/Male N 30993901). DNA was labeled by random priming with CY5-dCTPs (tumor DNA) and CY3-dCTPs (control DNA), and was hybridized to 4x180K whole-genome Agilent arrays (G4448A). Agilent G2565BA DNA Microarray Scanner was used to scan the chips. Image analysis and fluorescent signal acquisition were performed using the Feature-Extraction V9.1.3 software (Agilent Technologies).

RNA Sequencing

RNA was extracted from fresh frozen RMC (n = 11 cases), CDC (n = 9 cases), UTUC (n = 22 cases), and adjacent normal kidney (n = 6 patients with RMC) tissue samples using the RNeasy Kit (Qiagen) according to the manufacturer's instructions. Normal kidney tissues were obtained from locations at least 2 cm away from the primary tumors and the absence of metastatic cells was confirmed by a genitourinary pathology expert (Priya Rao). As a comparator, we used previously published RNA sequencing data (Chun et al., 2016) from 56 patients with MRT originating from the kidney (Table S4). As an additional control we randomly selected a dataset from The Cancer Genome Atlas (TCGA), comprised of ccRCC (n = 20 cases) (Cancer Genome Atlas Research Network, 2013), PRCC (n = 20 cases) (Cancer Genome Atlas Research Network et al., 2016), and ChRCC (n = 20 cases) (Davis et al., 2014) listed in Table S4.

After controlling for the quality of the initial samples, rRNA depletion was performed for the total RNA for each sample, followed by random-primed and stranded cDNA preparation and quality control. Total RNA was converted into a library of template molecules for sequencing on Illumina HiSeq2000, with a paired-end read length of 100 to 125 nt. The quality of the FASTQ reads was evaluated using the FastQC software (Andrews, 2014). The raw reads in FASTQ format were aligned to the reference human genome, hg19, using the MOSAIK alignment software (Lee et al., 2014). Gap alignment was performed using the Smith-Waterman algorithm in MOSAIK. Gene-level annotation was carried out using the GENCODE annotation, which was downloaded from the GENCODE project (Harrow et al., 2012). The overlaps between aligned reads and annotated genes were counted using HTSeq software (Anders et al., 2015). Gene counts were normalized using the scaling factor method. If the number of overlapped reads of any given gene was less than one per million total mapped reads for all samples, this gene was excluded from further analysis. Hierarchical clustering analyses were performed using the Pearson correlation coefficient as the distance metric and the ward's linkage rule. Principle component analyses (PCA) were also performed to explore the multi-gene structure. A negative binomial model was fit to the read counts of each gene. Then a Wald test was used to test the null hypothesis of no difference in gene expression between two conditions, e.g., tumor vs normal samples. The Benjamini & Hochberg (BH) method was used to control false discovery rate (FDR). These methods were implemented in the DESeq2 (Love et al., 2014) run on R version 3.2.3. Pathway diagram templates were taken from Chen et al. (Chen et al., 2018).

Virus Integration Analyses

The VirusSeq algorithmic method (<http://odin.mdacc.tmc.edu/~xsu1/VirusSeq.html>) was used to identify, as previously described (Chen et al., 2013), the following viruses and their integration sites from RNA-seq data: BK polyomavirus, cytomegalovirus, Epstein-Barr virus, hepatitis B virus, hepatitis C virus, human herpesvirus 1, human T-lymphotropic virus, human polyomavirus 2 (JC virus), Kaposi's sarcoma-associated herpesvirus, as well as human papillomavirus strains 6, 16, 18, 26, 30, 31, 33, 34, 35, 45, 52, 56, 58, 59, 68, 69, and 70.

Analysis of Kidney Nephron Atlas Expression Data

We used the gene expression profiles from different nephron sites (both human and mouse) obtained from the study by Cheval et al (Cheval et al., 2012). For each gene in our kidney cancer dataset (combined RMC, CDC, ccRCC, PRCC, ChRCC, and kidney MRT) we centered expression values on the mean centroid of these malignancies. Within each of the human and mouse datasets from the Cheval et al study, we centered values on the median across samples. Using the centered datasets for each kidney malignancy and the Cheval et al mRNA profile, we computed the global inter-profile correlation (by Pearson's), using all ~4000 genes in common, as previously described (Davis et al., 2014).

Gene Set Enrichment Analysis (GSEA)

We performed GSEA (Subramanian et al., 2005) of RNA-seq data using the R-GSEA script run in R version 3.2.3 using the following gene sets collected at the Molecular Signatures Database (MSigDB) (<http://software.broadinstitute.org/gsea/msigdb/collections.jsp>): (i) Fifty hallmark gene sets, which summarize and represent specific well-defined biological states or processes and display coherent expression. These gene sets were generated by a computational methodology based on identifying overlaps between gene sets in other MSigDB collections and retaining genes that display coordinate expression (Liberzon et al., 2015); (ii) Canonical pathway gene sets curated from online databases including BIOCARTEA, KEGG, and REACTOME; (iii) Gene Ontology (GO) gene sets.

Deconvolution of Tissue-Infiltrating Immune and Stromal Cell Populations

We used the Microenvironment Cell Populations-counter (MCP-counter) method (MCPcounter 1.1.0 package run on R version 3.2.3) to deconvolute and quantify eight immune and two stromal cell populations from RNA-seq data. The resulting scores for each cell

type were then Z-transformed. For each sample, MCP-counter produces an abundance score for CD3⁺ T cells, CD8⁺ T cells, cytotoxic lymphocytes, NK cells, B lymphocytes, monocytic lineage cells, myeloid dendritic cells, neutrophils, endothelial cells, and fibroblasts. Because MCP-counter scores are independently computed for each individual sample, they can be used for direct comparisons of cell type abundance across different samples (Becht et al., 2016).

DNA Methylation Analysis

DNA methylation was assessed using the Illumina Infinium HumanMethylation450 (HM450) BeadChip array in three untreated primary RMC tumor samples (PED4T, MED3T, and RMC8T), as well as normal kidney control samples from four patients with RMC (RMC2N, RMC4N, RMC5N, and RMC8N). Bisulfite conversion of genomic DNA (500–1000 ng) was performed using the Zymo EZ DNA methylation kit (Zymo Research, Irvine, CA) according to the manufacturer's recommendations. The quantity of bisulfite-converted DNA and the completeness of bisulfite conversion for each sample were assessed using a panel of MethyLight-based real-time PCR quality control assays as previously described (Campan et al., 2009). Bisulfite-converted DNA was subsequently used as a substrate for the HM450 BeadArrays, as recommended by the manufacturer. Specifically, each sample was whole-genome amplified (WGA), enzymatically fragmented, and then hybridized overnight to an 8-sample BeadArray, in which the WGA-DNA molecules annealed to locus-specific DNA oligomers linked to individual bead types. After the chemical processes, BeadArrays were scanned and the 'noob' function in the minfi R package (Aryee et al., 2014), which corrects for background fluorescence intensities and red-green dye bias (Triche et al., 2013), was used to extract raw signal intensities from the *.IDAT files. Probe alignment was performed using the hg19/GRCh37 human genome assembly. The beta (β) value for each probe was calculated using the formula $\beta = M/(M+U)$, in which M and U respectively refer to the (pre-processed) mean methylated and unmethylated probe signal intensities. The average β value reports a methylation signal ranging from 0 to 1, respectively representing completely unmethylated to completely methylated values. Probes in promoter CpG islands of *SMARCB1* with β -value ≤ 0.2 were considered unmethylated and those with β -value ≥ 0.3 were considered methylated.

Fluorescence In Situ Hybridization (FISH)

FISH was performed on paraffin sections according to the manufacturer's protocol using *SMARCB1*BA-20-GROR Break Apart probe (Empire Genomics) which is telomeric (orange label) and centromeric (green label) to the *SMARCB1* gene. Signal counts were performed on captured images of at least 50 non-overlapping tumor nuclei in two separate areas of a population of tumor cells. Samples with break-apart in $\geq 15\%$ of tumor nuclei were considered positive for *SMARCB1* translocation. Partial *SMARCB1* deletion was defined as loss of either green or orange probes in $\geq 15\%$ of tumor nuclei. Whole *SMARCB1* allele deletion was defined as $\geq 60\%$ loss of both green and orange probes.

Multiplex Ligation-Dependent Probe Amplification (MLPA)

MLPA was performed on genomic DNA according to the manufacturer's protocol using the SALSA MLPA P258 (*SMARCB1*) kit (MRC-Holland). This kit includes 2 probes for each of the 9 exons of *SMARCB1*, as well as probes for 9 other genes on chromosome 22 (*TBX1* exons 2 and 7, *DGCR8* exon 2, *SNAP29* exon 3, *LZTR1* exon 16, *PPIL2* exon 20, *GNAZ* exon 2, *SNRPD3* exon 2, *SEZ6L* exon 2, and *NIPSNAP1* exon 10), as well as 14 control probes for genes located on other chromosomes: *TNNT2* (chromosome 1), *POMC* (chromosome 2), *EDAR* (chromosome 2), *BMP2* (chromosome 2), *CASR* (chromosome 3), *IL4* (chromosome 5), *PKHD1* (chromosome 6), *PCDH15* (chromosome 10), *BEST1* (chromosome 11), *CSK* (chromosome 15), *FANCA* (chromosome 16), *CACNA1A* (chromosome 19), *JAG1* (chromosome 20), and *KCNJ6* (chromosome 21). Samples were processed and data were analyzed as previously described (Jalali et al., 2008). Dosage quotient (DQ) ratios were calculated and interpreted as follows: DQ = 0: homozygous deletion; $0.4 \leq DQ \leq 0.65$: heterozygous deletion; $0.7 < DQ < 1.3$: normal (identical to reference samples); $1.3 < DQ < 1.65$: heterozygous duplication; $1.75 < DQ < 2.15$: duplication; all other values: ambiguous result. All MLPA assays were performed in duplicate.

Spectral Karyotyping and G-banding

Exponentially growing cells were exposed to Colcemid (0.04 μ g/mL) for one hour at 37°C and to hypotonic treatment (0.075 M KCl) for 20 minutes at room temperature. Cells were fixed in a methanol and acetic acid (3:1 by volume) mixture for 15 min and washed three times in the fixative. Slides were prepared by dropping the cell suspension on wet slides and air drying.

G-banding was performed using trypsin solution and stained in Giemsa. Spectral karyotyping (SKY) was conducted according to the manufacturer's protocol using the human chromosome HiSKY probe (Applied Spectral Imaging, Inc.). A minimum of 18 metaphases were analyzed. Images were captured using a Nikon 80i microscope equipped with the HiBand spectral karyotyping software from Applied Spectral Imaging, Inc (Vista, CA).

SMARCB1 Re-expression Experiments

We used the tetracycline-inducible pIND20-fSNF5-HA vector (Wei et al., 2014) kindly donated by Dr. Bernard E. Weissman. The pInducer20 empty backbone (Meerbrey et al., 2011) was a gift from Stephen Elledge (Addgene plasmid # 44012 ; <http://n2t.net/addgene:44012> ; RRID:Addgene_44012). Lentivirus was generated in HEK-293FT cells and used to generate stable tet-inducible cell lines as previously described (Xu et al., 2001). All plasmid vectors were propagated in the E. coli strain DH5 α (Invitrogen; Cat#18265017). For all *SMARCB1* re-expression experiments, unless otherwise specified, a doxycycline concentration of 0.5 μ g/

mL was used for 3 days in cells harboring the tetracycline-inducible pIND20-fSNF5-HA vector or the pInducer20 empty backbone control.

Western Blot Analyses

Protein concentrations were measured by Pierce BCA protein assay kit. Before loading, samples were mixed with an equal volume of Laemmli Sample Buffer (Bio-Rad), heat denatured (100°C, 10 min) with β -mercaptoethanol (β -ME; Sigma-Aldrich), loaded in precast SDS/PAGE gels (Bio-Rad), transferred to PVDF membranes, and probed with specific primary antibodies overnight at 4°C. The following day, they were probed with secondary anti-mouse or anti-rabbit IgG conjugated horseradish peroxidase antibody, and chemiluminescence was detected by film exposure. The following primary antibodies were used: mouse monoclonal anti-SMARCB1 antibody clone 2C2 (Sigma-Aldrich; SAB4200202), rabbit polyclonal anti-phospho-Histone H2A.X at serine 139 (γ H2AX; Cell Signaling Technology; 2577), mouse monoclonal anti-c-MYC antibody 9E10 (Santa Cruz Biotechnology; sc-40), rabbit polyclonal anti-PARP (Cell Signaling Technology; 9542), goat polyclonal anti-ATR (Santa Cruz Biotechnology; sc-1887), rabbit polyclonal anti-phospho-ATR at serine 428 (Cell Signaling Technology; 2853), mouse monoclonal anti-TP53 (Santa Cruz Biotechnology; sc-126), rabbit polyclonal anti-phospho-TP53 at serine 15 (Cell Signaling Technology; 9284), mouse monoclonal anti-actin (Santa Cruz Biotechnology; sc-47778), rabbit polyclonal anti-phospho-CDK1 at tyrosine 15 (Cell Signaling Technology; 9111), mouse monoclonal anti-RPA 32 kDa subunit 9H8 (Santa Cruz Biotechnology; sc-56770), rabbit polyclonal anti-phospho-RPA32 at serines 4 and 8 (Bethyl Laboratories; A300-245A), mouse monoclonal anti-FANCD2 (Santa Cruz Biotechnology; sc-20022).

To reduce non-specific signals, membranes were blocked in 3% bovine serum albumin (BSA) or Odyssey blocking buffer (Licor). Membranes were incubated with indicated primary antibodies overnight at 4°C, washed in TBST buffer, and probed with HRP-conjugated secondary antibodies at room temperature for one hour. The detection of bands was carried out upon chemiluminescence reaction followed by film exposure. Western blots in the SMARCB1 rescue experiments were obtained after 5 days of doxycycline treatment. Western blots in the c-MYC knockdown experiments were obtained 3 days after MYC siRNA inhibition.

Co-immunoprecipitation Experiments

SMARCB1 was immunoprecipitated from cell extracts using anti-SMARCB1 antibody (Sigma-Aldrich; SAB4200202) and protein A/G agarose beads (Santa Cruz Biotechnology) using 1X cell lysis buffer [20 mM Tris-HCl (pH 7.5), 150 mM NaCl, 1 mM EDTA, 1 mM EGTA, 1% Triton X-100, and protease inhibitor cocktail (Roche)]. The immunoprecipitated complex was washed using phosphate-buffered saline (PBS) (3.2 mM Na₂HPO₄, 0.5 mM KH₂PO₄, 1.3 mM KCl, 135 mM NaCl, pH 7.4) containing 1% Triton X-100 (PBST). Following immunoprecipitation, the samples were subjected to SDS-PAGE gel electrophoresis under denaturing conditions, and subsequently immunoblotted using antibodies against PBRM1 (rabbit polyclonal; Bethyl Laboratories, A301-591A), SMARCA4 (rabbit monoclonal; Abcam; ab110641), and ARID1A (mouse monoclonal; Santa Cruz Biotechnology; sc-32761). TrueBlot anti-rabbit or mouse IgG-HRP (Rockland) were used as secondary antibodies.

Immunohistochemistry

Immunohistochemistry (IHC) was performed on FFPE tumor tissue sections. The tumor tissues were fixed in 10% formalin, embedded in paraffin, and transversely sectioned. Four- μ m sections were used for the IHC analyses. The sections were stained with a rabbit anti-human monoclonal antibody against STING (Cell Signaling, clone D2P2F; 13647S, dilution 1:100), PD-L1 (Cell Signaling, 13684S; 1:100), and PD-1 (Abcam, AB201825; 1:250), rabbit anti-human polyclonal antibody against CD3 (Agilent, A0452, 1:100), and mouse anti-human monoclonal antibodies against CD4 (Leica Biosystems, NCL-L-CD4-368; 1:80), CD8 (Thermo Scientific, MS-457-S; 1:25), FOXP3 (BioLegend, clone 206D, dilution 1:50), CD20 (Agilent; L26, 1:1,400), and CD68 (Agilent, M0876; 1:450). All slides were stained as previously described (Chen et al., 2016) using previously optimized conditions with appropriate positive and negative controls. The IHC reaction was detected using the Leica Bond Polymer Refine detection kit (Leica Biosystems) with diaminobenzidine (DAB) used as chromogen. Counterstaining was done using hematoxylin. IHC and hematoxylin- and eosin-stained slides were converted into high-resolution digital images using an Aperio slide scanner (Aperio AT Turbo, Leica Biosystems). Quantitative IHC staining of CD3, CD4, CD8, CD20, CD68, FOXP3, PD-1, and PD-L1 was evaluated by quantification of the density of positive cells (defined as the number of positive cells per mm²), percentage of positive cells, and H-score as previously described (Parra et al., 2016). Quantitative analysis of STING expression was performed using ImageJ according to the provider's instructions (Schneider et al., 2012). To facilitate the identification of malignant cells and direct quantification, all IHC stains were interpreted in conjunction with H&E-stained sections. This approach can help distinguish tumor cells from immune cells and thus allow reliable PD-L1 immune quantification on different cell subsets as previously established (Herbst et al., 2014; Tumei et al., 2014; Twyman-Saint Victor et al., 2015).

Small Interfering RNA (siRNA) Knockdown

Knockdown of c-MYC was achieved using siGENOME Human MYC siRNA SMARTpool at a concentration of 10 nM or sham control obtained by Horizon Discovery (Lafayette, CO).

CRISPR/Cas9 Knockout

Knockout of *SMARCB1* was achieved by lentivirus generated in HEK-293FT cells using pLentiCRISPR v2 plasmids harboring gRNA sequences against *SMARCB1* obtained from Genscript (Piscataway, NJ, USA). We used psPAX2, a gift from Didier Trono (Addgene

plasmid # 12260 ; <http://n2t.net/addgene:12260> ; RRID:Addgene_12260) for lentiviral packaging, as well as pMD2.G, also a gift from Didier Trono (Addgene plasmid # 12259 ; <http://n2t.net/addgene:12259> ; RRID:Addgene_12259) for lentiviral envelope expression. Lentiviral transduced cells were selected with puromycin. As negative control, we used cells transduced by lentivirus generated using a pLentiCRISPR v2 plasmid harboring non-targeting control gRNA (BRDN0001145885) (Doench et al., 2016), a gift from John Doench & David Root (Addgene plasmid # 80196 ; <http://n2t.net/addgene:80196> ; RRID:Addgene_80196). Propagation of all plasmid vectors was performed using the E. coli strain DH5 α (Invitrogen; Cat#18265017).

gRNA target sequences used for human *SMARCB1* knockout:

- TGAGAACGCATCTCAGCCCG
- CATCGATCTCCATGTCCAGC

Non-targeting control gRNA sequence:

- GGGACGCGAAAGAAACCAGT

Immunofluorescence Staining

RMC2C and RMC219 cells were plated onto a 6-well culture dish on a coverslip and fixed in 4% paraformaldehyde for 20 minutes, then washed 2 times with PBS. After washing again, cells were permeabilized and stained with a solution of 0.5% Triton X-100 for 15 minutes, then washed 2 times after permeabilization with PBS and blocked for one hour using 3.75% BSA. After blocking, the primary rabbit γ H2AX antibody (Cell Signaling Technology; catalogue#2577) was added in 3.75% BSA solution at a ratio of 1:500 and incubated overnight at 4°C. After the overnight incubation, cells were washed 3 times and then incubated for one hour with Alexa Fluor 546 anti-rabbit secondary fluorescent antibody purchased from Invitrogen (Life Technologies). The nuclear content was stained with DAPI reagent (Invitrogen, Life Technologies) for 10 minutes at room temperature. Cells were washed again 3 times with PBS and mounted on a slide using slowfade gold antifade solution (Thermo Fisher Scientific). The corners were sealed using nail polish and images were taken using a Nikon Eclipse Ti2 deconvolution microscope. γ H2AX foci within nuclei were quantified using the FindFoci plugin in ImageJ (Herbert et al., 2014).

Chromatin Immunoprecipitation Sequencing (ChIP)

We analyzed previously published c-MYC chromatin immunoprecipitation sequencing (ChIP-Seq) data from *SMARCB1*-negative G401 cells expressing tetracycline-inducible enhanced fluorescent protein (EGFP) control or *SMARCB1* (Weissmiller et al., 2019). ChIP-seq maps were generated by mapping reads to the human genome GRCh38 using bowtie2 (Langmead and Salzberg, 2012), and visualizing genome-wide maps using the Integrative Genome Viewer software (Thorvaldsdottir et al., 2013). c-MYC peaks were called using MACS2 (Zhang et al., 2008) at an FDR < 0.05. We first determined the union of peaks over the two replicates of each experiment, then determined the lost c-MYC peaks after *SMARCB1* re-expression using BEDTOOLS (Quinlan and Hall, 2010). Finally, lost c-MYC peaks were annotated for nearby genes, within a 10 kbp window from the gene body, using BEDTOOLS (Quinlan and Hall, 2010). Enriched pathways were determined using the hypergeometric distribution, with significance achieved at FDR-adjusted p value < 0.05 against the Hallmark and REACTOME compendia of pathways (Fabregat et al., 2018; Liberzon et al., 2015).

For the chromatin immunoprecipitation quantitative polymerase chain reaction (ChIP-qPCR) experiments, RMC2C cells expressing tetracycline-inducible *SMARCB1* or empty vector control were plated at 10×10^6 cells per plate and treated with 0.5 μ g/mL doxycycline for 48 hours. The cells were crosslinked using 0.4% paraformaldehyde for 10 minutes, quenched with 0.125M glycine for 10 minutes, washed with ice-cold PBS two times, and collected by centrifugation. Nuclei were extracted in 50 mM Tris HCl, pH8, 10 mM EDTA, 1% SDS for 15 minutes on ice. Chromatin was fragmented using a Covaris E220 ultrasonicator, and debris were removed by centrifugation. Chromatin was frozen at -80°C until ready to use. Each immuno-precipitation was performed on chromatin collected from 10×10^6 cells by dilution in 8 volumes of ChIP dilution buffer (16.7 mM Tris HCl, pH 8, 167 mM NaCl, 1.2 mM EDTA, 1.1% Triton, 0.01% SDS) using 5 μ g of rabbit polyclonal antibody against c-MYC (Santa Cruz Biotechnology, sc-764) or normal rabbit IgG control (Cell Signaling, 2729; 5 μ g). Immunoprecipitated chromatin was bound to protein A Dynabeads (Thermo-Fisher Scientific) and washed twice sequentially with low salt buffer (20 mM Tris HCl, pH 8, 150 mM NaCl, 2 mM EDTA, 1% Triton, 0.1% SDS), high salt buffer (20 mM Tris HCl, pH 8, 500 mM NaCl, 2mM EDTA, 1% Triton, 0.1% SDS), lithium chloride buffer (10 mM Tris HCl, pH 8, 0.25 M LiCl, 1 mM EDTA, 1% NP-40, 1% sodium deoxycholate) and TE (10 mM Tris HCl, pH 8, 1 mM EDTA). Dynabead-bound chromatin was eluted in 1% SDS and 0.1 M NaHCO₃ two times for 15 minutes at room temperature, before being treated with 10 μ g RNase A overnight at 65°C. DNA was then decrosslinked with 20 μ g proteinase K for 1hr at 42°C before extraction using a classical phenol/chloroform protocol. Samples were diluted in distilled water and quantified by Q-PCR using the following primers targeting the transcription start sites of each gene:

- *CCNE2* : CAGCACAACGTGGAGTGG and AGAGCAGAGCCGCACTTG
- *CDK4* : ATGTGACCAGCTGCCAAAG and TTACTCTTCGCCCTCCTC
- *ATF4* : CGAAGGAAAGAACGGACTCTG and TTATGGCCTCACGAAAGGAG
- *PRM1* : ACAGAGCGACACCCTGTCAT and AGGCGGTGGTTACACAACAT

Chemical Compounds

Olaparib, niraparib, VX970, AZD6738, and adavosertib were obtained from Selleckchem (Houston, TX, USA) and dissolved in DMSO. Clinical-grade doxorubicin, gemcitabine, carboplatin, cisplatin, and paclitaxel were obtained from the Department of Pharmacy at The University of Texas MD Anderson Cancer Center (Houston, TX, USA).

Cell Viability Experiments

Cell viability was determined using the cell proliferation kit 3-(4,5-dimethylthiazol-2-yl)-2,5-diphenyltetrazolium bromide (MTT) colorimetric assay (Sigma-Aldrich). Cells were plated in 96-well plates at a density of 5.0×10^3 cells/well. Twenty-four hours after seeding, the cells were treated with different drug concentrations ranging from 0.01 to 20 μM . The MTT assay was performed at 120 hours after treatment. The cells were incubated with 10% MTT added directly to the medium for 4 hours at 37°C, followed by cell lysis with detergent reagent overnight in the dark at room temperature. Absorbance was determined at 570 nm in three independent wells per condition for each experiment and results are presented as the means of at least three independent experiments. Dose response curves and the half maximal inhibitory concentration (IC_{50}) were calculated using the Dr Fit software (Di Veroli et al., 2015). For all SMARCB1 re-expression cell viability experiments, a doxycycline concentration of 0.5 $\mu\text{g}/\text{mL}$ was used for 3 days in cells harboring the tetracycline-inducible pIND20-fSNF5-HA vector or the plnducer20 empty backbone control prior to initiating drug treatments. For siRNA knockdown cell viability experiments, cells were first treated with siRNA against c-MYC or sham control for 72 hours prior to initiating drug treatments. Chemotherapy drug concentrations used for *in vitro* experiments were all chosen to be less than their respective peak plasma concentrations in humans (Ciccolini et al., 2016; Pavlik et al., 1982; Swift and Golsteyn, 2014; Von Hoff et al., 1986).

DNA Fiber Assay

DNA fiber assays were performed as previously described (Jackson and Pombo, 1998; Schlacher et al., 2011). Briefly, cells were labeled with IdU (50 μM , 25 min), followed by labeling with CldU (50 μM , 25 min) and spread as described before standard detection of IdU and CldU tracts using primary antibodies against anti-IdU / anti-BrdU (mouse monoclonal; BD Biosciences; clone B44, 1:100 in blocking buffer) and anti-CldU / anti-BrdU [rat monoclonal; Santa Cruz Biotechnology; BU1/75(ICR1), sc-56258, 1:200 in blocking buffer], as well as secondary antibodies goat polyclonal anti-mouse Alexa Fluor 488 (ThermoFisher; A-11001, 1:200 in blocking buffer) and goat polyclonal anti-rat Alexa Fluor 555 (ThermoFisher; A-21434, 1:300 in blocking buffer), respectively. Fibers were imaged (Nikon microscope) and analyzed using ImageJ software (Schneider et al., 2012). The rate for nascent tract replication was estimated using the conversion of 2.59 kb/ μm (Jackson and Pombo, 1998).

In Vivo Treatments

Studies involving animals, including housing and care, method of euthanasia, and experimental protocols were approved by the University of Texas MD Anderson Cancer Center Animal Care and Use Committee and were in accordance with appropriate guidelines (protocol ACUF 00000884-RN02). To test the *in vivo* efficacy of drugs targeting DDR pathways, CB-17 female scid mice aged 6–9 weeks old and harboring subcutaneous RMC PDX tumors were randomly assigned to one of four treatment groups ($n = 5$ mice/group): 1) oral administration of the PARP inhibitor niraparib (50 mg/kg/day) + oral vehicle control (DMSO) once daily, 2) oral administration of the ATR inhibitor AZD6738 (25 mg/kg/day) + oral vehicle control (DMSO) once daily, 3) oral administration of niraparib (50 mg/kg/day) + oral AZD6738 (25 mg/kg/day) once daily, 4) oral administration of only vehicle control (DMSO) once daily. Mice were treated daily for 5 days with 2 days off treatment for a total period of 25 days. For preclinical *in vivo* testing of niraparib alone or in combination with cisplatin, mice were randomly assigned to one of four treatment groups ($n = 10$ mice/group): 1) Oral administration of niraparib (50 mg/kg/day) once daily + cisplatin 1.25 mg/kg intraperitoneally weekly, 2) oral vehicle control (DMSO) once daily + cisplatin 1.25 mg/kg intraperitoneally weekly, 3) Oral administration of niraparib (50 mg/kg/day) once daily + vehicle control (normal saline) intraperitoneally weekly, 4) oral vehicle control (DMSO) once daily + vehicle control (normal saline) intraperitoneally weekly. Niraparib or oral vehicle control were administered daily for 5 days with 2 days off treatment for a total period of 25 days. Cisplatin or intraperitoneal vehicle control were administered weekly x3 weeks. Treatments were started when tumor volume reached 100 to 200 mm^3 . Tumor volume was measured twice weekly using Vernier calipers and calculated by the formula: volume = [(smallest diameter)² × (largest diameter)]/2.

QUANTIFICATION AND STATISTICAL ANALYSIS

All statistical analyses were performed using R (R Core Team, 2019). Continuous measures are presented as the mean \pm standard error of the mean of biological replicates. Differences in means between two groups for all *in vitro* experiments were compared using a two-tailed Welch's *t* test unless otherwise specified in the text and figures. The *p* values for the pathway diagrams in Figures 4E, 4F, and 5F were generated using the Wald test. The *p* values for STING IHC quantification levels in Figure 5E, the ChIP-qPCR in Figure 6G, and the comparisons between DNA fiber tract lengths in Figure 6H were generated using the Mann-Whitney U test. For *in vivo* tumor growth assessment, groups of mice randomized to each treatment ($n = 5$ per group) were monitored twice weekly. We performed semiparametric ANCOVA by generating proportional odds models using the regression modeling strategies (rms) statistical package in R (version 3.2.3). Regression imputation was used for missing data. A smooth nonlinear relationship was assumed between baseline and final tumor volumes at the end of treatment, using restricted cubic splines with three knots (Harrell, 2015). Power analyses were performed using the popower function in the Hmisc package in R (version 3.2.3). With $n = 5$ mice per group, we had

approximately 80% power at the 0.05 alpha level to detect a difference in tumor volume between two groups by an effect size of 1.875 (Cohen's *d*) at the end of treatment. With $n = 10$ mice per group, we had approximately 80% power at the 0.05 alpha level to detect a difference in tumor volume between two groups by an effect size of 1.27 (Cohen's *d*) at the end of treatment.

DATA AND CODE AVAILABILITY

Sequencing data generated in this paper have been deposited at the NCBI Sequence Read Archive (SRA) hosted by the NIH (SRA accession: PRJNA605003). Clear cell renal cell carcinoma, papillary renal cell carcinoma, and chromophobe renal cell carcinoma sequencing data were obtained from the Cancer Genome Atlas (<https://portal.gdc.cancer.gov/projects/>). Kidney MRT sequencing data were generated by [Chun et al. \(2016\)](#) (dbGaP accession number phs000470.v18.p7). MRT and ATRT sequencing data were generated by [Lee et al. \(2012\)](#) (dbGaP accession number phs000508). G401 c-MYC ChIP-seq data were generated by [Weissmiller et al. \(2019\)](#) (GEO accession number GSE109310).

BIBLIOGRAPHY

Bibliography Chapter I.....	378
Bibliography Chapter II.....	388
Bibliography Chapter III.....	403

BIBLIOGRAPHY CHAPTER I

- Adelman, K. and Lis, J. T. (2012) 'Promoter-proximal pausing of RNA polymerase II: emerging roles in metazoans.', *Nature reviews. Genetics*. Nature Publishing Group, 13(10), pp. 720–731. doi: 10.1038/nrg3293.
- Aiyar, S. E. *et al.* (2004) 'Attenuation of estrogen receptor α -mediated transcription through estrogen-stimulated recruitment of a negative elongation factor', *Genes and Development*. Cold Spring Harbor Laboratory Press, 18(17), pp. 2134–2146. doi: 10.1101/gad.1214104.
- Armache, K. J. *et al.* (2005) 'Structures of complete RNA polymerase II and its subcomplex, Rpb4/7', *Journal of Biological Chemistry*. J Biol Chem, 280(8), pp. 7131–7134. doi: 10.1074/jbc.M413038200.
- Ballas, N. *et al.* (2005) 'REST and its corepressors mediate plasticity of neuronal gene chromatin throughout neurogenesis', *Cell*, 121(4), pp. 645–657. doi: 10.1016/j.cell.2005.03.013.
- Banani, S. F. *et al.* (2017) 'Biomolecular condensates: Organizers of cellular biochemistry', *Nature Reviews Molecular Cell Biology*. Nature Publishing Group, 18(5), pp. 285–298. doi: 10.1038/nrm.2017.7.
- Banerji, J., Rusconi, S. and Schaffner, W. (1981) 'Expression of a β -globin gene is enhanced by remote SV40 DNA sequences', *Cell*, 27(2 PART 1), pp. 299–308. doi: 10.1016/0092-8674(81)90413-X.
- Bannister, A. J. and Kouzarides, T. (2011) 'Regulation of chromatin by histone modifications', *Cell Research*. Nature Publishing Group, 21(3), pp. 381–395. doi: 10.1038/cr.2011.22.
- Barski, A. *et al.* (2007) 'High-Resolution Profiling of Histone Methylations in the Human Genome', *Cell*. Elsevier, 129(4), pp. 823–837. doi: 10.1016/j.cell.2007.05.009.
- Bartkowiak, B. and Greenleaf, A. L. (2011) 'Phosphorylation of RNAPII: To P-TEFb or not to P-TEFb?', *Transcription*. Taylor and Francis Inc., 2(3), pp. 115–119. doi: 10.4161/trns.2.3.15004.
- Basehoar, A. D., Zanton, S. J. and Pugh, B. F. (2004) 'Identification and distinct regulation of yeast TATA box-containing genes', *Cell*. Cell, 116(5), pp. 699–709. doi: 10.1016/S0092-8674(04)00205-3.
- Bellush, J. M. and Whitehouse, I. (2017) 'DNA replication through a chromatin environment', *Philosophical Transactions of the Royal Society B: Biological Sciences*. Royal Society Publishing. doi: 10.1098/rstb.2016.0287.
- Benoist, C. and Chambon, P. (1981) 'In vivo sequence requirements of the SV40 early promoter region', *Nature*, 290(5804), pp. 304–310. doi: 10.1038/290304a0.
- Bentwich, I. *et al.* (2005) 'Identification of hundreds of conserved and nonconserved human microRNAs', *Nature Genetics*, 37(7), pp. 766–770. doi: 10.1038/ng1590.
- Bernstein, B. E. *et al.* (2006) 'A Bivalent Chromatin Structure Marks Key Developmental Genes in Embryonic Stem Cells', *Cell*. Elsevier, 125(2), pp. 315–326. doi: 10.1016/j.cell.2006.02.041.
- Bian, C. *et al.* (2011) 'Sgf29 binds histone H3K4me2/3 and is required for SAGA complex recruitment and histone H3 acetylation', *EMBO Journal*. European Molecular Biology Organization, 30(14), pp. 2829–2842. doi: 10.1038/emboj.2011.193.
- Bonnet, J. *et al.* (2014) 'The SAGA coactivator complex acts on the whole transcribed genome and is required for RNA polymerase II transcription', *Genes and Development*, 28(18), pp. 1999–2012. doi: 10.1101/gad.250225.114.
- Buratowski, S. (2009) 'Progression through the RNA Polymerase II CTD Cycle', *Molecular Cell*. Mol Cell, pp. 541–546. doi: 10.1016/j.molcel.2009.10.019.
- Cattoni, D. I. *et al.* (2017) 'Single-cell absolute contact probability detection reveals chromosomes are organized by multiple low-frequency yet specific interactions', *Nature Communications*. Nature Publishing Group, 8(1), pp. 1–10. doi: 10.1038/s41467-017-01962-x.
- Chandy, M. *et al.* (2006) 'SWI/SNF displaces SAGA-acetylated nucleosomes', *Eukaryotic Cell*.

- American Society for Microbiology Journals, 5(10), pp. 1738–1747. doi: 10.1128/EC.00165-06.
- Chatterjee, N., Walker, G. C. (2017) ‘Mechanisms of DNA damage, repair, and mutagenesis. Environmental and molecular mutagenesis’, *Physiology & behavior*, 58(5), pp. 235–263. doi: 10.1002/em.22087.Mechanisms.
- Chen, C. Y. A. and Shyu, A. Bin (2011) ‘Mechanisms of deadenylation-dependent decay’, *Wiley Interdisciplinary Reviews: RNA*, 2(2), pp. 167–183. doi: 10.1002/wrna.40.
- Chen, D. *et al.* (2018) ‘Super enhancer inhibitors suppress MYC driven transcriptional amplification and tumor progression in osteosarcoma’, *Bone Research*. Sichuan University, 6(1). doi: 10.1038/s41413-018-0009-8.
- Chen, F. X., Smith, E. R. and Shilatifard, A. (2018) ‘Born to run: Control of transcription elongation by RNA polymerase II’, *Nature Reviews Molecular Cell Biology*. Springer US, 19(7), pp. 464–478. doi: 10.1038/s41580-018-0010-5.
- Chen, J. *et al.* (2014) ‘Single-molecule dynamics of enhanceosome assembly in embryonic stem cells’, *Cell*. Cell Press, 156(6), pp. 1274–1285. doi: 10.1016/j.cell.2014.01.062.
- Chen, Y. *et al.* (2004) ‘A constitutive super-enhancer: Homologous region 3 of Bombyx mori nucleopolyhedrovirus’, *Biochemical and Biophysical Research Communications*, 318(4), pp. 1039–1044. doi: 10.1016/j.bbrc.2004.04.136.
- Coin, F. *et al.* (1998) ‘Mutations in the XPD helicase gene result in XP and TTD phenotypes, preventing interaction between XPD and the p44 subunit of TFIIH’, *Nature Genetics*, 20(2), pp. 184–188. doi: 10.1038/2491.
- Coin, F., Oksenysh, V. and Egly, J. M. (2007) ‘Distinct Roles for the XPB/p52 and XPD/p44 Subcomplexes of TFIIH in Damaged DNA Opening during Nucleotide Excision Repair’, *Molecular Cell*. Cell Press, 26(2), pp. 245–256. doi: 10.1016/j.molcel.2007.03.009.
- Compe, E. *et al.* (2019) ‘TFIIE orchestrates the recruitment of the TFIIH kinase module at promoter before release during transcription’, *Nature Communications*. Springer US, 10(1). doi: 10.1038/s41467-019-10131-1.
- Compe, E. and Egly, J. M. (2012) ‘TFIIH: When transcription met DNA repair’, *Nature Reviews Molecular Cell Biology*. Nat Rev Mol Cell Biol, pp. 343–354. doi: 10.1038/nrm3350.
- Cramer, P. *et al.* (2000) ‘Architecture of RNA polymerase II and implications for the transcription mechanism’, *Science*, 288(5466), pp. 640–649. doi: 10.1126/science.288.5466.640.
- Cramer, P. (2019) ‘Organization and regulation of gene transcription’, *Nature*. Springer US, 573(7772), pp. 45–54. doi: 10.1038/s41586-019-1517-4.
- Crick, F. and Watson, J. (1953) ‘© 1953 Nature Publishing Group’.
- Danino, Y. M. *et al.* (2015) ‘The core promoter: At the heart of gene expression’, *Biochimica et Biophysica Acta - Gene Regulatory Mechanisms*. Elsevier B.V., 1849(8), pp. 1116–1131. doi: 10.1016/j.bbagr.2015.04.003.
- Dekker, J. and Mirny, L. (2016) ‘The 3D Genome as Moderator of Chromosomal Communication’, *Cell*. Cell Press, pp. 1110–1121. doi: 10.1016/j.cell.2016.02.007.
- Dodonova, S. O. *et al.* (2020) ‘Nucleosome-bound SOX2 and SOX11 structures elucidate pioneer factor function’, *Nature*. Springer US, 580(7805), pp. 669–672. doi: 10.1038/s41586-020-2195-y.
- Donner, A. J. *et al.* (2010) ‘CDK8 is a positive regulator of transcriptional elongation within the serum response network’, *Nature Structural and Molecular Biology*. Nature Publishing Group, 17(2), pp. 194–201. doi: 10.1038/nsmb.1752.
- Egly, J. M. and Coin, F. (2011) ‘A history of TFIIH: Two decades of molecular biology on a pivotal transcription/repair factor’, *DNA Repair*. Elsevier B.V., 10(7), pp. 714–721. doi: 10.1016/j.dnarep.2011.04.021.

- van Emmerik, C. L. and van Ingen, H. (2019) ‘Unspinning chromatin: Revealing the dynamic nucleosome landscape by NMR’, *Progress in Nuclear Magnetic Resonance Spectroscopy*. The Authors, 110, pp. 1–19. doi: 10.1016/j.pnmrs.2019.01.002.
- Erdel, F. and Rippe, K. (2018) ‘Formation of Chromatin Subcompartments by Phase Separation’, *Biophysical Journal*. Biophysical Society, pp. 2262–2270. doi: 10.1016/j.bpj.2018.03.011.
- Ernst, J. *et al.* (2011) ‘Mapping and analysis of chromatin state dynamics in nine human cell types’, *Nature*. Nature Publishing Group, 473(7345), pp. 43–49. doi: 10.1038/nature09906.
- Ernst, J. and Kellis, M. (2013) ‘Interplay between chromatin state, regulator binding, and regulatory motifs in six human cell types’, *Genome Research*. Genome Res, 23(7), pp. 1142–1154. doi: 10.1101/gr.144840.112.
- Evangelista, F. M. *et al.* (2018) ‘Transcription and mRNA export machineries SAGA and TREX-2 maintain monoubiquitinated H2B balance required for DNA repair’, *Journal of Cell Biology*. Rockefeller University Press, 217(10), pp. 3382–3397. doi: 10.1083/jcb.201803074.
- Evrin, C. *et al.* (2018) ‘Histone H2A-H2B binding by Pol α in the eukaryotic replisome contributes to the maintenance of repressive chromatin’, *The EMBO Journal*. EMBO, 37(19). doi: 10.15252/emj.201899021.
- Feller, C. *et al.* (2015) ‘Global and specific responses of the histone acetylome to systematic perturbation’, *Molecular Cell*, 57(3), pp. 559–571. doi: 10.1016/j.molcel.2014.12.008.
- Fica, S. M. and Nagai, K. (2017) ‘Cryo-electron microscopy snapshots of the spliceosome: Structural insights into a dynamic ribonucleoprotein machine’, *Nature Structural and Molecular Biology*, 24(10), pp. 791–799. doi: 10.1038/nsmb.3463.
- Finn, E. H. and Misteli, T. (2019) ‘Molecular basis and biological function of variability in spatial genome organization’, *Science*, 365(6457). doi: 10.1126/science.aaw9498.
- Flavahan, W. A. *et al.* (2016) ‘Insulator dysfunction and oncogene activation in IDH mutant gliomas’, *Nature*. Nature Publishing Group, 529(7584), pp. 110–114. doi: 10.1038/nature16490.
- Foltz, D. R. *et al.* (2006) ‘The human CENP-A centromeric nucleosome-associated complex’, *Nature Cell Biology*, 8(5), pp. 458–469. doi: 10.1038/ncb1397.
- Fouse, S. D. *et al.* (2008) ‘Promoter CpG Methylation Contributes to ES Cell Gene Regulation in Parallel with Oct4/Nanog, PcG Complex, and Histone H3 K4/K27 Trimethylation’, *Cell Stem Cell*, 2(2), pp. 160–169. doi: 10.1016/j.stem.2007.12.011.
- Gannon, F. *et al.* (1979) ‘Gene, Organisation and sequences at the 5’ end of a cloned complete ovalbumin’, *Saudi Med J*, (278), pp. 428–434.
- Garvie, C. W. and Wolberger, C. (2001) ‘Recognition of specific DNA sequences’, *Molecular Cell*. Cell Press, pp. 937–946. doi: 10.1016/S1097-2765(01)00392-6.
- Gavrilov, A. A. *et al.* (2020) ‘Studying RNA-DNA interactome by Red-C identifies noncoding RNAs associated with various chromatin types and reveals transcription dynamics’, *Nucleic acids research*. NLM (Medline), 48(12), pp. 6699–6714. doi: 10.1093/nar/gkaa457.
- Goldman, J. A., Garlick, J. D. and Kingston, R. E. (2010) ‘Chromatin remodeling by imitation switch (ISWI) class ATP-dependent remodelers is stimulated by histone variant H2A.Z’, *Journal of Biological Chemistry*, 285(7), pp. 4645–4651. doi: 10.1074/jbc.M109.072348.
- Guillemette, B. *et al.* (2005) ‘Variant histone H2A.z is globally localized to the promoters of inactive yeast genes and regulates nucleosome positioning’, *PLoS Biology*, 3(12), pp. 1–11. doi: 10.1371/journal.pbio.0030384.
- Haberle, V. and Stark, A. (2018) ‘Eukaryotic core promoters and the functional basis of transcription initiation’, *Nature Reviews Molecular Cell Biology*. Nature Publishing Group, pp. 621–637. doi: 10.1038/s41580-018-0028-8.

- Hahn, S. (2004) ‘Structure and mechanism of the RNA polymerase II transcription machinery’, *Nature Structural and Molecular Biology*. Nat Struct Mol Biol, pp. 394–403. doi: 10.1038/nsmb763.
- Hantsche, M. and Cramer, P. (2017) ‘Conserved RNA polymerase II initiation complex structure’, *Current Opinion in Structural Biology*. Elsevier Ltd, 47, pp. 17–22. doi: 10.1016/j.sbi.2017.03.013.
- Hegi, M. E. *et al.* (2005) ‘MGMT gene silencing and benefit from temozolomide in glioblastoma’, *New England Journal of Medicine*. N Engl J Med, 352(10), pp. 997–1003. doi: 10.1056/NEJMoa043331.
- Helmlinger, D. and Tora, L. (2017) ‘Sharing the SAGA’, *Trends in Biochemical Sciences*. Elsevier Ltd, 42(11), pp. 850–861. doi: 10.1016/j.tibs.2017.09.001.
- Hsin, J. P. and Manley, J. L. (2012) ‘The RNA polymerase II CTD coordinates transcription and RNA processing’, *Genes and Development*. Cold Spring Harbor Laboratory Press, pp. 2119–2137. doi: 10.1101/gad.200303.112.
- Huang, R. X. and Zhou, P. K. (2020) ‘DNA damage response signaling pathways and targets for radiotherapy sensitization in cancer’, *Signal Transduction and Targeted Therapy*. Springer US, 5(1). doi: 10.1038/s41392-020-0150-x.
- Inoue, D. *et al.* (2019) ‘Spliceosomal disruption of the non-canonical BAF complex in cancer’, *Nature*. Nature Publishing Group, 574(7778), pp. 432–436. doi: 10.1038/s41586-019-1646-9.
- Janssen, A., Colmenares, S. U. and Karpen, G. H. (2018) ‘Heterochromatin: Guardian of the Genome’, *Annual Review of Cell and Developmental Biology*. Annual Reviews, 34(1), pp. 265–288. doi: 10.1146/annurev-cellbio-100617-062653.
- Jeggo, P. A., Downs, J. A. and Gasser, S. M. (2017) ‘Chromatin modifiers and remodellers in DNA repair and signalling’, *Philosophical Transactions of the Royal Society B: Biological Sciences*, 372(1731). doi: 10.1098/rstb.2016.0279.
- Jia, Q. *et al.* (2020) ‘Oncogenic super-enhancer formation in tumorigenesis and its molecular mechanisms’, *Experimental and Molecular Medicine*. Springer Nature, pp. 713–723. doi: 10.1038/s12276-020-0428-7.
- Jin, V. X. *et al.* (2006) ‘Genome-wide analysis of core promoter elements from conserved human and mouse orthologous pairs’, *BMC Bioinformatics*. BioMed Central, 7, p. 114. doi: 10.1186/1471-2105-7-114.
- Juven-Gershon, T. and Kadonaga, J. T. (2010) ‘Regulation of gene expression via the core promoter and the basal transcriptional machinery’, *Developmental Biology*. Academic Press Inc., pp. 225–229. doi: 10.1016/j.ydbio.2009.08.009.
- Kadonaga, J. T. (2012) ‘Perspectives on the RNA polymerase II core promoter’, *Wiley Interdisciplinary Reviews: Developmental Biology*. NIH Public Access, pp. 40–51. doi: 10.1002/wdev.21.
- Kalkat, M. *et al.* (2018) ‘MYC Protein Interactome Profiling Reveals Functionally Distinct Regions that Cooperate to Drive Tumorigenesis’, *Molecular Cell*, 72, pp. 836–848.e7. doi: 10.1016/j.molcel.2018.09.031.
- Kedinger, C. *et al.* (1970) ‘ α -Amanitin: A specific inhibitor of one of two DNA-dependent RNA polymerase activities from calf thymus’, *Biochemical and Biophysical Research Communications*, 38(1), pp. 165–171. doi: 10.1016/0006-291X(70)91099-5.
- Kempfer, R. and Pombo, A. (2020) ‘Methods for mapping 3D chromosome architecture’, *Nature Reviews Genetics*. Springer US, 21(4), pp. 207–226. doi: 10.1038/s41576-019-0195-2.
- El Khattabi, L. *et al.* (2019) ‘A Pliable Mediator Acts as a Functional Rather Than an Architectural Bridge between Promoters and Enhancers’, *Cell*. Cell Press, 178(5), pp. 1145–1158.e20. doi: 10.1016/j.cell.2019.07.011.
- Kim, Y. J. *et al.* (1994) ‘A multiprotein mediator of transcriptional activation and its interaction with the C-terminal repeat domain of RNA polymerase II’, *Cell*, 77(4), pp. 599–608. doi: 10.1016/0092-8674(94)90221-6.

- Kimura, K. *et al.* (2006) ‘Diversification of transcriptional modulation: Large-scale identification and characterization of putative alternative promoters of human genes’, *Genome Research*. *Genome Res*, 16(1), pp. 55–65. doi: 10.1101/gr.4039406.
- Kleaveland, B. *et al.* (2018) ‘A Network of Noncoding Regulatory RNAs Acts in the Mammalian Brain’, *Cell*. Elsevier Inc., 174(2), pp. 350–362.e17. doi: 10.1016/j.cell.2018.05.022.
- Klose, R. J. and Bird, A. P. (2006) ‘Genomic DNA methylation: The mark and its mediators’, *Trends in Biochemical Sciences*, 31(2), pp. 89–97. doi: 10.1016/j.tibs.2005.12.008.
- Klug, W. S. *et al.* (2016) *Concepts of genetics 12th*.
- Kohli, R. M. and Zhang, Y. (2013) ‘TET enzymes, TDG and the dynamics of DNA demethylation’, *Nature*, 502(7472), pp. 472–479. doi: 10.1038/nature12750.
- Kornberg, R. (1974) ‘Chromatin Structure : A Repeating Unit of Histones and DNA Chromatin structure is based on a repeating unit of eight’, *Science*, 184, pp. 868–871.
- Kulkarni, M. M. and Arnosti, D. N. (2003) ‘Information display by transcriptional enhancers’, *Development*. *Development*, 130(26), pp. 6569–6575. doi: 10.1242/dev.00890.
- Kurat, C. F. *et al.* (2017) ‘Chromatin Controls DNA Replication Origin Selection, Lagging-Strand Synthesis, and Replication Fork Rates’, *Molecular Cell*. Cell Press, 65(1), pp. 117–130. doi: 10.1016/j.molcel.2016.11.016.
- Kuzmiak, H. A. and Maquat, L. E. (2006) ‘Applying nonsense-mediated mRNA decay research to the clinic: progress and challenges’, *Trends in Molecular Medicine*. Elsevier, pp. 306–316. doi: 10.1016/j.molmed.2006.05.005.
- Lander, E. S. *et al.* (2001) ‘Initial sequencing and analysis of the human genome’, *Nature*. *Nature*, 409(6822), pp. 860–921. doi: 10.1038/35057062.
- Lang, S. E. *et al.* (2001) ‘E2F Transcriptional Activation Requires TRRAP and GCN5 Cofactors’, *Journal of Biological Chemistry*. *J Biol Chem*, 276(35), pp. 32627–32634. doi: 10.1074/jbc.M102067200.
- Larson, A. G. *et al.* (2017) ‘Liquid droplet formation by HP1 α suggests a role for phase separation in heterochromatin’, *Nature*. Nature Publishing Group, 547(7662), pp. 236–240. doi: 10.1038/nature22822.
- Lemieux, K. and Gaudreau, L. (2004) ‘Targeting of Swi/Snf to the yeast GAL1 UASG requires the Mediator, TAFIIIs, and RNA polymerase II’, *EMBO Journal*. *EMBO J*, 23(20), pp. 4040–4050. doi: 10.1038/sj.emboj.7600416.
- Lenhard, B., Sandelin, A. and Carninci, P. (2012) ‘Metazoan promoters: Emerging characteristics and insights into transcriptional regulation’, *Nature Reviews Genetics*. Nature Publishing Group, 13(4), pp. 233–245. doi: 10.1038/nrg3163.
- Levens, D., Baranello, L. and Kouzine, F. (2016) ‘Controlling gene expression by DNA mechanics: emerging insights and challenges’, *Biophysical Reviews*. Springer Verlag, pp. 259–268. doi: 10.1007/s12551-016-0216-8.
- Levine, M. (2011) ‘Paused RNA polymerase II as a developmental checkpoint’, *Cell*. Elsevier, pp. 502–511. doi: 10.1016/j.cell.2011.04.021.
- Li, B., Carey, M. and Workman, J. L. (2007) ‘The Role of Chromatin during Transcription’, *Cell*, 128(4), pp. 707–719. doi: 10.1016/j.cell.2007.01.015.
- Lomberk, G., Wallrath, L. L. and Urrutia, R. (2006) ‘The Heterochromatin Protein 1 family’, *Genome Biology*, 7(7), pp. 1–8. doi: 10.1186/gb-2006-7-7-228.
- Lorberbaum, D. S. and Barolo, S. (2013) ‘Gene regulation: When analog beats digital’, *Current Biology*. Cell Press. doi: 10.1016/j.cub.2013.10.004.
- Lovén, J. *et al.* (2013) ‘Selective inhibition of tumor oncogenes by disruption of super-enhancers’, *Cell*.

- Elsevier, 153(2), pp. 320–334. doi: 10.1016/j.cell.2013.03.036.
- Luecke, H. F. and Yamamoto, K. R. (2005) ‘The glucocorticoid receptor blocks P-TEFb recruitment by NFκB to effect promoter-specific transcriptional repression’, *Genes and Development*. Cold Spring Harbor Laboratory Press, 19(9), pp. 1116–1127. doi: 10.1101/gad.1297105.
- Lupiáñez, D. G. *et al.* (2015) ‘Disruptions of topological chromatin domains cause pathogenic rewiring of gene-enhancer interactions’, *Cell*. Cell Press, 161(5), pp. 1012–1025. doi: 10.1016/j.cell.2015.04.004.
- Lupiáñez, D. G., Spielmann, M. and Mundlos, S. (2016) ‘Breaking TADs: How Alterations of Chromatin Domains Result in Disease’, *Trends in Genetics*. Elsevier Ltd, 32(4), pp. 225–237. doi: 10.1016/j.tig.2016.01.003.
- MacAlpine, D. M. and Almouzni, G. (2013) ‘Chromatin and DNA replication’, *Cold Spring Harbor Perspectives in Biology*. Cold Spring Harb Perspect Biol, 5(8). doi: 10.1101/cshperspect.a010207.
- Magnani, L. *et al.* (2011) ‘PBX1 genomic pioneer function drives ERα signaling underlying progression in breast cancer’, *PLoS Genetics*. Public Library of Science, 7(11), p. 1002368. doi: 10.1371/journal.pgen.1002368.
- Marques, M. *et al.* (2010) ‘Reconciling the positive and negative roles of histone H2A.Z in gene transcription’, *Epigenetics*, 5(4), pp. 267–272. doi: 10.4161/epi.5.4.11520.
- Mathsyaraja, H. *et al.* (2019) ‘Max deletion destabilizes MYC protein and abrogates Eμ-Myc lymphomagenesis’, *Genes and Development*, 33(17–18), pp. 1252–1264. doi: 10.1101/gad.325878.119.
- Mayer, A., Landry, H. M. and Churchman, L. S. (2017) ‘Pause & go: from the discovery of RNA polymerase pausing to its functional implications’, *Current Opinion in Cell Biology*. Elsevier Ltd, 46, pp. 72–80. doi: 10.1016/j.ceb.2017.03.002.
- McGinty, R. K. and Tan, S. (2015) ‘Nucleosome structure and function’, *Chemical Reviews*, 115(6), pp. 2255–2273. doi: 10.1021/cr500373h.
- Menezes, R. A. *et al.* (2017) ‘Mediator, SWI/SNF and SAGA complexes regulate Yap8-dependent transcriptional activation of ACR2 in response to arsenate’, *Biochimica et Biophysica Acta - Gene Regulatory Mechanisms*. Elsevier B.V., 1860(4), pp. 472–481. doi: 10.1016/j.bbagr.2017.02.001.
- Meselson, M. and Stahl, F. W. (1958) ‘The replication of DNA in Escherichia coli’, *Proceedings of the National Academy of Sciences*. Proceedings of the National Academy of Sciences, 44(7), pp. 671–682. doi: 10.1073/pnas.44.7.671.
- Mi, W. *et al.* (2017) ‘YEATS2 links histone acetylation to tumorigenesis of non-small cell lung cancer’, *Nature Communications*. Nature Publishing Group, 8(1), p. 1088. doi: 10.1038/s41467-017-01173-4.
- Minnoye, L. *et al.* (2019) ‘Cross-species analysis of melanoma enhancer logic using deep learning’, pp. 1–36. doi: 10.1101/2019.12.21.885715.
- Moras, D. G. H. (1998) ‘The nuclear receptor ligand-binding domain: structure and function Dino Moras * and Hinrich Gronemeyer I-IAT’, *Cell Biology*, 10, pp. 384–391.
- Murakami, M., Iwata, Y. and Funaba, M. (2007) ‘Expression and transcriptional activity of alternative splice variants of Mitf exon 6’, *Molecular and Cellular Biochemistry*. Mol Cell Biochem, 303(1–2), pp. 251–257. doi: 10.1007/s11010-007-9474-x.
- Murre, C. *et al.* (1989) ‘Interactions between heterologous helix-loop-helix proteins generate complexes that bind specifically to a common DNA sequence’, *Cell*, 58(3), pp. 537–544. doi: 10.1016/0092-8674(89)90434-0.
- Myers, L. C. and Kornberg, R. D. (2000) ‘Ediator of’, *Yeast*.
- Näär, A. M., Lemon, B. D. and Tjian, R. (2001) ‘Transcriptional Coactivator Complexes’, *Annual Review of Biochemistry*. Annual Reviews 4139 El Camino Way, P.O. Box 10139, Palo Alto, CA 94303-0139, USA , 70(1), pp. 475–501. doi: 10.1146/annurev.biochem.70.1.475.
- Nair, S. K. and Burley, S. K. (2003) ‘X-ray structures of Myc-Max and Mad-Max recognizing DNA:

- Molecular bases of regulation by proto-oncogenic transcription factors', *Cell*. Cell Press, 112(2), pp. 193–205. doi: 10.1016/S0092-8674(02)01284-9.
- Nechaev, S. and Adelman, K. (2011) 'Pol II waiting in the starting gates: Regulating the transition from transcription initiation into productive elongation', *Biochimica et Biophysica Acta - Gene Regulatory Mechanisms*. Elsevier B.V., 1809(1), pp. 34–45. doi: 10.1016/j.bbagr.2010.11.001.
- Oksenysh, V. *et al.* (2009) 'Molecular insights into the recruitment of TFIIH to sites of DNA damage', *EMBO Journal*, 28(19), pp. 2971–2980. doi: 10.1038/emboj.2009.230.
- Olins, D. E. and Olins, A. L. (2003) 'Chromatin history: our view from the bridge', *Nature Reviews Molecular Cell Biology*, 4(10), pp. 809–814. doi: 10.1038/nrm1225.
- Oudet, P. (1975) 'and Biochemical that Chromatin Structure Is a Repeating Unit"', 4(April), pp. 281–300.
- Papatsenko, D. and Levine, M. (2007) 'A rationale for the enhanceosome and other evolutionarily constrained enhancers', *Current Biology*. Cell Press, pp. R955–R957. doi: 10.1016/j.cub.2007.09.035.
- Plaschka, C. *et al.* (2015) 'Architecture of the RNA polymerase II-Mediator core initiation complex', *Nature*, 518(7539), pp. 376–380. doi: 10.1038/nature14229.
- Ponjavic, J., Ponting, C. P. and Lunter, G. (2007) 'Functionality or transcriptional noise? Evidence for selection within long noncoding RNAs', *Genome Research*. Cold Spring Harbor Laboratory Press, 17(5), pp. 556–565. doi: 10.1101/gr.6036807.
- Porra, O. and Libri, D. (2015) 'Transcription termination and the control of the transcriptome: Why, where and how to stop', *Nature Reviews Molecular Cell Biology*. Nature Publishing Group, 16(3), pp. 190–202. doi: 10.1038/nrm3943.
- Pradeepa, M. M. *et al.* (2016) 'Histone H3 globular domain acetylation identifies a new class of enhancers', *Nature Genetics*. Nature Publishing Group, 48(6), pp. 681–686. doi: 10.1038/ng.3550.
- Quinodoz, S. A. *et al.* (2018) 'Higher-Order Inter-chromosomal Hubs Shape 3D Genome Organization in the Nucleus', *Cell*. Cell Press, 174(3), pp. 744–757.e24. doi: 10.1016/j.cell.2018.05.024.
- Rada-Iglesias, A. *et al.* (2012) 'Epigenomic annotation of enhancers predicts transcriptional regulators of human neural crest', *Cell Stem Cell*. Cell Stem Cell, 11(5), pp. 633–648. doi: 10.1016/j.stem.2012.07.006.
- Richard, P. and Manley, J. L. (2009) 'Transcription termination by nuclear RNA polymerases', *Genes and Development*. Cold Spring Harbor Laboratory Press, pp. 1247–1269. doi: 10.1101/gad.1792809.
- Riss, A. *et al.* (2015) 'Subunits of ADA-two-A-containing (ATAC) or Spt-Ada-Gcn5-acetyltransferase (SAGA) coactivator complexes enhance the acetyltransferase activity of GCN5', *Journal of Biological Chemistry*. American Society for Biochemistry and Molecular Biology Inc., 290(48), pp. 28997–29009. doi: 10.1074/jbc.M115.668533.
- Roeder and Rutter, 1969 (1969) 'Multiple forms of DNA-dependent RNA polymerase in eukaryotic organisms', *Group*, 224, pp. 177–178. Available at: <http://adsabs.harvard.edu/abs/1969Natur.224..177K>.
- Rohs, R. *et al.* (2010) 'Origins of specificity in protein-DNA recognition', *Annual Review of Biochemistry*. NIH Public Access, pp. 233–269. doi: 10.1146/annurev-biochem-060408-091030.
- Rowley, M. J. and Corces, V. G. (2018) 'Organizational principles of 3D genome architecture', *Nature Reviews Genetics*. Springer US, 19(12), pp. 789–800. doi: 10.1038/s41576-018-0060-8.
- Ruf, I. K. *et al.* (2000) 'Epstein-Barr Virus Small RNAs Potentiate Tumorigenicity of Burkitt Lymphoma Cells Independently of an Effect on Apoptosis', *Journal of Virology*. American Society for Microbiology, 74(21), pp. 10223–10228. doi: 10.1128/jvi.74.21.10223-10228.2000.
- Sainsbury, S., Bernecky, C. and Cramer, P. (2015) 'Structural basis of transcription initiation by RNA polymerase II', *Nature Reviews Molecular Cell Biology*. Nature Publishing Group, 16(3), pp. 129–143.

doi: 10.1038/nrm3952.

Sanz, A. B. *et al.* (2016) ‘Cooperation between SAGA and SWI/SNF complexes is required for efficient transcriptional responses regulated by the yeast MAPK Slt2’, *Nucleic Acids Research*. Oxford University Press, 44(15), pp. 7159–7172. doi: 10.1093/nar/gkw324.

Sati, S. *et al.* (2020) ‘4D Genome Rewiring during Oncogene-Induced and Replicative Senescence’, *Molecular Cell*. Elsevier Inc., 78(3), pp. 522–538.e9. doi: 10.1016/j.molcel.2020.03.007.

Schoenfelder, S. and Fraser, P. (2019) ‘Long-range enhancer–promoter contacts in gene expression control’, *Nature Reviews Genetics*. Springer US, 20(8), pp. 437–455. doi: 10.1038/s41576-019-0128-0.

Shabalina, S. A. and Koonin, E. V. (2008) ‘Origins and evolution of eukaryotic RNA interference’, *Trends in Ecology and Evolution*, 23(10), pp. 578–587. doi: 10.1016/j.tree.2008.06.005.

Singh, J. and Padgett, R. A. (2009) ‘Rates of in situ transcription and splicing in large human genes’, *Nature Structural and Molecular Biology*. Nature Publishing Group, 16(11), pp. 1128–1133. doi: 10.1038/nsmb.1666.

Slattery, M. *et al.* (2014) ‘Absence of a simple code: How transcription factors read the genome’, *Trends in Biochemical Sciences*. Elsevier Ltd, pp. 381–399. doi: 10.1016/j.tibs.2014.07.002.

Soutourina, J. *et al.* (2011) ‘Direct interaction of RNA polymerase II and mediator required for transcription in vivo’, *Science*. American Association for the Advancement of Science, 331(6023), pp. 1451–1454. doi: 10.1126/science.1200188.

Spector, D. L. and Lamond, A. I. (2011) ‘Nuclear speckles’, *Cold Spring Harbor Perspectives in Biology*. Cold Spring Harbor Laboratory Press, 3(2), pp. 1–12. doi: 10.1101/cshperspect.a000646.

Spencer, C. A. and Groudine, M. (1990) ‘Transcription elongation and eukaryotic gene regulation’, *Oncogene*. *Oncogene*, pp. 777–785. Available at: <https://pubmed-ncbi-nlm-nih-gov.proxy.insermbiblio.inist.fr/2193290/> (Accessed: 27 October 2020).

spicuglia, salvatore and Vanhille, L. (2012) ‘Chromatin signatures of active enhancers’, *Nucleus*. Informa UK Limited, 3(2), pp. 126–131. doi: 10.4161/nucl.19232.

Stadler, J. and Richly, H. (2017) ‘Regulation of DNA repair mechanisms: How the chromatin environment regulates the DNA damage response’, *International Journal of Molecular Sciences*. MDPI AG. doi: 10.3390/ijms18081715.

Staněk, D. and Fox, A. (2017) ‘Nuclear bodies: news insights into structure and function’, *Current Opinion in Cell Biology*, 46, pp. 94–101. doi: 10.1016/j.ceb.2017.05.001.

Stella, S., Cascio, D. and Johnson, R. C. (no date) ‘The shape of the DNA minor groove directs binding by the DNA-bending protein Fis’. doi: 10.1101/gad.1900610.

Steurer, B. *et al.* (2018) ‘Live-cell analysis of endogenous GFP-RPB1 uncovers rapid turnover of initiating and promoter-paused RNA Polymerase II’, *Proceedings of the National Academy of Sciences of the United States of America*, 115(19), pp. E4368–E4376. doi: 10.1073/pnas.1717920115.

Stine, Z. E. and Dang, C. V. (2015) ‘Splicing and Dicing MYC-Mediated Synthetic Lethality’, *Cancer Cell*. Cell Press, pp. 405–406. doi: 10.1016/j.ccell.2015.09.016.

Suganuma, T. *et al.* (2008) ‘ATAC is a double histone acetyltransferase complex that stimulates nucleosome sliding’, *Nature Structural and Molecular Biology*, 15(4), pp. 364–372. doi: 10.1038/nsmb.1397.

Takahashi, K. *et al.* (2007) ‘Induction of Pluripotent Stem Cells from Adult Human Fibroblasts by Defined Factors’, *Cell*. Elsevier, 131(5), pp. 861–872. doi: 10.1016/j.cell.2007.11.019.

Takahashi, K. and Yamanaka, S. (2006) ‘Induction of Pluripotent Stem Cells from Mouse Embryonic and Adult Fibroblast Cultures by Defined Factors’, *Cell*. Elsevier, 126(4), pp. 663–676. doi: 10.1016/j.cell.2006.07.024.

Talbert, P. B. and Henikoff, S. (2010) ‘Histone variants ancient wrap artists of the epigenome’, *Nature*

Reviews Molecular Cell Biology, 11(4), pp. 264–275. doi: 10.1038/nrm2861.

Talbert, P. B. and Henikoff, S. (2017) ‘Histone variants on the move: Substrates for chromatin dynamics’, *Nature Reviews Molecular Cell Biology*. Nature Publishing Group, pp. 115–126. doi: 10.1038/nrm.2016.148.

Tee, W. W. and Reinberg, D. (2014) ‘Chromatin features and the epigenetic regulation of pluripotency states in ESCs’, *Development (Cambridge)*. Company of Biologists Ltd, pp. 2376–2390. doi: 10.1242/dev.096982.

Thanos, D. and Maniatis, T. (1995) ‘Virus induction of human IFN β gene expression requires the assembly of an enhanceosome’, *Cell*, 83(7), pp. 1091–1100. doi: 10.1016/0092-8674(95)90136-1.

Thiagalingam, S. (no date) *Systems biology of cancer*.

Timmers, H. T. M. and Tora, L. (2018) ‘Transcript Buffering: A Balancing Act between mRNA Synthesis and mRNA Degradation’, *Molecular Cell*. Cell Press, pp. 10–17. doi: 10.1016/j.molcel.2018.08.023.

De Toeuf, B. *et al.* (2018) ‘ARE-mediated decay controls gene expression and cellular metabolism upon oxygen variations’, *Scientific Reports*, 8(1), pp. 1–17. doi: 10.1038/s41598-018-23551-8.

Tsai, C. C. *et al.* (2012) ‘Oct4 and Nanog Directly Regulate Dnmt1 to Maintain Self-Renewal and Undifferentiated State in Mesenchymal Stem Cells’, *Molecular Cell*. Elsevier Inc., 47(2), pp. 169–182. doi: 10.1016/j.molcel.2012.06.020.

Vo Ngoc, L. *et al.* (2017) ‘The punctilious RNA polymerase II core promoter’, *Genes and Development*. Cold Spring Harbor Laboratory Press, pp. 1289–1301. doi: 10.1101/gad.303149.117.

Wahl, M. C., Will, C. L. and Lührmann, R. (2009) ‘The Spliceosome: Design Principles of a Dynamic RNP Machine’, *Cell*, 137(2), pp. 701–718. doi: 10.1016/j.cell.2009.02.009.

Wang, X., Cairns, M. J. and Yan, J. (2019) ‘Super-enhancers in transcriptional regulation and genome organization’, *Nucleic Acids Research*. Oxford University Press, pp. 11481–11496. doi: 10.1093/nar/gkz1038.

Wang, Y. L. *et al.* (2008) ‘Human ATAC is a GCN5/PCAF-containing acetylase complex with a novel NC2-like histone fold module that interacts with the TATA-binding protein’, *Journal of Biological Chemistry*. JBC Papers in Press, 283(49), pp. 33808–33815. doi: 10.1074/jbc.M806936200.

Weber, C. M. and Henikoff, S. (2014) ‘Histone variants: Dynamic punctuation in transcription’, *Genes and Development*, 28(7), pp. 672–682. doi: 10.1101/gad.238873.114.

Wei-Lin Popp, M. and Maquat, L. E. (2013) ‘Organizing principles of Mammalian nonsense-mediated mRNA decay’, *Annual Review of Genetics*. Annual Reviews Inc., pp. 139–165. doi: 10.1146/annurev-genet-111212-133424.

Werner, F. and Grohmann, D. (2011) ‘Evolution of multisubunit RNA polymerases in the three domains of life’, *Nature Reviews Microbiology*. Nature Publishing Group, 9(2), pp. 85–98. doi: 10.1038/nrmicro2507.

Whyte, W. A. *et al.* (2013) ‘Master transcription factors and mediator establish super-enhancers at key cell identity genes’, *Cell*. Elsevier, 153(2), pp. 307–319. doi: 10.1016/j.cell.2013.03.035.

Yang, C. *et al.* (2007) ‘Prevalence of the initiator over the TATA box in human and yeast genes and identification of DNA motifs enriched in human TATA-less core promoters’, *Gene*. NIH Public Access, 389(1), pp. 52–65. doi: 10.1016/j.gene.2006.09.029.

Yuan, G. and Zhu, B. (2012) ‘Histone variants and epigenetic inheritance’, *Biochimica et Biophysica Acta - Gene Regulatory Mechanisms*. Elsevier B.V., 1819(3–4), pp. 222–229. doi: 10.1016/j.bbagr.2011.06.007.

Zaret, K. S. and Carroll, J. S. (2011) ‘Pioneer transcription factors: Establishing competence for gene expression’, *Genes and Development*. Genes Dev, pp. 2227–2241. doi: 10.1101/gad.176826.111.

Zhang, N. *et al.* (2014) 'MYC interacts with the human STAGA coactivator complex via multivalent contacts with the GCN5 and TRRAP subunits', *Biochimica et Biophysica Acta - Gene Regulatory Mechanisms*. Elsevier, 1839(5), pp. 395–405. doi: 10.1016/j.bbagr.2014.03.017.

Zhang, T. *et al.* (2020) 'Histone H3K27 acetylation is dispensable for enhancer activity in mouse embryonic stem cells', *Genome Biology*. BioMed Central Ltd., 21(1), p. 45. doi: 10.1186/s13059-020-01957-w.

Zhao, B. *et al.* (2020) 'The molecular basis and disease relevance of non-homologous DNA end joining', *Nature Reviews Molecular Cell Biology*. Springer US. doi: 10.1038/s41580-020-00297-8.

BIBLIOGRAPHY CHAPTER II

- Akbani, R. *et al.* (2015) 'Genomic Classification of Cutaneous Melanoma', *Cell*, 161(7), pp. 1681–1696. doi: 10.1016/j.cell.2015.05.044.
- Al, Y. a O. E. T. (1998) 'Tetracycline Repressor, tetR, rather than the Cell Transcription Factor Fusion Derivatives, Regulates Inducible Gene Expression in Mammalian Cells FENG YAO, i TOR SVENSJO, ' ^ T H O M A S WINKLER, ' MICH', 1950, pp. 1939–1950.
- Albini, A. *et al.* (2015) 'Cancer stem cells and the tumor microenvironment: Interplay in tumor heterogeneity', *Connective Tissue Research*. Taylor and Francis Ltd, 56(5), pp. 414–425. doi: 10.3109/03008207.2015.1066780.
- Alfert, A., Moreno, N. and Kerl, K. (2019) 'The BAF complex in development and disease', *Epigenetics and Chromatin*. BioMed Central Ltd. doi: 10.1186/s13072-019-0264-y.
- Alhazmi, A. S. *et al.* (2018) 'WITHDRAWN: The chromatin remodeling complex NURF localizes to gene bodies and is required for mRNA processing.', *Journal of Biological Chemistry*. American Society for Biochemistry & Molecular Biology (ASBMB), p. jbc.RA118.004382. doi: 10.1074/jbc.ra118.004382.
- Alkhatib, S. G. and Landry, J. W. (2011) 'The nucleosome remodeling factor', *FEBS Letters*. FEBS Lett, pp. 3197–3207. doi: 10.1016/j.febslet.2011.09.003.
- Allen, M. D. *et al.* (2015) 'The SWI/SNF Subunit INI1 Contains an N-Terminal Winged Helix DNA Binding Domain that Is a Target for Mutations in Schwannomatosis', *Structure*. Cell Press, 23(7), pp. 1344–1349. doi: 10.1016/j.str.2015.04.021.
- ALLFREY, V. G., FAULKNER, R. and MIRSKY, A. E. (1964) 'ACETYLATION AND METHYLATION OF HISTONES AND THEIR POSSIBLE ROLE IN THE', *Proceedings of the National Academy of Sciences of the United States of*. National Academy of Sciences, 51(5), pp. 786–794. doi: 10.1073/pnas.51.5.786.
- Alomer, R. M. *et al.* (2017) 'Esco1 and Esco2 regulate distinct cohesin functions during cell cycle progression', *Proceedings of the National Academy of Sciences of the United States of America*. National Academy of Sciences, 114(37), pp. 9906–9911. doi: 10.1073/pnas.1708291114.
- Alpsoy, A. and Dykhuizen, E. C. (2018) 'Glioma tumor suppressor candidate region gene 1 (GLTSCR1) and its paralog GLTSCR1-like form SWI/SNF chromatin remodeling subcomplexes', *Journal of Biological Chemistry*, 293(11), pp. 3892–3903. doi: 10.1074/jbc.RA117.001065.
- Asturias, F. J. *et al.* (2002) 'Structural analysis of the RSC chromatin-remodeling complex', *Proceedings of the National Academy of Sciences of the United States of America*. National Academy of Sciences, 99(21), pp. 13477–13480. doi: 10.1073/pnas.162504299.
- Aydin, Ö. Z. *et al.* (2014) 'Human ISWI complexes are targeted by SMARCA5 ATPase and SLIDE domains to help resolve lesion-stalled transcription', *Nucleic Acids Research*. Oxford University Press, 42(13), pp. 8473–8485. doi: 10.1093/nar/gku565.
- Baliñas-Gavira, C. *et al.* (2020) 'Frequent mutations in the amino-terminal domain of BCL7A impair its tumor suppressor role in DLBCL', *Leukemia*. Springer US, 34(10), pp. 2722–2735. doi: 10.1038/s41375-020-0919-5.
- Bannister, A. J. and Kouzarides, T. (2011) 'Regulation of chromatin by histone modifications', *Cell Research*. Cell Res, pp. 381–395. doi: 10.1038/cr.2011.22.
- Bao, Y. and Shen, X. (2007) 'INO80 subfamily of chromatin remodeling complexes', *Mutation Research - Fundamental and Molecular Mechanisms of Mutagenesis*. NIH Public Access, 618(1–2), pp. 18–29. doi: 10.1016/j.mrfmmm.2006.10.006.
- Barnett, C. and Krebs, J. E. (2011a) 'WSTF does it all: A multifunctional protein in transcription, repair, and replication', *Biochemistry and Cell Biology*. NIH Public Access, pp. 12–23. doi: 10.1139/O10-114.

- Barnett, C. and Krebs, J. E. (2011b) 'WSTF does it all: A multifunctional protein in transcription, repair, and replication', *Biochemistry and Cell Biology*. NIH Public Access, pp. 12–23. doi: 10.1139/O10-114.
- Becker, P. B. and Workman, J. L. (2013) 'Nucleosome remodeling and epigenetics', *Cold Spring Harbor Perspectives in Biology*. Cold Spring Harb Perspect Biol, 5(9). doi: 10.1101/cshperspect.a017905.
- Belotserkovskaya, R. *et al.* (2003) 'FACT facilitates transcription-dependent nucleosome alteration', *Science*. American Association for the Advancement of Science, 301(5636), pp. 1090–1093. doi: 10.1126/science.1085703.
- Bennett, G., Papamichos-Chronakis, M. and Peterson, C. L. (2013) 'DNA repair choice defines a common pathway for recruitment of chromatin regulators', *Nature Communications*. Nature Publishing Group, 4(1), pp. 1–10. doi: 10.1038/ncomms3084.
- Bennett, G. and Peterson, C. L. (2015) 'SWI/SNF recruitment to a DNA double-strand break by the NuA4 and Gcn5 histone acetyltransferases'. doi: 10.1016/j.dnarep.2015.03.006.
- Bergamin, E. *et al.* (2017) 'Molecular basis for the methylation specificity of ATXR5 for histone H3', *Nucleic Acids Research*. Oxford University Press, 45(11), pp. 6375–6387. doi: 10.1093/nar/gkx224.
- Bergamin, E., Blais, A. and Couture, J. F. (2014) 'Keeping them all together: β -Propeller domains in histone methyltransferase complexes', *Journal of Molecular Biology*. Elsevier Ltd, 426(20), pp. 3363–3375. doi: 10.1016/j.jmb.2014.05.010.
- Biggar, K. K. and Li, S. S. C. (2015) 'Non-histone protein methylation as a regulator of cellular signalling and function', *Nature Reviews Molecular Cell Biology*. Nature Publishing Group, 16(1), pp. 5–17. doi: 10.1038/nrm3915.
- Bischof, M. *et al.* (2015) 'Brg1-dependent chromatin remodelling is not essentially required during oligodendroglial differentiation', *Journal of Neuroscience*. Society for Neuroscience, 35(1), pp. 21–35. doi: 10.1523/JNEUROSCI.1468-14.2015.
- Bledau, A. S. *et al.* (2014) 'The H3K4 methyltransferase Setd1a is first required at the epiblast stage, whereas Setd1b becomes essential after gastrulation', *Development (Cambridge)*. Development, 141(5), pp. 1022–1035. doi: 10.1242/dev.098152.
- Boeger, H. *et al.* (2004) 'Removal of promoter nucleosomes by disassembly rather than sliding in vivo', *Molecular Cell*. Cell Press, 14(5), pp. 667–673. doi: 10.1016/j.molcel.2004.05.013.
- Bowen, N. J. *et al.* (2004) 'Mi-2/NuRD: Multiple complexes for many purposes', *Biochimica et Biophysica Acta - Gene Structure and Expression*. Biochim Biophys Acta, pp. 52–57. doi: 10.1016/j.bbaexp.2003.10.010.
- Brachmann, C. B. *et al.* (1995) 'The SIR2 gene family, conserved from bacteria to humans, functions in silencing, cell cycle progression, and chromosome stability', *Genes and Development*. Cold Spring Harbor Laboratory Press, 9(23), pp. 2888–2902. doi: 10.1101/gad.9.23.2888.
- Bracken, A. P. *et al.* (2003) 'EZH2 is downstream of the pRB-E2F pathway, essential for proliferation and amplified in cancer', *EMBO Journal*, 22(20), pp. 5323–5335. doi: 10.1093/emboj/cdg542.
- Bracken, A. P., Brien, G. L. and Verrijzer, C. P. (2019) 'Dangerous liaisons: Interplay between SWI/SNF, NURD, and polycomb in chromatin regulation and cancer', *Genes and Development*, 33(15–16), pp. 936–959. doi: 10.1101/gad.326066.119.
- Brahma, S. *et al.* (2017) 'INO80 exchanges H2A.Z for H2A by translocating on DNA proximal to histone dimers', *Nature Communications*. Nature Publishing Group, 8(1), pp. 1–12. doi: 10.1038/ncomms15616.
- Braun, T. P. *et al.* (2019) 'Myeloid lineage enhancers drive oncogene synergy in CEBPA/CSF3R mutant acute myeloid leukemia', *Nature Communications*. Nature Research, 10(1), pp. 1–15. doi: 10.1038/s41467-019-13364-2.
- Brien, G. L. *et al.* (2018) 'Targeted degradation of BRD9 reverses oncogenic gene expression in

synovial sarcoma', *eLife*. eLife Sciences Publications Ltd, 7. doi: 10.7554/eLife.41305.

Bultman, S. *et al.* (2000) 'A Brg1 null mutation in the mouse reveals functional differences among mammalian SWI/SNF complexes', *Molecular Cell*. Cell Press, 6(6), pp. 1287–1295. doi: 10.1016/S1097-2765(00)00127-1.

Bultman, S. J. *et al.* (2006) 'Maternal BRG1 regulates zygotic genome activation in the mouse', *Genes and Development*. Cold Spring Harbor Laboratory Press, 20(13), pp. 1744–1754. doi: 10.1101/gad.1435106.

Cairns, B. R. *et al.* (1994) 'A multisubunit complex containing the SWI1/ADR6, SWI2/SNF2, SWI3, SNF5, and SNF6 gene products isolated from yeast', *Proceedings of the National Academy of Sciences of the United States of America*, 91(5), pp. 1950–1954. doi: 10.1073/pnas.91.5.1950.

Cakiroglu, A. *et al.* (2019) 'Genome-wide reconstitution of chromatin transactions reveals that RSC preferentially disrupts H2AZ-containing nucleosomes', *Genome Research*. Cold Spring Harbor Laboratory Press, 29(6), pp. 988–998. doi: 10.1101/gr.243139.118.

Centore, R. C. *et al.* (2020) 'Mammalian SWI/SNF Chromatin Remodeling Complexes: Emerging Mechanisms and Therapeutic Strategies', *Trends in Genetics*. Elsevier Ltd, xx(xx), pp. 1–15. doi: 10.1016/j.tig.2020.07.011.

Chaban, Y. *et al.* (2008) 'Structure of a RSC-nucleosome complex and insights into chromatin remodeling', *Nature Structural and Molecular Biology*. NIH Public Access, 15(12), pp. 1272–1277. doi: 10.1038/nsmb.1524.

Chabanon, R. M., Morel, D. and Postel-Vinay, S. (2020) 'Exploiting epigenetic vulnerabilities in solid tumors: Novel therapeutic opportunities in the treatment of SWI/SNF-defective cancers', *Seminars in Cancer Biology*. Academic Press, pp. 180–198. doi: 10.1016/j.semcancer.2019.09.018.

Chambers, S. M. *et al.* (2012) 'Combined small-molecule inhibition accelerates developmental timing and converts human pluripotent stem cells into nociceptors', *Nature Biotechnology*. Nature Publishing Group, 30(7), pp. 715–720. doi: 10.1038/nbt.2249.

Chan, H. M. and La Thangue, N. B. (2001) 'p300/CBP proteins: HATs for transcriptional bridges and scaffolds', *Journal of Cell Science*, 114(13), pp. 2363–2373.

Cheng, X., Collins, R. E. and Zhang, X. (2005) 'Structural and sequence motifs of protein (histone) methylation enzymes', *Annual Review of Biophysics and Biomolecular Structure*, 34, pp. 267–294. doi: 10.1146/annurev.biophys.34.040204.144452.

Cheung, H. W. *et al.* (2011) 'Systematic investigation of genetic vulnerabilities across cancer cell lines reveals lineage-specific dependencies in ovarian cancer', *Proceedings of the National Academy of Sciences of the United States of America*. Proc Natl Acad Sci U S A, 108(30), pp. 12372–12377. doi: 10.1073/pnas.1109363108.

Choi, J. *et al.* (2012) 'The SWI/SNF-like BAF Complex Is Essential for Early B Cell Development', *The Journal of Immunology*, 188(8), pp. 3791–3803. doi: 10.4049/jimmunol.1103390.

Clapier, C. R. *et al.* (2017) 'Mechanisms of action and regulation of ATP-dependent chromatin-remodelling complexes', *Nature Reviews Molecular Cell Biology*. Nature Publishing Group, 18(7), pp. 407–422. doi: 10.1038/nrm.2017.26.

Clapier, C. R. and Cairns, B. R. (2009) 'The biology of chromatin remodeling complexes', *Annual Review of Biochemistry*, 78, pp. 273–304. doi: 10.1146/annurev.biochem.77.062706.153223.

Cohet, N. *et al.* (2010) 'SWI/SNF chromatin remodeling enzyme ATPases promote cell proliferation in normal mammary epithelial cells', *Journal of Cellular Physiology*, 223(3), pp. 667–678. doi: 10.1002/jcp.22072.

Connor, Y. D. *et al.* (2020) 'Germline mutations of SMARCA4 in small cell carcinoma of the ovary, hypercalcemic type and in SMARCA4-deficient undifferentiated uterine sarcoma: Clinical features of a single family and comparison of large cohorts', *Gynecologic Oncology*. Elsevier Ltd, 157(1), pp. 106–

114. doi: 10.1016/j.ygyno.2019.10.031.

Corona, D. F. V. *et al.* (1999) 'ISWI is an ATP-dependent nucleosome remodeling factor', *Molecular Cell*. Cell Press, 3(2), pp. 239–245. doi: 10.1016/S1097-2765(00)80314-7.

Cuthbert, G. L. *et al.* (2004) 'Histone deimination antagonizes arginine methylation', *Cell*. Cell, 118(5), pp. 545–553. doi: 10.1016/j.cell.2004.08.020.

Dar, A. A. *et al.* (2015) 'The role of BPTF in melanoma progression and in response to BRAF-targeted therapy', *Journal of the National Cancer Institute*. Oxford University Press, 107(5), p. 34. doi: 10.1093/jnci/djv034.

Dechassa, M. L. *et al.* (2008) 'Architecture of the SWI/SNF-Nucleosome Complex', *Molecular and Cellular Biology*. American Society for Microbiology, 28(19), pp. 6010–6021. doi: 10.1128/mcb.00693-08.

Delmas, V., Stokes, D. G. and Perry, R. P. (1993) 'A mammalian DNA-binding protein that contains a chromodomain and an SNF2/SWI2-like helicase domain', *Proceedings of the National Academy of Sciences of the United States of America*. National Academy of Sciences, 90(6), pp. 2414–2418. doi: 10.1073/pnas.90.6.2414.

Dhami, G. K. *et al.* (2013) 'Dynamic Methylation of Numb by Set8 Regulates Its Binding to p53 and Apoptosis', *Molecular Cell*. Mol Cell, 50(4), pp. 565–576. doi: 10.1016/j.molcel.2013.04.028.

Dillon, S. C. *et al.* (2005) 'The SET-domain protein superfamily: Protein lysine methyltransferases', *Genome Biology*, 6(8). doi: 10.1186/gb-2005-6-8-227.

Dodonova, S. O. *et al.* (2020) 'Nucleosome-bound SOX2 and SOX11 structures elucidate pioneer factor function', *Nature*. Springer US, 580(7805), pp. 669–672. doi: 10.1038/s41586-020-2195-y.

Downey, M. (2020) 'Non-histone protein acetylation by the evolutionarily conserved GCN5 and PCAF acetyltransferases', *Biochimica et Biophysica Acta - Gene Regulatory Mechanisms*. Elsevier, (July), p. 194608. doi: 10.1016/j.bbagr.2020.194608.

Doyon, Y. *et al.* (2004) 'Structural and Functional Conservation of the NuA4 Histone Acetyltransferase Complex from Yeast to Humans', *Molecular and Cellular Biology*. American Society for Microbiology, 24(5), pp. 1884–1896. doi: 10.1128/mcb.24.5.1884-1896.2004.

Du, J. *et al.* (2011) 'Sirt5 is a NAD-dependent protein lysine demalonylase and desuccinylase', *Science*. American Association for the Advancement of Science, 334(6057), pp. 806–809. doi: 10.1126/science.1207861.

Duran, A., Diaz-Meco, M. T. and Moscat, J. (2003) 'Essential role of RelA Ser311 phosphorylation by ζ PKC in NF- κ B transcriptional activation', *EMBO Journal*, 22(15), pp. 3910–3918. doi: 10.1093/emboj/cdg370.

Eroglu, B. *et al.* (2006) 'Critical role of Brg1 member of the SWI/SNF chromatin remodeling complex during neurogenesis and neural crest induction in zebrafish', *Developmental Dynamics*. John Wiley & Sons, Ltd, 235(10), pp. 2722–2735. doi: 10.1002/dvdy.20911.

Ewart, A. K. *et al.* (1994) 'Supravalvular Aortic Stenosis Associated with a', *Journal of Clinical Investigation*, 93(March), pp. 1071–1077.

Fang, R. *et al.* (2020) 'Inactivation of BRM/SMARCA2 sensitizes clear cell renal cell carcinoma to histone deacetylase complex inhibitors', *Pathology Research and Practice*. Elsevier, 216(4), p. 152867. doi: 10.1016/j.prp.2020.152867.

Filippakopoulos, P. *et al.* (2012) 'Histone recognition and large-scale structural analysis of the human bromodomain family', *Cell*. Cell, 149(1), pp. 214–231. doi: 10.1016/j.cell.2012.02.013.

Ford, J., Odeyale, O. and Shen, C. H. (2008) 'Activator-dependent recruitment of SWI/SNF and INO80 during INO1 activation', *Biochemical and Biophysical Research Communications*. NIH Public Access, 373(4), pp. 602–606. doi: 10.1016/j.bbrc.2008.06.079.

- Frye, R. A. (1999) 'Characterization of five human cDNAs with homology to the yeast SIR2 gene: Sir2-like proteins (Sirtuins) metabolize NAD and may have protein ADP-ribosyltransferase activity', *Biochemical and Biophysical Research Communications*, 260(1), pp. 273–279. doi: 10.1006/bbrc.1999.0897.
- Fuhrmann, J. and Thompson, P. R. (2016) 'Protein Arginine Methylation and Citrullination in Epigenetic Regulation', *ACS Chemical Biology*. American Chemical Society, pp. 654–668. doi: 10.1021/acscchembio.5b00942.
- Gao, L. *et al.* (2002) 'Cloning and functional characterization of HDAC11, a novel member of the human histone deacetylase family', *Journal of Biological Chemistry*. American Society for Biochemistry and Molecular Biology, 277(28), pp. 25748–25755. doi: 10.1074/jbc.M111871200.
- Gatchalian, J. *et al.* (2018) 'A non-canonical BRD9-containing BAF chromatin remodeling complex regulates naive pluripotency in mouse embryonic stem cells', *Nature Communications*. Springer US, 9(1). doi: 10.1038/s41467-018-07528-9.
- Goldknopf, I. L. and Busch, H. (1977) 'Isopeptide linkage between nonhistone and histone 2A polypeptides of chromosomal conjugate protein A24', *Proceedings of the National Academy of Sciences of the United States of America*. National Academy of Sciences, 74(3), pp. 864–868. doi: 10.1073/pnas.74.3.864.
- Goodman, R. H. and Smolik, S. (2000) 'CBP/p300 in cell growth, transformation, and development', *Genes and Development*. Cold Spring Harbor Laboratory Press, pp. 1553–1577. doi: 10.1101/gad.14.13.1553.
- Gramling, S. *et al.* (2011) 'Pharmacologic reversal of epigenetic silencing of the anticancer protein BRM: A novel targeted treatment strategy', *Oncogene*. Nature Publishing Group, 30(29), pp. 3289–3294. doi: 10.1038/onc.2011.80.
- Gregoretta, I. V., Lee, Y. M. and Goodson, H. V. (2004) 'Molecular evolution of the histone deacetylase family: Functional implications of phylogenetic analysis', *Journal of Molecular Biology*, 338(1), pp. 17–31. doi: 10.1016/j.jmb.2004.02.006.
- Gurard-Levin, Z. A., Quivy, J. P. and Almouzni, G. (2014) 'Histone chaperones: Assisting histone traffic and nucleosome dynamics', *Annual Review of Biochemistry*, 83, pp. 487–517. doi: 10.1146/annurev-biochem-060713-035536.
- Habibian, J. and Ferguson, B. S. (2019) 'The crosstalk between acetylation and phosphorylation: Emerging new roles for HDAC inhibitors in the heart', *International Journal of Molecular Sciences*, 20(1), pp. 1–15. doi: 10.3390/ijms20010102.
- Han, Y. *et al.* (2020) 'Cryo-EM structure of SWI/SNF complex bound to a nucleosome', *Nature*. Nature Research, 579(7799), pp. 452–455. doi: 10.1038/s41586-020-2087-1.
- Hassa, P. O. *et al.* (2006) 'Nuclear ADP-Ribosylation Reactions in Mammalian Cells: Where Are We Today and Where Are We Going?', *Microbiology and Molecular Biology Reviews*. American Society for Microbiology, 70(3), pp. 789–829. doi: 10.1128/mmbr.00040-05.
- He, S. *et al.* (2020) 'Structure of nucleosome-bound human BAF complex', *Science*, 367(6480), pp. 875–881. doi: 10.1126/science.aaz9761.
- Helming, K. C., Wang, X. and Roberts, C. W. M. (2014) 'Vulnerabilities of mutant SWI/SNF complexes in cancer', *Cancer Cell*. Cell Press, pp. 309–317. doi: 10.1016/j.ccr.2014.07.018.
- Helmlinger, D. and Tora, L. (2017) 'Sharing the SAGA', *Trends in Biochemical Sciences*. Elsevier Ltd, 42(11), pp. 850–861. doi: 10.1016/j.tibs.2017.09.001.
- Ho, L. *et al.* (2009) 'An embryonic stem cell chromatin remodeling complex, esBAF, is essential for embryonic stem cell self-renewal and pluripotency', *Proceedings of the National Academy of Sciences of the United States of America*. National Academy of Sciences, 106(13), pp. 5181–5186. doi: 10.1073/pnas.0812889106.

- Hoffman, G. R. *et al.* (2014) 'Functional epigenetics approach identifies BRM/SMARCA2 as a critical synthetic lethal target in BRG1-deficient cancers', *Proceedings of the National Academy of Sciences of the United States of America*. National Academy of Sciences, 111(8), pp. 3128–3133. doi: 10.1073/pnas.1316793111.
- Hohmann, A. F. and Vakoc, C. R. (2014) 'A rationale to target the SWI/SNF complex for cancer therapy', *Trends in Genetics*. Elsevier Ltd, 30(8), pp. 356–363. doi: 10.1016/j.tig.2014.05.001.
- Hota, S. K. and Bruneau, B. G. (2016) 'ATP-dependent chromatin remodeling during mammalian development', *Development (Cambridge)*. Company of Biologists Ltd, pp. 2882–2897. doi: 10.1242/dev.128892.
- Houtkooper, R. H., Pirinen, E. and Auwerx, J. (2012) 'Sirtuins as regulators of metabolism and healthspan', *Nature Reviews Molecular Cell Biology*. Europe PMC Funders, pp. 225–238. doi: 10.1038/nrm3293.
- Hu, B. *et al.* (2020) 'The roles of mutated SWI/SNF complexes in the initiation and development of hepatocellular carcinoma and its regulatory effect on the immune system: A review', *Cell Proliferation*. Blackwell Publishing Ltd, 53(4). doi: 10.1111/cpr.12791.
- Huang, F. *et al.* (2016) 'The enok acetyltransferase complex interacts with Elg1 and negatively regulates PCNA unloading to promote the G1/S transition', *Genes and Development*. Cold Spring Harbor Laboratory Press, 30(10), pp. 1198–1210. doi: 10.1101/gad.271429.115.
- Huber, F. M. *et al.* (2017) 'Histone-binding of DPF2 mediates its repressive role in myeloid differentiation', *Proceedings of the National Academy of Sciences of the United States of America*. National Academy of Sciences, 114(23), pp. 6016–6021. doi: 10.1073/pnas.1700328114.
- Husmann, D. and Gozani, O. (2019) 'Histone lysine methyltransferases in biology and disease', *Nature Structural and Molecular Biology*. Springer US, 26(10), pp. 880–889. doi: 10.1038/s41594-019-0298-7.
- Ikura, T. *et al.* (2000) 'Involvement of the TIP60 histone acetylase complex in DNA repair and apoptosis', *Cell*. Cell Press, 102(4), pp. 463–473. doi: 10.1016/S0092-8674(00)00051-9.
- Ingham, P. W. (1983) 'Differential expression of bithorax complex genes in the absence of the extra sex combs and trithorax genes', *Nature*. Nature Publishing Group, 306(5943), pp. 591–593. doi: 10.1038/306591a0.
- Jancewicz, I. *et al.* (2019) 'BRM: The core ATPase subunit of SWI/SNF chromatin-remodelling complex - A tumour suppressor or tumour-promoting factor?', *Epigenetics and Chromatin*. BioMed Central Ltd., pp. 1–17. doi: 10.1186/s13072-019-0315-4.
- Janknecht, R. (2002) 'The versatile functions of the transcriptional coactivators p300 and CBP and their roles in disease', *Histology and Histopathology*, 17(2), pp. 657–668. doi: 10.14670/HH-17.657.
- Jelinic, P. *et al.* (2016) 'Concomitant loss of SMARCA2 and SMARCA4 expression in small cell carcinoma of the ovary, hypercalcemic type', *Modern Pathology*. Nature Publishing Group, 29(1), pp. 60–66. doi: 10.1038/modpathol.2015.129.
- Jenuwein, T. (2006) 'The epigenetic magic of histone lysine methylation: Delivered on 6 July 2005 at the 30th FEBS Congress in Budapest, Hungary', in *FEBS Journal*. John Wiley & Sons, Ltd, pp. 3121–3135. doi: 10.1111/j.1742-4658.2006.05343.x.
- Jones, M. H., Hamana, N. and Shimane, M. (2000) 'Identification and characterization of BPTF, a novel bromodomain transcription factor', *Genomics*, 63(1), pp. 35–39. doi: 10.1006/geno.1999.6070.
- Jürgens, G. (1985) 'A group of genes controlling the spatial expression of the bithorax complex in *Drosophila*', *Nature*. Nature Publishing Group, 316(6024), pp. 153–155. doi: 10.1038/316153a0.
- Kadam, S. and Emerson, B. M. (2003) 'Transcriptional specificity of human SWI/SNF BRG1 and BRM chromatin remodeling complexes', *Molecular Cell*. Cell Press, 11(2), pp. 377–389. doi: 10.1016/S1097-2765(03)00034-0.

- Kadoch, C. *et al.* (2013) 'Proteomic and bioinformatic analysis of mammalian SWI/SNF complexes identifies extensive roles in human malignancy', *Nature Genetics*. Nat Genet, 45(6), pp. 592–601. doi: 10.1038/ng.2628.
- Kadoch, C. *et al.* (2017) 'Dynamics of BAF-Polycomb complex opposition on heterochromatin in normal and oncogenic states', *Nature Genetics*. Nature Publishing Group, 49(2), pp. 213–222. doi: 10.1038/ng.3734.
- Kadoch, C. and Crabtree, G. R. (2013) 'Reversible disruption of mSWI/SNF (BAF) complexes by the SS18-SSX oncogenic fusion in synovial sarcoma', *Cell*. Cell Press, 153(1), pp. 71–85. doi: 10.1016/j.cell.2013.02.036.
- Kaesler, M. D. *et al.* (2008) 'BRD7, a novel PBAF-specific SWI/SNF subunit, is required for target gene activation and repression in embryonic stem cells', *Journal of Biological Chemistry*. American Society for Biochemistry and Molecular Biology, 283(47), pp. 32254–32263. doi: 10.1074/jbc.M806061200.
- Kahali, S. *et al.* (2012) 'Class I histone deacetylases localize to the endoplasmic reticulum and modulate the unfolded protein response', *The FASEB Journal*. Wiley, 26(6), pp. 2437–2445. doi: 10.1096/fj.11-193706.
- Kang, H. *et al.* (2009) 'CK2 Is the Regulator of SIRT1 Substrate-Binding Affinity, Deacetylase Activity and Cellular Response to DNA-Damage', *PLoS ONE*. Edited by A.-K. Bielinsky. Public Library of Science, 4(8), p. e6611. doi: 10.1371/journal.pone.0006611.
- Kawasumi, R. *et al.* (2017) 'ESCO1/2's roles in chromosome structure and interphase chromatin organization', *Genes and Development*. Cold Spring Harbor Laboratory Press, 31(21), pp. 2136–2150. doi: 10.1101/gad.306084.117.
- Keenen, B. *et al.* (2010) 'Heterogeneous SWI/SNF chromatin remodeling complexes promote expression of microphthalmia-associated transcription factor target genes in melanoma', *Oncogene*. Nature Publishing Group, 29(1), pp. 81–92. doi: 10.1038/onc.2009.304.
- Khavari, P. A. *et al.* (1993) 'BRG1 contains a conserved domain of the SWI2/SNF2 family necessary for normal mitotic growth and transcription', *Nature*. Nature Publishing Group, 366(6451), pp. 170–174. doi: 10.1038/366170a0.
- Kim, J. and Kim, H. (2012) 'Recruitment and biological consequences of histone modification of H3K27me3 and H3K9me3.', *ILAR journal / National Research Council, Institute of Laboratory Animal Resources*. Oxford University Press, 53(3–4), pp. 232–239. doi: 10.1093/ilar.53.3-4.232.
- Kingston, R. E. and Narlikar, G. J. (1999) 'ATP-dependent remodeling and acetylation as regulators of chromatin fluidity', *Genes and Development*, 13(18), pp. 2339–2352. doi: 10.1101/gad.13.18.2339.
- Klein, D. C. and Hainer, S. J. (2020) 'Chromatin regulation and dynamics in stem cells', in *Current Topics in Developmental Biology*. Academic Press Inc., pp. 1–71. doi: 10.1016/bs.ctdb.2019.11.002.
- Kleinsmith, B. Y. L. J., Allfrey, V. G. and Mirsky, A. E. (1966) 'PHOSPHOPROTEIN METABOLISM IN ISOLATED LYMPHOCYTE NUCLEI * phosphate incorporation and " exchange " on serine and threonine residues in nuclear The existence of phosphoprotein fractions which rapidly incorporate P32-phosphate has been known in a variety ', 1064(1965), pp. 1182–1189.
- Kloet, S. L. *et al.* (2015) 'Towards elucidating the stability, dynamics and architecture of the nucleosome remodeling and deacetylase complex by using quantitative interaction proteomics', *FEBS Journal*. Blackwell Publishing Ltd, 282(9), pp. 1774–1785. doi: 10.1111/febs.12972.
- Kolla, V. *et al.* (2014) 'Role of CHD5 in human cancers: 10 years later', *Cancer Research*. Cancer Res, pp. 652–658. doi: 10.1158/0008-5472.CAN-13-3056.
- Koludrovic, D. *et al.* (2015) 'Chromatin-Remodelling Complex NURF Is Essential for Differentiation of Adult Melanocyte Stem Cells', *PLOS Genetics*. Edited by W. A. Bickmore. Public Library of Science, 11(10), p. e1005555. doi: 10.1371/journal.pgen.1005555.
- Kwon, C. S. and Wagner, D. (2007) 'Unwinding chromatin for development and growth: a few genes

at a time', *Trends in Genetics*, 23(8), pp. 403–412. doi: 10.1016/j.tig.2007.05.010.

Kwon, Y. C. and Jewett, M. C. (2015) 'High-throughput preparation methods of crude extract for robust cell-free protein synthesis', *Scientific Reports*. Nature Publishing Group, 5(1), pp. 1–8. doi: 10.1038/srep08663.

De La Serna, I. L., Ohkawa, Y. and Imbalzano, A. N. (2006) 'Chromatin remodelling in mammalian differentiation: Lessons from ATP-dependent remodellers', *Nature Reviews Genetics*, 7(6), pp. 461–473. doi: 10.1038/nrg1882.

Latrick, C. M. *et al.* (2016) 'Molecular basis and specificity of H2A.Z-H2B recognition and deposition by the histone chaperone YL1', *Nature Structural and Molecular Biology*. Nature Publishing Group, 23(4), pp. 309–316. doi: 10.1038/nsmb.3189.

Laurette, P. *et al.* (2015) 'Transcription factor MITF and remodeler BRG1 define chromatin organisation at regulatory elements in melanoma cells', *eLife*. eLife Sciences Publications Ltd, 2015(4), pp. 1–40. doi: 10.7554/eLife.06857.

Lee, J. E. *et al.* (2013) 'H3K4 mono- And di-methyltransferase MLL4 is required for enhancer activation during cell differentiation', *eLife*, 2013(2), pp. 1–25. doi: 10.7554/eLife.01503.

Li, Y. and Seto, E. (2016) 'HDACs and HDAC inhibitors in cancer development and therapy', *Cold Spring Harbor Perspectives in Medicine*. Cold Spring Harbor Laboratory Press, 6(10). doi: 10.1101/cshperspect.a026831.

Liu, J., Kim, J. and Oberdoerffer, P. (2013) 'Metabolic modulation of chromatin: Implications for DNA repair and genomic integrity', *Frontiers in Genetics*. Frontiers, p. 182. doi: 10.3389/fgene.2013.00182.

Lorch, Y. and Kornberg, R. D. (2017) 'Chromatin-remodeling for transcription', *Quarterly Reviews of Biophysics*, 50, pp. 1–15. doi: 10.1017/S003358351700004X.

Lu, J. Y. *et al.* (2011) 'Protein acetylation and aging', *Aging*. Impact Journals LLC, pp. 911–912. doi: 10.18632/aging.100398.

Lu, X. *et al.* (1998) 'A novel human gene, WSTF, is deleted in Williams syndrome', *Genomics*. Academic Press Inc., 54(2), pp. 241–249. doi: 10.1006/geno.1998.5578.

Marathe, H. G. *et al.* (2013) 'SWI/SNF Enzymes Promote SOX10-Mediated Activation of Myelin Gene Expression', *PLoS ONE*. Public Library of Science, 8(7), p. 69037. doi: 10.1371/journal.pone.0069037.

Marfella, C. G. A. and Imbalzano, A. N. (2007) 'The Chd family of chromatin remodelers', *Mutation Research - Fundamental and Molecular Mechanisms of Mutagenesis*. Mutat Res, 618(1–2), pp. 30–40. doi: 10.1016/j.mrfmmm.2006.07.012.

Margueron, R. and Reinberg, D. (2011) 'The Polycomb complex PRC2 and its mark in life', *Nature*. NIH Public Access, pp. 343–349. doi: 10.1038/nature09784.

Mari, F. *et al.* (2015) 'Coffin-Siris and Nicolaides-Baraitser syndromes are a common well recognizable cause of intellectual disability', *Brain and Development*. Elsevier, 37(5), pp. 527–536. doi: 10.1016/j.braindev.2014.08.009.

Marsh, J. A. and Teichmann, S. A. (2015) 'Structure, dynamics, assembly, and evolution of protein complexes', *Annual Review of Biochemistry*, 84(November), pp. 551–575. doi: 10.1146/annurev-biochem-060614-034142.

Mashtalir, N. *et al.* (2018) 'Modular Organization and Assembly of SWI/SNF Family Chromatin Remodeling Complexes', *Cell*. Cell Press, 175(5), pp. 1272–1288.e20. doi: 10.1016/j.cell.2018.09.032.

Mashtalir, N. *et al.* (2020) 'A Structural Model of the Endogenous Human BAF Complex Informs Disease Mechanisms', *Cell*. Elsevier Inc., pp. 1–16. doi: 10.1016/j.cell.2020.09.051.

Matsumoto, S. *et al.* (2006) 'Brg1 is required for murine neural stem cell maintenance and gliogenesis', *Developmental Biology*. Academic Press Inc., 289(2), pp. 372–383. doi: 10.1016/j.ydbio.2005.10.044.

McBride, M. J. *et al.* (2018) 'The SS18-SSX Fusion Oncoprotein Hijacks BAF Complex Targeting and

- Function to Drive Synovial Sarcoma', *Cancer Cell*. Elsevier Inc., 33(6), pp. 1128-1141.e7. doi: 10.1016/j.ccell.2018.05.002.
- Meeks, J. J. and Shilatifard, A. (2017) 'Multiple Roles for the MLL/COMPASS Family in the Epigenetic Regulation of Gene Expression and in Cancer', *Annual Review of Cancer Biology*. Annual Reviews Inc., 1(1), pp. 425–446. doi: 10.1146/annurev-cancerbio-050216-034333.
- Miao, D. *et al.* (2018) 'Genomic correlates of response to immune checkpoint therapies in clear cell renal cell carcinoma', *Science*. American Association for the Advancement of Science, 359(6377), pp. 801–806. doi: 10.1126/science.aan5951.
- Michel, B. C. *et al.* (2018) 'A non-canonical SWI/SNF complex is a synthetic lethal target in cancers driven by BAF complex perturbation', *Nature Cell Biology*. Nature Publishing Group, 20(12), pp. 1410–1420. doi: 10.1038/s41556-018-0221-1.
- Middeljans, E. *et al.* (2012) 'SS18 together with animal-specific factors defines human BAF-type SWI/SNF complexes', *PLoS ONE*. PLoS One, 7(3). doi: 10.1371/journal.pone.0033834.
- Mittal, P. and Roberts, C. W. M. (2020) 'The SWI/SNF complex in cancer — biology, biomarkers and therapy', *Nature Reviews Clinical Oncology*. Springer US, 17(7), pp. 435–448. doi: 10.1038/s41571-020-0357-3.
- Mohd-Sarip, A. *et al.* (2017) 'DOC1-Dependent Recruitment of NURD Reveals Antagonism with SWI/SNF during Epithelial-Mesenchymal Transition in Oral Cancer Cells', *Cell Reports*. Elsevier B.V., 20(1), pp. 61–75. doi: 10.1016/j.celrep.2017.06.020.
- Moore, K. E. and Gozani, O. (2014) 'An unexpected journey: Lysine methylation across the proteome', *Biochimica et Biophysica Acta - Gene Regulatory Mechanisms*. Elsevier B.V., 1839(12), pp. 1395–1403. doi: 10.1016/j.bbagr.2014.02.008.
- Morrison, E. A. *et al.* (2017) 'DNA binding drives the association of BRG1/hBRM bromodomains with nucleosomes', *Nature Communications*. Nature Publishing Group, 8(1), pp. 1–14. doi: 10.1038/ncomms16080.
- Muchardt, C. and Yaniv, M. (2001) 'When the SWI/SNF complex remodels ... the cell cycle', *Oncogene*. Oncogene, pp. 3067–3075. doi: 10.1038/sj.onc.1204331.
- Munshi, N. *et al.* (1998) 'Acetylation of HMG I(Y) by CBP turns off IFN β expression by disrupting the enhanceosome', *Molecular Cell*. Cell Press, 2(4), pp. 457–467. doi: 10.1016/S1097-2765(00)80145-8.
- Murray, K. (1964) 'The Occurrence of ϵ -N-Methyl Lysine in Histones', *Biochemistry*, 3(1), pp. 10–15. doi: 10.1021/bi00889a003.
- Narita, T., Weinert, B. T. and Choudhary, C. (2019) 'Functions and mechanisms of non-histone protein acetylation', *Nature Reviews Molecular Cell Biology*. Springer US, 20(3), pp. 156–174. doi: 10.1038/s41580-018-0081-3.
- Nathan, D. *et al.* (2006) 'Histone sumoylation is a negative regulator in *Saccharomyces cerevisiae* and shows dynamic interplay with positive-acting histone modifications', *Genes and Development*. Genes Dev, 20(8), pp. 966–976. doi: 10.1101/gad.1404206.
- Neigeborn, L. and Carlson, M. (1984) 'Genes affecting the regulation of SUC2 gene expression by glucose repression in *Saccharomyces cerevisiae*', *Genetics*, 108(4), pp. 845–858.
- Nguyen, A. T. and Zhang, Y. (2011) 'The diverse functions of Dot1 and H3K79 methylation', *Genes and Development*. Genes Dev, pp. 1345–1358. doi: 10.1101/gad.2057811.
- Nie, Z. *et al.* (2000) 'A Specificity and Targeting Subunit of a Human SWI/SNF Family-Related Chromatin-Remodeling Complex', *Molecular and Cellular Biology*. American Society for Microbiology, 20(23), pp. 8879–8888. doi: 10.1128/mcb.20.23.8879-8888.2000.
- O'Neill, C. *et al.* (1999) 'Colour in textile effluents - Sources, measurement, discharge consents and simulation: A review', *Journal of Chemical Technology and Biotechnology*, 74(11), pp. 1009–1018. doi: 10.1002/(SICI)1097-4660(199911)74:11<1009::AID-JCTB153>3.0.CO;2-N.

- Obri, A. *et al.* (2014) ‘ANP32E is a histone chaperone that removes H2A.Z from chromatin’, *Nature*. Nature Publishing Group, 505(7485), pp. 648–653. doi: 10.1038/nature12922.
- Palomera-Sanchez, Z. and Zurita, M. (2011) ‘Open, repair and close again: Chromatin dynamics and the response to UV-induced DNA damage’, *DNA Repair*. Elsevier B.V., 10(2), pp. 119–125. doi: 10.1016/j.dnarep.2010.10.010.
- Pan, D. *et al.* (2018) ‘A major chromatin regulator determines resistance of tumor cells to T cell-mediated killing’, *Science*, 359(6377), pp. 770–775. doi: 10.1126/science.aao1710.
- Pan, J. *et al.* (2019) ‘The ATPase module of mammalian SWI/SNF family complexes mediates subcomplex identity and catalytic activity-independent genomic targeting’, *Nature Genetics*. Nature Publishing Group, pp. 618–626. doi: 10.1038/s41588-019-0363-5.
- Papamichos-Chronakis, M. *et al.* (2011) ‘Global regulation of H2A.Z localization by the INO80 chromatin-remodeling enzyme is essential for genome integrity’, *Cell*. Cell, 144(2), pp. 200–213. doi: 10.1016/j.cell.2010.12.021.
- Parnell, T. J. *et al.* (2015) ‘The chromatin remodelers RSC and ISW1 display functional and chromatin-based promoter antagonism’, *eLife*. eLife Sciences Publications Ltd, 2015(4). doi: 10.7554/eLife.06073.
- Patel, A. B. *et al.* (2019) ‘Architecture of the chromatin remodeler RSC and insights into its nucleosome engagement’, *eLife*, 8, pp. 1–24. doi: 10.7554/eLife.54449.
- Pegoraro, G. *et al.* (2009) ‘Ageing-related chromatin defects through loss of the NURD complex’, *Nature Cell Biology*. Nat Cell Biol, 11(10), pp. 1261–1267. doi: 10.1038/ncb1971.
- Peterson, C. L., Dingwall, A. and Scott, M. P. (1994) ‘Five SWI/SNF gene products are components of a large multisubunit complex required for transcriptional enhancement’, *Proceedings of the National Academy of Sciences of the United States of America*, 91(8), pp. 2905–2908. doi: 10.1073/pnas.91.8.2905.
- Peterson, C. L. and Herskowitz, I. (1992) ‘Characterization of the yeast SWI1, SWI2, and SWI3 genes, which encode a global activator of transcription’, *Cell*, 68(3), pp. 573–583. doi: 10.1016/0092-8674(92)90192-F.
- Petrif, F. *et al.* (1995) ‘Rubinstein-Taybi syndrome caused by mutations in the transcriptional co-activator CBP’, *Nature*, pp. 348–351. doi: 10.1038/376348a0.
- Phelan, M. L. *et al.* (1999) ‘Reconstitution of a core chromatin remodeling complex from SWI/SNF subunits’, *Molecular Cell*. Cell Press, 3(2), pp. 247–253. doi: 10.1016/S1097-2765(00)80315-9.
- Pierre, R. S. and Kadoch, C. (2017) ‘Mammalian SWI/SNF complexes in cancer: emerging therapeutic opportunities’, *Current Opinion in Genetics and Development*. Elsevier Ltd, pp. 56–67. doi: 10.1016/j.gde.2017.02.004.
- Poli, J., Gasser, S. M. and Papamichos-Chronakis, M. (2017) ‘The INO80 remodeller in transcription, replication and repair’, *Philosophical Transactions of the Royal Society B: Biological Sciences*. Royal Society Publishing. doi: 10.1098/rstb.2016.0290.
- Raab, J. R. *et al.* (2019) ‘SWI/SNF remains localized to chromatin in the presence of SCHLAP1’, *Nature Genetics*. Nature Publishing Group, 51(1), pp. 26–29. doi: 10.1038/s41588-018-0272-z.
- Randazzo, F. M. *et al.* (1994) ‘brg1: A putative murine homologue of the Drosophila brahma gene, a homeotic gene regulator’, *Developmental Biology*, pp. 229–242. doi: 10.1006/dbio.1994.1023.
- Rea, S. *et al.* (2000) ‘Regulation of chromatin structure by site-specific histone H3 methyltransferases’, *Nature*, 406(6796), pp. 593–599. doi: 10.1038/35020506.
- Reyes, J. C. *et al.* (1998) ‘Altered control of cellular proliferation in the absence of mammalian brahma (SNF2 α)’, *EMBO Journal*. Oxford University Press, 17(23), pp. 6979–6991. doi: 10.1093/emboj/17.23.6979.
- Riggs, M. G. *et al.* (1977) ‘n-Butyrate causes histone modification in HeLa and Friend erythroleukaemia

- cells', *Nature*, 268(5619), pp. 462–464. doi: 10.1038/268462a0.
- Roberts, C. W. M. *et al.* (2000) 'Haploinsufficiency of Snf5 (integrase interactor 1) predisposes to malignant rhabdoid tumors in mice', *Proceedings of the National Academy of Sciences of the United States of America*. National Academy of Sciences, 97(25), pp. 13796–13800. doi: 10.1073/pnas.250492697.
- Ruthenburg, A. J. *et al.* (2007) 'Multivalent engagement of chromatin modifications by linked binding modules', *Nature Reviews Molecular Cell Biology*, 8(12), pp. 983–994. doi: 10.1038/nrm2298.
- Ruthenburg, A. J. *et al.* (2011) 'Recognition of a mononucleosomal histone modification pattern by BPTF via multivalent interactions', *Cell*. Cell, 145(5), pp. 692–706. doi: 10.1016/j.cell.2011.03.053.
- Sabbattini, P. *et al.* (2014) 'An H3K9/S10 methyl-phospho switch modulates Polycomb and Pol II binding at repressed genes during differentiation', *Molecular Biology of the Cell*. American Society for Cell Biology, 25(6), pp. 904–915. doi: 10.1091/mbc.E13-10-0628.
- Salceda, J., Fernández, X. and Roca, J. (2006) 'Topoisomerase II, not topoisomerase I, is the proficient relaxase of nucleosomal DNA', *EMBO Journal*. European Molecular Biology Organization, 25(11), pp. 2575–2583. doi: 10.1038/sj.emboj.7601142.
- Sandhya, S. *et al.* (2018) 'Domain architecture of BAF250a reveals the ARID and ARM-repeat domains with implication in function and assembly of the BAF remodeling complex', *PLoS ONE*, 13(10), pp. 1–26. doi: 10.1371/journal.pone.0205267.
- Sandoz, J. *et al.* (2019) 'Functional interplay between TFIID and KAT2A regulates higher-order chromatin structure and class II gene expression', *Nature Communications*. Nature Publishing Group, 10(1), pp. 1–14. doi: 10.1038/s41467-019-09270-2.
- Sapountzi, V. and Côté, J. (2011) 'MYST-family histone acetyltransferases: Beyond chromatin', *Cellular and Molecular Life Sciences*, 68(7), pp. 1147–1156. doi: 10.1007/s00018-010-0599-9.
- Sasaki, K., Yamagata, T. and Mitani, K. (2008) 'Histone deacetylase inhibitors trichostatin A and valproic acid circumvent apoptosis in human leukemic cells expressing the RUNX1 chimera', *Cancer Science*, 99(2), pp. 414–422. doi: 10.1111/j.1349-7006.2007.00699.x.
- Savkur, R. S. and Burris, T. P. (2004) 'The coactivator LXXLL nuclear receptor recognition motif', *Journal of Peptide Research*. John Wiley & Sons, Ltd, pp. 207–212. doi: 10.1111/j.1399-3011.2004.00126.x.
- Schick, S. *et al.* (2019) 'Systematic characterization of BAF mutations provides insights into intracomplex synthetic lethality in human cancers', *Nature Genetics*. Nature Publishing Group, 51(9), pp. 1399–1410. doi: 10.1038/s41588-019-0477-9.
- Schotta, G. *et al.* (2004) 'A silencing pathway to induce H3-K9 and H4-K20 trimethylation at constitutive heterochromatin', *Genes and Development*. Cold Spring Harbor Laboratory Press, 18(11), pp. 1251–1262. doi: 10.1101/gad.300704.
- Schubert, H. L. *et al.* (2013) 'Structure of an actin-related subcomplex of the SWI/SNF chromatin remodeler', *Proceedings of the National Academy of Sciences of the United States of America*. National Academy of Sciences, 110(9), pp. 3345–3350. doi: 10.1073/pnas.1215379110.
- Sen, P. *et al.* (2017) 'Loss of Snf5 Induces Formation of an Aberrant SWI/SNF Complex', *Cell Reports*. Elsevier Company., 18(9), pp. 2135–2147. doi: 10.1016/j.celrep.2017.02.017.
- Seto, E. and Yoshida, M. (2014) 'Erasers of histone acetylation: The histone deacetylase enzymes', *Cold Spring Harbor Perspectives in Biology*. Cold Spring Harbor Laboratory Press, 6(4). doi: 10.1101/cshperspect.a018713.
- Shain, A. H. and Pollack, J. R. (2013) 'The Spectrum of SWI/SNF Mutations, Ubiquitous in Human Cancers', *PLoS ONE*. PLoS One, 8(1). doi: 10.1371/journal.pone.0055119.
- Shen, W. *et al.* (2007) 'Solution structure of human Brg1 bromodomain and its specific binding to acetylated histone tails', *Biochemistry*, 46(8), pp. 2100–2110. doi: 10.1021/bi0611208.

- Shi, Y. and Whetstone, J. R. (2007) 'Dynamic Regulation of Histone Lysine Methylation by Demethylases', *Molecular Cell*. Cell Press, pp. 1–14. doi: 10.1016/j.molcel.2006.12.010.
- Shi, Yujiang *et al.* (2004) 'Histone demethylation mediated by the nuclear amine oxidase homolog LSD1', *Cell*. Cell, 119(7), pp. 941–953. doi: 10.1016/j.cell.2004.12.012.
- Shin, H. *et al.* (2018) 'Transcriptional regulation mediated by H2A.Z via ANP32e-dependent inhibition of protein phosphatase 2A', *Biochimica et Biophysica Acta - Gene Regulatory Mechanisms*. Elsevier B.V., 1861(5), pp. 481–496. doi: 10.1016/j.bbagr.2018.03.002.
- Shintani, S. *et al.* (2001) 'Cyclin D1 overexpression associates with radiosensitivity in oral squamous cell carcinoma', *International Journal of Cancer*. John Wiley & Sons, Ltd, 96(3), pp. 159–165. doi: 10.1002/ijc.1014.
- Shukla, M. S. *et al.* (2019) 'Generation of Remosomes by the SWI/SNF Chromatin Remodeler Family', *Scientific Reports*. Nature Publishing Group, 9(1), pp. 1–13. doi: 10.1038/s41598-019-50572-8.
- Smith, S. and Stillman, B. (1989) 'Purification and characterization of CAF-I, a human cell factor required for chromatin assembly during DNA replication in vitro', *Cell*, 58(1), pp. 15–25. doi: 10.1016/0092-8674(89)90398-X.
- Soutoglou, E., Katrakili, N. and Talianidis, I. (2000) 'Acetylation regulates transcription factor activity at multiple levels', *Molecular Cell*. Mol Cell, 5(4), pp. 745–751. doi: 10.1016/S1097-2765(00)80253-1.
- Stanton, B. Z. *et al.* (2017) 'Smarca4 ATPase mutations disrupt direct eviction of PRC1 from chromatin', *Nature Genetics*. Nature Publishing Group, 49(2), pp. 282–288. doi: 10.1038/ng.3735.
- Strub, T., Ballotti, R. and Bertolotto, C. (2020) 'The “ART” of epigenetics in melanoma: From histone “alterations, to resistance and therapies”', *Theranostics*. Ivyspring International Publisher, pp. 1777–1797. doi: 10.7150/thno.36218.
- Sura, W. *et al.* (2017) 'Dual role of the histone variant H2A.Z in transcriptional regulation of stress-response genes', *Plant Cell*, 29(4), pp. 791–807. doi: 10.1105/tpc.16.00573.
- Takeuchi, J. K. *et al.* (2011) 'Chromatin remodelling complex dosage modulates transcription factor function in heart development', *Nature Communications*. Nature Publishing Group, 2(1), p. 187. doi: 10.1038/ncomms1187.
- Tamkun, J. W. *et al.* (1992) 'brahma: A regulator of Drosophila homeotic genes structurally related to the yeast transcriptional activator SNF2 SWI2', *Cell*. Cell Press, 68(3), pp. 561–572. doi: 10.1016/0092-8674(92)90191-E.
- Tanaka, Y. *et al.* (2000) 'Extensive brain hemorrhage and embryonic lethality in a mouse null mutant of CREB-binding protein', *Mechanisms of Development*. Elsevier, 95(1–2), pp. 133–145. doi: 10.1016/S0925-4773(00)00360-9.
- Tando, T. *et al.* (2010) 'Requiem protein links RelB/p52 and the Brm-type SWI/SNF complex in a noncanonical NF- κ B pathway', *Journal of Biological Chemistry*. J Biol Chem, 285(29), pp. 21951–21960. doi: 10.1074/jbc.M109.087783.
- Tang, J. *et al.* (2000) 'PRMT1 is the predominant type I protein arginine methyltransferase in mammalian cells', *Journal of Biological Chemistry*. American Society for Biochemistry and Molecular Biology, 275(11), pp. 7723–7730. doi: 10.1074/jbc.275.11.7723.
- Taunton, J., Hassig, C. A. and Schreiber, S. L. (1996) 'A mammalian histone deacetylase related to the yeast transcriptional regulator Rpd3p', *Science*. American Association for the Advancement of Science, 272(5260), pp. 408–411. doi: 10.1126/science.272.5260.408.
- Tomar, R. S. *et al.* (2009) 'A Novel Mechanism of Antagonism between ATP-Dependent Chromatin Remodeling Complexes Regulates RNR3 Expression', *Molecular and Cellular Biology*. American Society for Microbiology, 29(12), pp. 3255–3265. doi: 10.1128/mcb.01741-08.
- Torchy, M. P., Hamiche, A. and Klaholz, B. P. (2015) 'Structure and function insights into the NuRD

- chromatin remodeling complex', *Cellular and Molecular Life Sciences*, 72(13), pp. 2491–2507. doi: 10.1007/s00018-015-1880-8.
- Tsukiyama, T. *et al.* (1995) 'ISWI, a member of the SWI2/SNF2 ATPase family, encodes the 140 kDa subunit of the nucleosome remodeling factor', *Cell*, 83(6), pp. 1021–1026. doi: 10.1016/0092-8674(95)90217-1.
- Tsukiyama, T. and Wu, C. (1995) 'Purification and properties of an ATP-dependent nucleosome remodeling factor', *Cell*, 83(6), pp. 1011–1020. doi: 10.1016/0092-8674(95)90216-3.
- Vaart, A. Van Der *et al.* (2020) 'Dose-dependent functions of SWI/SNF BAF in permitting and inhibiting cell proliferation in vivo', *Science Advances*. American Association for the Advancement of Science, 6(21). doi: 10.1126/sciadv.aay3823.
- Valekunja, U. K. *et al.* (2013) 'Histone methyltransferase MLL3 contributes to genome-scale circadian transcription', *Proceedings of the National Academy of Sciences of the United States of America*. National Academy of Sciences, 110(4), pp. 1554–1559. doi: 10.1073/pnas.1214168110.
- Vangamudi, B. *et al.* (2015) 'The SMARCA2/4 ATPase domain surpasses the bromodomain as a drug target in SWI/SNF-mutant cancers: Insights from cDNA rescue and PFI-3 inhibitor studies', *Cancer Research*, 75(18), pp. 3865–3878. doi: 10.1158/0008-5472.CAN-14-3798.
- Vardabasso, C. *et al.* (2015) 'Histone Variant H2A.Z.2 Mediates Proliferation and Drug Sensitivity of Malignant Melanoma', *Molecular Cell*. Cell Press, 59(1), pp. 75–88. doi: 10.1016/j.molcel.2015.05.009.
- Versteeg, I. *et al.* (1998) 'Truncating mutations of hSNF5/INI1 in aggressive paediatric cancer', *Nature*. Nature, 394(6689), pp. 203–206. doi: 10.1038/28212.
- Vorobyeva, N. E. *et al.* (2009) 'Transcription coactivator SAYP combines chromatin remodeler Brahma and transcription initiation factor TFIID into a single supercomplex', *Proceedings of the National Academy of Sciences of the United States of America*. National Academy of Sciences, 106(27), pp. 11049–11054. doi: 10.1073/pnas.0901801106.
- Vradii, D. *et al.* (2006) 'Brg1, the ATPase subunit of the SWI/SNF chromatin remodeling complex, is required for myeloid differentiation to granulocytes', *Journal of Cellular Physiology*, 206(1), pp. 112–118. doi: 10.1002/jcp.20432.
- Wagner, F. R. *et al.* (2020) 'Structure of SWI/SNF chromatin remodeller RSC bound to a nucleosome', *Nature*. Nature Research, 579(7799), pp. 448–451. doi: 10.1038/s41586-020-2088-0.
- Wang, L. *et al.* (2014) 'INO80 facilitates pluripotency gene activation in embryonic stem cell self-renewal, reprogramming, and blastocyst development', *Cell Stem Cell*. Cell Press, 14(5), pp. 575–591. doi: 10.1016/j.stem.2014.02.013.
- Wang, R. R. *et al.* (2018) 'The SWI/SNF chromatin-remodeling factors BAF60a, b, and c in nutrient signaling and metabolic control', *Protein and Cell*. Higher Education Press, pp. 207–215. doi: 10.1007/s13238-017-0442-2.
- Wang, W. (2003) 'The SWI/SNF family of ATP-dependent chromatin remodelers: Similar mechanisms for diverse functions', *Current Topics in Microbiology and Immunology*. Springer Verlag, pp. 143–169. doi: 10.1007/978-3-642-55747-7_6.
- Wang, X. *et al.* (2019) 'BRD9 defines a SWI/SNF sub-complex and constitutes a specific vulnerability in malignant rhabdoid tumors', *Nature Communications*. Nature Publishing Group, 10(1), pp. 1–11. doi: 10.1038/s41467-019-09891-7.
- Watanabe, S. *et al.* (2010) 'Structural characterization of H3K56Q nucleosomes and nucleosomal arrays', *Biochimica et Biophysica Acta - Gene Regulatory Mechanisms*. Elsevier B.V., 1799(5–6), pp. 480–486. doi: 10.1016/j.bbagr.2010.01.009.
- Weider, M. *et al.* (2012) 'Chromatin-Remodeling Factor Brg1 Is Required for Schwann Cell Differentiation and Myelination', *Developmental Cell*. Cell Press, 23(1), pp. 193–201. doi: 10.1016/j.devcel.2012.05.017.

- Weirich, S. *et al.* (2015) ‘Investigation of the methylation of Numb by the SET8 protein lysine methyltransferase’, *Scientific Reports*. Nature Publishing Group, 5(1), p. 13813. doi: 10.1038/srep13813.
- Willis, M. S. *et al.* (2012) ‘Functional redundancy of SWI/SNF catalytic subunits in maintaining vascular endothelial cells in the adult heart’, *Circulation Research*. NIH Public Access, 111(5), p. e111. doi: 10.1161/CIRCRESAHA.112.265587.
- Wilson, B. G. *et al.* (2010) ‘Epigenetic antagonism between polycomb and SWI/SNF complexes during oncogenic transformation’, *Cancer Cell*. NIH Public Access, 18(4), pp. 316–328. doi: 10.1016/j.ccr.2010.09.006.
- Wilson, B. G. *et al.* (2014) ‘Residual Complexes Containing SMARCA2 (BRM) Underlie the Oncogenic Drive of SMARCA4 (BRG1) Mutation’, *Molecular and Cellular Biology*. American Society for Microbiology, 34(6), pp. 1136–1144. doi: 10.1128/mcb.01372-13.
- Winkler, D. D. and Luger, K. (2011) ‘The histone chaperone FACT: Structural insights and mechanisms for nucleosome reorganization’, *Journal of Biological Chemistry*. J Biol Chem, pp. 18369–18374. doi: 10.1074/jbc.R110.180778.
- Workman, J. L. and Kingston, R. E. (1992) ‘Nucleosome core displacement in vitro via a metastable transcription factor-nucleosome complex’, *Science*. Science, 258(5089), pp. 1780–1784. doi: 10.1126/science.1465613.
- Wysocka, J. *et al.* (2006) ‘A PHD finger of NURF couples histone H3 lysine 4 trimethylation with chromatin remodelling’, *Nature*. Nature Publishing Group, 442(7098), pp. 86–90. doi: 10.1038/nature04815.
- Xiao, H. *et al.* (2001) ‘Dual functions of largest NURF subunit NURF301 in nucleosome sliding and transcription factor interactions’, *Molecular Cell*. Cell Press, 8(3), pp. 531–543. doi: 10.1016/S1097-2765(01)00345-8.
- Yan, Z. *et al.* (2005) ‘PBAF chromatin-remodeling complex requires a novel specificity subunit, BAF200, to regulate expression of selective interferon-responsive genes’, *Genes and Development*. Genes Dev, 19(14), pp. 1662–1667. doi: 10.1101/gad.1323805.
- Yang, X. J. and Seto, E. (2008) ‘The Rpd3/Hda1 family of lysine deacetylases: From bacteria and yeast to mice and men’, *Nature Reviews Molecular Cell Biology*. NIH Public Access, pp. 206–218. doi: 10.1038/nrm2346.
- Ye, Y. *et al.* (2019) ‘Structure of the RSC complex bound to the nucleosome’, *Science*. American Association for the Advancement of Science, 366(6467), pp. 838–843. doi: 10.1126/science.aay0033.
- Yoshimura, T. *et al.* (2009) ‘Comprehensive Analysis of Inflammatory Immune Mediators in Vitreoretinal Diseases’, *PLoS ONE*. Edited by R. Linden. Public Library of Science, 4(12), p. e8158. doi: 10.1371/journal.pone.0008158.
- Yu, Y. *et al.* (2012) ‘Bcl11a is essential for lymphoid development and negatively regulates p53’, *Journal of Experimental Medicine*. The Rockefeller University Press, 209(13), pp. 2467–2483. doi: 10.1084/jem.20121846.
- Zeng, L. *et al.* (2010) ‘Mechanism and regulation of acetylated histone binding by the tandem PHD finger of DPF3b’, *Nature*. Nature, 466(7303), pp. 258–262. doi: 10.1038/nature09139.
- Zhang, W. *et al.* (2019) ‘The BAF and PRC2 Complex Subunits Dpf2 and Eed Antagonistically Converge on Tbx3 to Control ESC Differentiation’, *Cell Stem Cell*. Cell Press, 24(1), pp. 138–152.e8. doi: 10.1016/j.stem.2018.12.001.
- Zhang, Y. *et al.* (1999) ‘Analysis of the NuRD subunits reveals a histone deacetylase core complex and a connection with DNA methylation’, *Genes and Development*. Cold Spring Harbor Laboratory Press, 13(15), pp. 1924–1935. doi: 10.1101/gad.13.15.1924.
- Zhou, H. *et al.* (2020) ‘PBRM1 mutation and preliminary response to immune checkpoint blockade

treatment in non-small cell lung cancer', *npj Precision Oncology*. Springer Science and Business Media LLC, 4(1), pp. 1–4. doi: 10.1038/s41698-020-0112-3.

BIBLIOGRAPHY CHAPTER III

- Alvarez, Ofelia, Maria M. Rodriguez, Lanetta Jordan, and Sharada Sarnaik. 2015. "Renal Medullary Carcinoma and Sickle Cell Trait: A Systematic Review." *Pediatric Blood and Cancer* 62(10):1694–99.
- Amin, Mahul B., Gladell P. Paner, Isabel Alvarado-Cabrero, Andrew N. Young, Hans J. Stricker, Robert H. Lyles, and Holger Moch. 2008. "Chromophobe Renal Cell Carcinoma: Histomorphologic Characteristics and Evaluation of Conventional Pathologic Prognostic Parameters in 145 Cases." *American Journal of Surgical Pathology* 32(12):1822–34.
- Arlo J. Miller and Martin C. Mihm, Jr. 2001. "Melanoma 2001." *Southern Medical Journal* 94(9):851–52.
- Balkwill, Fran and Alberto Mantovani. 2001. "Inflammation and Cancer: Back to Virchow?" *Lancet* 357(9255):539–45.
- Ballas, S. K. and E. D. Smith. 1992. "Red Blood Cell Changes during the Evolution of the Sickle Cell Painful Crisis." *Blood* 79(8):2154–63.
- Barnes, Zoa, Isaiah J. Fidler, Eilene Gruys, Maria A. Cifone, and Corazon Bucana. 1981. "Demonstration of Multiple Phenotypic Diversity in a Murine Melanoma of Recent Origin 1, 2, 3, 4." *Journal of the National Cancer Institute* 67(4):947–56.
- Baroni, Adone, Elisabetta Buommino, Vincenza De Gregorio, Eleonora Ruocco, Vincenzo Ruocco, and Ronni Wolf. 2012. "Structure and Function of the Epidermis Related to Barrier Properties." *Clinics in Dermatology* 30(3):257–62.
- Batus, Marta, Salman Waheed, Carl Ruby, Lindsay Petersen, Steven D. Bines, and Howard L. Kaufman. 2013. "Optimal Management of Metastatic Melanoma: Current Strategies and Future Directions." *American Journal of Clinical Dermatology* 14(3):179–94.
- Beckerman, Pazit, Chengxiang Qiu, Jihwan Park, Nora Ledo, Yi An Ko, Ae Seo Deok Park, Sang Youb Han, Peter Choi, Matthew Palmer, and Katalin Susztak. 2017. "Human Kidney Tubule-Specific Gene Expression Based Dissection of Chronic Kidney Disease Traits." *EBioMedicine* 24:267–76.
- Bentley, N. J., T. Eisen, and C. R. Goding. 1994. "Melanocyte-Specific Expression of the Human Tyrosinase Promoter: Activation by the Microphthalmia Gene Product and Role of the Initiator." *Molecular and Cellular Biology* 14(12):7996–8006.
- Bertolotto, Corine, Patricia Abbe, Timothy J. Hemesath, Karine Bille, David E. Fisher, Jean Paul Ortonne, and Robert Ballotti. 1998. "Microphthalmia Gene Product as a Signal Transducer in CAMP-Induced Differentiation of Melanocytes." *Journal of Cell Biology* 142(3):827–35.
- Birkeland, E., S. Zhang, D. Poduval, J. Geisler, S. Nakken, D. Vodak, L. A. Meza-Zepeda, E. Hovig, O. Myklebost, S. Knappskog, and P. E. Lønning. 2018. "Patterns of Genomic Evolution in Advanced Melanoma." *Nature Communications* 9(1).
- Boshuizen, Julia, Louise A. Koopman, Oscar Krijgsman, Aida Shahrabi, Elke Gresnigt Van Den Heuvel, Maarten A. Ligtenberg, David W. Vredevogd, Kristel Kemper, Thomas Kuilman, Ji Ying Song, Nora Pencheva, Jens Thing Mortensen, Marnix Geukes Foppen, Elisa A. Rozeman, Christian U. Blank, Maarten L. Janmaat, David Satijn, Esther C. W. Breij, Daniel S. Peeper, and Paul W. H. I. Parren. 2018. "Cooperative Targeting of Melanoma Heterogeneity with an AXL Antibody-Drug Conjugate and BRAF/MEK Inhibitors." *Nature Medicine* 24(2):203–12.
- Brenner, Michaela and Vincent J. Hearing. 2008. "The Protective Role of Melanin against UV Damage in Human Skin." *Photochemistry and Photobiology* 84(3):539–49.
- Bronner, Marianne E. and Nicole M. LeDouarin. 2012. "Development and Evolution of the Neural Crest: An Overview." *Developmental Biology* 366(1):2–9.
- Bush, William D. and John D. Simon. 2007. "Quantification of Ca²⁺ Binding to Melanin Supports the Hypothesis That Melanosomes Serve a Functional Role in Regulating Calcium Homeostasis." *Pigment Cell Research* 20(2):134–39.

- Caliò, Anna, Diego Segala, Enrico Munari, Matteo Brunelli, and Guido Martignoni. 2019. “MiT Family Translocation Renal Cell Carcinoma: From the Early Descriptions to the Current Knowledge.” *Cancers* 11(8).
- Capitanio, Umberto and Francesco Montorsi. 2016. “Renal Cancer.” *The Lancet* 387(10021):894–906.
- Caramel, J., S. Medjkane, F. Quignon, and O. Delattre. 2008. “The Requirement for SNF5/INI1 in Adipocyte Differentiation Highlights New Features of Malignant Rhabdoid Tumors.” *Oncogene* 27(14):2035–44.
- Caramel, Julie, Eftychios Papadogeorgakis, Louise Hill, Gareth J. Browne, Geoffrey Richard, Anne Wierinckx, Gerald Saldanha, Joy sborne, Peter Hutchinson, Gina Tse, Joël Lachuer, Alain Puisieux, J. Howard Pringle, Stéphane Ansieau, and Eugene Tulchinsky. 2013. “A Switch in the Expression of Embryonic EMT-Inducers Drives the Development of Malignant Melanoma.” *Cancer Cell* 24(4):466–80.
- Carreira, Suzanne, Jane Goodall, Laurence Denat, Mercedes Rodriguez, Paolo Nuciforo, Keith S. Hoek, Alessandro Testori, Lionel Larue, and Colin R. Goding. 2006. “Mitf Regulation of Dial Controls Melanoma Proliferation and Invasiveness.” *Genes and Development* 20(24):3426–39.
- Carroll, Thomas J. and Amrita Das. 2011. “Planar Cell Polarity in Kidney Development and Disease.” *Organogenesis* 7(3):180–90.
- Casascelli, Jozefina, Nils Weinhold, Gunes Gundem, Lu Wang, Emily C. Zabor, Esther Drill, Patricia I. Wang, Gouri J. Nanjangud, Almedina Redzematovic, Amrita M. Nargund, Brandon J. Manley, Maria E. Arcila, Nicholas M. Donin, John C. Cheville, R. Houston Thompson, Allan J. Pantuck, Paul Russo, Emily H. Cheng, William Lee, Satish K. Tickoo, Irina Ostrovnaya, Chad J. Creighton, Elli Papaemmanuil, Venkatraman E. Seshan, A. Ari Hakimi, and James J. Hsieh. 2017. “Genomic Landscape and Evolution of Metastatic Chromophobe Renal Cell Carcinoma.” *JCI Insight* 2(12).
- Chapman, Paul B., Axel Hauschild, Caroline Robert, John B. Haanen, Paolo Ascierto, James Larkin, Reinhard Dummer, Claus Garbe, Alessandro Testori, Michele Maio, David Hogg, Paul Lorigan, Celeste Lebbe, Thomas Jouary, Dirk Schadendorf, Antoni Ribas, Steven J. O’Day, Jeffrey A. Sosman, John M. Kirkwood, Alexander M. M. Eggermont, Brigitte Dreno, Keith Nolop, Jiang Li, Betty Nelson, Jeannie Hou, Richard J. Lee, Keith T. Flaherty, and Grant A. McArthur. 2011. “Improved Survival with Vemurafenib in Melanoma with BRAF V600E Mutation.” *New England Journal of Medicine* 364(26):2507–16.
- Chappell, William H., Linda S. Steelman, Jacquelyn M. Long, Ruth C. Kempf, Stephen L. Abrams, Richard A. Franklin, Jörg Bäsecke, Franca Stivala, Marco Donia, Paolo Fagone, Graziella Malaponte, Maria C. Mazzarino, Ferdinando Nicoletti, Massimo Libra, Danijela Maksimovic-Ivanic, Sanja Mijatovic, Giuseppe Montalto, Melchiorre Cervello, Piotr Laidler, Michele Milella, Agostino Tafuri, Antonio Bonati, Camilla Evangelisti, Lucio Cocco, Alberto M. Martelli, and James A. McCubrey. 2011. “Ras/Raf/MEK/ERK and PI3K/PTEN/Akt/MTOR Inhibitors: Rationale and Importance to Inhibiting These Pathways in Human Health.” *Oncotarget* 2(3):135–64.
- Cheli, Yann, Mickael Ohanna, Robert Ballotti, and Corine Bertolotto. 2010. “Fifteen-Year Quest for Microphthalmia-Associated Transcription Factor Target Genes.” *Pigment Cell and Melanoma Research* 23(1):27–40.
- Chen, Lihe, Jevin Z. Clark, Jonathan W. Nelson, Brigitte Kaissling, David H. Ellison, and Mark A. Knepper. 2019. “Renal-Tubule Epithelial Cell Nomenclature for Single-Cell Rna-Sequencing Studies.” *Journal of the American Society of Nephrology* 30(8):1358–64.
- Chen, Wei, Senlin Li, Huansha Yu, Xing Liu, Lulu Huang, Qiang Wang, Heng Liu, Ye Cui, Yijun Tang, Peng Zhang, and Chen Wang. 2016. “ER Adaptor SCAP Translocates and Recruits IRF3 to Perinuclear Microsome Induced by Cytosolic Microbial DNAs.” *PLoS Pathogens* 12(2):1–22.
- Clark, Wallace H., Lynn From, Evelina A. Bernardino, and Martin C. Mihm. 1969. “The Histogenesis and Biologic Behavior of Primary Human Malignant Melanomas of the Skin.” *Cancer Research* 29(3).

- Costin, Gertrude-E. and Vincent J. Hearing. 2007. "Human Skin Pigmentation: Melanocytes Modulate Skin Color in Response to Stress." *The FASEB Journal* 21(4):976–94.
- Cully, Megan, Han You, Arnold J. Levine, and Tak W. Mak. 2006. "Beyond PTEN Mutations: The PI3K Pathway as an Integrator of Multiple Inputs during Tumorigenesis." *Nature Reviews Cancer* 6(3):184–92.
- Curtin, John A., Jane Fridlyand, Toshiro Kageshita, Hetal N. Patel, Klaus J. Busam, Heinz Kutzner, Kwang-Hyun Cho, Setsuya Aiba, Eva-Bettina Bröcker, Philip E. LeBoit, Dan Pinkel, and Boris C. Bastian. 2005. "Distinct Sets of Genetic Alterations in Melanoma." *New England Journal of Medicine* 353(20):2135–47.
- Davidson, Guillaume, Sébastien Coassolo, A. Kieny, M. Ennen, E. Pencreach, Gabriel G. Malouf, Dan Lipsker, and I. Davidson. 2019. "Dynamic Evolution of Clonal Composition and Neoantigen Landscape in Recurrent Metastatic Melanoma with a Rare Combination of Driver Mutations." *Journal of Investigative Dermatology* 139(8):1769-1778.e2.
- Davies, Helen, Graham R. Bignell, Charles Cox, Philip Stephens, Sarah Edkins, Sheila Clegg, Jon Teague, Hayley Woffendin, Mathew J. Garnett, William Bottomley, Neil Davis, Ed Dicks, Rebecca Ewing, Yvonne Floyd, Kristian Gray, Sarah Hall, Rachel Hawes, Jaime Hughes, Vivian Kosmidou, Andrew Menzies, Catherine Mould, Adrian Parker, Claire Stevens, Stephen Watt, Steven Hooper, Hiran Jayatilake, Barry A. Gusterson, Colin Cooper, Janet Shipley, Darren Hargrave, Katherine Pritchard-Jones, Norman Maitland, Georgia Chenevix-Trench, Gregory J. Riggins, Darell D. Bigner, Giuseppe Palmieri, Antonio Cossu, Adrienne Flanagan, Andrew Nicholson, Judy W. C. Ho, Suet Y. Leung, Siu T. Yuen, Barbara L. Weber, Hilliard F. Seigler, Timothy L. Darrow, Hugh Paterson, Richard Wooster, Michael R. Stratton, and P. Andrew Futreal. 2002. "Mutations of the BRAF Gene in Human Cancer." *Nature* 417(6892):949–54.
- Davis, C. J., F. K. Mostofi, and I. A. Sesterhenn. 1995. "Renal Medullary Carcinoma: The Seventh Sickle Cell Nephropathy." *American Journal of Surgical Pathology* 19(1):1–11.
- Dell'Angelica, Esteban C. 2003. "Melanosome Biogenesis: Shedding Light on the Origin of an Obscure Organelle." *Trends in Cell Biology* 13(10):503–6.
- Dimashkieh, Haytham, Jong Choe, and George Mutema. 2003. *Renal Medullary Carcinoma A Report of 2 Cases and Review of the Literature*. Vol. 127. Allen Press.
- Dituri, Francesco, Carla Cossu, Serena Mancarella, and Gianluigi Giannelli. 2019. "The Interactivity between TGF β and BMP Signaling in Organogenesis, Fibrosis, and Cancer Activated Protein Kinases (MAPKs, Namely Extracellular Receptor Kinase 1 and 2-ERK1/2)." *Cells* 8(I):1–21.
- Domingues, Beatriz, Jose Lopes, Paula Soares, and Helena Populo. 2018. "Melanoma Treatment in Review." *ImmunoTargets and Therapy* Volume 7:35–49.
- Dorsky, Richard I., Randall T. Moon, and David W. Raible. 1998. "Control of Neural Crest Cell Fate by the Wnt Signalling Pathway." *Nature* 396(6709):370–72.
- Drummond, Iain A. and Alan J. Davidson. 2010. *Zebrafish Kidney Development*. Vol. 100. Third Edit. Elsevier Inc.
- Duman, Nilay, Gökçe Erkin, Özgür Gökçöz, Sevilay Karahan, Aycan Ugur Kayıkçıoğlu, and Ismail Çelik. 2015. "Nevus-Associated versus de Novo Melanoma: Do They Have Different Characteristics and Prognoses?" *Dermatopathology* 2(1):46–51.
- Dupin, Elisabeth, Sophie Cruzet, and Nicole M. Le Douarin. 2006. "The Contribution of the Neural Crest to the Vertebrate Body." *Advances in Experimental Medicine and Biology* 589:96–119.
- Eichhoff, Ossia M., Marie C. Zipser, Mai Xu, Ashani T. Weeraratna, Daniela Mihic, Reinhard Dummer, and Keith S. Hoek. 2010. "The Immunohistochemistry of Invasive and Proliferative Phenotype Switching in Melanoma: A Case Report." *Melanoma Research* 20(4):349–55.
- Elliott, Alexis and Evelyn Bruner. 2019. "Renal Medullary Carcinoma." *Archives of Pathology and Laboratory Medicine* 143(12):1556–61.

- Epstein, Murray. 1997. "Alcohol's Impact on Kidney Function." *Alcohol Research and Health* 21(1):84–91.
- Ernfors, Patrik. 2010. "Cellular Origin and Developmental Mechanisms during the Formation of Skin Melanocytes." *Experimental Cell Research* 316(8):1397–1407.
- Evans, Roger G. 2019. "Another Step Forward for Methods for Studying Renal Oxygenation." *Kidney International* 96(3):552–54.
- Fedorenko, I. V., G. T. Gibney, and K. S. M. Smalley. 2013. "NRAS Mutant Melanoma: Biological Behavior and Future Strategies for Therapeutic Management." *Oncogene* 32(25):3009–18.
- Fife, Brian T. and Jeffrey A. Bluestone. 2008. "Control of Peripheral T-Cell Tolerance and Autoimmunity via the CTLA-4 and PD-1 Pathways." *Immunological Reviews* 224(1):166–82.
- Fitzpatrick, T. B. 1988. "The Validity and Practicality of Sun-Reactive Skin Types I through VI." *Archives of Dermatology* 124(6):869–71.
- Flaherty, Keith T., Jeffery R. Infante, Adil Daud, Rene Gonzalez, Richard F. Kefford, Jeffrey Sosman, Omid Hamid, Lynn Schuchter, Jonathan Cebon, Nageatte Ibrahim, Ragini Kudchadkar, Howard A. Burris, Gerald Falchook, Alain Algazi, Karl Lewis, Georgina V. Long, Igor Puzanov, Peter Lebowitz, Ajay Singh, Shonda Little, Peng Sun, Alicia Allred, Daniele Ouellet, Kevin B. Kim, Kiran Patel, and Jeffrey Weber. 2012. "Combined BRAF and MEK Inhibition in Melanoma with BRAF V600 Mutations." *New England Journal of Medicine* 367(18):1694–1703.
- Fry, Brendan C., Aurélie Edwards, Ioannis Sgouralis, and Anita T. Layton. 2014. "Impact of Renal Medullary Three-Dimensional Architecture on Oxygen Transport." *American Journal of Physiology - Renal Physiology* 307(3):F263.
- Gallo, Richard L. 2017. "Human Skin Is the Largest Epithelial Surface for Interaction with Microbes." *Journal of Investigative Dermatology* 137(6):1213–14.
- Gandini, Sara, Francesco Sera, Maria Sofia Cattaruzza, Paolo Pasquini, Orietta Picconi, Peter Boyle, and Carmelo Francesco Melchi. 2005. "Meta-Analysis of Risk Factors for Cutaneous Melanoma: II. Sun Exposure." *European Journal of Cancer* 41(1):45–60.
- Garbe, Claus, Ketty Peris, Axel Hauschild, Philippe Saiag, Mark Middleton, Lars Bastholt, Jean Jacques Grob, Josep Malvehy, Julia Newton-Bishop, Alexander J. Stratigos, Hubert Pehamberger, and Alexander M. Eggermont. 2016. "Diagnosis and Treatment of Melanoma. European Consensus-Based Interdisciplinary Guideline - Update 2016." *European Journal of Cancer* 63:201–17.
- Geissinger, Eva, Christin Weisser, Petra Fischer, Manfred Scharl, and Claudia Wellbrock. 2002. "Autocrine Stimulation by Osteopontin Contributes to Antiapoptotic Signalling of Melanocytes in Dermal Collagen." *Cancer Research* 62(16):4820–28.
- Gershenwald, Jeffrey E. and Merrick I. Ross. 2011. "Sentinel-Lymph-Node Biopsy for Cutaneous Melanoma." *New England Journal of Medicine* 364(18):1738–45.
- Goding, Colin R. 2000. "Mitf from Neural Crest to Melanoma: Signal Transduction and Transcription in the Melanocyte Lineage." *Genes and Development* 14(14):1712–28.
- Goding, Colin R. 2007. "Melanocytes: The New Black." *International Journal of Biochemistry and Cell Biology* 39(2):275–79.
- Goodall, Jane, Suzanne Carreira, Laurence Denat, Dominique Kobi, Irwin Davidson, Paolo Nuciforo, Richard A. Sturm, Lionel Larue, and Colin R. Goding. 2008. "Brn-2 Represses Microphthalmia-Associated Transcription Factor Expression and Marks a Distinct Subpopulation of Microphthalmia-Associated Transcription Factor-Negative Melanoma Cells." *Cancer Research* 68(19):7788–94.
- Green, Stephen A., Marcos Simoes-Costa, and Marianne E. Bronner. 2015. "Evolution of Vertebrates as Viewed from the Crest." *Nature* 520(7548):474–82.
- Greene, Mark H., David E. Elder, Dupont Guerry, Martin N. Epstein, Mark H. Greene, and Marie Van Horn. 1984. "A Study of Tumor Progression: The Precursor Lesions of Superficial Spreading and

Nodular Melanoma.” *Human Pathology* 15(12):1147–65.

Grote, David, Sami Kamel Boualia, Abdallah Souabni, Calli Merkel, Xuan Chi, Frank Costantini, Thomas Carroll, and Maxime Bouchard. 2008. “Gata3 Acts Downstream of β -Catenin Signaling to Prevent Ectopic Metanephric Kidney Induction” edited by V. van Heyningen. *PLoS Genetics* 4(12):e1000316.

Grubb, Robert L., Peter L. Choyke, Peter A. Pinto, W. Marston Linehan, and McClellan M. Walther. 2005. “Management of von Hippel-Lindau-Associated Kidney Cancer.” *Nature Clinical Practice Urology* 2(5):248–54.

Guo, Xing and Xiao Fan Wang. 2009. “Signaling Cross-Talk between TGF- β /BMP and Other Pathways.” *Cell Research* 19(1):71–88.

Gupta, Jayanta, Nandita Mitra, Peter A. Kanetsky, Joe Devaney, Maria R. Wing, Muredach Reilly, Vallabh O. Shah, Vaidyanathapura S. Balakrishnan, Nicolas J. Guzman, Matthias Girndt, Brian G. Periera, Harold I. Feldman, John W. Kusek, Marshall M. Joffe, Dominic S. Raj, and CRIC Study Investigators. 2012. “Association between Albuminuria, Kidney Function, and Inflammatory Biomarker Profile in CKD in CRIC.” *Clinical Journal of the American Society of Nephrology : CJASN* 7(12):1938–46.

Hartman, Mariusz L. and Malgorzata Czyz. 2015. “Pro-Survival Role of MITF in Melanoma.” *Journal of Investigative Dermatology* 135(2):352–58.

Hauschild, Axel, Jean Jacques Grob, Lev V. Demidov, Thomas Jouary, Ralf Gutzmer, Michael Millward, Piotr Rutkowski, Christian U. Blank, Wilson H. Miller, Eckhart Kaempgen, Salvador Martín-Algarra, Boguslawa Karaszewska, Cornelia Mauch, Vanna Chiarion-Sileni, Anne Marie Martin, Suzanne Swann, Patricia Haney, Beloo Mirakhur, Mary E. Guckert, Vicki Goodman, and Paul B. Chapman. 2012. “Dabrafenib in BRAF-Mutated Metastatic Melanoma: A Multicentre, Open-Label, Phase 3 Randomised Controlled Trial.” *The Lancet* 380(9839):358–65.

Hemesath, Timothy J., Eiríkur Steingrímsson, Gaël McGill, Michael J. Hansen, James Vaught, Colin A. Hodgkinson, Heinz Arnheiter, Neal G. Copeland, Nancy A. Jenkins, and David E. Fisher. 1994. “Microphthalmia, A Critical Factor in Melanocyte Development, Defines a Discrete Transcription Factor Family.” *Genes and Development* 8(22):2770–80.

Hershey, Christine L. and David E. Fisher. 2005. “Genomic Analysis of the Microphthalmia Locus and Identification of the MITF-J/Mitf-J Isoform.” *Gene* 347(1):73–82.

Heyman, Samuel N., Christian Rosenberger, and Seymour Rosen. 2010. “Experimental Ischemia-Reperfusion: Biases and Myths: The Proximal vs. Distal Hypoxic Tubular Injury Debate Revisited.” *Kidney International* 77(1):9–16.

Hodis, Eran, Ian R. Watson, Gregory V. Kryukov, Stefan T. Arold, Marcin Imielinski, Jean Philippe Theurillat, Elizabeth Nickerson, Daniel Auclair, Liren Li, Chelsea Place, Daniel Dicara, Alex H. Ramos, Michael S. Lawrence, Kristian Cibulskis, Andrey Sivachenko, Douglas Voet, Gordon Saksena, Nicolas Stransky, Robert C. Onofrio, Wendy Winckler, Kristin Ardlie, Nikhil Wagle, Jennifer Wargo, Kelly Chong, Donald L. Morton, Katherine Stemke-Hale, Guo Chen, Michael Noble, Matthew Meyerson, John E. Ladbury, Michael A. Davies, Jeffrey E. Gershenwald, Stephan N. Wagner, Dave S. B. Hoon, Dirk Schadendorf, Eric S. Lander, Stacey B. Gabriel, Gad Getz, Levi A. Garraway, and Lynda Chin. 2012. “A Landscape of Driver Mutations in Melanoma.” *Cell* 150(2):251–63.

Hoek, Keith S. and Colin R. Goding. 2010. “Cancer Stem Cells versus Phenotype-Switching in Melanoma.” *Pigment Cell and Melanoma Research* 23(6):746–59.

Hoek, Keith S., Natalie C. Schlegel, Patricia Brafford, Antje Sucker, Selma Ugurel, Rajiv Kumar, Barbara L. Weber, Katherine L. Nathanson, David J. Phillips, Meenhard Herlyn, Dirk Schadendorf, and Reinhard Dummer. 2006. “Metastatic Potential of Melanomas Defined by Specific Gene Expression Profiles with No BRAF Signature.” *Pigment Cell Research* 19(4):290–302.

Hoek, Keith S., Natalie C. Schlegel, Ossia M. Eichhoff, Daniel S. Widmer, Christian Praetorius,

- Steingrímur O. Einarsson, Sigríður Valgeirsdóttir, Kristín Bergsteinsdóttir, Alexander Schepsky, Reinhard Dummer, and Eiríkur Steingrímsson. 2008. “Novel MITF Targets Identified Using a Two-Step DNA Microarray Strategy.” *Pigment Cell and Melanoma Research* 21(6):665–76.
- Hong, Andrew L., Yuen Yi Tseng, Jeremiah A. Wala, Won Jun Kim, Bryan D. Kynnap, Mihir B. Doshi, Guillaume Kugener, Gabriel J. Sandoval, Thomas P. Howard, Ji Li, Xiaoping Yang, Michelle Tillgren, Mahmoud Ghandi, Abeer Sayeed, Rebecca Deasy, Abigail Ward, Brian McSteen, Katherine M. Labella, Paula Keskula, Adam Tracy, Cora Connor, Catherine M. Clinton, Alanna J. Church, Brian D. Crompton, Katherine A. Janeway, Barbara Van Hare, David Sandak, Ole Gjoerup, Pratiti Bandopadhyay, Paul A. Clemons, Stuart L. Schreiber, David E. Root, Prafulla C. Gokhale, Susan N. Chi, Elizabeth A. Mullen, Charles W. M. Roberts, Cigall Kadoch, Rameen Beroukhi, Keith L. Ligon, Jesse S. Boehm, and William C. Hahn. 2019. “Renal Medullary Carcinomas Depend upon SMARCB1 Loss and Are Sensitive to Proteasome Inhibition.” *ELife* 8.
- Hsueh, Eddy C. and Kalyan C. Gorantla. 2016. “Novel Melanoma Therapy.” *Experimental Hematology and Oncology* 5(1):23.
- Iacovelli, Roberto, Daniela Modica, Antonella Palazzo, Patrizia Trenta, Gabriele Piesco, and Enrico Cortesi. 2015. “Clinical Outcome and Prognostic Factors in Renal Medullary Carcinoma: A Pooled Analysis from 18 Years of Medical Literature.” *Journal of the Canadian Urological Association* 9(3-4APRIL):E172–77.
- Jemal, Ahmedin, Freddie Bray, Melissa M. Center, Jacques Ferlay, Elizabeth Ward, and David Forman. 2011. “Global Cancer Statistics.” *CA: A Cancer Journal for Clinicians* 61(2):69–90.
- Jerby-Arnon, Livnat, Parin Shah, Michael S. Cuoco, Christopher Rodman, Mei Ju Su, Johannes C. Melms, Rachel Leeson, Abhay Kanodia, Shaolin Mei, Jia Ren Lin, Shu Wang, Bokang Rabasha, David Liu, Gao Zhang, Claire Margolais, Orr Ashenberg, Patrick A. Ott, Elizabeth I. Buchbinder, Rizwan Haq, F. Stephen Hodi, Genevieve M. Boland, Ryan J. Sullivan, Dennie T. Frederick, Benchun Miao, Tabea Moll, Keith T. Flaherty, Meenhard Herlyn, Russell W. Jenkins, Rohit Thummalapalli, Monika S. Kowalczyk, Israel Cañadas, Bastian Schilling, Adam N. R. Cartwright, Adrienne M. Luoma, Shruti Malu, Patrick Hwu, Chantale Bernatchez, Marie Andrée Forget, David A. Barbie, Alex K. Shalek, Itay Tirosh, Peter K. Sorger, Kai Wucherpfennig, Eliezer M. Van Allen, Dirk Schadendorf, Bruce E. Johnson, Asaf Rotem, Orit Rozenblatt-Rosen, Levi A. Garraway, Charles H. Yoon, Benjamin Izar, and Aviv Regev. 2018. “A Cancer Cell Program Promotes T Cell Exclusion and Resistance to Checkpoint Blockade.” *Cell* 175(4):984-997.e24.
- Jimbrow, K., W. C. Quevedo, T. B. Fitzpatrick, and G. Szabo. 1976. “Some Aspects of Melanin Biology: 1950-1975.” *Journal of Investigative Dermatology* 67(1):72–89.
- Joseph, Avenel, Humphrey Yao, and Barry T. Hinton. 2009. “Development and Morphogenesis of the Wolffian/Epididymal Duct, More Twists and Turns.” *Developmental Biology* 325(1):6–14.
- Kaunitz, Genevieve J., Tricia R. Cottrell, Mohammed Lilo, Valliammai Muthappan, Jessica Esandrio, Sneha Berry, Haiying Xu, Aleksandra Ogurtsova, Robert A. Anders, Alexander H. Fischer, Stefan Kraft, Meg R. Gerstenblith, Cheryl L. Thompson, Kord Honda, Jonathan D. Cuda, Charles G. Eberhart, James T. Handa, Evan J. Lipson, and Janis M. Taube. 2017. “Melanoma Subtypes Demonstrate Distinct PD-L1 Expression Profiles.” *Laboratory Investigation* 97(9):1063–71.
- Kawasumi, Ryotaro, Takuya Abe, Hiroshi Arakawa, Massimiliano Garre, Kouji Hirota, and Dana Branzei. 2017. “ESCO1/2’s Roles in Chromosome Structure and Interphase Chromatin Organization.” *Genes and Development* 31(21):2136–50.
- King, Alastair J., Marc R. Arnone, Maureen R. Bleam, Katherine G. Moss, Jingsong Yang, Kelly E. Fedorowicz, Kimberly N. Smitheman, Joseph A. Erhardt, Angela Hughes-Earle, Laurie S. Kane-Carson, Robert H. Sinnamon, Hongwei Qi, Tara R. Rheault, David E. Uehling, and Sylvie G. Laquerre. 2013. “Dabrafenib; Preclinical Characterization, Increased Efficacy When Combined with Trametinib, While BRAF/MEK Tool Combination Reduced Skin Lesions.” *PLoS ONE* 8(7).
- Knutson, Sarah K., Natalie M. Warholic, Tim J. Wigle, Christine R. Klaus, Christina J. Allain, Alejandra

- Raimondi, Margaret Porter Scott, Richard Chesworth, Mikel P. Moyer, Robert A. Copeland, Victoria M. Richon, Roy M. Pollock, Kevin W. Kuntz, and Heike Keilhack. 2013. “Durable Tumor Regression in Genetically Altered Malignant Rhabdoid Tumors by Inhibition of Methyltransferase EZH2.” *Proceedings of the National Academy of Sciences of the United States of America* 110(19):7922–27.
- Kobayashi, Akio, M. Todd Valerius, Joshua W. Mugford, Thomas J. Carroll, Michelle Self, Guillermo Oliver, and Andrew P. McMahon. 2008. “Six2 Defines and Regulates a Multipotent Self-Renewing Nephron Progenitor Population throughout Mammalian Kidney Development.” *Cell Stem Cell* 3(2):169–81.
- Koludrovic, Dana, Patrick Laurette, Thomas Strub, Céline Keime, Madeleine Le Coz, Sebastien Coassolo, Gabrielle Mengus, Lionel Larue, and Irwin Davidson. 2015. “Chromatin-Remodelling Complex NURF Is Essential for Differentiation of Adult Melanocyte Stem Cells” edited by W. A. Bickmore. *PLOS Genetics* 11(10):e1005555.
- Kondo, Taisuke and Vincent J. Hearing. 2011. “Update on the Regulation of Mammalian Melanocyte Function and Skin Pigmentation.” *Expert Review of Dermatology* 6(1):97–108.
- Konieczkowski, David J., Cory M. Johannessen, Omar Abudayyeh, Jong Wook Kim, Zachary A. Cooper, Adriano Piris, Dennie T. Frederick, Michal Barzily-Rokni, Ravid Straussman, Rizwan Haq, David E. Fisher, Jill P. Mesirov, William C. Hahn, Keith T. Flaherty, Jennifer A. Wargo, Pablo Tamayo, and Levi A. Garraway. 2014. “A Melanoma Cell State Distinction Influences Sensitivity to MAPK Pathway Inhibitors.” *Cancer Discovery* 4(7):816–27.
- Krauthammer, Michael, Yong Kong, Antonella Bacchiocchi, Perry Evans, Natapol Pornputtpong, Cen Wu, James P. McCusker, Shuangge Ma, Elaine Cheng, Robert Straub, Merdan Serin, Marcus Bosenberg, Stephan Ariyan, Deepak Narayan, Mario Sznol, Harriet M. Kluger, Shrikant Mane, Joseph Schlessinger, Richard P. Lifton, and Ruth Halaban. 2015. “Exome Sequencing Identifies Recurrent Mutations in NF1 and RASopathy Genes in Sun-Exposed Melanomas.” *Nature Genetics* 47(9):996–1002.
- Lamley, K. V. and W. Kriz. 1991. “Anatomy of the Renal Interstitium.” *Kidney International* 39(3):370–81.
- Land, Edward J., Christopher A. Ramsden, and Patrick A. Riley. 2003. “Tyrosinase Autoactivation and the Chemistry of Ortho-Quinone Amines.” *Accounts of Chemical Research* 36(5):300–308.
- Larue, Lionel, Mayuko Kumasaka, and Colin R. Goding. 2003. “B-Catenin in the Melanocyte Lineage.” *Pigment Cell Research* 16(3):312–17.
- Laurette, Patrick, Thomas Strub, Dana Koludrovic, Celine Keime, Stephanie Le Gras, Hannah Seberg, Eric Van Otterloo, Hana Imrichova, Robert Siddaway, Stein Aerts, Robert A. Cornell, Gabrielle Mengus, and Irwin Davidson. 2015. “Transcription Factor MITF and Remodeller BRG1 Define Chromatin Organisation at Regulatory Elements in Melanoma Cells.” *ELife* 2015(4):1–40.
- Lee, Chang Joon, David W. Smith, Bruce S. Gardiner, and Roger G. Evans. 2019. “Stimulation of Erythropoietin Release by Hypoxia and Hypoxemia: Similar but Different.” *Kidney International* 95(1):23–25.
- Lee Hamm, L., Nazih Nakhoul, and Kathleen S. Hering-Smith. 2015. “Acid-Base Homeostasis.” *Clinical Journal of the American Society of Nephrology* 10(12):2232–42.
- Leibovich, Bradley C., Christine M. Lohse, Paul L. Crispen, Stephen A. Boorjian, R. Houston Thompson, Michael L. Blute, and John C. Cheville. 2010. “Histological Subtype Is an Independent Predictor of Outcome for Patients With Renal Cell Carcinoma.” *Journal of Urology* 183(4):1309–16.
- Levy, Carmit, Mehdi Khaled, and David E. Fisher. 2006. “MITF: Master Regulator of Melanocyte Development and Melanoma Oncogene.” *Trends in Molecular Medicine* 12(9):406–14.
- Liebich, H. M. and C. Först. 1990. “Basic Profiles of Organic Acids in Urine.” *Journal of Chromatography B: Biomedical Sciences and Applications* 525(C):1–14.
- Lin, Jennifer Y. and David E. Fisher. 2007. “Melanocyte Biology and Skin Pigmentation.” *Nature*

445(7130):843–50.

Linehan, W. Marston, James Vasselli, Ramaprasad Srinivasan, McClellan M. Walther, Maria Merino, Peter Choyke, Cathy Vocke, Laura Schmidt, Jennifer S. Isaacs, Gladys Glenn, Jorge Toro, Berton Zbar, Donald Bottaro, Len Neckers, Robert Figlin, Michael Gordon, Janice Dutcher, and Michael Atkins. 2004. “Genetic Basis of Cancer of the Kidney: Disease-Specific Approaches to Therapy.” in *Clinical Cancer Research*. Vol. 10. Clin Cancer Res.

Liu, Youxia, Xinxin Ma, Jie Zheng, Xiangchun Liu, and Tiekun Yan. 2017. “Pregnancy Outcomes in Patients with Acute Kidney Injury during Pregnancy: A Systematic Review and Meta-Analysis.” *BMC Pregnancy and Childbirth* 17(1).

Louphrasitthiphol, Pakavarin, Ioanna Ledaki, Jagat Chauhan, Paola Falletta, Robert Siddaway, Francesca M. Buffa, David R. Mole, Tomoyoshi Soga, and Colin R. Goding. 2019. “MITF Controls the TCA Cycle to Modulate the Melanoma Hypoxia Response.” *Pigment Cell & Melanoma Research* 32(6):792–808.

Luskin, Marlise R., Mark A. Murakami, Scott R. Manalis, and David M. Weinstock. 2018. “Targeting Minimal Residual Disease: A Path to Cure?” *Nature Reviews Cancer* 18(4):255–63.

MacCallum, Robert N., Edward C. Lynch, J. David Hellums, and Clarence P. Alfrey. 1975. “Fragility of Abnormal Erythrocytes Evaluated by Response to Shear Stress.” *The Journal of Laboratory and Clinical Medicine* 85(1):67–74.

Madison, Kathi C. 2003. “Barrier Function of the Skin: ‘La Raison d’Être’ of the Epidermis.” *Journal of Investigative Dermatology* 121(2):231–41.

Maertens, Ophélie, Bryan Johnson, Pablo Hollstein, Dennie T. Frederick, Zachary A. Cooper, Ludwine Messiaen, Roderick T. Bronson, Martin McMahon, Scott Granter, Keith Flaherty, Jennifer A. Wargo, Richard Marais, and Karen Cichowski. 2013. “Elucidating Distinct Roles for NF1 in Melanomagenesis.” *Cancer Discovery* 3(3):339–49.

Makoto, Ikeya, Scott M. K. Lee, Jane E. Johnson, Andrew P. Mc Mahon, and Shinji Takada. 1997. “Wnt Signalling Required for Expansion of Neural Crest and Cns Progenitors.” *Nature* 389(6654):966–70.

Malouf, Gabriel G., Siraj M. Ali, Kai Wang, Sohail Balasubramanian, Jeffrey S. Ross, Vincent A. Miller, Philip J. Stephens, David Khayat, Sumanta K. Pal, Xiaoping Su, Kanishka Sircar, Pheroze Tamboli, Eric Jonasch, Nizar M. Tannir, Christopher G. Wood, and Jose A. Karam. 2016. “Genomic Characterization of Renal Cell Carcinoma with Sarcomatoid Dedifferentiation Pinpoints Recurrent Genomic Alterations.” *European Urology* 70(2):348–57.

Mayor, Roberto and Eric Theveneau. 2012. “The Neural Crest.” *Development (Cambridge)* 140(11):2247–51.

Melero, Ignacio, Antonio M. Grimaldi, Jose L. Perez-Gracia, and Paolo A. Ascierto. 2013. “Clinical Development of Immunostimulatory Monoclonal Antibodies and Opportunities for Combination.” *Clinical Cancer Research* 19(5):997–1008.

Michaloglou, C., L. C. W. Vredeveld, W. J. Mooi, and D. S. Peeper. 2008. “BRAFE600 in Benign and Malignant Human Tumours.” *Oncogene* 27(7):877–95.

Moch, Holger, Antonio L. Cubilla, Peter A. Humphrey, Victor E. Reuter, and Thomas M. Ulbright. 2016. “The 2016 WHO Classification of Tumours of the Urinary System and Male Genital Organs—Part A: Renal, Penile, and Testicular Tumours.” *European Urology* 70(1):93–105.

Msaouel, Pavlos, Gabriel G. Malouf, Xiaoping Su, Hui Yao, Durga N. Tripathi, Melinda Soeung, Jianjun Gao, Priya Rao, Cristian Coarfa, Chad J. Creighton, Jean Philippe Bertocchio, Selvi Kunnimalaiyaan, Asha S. Multani, Jorge Blando, Rong He, Daniel D. Shapiro, Luigi Perelli, Sanjana Srinivasan, Federica Carbone, Patrick G. Pilié, Menuka Karki, Riyad N. H. Seervai, Bujamin H. Vokshi, Dolores Lopez-Terrada, Emily H. Cheng, Ximing Tang, Wei Lu, Ignacio I. Wistuba, Timothy C. Thompson, Irwin Davidson, Virginia Giuliani, Katharina Schlacher, Alessandro Carugo, Timothy P. Heffernan, Padmanee Sharma, Jose A. Karam, Christopher G. Wood, Cheryl L. Walker, Giannicola

- Genovese, and Nizar M. Tannir. 2020. “Comprehensive Molecular Characterization Identifies Distinct Genomic and Immune Hallmarks of Renal Medullary Carcinoma.” *Cancer Cell* 37(5):720-734.e13.
- Msaouel, Pavlos, Nizar M. Tannir, and Cheryl Lyn Walker. 2018. “A Model Linking Sickle Cell Hemoglobinopathies and Smarcb1 Loss in Renal Medullary Carcinoma.” *Clinical Cancer Research* 24(9):2044–49.
- Mukherjee, Nabanita, Yan Lu, Adam Almeida, Karoline Lambert, Chung Wai Shiau, Jung Chen Su, Yuchun Luo, Mayumi Fujita, William A. Robinson, Steven E. Robinson, David A. Norris, and Yiqun G. Shellman. 2017. “Use of a MCL-1 Inhibitor Alone to de-Bulk Melanoma and in Combination to Kill Melanoma Initiating Cells.” *Oncotarget* 8(29):46801–17.
- Müller, Judith, Oscar Krijgsman, Jennifer Tsoi, Lidia Robert, Willy Hugo, Chunying Song, Xiangju Kong, Patricia A. Possik, Paulien D. M. Cornelissen-Steijger, Marnix H. Geuke, Foppen, Kristel Kemper, Colin R. Goding, Ultan McDermott, Christian Blank, John Haanen, Thomas G. Graeber, Antoni Ribas, Roger S. Lo, and Daniel S. Peeper. 2014. “Low MITF/AXL Ratio Predicts Early Resistance to Multiple Targeted Drugs in Melanoma.” *Nature Communications* 5(1):1–15.
- Murayama, Makio. 1966. “Tertiary Structure of Sickle Cell Hemoglobin and Its Functional Significance.” *Journal of Cellular Physiology* 67(S1):21–31.
- Murukesh, N., C. Dive, and G. C. Jayson. 2010. “Biomarkers of Angiogenesis and Their Role in the Development of VEGF Inhibitors.” *British Journal of Cancer* 102(1):8–18.
- Nakayama, Robert T., John L. Pulice, Alfredo M. Valencia, Matthew J. McBride, Zachary M. McKenzie, Mark A. Gillespie, Wai Lim Ku, Mingxiang Teng, Kairong Cui, Robert T. Williams, Seth H. Cassel, He Qing, Christian J. Widmer, George D. Demetri, Rafael A. Irizarry, Keji Zhao, Jeffrey A. Ranish, and Cigall Kadoch. 2017. “SMARCB1 Is Required for Widespread BAF Complex-Mediated Activation of Enhancers and Bivalent Promoters.” *Nature Genetics* 49(11):1613–23.
- Nickerson, Michael L., Erich Jaeger, Yangu Shi, Jeffrey A. Durocher, Sunil Mahurkar, David Zaridze, Vsevolod Matveev, Vladimir Janout, Hellena Kollarova, Vladimir Bencko, Marie Navratilova, Neonilia Szeszenia-Dabrowska, Dana Mates, Anush Mukeria, Ivana Holcatova, Laura S. Schmidt, Jorge R. Toro, Sara Karami, Rayjean Hung, Gary F. Gerard, W. Marston Linehan, Maria Merino, Berton Zbar, Paolo Boffetta, Paul Brennan, Nathaniel Rothman, Wong Ho Chow, Frederic M. Waldman, and Lee E. Moore. 2008. “Improved Identification of von Hippel-Lindau Gene Alterations in Clear Cell Renal Tumors.” *Clinical Cancer Research* 14(15):4726–34.
- Nissan, Moriah H., Christine A. Pratilas, Alexis M. Jones, Ricardo Ramirez, Helen Won, Cailian Liu, Shakuntala Tiwari, Li Kong, Aphrothiti J. Hanrahan, Zhan Yao, Taha Merghoub, Antoni Ribas, Paul B. Chapman, Rona Yaeger, Barry S. Taylor, Nikolaus Schultz, Michael F. Berger, Neal Rosen, and David B. Solit. 2014. “Loss of NF1 in Cutaneous Melanoma Is Associated with RAS Activation and MEK Dependence.” *Cancer Research* 74(8):2340–50.
- Padala, Sandeep Anand, Adam Barsouk, Krishna Chaitanya Thandra, Kalyan Saginala, Azeem Mohammed, Anusha Vakiti, Prashanth Rawla, and Alexander Barsouk. 2020. “Epidemiology of Renal Cell Carcinoma.” *World Journal of Oncology* 11(3):79–87.
- Pallone, Thomas L. 2014. “Complex Vascular Bundles, Thick Ascending Limbs, and Aquaporins: Wringing out the Outer Medulla.” *American Journal of Physiology - Renal Physiology* 306(5):F505.
- Pallone, Thomas L., Channing R. Robertson, and Rex L. Jamison. 1990. “Renal Medullary Microcirculation.” *Physiological Reviews* 70(3):885–920.
- Patard, Jean Jacques, Emmanuelle Leray, Nathalie Rioux-Leclercq, Luca Cindolo, Vincenzo Ficarra, Amnon Zisman, Alexandre De La Taille, Jacques Tostain, Walter Artibani, Claude C. Abbou, Bernard Lobel, François Guillé, Dominique K. Chopin, Peter F. A. Mulders, Christopher G. Wood, David A. Swanson, Robert A. Figlin, Arie S. Belldegrun, and Allan J. Pantuck. 2005. “Prognostic Value of Histologic Subtypes in Renal Cell Carcinoma: A Multicenter Experience.” *Journal of Clinical Oncology* 23(12):2763–71.

- Pavlick, Anna C., Antoni Ribas, Rene Gonzalez, Omid Hamid, Thomas Gajewski, Adil Daud, Igor Puzanov, Jessie J. Hsu, Nicholas W. Choong, and Grant A. McArthur. 2015. “Extended Follow-up Results of Phase Ib Study (BRIM7) of Vemurafenib (VEM) with Cobimetinib (COBI) in BRAF -Mutant Melanoma. ” *Journal of Clinical Oncology* 33(15_suppl):9020–9020.
- Pla, Patrick and Anne H. Monsoro-Burq. 2018. “The Neural Border: Induction, Specification and Maturation of the Territory That Generates Neural Crest Cells.” *Developmental Biology* 444:S36–46.
- Pogenberg, Vivian, Margrét H. Ögmundsdóttir, Kristín Bergsteinsdóttir, Alexander Schepsky, Bengt Phung, Viktor Deineko, Morlin Milewski, Eiríkur Steingrímsson, and Matthias Wilmanns. 2012. “Restricted Leucine Zipper Dimerization and Specificity of DNA Recognition of the Melanocyte Master Regulator MITF.” *Genes and Development* 26(23):2647–58.
- Polakovicova, S., H. Seidenberg, R. Mikusova, S. Polak, and V. Pospisilova. 2011. “Merkel Cells - Review on Developmental, Functional and Clinical Aspects.” *Bratislava Medical Journal* 112(2):80–87.
- Pollock, Pamela M., Ursula L. Harper, Katherine S. Hansen, Laura M. Yudt, Mitchell Stark, Christiane M. Robbins, Tracy Y. Moses, Galen Hostetter, Urs Wagner, John Kakareka, Ghadi Salem, Tom Pohida, Peter Heenan, Paul Duray, Olli Kallioniemi, Nicholas K. Hayward, Jeffrey M. Trent, and Paul S. Meltzer. 2003. “High Frequency of BRAF Mutations in Nevi.” *Nature Genetics* 33(1):19–20.
- Prince, Sharon, Suzanne Carreira, Keith W. Vance, Amaal Abrahams, and Colin R. Goding. 2004. “Tbx2 Directly Represses the Expression of the P21WAF1 Cyclin-Dependent Kinase Inhibitor.” *Cancer Research* 64(5):1669–74.
- Proksch, Ehrhardt, Regina Fölster-Holst, Matthias Bräutigam, Marjan Sepehrmanesh, Stephan Pfeiffer, and Jens Michael Jensen. 2009. “Role of the Epidermal Barrier in Atopic Dermatitis: Academy CME.” *JDDG - Journal of the German Society of Dermatology* 7(10):899–910.
- Prommer, Hans Ulrich, Johannes Maurer, Karoline Von Websky, Christian Freise, Kerstin Sommer, Hamoud Nasser, Rudi Samapati, Bettina Reglin, Pedro Guimarães, Axel Radlach Pries, and Uwe Querfeld. 2018. “Chronic Kidney Disease Induces a Systemic Microangiopathy, Tissue Hypoxia and Dysfunctional Angiogenesis.” *Scientific Reports* 8(1):1–14.
- Qian, Xiaoyuan, Zhixian Wang, Jiaqiao Zhang, Qing Wang, Peng Zhou, Shaogang Wang, Bo Wang, and Can Qian. 2020. “Clinical Features and Prognostic Outcome of Renal Collecting Duct Carcinoma: 12 Cases from a Single Institution.” *Cancer Management and Research* 12:3589–95.
- Quintana, Elsa, Mark Shackleton, Hannah R. Foster, Douglas R. Fullen, Michael S. Sabel, Timothy M. Johnson, and Sean J. Morrison. 2010. “Phenotypic Heterogeneity among Tumorigenic Melanoma Cells from Patients That Is Reversible and Not Hierarchically Organized.” *Cancer Cell* 18(5):510–23.
- Rambow, Florian, Jean Christophe Marine, and Colin R. Goding. 2019. “Melanoma Plasticity and Phenotypic Diversity: Therapeutic Barriers and Opportunities.” *Genes and Development* 33(19–20):1295–1318.
- Rambow, Florian, Aljosja Rogiers, Oskar Marin-Bejar, Sara Aibar, Julia Femel, Michael Dewaele, Panagiotis Karras, Daniel Brown, Young Hwan Chang, Maria Debiec-Rychter, Carmen Adriaens, Enrico Radaelli, Pascal Wolter, Oliver Bechter, Reinhard Dummer, Mitchell Levesque, Adriano Piris, Dennie T. Frederick, Genevieve Boland, Keith T. Flaherty, Joost van den Oord, Thierry Voet, Stein Aerts, Amanda W. Lund, and Jean Christophe Marine. 2018. “Toward Minimal Residual Disease-Directed Therapy in Melanoma.” *Cell* 174(4):843-855.e19.
- Ranieri, Marianna. 2019. “Renal Ca²⁺ and Water Handling in Response to Calcium Sensing Receptor Signaling: Physiopathological Aspects and Role of CaSR-Regulated MicroRNAs.” *International Journal of Molecular Sciences* 20(21):1–15.
- Rao, Guanhua, Hongyi Wang, Baowei Li, Li Huang, Danfeng Xue, Xiaohui Wang, Haijing Jin, Jun Wang, Yushan Zhu, Youyong Lu, Lei Du, and Quan Chen. 2013. “Reciprocal Interactions between Tumor-Associated Macrophages and CD44-Positive Cancer Cells via Osteopontin/CD44 Promote

Tumorigenicity in Colorectal Cancer.” *Clinical Cancer Research* 19(4):785–97.

Ribas, Antoni, Igor Puzanov, Reinhard Dummer, Dirk Schadendorf, Omid Hamid, Caroline Robert, F. Stephen Hodi, Jacob Schachter, Anna C. Pavlick, Karl D. Lewis, Lee D. Cranmer, Christian U. Blank, Steven J. O’Day, Paolo A. Ascierto, April K. S. Salama, Kim A. Margolin, Carmen Loquai, Thomas K. Eigentler, Tara C. Gangadhar, Matteo S. Carlino, Sanjiv S. Agarwala, Stergios J. Moschos, Jeffrey A. Sosman, Simone M. Goldinger, Ronnie Shapira-Frommer, Rene Gonzalez, John M. Kirkwood, Jedd D. Wolchok, Alexander Eggermont, Xiaoyun Nicole Li, Wei Zhou, Adriane M. Zernhelt, Joy Lis, Scot Ebbinghaus, S. Peter Kang, and Adil Daud. 2015. “Pembrolizumab versus Investigator-Choice Chemotherapy for Ipilimumab-Refractory Melanoma (KEYNOTE-002): A Randomised, Controlled, Phase 2 Trial.” *The Lancet Oncology* 16(8):908–18.

Richtig, G., C. Hoeller, K. Kashofer, A. Aigelsreiter, A. Heinemann, L. N. Kwong, M. Pichler, and E. Richtig. 2017. “Beyond the BRAFV600E Hotspot: Biology and Clinical Implications of Rare BRAF Gene Mutations in Melanoma Patients.” *British Journal of Dermatology* 177(4):936–44.

Riesenberg, Stefanie, Angela Groetchen, Robert Siddaway, Tobias Bald, Julia Reinhardt, Denise Smorra, Judith Kohlmeyer, Marcel Renn, Bengt Phung, Pia Aymans, Tobias Schmidt, Veit Hornung, Irwin Davidson, Colin R. Goding, Göran Jönsson, Jennifer Landsberg, Thomas Tüting, and Michael Hölzel. 2015. “MITF and C-Jun Antagonism Interconnects Melanoma Dedifferentiation with pro-Inflammatory Cytokine Responsiveness and Myeloid Cell Recruitment.” *Nature Communications* 6.

Robert, Caroline, Jacob Schachter, Georgina V. Long, Ana Arance, Jean Jacques Grob, Laurent Mortier, Adil Daud, Matteo S. Carlino, Catriona McNeil, Michal Lotem, James Larkin, Paul Lorigan, Bart Neyns, Christian U. Blank, Omid Hamid, Christine Mateus, Ronnie Shapira-Frommer, Michele Kosh, Honghong Zhou, Nageatte Ibrahim, Scot Ebbinghaus, and Antoni Ribas. 2015. “Pembrolizumab versus Ipilimumab in Advanced Melanoma.” *New England Journal of Medicine* 372(26):2521–32.

Saito-Diaz, Kenyi, Tony W. Chen, Xiaoxi Wang, Curtis A. Thorne, Heather A. Wallace, Andrea Page-Mccaw, and Ethan Lee. 2013. “The Way Wnt Works: Components and Mechanism.” *Growth Factors* 31(1):1–31.

Sanchez, M. P., I. Silos-Santiago, J. Frisen, B. He, S. A. Lira, and M. Barbacid. 1996. “Renal Agenesis and the Absence of Enteric Neurons in Mice Lacking GDNF.” *Nature* 382(6586):70–73.

Sands, Jeff M. and Harold E. Layton. 2009. “The Physiology of Urinary Concentration: An Update.” *Seminars in Nephrology* 29(3):178–95.

Schiaffino, Maria Vittoria. 2010. “Signaling Pathways in Melanosome Biogenesis and Pathology.” *International Journal of Biochemistry and Cell Biology* 42(7):1094–1104.

Schwartz, J. I., K. Vandormael, M. P. Malice, R. N. Kalyani, K. C. Lasseter, G. B. Holmes, B. J. Gertz, K. M. Gottesdiener, M. Laurenzi, K. J. Redfern, and K. Brune. 2002. “Comparison of Rofecoxib, Celecoxib, and Naproxen on Renal Function in Elderly Subjects Receiving a Normal-Salt Diet*.” *Clinical Pharmacology & Therapeutics* 72(1):50–61.

Shaffer, Sydney M., Margaret C. Dunagin, Stefan R. Torborg, Eduardo A. Torre, Benjamin Emert, Clemens Krepler, Marilda Beqiri, Katrin Sproesser, Patricia A. Brafford, Min Xiao, Elliott Egan, Ioannis N. Anastopoulos, Cesar A. Vargas-Garcia, Abhyudai Singh, Katherine L. Nathanson, Meenhard Herlyn, and Arjun Raj. 2017. “Rare Cell Variability and Drug-Induced Reprogramming as a Mode of Cancer Drug Resistance.” *Nature* 546(7658):431–35.

Shah, Amishi Y., Jose A. Karam, Gabriel G. Malouf, Priya Rao, Zita D. Lim, Eric Jonasch, Lianchun Xiao, Jianjun Gao, Ulka N. Vaishampayan, Daniel Y. Heng, Elizabeth R. Plimack, Elizabeth A. Guancial, Chunkit Fung, Stefanie R. Lowas, Pheroze Tamboli, Kanishka Sircar, Surena F. Matin, W. Kimryn Rathmell, Christopher G. Wood, and Nizar M. Tannir. 2017. “Management and Outcomes of Patients with Renal Medullary Carcinoma: A Multicentre Collaborative Study.” *BJU International* 120(6):782–92.

Shah, Darshil J. and Roxana S. Dronca. 2014. “Latest Advances in Chemotherapeutic, Targeted, and Immune Approaches in the Treatment of Metastatic Melanoma.” *Mayo Clinic Proceedings* 89(4):504–

19.

Shah, Mita M., James B. Tee, Tobias Meyer, Catherine Meyer-Schwesinger, Yohan Choi, Derina E. Sweeney, Thomas F. Gallegos, Kohei Johkura, Eran Rosines, Valentina Kouznetsova, David W. Rose, Kevin T. Bush, Hiroyuki Sakurai, and Sanjay K. Nigam. 2009. "The Instructive Role of Metanephric Mesenchyme in Ureteric Bud Patterning, Sculpting, and Maturation and Its Potential Ability to Buffer Ureteric Bud Branching Defects." *American Journal of Physiology - Renal Physiology* 297(5):1330–41.

Shain, A. Hunter and Boris C. Bastian. 2016. "From Melanocytes to Melanomas." *Nature Reviews Cancer* 16(6):345–58.

Shibahara, Shigeki. 2001. "Microphthalmia-Associated Transcription Factor (MITF): Multiplicity in Structure, Function, and Regulation." *Journal of Investigative Dermatology Symposium Proceedings* 6(1):99–104.

Shuch, Brian, Ali Amin, Andrew J. Armstrong, John N. Eble, Vincenzo Ficarra, Antonio Lopez-Beltran, Guido Martignoni, Brian I. Rini, and Alexander Kutikov. 2015. "Understanding Pathologic Variants of Renal Cell Carcinoma: Distilling Therapeutic Opportunities from Biologic Complexity." *European Urology* 67(1):85–97.

Simon, Camille, Jalila Chagraoui, Jana Kroschl, Patrick Gendron, Brian Wilhelm, Sébastien Lemieux, Geneviève Boucher, Pierre Chagnon, Simon Drouin, Raphaëlle Lambert, Claude Rondeau, Annie Bilodeau, Sylvie Lavallée, Martin Sauvageau, Josée Hébert, and Guy Sauvageau. 2012. "A Key Role for EZH2 and Associated Genes in Mouse and Human Adult T-Cell Acute Leukemia." *Genes and Development* 26(7):651–56.

Smith, Lynne T. and Karen A. Holbrook. 1986. "Embryogenesis of the Dermis in Human Skin." *Pediatric Dermatology* 3(4):271–80.

Specenier, Pol. 2016. "Nivolumab in Melanoma." *Expert Review of Anticancer Therapy* 16(12):1247–61.

Steffens, Sandra, Martin Janssen, Frederik C. Roos, Frank Becker, Simon Schumacher, Christoph Seidel, Gerd Wegener, Joachim W. Thüroff, Rainer Hofmann, Michael Stöckle, Stefan Siemer, Mark Schrader, Arndt Hartmann, Markus A. Kuczyk, Kerstin Junker, and Andres J. Schrader. 2012. "Incidence and Long-Term Prognosis of Papillary Compared to Clear Cell Renal Cell Carcinoma - A Multicentre Study." *European Journal of Cancer* 48(15):2347–52.

Steingrímsson, Eiríkur. 2008. "All for One, One for All: Alternative Promoters and Mitf." *Pigment Cell and Melanoma Research* 21(4):412–14.

Strub, T., S. Giuliano, T. Ye, C. Bonet, C. Keime, D. Kobi, S. Le Gras, M. Cormont, R. Ballotti, C. Bertolotto, and I. Davidson. 2011. "Essential Role of Microphthalmia Transcription Factor for DNA Replication, Mitosis and Genomic Stability in Melanoma." *Oncogene* 30(20):2319–32.

Sullivan, Ryan J. and Keith T. Flaherty. 2015. "New Strategies in Melanoma: Entering the Era of Combinatorial Therapy." *Clinical Cancer Research* 21(11):2424–35.

Sviderskaya, Elena V., Vanessa C. Gray-Schopfer, Simon P. Hill, Nico P. Smit, Tracy J. Evans-Whipp, Jane Bond, Lucy Hill, Veronique Bataille, Gordon Peters, David Kipling, David Wynford-Thomas, and Dorothy C. Bennett. 2003. "P16/Cyclin-Dependent Kinase Inhibitor 2A Deficiency in Human Melanocyte Senescence, Apoptosis, and Immortalization: Possible Implications for Melanoma Progression." *Journal of the National Cancer Institute* 95(10):723–32.

Thomas, Aaron J. and Carol A. Erickson. 2008. "The Making of a Melanocyte: The Specification of Melanoblasts from the Neural Crest." *Pigment Cell and Melanoma Research* 21(6):598–610.

Thomas, Aaron J. and Carol A. Erickson. 2009. "FOXD3 Regulates the Lineage Switch between Neural Crest-Derived Glial Cells and Pigment Cells by Repressing MITF through a Non-Canonical Mechanism." *Development* 136(11):1849–58.

Tirosch, Itay, Andrew S. Venteicher, Christine Hebert, Leah E. Escalante, Anoop P. Patel, Keren Yizhak, Jonathan M. Fisher, Christopher Rodman, Christopher Mount, Mariella G. Filbin, Cyril Neftel, Niyati

- Desai, Jackson Nyman, Benjamin Izar, Christina C. Luo, Joshua M. Francis, Aanand A. Patel, Maristela L. Onozato, Nicolo Riggi, Kenneth J. Livak, Dave Gennert, Rahul Satija, Brian V. Nahed, William T. Curry, Robert L. Martuza, Ravindra Mylvaganam, A. John Iafrate, Matthew P. Frosch, Todd R. Golub, Miguel N. Rivera, Gad Getz, Orit Rozenblatt-Rosen, Daniel P. Cahill, Michelle Monje, Bradley E. Bernstein, David N. Louis, Aviv Regev, and Mario L. Suvà. 2016. "Single-Cell RNA-Seq Supports a Developmental Hierarchy in Human Oligodendroglioma." *Nature* 539(7628):309–13.
- Tsoi, Jennifer, Lidia Robert, Kim Paraiso, Carlos Galvan, Katherine M. Sheu, Johnson Lay, Deborah J. L. Wong, Mohammad Atefi, Roksana Shirazi, Xiaoyan Wang, Daniel Braas, Catherine S. Grasso, Nicolaos Palaskas, Antoni Ribas, and Thomas G. Graeber. 2018. "Multi-Stage Differentiation Defines Melanoma Subtypes with Differential Vulnerability to Drug-Induced Iron-Dependent Oxidative Stress." *Cancer Cell* 33(5):890-904.e5.
- Ullrich, Nico, Stefanie Löffek, Susanne Horn, Marie Ennen, Luis Sánchez-del-Campo, Fang Zhao, Frank Breitenbuecher, Irwin Davidson, Bernhard B. Singer, Dirk Schadendorf, Colin R. Goding, and Iris Helfrich. 2015. "MITF Is a Critical Regulator of the Carcinoembryonic Antigen-Related Cell Adhesion Molecule 1 (CEACAM1) in Malignant Melanoma." *Pigment Cell & Melanoma Research* 28(6):736–40.
- Vandamme, Niels and Geert Berx. 2019. "From Neural Crest Cells to Melanocytes: Cellular Plasticity during Development and Beyond." *Cellular and Molecular Life Sciences* 76(10):1919–34.
- Vega-Lopez, Guillermo A., Santiago Cerrizuela, and Manuel J. Aybar. 2017. "Trunk Neural Crest Cells: Formation, Migration and Beyond." *International Journal of Developmental Biology* 61(1–2):5–15.
- Verfaillie, Annelien, Hana Imrichova, Zeynep Kalender Atak, Michael Dewaele, Florian Rambow, Gert Hulselmans, Valerie Christiaens, Dmitry Svetlichnyy, Flavie Luciani, Laura Van Den Mooter, Sofie Claerhout, Mark Fiers, Fabrice Journe, Ghanem Elias Ghanem, Carl Herrmann, Georg Halder, Jean Christophe Marine, and Stein Aerts. 2015. "Decoding the Regulatory Landscape of Melanoma Reveals TEADS as Regulators of the Invasive Cell State." *Nature Communications* 6.
- Versteeg, Isabella, Nicolas Sévenet, Julian Lange, Marie Françoise Rousseau-Merck, Peter Ambros, Rupert Handgretinger, Alain Aurias, and Olivier Delattre. 1998. "Truncating Mutations of HSNF5/INI1 in Aggressive Paediatric Cancer." *Nature* 394(6689):203–6.
- Wallace, M. A. 1998. "Anatomy and Physiology of the Kidney." *AORN Journal* 68(5):799–800.
- Wan, Paul T. C., Mathew J. Garnett, S. Mark Roe, Sharlene Lee, Dan Niculescu-Duvaz, Valerie M. Good, Cancer Genome Project, C. Michael Jones, Christopher J. Marshall, Caroline J. Springer, David Barford, and Richard Marais. 2004. "Mechanism of Activation of the RAF-ERK Signaling Pathway by Oncogenic Mutations of B-RAF." *Cell* 116(6):855–67.
- Wasmeier, Christina, Alistair N. Hume, Giulia Bolasco, and Miguel C. Seabra. 2008. "Melanosomes at a Glance." *Journal of Cell Science* 121(24):3995–99.
- Weatherhead, S. C., M. Haniffa, and C. M. Lawrence. 2007. "Melanomas Arising from Naevi and de Novo Melanomas - Does Origin Matter?" *British Journal of Dermatology* 156(1):72–76.
- Wellbrock, Claudia, Lesley Ogilvie, Douglas Hedley, Maria Karasarides, Jan Martin, Dan Niculescu-Duvaz, Caroline J. Springer, and Richard Marais. 2004. "V599EB-RAF Is an Oncogene in Melanocytes." *Cancer Research* 64(7):2338–42.
- WH, Ward and Farma JM. 2017. *Cutaneous Melanoma: Etiology and Therapy*. Codon Publications.
- Whittaker, Steven R., Jean Philippe Theurillat, Eliezer Van Allen, Nikhil Wagle, Jessica Hsiao, Glenn S. Cowley, Dirk Schadendorf, David E. Root, and Levi A. Garraway. 2013. "A Genome-Scale RNA Interference Screen Implicates NF1 Loss in Resistance to RAF Inhibition." *Cancer Discovery* 3(3):351–62.
- Widmer, Daniel S., Phil F. Cheng, Ossia M. Eichhoff, Benedetta C. Belloni, Marie C. Zipser, Natalie C. Schlegel, Delphine Javelaud, Alain Mauviel, Reinhard Dummer, and Keith S. Hoek. 2012. "Systematic Classification of Melanoma Cells by Phenotype-Specific Gene Expression Mapping."

Pigment Cell and Melanoma Research 25(3):343–53.

Wilson, Paul A., Giorgio Lagna, Atsushi Suzuki, and Ali Hemmati-Brivanlou. 1997. “Concentration-Dependent Patterning of the *Xenopus* Ectoderm by BMP4 and Its Signal Transducer Smad1.” *Development* 124(16):3177–84.

Wood, Kevin and Jason Luke. 2017. “The Biology and Therapeutic Approach to BRAF-Mutant Cutaneous Melanoma.” *The American Journal of Hematology/Oncology* 13(1):4–10.

Wouters, Jasper, Zeynep Kalender-Atak, Liesbeth Minnoye, Katina I. Spanier, Maxime De Waegeneer, Carmen Bravo González-Blas, David Mauduit, Kristofer Davie, Gert Hulselmans, Ahmad Najem, Michael Dewaele, Dennis Pedri, Florian Rambow, Samira Makhzami, Valerie Christiaens, Frederik Ceyskens, Ghanem Ghanem, Jean Christophe Marine, Suresh Poovathingal, and Stein Aerts. 2020. “Robust Gene Expression Programs Underlie Recurrent Cell States and Phenotype Switching in Melanoma.” *Nature Cell Biology* 22(8):986–98.

Wu, Heng, Vikas Goel, and Frank G. Haluska. 2003. “PTEN Signaling Pathways in Melanoma.” *Oncogene* 22(20):3113–22.

Yu, Chune, Xiaowei Liu, Jiqiao Yang, Min Zhang, Hongyu Jin, Xuelei Ma, and Hubing Shi. 2019. “Combination of Immunotherapy with Targeted Therapy: Theory and Practice in Metastatic Melanoma.” *Frontiers in Immunology* 10(MAY):990.

Zhong, Minghao, Patricia De Angelo, Lisa Osborne, Alberto E. Paniz-Mondolfi, Matthew Geller, Youfeng Yang, W. Marston Linehan, Maria J. Merino, Carlos Cordon-Cardo, and Dongming Cai. 2012. “Translocation Renal Cell Carcinomas in Adults: A Single-Institution Experience.” *American Journal of Surgical Pathology* 36(5):654–62.

Zimmerman, Amanda, Ling Bai, and David D. Ginty. 2014. “The Gentle Touch Receptors of Mammalian Skin.” *Science* 346(6212):950–54.

Role of SWI/SNF chromatin-remodeling complexes in tumorigenesis: insights in dedifferentiated melanoma cells and renal medullary carcinoma

Résumé

Les complexes de remodelage de la chromatine SWI/SNF sont composés de 10 à 15 sous-unités et utilisent l'énergie fournie par l'hydrolyse de l'ATP afin de remodeler la structure de la chromatine dans le but de réguler l'expression génique. Ce manuscrit présente l'étude des rôles de SMARCA4 et SMARCB1, deux sous-unités centrales de SWI/SNF, dans les cellules dédifférenciées de mélanome et dans le carcinome du rein médullaire respectivement.

Nos résultats démontrent qu'à la fois SMARCA4 et SMARCB1 ont des fonctions importantes, mais opposées, dans l'oncogenèse. D'une part, SMARCA4 régule et agit en conjonction avec le facteur de transcription mésodermique PRRX1 afin de promouvoir la croissance tridimensionnelle des cellules dédifférenciées de mélanome, un type mésenchymateux de mélanome aux fortes capacités invasives et résistantes aux traitements. D'autre part, SMARCB1 agit comme un suppresseur de tumeur dans le carcinome du rein médullaire, une forme rare mais létale de cancers rénaux, en bloquant MYC et en coopérant avec le facteur de transcription rénal TFCP2L1 afin d'induire la mort cellulaire par ferroptose et la transition mésenchymato-épithéliale (TME).

L'ensemble de ce travail de thèse a permis de mettre en évidence de nouveaux mécanismes de régulation épigénétique de l'oncogenèse par les complexes SWI/SNF contenant SMARCA4 ou SMARCB1 dans deux types de cancers très agressifs et résistants aux traitements conventionnels. Ces résultats préliminaires pourront servir de base pour le développement de nouvelles approches thérapeutiques à travers l'exploitation des vulnérabilités intrinsèques qui ont été identifiées, notamment CLDN1 dans le mélanome dédifférencié et GPX4 dans le carcinome du rein médullaire.

Mots-clés: SWI/SNF, remodelage de la chromatine, épigénétique, BRG1, SMARCB1, cancer, TEM

Abstract

The Switch/Sucrose non-fermentable (SWI/SNF) chromatin-remodeling complexes, comprising 10-15 subunits, that use the energy delivered by ATP hydrolysis to remodel the structure of chromatin and in turn regulate gene expression. Here we investigated the role of SMARCA4 and SMARCB1, two SWI/SNF core subunits, in dedifferentiated melanoma and renal medullary carcinoma respectively.

Our results show that both SMARCA4 and SMARCB1 are important regulators of tumorigenesis, despite displaying distinct functions. On one hand, SMARCA4 regulates and acts in conjunction with a mesoderm-specific transcription factor PRRX1 to promote tridimensional spheroid growth in dedifferentiated melanoma cells, a type of melanoma that displays a mesenchymal signature with highly invasive and drug-resistant properties. On the other hand, SMARCB1 acts as a tumor-suppressor in renal medullary carcinoma, a rare but lethal form of kidney cancer, by antagonizing MYC and cooperates with a renal-specific transcription factor TFCP2L1 to induce cell death by ferroptosis and mesenchymal-to-epithelial transition (MET).

We have shed lights on new mechanisms of epigenetic regulation of tumorigenesis by the SMARCB1- and SMARCA4-containing SWI/SNF complexes in two types of highly aggressive and hard-to-treat cancers. Furthermore, these works have paved the way for developing novel therapeutic approaches by exploiting tumor-intrinsic vulnerabilities, namely CLDN1 in dedifferentiated melanoma and GPX4 in renal medullary carcinoma.

Keywords : SWI/SNF, chromatin-remodeling, epigenetics, BRG1, SMARCB1, cancer, EMT